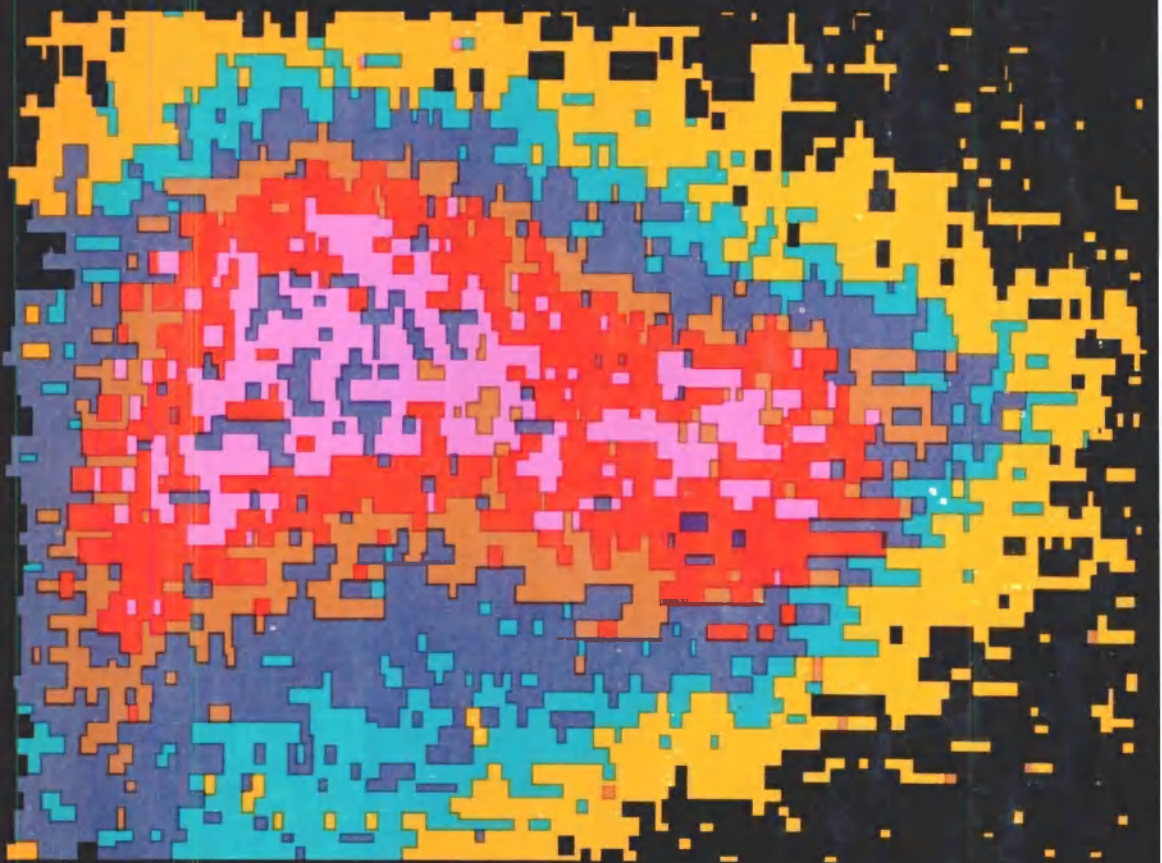

Proceedings of a Symposium, Athens, 20-24 April 1964

MEDICAL RADIOISOTOPE SCANNING

VOL. I

INTERNATIONAL ATOMIC ENERGY AGENCY, VIENNA, 1964

The following States are Members of the International Atomic Energy Agency:

AFGHANISTAN
ALBANIA
ALGERIA
ARGENTINA
AUSTRALIA
AUSTRIA
BELGIUM
BOLIVIA
BRAZIL
BULGARIA
BURMA
BYELORUSSIAN SOVIET SOCIALIST REPUBLIC
CAMBODIA
CAMEROUN
CANADA
CEYLON
CHILE
CHINA
COLOMBIA
CONGO (LÉOPOLDVILLE)
CUBA
CZECHOSLOVAK SOCIALIST REPUBLIC
DENMARK
DOMINICAN REPUBLIC
ECUADOR
EL SALVADOR
ETHIOPIA
FINLAND
FRANCE
FEDERAL REPUBLIC OF GERMANY
GABON
GHANA
GREECE
GUATEMALA
HAITI
HOLY SEE
HONDURAS
HUNGARY
ICELAND
INDIA
INDONESIA
IRAN
IRAQ
ISRAEL
ITALY
IVORY COAST
JAPAN
REPUBLIC OF KOREA
LEBANON
LIBERIA
LIBYA
LUXEMBOURG
MALI
MEXICO
MONACO
MOROCCO
NETHERLANDS
NEW ZEALAND
NICARAGUA
NIGERIA
NORWAY
PAKISTAN
PARAGUAY
PERU
PHILIPPINES
POLAND
PORTUGAL
ROMANIA
SAUDI ARABIA
SENEGAL
SOUTH AFRICA
SPAIN
SUDAN
SWEDEN
SWITZERLAND
SYRIA
THAILAND
TUNISIA
TURKEY
UKRAINIAN SOVIET SOCIALIST REPUBLIC
UNION OF SOVIET SOCIALIST REPUBLICS
UNITED ARAB REPUBLIC
UNITED KINGDOM OF GREAT BRITAIN AND NORTHERN IRELAND
UNITED STATES OF AMERICA
URUGUAY
VENEZUELA
VIET-NAM
YUGOSLAVIA

The Agency's Statute was approved on 23 October 1956 by the Conference on the Statute of the IAEA held at United Nations Headquarters, New York; it entered into force on 29 July 1957. The Headquarters of the Agency are situated in Vienna. Its principal objective is "to accelerate and enlarge the contribution of atomic energy to peace, health and prosperity throughout the world".

Printed by the IAEA in Austria
October 1964

MEDICAL RADIOISOTOPE SCANNING

VOL. I

PROCEEDINGS SERIES

MEDICAL RADIOISOTOPE SCANNING

PROCEEDINGS OF THE SYMPOSIUM ON
MEDICAL RADIOISOTOPE SCANNING
HELD BY THE
INTERNATIONAL ATOMIC ENERGY AGENCY
IN ATHENS, 20-24 APRIL 1964

In two volumes

VOL.I

INTERNATIONAL ATOMIC ENERGY AGENCY
VIENNA, 1964

Symposium on Medical Radioisotope Scanning, Athens, 20 - 26 April 1964.
Proceedings ... held by the International Atomic Energy Agency ... Vienna, the Agency, 1964.
2 vols. (IAEA, Proceedings series)

616.073.75
612.014.483
621.039.85

MEDICAL RADIOISOTOPE SCANNING,
IAEA, VIENNA, 1964
STI/PUB/82

FOREWORD

Medical applications of radioisotopes continue to grow in number and importance and medical centres in almost all countries of the world are now using radioactive materials both in the diagnosis and treatment of disease. An increasing proportion of these applications involves studies of the spatial distribution of radioactive material within the human body, for which purpose highly specialized scanning methods have been elaborated. By these methods it is possible to study the position, size and functional state of different organs, to detect tumours, cysts and other abnormalities and to obtain much useful information about regions of the body that are otherwise inaccessible, except by surgery.

Progress in scanning methods in recent years has been very rapid and there have been many important advances in instrumentation and technique. The development of new forms of the gamma camera and of colour-scanning techniques are but two examples of recent improvements. The production of new radioisotopes and new labelled compounds has further extended the scope of these methods.

To survey these new advances the International Atomic Energy Agency held a Symposium on Medical Radioisotope Scanning in Athens from 20 - 24 April 1964. The scientific programme of the meeting covered all aspects of scanning methods including theoretical principles, instrumentation, techniques and clinical applications. The World Health Organization assisted in the selection of papers by providing a consultant to the selection committee.

The meeting followed the earlier IAEA/WHO Seminar on Medical Radioisotope Scanning in Vienna in 1959, which was attended by 36 participants and at which 14 papers were presented. Some idea of the growth of interest in the subject may be gained from the fact that the Symposium was attended by 160 participants from 26 countries and 4 international organizations, and that 58 papers were presented.

The published proceedings, comprising two volumes, contain all the scientific papers presented at the Symposium together with the subsequent discussions. Volume I covers the sessions devoted to theoretical principles, instrumentation and techniques, whilst Volume II deals with choice of radioisotopes and labelled compounds, clinical applications and interpretation of results. It is hoped that together they will provide a valuable guide to the present status and likely future development of medical radioisotope scanning and its applications.

The Agency gratefully acknowledges the co-operation of the staff of the Greek Atomic Energy Commission.

EDITORIAL NOTE

The papers and discussions incorporated in the proceedings published by the International Atomic Energy Agency are edited by the Agency's editorial staff to the extent considered necessary for the reader's assistance. The views expressed and the general style adopted remain, however, the responsibility of the named authors or participants.

For the sake of speed of publication the present Proceedings have been printed by composition typing and photo-offset lithography. Within the limitations imposed by this method, every effort has been made to maintain a high editorial standard; in particular, the units and symbols employed are to the fullest practicable extent those standardized or recommended by the competent international scientific bodies.

The affiliations of authors are those given at the time of nomination.

The use in these Proceedings of particular designations of countries or territories does not imply any judgement by the Agency as to the legal status of such countries or territories, of their authorities and institutions or of the delimitation of their boundaries.

The mention of specific companies or of their products or brand-names does not imply any endorsement or recommendation on the part of the International Atomic Energy Agency.

CONTENTS OF VOL. I

I. THEORY OF SCANNING

Theory of radioisotope scanning (SM-51/58) 3
G. L. Brownell
Discussion 33
A theory of radioisotope scanning systems (SM-51/52) 35
R. N. Beck
Discussion 55
Information theory and radioisotope scanning (SM-51/29) 57
J. Cederlund
Discussion 75
Theory of scanning and imaging of radioisotope distributions (SM-51/60) 77
B. Cassen
Discussion 86

II. MOVING DETECTORS AND COLLIMATORS

Note sur la sensibilité et le pouvoir de résolution en scintigraphie (SM-51/88) 91
J. Courtial et A. Gandy
Discussion 114
A comparison between collimator theory, extended to allow for the effect of wall penetration, and experiment (SM-51/28) 115
H. A. B. Simons
Studies on the relationship of organ size and scanning picture (SM-51/33) 141
R. Wolf and J. Fischer
The evaluation of straight-bore, tapered and focusing collimators as a function of gamma-ray energy (SM-51/72) 153
W. J. MacIntyre, J. H. Christie and I. Tatsuno
Discussion 172
Collimator evaluation with the IAEA scanning phantom (SM-51/69) ... 175
M. A. Bender and M. Blau
Discussion 189
The design and performance of a large high-resolution focusing collimator (SM-51/59) 193
C. C. Harris, P. R. Bell, M. M. Satterfield, D. A. Ross and J. C. Jordan
Discussion 208

III. MOVING DETECTORS AND COLLIMATORS (cont.)

Collimators for radioisotope scanning systems (SM-51/53) 211
R. N. Beck
Discussion 231

Construction of a high-efficiency, low-energy collimator (SM-51/45). 233
R. Höfer and A. Roszuczky
Discussion 240
A depth-focussing collimator for the investigation of the brain cortex (SM-51/27) 243
H. I. Glass
Discussion 251
Localization and total body high-energy gamma-ray scanning studies in cancer patients (SM-51/47) 253
J. S. Laughlin, P. J. Kenny, K. R. Corey, E. Greenberg and D. A. Weber
Discussion 268
A clinical radioisotope scanner for cylindrical and section scanning (SM-51/48) 273
D. E. Kuhl
Discussion 289
Clinical photoscintillography: technique and applications (SM-51/43). 291
K. H. Ephraim
An automatic scanning system, using a tape perforator and computer techniques (SM-51/36) 321
H. Schepers and C. Winkler
Discussion 329

IV. STATIONARY DETECTORS

Deux nouveaux types de détecteur pour camera à rayons X ou γ (SM-51/86) 333
C. Kellershohn, A. Lansiart et A. Desgrez
Étude d'une caméra à scintillations: description et applications cliniques (SM-51/83) 355
H. Jammet, R. Gongora, J. Morichère et P. Desneiges
Dynamic studies with a gamma-ray scintillation camera (SM-51/98). 377
W. G. Myers
Discussions 388
The digital autofluoroscope (SM-51/70) 391
M. A. Bender
Discussion 398
A scintillation camera for kinetic studies of the distribution of radioactive nuclides in the brain (SM-51/71) 401
W. Gross, E. B. Schlesinger and S. de Boves
Discussion 410
Autofluorography with an X-ray image amplifier (SM-51/77) 411
M. M. Ter-Pogossian and J. O. Eichling
Discussion 416

V. DISPLAY SYSTEMS

An analysis of quantitative colour display for scanning (SM-51/25) ... 423
J. R. Mallard, M. H. Duggan, M. J. Myers and R. J. Wilks

A new method for colour scanning (SM-51/7) 451
H. Kakehi, N. Arimizu and G. Uchiyama
Discussion 462
Contrast enhancement by multicolour print-out of thyroid, kidney, liver and brain scans (SM-51/57) 465
G. J. Hine, D. H. Patten and B. A. Burrows
Le scintigramme en couleurs du foie (SM-51/101) 473
T. Spârchez, B. Gheorghescu, A. Steclaci, E. Merculiev et M. Popovici
Discussion 484
Electronic modification of the scintigram and its limitations (SM-51/82) 491
B. Conrad and W. Horst
Discussion 506
Techniques which aid in quantitative interpretation of scan data (SM-51/63) 509
D. B. Charleston, R. N. Beck, P. Eidelberg and M. W. Schuh
Discussion 524

VI. DISPLAY SYSTEMS (cont.)

Analysis of scan records with a recording densitometer - the "re-scanner" (SM-51/66) 529
C. C. Harris, P. R. Bell, M. M. Satterfield, D. A. Ross and J. C. Jordan
Discussion 542
Perspectives d'emploi d'un nouveau système d'enregistrement à contraste accentué (SM-51/94) 545
I. Baschieri et A. Scognamiglio

List of Chairmen of Sessions and Secretariat of the Symposium 559

I

THEORY OF SCANNING

THEORY OF RADIOISOTOPE SCANNING

G. L. BROWNELL
MASSACHUSETTS GENERAL HOSPITAL,
BOSTON, MASS., UNITED STATES OF AMERICA

Abstract — Résumé — Аннотация — Resumen

THEORY OF RADIOISOTOPE SCANNING. All scanning techniques, whether utilizing focusing collimators, positron detectors or the newer camera techniques, have certain basic problems. The success of these techniques depends in large measure upon the correct choice of various parameters of the collimating system, of which the most important is the resolution. In this paper the relationship of optimum resolution to radioisotope content and distribution are discussed.

Radioisotope scanning may be considered as a process of information extraction and presentation. The primary information lies in the original radioisotope distribution. The collimator and detecting system provide the information transfer mechanism and the final scan presents the resultant information. As with all such techniques, only a small fraction of the information is retained in the final scan.

It can be shown that for focusing collimator and scintillation camera systems, the number of counts per resolution area varies as the fourth power of the resolution distance. For certain radioisotope distributions it is possible to derive analytically an optimum value of resolution distance. However, for most systems the optimum resolution must be determined by trial and error. The problems here are similar to those of pattern recognition in other fields.

A computer programme has been prepared to aid in determining the optimum resolution for various types of patterns. This computer is unique in having intermediate disc storage and CRT read-out. The results have general applicability to the design of many scanning systems.

THÉORIE DE L'EXPLORATION AU MOYEN D'UN RADIOISOTOPE. Toutes les méthodes d'exploration au moyen d'un radioisotope, celles qui font appel aux collimateurs à focalisation, aux détecteurs de positons ou les techniques plus récentes utilisant des caméras à scintillation, posent certains problèmes fondamentaux. Le succès de ces techniques dépend beaucoup du choix des différents paramètres du dispositif de collimation, dont le plus important est la résolution. L'auteur étudie les relations qui existent entre la résolution optimum, d'une part, la concentration du radioisotope et sa répartition, d'autre part.

L'exploration au moyen d'un radioisotope peut être considérée comme un moyen d'extraire et de présenter des informations. Les informations primaires se trouvent dans la répartition initiale du radioisotope. Le collimateur et le détecteur constituent le mécanisme de transfert de l'information et le scintigramme final présente les informations obtenues. Comme dans toutes les techniques de ce genre, le scintigramme final ne contient qu'une faible partie des informations.

On peut montrer que, dans le cas d'ensembles comportant un collimateur à focalisation ou une caméra à scintillation, le nombre de coups par surface de résolution varie comme la quatrième puissance du diamètre de résolution. Pour certaines répartitions du radioisotope, il est possible de déduire analytiquement une valeur optimum du diamètre de résolution. Toutefois, avec la plupart des ensembles, cette valeur optimum doit être déterminée par approximations successives. Dans ce cas, les problèmes qui se posent sont analogues à ceux que pose la détermination d'une répartition dans d'autres domaines.

L'auteur a établi un programme pour calculatrice, qui doit permettre de déterminer plus facilement la résolution optimum pour différents types de répartitions. La calculatrice utilisée est le seul appareil de ce genre qui comporte une mémoire intermédiaire à disques et une tête de lecture à tube à rayons cathodiques. Les résultats pourront être appliqués à l'étude d'un grand nombre d'ensembles de scintigraphie.

МАТЕМАТИЧЕСКАЯ ОСНОВА РАДИОИЗОТОПНОГО СКЕННИРОВАНИЯ. Все методы сканнирования как с использованием фокусирующих коллиматоров, позитронных детекторов, так и новых методов с применением камеры, выдвигают определенные основные проблемы. Успешное применение этих методов зависит в большой степени от правильного выбора раз-

личных параметров коллимирующих систем, из которых наиболее важным является разрешение. В настоящем докладе обсуждается взаимоотношение оптимального разрешения и содержания и распределения радиоизотопов.

Радиоизотопное сканнирование можно рассматривать как процесс сбора информации и представления данных. Первичная информация зависит от первоначального распределения радиоизотопов. Коллиматор и система детектирования обеспечивают механизм передачи информации, а окончательная сканнограмма дает результирующую информацию. В случае применения всех этих методов лишь небольшая часть информации попадает на окончательную сканнограмму.

Можно видеть, что для системы фокусирующего коллиматора и сцинтилляционной камеры число отсчетов на площадь разрешения колеблется как четвертая степень расстояния разрешения. Для некоторых видов распределения изотопов можно получить аналитически оптимальную величину расстояния разрешения. Однако для большинства систем оптимальное разрешение должно определяться опытным путем и с погрешностями. Настоящие проблемы аналогичны проблемам расшифровки снимков в других областях. Программа вычислительной машины была подготовлена с тем, чтобы содействовать определению оптимального разрешения для различных моделей. Настоящая вычислительная машина является уникальной, поскольку в ней имеется промежуточный отсек для диска и для считывания электронно-лучевой трубки. Результаты применимы к конструкции многих сканнирующих систем.

TEORÍA DE LA EXPLORACIÓN RADIOISOTÓPICA. Todas las técnicas de exploración radioisotópica con colimadores enfocados, detectores de positrones o cámaras de centelleo de los modelos más recientes plantean ciertos problemas básicos. Su éxito depende en gran medida de la elección acertada de varios parámetros del dispositivo de colimación, el más importante de los cuales es el poder de resolución. El autor examina la relación que existe entre el poder de resolución óptimo, por una parte, y, por otra, el contenido de radioisótopos y su distribución.

La exploración radioisotópica puede considerarse como un medio para acopiar y presentar ciertos datos. La información primaria se refiere a la distribución original del radioisótopo. El colimador y el detector constituyen el mecanismo de transferencia de la información y el gammagrama final presenta los datos resultantes. Como en todas las técnicas de esa índole, el gammagrama sólo recoge una pequeña parte de la información.

Puede demostrarse que cuando se utiliza un colimador enfocado y una cámara de centelleo, el número de impulsos por superficie de resolución varía como la cuarta potencia de la distancia de resolución. Para ciertas distribuciones del radioisótopo es possible deducir analíticamente un valor óptimo de la distancia de resolución. Sin embargo, para la mayoría de los sistemas de colimación el poder de resolución óptimo debe determinarse por tanteo. En este caso los problemas son análogos a los que plantea la identificación de esquemas en otras disciplinas.

El autor ha preparado un programa para calculadora destinado a determinar más fácilmente el poder de resolución óptimo correspondiente a diversos esquemas. La calculadora utilizada es la única que posee una memoria intermedia sobre disco y un tubo de rayos catódicos para la lectura. Los resultados así obtenidos son de validez general para el diseño de diversos dispositivos de exploración centelleográfica.

1. INTRODUCTION

Radioisotope scanning is assuming an increasingly important role in medical diagnosis with the advent of new scanning techniques and new radioisotopes and compounds. In particular, the development of various camera concepts has considerably broadened the scope of radioisotope scanning and permitted the extension of scanning into the study of dynamic processes. These developments have emphasized the importance of optimizing the parameters of radioisotope scanners, a procedure which has historically proceeded along empirical lines. It is of considerable interest, therefore, to examine some of the fundamental problems involved in producing scans with maximum information content. Although in certain cases information content

or capacity will be given a quantitative definition, the meaning of the term as used here is principally to indicate the degree of usefulness of a scan to a physician in performing a diagnosis.

In previous papers [1-3] some general principles of radioisotope scanning were developed. In particular, collimator point-source sensitivity distributions were presented and the problem of determining the optimum resolution of a device was discussed. In this paper these concepts will be developed further, and a treatment of the design of focusing collimators and collimating devices for scintillation cameras will be presented. The similarities between the important parameters of mechanical scanners and cameras is emphasized, and a unified procedure for determining the optimum resolution distance for maximum information capacity is developed. This problem, the treatment of which occupies much of the present paper, is felt to be one of the most important facing the designer of any type of scanning device.

It has become popular to attempt to derive a single quantity to reflect the performance of a scanner. This seems to be a pointless task which only serves to cloud a true evaluation of the problems, most of which can be better evaluated on an individual basis. The biological properties and relative concentration of radioisotopes and compounds and radiation dose to the patient clearly form one area of consideration. The design of collimators, sensitivity of detectors, and optimum resolution are clearly inter-related topics. Finally, read-out devices and methods of data storage and treatment can be considered together. Attempts to combine all of these factors into a single number simply invite confusion. All of these factors must be considered, but it is a relatively straightforward task to examine them in detail with reference to a specific scanning problem and a specific isotope or compound.

2. POINT-SOURCE SENSITIVITY DISTRIBUTIONS

The point-source geometrical efficiency distributions for various collimators have been presented in previous reports [1-3]. The types of collimators studied include cylindrical and tapered apertures, focusing collimators and positron detection. Such distributions, whether calculated or determined experimentally, form the bases for determining the performance of a scanning device to any source distribution, as the response of a detector to a continuous source distribution can be obtained by integration over the appropriate point-source distributions. Other factors such as source attenuation, septa penetration and detector sensitivity can be introduced using theoretical or experimental factors.

It is convenient to approximate the response to a point source on a plane by a Gaussian distribution. If this approximation is made, the distribution on a plane may be completely characterized by two parameters, the peak sensitivity, when the source is directly on the axis of the detector, and the full width at half-maximum or the distance between the two positions of a point source at which the response is one half the maximum. These values can readily be measured by moving a point source on a plane normal to the axis of the collimator on a line intersecting the axis. If the plane is the focal plane, a plane containing the focal point of a focusing detector or the

mid-plane of a positron detector, the two parameters are referred to as the focal geometrical efficiency, g_0, and the resolution, d. The values will differ on different planes, but these two quantities can often be used to characterize a collimator.

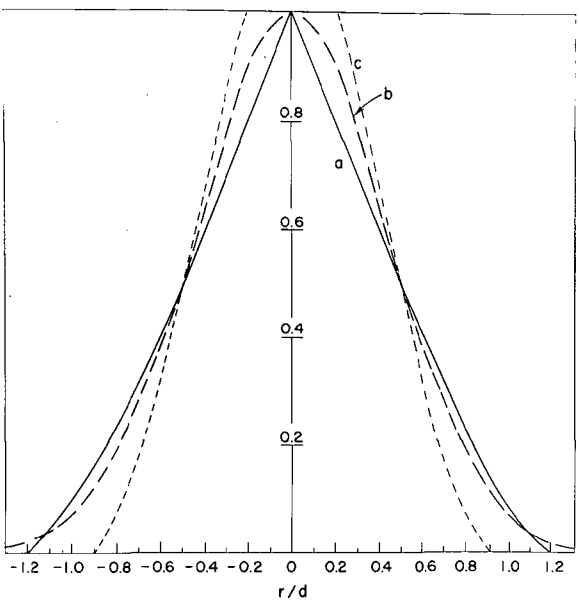

Fig. 1

Calculated point-source response for (a) focusing colimator or positron detector with source on focal plane, (b) focusing collimator or positron detector with source on plane 0.43 of distance to focal plane and (c) Gaussian curve

Figure 1 shows the calculated point-source response for two situations. Curve (a) represents the response of a tapered aperture or a focusing collimator with the point source on the source plane while curve (b) represents the response of a tapered aperture with the source on a plane 0.43 of the distance to the focal plane. Curve (c) shows a Gaussian distribution; all curves having been normalized to a geometrical efficiency of 1.0 at the midpoint and to equal half-widths. In actual fact, many minor effects such as small-angle scattering and side-wall penetration of the taper make the resultant response curve much more nearly Gaussian. In some of the discussion to be presented later, the approximation of a Gaussian curve and its two parameters to the true point source data will be used.

The definition of resolution of a collimator as the full width at half maximum on the focal plane is, of course, arbitrary. However, it is a logical choice and in conformity with the definition of resolution in other fields.

3. PLANE-SOURCE RESPONSE

One of the most useful concepts in the analysis of collimator response is that involving plane source, as any three-dimensional source distribution

can be considered as being composed of thin slabs of activity. Neglecting source attenuation and making certain approximations, it can be shown that the response of a detector to a thin slab having constant activity per unit area is independent of distance from the collimator [3,4]. This response may be determined by integrating the point source geometrical efficiency over any plane. In the case of axially symmetrical distributions, this becomes:

$$G_s = \int_0^\infty g(r)\, 2\pi r\, dr \qquad (1)$$

where g(r) is the radial point source geometric efficiency on a given plane. Further, the concept holds for non-axially symmetrical distributions, although integration over two dimensions is required. The slab response can often be calculated most simply by considering a plane at the front surface of the collimator.

As the point-source distribution on a plane can be approximated by a Gaussian distribution with two parameters, it is logical that the slab-source response could be expressed in terms of these two parameters. Table I

TABLE I

RATIO OF PLANE SOURCE GEOMETRICAL EFFICIENCY, G_s, TO $g_0 d^2$

	$G_s/g_0 d^2$
Focus or positron detector with round apertures on focal plane	1.03
Focus or positron detector with round apertures at 0.43 of distance to focal plane	0.93
Focus or positron detector with square apertures on focal plane	1.05
Gaussian distribution	1.18

shows that the slab-source response can be closely approximated by $g_0 d^2$ for a variety of collimators and distances. Although the slab-source response for a Gaussian distribution is somewhat higher than $g_0 d^2$, principally because of its relatively long tail, the approximation is seen to be adequate for many purposes.

As G_s is independent of the collimator-slab distance, in air, the product $g_0 d^2$ must remain constant and d will vary as $g_0^{-1/2}$ for different distances from the collimator. Consequently, if g_0 is measured along the axis of a collimator and d measured on the focal plane, the point source and slab-source response can be completely determined.

The overall efficiency, ϵ, will include other factors than the geometrical efficiency.

$$\epsilon = g\eta\, sf \tag{2}$$

where η is the attenuation in the source, s is the detection efficiency of the crystal, and f is the fraction of disintegrations of the radioisotope which give rise to detectable radiation. In the case of a slab source, a similar expression can be derived:

$$\xi_s = G_s\, \eta sf. \tag{3}$$

The response of a detector, R, to a slab of thickness Δx containing an activity concentration ρ (dpm/cm^3) at a depth x in an absorbing medium will be:

$$R = \xi_s \rho \Delta x = G_s\, sf\rho\, e^{-\mu x} \Delta x \tag{4}$$

where exponential adsorption with an absorption coefficient, μ, is assumed. If the activity is distributed in depth, $\rho(x)$, equation (4) becomes:

$$R = G_s\, sf \int_0^{\ell} \rho(x) e^{-\mu x}\, dx \tag{5}$$

where ℓ is the thickness of the object. It is convenient to define a flux, F, which gives the density of detectable radiation emerging from the object being scanned.

$$F = f \int_0^{\ell} \rho(x) e^{-\mu x}\, dx\,. \tag{6a}$$

The corresponding equation for positron detection is:

$$F = f\, e^{-\mu \ell} \int_0^{\ell} \rho(x)\, dx\,. \tag{6b}$$

Introducing this quantity into equation (5) we find

$$R = G_s\, sF \tag{7}$$

where G_s is generally determined from the quantity $g_0 d^2$ as measured on the focal plane. Table II shows calculated values of g_0, d, and G_s for various collimators calculated under the specific conditions indicated.

4. COMPARISON OF COLLIMATORS

From equation (7), it can be seen that scanner response is dependent on two factors, G_s and F, assuming that the detection efficiency of the crystal,

TABLE II

PARAMETERS FOR VARIOUS TYPES OF COLLIMATORS

Collimator	Geometrical efficiency g_0	Resolution d	Slab geometrical efficiency $G_s = g_0 d^2$	G_s(relative) normalized to equal d
Cylinder	$b^2/16a^2$	4.00 b	b^4/a^2	1
Taper	$b^2/16a^2$	1.75 b	$0.191\ b^4/a^2$	5.15
Focus (n apertures)	$nb^2/16a^2$	1.75 b	$0.191\ n\ b^4/a^2$	5.15 n
Coincidence	$b^2/4a^2$	0.82 b	$0.168\ b^4/a^2$	96.5

b is radius of cylindrical collimator, radius of large end of taper in single taper or focus collimator, and radius of crystal in coincidence detector.
a is length of collimator and collimator – focal-plane distance for cylindrical, taper, and focus collimator and is crystal-source distance for coincidence detector.

s, is constant. A meaningful comparison of collimator response can be made only at equal resolution because the detection efficiency and the resultant information content of a scan is strongly dependent on resolution. Thus G_s for different collimators must be compared at equal resolution. This quantity, however, is independent of the source distribution and isotope used. The flux, F, is independent of collimator resolution and efficiency, but is dependent on the type of radiation, i.e., the energy of a gamma-ray or the use of positron annihilation radiation.

The flux, F, will directly affect the overall response. However, F will also yield the relative increase in response over areas of increased activity or the "target:non-target" ratio. This latter factor may be even more important than the overall response itself as the response can be compensated by increasing the level of activity and in any case is meaningful in comparing isotopes or scanning techniques only when referred to some absolute criteria such as tolerance dose to a critical organ resulting from a certain level of radioactivity.

To determine optimum energy of gamma emitters for brain tumour localization and to compare the use of gamma emitters with positron emitters, we have examined the model shown in Fig. 2. The increased activity at the surface of the model is quite typical of radioisotope distributions in the head as the activity in scalp, skull and dura is generally considerably greater than that in normal brain tissue. A tumour of area large compared to the resolution distance of the scanning device is indicated in one of three locations; front, centre and back. The relative responses of focusing and positron detectors at constant resolution for tumour to normal regions as calculated by equations (6a) and (6b) are shown on Fig. 3. The relative response for positron emitters is independent of location because the sum of the distances traversed by the two annihilation quanta is constant. In the case of gamma

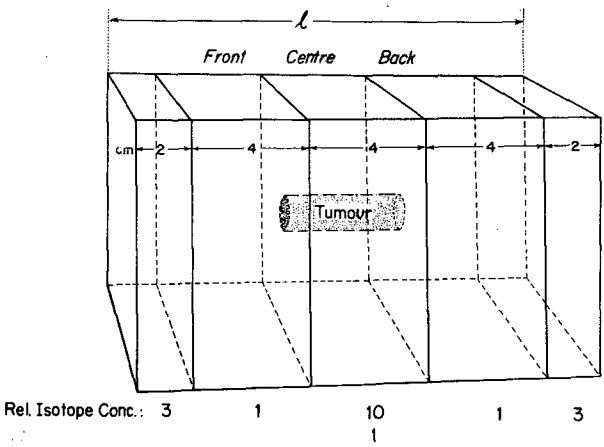

Fig. 2

Model used for comparison of gamma energy and gamma and positron detection for brain-tumour localization

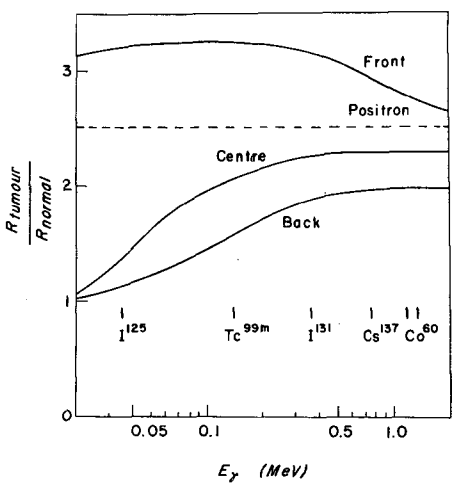

Fig. 3

Response over "tumour" area relative to "normal" area of model of Fig. 2 for gamma-rays of various energy and for positron annihilation radiation

detection the ratio of tumour response to normal depends strongly on the location. As would be expected, a tumour adjacent to the surface will be detected with high sensitivity and consequently the tumour-normal ratio will be increased. However, if it is in the centre or back location, the ratio will be decreased. The centre location is perhaps the most significant for brain-tumour scanning as superficial tumours are relatively easy to detect. In general, the tumours which are missed tend to lie near the midline and near the area of increased activity resulting from face muscle. In this case it is

seen that positron detection offers a small but distinct advantage over even high-energy gamma-rays. Low-energy gamma-rays, i.e., below 100 keV, would be poor for this task.

Although it is felt that positron detection offers some advantage in this situation, there are other situations where gamma detection would be markedly superior. An obvious case is in thyroid scanning where the area of interest is relatively near the surface.

The absolute response of a collimator system will depend on G_s, s, and F. In Table II, values of G_s normalized to equal resolution (a requirement in any comparison of this type) is shown for four collimating devices. The response of a focusing detector depends on the number of apertures which will usually be dictated by the crystal size. The value of relative geometrical efficiency for a focus detector with about 18 apertures will be equal to that of a positron detector.

F will depend on gamma energy and source distribution and must, in general, be calculated for each case. However, two cases may be readily compared; an I^{131} concentration and a positron emitter concentration located in the mid-slab of Fig. 2. The transmission of the 364-keV gamma-ray from I^{131} will be about 41% while that of both annihilation quanta will be 24%. Values of s for the two cases will be similar, in the range of 0.5 for both detectors if photopeak selection is used in I^{131} detection and all pulses are retained in coincidence detection. The conclusion reached is that for an equal number of emitted detectable radiations and for equal resolution the response of a positron detector is comparable to that of a focused detector having about 10 apertures.

Table III shows a comparison of theoretical calculations with the experimental values of DEWEY and SINCLAIR [5] for three focusing collimators. Appropriate factors for detection efficiency, photopeak ratio, and f were employed in the calculation. In general, the agreement between theory and experiment is adequate. The progressive discrepancy in efficiency for the 19- and 7-hole collimators can be explained on the basis that the scintillation detector did not completely cover the area of the apertures. The plane-source calculations further give adequate agreement when the experimental data is corrected for the shielding parameter. This correction essentially eliminates the detected gammas which have penetrated the collimator.

To compare the sensitivity of a typical focus collimator with that of positron detection, the seven-hole collimator may be considered. The positron detector having a theoretical resolution of 1.40 cm will have a crystal radius of 2.0 cm. Assuming a source plane to crystal surface distance of 10 cm and a detection efficiency of 25%, the response of the system would be 11 000 cpm/μc/cm^2 of a pure positron emitter. Experimental values confirm this theoretical calculation. In the case of absorbing media the positron detection efficiency would be reduced more than that of gamma detection so that the efficiency of the two systems would be comparable.

For obvious reasons the efficiency of positron detection at high resolution is less than that of focusing collimators. In the case of positron detection the increased resolution would be achieved by masking the crystal and consequently the sensitivity would be markedly reduced. It is obvious that if positrons are to be used at high resolution, they must be employed in a multiple crystal matrix. A number of very interesting possibilities suggest

TABLE III

COMPARISON OF EXPERIMENTAL COLLIMATOR RESOLUTIONS AND SENSITIVITIES OF DEWEY AND SINCLAIR [5] WITH THEORETICAL VALUES

Point source				
Resolution (cm)			ξ_0(cpm/μc)	
Collimator	Theoretical	Experimental	Theoretical	Experimental
91-hole	0.40	0.50	2950	2550
19-hole	0.79	0.90	3290	2410
7-hole	1.40	1.65	3820	2200

Plane source			
ξ_s(cpm/μc/cm²)			
Collimator	Experimental	Exp × SP	Theoretical
91-hole	3240	615	583
19-hole	4268	1840	2320
7-hole	8627	5610	7830

themselves for this purpose. However, the even more striking possibilities of positron cameras have precluded work along these lines.

5. FOCUSING COLLIMATOR DESIGN

In this section are outlined briefly techniques that we have used for designing focusing collimators. A more complete report is being prepared for publication elsewhere. The principal question involved in the design of multi-aperture collimators is the choice of the number, n, and size of the tapered apertures. This in turn depends on the choice of optimum resolution distance; which is discussed in section 6. However, to illustrate the procedure, calculations are presented using the following assumptions:

(a) 25 recorded quanta per resolution area – defined as d^2 – will be assumed to be optimum;

(b) The focal distance will be assumed to be equal to the collimator length;

(c) One half of the crystal area will be assumed to be exposed to gamma radiation. The other half will be covered by the septa of the collimator.

In previous papers [1-3], the following relation was derived:

$$d^4\epsilon_0 = 25A/\ell\rho T \tag{8}$$

d = resolution distance,

ϵ_0 = maximum detection efficiency for point source on the focal plane,

A = scanned area,
ρ = average concentration of radioactivity,
T = scanning time.

Introducing equations (2) and (6), we have:

$$d^4 g_0 = 25A/FsT \tag{9}$$

where all of the factors (except s) on the right depend on the source configuration and are independent of collimator design.

From Table II, values of d and g_0 can be obtained in terms of b and a, the maximum diameter and length of the tapered apertures. If it is assumed that one half of the area of a large crystal of radius b_0 is exposed to the apertures, $nb^2 = b_0^2/2$ and

$$d^4 g_0 = 7.35 \times 10^{-2} \frac{b_0^6}{n^2 a^2} . \tag{10}$$

Figure 4 shows a family of plots of n, the number of apertures, as a function $d^4 g_0$ and the parameter $u = b_0^3/a$. In use, the value, u, would first be determined by the size of the crystal available and the desired focal length. The parameter $d^4 g_0$ would be determined from the source configuration by

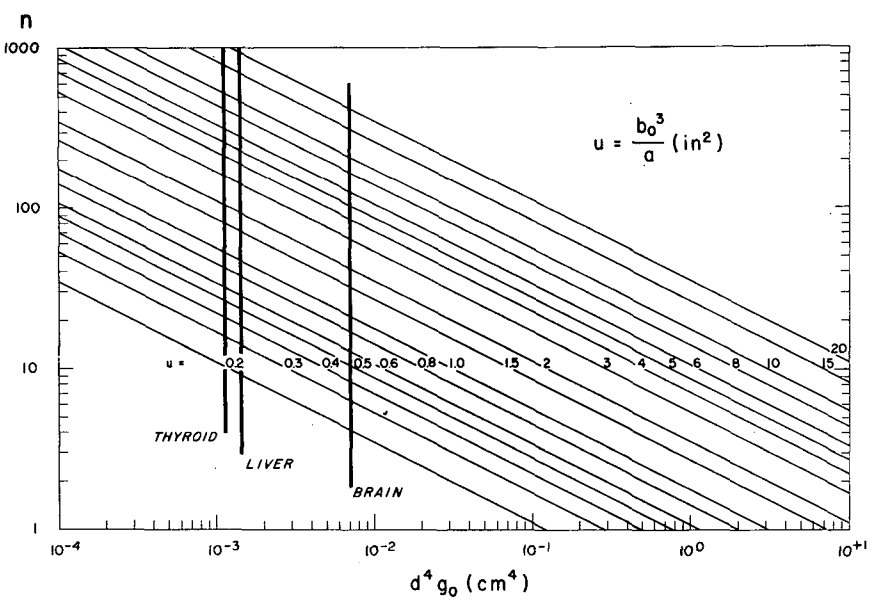

Fig. 4

Family of plots of n as function of $d^4 g_0$ and $u = b_0^3/a$ for design of focusing collimator

TABLE IV

TYPICAL PARAMETERS FOR VARIOUS SCANNING OPERATIONS

Organ	Isotope	Total activity (μc)	Area (cm^2)	T (sec)	$\bar{n}$	s	f	$g_0 d^4$ (cm^4)
Thyroid	I^{131}	10	70	1000	0.80	0.75	0.80	1.11×10^{-3}
Liver	I^{131}	200	400	2000	0.50	0.75	0.80	1.42×10^{-3}
Brain	I^{131}	40	400	2000	0.50	0.75	0.80	7.15×10^{-2}

means of equation (9). Typical values of $d^4 g_0$ are shown on Fig. 4 calculated from the estimates shown in Table IV. The intersection of the curve for the desired value of u and $g_0 d^4$ gives the optimum number of apertures and consequently their dimensions.

The effect of gamma penetration through the walls of the collimator has been discussed in a previous report [1]. In general, the effect is equivalent to an apparent increase in the radius of the collimator. An approximate expression for this increase is

$$\Delta d/d = \Delta b/b = 1/\mu a \qquad (11)$$

where μ is the absorption coefficient of the collimator material. To correct for sidewall penetration, the collimator should be designed with a somewhat smaller value of b than calculated geometrically to give the desired resolution. In general, the correction must be kept less than 10% for the collimator design to be successful.

Septa penetration presents a somewhat more complex calculation problem. However, we have used a simple ray-tracing technique which is adequate to indicate the magnitude of this effect. The procedure is indicated on Fig. 5 where a typical aperture is considered to be surrounded by concentric rings of identical apertures. The activity in volume V_0 will be detected with a geometrical efficiency, g_0. If it is assumed that an equal volume is seen by an aperture in the next ring such that rays coming from this volume penetrate one septa and strike the crystal at the base of the centre aperture, the total source volume for single penetration will be six times that of the central aperture. The relative attenuation through each septa will be $\exp^{-\mu a_1}$, and the contribution of the response resulting from septa penetration from the first ring to the true response will be $6 \exp^{-\mu a_1}$. The same argument can be applied to the next ring, in which case the total distance of septa penetration will be a_2 and there will be twelve equivalent volumes giving a total relative contribution of $12 \exp^{-\mu a_2}$. The procedure can be repeated for succeeding rings, and the sum of these relative contributions ($6 \exp^{-\mu a_1} + 12 \exp^{-\mu a_2} + \cdots$) gives an estimate of the fractional septa penetration. The septa should be designed so that fractional septa penetration is less than 20%.

The above procedure can be improved by using the distance between hexagonal holes of equal area to the round hole, calculating the exact pene-

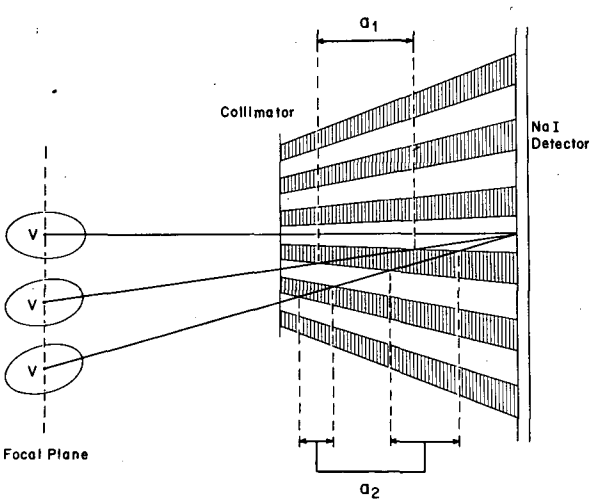

Fig. 5

Calculation of septa penetration by means of simple ray-tracing technique

tration distance for second and succeeding rings of holes, and using more rays to characterize the penetration. More thorough treatments of this effect have been reported (e.g. 5). BECK [6] has presented a more detailed optimization procedure for collimator design.

6. DETERMINATION OF OPTIMUM RESOLUTION

6.1. Figure of merit

A number of authors [6, 7] have applied a theory developed for sample counting directly to scanning problems. In this theory, the time (or the reciprocal of the time) required to statistically determine a sample of increased activity from a sample with no activity (background) is employed as a measure of the usefulness of a counting device. This quantity, usually defined as the figure of merit, is quite useful in the analysis of sample counting devices, but has severe limitations in scanner theory as it does not directly consider the most important parameter in scanner design, namely the resolution. In this theory resolution enters only indirectly in that if the resolution distance exceeds the dimensions of the target volume, the contrast ratio is decreased, affecting adversely the figure of merit.

In general, any procedure which increases the counting rate will improve the figure of merit. This often leads to anomalous results. For example, the figure of merit will usually be improved if pulse-height selection is omitted in gamma scanners. Factors such as septa penetration and sidewall penetration can improve the figure of merit and, indeed, dispensing with the collimator entirely can lead to an apparent improvement in the figure of merit. In specific cases where resolution is maintained constant, the

figure of merit may have some application in comparing different systems or isotopes. However, even here it is usually preferable to examine separately the factors of contrast ratio and sensitivity which determine the figure of merit.

6.2. Relation between sensitivity and resolution

Equation (7) gives the response of a detector to an isotope distribution. If an average flux, $\bar{F}$, is assumed and a scanning time T employed, the total number of recorded quanta N, will be

$$N = G_s \, s \bar{F} T = g_0 d^2 \bar{F} s T \, . \tag{12}$$

Scanners can be categorized by the dependence of N on d, the resolution distance. In general, they can be considered as d^4 detectors if N varies as d^4, d^2 detectors if N varies as d^2 and resolution independent detectors, or d^0 detectors, if N is independent of d.

In the following sections, the dependence of N on d is derived for a number of scanning systems. The assumptions stated in section 4 will be used here, but it should be noted that the dependence on d and subsequent analysis of information capacity are considerably more general than these assumptions.

6.2.1. d^4 scanners

Single cylindrical or tapered aperture collimators or single pair positron detectors fall into the first category. For a single cylindrical collimator (Table II) $g_0 = b^2/16a^2$ and $d = 4b$. Consequently $g_0 = d^2/256a^2$, and the number of recorded quanta is from equation (12).

$$N = K d^4/A^2 \tag{13}$$

where $K = 3.90 \times 10^{-3} \bar{F} s T A^2/a^2$ cylindrical apertures,

$K = 2.04 \times 10^{-2} \bar{F} s T A^2/a^2$ tapered aperture,

$K = 3.72 \times 10^{-1} \bar{F} s T A^2/a^2$ positron detection,

where A is the scanned area.

The dimensionless quantity K is proportional to average activity level ($\bar{F}$) and to time as well as to the collimator parameters. Thus, activity and time may be traded for each other and either or both may be decreased without affecting the scan if it is possible to increase the scanner sensitivity without decreasing the resolution.

A radioisotope scan may be considered as a series of observations of activity in resolution areas or cells of area d^2. This area is arbitrarily defined as d was arbitrarily defined. Therefore, the number of observations is A/d^2 and the number of recorded quanta per resolution area, m, for a d^4 scanner will be:

$$m = d^2N/A = K\,d^6/A^3 \tag{14}$$

where K may assume any of the values shown in equation (13).

6.2.2. d^2 scanner

A focusing collimator can, under certain assumptions, be considered a d^2 scanner. If it is assumed that one-half of the area of a detector of radius b_0 is exposed to apertures, the number of apertures, n, will be $b_0^2/2b^2$, and N the total number of recorded quanta will be:

$$N = K\,d^2/A \tag{15}$$

where $K = 3.18 \times 10^{-2}\,\bar{F}sTb_0^2A/a^2$.
The number of recorded quanta per resolution area will be:

$$m = K\,d^4/A^2. \tag{16}$$

6.2.3. d^2 cameras

The pinhole camera [8] and the multi-aperture camera [9] fall in the d^2 category and may be analysed by entirely analogous means. Some care must, however, be taken in the definition of resolution. In the case of the pinhole camera, the definition is illustrated in Fig. 6 where two points, a distance d apart, project circular images on the detector whose area of overlap is one-half the area of the circle. This definition is symmetrical with the definition of resolution as full-width at half maximum as used with conventional collimators.

The resolution of the camera for an object at a distance, a, from the pinhole which is, in turn, at a distance, a, from the detector is $d = 0.84b$ where $b/2$ is the pinhole radius or the effective radius if gamma-ray penetration is appreciable. The point source efficiency is: $g_0 = b^2/16a^2$. The number of recorded quanta will be:

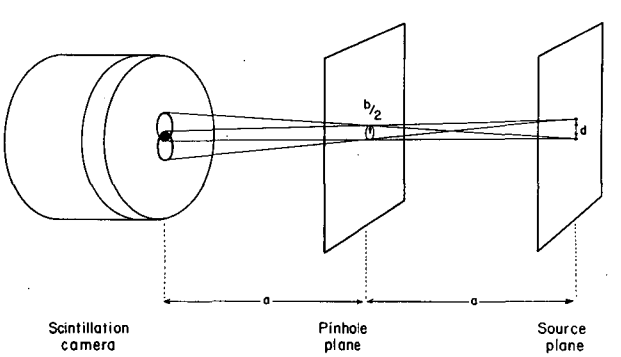

Fig. 6

Illustration of definition of resolution for pinhole camera

$$N = K d^2/A \tag{17}$$

where $K = 8.86 \times 10^{-2} \bar{F} s T A^2/a^2$.

The relation for m will be the same as in equation (16).

The multi-aperture camera consists of a matrix of tapered apertures placed in front of a large area camera detector. If the apertures have a length, a, and the distance from the front of the aperture to the source plane is also a, and if one half of the area of a detector of radius b_0 is exposed to tapers, the number of recorded quanta will be

$$N = K d^2/A \tag{18}$$

where

$$K = 3.12 \times 10^{-2} \bar{F} s T b_0^2 A/a^2$$

and the relation for m will be of the same form as equation (16).

6.2.4. Resolution independent camera – positron camera

A number of devices have been proposed or built to combine the camera concept with use of positron emitting radioisotopes. The positron camera of ANGER [10] will be discussed in this section. Figure 7 shows a schematic

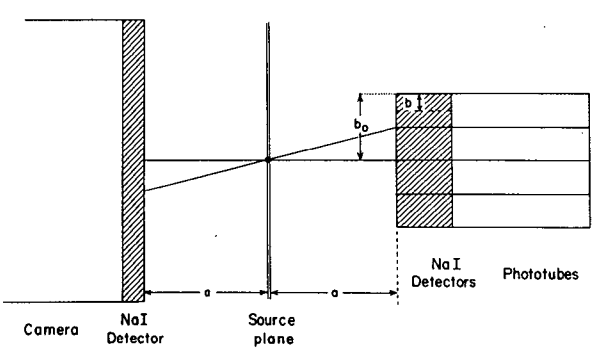

Fig. 7

Diagram of positron camera

diagram of this device which uses a large crystal in a scintillation camera and a matrix of small crystals. Pulses from a small crystal gate the camera to select annihilation radiation, and imaging is achieved by displacing the positron of the observed scintillation on the oscilloscope screen according to the location of the small crystal in which a pulse is observed. If it is assumed that the radius of the small crystals, b, can be varied while maintaining the radius of the matrix, b_0, constant, it can be shown that

$$N = K d^2/A \tag{19}$$

$$K = \overline{F}sTb_0^2/4a^2 \tag{20}$$

and

$$m = K.$$

In the case of camera designs, other factors than geometrical consideration can limit resolution. In particular, statistical variations in the number of emitted photoelectrons impose a resolution limit in the multiple phototube imaging device. This will not affect N but will make the positioning of the pulses less precise. If d_g is the geometrical resolution defined above and d_0 is a constant resolution distance imposed from any other source,

$$d^2 = d_g^2 + d_0^2. \tag{21}$$

This effect will also be observed with other types of scanners where it is usually less important.

6.3. Information theory applied to scanning

A radioisotope scanner may be considered as an information transfer device. The original information lies in the distribution and intensity of the radioisotope within the object being scanned. The detector and electronic system presents a portion of this information on the radioisotope scan. In general, the more information that is retained and presented on the scan, the better the system.

Each step of the process of radioisotope scanning results in a loss of information. Perhaps the greatest loss lies in the collimator itself, because such a device achieves resolution by rejecting a large fraction of the original quanta. Some information may be lost in the detector and electronic system although this is usually the most efficient portion of the scanner. The presentation of the data may result in a marked information loss. In general, any processing of information such as scaling, finite line structure, nonlinear presentation will result in information loss. These factors wil not be considered in detail in the present study, but are obvious extensions for further study. The present study is limited to the scanner itself, and in particular to the choice of optimum resolution distance.

That the information content of a scan is a function of resolution can be seen from the following argument. In the case of a d^2 detector, the total number of dots appearing on the scan will vary as d^2. Consequently, at very high resolution, small values of d, the number of dots appearing on the scan will approach 0 and the information content will obviously be negligible. At the other extreme, the resolution could increase to approach the dimension of the scan and, although the number of dots would be very large, no useful information on the isotope distribution would be obtained. Between these two extremes there must lie an optimum value of resolution d and number of dots N. The determination of this optimum value is an interesting and important aspect of scanning theory. The discussion to be presented here represents an extension of a previous preliminary analysis [11].

6.4. Information capacity of a scan

Although information content has a precise scientific meaning, it is rarely possible to set up practical problems in a form which can be analytically solved. This is particularly true of any problem involving human interpretation or pattern recognition. The information capacity of a scan can be defined in somewhat more precise terms in that it will not depend on the information content of the original distribution. The derivation here has some similarities to the analysis of JONES [12] for information capacity of photographic films. A scan of high information capacity would actually contain very little information if the original distribution contained very little information. On the other hand, the greater the information capacity, the more detail of the original distribution will be retained. This raises a basic and somewhat controversial point. From one point of view, the object of a scan is to distinguish abnormal from normal; essentially a yes-no decision involving one bit of information. Thus an attempt is made to make abnormal black and normal white even though most of the original information is lost in the process. The assumption is made here that a scan having maximum information capacity, based on both geometrical and statistical limitations, will indeed be of greatest aid in interpreting scans. Although this statement will be modified later on the basis of data obtained with our simulation programme, we believe it is a valid starting point.

A radioisotope scan with a resolution, d, may be considered equivalent to a series of A/d^2 observations, each having an expectation value of m counts for a given average isotope level and $\bar{F}$. Whether the observations are made sequentially or simultaneously is immaterial for this analysis. The information capacity of each cell, H(m), is defined by the relation [13,14].

$$H(m) = -\sum_{i=0}^{\infty} P_m(i) \log_2 P_m(i) \tag{22}$$

where $P_m(i)$ is the Poisson distribution of probabilities that exactly i dots appear in a cell with an expectation value of m. Equation (22) states that the information capacity of a cell is equal to the sum of the information capacity of each state defined as $\log_2 P_m(i)$ and weighted by the probability of that state $P_m(i)$.

Since a total of A/d^2 cells are measured, the total information capacity of the scan may be found by summing over all cells.

$$H = A\,H(m)/d^2. \tag{23}$$

This is, however, a rather crude approximation because only one half of the area of the assumed Gaussian response function is contained within d^2 so that only half of the quanta originating in a cell of the source distribution fall into the corresponding cell of the scan. A better approximation would be to assume that m/2 of the expected number m fall in the correct cell and the remainder fall in neighbouring cells. Thus in each cell there are m/2 dots with a resolution d and m/2 with a resolution 2d. Therefore, equation (23) can be rewritten:

$$H = A\,H(m/2)/d^2 + A\,H(m/2)/(2d)^2$$

$$= 1.25\ A\,H(m/2)/d^2. \tag{24}$$

From equations (14), (16), and (20), it may easily be shown that:

$$\frac{H}{1.25K^{1/3}} = \frac{1}{m^{1/3}}\,H(m/2)\ d^4 \text{ detector,} \tag{25}$$

$$\frac{H}{1.25K^{1/2}} = \frac{1}{m^{1/2}}\,H(m/2)\ d^2 \text{ detector,} \tag{26}$$

$$\frac{H}{1.25K} = \frac{1}{m}\,H(m/2)\ d^0 \text{ detector.} \tag{27}$$

Figure 8 shows a plot of information capacity as a function of m for the three types of detectors. As would be expected, the information capacity of the resolution independent detector does not peak but increases steadily at small values of m corresponding to small values of d. At first sight, this would seem to be an anomaly as the scan would appear unchanged with decreasing values of d and constant N after the points have been determined to a certain precision. In other words, if the number of dots remained constant, it would seem to make little improvement to determine the precise location of the dots, i.e. decrease $d/\sqrt{A}$, to 10^{-6} or less. This, however, depends on the problem at hand as such precision may be required for other purposes, i.e. for the storage of information on photographic film. Therefore, even the concept of information capacity must be qualified so that only the storage of useful information is considered. In the case of d^2 and d^4 detectors, statistical considerations limit the range of d so that total information capacity and useful information capacity are more nearly the same.

It is interesting to note that the quantity $H/1.25K$ for the resolution independent curve of Fig. 8 may be considered proportional to the information content per dot as N equals K. Over much of the range where resolution distance is important, $H/1.25K$ is seen to decrease by one bit per bit of m. As m varies as d^2/A there is one bit per dot loss of information for each $\sqrt{2}$ increase in $d/\sqrt{A}$. This clearly defines the relation between the information content of a dot and its precision in location.

The curves for the d^2 and d^4 detectors on Fig. 8 are seen to peak at values of 0.5 and 2.2 bits respectively. (The number of bits in m is defined as $\log_2 m$). The fact that these curves have a maximum confirms the previous intuitive analysis. The optimum value of m maximizes the information capacity of the scan for the set of imposed conditions. Presumably, a scan obtained with this value of m would portray the greatest detail in a radioisotope distribution, if such detail exists. Alternatively, such a scan would have the highest likelihood of detecting and correctly locating a small area of increased activity above a uniform background.

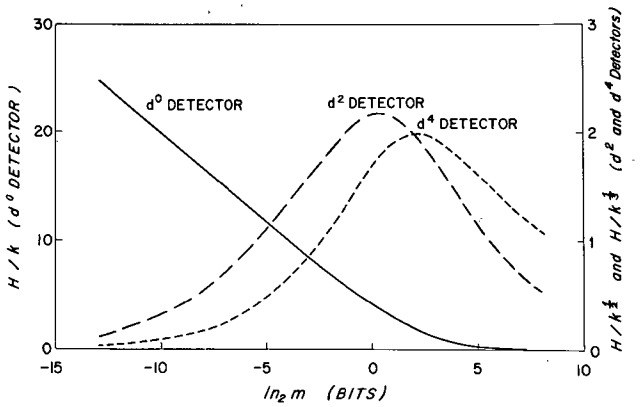

Fig. 8

Information capacity of scan for d^4, d^2, and d^0 scanners

An important result of this analysis is not only that a numerical value of m for maximum information content is found but that an optimum in information capacity exists only as a function of m. This states that if the activity level, time of scan, or sensitivity of the scanner is increased, the resolution distance should be decreased until the counts per resolution area again reaches this value. The simplicity and beauty of this concept and its immediate application to scanning problems has led us to study this approach further, particularly with regard to the determination of the optimum value of m for different source distributions.

6.5. Scanner simulation programme

In general, expressions such as equations (25), (26), (27) cannot be derived for more complex source distributions, although CEDERLUND [15] has discussed the approach to simple patterns. However, one could perform a similar analysis by constructing a large series of scanners having different resolutions and scanning an actual source distribution at varying activity levels. For each level, the best scan could be selected and the corresponding value of m determined. The procedure could then be repeated at different activity levels. Even if the practical problem of performing such a study were overcome, it would be unlikely that extraneous effects could be reduced to a point where they would not interfere with the study.

A study of this type can, however, be performed by using a digital computer to simulate the performance of a scanner. For this purpose, we have prepared a programme for use with the PDP-1 computer at ITEK Corporation. This computer was chosen because of its particularly flexible display facilities. Its output may be displayed on a point plotter or as dots on an oscilloscope screen which can then be photographed. The latter method is preferred because of the higher speed of presentation. The computer also has a flicker-free display of stored data, but this was not required in most of the studies.

The simulation programme produces a picture analogous to a radioisotope scan by the following process. A pattern to be scanned is selected. At the present time the pattern is limited to a circle of arbitrary radius and arbitrary centre location and a line of arbitrary slope and intercept. The relative activity level of three areas and three-line segments is selected. Although a considerable variety of patterns can be constructed from these elements, any number of simple patterns could be used as input data.

The first section of the simulation programme scans the pattern into grid elements (fine compared to the resolution distance) and assigns a relative density to each. Each element is assigned an address in the core memory together with its relative density. The second section of the simulation programme has the total number of dots on the scan and resolution distance as input parameters. Each grid element is analysed separately and the number of dots originating within the element is selected on the basis of the total number of dots, the relative density, and a statistical selection process. These dots are then distributed about the grid element following a Gaussian distribution in two dimensions by means of random-number selection. A dot appears on the scope face at the selected location which may be retained in display memory or may be recorded with a camera. The process is continued until all of the dots originating in an element have been presented. The next element is then treated in the same manner and the process continued until all grid elements have been covered.

A study is carried out by selecting a pattern and the relative density levels. A family of scans is then made by varying N and d such that $N = Kd^2/A$. This corresponds to holding activity and time constant and varying scanner resolution for a d^2 scanner. The next family of scans is made at a larger value of K corresponding to higher activity, longer time, or greater intrinsic sensitivity. Table V shows the scans performed in a typical study for a given pattern.

Although the study was specifically aimed at d^2 detectors, the scans can be sorted to represent other types of scanners. In particular, families of scans for resolution independent detectors can be obtained by simply interchanging the sets and cases. As would be expected in this case, the highest resolution gave the best scan in each of these families.

6.6. Disc pattern

The first pattern to be studied (Fig. 9) consisted of a disc of uniform activity in a region of lower uniform activity. The radius of the disc was 256 units compared to a side length of the scan of 1024 units, and the ratio of activity inside relative to background was 5:1. Figure 10 shows a selection of scans from set 4 for this pattern.

The criteria used to determine the optimum scan will, of course, influence the result. The criteria we have used is the selection of the scan which best represented a known pattern. In general, there was a good deal of unanimity in the choice of the optimum scan by six readers with varying degrees of experience in reading scan. The readers almost always came within one case of each other. Though there did not appear to be a significant trend with experience of the reader, there was a very clear trend towards choice of scans of higher resolution after careful study of the scans.

TABLE V

PARAMETERS OF SIMULATED SCANS

Set No.		0	1	2	3	4	5	6
K		5.45×10^4	1.09×10^5	2.18×10^5	4.37×10^5	8.74×10^5	1.75×10^6	3.50×10^6
K (relative)		1	2	4	8	16	32	64
$\ln_2 K$ (relative)		0	1	2	3	4	5	6
Case No.	N	Resolution						
1	375	85	60	42	30	21	15	11
2	750	120	85	60	42	30	21	15
3	1500	170	120	85	60	42	30	21
4	3000	240	170	120	85	60	42	30
5	6000	340	240	170	120	85	60	42
6	12000	480	340	240	170	120	85	60
7	24000	680	480	340	240	170	120	85
8	48000	960	680	480	340	240	170	120

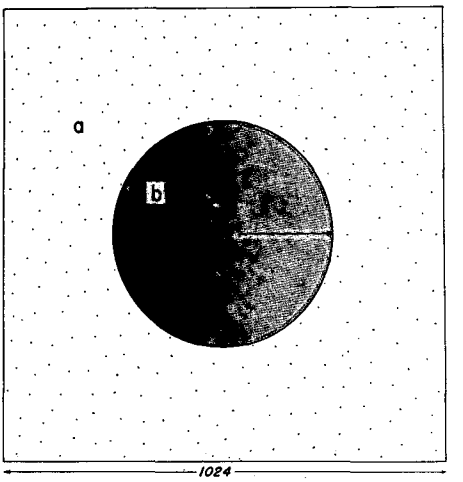

Fig. 9

Disc pattern for scanning simulation

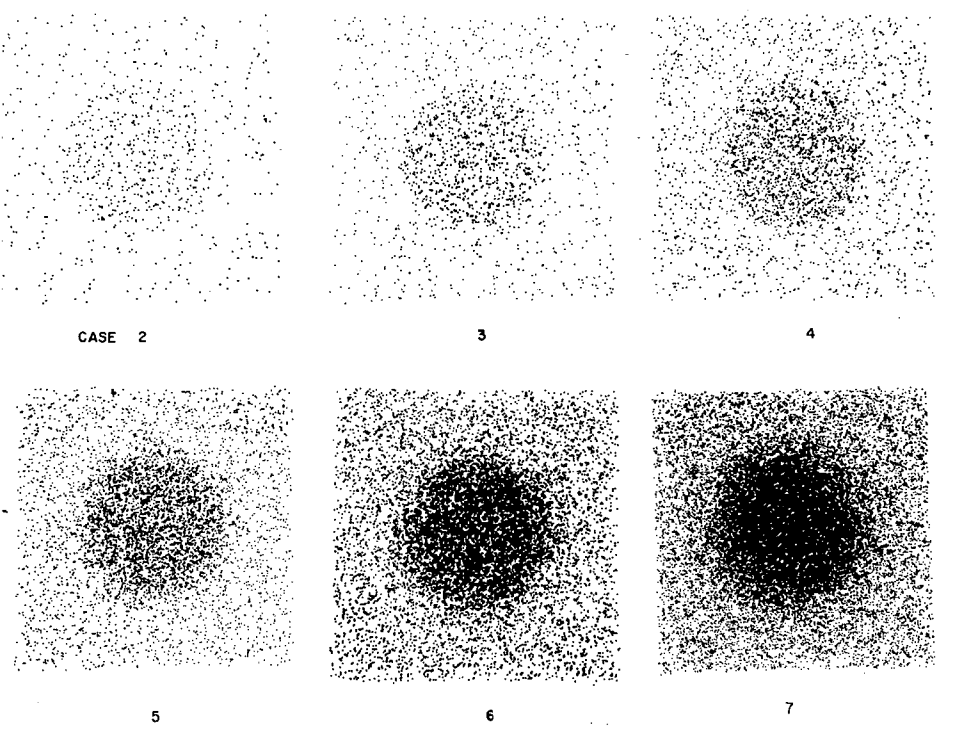

Fig. 10

Family of scans for Set 4 with disc source; 5 : 1 activity ratio

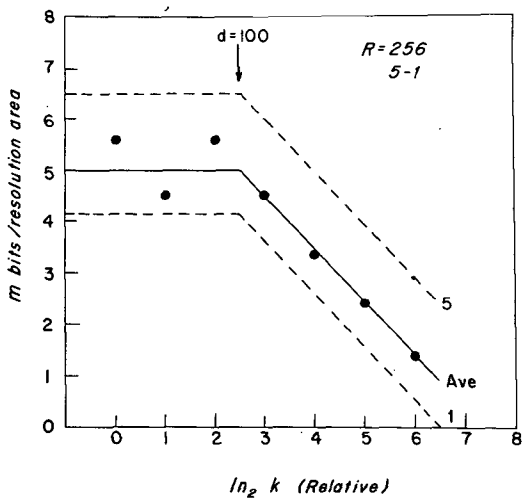

Fig. 11

Optimum value of m as a function of K for disc pattern with 5 : 1 density ratio

The results of the study on the 5:1 disc source are shown on Fig. 11. The optimum value of m (dots per resolution area) is shown for each level of activity studied. As would be expected in a study of this type, there is considerable fluctuation in m from one activity level to the next. This results from the fact that the observer may be influenced by many subjective factors as well as the rather coarse steps between cases. Even with 8 cases per set, the step in m between cases is a factor of 4 or 2 bits. However, Fig. 11 appears to show two distinct regions. At low activity, the optimum value of ln_2m remains fairly constant at approximately 5 bits per resolution area. This is consistent with the previous analysis of information capacity although the optimum value of m is considerably higher. The corresponding values inside and outside the disc are about 6.5 and 4.1 bits per resolution area respectively.

At higher activity levels, the optimum value of m decreases such that the number of dots on the scan remain relatively constant at about 3000. Over this region, ln_2m decreases by 1 bit per factor of 2 increase in activity, K.

This study was repeated using a 2:1 density ratio. Fig. 12 shows the results of this study. Again two regions are apparent although the constant m region appears to extend to somewhat higher m values. The average value of ln_2m is also somewhat lower, i.e. 4.5 bits compared to 5 bits for the 5:1 case, but it is interesting to note that the optimum value for the background region is essentially the same, i.e. 4.1 bits per resolution area. At higher activity levels, the optimum value of m decreases in a manner similar to Fig. 11.

A logical explanation of the data shown on Figs. 11 and 12 is related to the distinction previously noted between information capacity and information content. At low-activity levels, a decrease in d is clearly of advantage in discerning the pattern subject to the limitation of decreasing N. Thus this

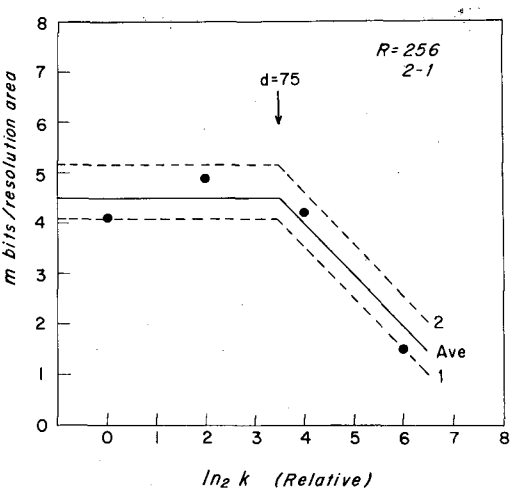

Fig. 12

Optimum value of m as a function of K for disc pattern with 2 : 1 density ratio

region is limited by information capacity, and the result of constant m is in agreement with that analysis. The fact that the numerical value is greater than shown on Fig. 8 for a uniform source is not surprising in view of the different criteria.

As the activity increases, a point is reached where the number of dots within the disc is sufficient to adequately define the pattern. Above this point this number seems to remain constant. This phenomena has been observed only for the simple disc pattern and the explanation at the present time is somewhat tenuous. It appears, however, that the eye examines an area somewhat smaller to, but comparable with, the area of the disc in distinguishing its edge. As the number of dots within this area becomes statistically significant compared to a comparable background region, the resolution no longer becomes the controlling parameter, but rather the total of dot in this area.

This type of behaviour is similar to the findings of ROSE [16] on the visual detection of areas on a photographic film. The study is not strictly analogous to the present study in that resolution was not involved and only small areas were considered (i.e. less than 100 min of arc). The results of Rose may be stated simply in that an area will be detected if the difference in the number of quanta received by the eye during its retention period exceeds that from an equal background area by five times the square root of the background number. In other words, the number of quanta required for detection is five times the standard deviation of the background over equal areas and all at equal retention time. If we neglect retention time in the present study and calculate an apparent circle of detection for the high activity region of Fig. 12, we find a value of about 90 units for the diameter of this region or about 18% of the diameter of the disc. (These dimensions are in computer units where the scan side is 1024 units). It is interesting that this is roughly equal to the value of resolution distance separating the

constant N region (or Rose region) and constant m region (75 units). This is consistent with, but by no means a proof of, the assumption stated previously that the eye examines a fixed area, the diameter of which is small compared to that of the pattern being detected, in determining the shape of the pattern. For the present case, the diameter of this region would appear to be about 15% of the diameter of the disc for the 2:1 case and 20% for the 5:1 case.

6.7. Disc and line pattern

The second pattern studied is shown on Fig. 13 and consists of three areas of activity of ratio 1:2:5. This pattern bears a general resemblance

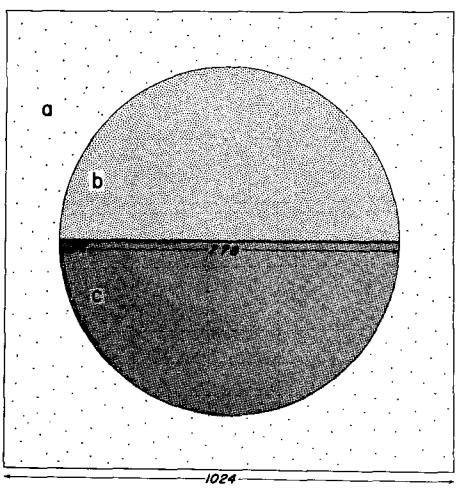

Fig. 13

Disc and line pattern (three area pattern) for scanning simulation

to the problem of brain scanning in that the lower 5 area is typical of the level of increased activity over the face. However, the pattern was not a direct attempt to simulate an actual scan, but rather to examine the next step in complexity – a line discontinuity. The intersection of the line and the circle also introduces considerably more detail than is present in the disc pattern.

Figure 14 shows a selection of scans from Set 4 with the disc and line pattern. The increased complexity considerably increases the difficulty in establishing selection criteria. However, a similar criteria was used, and again there was considerable unanimity of opinion that one case of each set conveyed the maximum useful information. Figure 15 shows the optimum value of m as a function of K and it is seen that no clear trend can be discerned. The actual value of $\log_2 m$ is about 4.7 bits for the average of the scan, and the value for the background area is again about 4.1 bits. The corresponding values for the 2 and 5 areas are 5.1 and 6.5 bits per resolution area.

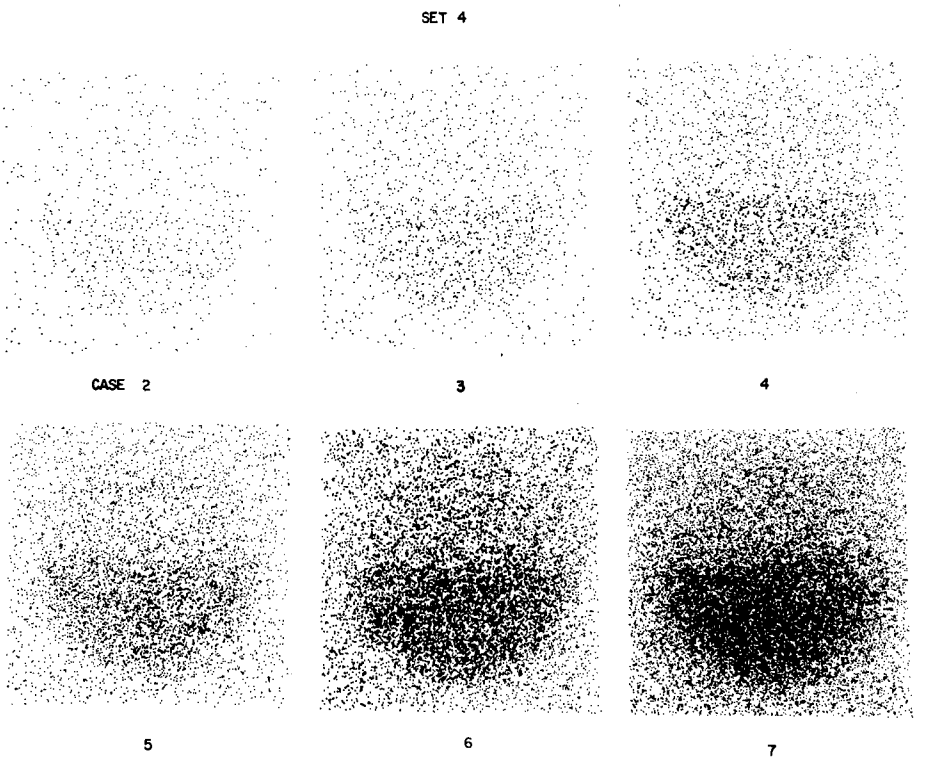

Fig. 14

Family of scans for Set 4 with disc and line pattern; 5 : 2 : 1 activity ratios

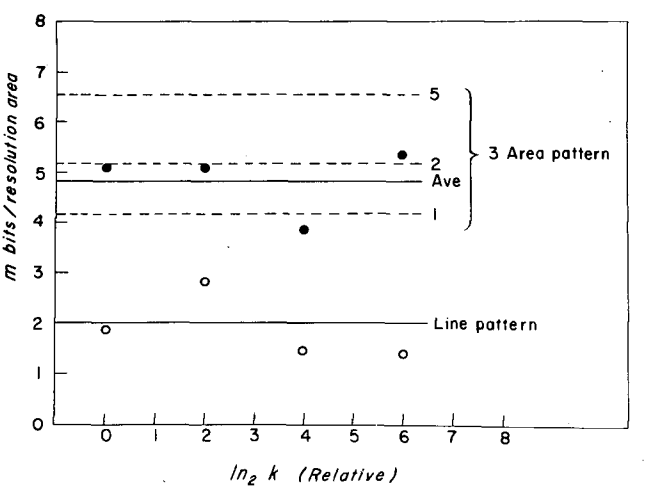

Fig. 15

Optimum value of m as a function of K for the disc and line pattern and for the line pattern

The tentative conclusion on the basis of this data is that the range of K studied corresponded only to the constant m region and that higher values of K would be required to reach the Rose region. Therefore, it would appear that the critical dimension on this scan is smaller than the diameter of the disc, so that a smaller value of resolution distance is necessary to reach the limit of the constant m region. As the value of d corresponding to the optimum value of m at the highest activity was 68 units (where the diameter of the disc was 768 units), presumably the diameter of the Rose area must be less than this value.

6.8. Line pattern

To pursue this question further, a pattern consisting of a line source on a uniform background was studied (Fig. 16). The activity levels were ad-

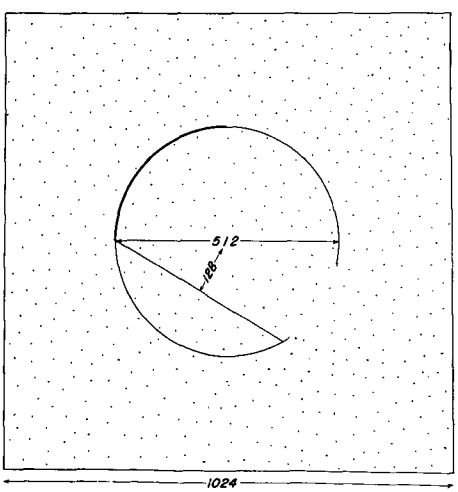

Fig. 16

Line pattern for scanning simulation

justed so that about 20% of the dots originated from the line source. A family of scans from Set 6 is shown on Fig. 17.

The results of this study are shown also on Fig. 15. Again, no clear trend can be discerned, although the average value of $\ln_2 m$ in this case is only about 2 bits. This reflects the fact that a higher resolution is required to visualize the detail in this pattern. The diameter of the Rose region in this case must be less than 29 units.

6.9 General conclusions from scanning simulation

The results to date with the scanning simulation programme are preliminary and further studies are planned. However, certain tentative conclusions can be stated. For simple patterns, m is maintained constant at a

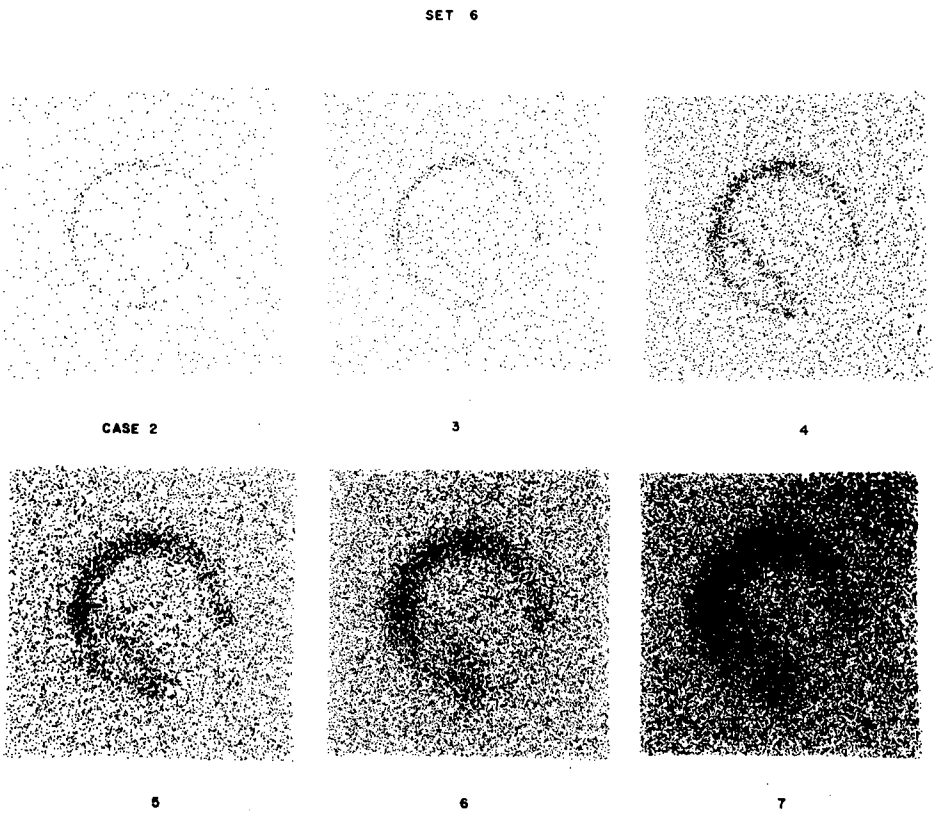

Fig. 17

Family of scans for Set 6 with line pattern of Fig. 16

value of about 4 bits/resolution area in the background area as long as d is greater than 20% of the diameter of the region. As activity is increased and d decreased below this value, the total number of dots is held constant such that the number in a circle of diameter 15-20% of the diameter of the region satisfies the Rose criteria.

For patterns of higher detail, the region of constant m is extended to higher values of K. It may be that the resolution distance must be small compared to an effective radius of curvature in the pattern for the Rose region to be seen. For patterns with a high level of detail, the average value of m decreases Presumably the value obtained for maximum information capacity will be the lower limit.

6.10. Future studies with simulation programme

The conclusions drawn here on the basis of the simulation programme are tentative and analysis of these scans and other patterns and density levels is required. Perhaps the most obvious extension of this study

is in alternate modes of read-out. It would be relatively easy to include scaling and line structure. Another simple extension would be to examine these scans through closed circuit television to investigate the effects of background suppression and intensification.

There are other interesting applications of this programme. It should be possible to treat problems of magnification as exists with the pinhole and positron camera. Further, methods of three-dimensional visualization such as those discussed by KUHL [17] could be studied. For example, a collimator with a highly convergent field of view tends to visualize the focal plane. By dividing a three-dimensional object into slabs and portraying each slab on the final scan with the appropriate resolution, the effectiveness of a highly convergent collimator for visualizing only the focal plane could be studied.

7. SUMMARY

Point-source sensitivity distributions provide the basic data for analysis of any collimating system. In many cases, such distributions on a plane can be characterized by two parameters, the focal sensitivity and the resolution, and the distribution can often be approximated by a Gaussian curve. The slab geometrical sensitivity can be approximated by $g_0 d^2$ and is independent of distance from collimator to slab, without absorber. In an absorbing medium it decreases as $\exp^{-\mu x}$.

Collimators and detectors can be characterized by the dependence of number of counts on the scan for given external conditions on resolution distance. In general, they can be grouped as d^4, d^2, and d^0 systems. An analysis of these systems on the basis of information capacity indicates that an optimum value of m, counts per resolution area, exists independent of activity level.

A scanning simulation programme was used to study the choice of optimum value of m as a function of activity level and pattern. It was tentatively observed that for patterns with high detail, the optimum value of m was relatively independent of activity level. For simple disc patterns, two regions exist. At low activity, m is relatively independent of activity level, but at high activity, N appears to be constant. The latter region is analogous to the observations of Rose on the detection of small dots on photographic film.

ACKNOWLEDGEMENTS

I wish to acknowledge valuable discussions with Dr. Saul Aronow and Mr. William Ellett of the Massachusetts General Hospital and Prof. George Wadsworth of MIT. The computer programme was prepared by Mr. Steven Pizer with the assistance of Dr. Arthur Callahan. Mr. Charles Burgess of ITEK was most helpful in assisting in the preparing of the simulated scans. Mr. Henri Vetter and Mr. Oscar Chomicki made many useful comments on this work.

This study was supported by the Atomic Energy Commission (AT-(30-1) 1242 and the National Institutes of Health (AM 05423).

REFERENCES

[1] BROWNELL, G.L., "Theory of Radioisotope Scanning", Int. J. appl. Rad. Isotopes 3 (1958) 181.
[2] BROWNELL, G.L., "Radioisotope Scanning" Proc. of the First National Biophysics Conference, Yale University Press (1959) 59.
[3] BROWNELL, G.L., "Theory of Isotope Scanning', Medical Radioisotope Scanning, IAEA, Vienna (1959) 1.
[4] MAYNEORD, W.V., "Some Applications of Nuclear Physics to Medicine", Brit. J. Radiol., Suppl. 2 (1950) 168.
[5] MYHILL, J., "Theory of Multichannel Collimator Scintillation Detectors", Int. J. appl. Rad. Isotopes 12 (1961) 10.
[6] BECK, R.N., "A Theoretical Evaluation of Brain Scanning Systems", J. nucl. Med. 2 (1961) 314.
[7] DEWEY, W.C. and SINCLAIR, W.K., "Criteria for Evaluating Collimators Used in In Vivo Distribution Studies with Radioisotopes", Int. J. appl. Rad. Isotopes 10 (1961) 1.
[8] ANGER, H.O. and ROSENTHAL, D.J., "Scintillation Camera and Positron Camera", Medical Radioisotope Scanning, IAEA, Vienna (1959) 59.
[9] BENDER, M.A. and BLAU, M., "The Autofluoroscope", Nucleonics 2, No. 10 (1963) 52.
[10] ANGER, H.O., "Gamma-ray and Positron Scintillation Camera", Nucleonics 2, No. 10 (1963) 56.
[11] BROWNELL, G.L., "Problems in Radioisotope Visualization", Progress in Med. Radioisotope Scanning, O.R.I.N.S. (1962) 158.
[12] JONES, R.C. "Information Capacity of Photographic Film", J. optical Soc. 51 (1961) 1159.
[13] SHANNON, C.E. and WEAVER, W., "The Mathematical Theory of Communication", University of Illinois Press (1963).
[14] WOODWARD, P.M., "Probability and Information Theory", McGraw-Hill Co., New York, (1953).
[15] CEDERLUND, J.F., "Image Quality in Radioisotope Scanning", 10th Int. Conf. of Radiol., Montreal (1962) 213.
[16] ROSE, A., "The Sensitivity Performance of the Human Eye on an Absolute Scale", J. optical Soc 38 (1948).
[17] KUHL, D.E. and EDWARDS, R.Q., "Image Separation Radioisotope Scanning", Radiology 80, No.4 (1963) 653.

DISCUSSION

C.M.E. MATTHEWS: I was very interested in Dr. Brownell's paper, but I do not agree with his remarks about figures of merit. What is usually required in scanning is to determine whether there is an area of increased or reduced uptake or not, i.e. to detect a lesion. The probability of detection will depend on the ratio of increase in count rate over tumour to standard error of the difference in count rate over tumour and brain. This can be calculated by using Dewey's and Sinclair's figure of merit (Int. J. appl. Radiat. Isotopes 10 1 (1961)), and the calculation of this ratio allows for the amount of the isotope which can be given to the patient. The result can be checked experimentally by using phantoms, and it is then found, as predicted, that when this ratio is greater than 3 the tumour can be detected. The effect of the background must be taken into account and this may seriously reduce the ratio. The low background obtained with coincidence counting seems to be one of the main advantages of using positron emitters. If, as Dr. Brownell says, penetration through the septa increases the figure of merit, does this not mean that the collimator being used is not optimum,

and that one with fewer holes would give better results in the detection of tumours?

Outlining the exact shape of the lesion presents a different problem, with regard to which this figure of merit does not apply.

G. BROWNELL: The question to be resolved is really whether the source configuration contains detail and, consequently, provides information. In my experience, source configurations, particularly in the case of brain tumours, do contain considerable detail. In particular, perhaps the most usual distribution of activities in brain tumours is a concentration in a spherical shell, as the activity often falls off within the middle of the volume. The resultant portrayal resembles a circle. Furthermore, such areas are seldom perfectly circular and may have very complex shapes. In such cases, improved resolution will make detection much easier, especially as the eye is particularly sensitive to discontinuities. Thus, the problem of detection cannot be separated from the problem of outlining the shape.

As to the phantom studies, the use of spherical regions of increased or decreased activity will not yield any information on the subject because the isotopes distribution does not contain detail. The use of a more complex shape, such as a ring, might yield different results.

A THEORY OF RADIOISOTOPE SCANNING SYSTEMS

R. N. BECK
ARGONNE CANCER RESEARCH HOSPITAL*
THE UNIVERSITY OF CHICAGO, CHICAGO, ILL.
UNITED STATES OF AMERICA

Abstract — Résumé — Аннотация — Resumen

A THEORY OF RADIOISOTOPE SCANNING SYSTEMS. The principal goal of a general theory of scanning systems is the prediction and evaluation of the performance of hypothetical systems, optimally designed for specific scanning applications, e.g. brain-tumour detection. Such a theory should provide quantitative answers to such questions as "How does a scanning system designed for I^{131} radiation compare with one designed for Hg^{203} in detecting brain tumours of a certain size, depth, etc.?"

This paper attempts to organize the various components of such a theory and to derive equations which relate the biological and physical parameters which must be considered. These include tumour size, depth, uptake ratio, collimator sensitivity, resolution, focal length, scan area, time, reliability, etc.

Central to such a theory is a criterion or figure of merit which can be computed for any system and used for comparison of different systems. Figures of merit based on visual perception and information theory are discussed and one based on statistics is adopted. This figure of merit is a function of detector sensitivity and resolution, which are treated in detail.

Collimator response to point, plane, and volume distributions of radioactivity is discussed in detail. The total response $[E_t = E(1+P+S)]$ of a collimated detector viewing a large distributed source consists of three components produced by gamma-rays which enter the collimator (1) "geometrically" or properly (E), (2) by penetrating the collimator septa (EP), and (3) by scattering in the source or collimator (ES). Exact equations for these components are very complex for multi-channel collimators. Useful approximate expressions are derived for E, P, and S; the limitations of these expressions are discussed.

Collimator resolution, as defined by some fraction of the width of the point-source response curve, is inadequate for predicting the response to a distributed source. An analogous situation exists in optics where "it has been increasingly realized that the advantages of resolving power as a criterion of quality are largely illusory". Borrowing from that field, the concept of "sine wave response" is introduced to define resolution of collimated scintillation detectors for distributed sources.

UNE THÉORIE DES SYSTÈMES DE SCINTIGRAPHIE AU MOYEN DES RADIOISOTOPES. Le principal objet d'une théorie générale des systèmes de scintigraphie est de prédire et d'évaluer les performances de systèmes hypothétiques conçus à des fins bien déterminées, par exemple pour la détection des tumeurs cérébrales. Une telle théorie devrait donner des résponses quantitatives à des questions telles que la suivante: «Pour la détection de tumeurs cérébrales d'une certaine dimension, profondeur, etc., faut-il utiliser un scintigraphe conçu pour ^{131}I ou pour ^{203}Hg?»

L'auteur cherche à coordonner les divers éléments d'une telle théorie et à établir des équations exprimant les rapports entre les paramètres biologiques et physiques à considérer: dimension et profondeur de la tumeur, taux de fixation, sensibilité du collimateur, pouvoir de résolution, distance focale, surface du scintigramme, temps d'exploration, fiabilité, etc.

L'élément essentiel de cette théorie est un critère ou indice de qualité pouvant être calculé pour n'importe quel système et utilisé pour la comparaison de divers systèmes. L'auteur discute des indices de qualité fondés sur la perception visuelle et la théorie de l'information et adopte un indice fondé sur la statistique. Cet indice est une fonction de la sensibilité et de la résolution du détecteur; l'une et l'autre sont étudiées de manière détaillée.

L'auteur analyse la réponse du collimateur pour des sources de radioactivité ponctuelles et pour des sources distribuées dans un plan ou dans l'espace. La réponse totale $[E_t = E(1+P+S)]$ d'un détecteur colli-

* Operated by the University of Chicago for the United States Atomic Energy Commission.

maté, dirigé sur une source de grande surface, est la somme de trois composantes dues aux rayons gamma qui pénètrent dans le collimateur: a) «géométriquement» ou de façon normale (E); b) à travers les parois du collimateur (EP); c) par dispersion dans la source ou le collimateur (ES). Dans le cas des collimateurs à canaux multiples, les équations exactes pour ces composantes sont très complexes. Des valeurs approchées, d'intérêt pratique, sont données pour E, P et S; l'auteur discute les conditions dans lesquelles on peut les utiliser.

La résolution du collimateur, définie par une fraction de la largeur de la courbe de réponse pour une source ponctuelle, ne suffit pas pour prévoir la réponse pour une source en volume. Une situation analogue se présente en optique où «l'on comprend de mieux en mieux que les avantages du pouvoir de résolution comme critère de qualité sont en grande partie illusoires». S'inspirant de cette considération, l'auteur introduit le concept de la «réponse à une onde sinusoïdale» pour définir la résolution des détecteurs à scintillation collimatés pour les sources non ponctuelles.

ТЕОРИЯ СИСТЕМ РАДИОИЗОТОПНОГО СКЕННИРОВАНИЯ. Главной целью общей теории систем сканнирования является предсказание и оценка характеристики гипотетических систем, оптимально предназначенных для конкретных целей применения сканнирования; например для обнаружения опухолей мозга. Такая теория должна дать количественные ответы на вопрос: "Как сравнивать систему сканнирования, предназначенную для йода-131 с системой, предназначенной для ртути-203 при обнаружении опухолей мозга определенного размера, глубины и т.д.?".

В докладе делаются попытки систематизации различных компонентов такой теории и выведения уравнений для рассматриваемых биологических и физических параметров. Они включают размер опухолей, глубину, коэффициент поглощения, чувствительность коллиматора, разрешающую способность, фокусное расстояние, площадь сканнирования, время, надежность и т.д.

Основой такой теории является критерий или цифровые параметры, которые могут быть вычислены для любой системы и использованы для сравнения различных систем. Обсуждаются цифровые параметры, основанные на визуальном восприятии и теории информации и принимается один из них, имеющий статистическую основу. Эти цифровые параметры являются функцией чувствительности детектора и его разрешающей способности, которые подробно рассматриваются.

Подробно обсуждается характеристика коллиматора относительно места, уровня и объема распределения радиоактивности. Общая характеристика [$E_t = E\ (+P+S)$] детектора, снабженного коллиматором, направленного на крупный распределенный источник, состоит из трех компонентов, производимых гамма-лучами, которые попадают в коллиматор 1) "геометрически" или правильно (E), 2) путем проникновения через перегородки коллиматора (EP), и путем рассеяния в источнике или коллиматоре (ES). Точные уравнения для этих компонентов являются очень сложными для многоканальных коллиматоров. Выведены полезные приблизительные выражения для E, P и S; обсуждается ограниченность применения этих выражений.

Разрешающая способность коллиматора, определяемая некоторой фракцией широты кривой чувствительности к точечному источнику, не адекватна для предсказания чувствительности к распределенному источнику. Аналогичное положение существует в оптике, где "все чаще признается, что преимущества разрешающей мощности как критерия качества являются в значительной степени иллюзорными". По аналогии вводится концепция "синусоидная волновая характеристика" для определения разрешающей способности сцинтилляционных детекторов, снабженных коллиматором, в отношении распределенных источников.

TEORÍA DE LOS SISTEMAS DE EXPLORACIÓN RADIOISOTÓPICA. El principal objetivo de una teoría general de los sistemas de exploración radioisotópica es predecir y evaluar el rendimiento de sistemas hipotéticos concebidos para fines bien determinados, por ejemplo, para la detección de tumores cerebrales. Dicha teoría debería dar respuestas cuantitativas a preguntas tales como la siguiente: «Para la detección de tumores cerebrales de un cierto tamaño, profundidad, etc., es necesario utilizar un aparato de exploración concebido para el ^{131}I o para el ^{203}Hg?».

El autor trata de coordinar los diversos elementos de una teoría de esa clase y de establecer ecuaciones que expresen las relaciones entre los parámetros biológicos y físicos que deben tenerse en cuenta: tamaño y profundidad del tumor, índice de captación, sensibilidad del colimador, poder de resolución, distancia focal, superficie del centelleograma, tiempo de exploración, exactitud de los resultados, etc.

El elemento esencial de esta teoría es un criterio o índice de calidad que se pueda calcular para cualquier sistema y sirva para comparar entre sí sistemas diversos. El autor discute índices de calidad basados en la percepción visual y en la teoría de la información, y adopta uno basado en la estadística. Este índice es una function de la sensibilidad y del poder de resolución del detector; los dos son estudiados detalladamente.

El autor analiza la respuesta del colimador a fuentes radiactivas puntuales, planas y tridimensionales. La respuesta total [$E_t = E(1+P+S)$] de un detector colimado dirigido sobre una fuente de gran extensión es la suma de tres componentes debidos a los rayos gamma que penetran en el colimador a) «geométricamente» o de una manera normal (E); b) atravesando los tabiques del colimador (EP); c) por dispersión en la fuente o en el colimador (ES). Las ecuaciones exactas de estos componentes son muy complejas para los colimadores multicanales. En la memoria se dan valores aproximados de interés práctico para E, P y S, y se discuten las condiciones en que estos valores pueden utilizarse.

El poder de resolución del colimador, definido por una fracción de la anchura de la curva de respuesta a una fuente puntual, no basta para prever la respuesta a una fuente tridimensional extensa. En óptica se produce una situación análoga y «cada vez se hace más patente que las ventajas del poder de resolución como criterio de la calidad son en gran parte ilusorias». Inspirándose en esta consideración el autor introduce el concepto de la «respuesta a una onda sinusoidal» para definir el poder de resolución de los detectores de centelleo colimados para fuentes no puntuales.

1. INTRODUCTION

An increasingly important application of radioisotopes in medicine is their use in diagnostic tests. Tests designed to detect lesions in the thyroid, brain, etc., employ radioisotope scanning systems to determine the distribution of a small quantity of radioactive material. In such procedures, the sensitivity and spatial resolution of the radiation detector are of prime importance, since these factors determine the quantity of radioactive material required for the test (and hence the radiation dosage to the patient) and the size of the smallest lesion that can be detected. Several fundamentally different systems have been developed for determining the distribution of radioisotopes. This paper deals with collimated scintillation detector systems, which scan the organ of interest in a systematic pattern, respond to gamma radiation and, ideally, produce an accurate picture of the three-dimensional distribution of radioactive material projected onto a plane, with lesions contrasted sharply to the surrounding normal tissue.

While the ultimate criterion must be based on clinical results, an adequate theory of scanning systems would permit one to predict and evaluate the performance of hypothetical systems, optimally designed for specific scanning applications. This paper attempts to organize the major components of such a theory, and to derive equations which relate the biological and physical parameters that must be considered. This organization is shown in Fig. 1, in which the parameters relating to the patient (source), detector, and scan procedure, are shown in relation to a system figure of merit, Q. By specifying a permitted radiation dosage to the patient, gamma energy of the isotope to be used, collimator radius of view, etc., one can compute the system figure of merit, Q_A, that can be attained. On the other hand, by specifying the area to be scanned, scanning time etc., a required figure of merit, Q_R, can be computed. From these it follows that the scan procedure is not possible unless $Q_A \geq Q_R$.

Systems not explicitly considered here, but which perform the same function are the positron scanner of BROWNELL [1], and the non-scanning gamma-ray cameras of ANGER [2], BENDER and BLAU [3].

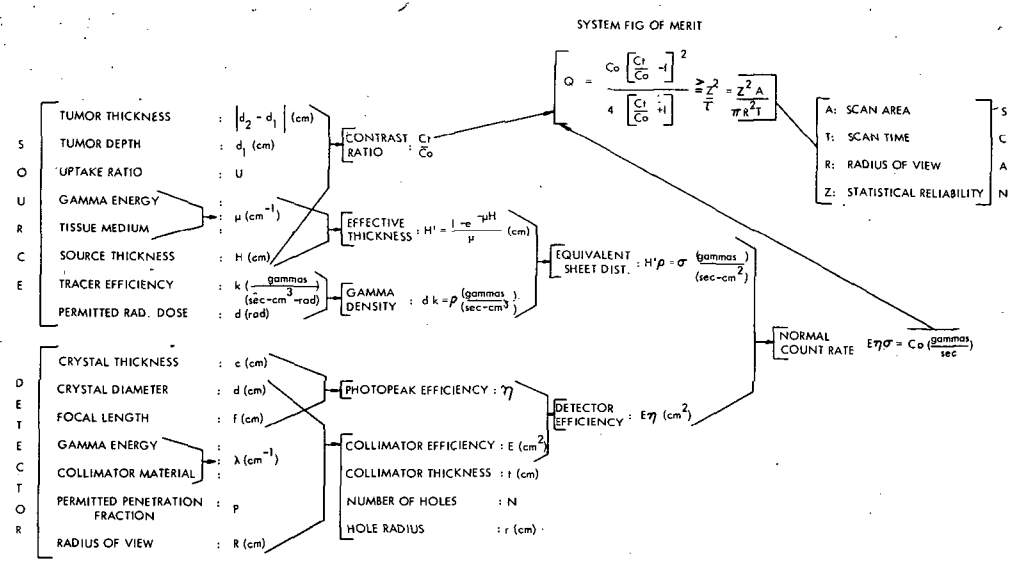

Fig. 1

Schematic diagram of the theory. If patient (source) and detector parameters are specified, an attainable system figure of merit Q can be computed. Similarly, a required Q can be determined from specified scan parameters. The scan procedure is feasible if $Q_A \geq Q_R$.

2. DETECTOR RESPONSE

Radiation detectors used in scanning systems are collimated scintillation detectors (Fig. 2) consisting of a dense metal (lead, gold or tungsten) collimator which defines a small field of view compared to the source dimensions;

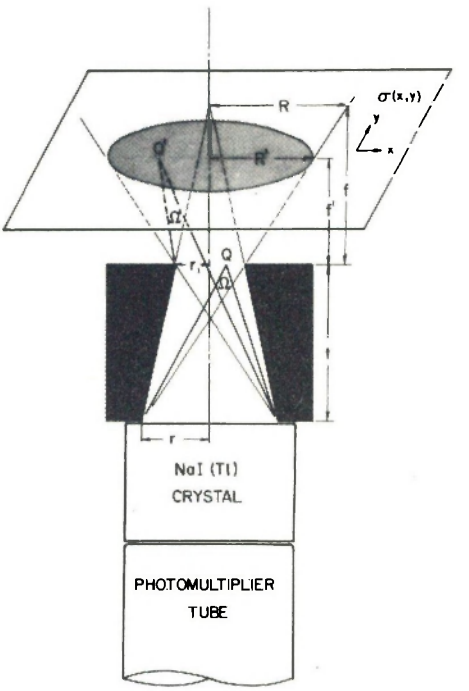

Fig. 2

Scintillation detector with single hole collimator viewing a sheet distribution of radioactivity.

a sodium iodide crystal, which converts gamma-ray energy into light photons; and a photomultiplier, which transforms the light into an output current pulse for each detected gamma ray. The total response can be thought of as a sum of signal and noise components. The signal component is the detector response to activity within the collimator field of view, while the noise component consists of detector response to all non-image-forming radiation sources, including the natural background of cosmic radiation, the gamma rays which penetrate the detector shield or collimator septa, and the gamma rays which are scattered in the source or collimator before entering the detector. Equations describing the principle components will be derived.

2.1. Response to a point source

Let us consider a gamma ray emitted at point Q' (Fig. 2) within the collimator field. The probability that it will pass through the collimator

properly (i.e. without penetration, etc.) and be detected is $(\Omega'/4\pi)\eta$ where $\Omega'(x, y, z)$ is the solid angle of view into the collimator and η is the crystal efficiency. The total "geometrical" response to a large distributed source can be found, in principle, by integrating this function (with an appropriate attenuation factor) over the source distribution $\rho(x, y, z)$ γ's emitted/cm^{3}s. In practice, this calculation is almost never carried out even for a uniform source distribution, because an accurate equation for $\Omega'(x, y, z)$ is quite complex.

2.2. Response to a sheet distribution

A much simpler approach is based on the geometrical response to a sheet distribution of activity $\sigma(x, y)$ γ's/cm^{2}s which is uniform over the collimator field.

As the sheet is moved away from the collimator, the geometrical response is constant [4]. This is essentially due to the fact that the response to activity at any point on the sheet decreases as the inverse square of the distance, while the amount of activity within the collimator field of view is proportional to the square of this distance; the product of these factors being constant. Perhaps less obvious, but nonetheless true, this argument also applies to focused collimators, such as the one shown in Fig. 3. Here the source is a uniform disc of activity just large enough to cover the field of view from the collimator face out to the focal distance at 4 in. When this source is placed against the collimator face it is effectively an infinitely large sheet distribution for all components of response to a source; however, when it is placed at the focal distance, this is true only for geometrical response. For penetration and scatter responses, it is more like a point source. For the 27.4-keV radiation from I^{125}, the geometrical response is the only significant component; hence for this energy the response is constant out to the focal distance. Beyond this point, the source no longer covers the field of view, and the response decreases. This collimator was designed for Hg^{203} (279 keV). For this energy, the septa are just thick enough to reduce the penetration response to a small fraction of geometrical response, so that when the source is at the focal distance, the response is 92% maximum. For higher energies the fraction of total response due to penetration and scatter is larger and therefore the response to this small source decreases rapidly with distance from the face of the collimator.

2.3. Response to a volume distribution

The fact that the geometrical response to a uniform sheet distribution is independent of distance can be used to compute the geometrical response to a large uniform volume distribution in which the concentration of activity is ρ γ's/cm^{3}s. The volume distribution can be thought of as a stack of sheets each having an activity concentration $\rho\, dz$ γ's/cm^{2}s. If attenuation could be neglected, all sheets would contribute equally to the total geometrical response, which would be the same as that from an equivalent single sheet with concentration ρH, where H is the volume thickness in the direction of

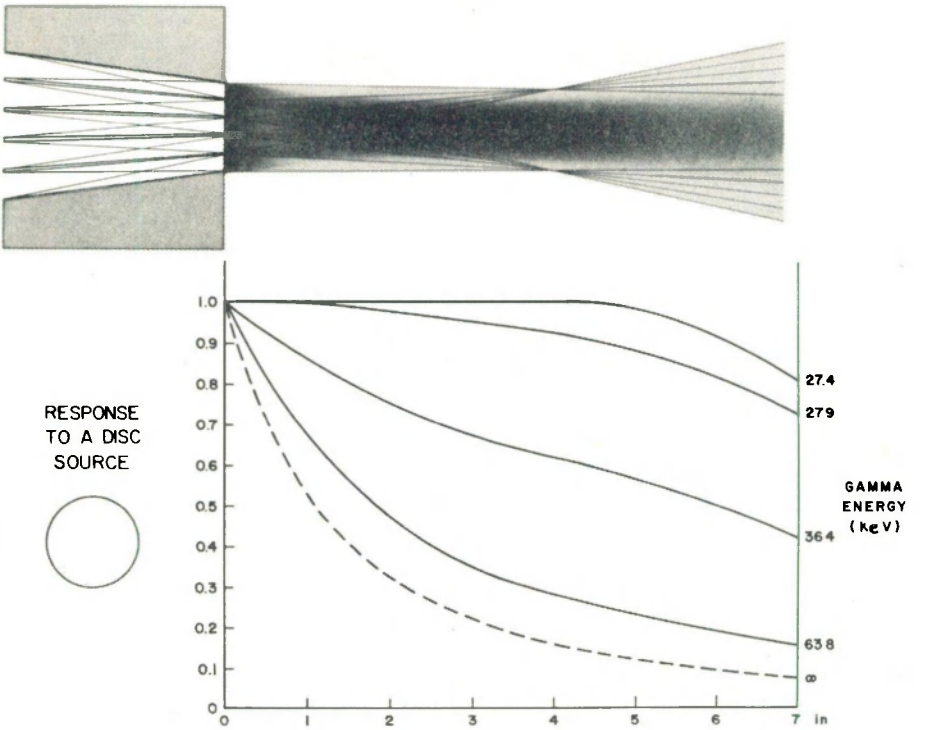

Fig.3

(a) Point source response pattern.
(b) Disc source response curves for a collimator designed for Hg^{203} (279 keV). Response to disc of I^{125} (27.4 keV) is constant from 0 in to 4 in. For higher energies an increasing proportion of the response at 0 in is due to septum penetration. At 279 keV, penetration is negligible.

the collimator axis. The actual geometrical response to a sheet depth z is reduced by the attenuation factor $e^{-\mu z}$, where μ is the attenuation coefficient in the overlying material. Summing over all sheets gives the equivalent single sheet:

$$\sigma_0 = \int_0^H \rho e^{-\mu z}\, dz = \rho \left[\frac{1 - e^{-\mu H}}{\mu} \right] = \rho H', \tag{1}$$

where H' is the effective or reduced source thickness. This procedure can be generalized at least to the extent that an equivalent sheet can be found even when the concentration $\rho(z)$ varies with depth in the source. For example, if the source contains a region, between depths d_1 and d_2, in which the concentration of activity is U times the normal concentration, the geometrical response will be the same as that for an equivalent sheet with

$$\sigma_t = \rho \left[H' + (U-1)\exp -\mu d_1 \left(\frac{1 - \exp -\mu |d_2 - d_1|}{\mu} \right) \right]. \tag{2}$$

This is used as the sheet distribution equivalent to volume distribution containing a lesion with uptake ratio U.

A formulation which requires that the source concentration be uniform over surfaces perpendicular to the collimator axis and within the field of view may appear to be such a radical simplification of the real source that its usefulness would be severely limited. On the other hand, there is little hope of resolving source structure which is very small compared to the collimator field of view. While no general theory exists which allows one to optimize the diameter of the field of view for a given lesion size, the tendency is to make them approximately equal [5]. In this case the simplification is not unreasonable.

The concept of "modulation transfer function" is introduced later to augment this formulation and to provide a convenient empirical procedure for the study of response to objects which may be smaller than the collimator field of view.

3. GEOMETRICAL EFFICIENCY E

The constancy of response to a uniform sheet with distance from the collimator not only facilitates the reduction of a volume distribution to an equivalent sheet σ it also simplifies the derivation of an equation for E, the geometrical efficiency. By placing the sheet against the collimator face ($f' = 0$ in Fig. 2), E can be derived in simplest form. Consider a gamma emitted at a point Q on the sheet at distance x from the axis. The probability that it will enter the crystal is $\Omega(x)/4\pi$. The total number, C, of gammas entering the crystal is found by integrating over the sheet.

$$C = \int_0^{r_1} \sigma \frac{\Omega(x)}{4\pi}(2\pi x)dx = \frac{\sigma}{2}\int_0^{r_1} \Omega(x)xdx = E\sigma\left(\frac{\gamma' s}{s}\right) \tag{3}$$

or

$$E(cm^2) \equiv \frac{1}{2}\int_0^{r_1} \Omega(x)xdx$$

Note that when E is multiplied by the sheet source strength, σ, we obtain C, the number of gammas per second which pass through the collimator properly; thus we call E "efficiency" despite its dimension of cm^2.

3.1. Exact solutions:

The integral used here to define E can be determined once $\Omega(x)$ is known. Exact expressions can be found for $\Omega(x)$ in terms of elliptic integrals or as an infinite series of Legendre polynomials [6]. It has been pointed out by GARRETT [7] that the derivation of E is mathematically equivalent to the problem of finding an equation for the mutual inductance between an in-

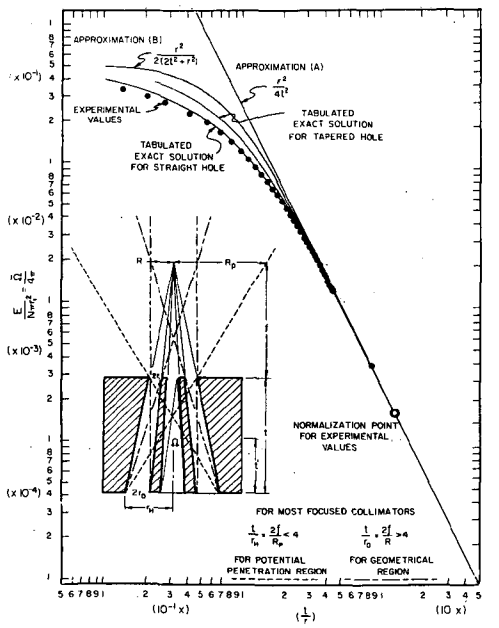

Fig.4

Mean probability ($\bar{\Omega}/4\pi$) of a gamma ray passing through a collimator hole versus hole ratio (t/r); exact solutions for straight and tapered holes and two approximations used in collimator design.

finitely long circular coil of radius r and a single filament of radius r_1 placed on the coil axis at distance t (using the notation of Fig. 2). This is important because an extensive literature on mutual inductance exists and accurate values have been tabulated for a variety of configurations. In Fig. 4 tabulated values (taken from Grover's tables [8]) are plotted against t/r for straight holes and for tapered holes with $2r_1 = r$. Experimental values, normalized to the theoretical value at t/r = 16, are plotted for the straight hole case. These measurements were made using a disc of Tm^{170} (84 keV) and a stack of lead sheets with a 1-in hole bored through them. Measured values fall on the theoretical curve except for small values of t/r where a variety of experimental difficulties become critical.

3.2. *Approximate solution:* E_A

In most scanning applications, adequate spatial resolution is obtained only when t/r is quite large, in which case the solid angle of view is almost constant and equal to $\Omega = \pi r^2/t^2$ which gives

$$E_A = \pi r^2 r_1^2/4\,t^2 \,. \tag{4}$$

3.3. *Approximate solution:* E_B

It will appear later (in connection with the septum penetration problem) that a better estimate of E is needed for relatively small values of t/r. For

the axial point, $\Omega(0) = 2\pi[1 - (1 + r^2/t^2)^{-1/2}]$. Setting $(1 + r^2/t^2)^{-1/2} \cong 1 + r^2/2t^2$ gives

$$E = \pi r^2 r_1^2/2(2t^2 + r^2). \tag{5}$$

The two approximations are equivalent (Fig. 4) for large values of t/r but for small values, E_A diverges and E_B is more accurate. As t approaches zero, E_B approaches $\pi r_1^2/2$ which is an exact asymptotic solution. This simply says that when t = 0, half of the gamma rays leaving the disc source ($\pi r_1^2 \sigma$), enter the crystal. Setting $r_1 = r$ in either of these equations gives E for a straight hole.

3.4. Maximizing E

In designing collimators for specific scanning applications we usually begin with some idea of the size and depth of the lesions to be detected. Thus we can estimate the radius of view R' required at distance f'. Referring to Fig. 2, it is clear that these conditions are satisfied by infinitely many tapered or straight holes. The problem is to find the hole dimensions for which the geometrical efficiency E is maximum, for a given R', f', and any other specified condition. Using equation (4) for geometrical efficiency, it is easily shown that, for a hole tapered to a distance f (which may not equal f')

$$E = (\pi r^2/4t^2)[(tR' - f'r)/(f' + t)]^2.$$

This is a very general equation which applies to both straight and tapered holes. For given values of R' and f', the geometrical efficiency E is maximum only when r and t are infinitely large; thus no proper maximum exists for the general case. However, three interesting special cases occur when an additional restriction is placed on the equation.

(a) If consideration is restricted to straight holes, and R' and f' are specified, it is easy to show that E is maximum when 2r = R' and t = 2f'. In this case, $E = \pi R'^4/256\, f'^2$.

(b) For tapered holes with specified values of R', f' and r (where r is given its maximum convenient value, E is maximum when $t = (rf'/R')[1 + (1 + R'/r)^{1/2}]$. In this case $f' \neq f$.

(c) For tapered holes with specified values of R', f' and t (where t is given its maximum value), E is maximum when $r = tR'/2f'$. This relation implies that f' = f (and consequently R' = R); thus $r = tR/2f$ and $E = \pi R^4/64f^2(1 + f/t)^2 = \pi r^4/4t^2(1 + t/f)^2$.

A comparison of straight and tapered holes indicates that, for given values of R', f' and t or r, it is always possible to obtain higher counting efficiency with a tapered hole. This point is discussed in more detail elsewhere [9].

For focused collimators consisting of N holes in hexagonal array, the most convenient taper is the one found in (c) above. Using this relation, the geometrical efficiency of a focused collimator is just N times the single hole efficiency.

4. PENETRATION AND SCATTER COMPONENTS

Since the absolute magnitude of response components other than geometrical response are not of primary interest, the other components are introduced as ratios taken with respect to E. Thus the total efficiency is written as $E_T = E(1+P+S)$ where EP and ES are penetration and scatter efficiencies respectively, and P and S are referred to as penetration and scatter fractions, respectively. Each of these fractions can be further resolved into more convenient components. Thus $P = P_o + P_i + P_s$ and $S = S_o + S_i + S_{so} + S_{si}$; where P_o and S_o refer to gammas that arise outside (and P_i and S_i to those which arise inside) the collimator field of view, and enter the detector by penetrating or scattering from the collimator septa. Similarly, S_{so} refers to the Compton spectrum of degraded photons due to scattering within the source of gammas which originate outside the collimator field of view, while S_{si} refers to photons resulting from scattering of gammas oridetector shielding (not the collimator septa).

If the source is a large volume distribution, all of these components are non-zero, even when only photopeak pulses are counted. Although the penetration and scatter components due to gammas arising within the collimator field, $E(P_i + S_i + S_{si})$, do not degrade the collimator resolution, there is no general method for increasing these components without increasing the "noise" component, $E(P_o + S_o + S_{so})$. The goal of detector design is then to make E as large as possible (for a given resolution, focal length, gamma energy, etc.) while keeping P+S small compared to 1.

4.1. Response to scattered photons

The energy spectrum of photons emanating from a large distributed source contains both scattered and unscattered components. The scattered component is a continuous spectrum of degraded photon energies, due primarily to Compton scattering events, which take place within the collimator field of view. However, the gamma rays which undergo Compton scattering may easily originate at points in the source well outside the collimator field. For this reason, the scatter component does not represent the concentration of activity within the field of view and is thought of as noise, to be rejected. The use of a pulse height analyser to select only photopeak pulses for recording does not entirely eliminate the scatter component since photons scattered through small angles tend to fall within the photopeak. The "source scatter fraction", S_s, is defined as the ratio of scattered to unscattered photons within the photopeak (when the septum penetration and collimator scatter components can be neglected). This fraction is a function of the source size, gamma energy E_0, detector energy resolution R_0, etc. To measure it, we must separate the scattered and unscattered components within the photopeak. The shape of the Compton spectrum of scattered photons (of energy E_s) entering the detector is given approximately by the normalized Klein-Nishina equation* [10]

* The Klein-Nishina equation was derived for photon interactions with "free" electrons and is not strictly applicable to the real case of bound electrons. However, the reduced probability of Compton scattering at small angles from bound electrons is more than compensated for by the increased probability of coherent scattering [11]. Also, the K-N equation describes the spectrum following single scattering events. To some extent multiple scattering occurs in a source of the size we are considering.

$$f(E_s) = \frac{1}{E_0^2}\left[\frac{E_s}{E_0} + \frac{E_0}{E_s} - 1.02\left[\frac{1}{E_s} - \frac{1}{E_0}\right] + 0.262\left[\frac{1}{E_s} - \frac{1}{E_0}\right]^2\right]$$

where $E_b \leq E_s \leq E_0$.

If the crystal of the scintillation detector is large enough to absorb totally the energy of incoming photons, the output pulse amplitude is approximately proportional (in the mean) to the photon energy. However, the response of such detectors to a monoenergetic beam of photons is a distribution of pulse amplitudes that is approximately Gaussian, with the standard deviation a function of photon energy. It is customary to define energy resolution of such detectors as the full width of the photopeak at half height divided by the mean energy. Assuming that the energy resolution is inversely proportional to the square root of photon energy [10] and is R_0 for the photopeak energy E_0, the equation for the "spread function" at some lower energy E_s is a Gaussian distribution $p(E_s, E)$ with mean E_s and standard deviation

$$\sigma = \frac{R_0}{2}\left[\frac{E_0 E_s}{2\log_e 2}\right]^{1/2} = K_0 E_s^{1/2}.$$

The theoretical detector output spectrum due to scattered radiation, F(E), is then found by using this spread function as the kernel of a convolution transform of the Klein-Nishina equation

$$F(E) = \int_{E_b}^{E_0} f(E_s)\, p(E_s, E)\, dE_s$$

where $p(E_s, E) = K_0^{-1}(2\pi E_s)^{-1/2} \exp[-(E - E_s)^2/2E_s K_0^2]$.

The simplest procedure from this point is to note that

$$F(E) = \lim_{n\to\infty} \sum_{i=1}^{n} f(E_{si})\, p(E_{si}, E)[E_0 - E_b]/n$$

with $E_{si} = E_b + (E_0 - E_b)(i - 1/2)/n$, $i = 1, 2, \ldots n$ and to approximate F(E) by a construction using some finite n. Fig. 5a illustrates this procedure for Hg^{203} using n = 20. Here the energy interval of scattered radiation (133 keV $= E_b \leq E_s \leq E_0 = 279$ keV) is divided into 20 sub-intervals, and for each a Gaussian distribution is constructed having the appropriate standard deviation. Each distribution is then weighted by the mean value of $F(E_{si})$ for that interval. The value of F(E) at each point is found by summing the weighted distributions. The result is a smooth "smeared" spectrum shown in Fig. 5a. The smooth, distorted, shape of this theoretical output spectrum is almost entirely due to the finite resolution of the detector rather than to the relatively small value of n; note that the "back scatter peak" is shifted from 133 to 146 keV while the "small angle scatter peak" is shifted from 279 to 255 keV. This theoretical spectrum can be used to strip the scattered

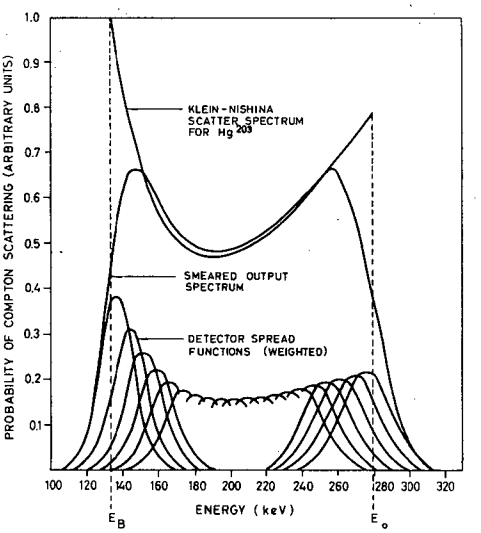

(a)

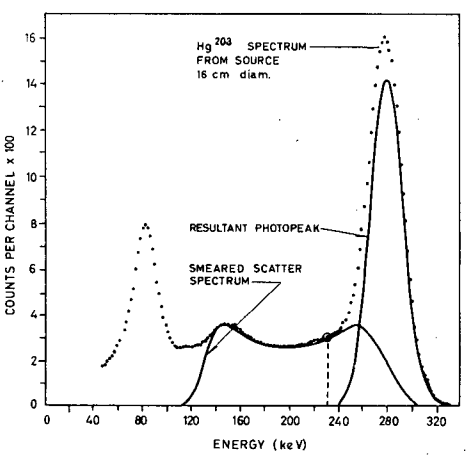

(b)

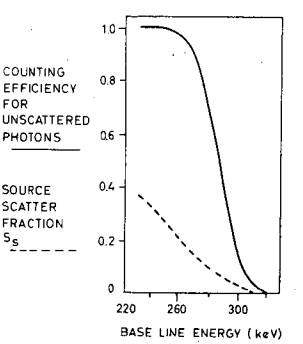

(c)

Fig.5

Method for determining fraction of photopeak pulses due to scatter in a large distributed source

(a) Construction of theoretical output spectrum from K - N equation.

(b) Theoretical output spectrum is subtracted from actual spectrum to obtain photopeak of unscattered gammas.

(c) Photopeak counting efficiency and source scatter fraction versus baseline discriminator setting.

component from an actual spectrum of Hg^{203} by normalizing the amplitude of F(E) at a point just below the photopeak and plotting the normalized F(E) for all energies. This is shown in Fig. 5b where 230 keV was selected as

the normalizing point. Subtracting F(E) from the experimental spectrum of Hg^{203} for E > 230 keV, the difference curve is the unscattered radiation component. This symmetrical unscattered photopeak shows 11.4% energy resolution. Using a point source, the measured resolution is 11.5%.

The effective source scatter fraction S_s depends on the energy setting of the base line discriminator; see Fig. 5c. While raising this setting decreases the scatter fraction, it also decreases the counting efficiency for unscattered radiation. A single setting, optimum for all source configurations, does not exist. For a given source (which includes a specified lesion size and uptake ratio) the system figure of merit Q (to be defined later) can be maximized for some baseline setting.

The similarity between the theoretical and actual scatter spectra is considered remarkable in that multiple scattering events have not been treated. While the occurrence of these events may be infrequent for the 16-cm diameter source of Hg^{203}, their frequency will increase for larger sources or lower gamma energies. The low energy limit of applicability of the procedure outlined here is not known.

In addition to the response to radiation scattered within the source, the detector also responds to radiation scattered within the collimator itself. This radiation may originate within (S_i) the collimator field of view, or outside (S_o) this field. In this case the Compton scattered photon spectrum, augmented by a coherent scattering component, is heavily skewed toward the high energy end. This distortion makes normalization difficult and the above method of stripping unsatisfactory. In fact, no satisfactory method is available for unambiguously separating collimator scatter components from their corresponding penetration components, P_i and P_o.

4.2. Response to penetrating radiation

No general formulation of detector shielding requirements will be attempted here; the solution to problems raised by the penetration component P_s is clear, if the scan mechanism is designed to carry on adequate shielding load.

To simplify the notation, the septum penetration fraction, $P_o + P_i$, will be denoted by P unless otherwise stated. Perhaps the most important and difficult problem in focused collimator design is this: gamma penetration of the collimator septa can be reduced by increasing the septum thickness; however, this reduces the hole size, which decreases the geometrical efficiency, E. If $E\sigma$ is the number of gammas per second that enters the collimator properly, the septa should be just thick enough to limit the penetration response to $PE\sigma$, where P is some small fraction, selected as negligible compared to 1. Consider the large hexagonal hole that would exist if all the septum material were removed, or were transparent to gamma radiation. This hole "sees" a region of radius R_p (see inset in Fig. 4) and has geometrical efficiency E_h. For E_h we use approximation B, since the equivalent round tapered hole has a small value of t/r_h. If the source is large enough to cover this region, the response to σ will be $E_h\sigma$. The difference, $(E_h - E)\sigma$ is thought of as the potential penetration response, which must be reduced to the actual penetration response $PE\sigma$ by the relatively opaque

septum material. The ratio $PE/(E_h - E) = M$ is the mean probability of a gamma ray penetrating the septa, from a large distributed source.

To complete the formulation, an equation is needed that expresses M as a function of collimator variables (hole size r, thickness t, etc.) and gamma energy. MYHILL [12] has formulated this problem for point sources, but his analysis is not easily extended to distributed sources. In an approach used by NEWELL [5] the effective mean path length through septa, t', is estimated by (collimator thickness) × (average density) or $t' = t(1-\tau)$ where the transmission ratio τ = base area of N holes/base area of hex array. With this estimate of t', $M = \exp -\lambda t(1-\tau)$, where λ is the attenuation coefficient in collimator material, and $P = [E_h - E)/E] \exp -\lambda t(1-\tau)$. This equation can be used [13] in a procedure for designing collimators that have maximum E for specified gamma energy, collimator material, crystal diameter, R'f' and P. Accurate experimental verification of the equation is difficult if the theoretical value of P is small, since no satisfactory method exists for separating P_o and S_o experimentally. For example, the collimator in Fig. 3 was designed for brain scanning with Hg^{203}, with P = 0.01. The total response to a disc of Hg^{203} at the focal distance is 0.08 less than its value when the source is at the collimator face. This decrease is due to a reduction in the P and $S_o + S_i$ responses; how much should be attributed to each of these components is not known. At worst, P is approximately 0.08. A better test of accuracy of the equation for P occurs when the theoretical value is quite large, since the scatter components are likely to be fairly small by comparison. For I^{131} (364 keV), the theoretical value is P = 0.33. When this source is at the focal distance, the response is 0.37 less its maximum value, which implies P is approximately 0.6. In general, for collimators that have been tested in this, and other ways, "order of magnitude" agreement is observed when the theoretical value of P is small, and better agreement is observed when the theoretical value of P is large.

When this equation for P is used in a programme of collimator design, it is advisable to select a small value, say 0.01, for P; it is found that this results in only a small decrease in E, from that obtained when P is chosen to be 0.1.

There is reason to believe that the accuracy of this equation for P decreases with decreasing gamma energy. For low energies, the theoretical septum thickness required to make P negligible is very small compared to the estimated effective mean path length used in the derivation of P. Should a more accurate equation for P be required, a promising approach is through the introduction of a probability distribution function of path lengths, p(w). Then the effective mean probability of penetration is $M = \int_0^\infty (\exp -\lambda w) p(w) dw$. While an exact derivation of p(w) is complex, an approximation which would lead to a more accurate estimate of P may not be difficult to obtain. To illustrate the procedure, suppose all path lengths, w, lie within the range $0 \leq w \leq t$; in the interval $0 \leq w \leq t(1-\tau)$ we take p(w) to be proportional to w^2, while in the interval $t(1-\tau) \leq w \leq t$ we suppose p(w) decreases linearly to p(t) = 0. This distribution function can be normalized and used to compute $P = 6N/[\lambda^3 t^3 (2+\tau)(1-\tau)^2 \tau^2]$.

5. RESOLUTION VERSUS MODULATION TRANSFER FUNCTION

From the earliest developments in radioisotope scanning it was recognized that the total response of a detector to any source could be found, in principle, if the point source response function and the source distribution were known. While this approach is conceptually clear and amenable to modern computer technology, little progress has been made in obtaining results of any generality, even for simple source distributions. This is due to no fallacy in the method, but to the complexity of the point source response function, which depends on distance from the collimator, gamma energy, focal length, thickness, hole size, etc. The approach to point source response functions for focused collimators has been primarily empirical (the notable exceptions are the work of BROWNELL [14] and MYHILL [12]). It has become common practice to represent these functions by the isoresponse contours. While these curves have contributed much to our qualitative understanding of collimator response, their principal quantitative use has been to define resolution as the width of the 50% contour. This definition is inadequate precisely because it does not indicate the shape of the response function.

The situation is analogous to that in optics, where the "resolving power" (or resolution) of a lens was first defined in terms of the minimum separation of point sources of light which could be distinguished. This measure was valuable in comparing lenses for astronomical observations, because of the interest in resolving double stars. In fact, double stars were used as test objects. It was recognized early that this criterion was not suitable for evaluating lenses for other purposes.

The concept of resolution was extended to distributed sources by Foucalt who introduced sets of closely spaced lines as a test pattern. Resolving power was then defined in terms of the closest spacing of lines that could be distinguished. The intuitive notion expressed in these concepts is that a lens which can resolve the smallest details should certainly produce the best images of larger objects. Compelling as this argument is, early experience proved it false. Nevertheless, resolving power, expressed in lines per millimeter, and measured by some form of the Foucalt test, is still the most widely used criterion for expressing the quality of an optical system [15].

In recent years the subject has been reformulated [16, 17] in a way that satisfies both intuition and observation. In the new approach, lens response is measured or computed at all "space frequencies" (expressed in lines/millimeter), using Foucalt test patterns or the equivalent. At some high space frequency the lines are no longer resolved (response falls to zero); however, it is recognized that this resolution limit does not determine the response at lower space frequencies. Thus, no attempt is made to characterize the frequency response by a single number (or resolving power). (If all point source response or "spread" functions had the same shape, a single number could be used to characterize the space frequency response function, but this is not the case for lenses or collimators.) However, certain conclusions can be drawn directly. If the response for lens A is greater than that for lens B at low space frequencies, then lens A will reproduce large details more sharply than lens B, even though the high frequency response (or resolving power) of lens B may be greater. While this

frequency response or transfer function contains no more information than was contained in the point source response function, the information is in a more convenient form for predicting the response to distributed objects or for comparing different lens systems.

This formulation can be directly applied to the analysis of focused collimator response. A test pattern that is widely used in optics for measuring frequency response is the sunburst pattern (or Siemens star) which consists of alternate light and dark pie-shaped wedges, forming a disc. For collimators, we introduce a pattern of alternate radioactive source and no-source wedges forming one quadrant of a disc. See Fig. 6. The space frequency is lowest at the perimeter and highest at the centre of the quadrant.

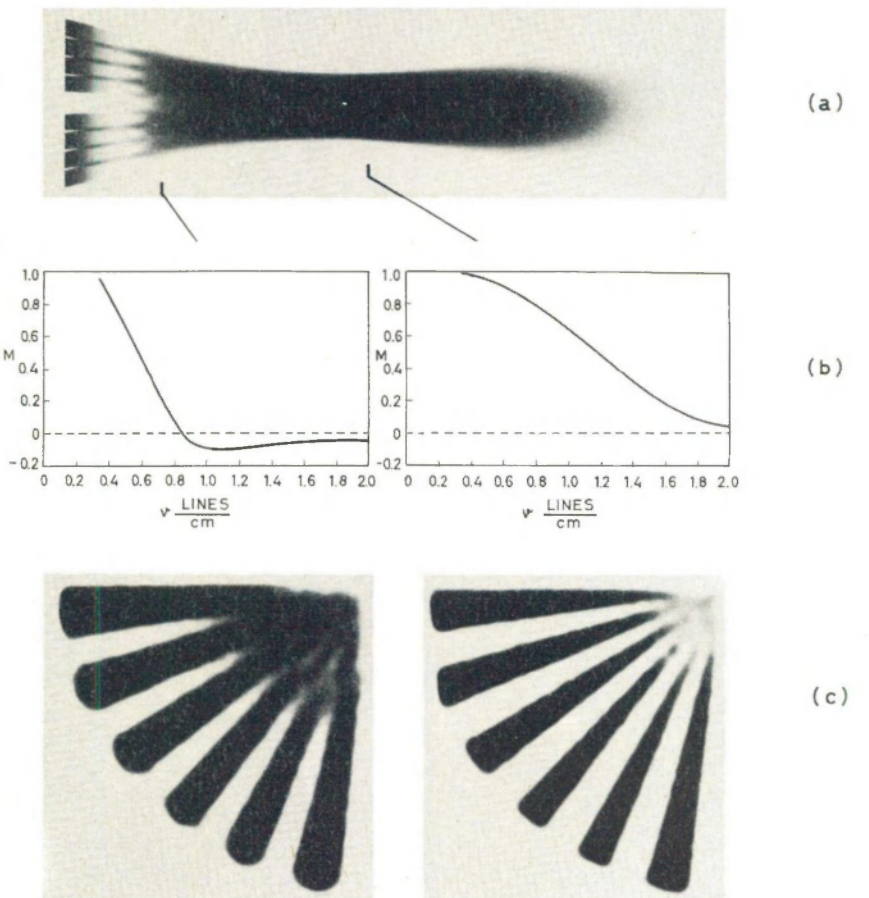

Fig. 6

(a) Point source sensitivity pattern for a focused collimator (centre hole obstructed).

(b and c) Modulation transfer functions, M, for two point source functions; "square" (near collimator) and "peaked" (at focal distance). When the point function is "square", collimators, like lenses, exhibit "spurious" resolution (note negative values of M and apparent reversal of source-no source wedges in the Siemens star test pattern in lower left photograph).

Let C_t and C_0 be the count rates observed at the same radius or space frequency, when the collimator axis is on the centre of a source and no-source wedge, respectively. The "image modulation" is defined by

$$m_i = \frac{C_t - C_0}{C_t + C_0} .$$

Similarly, the "source or object modulation" is defined by $m_0 = (\sigma_t - \sigma_0)/(\sigma_t + \sigma_0)$. These quantities are related by the "modulation transfer function" M, defined by the equation

$$Mm_0 = m_i .$$

We have chosen a simple test pattern in which $\sigma_0 = 0$. Thus $m_0 = 1$ and $M = m_i$. We can measure C_t and C_0 for all space frequencies ν represented on the test pattern and plot M versus ν, which is simply the space frequency response function.

In addition to serving as a basis for comparing collimators, this response function can be used to study the detrimental effects of background, scatter and penetration, since it is reduced by all of these response components.

6. FIGURE OF MERIT: Q

When the collimator region of view has a diameter that is larger than the wedge width, the observed count rates are not given by $C_t = E\sigma_t$, etc., even in the absence of scatter, penetration and background. This is simply because the source and no-source regions do not cover the field of view. In this case $C_t - C_0$ is reduced and approaches zero as the space frequency increases. Even at lower frequencies, the structure is seen reliably only if enough counts are accumulated to resolve C_t and C_0 statistically. If τ is the time spent in observing each count rate, the best estimates of the true mean rates are $C_t \pm (C_t/\tau)^{1/2}$ and $C_0 \pm (C_0/\tau)^{1/2}$, and of the difference, $(C_t - C_0) \pm [(C_t + C_0)/\tau]^{1/2}$. Considering α and β errors equally serious, we require that $(C_t - C_0) \geqq 2z[(C_t + C_0)/\tau]^{1/2}$. Thus, if we wish to distinguish C_t and C_0 with a reliability that is associated with Z standard deviations, the required counting time is $\tau \geqq Z^2/Q$ where $Q \equiv C_0(C_t/C_0 - 1)^2/4(C_t/C_0 + 1)$. Since the modulation transfer function is also a function of C_t and C_0, we can write $Q = C_0M^2/2(1 - M) = C_tM^2/2(1 + M)$. This system figure of merit can be used in many ways. For example, having measured $M(\nu)$ and $C_0(\nu)$ for two collimators having different radii of view, R, the Q of each can be plotted against ν to obtain a comparison of performances expected for different lesion sizes. In this sense, the radius of view can be optimized for a given lesion size.

If the total scan is to occupy an area A, and is to be completed in time T, with statistical reliability associated with Z standard deviations, then these conditions require a figure of merit $Q_R = Z^2A/\pi R^2T$. If the attainable figure of merit is equal to or greater than Q_R, the scan procedure is feasible.

7. INFORMATION THEORY AND OPTIMUM RADIUS OF VIEW

An alternative procedure for optimizing R applies in the absence of any knowledge whatever of the lesion size to be detected. We consider a region of area A, with mean concentration of activity σ, which is to be scanned in time T using a detector having a radius of view R. The question arises "for what value of R is the scan picture 'best' as judged by some reasonable critterion"? Ideally, a scanning system produces a precise picture of the concentration of radioactivity at each point in A. Such a picture answers two questions concerning the distribution of radioactivity: "how much activity is present"? and "where is it located"? If R is extremely small, the observed count rates will be so low that the quantity of activity cannot be measured accurately, while if R is very large we have no precise knowledge about where the activity is located. For intermediate values of R, the system will produce "better" pictures of the distribution. Establishing a criterion for the "best" picture is clearly somewhat arbitrary. Our approach is to define the information content, I, in the picture by a suitable (though somewhat arbitrary) function of R and further, to define the optimum radius of view as that R which maximizes the information content. Following modern practice in the optical and photographic arts [18] we divide the area A into M cells, each of area πR^2, and define the information content, I, in the picture as M times the mean information content, i, per cell.

If we think of the information content of a cell as the information gained through observation, then we can write $i = \log b - \log a = \log b/a$, where b and a = the number of equally probable possibilities before and after the observation, respectively. Thus, before making an observation of the number, m, of counts in a cell, we may estimate that the observation will surely yield a number in the range $0 \leq m \leq b$. Having observed some specific number, m, our best estimate of the true mean number we should observe on many repetitions of the observation is m with standard deviation $(m)^{1/2}$ (since observed numbers of counts are Poisson distributed). It is easy to show [19] that the information content in a normal distribution is the same as that in a rectangular distribution having a width of $(2\pi e)^{1/2}$ standard deviations, within which all possible values are equally probable. Assuming the observed count m is large enough so that the Poisson distribution is approximately normal, we can set $a = (2\pi em)^{1/2}$ and write $i = \log (b/2\pi em)^{1/2}$. The smallest gain in information (and thus the most conservative estimate of i) occurs when $b = m$ giving $i = \log (m/2\pi e)^{1/2}$ and $I = M \log (m/2\pi e)^{1/2}$. To express I as a function of R we substitute $M = A/\pi R^2$ and $m = C\tau = CT\pi R^2/A$. The count rate $C = E\eta H'\rho$ is also a function of R through collimator efficiency E. Here, two interesting cases occur. For a set of single (tapered or straight) hole collimators having the same thickness, $E = KR^4$ where K is a proportionality factor. For a set of focused collimators, designed for a fixed crystal diameter, gamma energy, penetration fraction etc., we find that $E \cong KR^2$. Using the latter relation the total information is: $I = A/\pi R^2 \log (K\eta H'\rho T/2eA)^{1/2} R^2$ and is maximum when the radius of view is: $R_{opt} = e^{1/2}(2eA/K\eta H'\rho T)^{1/4}$. Using this value in the expression for m, we find that the optimum number of counts per cell is $m_{opt} = 2\pi e^3 = 126$. In this case, the optimum information content per cell is $i_{opt} = \log (m_{opt}/2\pi e)^{1/2} = \log e = 1$

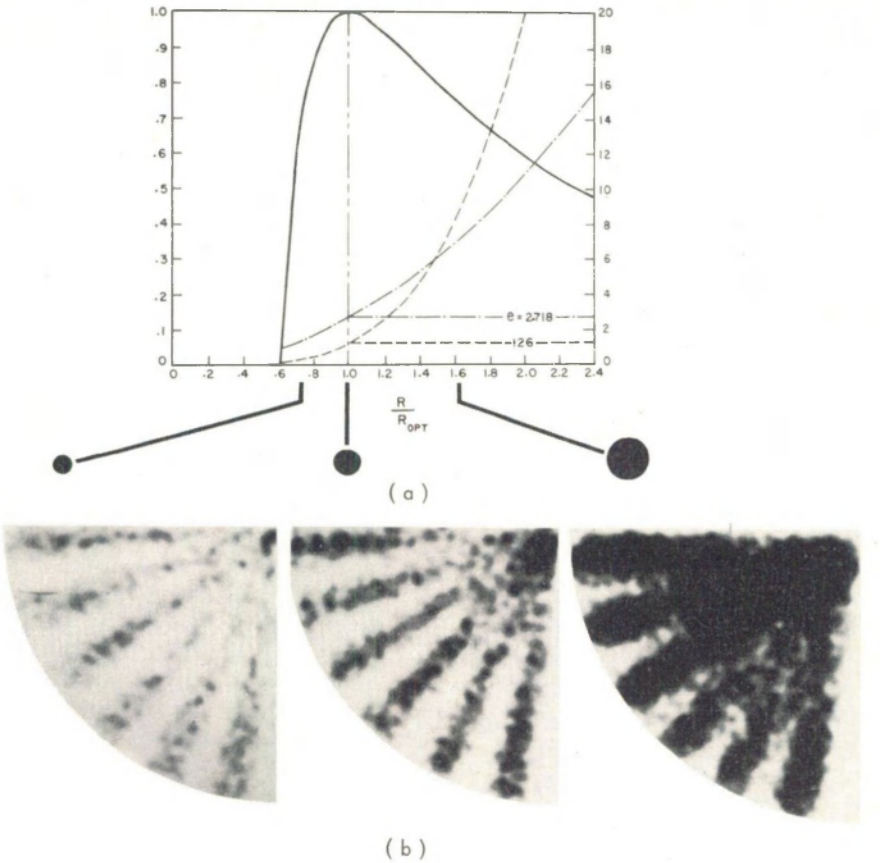

Fig. 7

For "optimum" balance between sensitivity and resolution, scan picture contains maximum information. This occurs when resolution is such that each "region of view" contains one natural unit (1.443 bits) of information. Scans, left and right, contain 25% less information than centre scan.
——— = I/I_{max}; —·—·— = No. of distinguishable states; - - - - = No. of counts/cell x 100.

natural unit*. Since information can also be thought of as the logarithm of the number of mutually distinguishable states, this means that the optimum number of such states is e = 2.718, the base of natural logarithms. Since 3 is the integer closest to e, this result may be interpreted very loosely as suggesting that the optimum picture of the distribution of activity is obtained when the radius of view is chosen so that the number of counts accumulated in a cell is sufficient to allow us to make one of three decisions for each cell: the concentration of activity is normal, above normal or below normal. Figure 7 summarizes these results.

Similar results are obtained for the straight hole, where $E = KR^4$. In this case the shape of the I/I max versus R/R_{opt} curve is identical to that in Fig. 7 while $m_{opt} = 2\pi e^4 = 342$ counts per cell. The optimum number of

* 1 natural unit of information = 1.443 binary units or bits.

distinguishable states is $e^{3/2}$ giving 1.5 natural units as the optimum information per cell.

8. CONCLUSION

The ultimate criterion for "optimizing" a scan procedure must be based on some measure that maximizes the probability of detecting the lesions of interest. To some extent this depends on how the information is analysed; whether it is manipulated by a computer or simply viewed as a picture. The measures discussed here (system figure of merit Q and information content I) affect a balance between sensitivity and resolution which may or may not be optimum from the point of view of human perception. Thus these measures must be evaluated in the context of the method of analysis.

ACKNOWLEDGEMENT

The author is indebted to L. O. Jacobson, D. Charleston, P. V. Harper, and L. Zimmer for their trust, constant assistance, stimulation, and helpful criticism.

REFERENCES

[1] BROWNELL, G.L., Medical Radioisotope Scanning, IAEA, Vienna (1959) 1-12.
[2] ANGER, H.O., Nucleonics 21 (1963) 56-59.
[3] BENDER, M.A. and BLAU, M., Nucleonics 21 (1963) 52-55.
[4] MAYNEORD, W.V., Brit. J. Radiol. (Suppl. 2) (1950) 168.
[5] NEWELL, R.R., SAUNDERS, W. and MILLER, E., Nucleonics 10 (1952) 36.
[6] JAFFEY, A.H., Rev. sci. Instrum. 25 (1954) 349.
[7] GARRETT, M.W., Rev. sci. Instrum. 25 (1954) 1208.
[8] GROVER, F.W., Inductance Calculations. D. Van Nostrand Co., Inc., Princeton, New Jersey (1946) 115.
[9] BECK, R.N., Collimators for Radioisotope Scanning Systems, these Proceedings.
[10] NELMS, A.T., National Bureau of Standards Circular 542 (1953).
[11] MANAGEN, W. and CROUTHAMEL, C.E., in Applied Gamma-Ray Spectrometry, Chap. 2 (CROUTHAMEL, C.E., Ed.) Pergamon Press, New York (1960) 31.
[12] MYHILL, J., Int. J. appl. Rad. Isotopes 12 (1961) 10-19.
[13] BECK, R.N., J. nucl. Med. 2 (1961) 314-324.
[14] BROWNELL, G.L., Int. J. appl. Rad. Isotopes 3 (1958) 181-192.
[15] WASHER, F.E. and GARDNER, I.C., National Bureau of Standards Circular 533 (1953).
[16] SCHADE, O.H., Optical Image Evaluation, Chap. 17, National Bureau of Standards Circular 526 (1954).
[17] PERRIN, F.H., J. Soc. Motion Picture Television Engrs 69 (1960) March 151-156; April 239-249.
[18] LINFOOT, E.H., J. Opt. Soc. Amer. 45 (1955) 808-819.
[19] BELL, D.A., Information Theory and its Engineering Applications, 2nd ed. Pitman Publishing Corp., New York (1956).

DISCUSSION

M. BLAU: Dr. Beck reports the optimal number of counts per resolution area as 126. Dr. Brownell's curves seem to indicate that the optimum

is much lower, perhaps less than 10. Can these two conclusions be reconciled?

R. BECK: I believe that the difference lies in our definitions of information content per cell. If this quantity is defined by the logarithm of the number of counts per cell, I believe Dr. Brownell's number is obtained. I have defined this quantity as the logarithm of the number of statistically distinguishable states, which gives 126 counts per cell as the optimum number.

G. BROWNELL: I believe that the optimum value of m will depend on the pattern. In general, the greater the detail, the smaller the value of m, as shown by the range of $\log_2 m$ from 2 to 5 bits found in our scanning simulation programme. The value found for maximum information capacity would represent a minimum.

INFORMATION THEORY AND RADIOISOTOPE SCANNING*

J. CEDERLUND
RADIOFYSISKA AVDELNINGEN, CENTRALLASARETTET,
BORÅS, SWEDEN

Abstract — Résumé — Аннотация — Resumen

INFORMATION THEORY AND RADIOISOTOPE SCANNING. The quality of a scintigram is often described in terms of resolution and contrast. Generally, these two parameters are not independent of each other. Increased resolution can usually only be achieved at the cost of decreased contrast. A fundamental problem in scanning theory is to find the best compromise between resolution and contrast. This problem can be solved if one can find a measure of the quality of a scintigram that considers both resolution and contrast. This paper discusses the possibility of defining the information content of a scintigram and using this as a quality measure.

First, an elementary introduction to information theory is presented in order to enable a reader with no previous knowledge of information theory to follow the rest of the paper. A heuristic approach to the main topic is criticized and some commonly met pitfalls during the application of the information theory are pointed out.

A mathematical model of a simplified scanning system consisting of a collimator and a detector is described. The amount of information available at the output of this system is calculated. The scanning system divides the scintigram into a number of image elements. With few image elements the contrast is good. If the number of elements is increased resolution is improved, but contrast is reduced. It can be shown that, under certain conditions, as the number of elements is increased the amount of information in the image first increases, reaches a maximum and then decreases.

A discussion follows on how much of the potentially available information is lost in the display system, for instance through the effect of contrast enhancement. Finally, it is pointed out that high information content is a necessary, but not sufficient, condition for good quality of a scintigram.

THÉORIE DE L'INFORMATION ET SCINTIGRAPHIE AU MOYEN DE RADIOISOTOPES. On exprime fréquemment la qualité d'un scintigramme en fonction de la résolution et du contraste. D'une manière générale, ces deux paramètres ne sont pas indépendants l'un de l'autre. Habituellement, on ne peut augmenter la résolution qu'en diminuant le contraste. Un des problèmes fondamentaux qui se posent dans la théorie de la scintigraphie consiste à trouver le meilleur compromis entre la résolution et le contraste. On peut résoudre ce problème à condition de pouvoir établir une mesure de la qualité du scintigramme qui tienne compte à la fois de la résolution et du contraste. Le mémoire étudie la possibilité de définir l'information contenue dans un scintigramme et de l'utiliser comme mesure de qualité.

L'auteur présente tout d'abord une introduction élémentaire à la théorie de l'information, afin de permettre à tout lecteur n'ayant pas de connaissances préalables dans ce domaine de comprendre le reste du mémoire. Il critique la conception euristique du thème principal et signale quelques dangers auxquels on se heurte souvent lorsqu'on applique la théorie de l'information.

L'auteur décrit un modèle mathématique d'un système d'exploration simplifié, composé d'un collimateur et d'un détecteur. Il calcule la quantité d'informations que l'on peut obtenir à l'aide de ce système. Le scintigramme comprend un certain nombre d'éléments d'image. Lorsque ces éléments sont peu nombreux, le contraste est bon. Si leur nombre augmente, la résolution est améliorée mais le contraste diminue. On peut démontrer que, sous certaines conditions, à mesure que le nombre d'éléments augmente, la quantité d'informations contenues dans l'image commence par augmenter, puis atteint un maximum et finit par diminuer.

* This work was supported by a grant from the Swedish Cancer Society.

L'auteur examine ensuite quelle est la proportion des informations potentiellement disponibles qui est perdue à la lecture du scintigramme, par exemple sous l'effet d'un accroissement du contraste. Enfin, il fait ressortir qu'une grande quantité d'informations est une condition nécessaire, mais non suffisante, pour assurer la bonne qualité d'un scintigramme.

ТЕОРИЯ ИНФОРМАЦИИ И РАДИОИЗОТОПНОЕ СКЕННИРОВАНИЕ. Качество сцинтиграммы часто характеризуют с точки зрения разрешающей способности и контрастности. Эти два параметра в общем зависят друг от друга. Разрешающую способность можно увеличить только за счет уменьшения контрастности. Основная проблема теории скеннирования заключается в том, чтобы найти наилучшее компромиссное решение проблемы зависимости между разрешающей способностью и контрастностью. Эта проблема может быть решена в том случае, если будет найдена мера качества сцинтиграммы, учитывающая разрешающую способность и контрастность. В этом докладе обсуждается возможность определения количества информации, содержащейся в сцинтиграмме и использование его для качественной характеристики.

Вначале дается элементарное описание теории информации, чтобы читатель, который до этого не был знаком с теорией информации, мог разобраться в содержании доклада.

Критикуется эвристический метод исследования главной темы и указываются некоторые источники ошибок, обычно встречающиеся при применении теории информации.

Описывается математическая модель упрощенной системы скеннирования, состоящей из коллиматора и детектора. Подсчитывается объем информации на выходе этой системы. Система скеннирования делит сцинтиграмму на ряд элементов изображения. При небольшом количестве элементов изображения контрастность хорошая. Если увеличивается число элементов, улучшается разрешающая способность, но контрастность снижается. Можно продемонстрировать, как при определенных условиях, по мере увеличения числа элементов, объем информации на изображении сначала увеличивается, достигает максимума, а потом снижается.

Затем обсуждается вопрос о том, какой объем потенциально доступной информации теряется в воспроизводящей системе, например, в результате усиления контрастности.

В заключение подчеркивается, что большое количество информации является необходимым, но не единственным условием для хорошего качества сцинтиграммы.

TEORÍA DE LA INFORMACIÓN Y EXPLORACIÓN MEDIANTE RADIOISÓTOPOS. La calidad de un centelleograma se expresa frecuentemente en función del poder de resolución y del contraste. Estos dos parámetros no suelen ser independientes uno de otro. Por lo general, el aumento del poder de resolución sólo puede lograrse disminuyendo el contraste. Uno de los problemas fundamentales que se plantean en la teoría de la exploración gammagráfica consiste en hallar la mejor fórmula de compromiso entre el poder de resolución y el contraste. Este problema puede resolverse si se encuentra una medida de la calidad del centelleograma que tenga en cuenta, a la vez, el poder de resolución y el contraste. En la memoria se examina la posibilidad de definir la información contenida en un centelleograma y de utilizarla como medida de calidad.

El autor presenta en primer lugar una introducción elemental a la teoría de la información a fin de que el lector que no posea conocimientos previos en esta esfera pueda comprender el resto de la memoria. Critica la concepción heurística del tema principal y señala algunos errores que suelen cometerse al aplicar la teoría de la información.

Describe un modelo matemático de un sistema simplificado de exploración compuesto de un colimador y de un detector. Calcula la cantidad de información que puede obtenerse con este sistema. El centelleograma comprende un cierto número de elementos de imagen. Cuando estos elementos son poco numerosos, el contraste es bueno. Si su número aumenta, se mejora el poder de resolución, pero el contraste disminuye. Se puede demostrar que, en ciertas condiciones, a medida que el número de elementos aumenta, la cantidad de información contenida en la imagen comienza por aumentar, luego alcanza un máximo y acaba por disminuir.

El autor examina a continuación cuál es la cantidad de información potencialmente disponible que se pierde en el sistema de representación, por ejemplo, por efecto de un aumento del contraste. Señala, por último, que una gran cantidad de información es una condición necesaria, pero no suficiente, de la buena calidad de un centelleograma.

1. THE DEFINITION OF INFORMATION

1.1. Introduction

In many papers on scintillation scanning the information content of a scintigram is discussed in general terms, but very few attempts have been made to measure this information quantitatively and discuss how it varies under different conditions. This paper represents such an attempt. In writing it I have borrowed freely from many sources, mainly from SHANNON's now classical paper "The mathematical theory of communication", [1], and also from [2-6].

The fundamental problem of communication is to reproduce at one point a message selected at another point. Message is here used in a broad sense. In our case the message is an image of the distribution of radioactivity in a certain region. Frequently the messages have a meaning, but this aspect is irrelevant to the engineering problem. The significant aspect is that the actual message (or image) is one selected from a set of possible messages (images). The system must be designed to operate for each possible selection, not just for the one which will actually be chosen since this is unknown at the time of design.

If the number of possible messages in the set is finite then this number, or any monotonic function of this number, can be regarded as a measure of the information produced when one message is chosen from the set, all choices being equally likely. For several reasons the most natural choice is the logarithmic function. Essentially then the information in a message (or image) is the logarithm of the number of possible messages (images) from among which it was chosen.

This definition will soon have to be generalized in order to take into consideration sets of messages which do not have equal a priori probabilities. In order to do so we must briefly discuss what is known as the entropy of finite schemes.

We will however first discuss an example that illustrates one of the reasons for choosing a logarithmic measure of information.

1.2. Example

With an alphabet of 26 different letters, with just one letter 26 different messages can be produced. With two letters $26.26 = 676$ different messages can be produced, with three $26.26.26 = 17576$ different messages. The number of possible messages therefore increases exponentially with the number of letters. Intuitively we feel, however, that the information increases linearly with the number of letters. For example, two pages of text contain twice as much information as one. Doubling the number of letters squares the number of possible messages, but only doubles the logarithm of the number of possible messages. Therefore, the logarithmic measure agrees with our intuitive notions.

1.3. Entropy of finite schemes

Consider a set of events $X_1, X_2, \ldots X_n$ such that one and only one of them must occur at each trial. Examples of such events are the appearance

of heads or tails in tossing a coin, the appearance of 1, 2, 3, 4, 5 or 6 points in throwing a die, the appearance of a letter at the receiving end of a teletypewriter or the appearance of a black or white dot on a T.V. screen. A complete system of events $X_1, X_2, \ldots X_n$, together with their probabilities of ocurrence $p_1, p_2, \ldots p_n$ (were $p_i \geq 0$ and $\sum_{i=1}^{n} p_i = 1$) is called a finite scheme

$$X = \begin{pmatrix} X_1, & X_2, \ldots & X_n \\ p_1, & p_2, \ldots & p_n \end{pmatrix}.$$

For instance the throwing of a die is associated with the finite scheme

$$X = \begin{pmatrix} X_1, & X_2, & X_3, & X_4, & X_5, & X_6 \\ 1/6 & 1/6 & 1/6 & 1/6 & 1/6 & 1/6 \end{pmatrix}.$$

Every finite scheme describes a state of uncertainty. It has been shown that the quantity

$$H(X) = -\sum_{i=1}^{n} p_i \log p_i$$

can serve as a very suitable measure of this uncertainty. The quantity H(X) is called entropy, because of its close analogy to a well-known quantity in the theory of thermodynamics.

The logarithms can be taken to any arbitrary base, the choice of base defines the unit. Usually the logarithms to the base of 2 are employed, in which case the unit is called a "bit" (binary unit). For mathematical convenience natural logarithms may be employed, in which case the unit is called "nit" (natural unit). In some special cases logarithms to the base of ten are used, the corresponding unit is then called "hartley" (in honour of R.V.L. Hartley).

The entropy $H(X) = -\sum_{i=1}^{n} p_i \log p_i = 0$ only if one of the probabilities p_i is one, and all the rest are zero (by definition both 0 log 0 and 1 log 1 is zero). This is just the case when the outcome of the experiment is known beforehand, therefore it is appropriate that the uncertainty in this case has the value zero.

It can be proved mathematically that if n is fixed the scheme with the most uncertainty is the one with equally likely results, i.e. $p_i = 1/n$. This also agrees with our intuitive notions. In the two alternatives

$$\begin{pmatrix} X_1 & X_2 \\ 0.5 & 0.5 \end{pmatrix} \qquad \begin{pmatrix} X_1 & X_2 \\ 0.99 & 0.01 \end{pmatrix}$$

the outcome of the first is much more uncertain than the second, which is "almost certainly" X_1.

1.4. Information as reduction of entropy

When performing an experiment the possible outcomes of which are described by a given scheme X, we obtain some information (i.e. we find out which of the events X_i actually occurs), and the uncertainty of the scheme is eliminated. We can say that the information gained by performing the experiment consists in removing the uncertainty which existed before the experiment.

1.5. Example

Before throwing a die the uncertainty is

$$-\sum_{i=1}^{n} p_i \log_2 p_i = -\left(\frac{1}{6}+\frac{1}{6}+\frac{1}{6}+\frac{1}{6}+\frac{1}{6}+\frac{1}{6}\right)\log_2\frac{1}{6} = \log_2 6 = 2.58 \text{ bits.}$$

After the throw, the uncertainty is zero and the information gained is 2.58 bits.

1.6. Example

An alphabet has 32 different letters which all occur with equal probability, i.e. $p_i = 1/32$. The entropy is

$$-\sum p_i \log_2 p_i = -(32/32)\log_2 1/32 = \log_2 32 = \log_2 2^5 = 5 \text{ bits.}$$

The amount of information is therefore 5 bits per received letter. Note that in this case the amount of information per letter is equal to the logarithm of the number of possible letters.

1.7. Example

If the 32 letters in the previous example do not have the same a priori probability but, for instance, 8 letters have the probability 1/16, 8 have probability 1/32 and the remaining 16 have probability 1/64 then the entropy is

$$-\sum_{i=1}^{n} p_i \log_2 p_j = \frac{8}{16}\log_2 16 + \frac{8}{32}\log_2 32 + \frac{16}{64}\log_2 64 = 4.75 \text{ bits.}$$

The average information per letter is thus 4.75 bits. In this case the information per letter is less than the logarithm of the number of letters. This is generally the case with practically used alphabets.

1.8. Redundancy

n practice the average amount of information per letter is further reduced by the fact that the probability of occurence of one letter is affected by the choice of the preceding letters. If for instance the letters "informatio" have been chosen, the probability that the next letter is l is practically zero, while the probability that it is n is practically one. In fact it is quite likely that after having read only the letters "infor..." one could guess that the rest of the word is "... mation". These last letters then carry very little information.

The fact that knowledge of the preceding letters somewhat decreases our uncertainty regarding the next letter reduces the average amount of information per letter. The actual information per letter in English written text has been calculated to be only about 50% of what would be possible if all letters were chosen independently and with equal probability. The difference between actual information and maximum information is called redundancy. This means that when we write English half of what we write is chosen freely, and half is determined by the structure of the language and represents redundant information.

1.9. Coding and noise

Because of redundancy a message can often be compressed by suitable coding. For instance if a code book is compiled where all the words to be used are listed and assigned numbers in such a way that frequently used words are assigned short numbers, and the longer numbers are reserved for the infrequently used words, then a considerable reduction in the length of the message can be achieved and the amount of redundancy is correspondingly reduced.

Redundancy, however, may in some cases have a beneficial effect. If the communication channel is noisy, i.e. if the received signal is not always identical with the transmitted, then redundancy helps to make a correct interpretation. In written English, for instance, the content of a message can be quite clear, even if many words are wrongly spelled.

If the message is coded in a redundancy-free manner, then one single error can completely change the content. In some cases redundancy is deliberately introduced in order to combat noise. An example is the practice of writing important words twice, when sending a telegram.

We will return to the problem of noise in a later section, and discuss how the information content of an image is reduced by noise.

2. INFORMATION CONTENT OF IMAGES

2.1. Model of an image-producing system

In order to estimate the information content of images we will discuss the following simplified model of an image producing system, due to LINFOOT [2]. We divide up the image surface of the system into a number

n of cells (square or hexagons), which we will call image elements. Each image element is supposed to be capable of taking on m density-values black and white. We suppose further that when an object is presented to the model each image element takes on that density value which most nearly corresponds to the mean brightness of the corresponding area of the object. The model thus produces an approximate image of the object by means of a kind of mosaic picture, and the larger m and n the more faithful the representation.

2. 2. *Number of different images*

With only one image element we can produce m different images. With two image elements, any one of the m different density values of the first element can be combined with any one of the m different density values of the second element. We can therefore produce m^2 different images. In the general case with n elements we can produce m^n different images.

If all of these are equally likely, then our uncertainty regarding which image the model will produce is $\log_2 m^n$ bits, or $n \log_2 m$ bits, and this is also the information gained when an image is produced. This means that the information content of an image is equal to the number of image elements, n, times the amount of information per image element, $\log_2 m$. Note that if the image elements only can take on two different density values, black and white, then the amount of information per element is $\log_2 2 = 1$ bit, thus the information in this image is equal to the number of image elements.

2. 3. *Application to the scanning problem*

In order to apply this model to the theory of scanning we must first define n and m. We can envisage a simplified model of a scanning system where the collimator defines a small area in the object. This area is made to cover the whole object stepwise, without overlapping. Each step corresponds to one image element, and the number of such steps needed to cover the object is n, the number of image elements.

The number of counts per element determines the density of the element. The greater the number of counts per element the greater is m, the number of different density values.

We can now approach one of the most fundamental problems of scanning theory, the relation between resolution and sensitivity. Resolution is related to n. The larger n is, the better the resolution. But large n means low sensitivity, few counts are registered per image element, and the amount of information per element is small.

The total amount of information in the image is n multiplied by $\log_2 m$, the amount of information per image element. In order to discuss how the information varies as n increases, we must know two relations, 1: the relation between the number of counts per element and m, the number of distinguishable density levels, 2: the relation between n and the number of counts per element.

In a recent article [5] BROWNELL has suggested that, as a gross oversimplification, we can equate m with the number of counts per element. If this is done one can show that the information of the image has a maximum

if n is chosen such that on the average 7.5 counts are registered per image element.

This result is interesting but can only be regarded as a first approximation. In order to obtain a result that is somewhat more realistic we must realize that the number of distinguishably different density levels is considerably less than the average number of counts per element. We know that if we have recorded say 10 counts a repeated measurement might result in only 9 counts, or in 11 counts. Therefore we do not feel convinced that these three counts really should be registered as different density levels.

This can be regarded as a noise problem and, in order to solve it, we must return again to the study of noisy communication channels.

3. NOISE AND INFORMATION

3.1. Introductory example

In order to show how information is destroyed by noise the following example from SHANNON [1] will be cited: Suppose there are two possible symbols 0 and 1, and we are transmitting at a rate of 1000 symbols/s with probabilities $p_0 = p_1 = 1/2$. Thus our source is producing information at the rate of 1000 bits/s. During transmission the noise introduces errors so that, on the average, 1 in 100 is received incorrectly (a 0 as 1, or 1 as 0). What is the rate of transmission of information? Certainly less than 1000 bits/s since about 1% of the received symbols are incorrect. Our first impulse might be to say the rate is 990 bits/s, merely subtracting the expected number of errors. This is not satisfactory since it fails to take into account the recipient's lack of knowledge of where the errors occur. We may carry it to an extreme case and suppose the noise so great that the received symbols are entirely independent of the transmitted symbols. The probability of receiving 1 is 1/2 whatever was transmitted and similarly for 0. Then about half of the received symbols are correct due to change alone, and we would be giving the system credit for transmitting 500 bits/s while actually no information is being transmitted at all. Equally "good transmission would be obtained by dispensing with the communication channel entirely and flipping a coin at the receiving point.

The proper correction to apply is calculated in the following way. Before any symbols are received the probability p_0 that 0 will be sent is 1/2 and the probability p_1 that 1 will be sent is also 1/2. The uncertainty before any symbol is sent is thus $\sum_i p_i \log p_i = -1/2 \log 1/2 - 1/2 \log 1/2 = 1$ bit symbol. If there was no noise this uncertainty would disappear completely on receiving a symbol and the information gained per received symbol would be 1 bit. With noise, however, the uncertainty is reduced, but does not disappear completely. If we receive a 0 the probability that 0 was sent is 0.99, and the probability that 1 was sent is 0.01. Our remaining uncertainty now is $-\Sigma p_i \log p_i = -(0.99 \log 0.99 + 0.01 \log 0.01) = 0.081$ bits/symbol. Our uncertainty is therefore reduced by the amount $1 - 0.081 = 0.919$ bits per received symbol. Since 1000 symbols/s were sent we receive 919 bits of information per second. It is interesting to note that although only 1% of the symbols are affected by noise 8% of the information is destroyed. This is

because we do not know which letters are affected. We will now consider a more general case of how noise affects the transmitted information

3.2. *Joint probability matrix*

Let us assume that we have a communication channel that is related to the two finite schemes X and Y

$$X = \begin{pmatrix} x_1 & x_2 & \dots & x_i & \dots & x_n \\ p(x_1) & p(x_2) & \dots & p(x_i) & \dots & p(x_n) \end{pmatrix}$$

$$Y = \begin{pmatrix} y_1 & y_2 & \dots & y_i & \dots & y_m \\ p(y_1) & p(y_2) & \dots & p(y_i) & \dots & p(y_m) \end{pmatrix} .$$

The scheme X refers to the transmitted symbols and Y to the received symbols. If the two schemes are independent, that is to say if the probability of receiving y_j is independent of which x_i is sent, then no information is transmitted. In a noiseless system the received symbol exactly specifies the transmitted symbol. If the system is slightly disturbed by noise then a received symbol gives a high probability for one transmitted symbol and a low probability for one or more of the other transmitted symbols. The probability of the joint event that the symbol x_i is transmitted and that y_i is received is denoted $p(x_i, y_i)$. The interdependence between the two schemes X and Y is specified by the joint probability matrix

$$\begin{bmatrix} p(x_1, y_1) & p(x_1, y_2) \dots & p(x_1, y_j) \dots & p(x_1, y_m) \\ p(x_2, y_1) & p(x_2, y_2) \dots & p(x_2, y_j) \dots & p(x_2, y_m) \\ \dots & \dots & \dots & \dots \\ p(x_i, y_1) & p(x_i, y_2) \dots & p(x_i, y_j) \dots & p(x_i, y_m) \\ \dots & \dots & \dots & \dots \\ p(x_n, y_1) & p(x_n, y_2) \dots & p(x_n, y_j) \dots & p(x_n, y_m) \end{bmatrix}$$

From this joint probability matrix we can compute the probability for x_i as

$$p(x_i) = \sum_{j=1}^{m} p(x_i, y_j)$$

and similarly

$$p(y_j) = \sum_{i=1}^{n} p(x_i, y_j).$$

3.3 Numerical example

As an illustration of a joint probability matrix we cite the following example from REZA [3]. A transmitter has an alphabet consisting of five letters (x_1, x_2, x_3, x_4, x_5) and the receiver has an alphabet of four letters (y_1, y_2, y_3, y_4). The joint probabilities are given below.

$$\begin{array}{c} \\ x_1 \\ x_2 \\ x_3 \\ x_4 \\ x_5 \end{array} \begin{array}{c} \begin{array}{cccc} y_1 & y_2 & y_3 & y_4 \end{array} \\ \begin{bmatrix} 0.25 & 0 & 0 & 0 \\ 0.10 & 0.30 & 0 & 0 \\ 0 & 0.05 & 0.10 & 0 \\ 0 & 0 & 0.05 & 0.10 \\ 0 & 0 & 0.05 & 0 \end{bmatrix} \end{array}.$$

Fig. 1 illustrates the situation.

3.4 *Conditional entropy*

A number of entropies can be computed for this system. We are interested in H(X) which is a measure of the average uncertainty regarding which letter is going to be transmitted, and in a new type of entropy which we will denote H(X/Y) which is the average uncertainty regarding which letter x was transmitted when it is known that a letter y has been received H(X/Y) is known as a conditional entropy, and is pronounced "the entropy of x when y is known", or "the entropy of x given y".

In order to compute H(X) for the above example we note that $p(x_1) = 0.25$, $p(x_2) = 0.10 + 0.30 = 0.4$, $p(x_3) = 0.05 + 0.10 = 0.15$, $p(x_4) = 0.05 + 0.10 = 0.15$, $p(x_5) = 0.05$.

$H(X) = -\sum_i p(x_i) \log p(x_i) = -0.25 \log 0.25 - 0.40 \log 0.40 - 0.15 \log 0.15 - 0.15 \log 0.15 - 0.05 \log 0.05 = 2.066$ bits.

Note that $H(X) = -\sum_i p(x_i) \log p(x_i)$ can be written

$$H(X) = \sum_i \sum_j p(x_i, y_j) \log p(x_i).$$

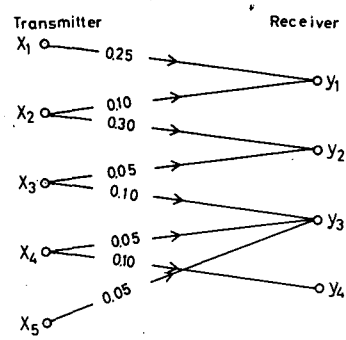

Fig. 1

Symbolic diagram of a transmitter with the alphabet $x_1 \ldots x_5$ and a receiver with the alphabet $y_1 \ldots y_4$. The number on the arrow from x_i to y_j is the joint probability $p(x_i, y_j)$ that y_j will be received when x_i is transmitted.

Next we have to compute $H(X|Y)$. We then first need to know the conditional probability $p(x_i/y_j)$, that is to say the probability for x_i when y_j has been received. This probability is computed from $p(x_i/y_j) = p(x_i, y_j)/p(y_j)$ which formula will not be derived, but only made plausible by the following example. If y_2 was received we know that either x_2 or x_3 was sent (see Fig. 1), the probability for x_2 is $0.30/(0.30 + 0.05) = 6/7$ and the probability for x_3 is $0.05/(0.30 + 0.05) = 1/7$. The probabilities for all the other letters are 0. The uncertainty regarding x when y_2 has been received is then $H(X/y_2) = -\sum_i p_i(x_i/y_2) \log p(x_i/y_j) = -(6/7)\log 6/7 - (1/7)\log 1/7 = 0.591$. Similarly we can compute $H(X/y_j) = -\Sigma[p(x_i, y_j)/p(y_j)] \log p(x_i, y_j)/p(y_j)$ for all the four letters (y_1, y_2, y_3, y_4). Finally the average conditional entropy for all four values of y_j is taken in order to obtain a measure of average conditional entropy of the whole system.

$$H(X|Y) = H(X|y_j) = \sum_{j=1}^{m} p(y_j) H(X|y_j)$$
$$= -\sum_{j=1}^{m} (p(y_j) \sum_{j=1}^{n} p(x_i|y_j) \log p(x_i|y_j)$$
$$= -\sum_{i=1}^{n} \sum_{j=1}^{m} p(x_i, y_j) \log p(x_i, y_j)/p(y_j) .$$

In the above example $H(X|Y) = -0.25 \log 5/7 - 0.10 \log 2/7 - 0.30 \log 6/7 - -0.05 \log 1/7 - 0.10 \log 1/2 - 0.05 \log 1/4 - 0.05 \log 1/4 = 0.809$ bits. Our average gain in information for each letter y we receive is then our uncertainty $H(x)$ regarding x before we received y, minus the smaller uncertainty $H(X|Y)$ regarding x when we have received y:

$I(X;Y) = H(X) - H(X|Y) = 2.066 - 0.809 = 1.157$ bits per letter. Note that the general expression for

$$I(X;Y) = H(X) - H(X|Y) = -\sum_i \sum_j p(x_i, y_j) \log p(x_i)$$

$$+ \sum_i \sum_j p(x_i, y_j) \log p(x_i, y_j)/p(y_j) \text{ can be written}$$

$$I(X;Y) = \sum_i \sum_j p(x_i, y_j) \log p(x_i, y_j)/p(x_i)\, p(y_j)$$

which is the expression we will use in the following sections. The reader who is not satisfied with this very sketchy derivation is referred to textbooks on information theory such as [3].

We will now apply these ideas to a rather hypothetical communication system, which will prove of value for our main theme.

3.5. A binary channel with Poisson noise

Consider a communication channel consisting of a radioactive source and a detector that registers k counts/s from the source. Between the source and the detector there is a shutter which can prevent any radiation from reaching the detector. It is assumed that messages are to be transmitted in a binary code (letters 0, 1) where the letters have equal probability of occuring. A time unit of t seconds is chosen, during each such time unit the shutter is either open or closed. A closed shutter is equivalent to transmitting the letter 0, an open shutter means the letter 1. If the detector registers no counts this is interpreted as receiving the letter 0. If one or more counts are registered it is interpreted as receiving the letter 1. It is assumed that there is no "background" counting rate.

The average number of counts registered during a time unit with open shutter is k t. The probability, that when the letter 1 is transmitted, it will be received as the letter 0 is calculated from the Poisson distribution $P(x) = \lambda^x \exp - \lambda / x!$ with $x = 0$ and $x = kt$; consequently $P(0) = \exp^{-kt}$. The situation is illustrated in Fig. 2. Nothing is lost in generality if we assume that $k = 1$. From the Figure we can compute the different probabilities as: $p(x_0) = 1/2$, $p(x_1) = 1/2$, $p(y_0) = (1 + \exp - t)/2$, $p(y_1) = (1 - \exp - t)/2$, $p(x_0, y_0) = 1/2$, $p(x_0, y_1) = 0$, $p(x_1, y_0) = (1/2) \exp - t$ and $p(x_1, y_1) = (1 - \exp - t)/2$. These probabilities inserted in the formula

$$I(X;Y) = \sum_i \sum_j p(x_i, y_j) \log p(x_i, y_j)/p(x_i)\, p(y_j)$$

yield after some algebraic work

$$I(X;Y) = 1 - \tfrac{1}{2} [(1 + e^{-t}) \log (1 + e^{-t}) - e^{-t} \log e^{-t}] \text{ bits/letter.}$$

Note that for $t \gg 1$ this approaches 1 bit/letter and for $t \ll 1$ it approaches $(1/2)t$ bit/letter.

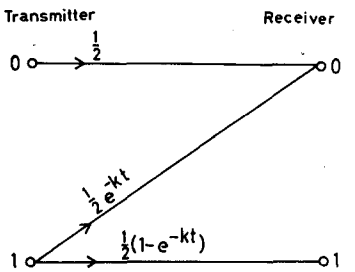

Fig. 2

Symbolic diagram of a communication system based on a radioactive source

Let us now consider which time unit should be chosen, in order to transmit as much information as possible per second. If we choose a long time unit t, so that many counts are recorded every time the shutter is open then we are almost sure that we can always recognize whether a 0 or a 1 was transmitted, and we receive one bit of information per letter. We have practically no noise, but on the other hand we only transmit at a rate of $1/t$ bits per second. If on the other hand we choose a time unit t much shorter than one second, a transmitted 0 will always be received as a 0. A 1 however will also mostly be received as a 0 and only now and again as a 1. On the average we will receive $t/2$ bits per transmitted letter. It is however worth noting that, even though the received information per letter approached zero linearly with t, the received information per second approaches $(1/2)t$ $1/t = 1/2$ bit per second, which is therefore the maximum rate of transmission we can achieve with this communication system. We will return to this system later, and show that it can serve as a simple model of a scanning system. However we must first attend to the collimating problem.

4. INFORMATION CONTENT OF SCINTIGRAMS

4. 1. Three different classes of ideal collimators

An ideal collimator would define a small area in the object, and allow all the counts from this area to be recorded, and reject all counts from outside. Real collimators are far from ideal, and much theoretical and experimental work has been carried out to investigate the properties of real collimators. In this paper, however, we are only concerned with ideal collimators, partly because the author feels that at present it is too difficult to apply information theory to real collimators, and partly because it is important to stress the fact that, even with ideal collimators, the fundamental problem of deciding the optimum resolution is very difficult. When discussing this problem it is helpful to consider a simple experiment that illustrates the fundamental collimation problem.

Let us assume that we want to know as much as possible about the distribution of radioactivity on a piece of paper. At our disposal we have a detector, say a well-counter, and a limited amount of time. The paper can be

cut into a number of pieces, and each counted for part of the time. A fundamental problem is to decide into how many pieces the paper should be cut.

Counting the whole paper all the available time corresponds to an image with only one image element, the resolution area is the whole paper. Let us denote the number of recorded counts C. Cutting the paper in two, and counting each piece half the available time corresponds to two image elements while the resolution area is now half the paper. This time however, the total number of counts is only C/2, and the average number of counts per image element is C/4.

If the paper is cut into n pieces, and each piece is counted for 1/n of the time, the resolution area is 1/n of the size of the paper, the total number of counts registered is C/n and the counts per image element is C/n^2.

Let us now focus attention on to the relation between the size of the image element (the resolution area) and the total number of counts recorded. In the described experiment, the total number of counts is directly proportional to the size of the resolution area. This is typical for a whole class of collimators. Both focussed multichannel collimators and pinhole collimators roughly behave in this manner.

In a sense a single-channel analyser can be regarded as a kind of one-dimensional scanner. The total number of counts recorded when a spectrum is "scanned" with uniform speed is directly proportional to channel-width.

However, there are two other classes of collimators, whose behaviour can be illustrated by the above experiment.

Let us assume that there are as many detectors as we want at our disposal. If the paper is cut into n pieces, we will use n of these detectors and count all the pieces simultaneously. In this manner the total number of recorded counts is always equal to C (disregarding background effects), independent of the number of image elements. It is somewhat more difficult to find practical approximations to collimating systems that behave in this manner. A multi-channel pulse-height analyser may in a sense be regarded as such a system. If we increase the number of channels, the total number of recorded counts is still the same.

These two classes of collimators will be described as zero-loss order, if the total number of counts do not decrease as the resolution area is made smaller, and first-loss order if the total number of counts decreases linearly with the resolution area. We will also consider collimators of second-loss order, if the total number of counts decreases in proportion to the square of the resolution area. This is approximately the case for single-hole collimators.

Roughly zero-loss order collimators are what we are aiming at, first-loss order collimators are the ones currently in use, while second-loss order collimators practically belong to the past.

We will now estimate the information content of the images of some simple objects, scanned with these three classes of collimators.

4.2. Image of a hard contrast object

Let us regard an object of uniform activity surrounded by a region of no activity. Let us further assume that we know that the object covers half the area to be scanned, that our detector has no background effect, and that we

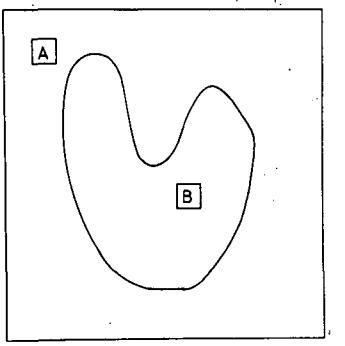

Fig. 3

A very simplified model of a scanning object. The resolution area A is in a region of no activity while B is in region of uniform activity.

employ a zero-loss order collimating system. In Fig. 3 the image element A is in a region of no activity, while B is in a region of uniform activity. The situation corresponds exactly to the example in section 3.5. We can think of the object as transmitting the signal 0 when the image element is in the region of no activity and as transmitting a 1 when the image element is in an activity region. Since the object covers half the area, the probability that 0 will be transmitted is 1/2 and that 1 will be transmitted is also 1/2. If no counts are received in an image element it will be coloured white, if one or more counts are registered it will be coloured black. The amount of information per element is given by the formula from section 355,

$$I(X;Y) = 1 - [(1+e^{-t}) \log (1+e^{-t}) - e^{-t} \log e^{-t}]/2 \text{ bits/element}$$

where t now should be taken to mean the average number of counts registered per image element (X stands for transmitting a 0 or a 1, Y stands for printing a white or a black mark).

Figure 4 is a plot of I(X;Y) as function of the average number of counts per element in the active region. It is seen that if this number is more than about 10 the information is practically 1 bit per image element. Since we get no more information for 1000 counts per element than for 10, it is a waste of information to make the element so large that 1000 counts are registered. It is better to have more elements and fewer counts per element. This is evident from curve A Fig. 5, which gives the total information in the image as function of the number of image elements, assuming that the total number counts (which is independent of the number of elements) is 1000. As we make the elements smaller and smaller but more and more of them the information approaches 500 bits. There is no limit to how small we can make the elements. If we employ a collimator of loss order 1 the situation is different. We now obtain a maximum of information of about 15 bits, and it is a disadvantage to use too large or too small image elements. With a second-loss order collimator, curve C shows that the information is still

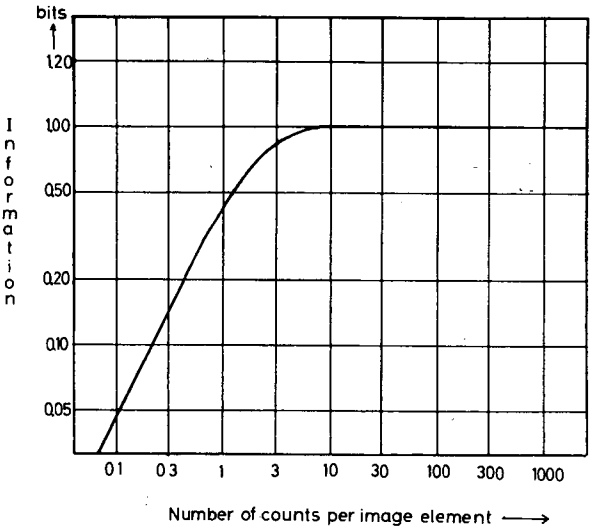

Fig. 4

Information content per image element of the object described in Fig. 3, as function of number of counts per element in the active region

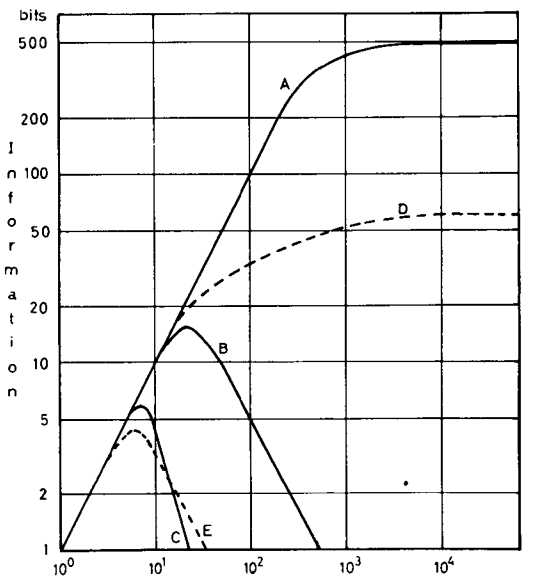

Fig. 5

Total information content of the object described in Fig. 3. Curves A, B and C refer to collimators of loss order 0, 1 and 2 respectively. D and E refer to the same object but in a background of uniform activity equal to half the activity over the object area for collimators of loss order 0 and 1 respectively.

less. Curves D and E show the effect if the region around the object has an activity equal to half the object activity. This illustrates the damaging effect of background.

4.3. Object with continous activity variation

Figures 6 and 7 refer to a more realistic object, in which it is assumed that the activity λ in each element can have any value from 0 up to a maximum N counts/element. It is furthermore assumed that all values of λ in the

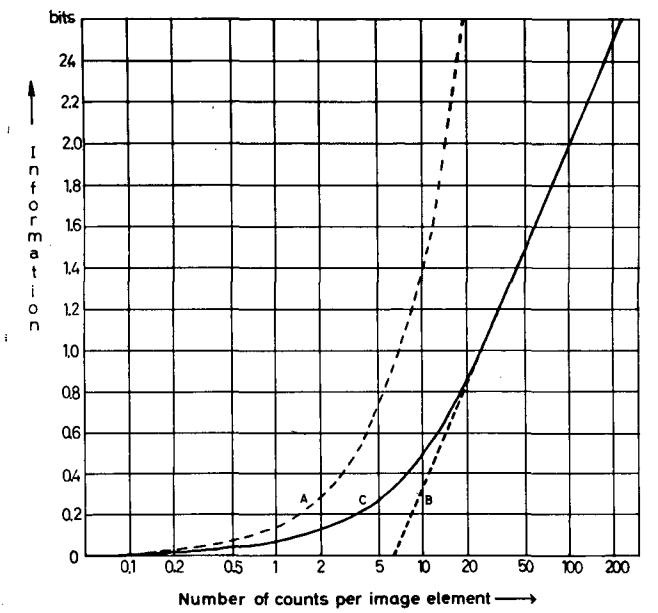

Fig. 6

Information content per image element, for an object, where each object element can, with equal probability, take on any average activity from zero up to a maximum N counts. Curve A is an extrapolation that is correct for small values of N, curve B applies for large values of N, and curve C is an estimate for intermediate values of N.

region 0 to N are equally probable. The computation of the information per element is somewhat more complicated, and cannot be presented here. Curve A, however, gives the result for small values of N, and B for large values of N, and C is an estimated curve in the intermediate region. Figure 7 shows total information in the image of such an object, assuming that the total number of counts for a zero-loss order collimator is 10^8.

4.4. The effect of background cut-off level

Figure 8 shows the information in an object of the hard contrast type described earlier, where the average background activity is 5 counts per element, and the average object activity is 10 counts per element. The back-

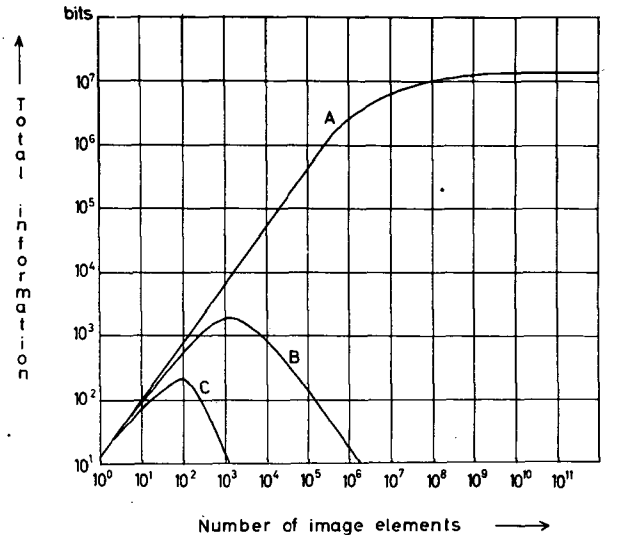

Fig. 7

Total information content of an image of the object described in Fig. 6. Curves A, B and C refer to collimators of loss order 0, 1 and 2 respectively.

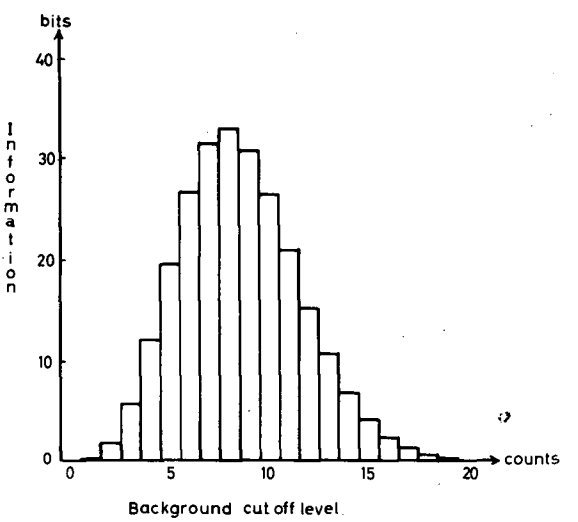

Fig. 8

Variation of information content as function of background cut-off level

ground cut-off level can be varied. For instance if it is set at 4, then a recorded count of less than 4 is registered as a white mark, while 4 or more is registered as a black mark. The diagram illustrates the importance of a correct setting of the background cut-off level.

5. CONCLUSION

Information theory can not solve all the problems in scanning theory. High information content does not necessarily guarantee an easily interpretable image. It may even be necessary to sacrifice some information in order to obtain a more easily interpretable image. Low information content on the other hand results in a poor image, and information once lost cannot be recovered by any artful tricks.

In this paper information theory has been applied to some simple problems. Much work is needed to obtain practically useful results. The author firmly believes that these efforts will prove of value, and eventually result in a clearer understanding of the theory of scanning.

REFERENCES

[1] SHANNON, C.E. and WEAVER, W., The Mathematical Theory of Communication, The University of Illinois Press, Urbana (1959).

[2] LINFOOT, E.H., Information Theory and Photographic Images, J. of Photographic Science 7 (1959) 148-156.

[3] REZA, F.M., An Introduction to Information Theory, McGraw-Hill Book Company, Inc., New York (1961).

[4] BRILLOUIN, L., Science and Information Theory, Academic Press Inc., New York, 2nd ed. (1962).

[5] BROWNELL, G.L., *Problems in Radioisotope Visualization*; Read at The Scanning Symposium, Oak Ridge, Tenn. 22-26 Oct. (1962).

[6] STERN, T.E., Some Quantum Effects in Information Channels, IRE Trans. on Information Theory IT-6 (1960) 435-440.

DISCUSSION

G. BROWNELL: In the treatment of background, was the object assumed to be hard (i.e. black or white) or was it assumed that it had a continuous distribution of density?

J. CEDERLUND: The object was assumed to have only two kinds of object elements.

THEORY OF SCANNING AND IMAGING OF RADIOISOTOPE DISTRIBUTIONS

B. CASSEN*
DEPARTMENT OF BIOPHYSICS AND NUCLEAR MEDICINE,
UNIVERSITY OF CALIFORNIA,
LOS ANGELES, CALIF., UNITED STATES OF AMERICA

Abstract — Résumé — Аннотация — Resumen

THEORY OF SCANNING AND IMAGING OF RADIOISOTOPE DISTRIBUTIONS. In a published paper, the author has presented a simplified basic theory of the quantitative performance characteristics of radioisotope imaging and scanning systems. A "figure of merit" is derived, depending partly on the instrument characteristics and partly on the methodology utilized. The factors involved in the figure of merit are: the count-rate sensitivity of the detector per unit solid angle subtended from a resolution element, the solid angle subtended from a resolution element, the number of resolution elements viewed simultaneously, the number of resolution elements in the total field scanned or imaged, the dose concentration, the total time taken to produce an image or scan and the background count-rate.

In the present presentation the basic theory is further refined and discussed to take into account factors such as "depth-of-focus" resolution, variable speed or variable dwell scanning, possibilities of variable or automatically variable resolution, relative resolvability of "cold" and "hot" nodules, field size and use of special radioisotopes and types of detectors.

Also, a discussion is presented on the handling and processing of data arising from scanning and imaging techniques. The relative merits of background eliminators and contrast enhancement procedures such as photoscanning and colour scanning are analysed. The advantages and possible disadvantages of tape recording original data and the repeated playback through contrast and background processing circuits is discussed.

Some experimentally determined figure-of-merit data are presented on a widely used commercial scanner and on some new developments, especially a new high quantum utilization scanner, which is briefly described in the above-mentioned article and has since undergone further development, improvement and testing.

THÉORIE DE LA SCINTIGRAPHIE A BALAYAGE OU FIXE. Dans une publication, l'auteur a exposé une théorie fondamentale simplifiée des caractéristiques quantitatives de rendement des divers systèmes de scintigraphie (à balayage ou fixes) au moyen des radioisotopes. Il en a déduit un «indice de qualité» qui varie selon les caractéristiques de l'appareillage et selon la méthodologie utilisée. Les facteurs intervenant dans l'indice de qualité sont notamment: l'angle solide unitaire sous-tendu par un élément de résolution, la sensibilité du détecteur pour cet angle solide unitaire, le nombre d'éléments de résolution «vus» simultanément, le nombre d'éléments de résolution dans l'ensemble du champ balayé ou autrement exploré, la concentration du radioisotope, le temps total nécessaire pour produire un scintigramme, ainsi que l'intensité du bruit de fond.

Dans la présentation actuelle, la théorie fondamentale a été encore perfectionnée et tient compte d'autres facteurs: résolution en fonction de la «profondeur focale», vitesse de balayage ou temps d'exposition, possibilités des résolution variable ou automatiquement variable, résolubilité relative des nodules «froids» et «chauds», dimension du champ, et utilisation de radioisotopes et de types de détecteurs spéciaux.

Ensuite, l'auteur fait un exposé sur le dépouillement et le traitement des données obtenues par les diverses techniques de scintigraphie. Il analyse les avantages relatifs des éliminateurs de bruits de fond et des méthodes d'accentuation du contraste, telles que la photoscintigraphie et la scintigraphie polychrome. Il examine les avantages qu'il y a, les inconvénients qu'il pourrait y avoir à enregistrer sur bandes des données originales et à faire repasser à volonté les bandes dans les circuits d'accentuation du contraste et d'élimination du bruit de fond.

---

* These studies were supported by Contract AT(04-1)GEN-12 between the Atomic Energy Commission and the University of California.

L'auteur donne des valeurs de l'indice de qualité déterminées expérimentalement pour un appareil d'exploration très courant vendu dans le commerce, et pour quelques appareils nouveaux, notamment un appareil très perfectionné, qui a été brièvement décrit dans l'article mentionné au début du résumé et qui a fait depuis lors l'objet de nouvelles mises au point et améliorations et d'essais.

ТЕОРИЯ СКЕННИРОВАНИЯ И ИЗОБРАЖЕНИЕ РАСПРЕДЕЛЕНИЯ РАДИОИЗОТОПОВ. Дается упрощенная основная теория количественного определения характеристик радиоизотопных систем изображения и скеннирования. Выводится "цифровой показатель", частично зависящий от характеристик прибора и частично от используемой методологии. Факторами, влияющими на цифровой показатель, являются: чувствительность детектора к скорости счета на единицу пространственного угла, противолежащего разрешающему элементу, пространственный угол, противолежащий разрешающему элементу, количество разрешающих элементов, наблюдаемых одновременно, количество элементов разложения во всем поле скеннирования или наблюдения, концентрация дозы, общее время, затраченное на получение изображения или скенограммы и скорость счета фона.

В настоящем представлении основная теория совершенствуется и обсуждается с тем, чтобы учитывать такие факторы, как "глубина фокуса" разложения, переменная скорость или переменное скеннирование,возможности переменного или автоматически изменяющегося разрешения, сравнительная разрешающая способность, "холодных" и "горячих" узлов, размер поля и использование специальных радиоизотопов и видов детекторов.

Дается также обсуждение вопросов обработки данных, получаемых методами скеннирования и проекции. Анализируется относительная особенность элиминаторов фона и процедур контрастного усиления таких как фотоскеннирование и цветное скеннирование. Обсуждаются преимущества и возможные недостатки записи на пленку оригинальных данных и повторное воспроизведение с помощью контрастных и фоновых обрабатывающих контуров.

Даются некоторые экспериментальные цифровые данные для широко используемого коммерческого скеннера, а также некоторые новые данные касающиеся нового скеннера, использующего кванты высокой энергии, который вкратце описывается в вышеупомянутой статье, и с того времени был усовершенствован и прошел испытания.

TEORÍA DE LA EXPLORACIÓN Y DE LA OBTENCIÓN DE IMÁGENES DE DISTRIBUCIONES RADIOISOTÓPICAS. En un artículo ya publicado el autor expuso una teoría fundamental simplificada de las características cuantitativas de funcionamiento de diversos sistemas de exploración y obtención de imágenes radioisotópicas. De ella ha deducido un «índice de calidad» que varía según las características del instrumento y según el método empleado. Los factores que intervienen en dicho índice de calidad son: la sensibilidad del detector para el ángulo sólido subtendido por un elemento de resolución, el número de elementos de resolución «vistos» simultáneamente, el número de elementos de resolución en el conjunto del campo que se explora o cuya imagen se obtiene, la concentración del radioisótopo, el tiempo total necesario para obtener una imagen y la intensidad de la actividad de fondo.

En la actual presentación, la teoría fundamental ha sido perfeccionada teniendo en cuenta otros factores: el poder de resolución en función de la «profundidad focal», la velocidad de la exploración o el tiempo de exposición, las posibilidades de un poder de resolución modificable o automáticamente variable, la resolubilidad relativa, los nódulos «fríos» y «calientes», la dimensión del campo y el empleo de radioisótopos y de tipos de detectores especiales.

A continuación, el autor expone la manera de tratar los datos obtenidos con las diferentes técnicas de centelleografía. Analiza las ventajas relativas de los eliminadores de la actividad de fondo y de los métodos de aumentar el contraste, tales como la fotoexploración, y la centelleografía policroma. Examina las ventajas y los inconvenientes de registrar en cinta los datos originales y de hacer pasar dicha cinta por circuitos electrónicos que aumenten el contraste o eliminen el fondo.

El autor da algunos valores del índice de calidad determinados experimentalmente par un aparato comercial de exploración y para algunos aparatos nuevos, especialmente para uno muy perfeccionado brevemente descrito en el artículo que se menciona al principio de este resumen y que, desde entonces, ha sido objeto de nuevos ensayos y perfeccionamientos.

We are all aware of the marginal information content of scans or other type images of radioisotope distributions in the current practice of clinical

nuclear medicine. Many types of clinically useful information, not easily obtained by radiographic or other methods, seem to be just within or just out of our reach. Many clinical investigators are pursuing possible advances with great enthusiasm, but a large part of their effort is directed towards the use of new agents. It would appear that any appreciable intrinsic advance in increasing the information-gathering ability of scanners or other imaging devices would in many cases enable the currently marginal applications to become of real practical utility.

With this in mind, we have made a basic theoretical analysis of the principal physical and methodological factors involved in imaging and scanning. In these studies little emphasis was given to the use of large administered doses of very short-lived radioisotopes. Of course, with suitable "cows" or suitable proximity to a reactor or accelerator some interesting applications might develop, but they would be currently out of reach of the vast majority of practitioners of nuclear medicine and clinical investigators. The practical difficulties of rapid chemical processing and the responsibilities for assuring sterile and pyrogen-free preparations would be appreciable.

The results of the basic theoretical study which will be amplified and refined in this communication appeared in the Journal of Nuclear Medicine, February 1964, under the title "Theory of the Performance Characteristics of Radioisotope Distribution Imaging Systems." To summarize briefly, it was shown for a given gamma-emitting radioisotope, a field of view of predetermined size and a relatively fixed type of information-seeking problem, that in the first approximation the relative quality of the image can be expressed by a statistical quality "figure of merit". As the term, "figure of merit", is now used with various meanings, we will refer to the quantity below as a system "performance index", to avoid confusion.

$$N^2/\sigma^2 = KWVDTn/F(1+2/R),$$

where the following symbols are used:

- D - dose density, $\mu c/cm^3$;
- V - effective resolution volume in cm^3;
- K - count-rate per unit volume per unit dose density per unit solid angle, counts/s/μc/sr;
- W - effective solid angle subtended by detectors to resolution volume, sr;
- F - number of resolution elements in field of view;
- n - number of resolution elements simultaneously detected;
- T - time taken to scan or build up image;
- N - total net counts per source resolution element during time of scan or build-up;
- B - total background counts during this time;
- σ - standard deviation of N;
- R - signal to background ratio, N/B;
- m - performance index of system and procedure performance index.

It should be emphasized that this performance index is for comparisons of systems with a predetermined field area, a predetermined resolution, and a predetermined radioisotope.

The factor KWVn/F of m is instrumental. The factor DT/(1+2/R) is methodological. The formula shows that better images can be obtained by increasing the dose, by increasing the time required for scanning or image build-up, and by decreasing the background. The background can also be frequently decreased by instrumental design. The principal instrumental factor can only be maximized for a fixed field of view and size of resolution element by maximizing the gamma quantum utilization factor KWn. A converging collimator increases W. An image build-up device such as an Anger camera maximizes n but leaves W relatively small and for most useful radioisotopes currently has a low value of K due to the use of a thin sodium iodide crystal. The "autofluoroscope" attempts to increase K by using thicker crystals in a mosaic. As far as the author is aware, to date such a system has a very limited number of resolution elements and field of view. Figure 1 shows diagrammatically the two ideal extremes of quantum utilization, maximizing n and maximizing W. A real break-through could be made if someone could devise a way of maximizing both n and W simultaneously. Increasing n by multichannel scanning has not been developed to the knowledge of the author. It would be very difficult to have a large W for multiple channel scanning. Figure 2 shows diagrammatically a high quantum utilization scanner with a large W, that is a 2200-hole spherical-cap collimator built at the UCLA. Laboratory of Nuclear Medicine and Radiation Biology and now undergoing clinical tests at the UCLA School of Medicine for stereotaxic brain-tumour localization. After discussing the theory of other possible auxiliary methods of improving scanning techniques, a description will be given of some of the performance characteristics of this new scanner compared with a commercially available scanner.

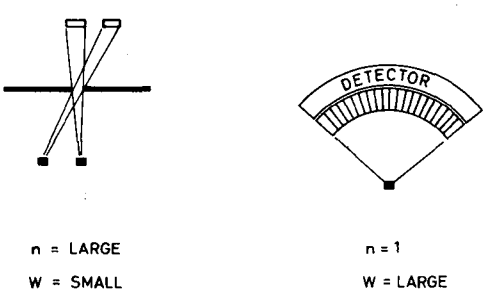

Fig. 1

Two possibilities of increasing figure of merit

Many users of scanners, especially when the size and shape of an organ, region of activity, or hole in a region of activity is the desired information to be acquired, have felt that it is a waste of time to scan over the usually considerably larger area external to the region of interest. Away back in the early days of the original scanner development at UCLA, CURTIS and CASSEN described a system [1], in a paper, entitled "Speeding Up and Improving Contrast of Thyroid Scintigrams." When a preset counting rate was not exceeded, the scanning motion was very rapid. As the preset rate

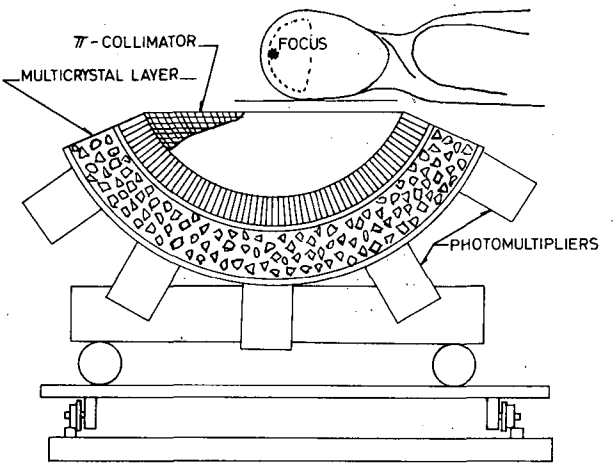

Fig. 2

Diagrammatic section of high quantum utilization scanner

was exceeded, the mechanical scanning speed was slowed down automatically. To the author's knowledge, this system has never been incorporated in commercial equipment. It would seem desirable to have at least manually controlled speed-up so that the operator can narrow down his detailed field of scan to meet his particular problem. The extension and refinement of variable speed scanning has some theoretical possibilities for special applications. Suggestions have been made by various individuals (most recently to the author by Dr. H. Katzenstein of Solid State Radiations Inc., Los Angeles) that there is considerable latitude for not unduly dwelling on a resolution element in scanning. In one form a system might be developed which dwells on a given resolution element in such a way that if a preset number of counts is not reached within a preset time interval, it will leave that resolution element and advance to the next element. Also, if the preset time is exceeded, it will dwell at that element until a preset number of counts is received before advancing. The recording system would then indicate zero for the first type of element and the inverse time for the fixed number of counts in the second type of element. In the latter type elements the counting statistics standard deviation σ will be uniform. In principle, the performance index could be considerably increased for certain types of scanning problems. Its practical utility is difficult to evaluate at the present time as its advantages depend on the essential distribution contrast in the radioisotope distribution being scanned. For search and location of a discrete source of activity this method or even more sophisticated versions of it might show up to maximum advantage in time saving or alternately in use of a smaller administered dose. A possible more sophisticated version would be to have a counting rate monitor automatically vary the resolution of the collimators so that in regions of sufficiently high activity more detail could be resolved. As far as the author is aware, no attempts have been made to explore such a possibility.

Commercial scanners, at least in the United States, have no new essential features over the original scanners except the use of the Oak Ridge-introduced converging collimator about 1954 and the single-channel spectrometer window which is useful for cutting down background in some scanning problems. They are much better engineered for smooth reliable operation and have various forms of data processing methods built into them. It should be emphasized that such features as ratemeter background eliminators, photoscanners, colour printers or recorders, local television contrast enhancement circuits, photographic contrast and other contrast enhancement procedures add no new information to that arriving from the detecting system. An experienced reader can see everything there is to be seen in a linear representation of the original data. These devices are useful in making certain features more easily observable to the extremely non-linear eye and brain. Actually, if they are not very carefully used, they reduce the information content of the original data. From this point of view, it would be most desirable to record the original data on magnetic tape (MacIntyre 1956) or magnetic plates so that it is not lost and then to play it back to various types of data processors. A typical photoscanner acts both as a background subtracter and contrast amplifier. On account of its frequently limited contrast range it often throws out information. If information is desired on the size or outline of a region of activity, such as size of a thyroid gland, this information can be, and often is, appreciably distorted by photoscanning.

THEORY OF DEPTH OF FOCUS OF A SPHERICAL-CAP CONVERGING COLLIMATOR

The exploratory 2200-hole large solid-angle spherical-cap collimator has an interesting feature which can be taken advantage of in certain types of scanning, such as brain-tumour scanning. The resolution depth is not much greater than the horizontal resolution width. This is in contrast with the well-known pattern obtained from small solid-angle Oak Ridge-type converging collimators. It is easy to see that in a theoretical limiting case of complete spherical symmetry the resolution pattern of a point source must be spherically symmetric.

The following theoretical analysis of the situation involves some explicit approximations which should be adequate in practical situations. In Fig. 3, O is the focus of a spherical-cap collimator of semiangle θ_0. A collimating channel EBFC is shown in section, the axis making an angle θ with the central axis. The half angle of a collimator is δ. x is the distance, which can be negative, of the source above the focus. β is the angle passed by the collimating channel from the source at X.

It can be shown by simple trigonometry that

$$\sin\omega = x\sin(\theta-\delta)/[x^2+(r+l)^2+2x(r+l)\cos(\theta-\delta)],$$

and if ω is small, $EA = l\omega$, $AB = 2r\delta - l\omega$, and the geometrical efficiency F of the collimating channel compared with the source at the focus is equal to $AB/EB = 1 - l\omega/2r\delta$.

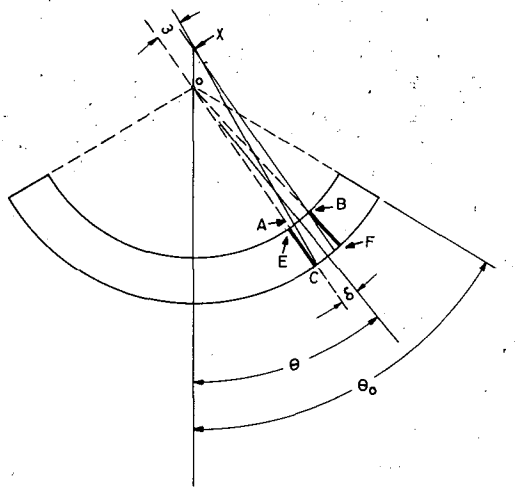

Fig. 3

Geometry of depth of focus
For analysis of depth of focus of spherical-cap collimator

When x is small compared with r

$$F = 1 - lx \sin(\theta - \delta)/2r\delta(r+l).$$

The cut-off angle θ_c for a fixed x is then given by

$$\sin(\theta_c - \delta) = 2r\delta(r+l)/lx,$$

or if θ_0 is the semiangle of the collimator, the value of x for which the peripheral collimators start cutting out is $x_c = 2r\delta(r+l)/l \sin\theta_0$. For a large angle collimator shown in Fig. 4, r = 0.3 cm, r = 17.7 cm, r + l = 22.8 cm, l = 5.1 cm, $\theta_0 = 0.866$. Therefore, $x_c = 3.1$ cm and there is no complete cut-off of any collimators for this vertical distance up or down from the focus. Within this range of x the combined efficiency of all collimators is given by

$$E = C\int_c^{\theta_0} [1 - lx \sin\theta/2r\delta(r+l)] \sin\theta d\theta,$$

where C is a normalizing constant to make E = 1 at x = 0.
Then integrating and normalizing

$$E = 1 - lx(\theta_0 - \sin\theta_0 \cos\theta_0)/4r\delta(r+l)(1 - \cos\theta_0).$$

For our spherical-cap collimator E will be equal to 0.5 at

$$x_{\frac{1}{2}} = 2r\delta(r+l)(1 - \cos\theta_0)/l(\theta_0 - \sin\theta_0 \cos\theta_0) = 2.19 \text{ cm}.$$

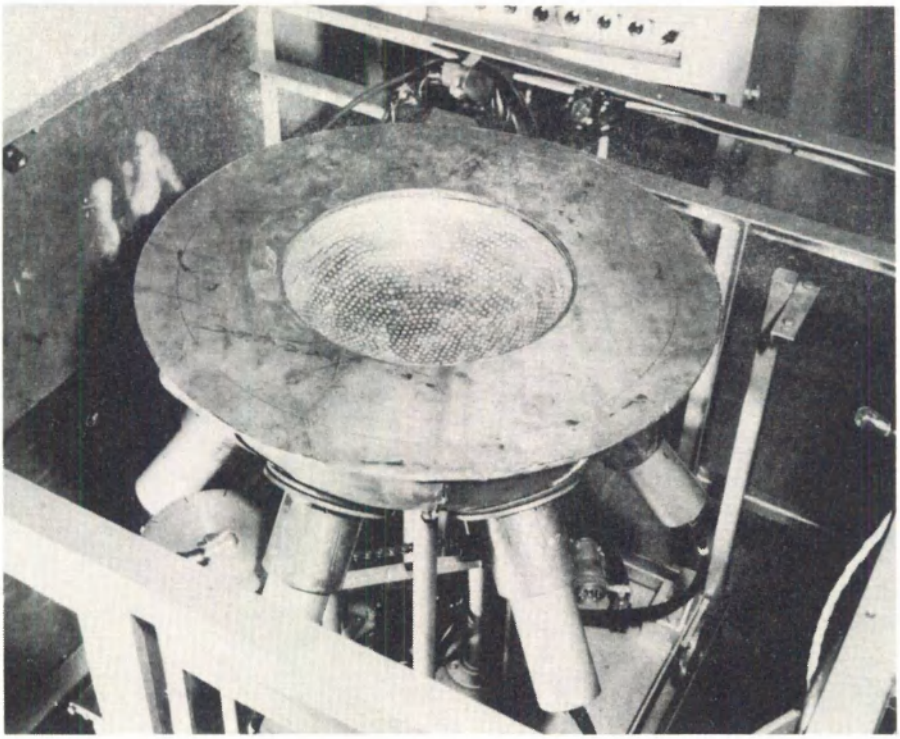

Fig. 4

Appearance of large-angle collimator

Therefore, the 50% response distance of the whole collimator is less than that at which any collimators are completely cut off.

In general, for θ_0 less than 60° and reasonable collimator design with the same r, l, δ, the fifty per cent vertical resolution distance will vary as $(1-\cos\theta_0)/(\theta_0-\sin\theta_0\cos\theta_0)$. This is plotted in Fig. 5, showing that the depth of focus rapidly decreases with the semiangle of the collimator.

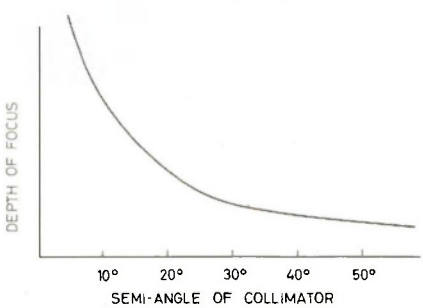

Fig. 5

Relative depth of focus of spherical-cap collimator

For the particular large angle collimator of Fig. 4, the experimental horizontal and vertical resolution with a point mercury-203 source is shown in Fig. 6. An estimate of $x_{1/2}$ from the experimental curve is less than 2.5 cm, compared with the theoretical 2.2 cm.

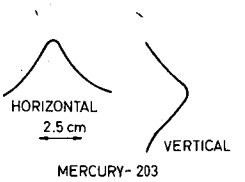

Fig. 6

Experimental resolution of spherical-cap collimator

Two approximately equal mercury-203 point sources of about one microcurie were prepared as indicated in the article in the Journal of Nuclear Medicine. The horizontal distance apart at which a counting rate minimum between them could just be recognized was considered to be the diameter of a resolution volume. For the converging collimator used on a commercial "Magnascanner" this distance was about 1.6 cm, making the arbitrarily defined resolution volume 2.15 cm^3. For the large solid-angle converging collimator the distance was about 2.9 cm, corresponding to a resolution volume of 26.5 cm^3. This collimator was not designed to have the resolution of the commercial scanner. The counting rate per microcurie on the commercial scanner was about 35 counts/s and that on the large angle collimator was 115 counts/s. This latter could be very much increased by opening the spectrometric window but with the inadequate shielding used at the time these measurements were made, the background increased faster than the signal when the window was opened. Additional shielding is being added. Geometrically, the solid angle of the large-angle collimator excluding septa was about 40 times that of the commercial collimator.

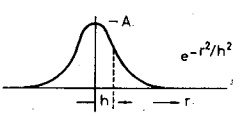

Fig. 7

Mathematically idealized resolution pattern

Finally, in what follows a brief theoretical discussion that was presented to the Society of Nuclear Medicine in 1957 but has not been published, is given to analyse the factors determining resolvability of a hole in a sea of activity compared with the resolvability of a region of activity surrounded by an absence of activity. If, as in Fig. 7, the horizontal resolution pattern of a point source for a given collimation system is idealized as $A \exp(-r^2/h^2)$, then in the centre of A hole of activity of radius a surrounded by uniform activity A per cm^2 the contribution of the continuous distribution will be

$$T = A \int_0^{2\pi} \int_a^{\infty} \exp(-r^2/h^2) r\, dr\, d\theta$$

$$= \pi A h^2 \exp(-a^2/h^2).$$

When a = 0 the response will be $\pi A h^2$. The response of activity in the centre of a uniform disc of radius A will then be $\pi A h^2(1 - \exp -a^2/h^2)$ and the response for large r is zero. For the case of the hole the contrast ratio from the centre of the hole to far away from the hole will be $\exp(-a^2/h^2)$. This approaches zero as a gets large with respect to h. If A is of the order of h, then the hole effectively fills up from the collimation tails of all the surrounding activity. It appears practically impossible to get sharp enough collimation and lack of a penumbra zone to avoid this filling-up effect even in a thin plan distribution, let alone a spherical hole in a sea of activity. Much sharper effective collimation can be obtained with coincidence techniques with positron emitters than with absorption collimators, thus indicating that greater sensitivity for holes in a sea of activity can be obtained by the use of positron emitters if they are otherwise applicable.

REFERENCE

[1] CURTIS, N. and CASSEN, B., Nucleonics 10 (1952) 58.

DISCUSSION

W. PAUL: Have you any experience in scanning brains?

B. CASSEN: We have made phantom studies and are now initiating a clinical testing programme. So far, tests have been carried out on three patients, but we have not yet any extensive experience.

H. A. B. SIMONS: How does resolution alter with quantum energy and septal penetration?

B. CASSEN: We have made resolution tests with Hg^{203} and I^{131}. They differ only very slightly.

H. GLASS: I should like to ask you, Dr. Cassen, what is the nature of the multi-crystal detector and how do you present your information, which is a three-dimensional plot in spherical co-ordinates, on a two-dimensional case sheet?

B. CASSEN: The detector whose possibilities we are exploring consists of a spherical cap, large solid angle (pi steradians), 2200-hole collimator, backed up by a 2-in thick layer of irregular broken pieces of sodium iodide immersed in a chlorinated hydrocarbon liquid. There are about 50 lb of crystal. They are viewed by seven 2-in photomultiplier tubes. The radius from the focus to the front of the collimators is 7 in. The focus can scan at a depth of up to 4 in from the patient's skin. The collimator scans under the patient and is driven hydraulically.

As to your second question, I should like to point out that, because of the relatively shallow depth of focus of a large solid angle collimator and

the very high counting rates obtained, scanning in the brain is done in a series of planes. The patient's head is positioned in such a way as to establish a stereotaxic co-ordinate system whose co-ordinates can be read off directly on the scans.

II

MOVING DETECTORS AND COLLIMATORS

NOTE SUR LA SENSIBILITÉ ET LE POUVOIR DE RÉSOLUTION EN SCINTIGRAPHIE

J. COURTIAL ET A. GANDY
FONDATION CURIE, PARIS, FRANCE

Abstract — Résumé — Аннотация — Resumen

SENSITIVITY AND RESOLVING POWER IN SCINTISCANNING. This paper attempts to assess theoretically the effect of collimator parameters on the quality of the scintigram.

The first part is devoted to a definition of the perfect collimator and to restating its properties when it is used to localize a point source.

The second part deals with plane sources. The sensitivity of the collimator is expressed as a function of its geometrical constants, followed by a definition of its "fineness"; this is related to its response curve in the case of a point source or its "transit curve" when crossing the contour of a plane source. The authors next discuss the images obtained with the scintiscanning device when used for exploring a number of plane sources having simple geometries. Since these images cannot be interpreted with certainty because of the statistical nature of the information recorded, recourse is had to the concepts of "linear resolving power" and "surface resolving power". The relationships between these resolving powers and the parameters of the scintiscanner are then established. These relationships provide a guide to the selection of operating conditions and make it possible to interpret the image obtained.

The third part considers the case of three-dimensional sources. It is first shown that the sensitivity of the perfect collimator can be expressed by the same formula as is used for plane sources. It is then shown that the concept of "surface resolving power" requires to be supplemented by that of "depth resolving power". The latter is derived from consideration of the image of an object of simple geometry and determines the dimensional limits below which the object is no longer perceptible. The curves illustrating this concept provide a comparison of the merits of the various perfect collimators.

The fourth part shows how the theoretical results can be applied in practice when certain properties of real collimators are stated. Finally, a comparison is made of the resolving powers yielded by the various methods of recording.

NOTE SUR LA SENSIBILITÉ ET LE POUVOIR DE RÉSOLUTION EN SCINTIGRAPHIE. La présente note cherche à préciser de façon théorique l'influence des paramètres qui caractérisent le collimateur sur les qualités du document scintigraphique.

La première partie est consacrée à la définition du collimateur parfait et au rappel de ses propriétés quand il est utilisé pour localiser une source ponctuelle.

Dans la seconde partie on étudie les sources planes. On donne l'expression de la sensibilité du collimateur en fonction de ses constantes géométriques. On définit ensuite sa «finesse» qui est en relation avec sa courbe de réponse pour une source ponctuelle ou avec sa «courbe de passage» au franchissement du contour d'une source plane. On considère alors les images obtenues à l'aide du dispositif scintigraphique lorsqu'il explore un certain nombre de sources planes de forme géométrique simple. L'interprétation de ces images étant rendue incertaine par la nature statistique des informations enregistrées, on est conduit à introduire les notions de «pouvoir de résolution linéaire» et de «pouvoir de résolution en surface». On établit alors les relations qui existent entre ces pouvoirs de résolution et les divers paramètres du dispositif scintigraphique. Celles-ci permettent d'orienter le choix des conditions opératoires et d'interpréter l'image obtenue.

Dans la troisième partie on envisage le cas de sources à trois dimensions. On montre d'abord que la sensibilité du collimateur parfait peut être exprimée par la même formule que dans le cas des sources planes. On montre ensuite que la notion de «pouvoir de résolution en surface» doit être complétée par celle de «pouvoir de résolution en profondeur».

Cette dernière se déduit de l'étude de l'image d'un objet de forme géométrique simple et précise les dimensions limites au dessous desquelles cet objet n'est plus perceptible. Les courbes qui illustrent cette notion permettent de comparer les mérites des divers collimateurs parfaits.

Dans la quatrième partie, on montre comment les résultats théoriques peuvent être appliqués aux cas réels en précisant certaines propriétés des collimateurs réels. On compare enfin les pouvoirs de résolution que permettent d'atteindre les diverses méthodes d'enregistrement.

К ВОПРОСУ О ЧУВСТВИТЕЛЬНОСТИ И РАЗРЕШАЮЩЕЙ СПОСОБНОСТИ В СЦИНТИГРАФИИ. Уточняются в теоретическом плане влияние параметров, характеризующих коллиматор, на качество сцинтиграфического документа.

Первая часть работы посвящена определению совершенного коллиматора и его свойствам, когда он используется для локализации точечного источника.

Во второй части исследуются плоские источники. Приводится выражение чувствительности коллиматора в зависимости от его геометрических констант. Затем дается определение "тонкости" коллиматора, которая соответствует его характеристике для точечного источника или его "кривой прохождения" через контур плоского источника.

Далее рассматриваются изображения, полученные с помощью сцинтиграфического устройства с использованием некоторого количества плоских источников простой геометрической формы. В связи с тем, что интерпретация этих изображений делает неопределенной зарегистрированную информацию в результате статистического характера, возникает необходимость ввести понятия "горизонтальной разрешающей способности" и "разрешающей способности в поверхности". Затем устанавливаются соотношения, которые существуют между этими разрешающими способностями и различными параметрами сцинтиграфического устройства. Эти способности позволяют определять выбор оперативных условий и интерпретировать полученное изображение.

В третьей части рассматривается случай с трехразмерными источниками. Вначале говорится, что чувствительность совершенного коллиматора может быть выражена той же формулой, что и в случае с плоскими источниками. Затем указывается, что понятие "разрешающая способность на поверхности" должна быть дополнена понятием " разрешающая способность в глубину". Это последнее выводится на основе изучения изображения предмета простой геометрической формы и уточняет предельные размеры, ниже которых этот предмет перестает быть воспринимаемым. Кривые, которые иллюстрируют это понятие, позволяют сравнивать достоинства различных совершенных коллиматоров.

В четвертой части показывается, как теоретические результаты могут быть применены к реальным случаям, уточняя при этом определенные свойства действительных коллиматоров. Затем проводится сравнение разрешающих способностей, которые могут быть получены различными методами регистрации.

SENSIBILIDAD Y PODER DE RESOLUCIÓN EN CENTELLEOGRAFÍA. La memoria trata de precisar teóricamente la influencia de los parámetros característicos del colimador sobre la calidad del centelleograma.

La primera parte se dedica a definir el colimador perfecto y a recordar sus propiedades cuando se utiliza para localizar una fuente puntiforme.

En la segunda parte se estudian las fuentes planas. Se expresa la sensibilidad del colimador en función de sus constantes geométricas. Seguidamente se define la «finura» del colimador, que está relacionada con su curva de respuesta para una fuente puntiforme o con su «curva de paso», al atravesar el contorno de una fuenta plana. Se estudian las imágenes obtenidas con un dispositivo centelleográfico al explorar cierto número de fuentes planas de forma geométrica sencilla. Como la interpretación de esas imágenes resulta insegura debido al carácter estadístico de las informaciones registradas, se introducen las nociones de «poder de resolución lineal» y de «poder de resolución en superficie». A continuación se establecen las relaciones existentes entre esos poderes de resolución y los diversos parámetros del dispositivo centelleográfico. Estas relaciones constituyen una guía para la selección de las condiciones de operación y para la interpretación de la imagen obtenida.

En la tercera parte se estudia el caso de las fuentes tridimensionales. Se muestra, en primer lugar, que la sensibilidad del colimador perfecto puede expresarse con la misma fórmula que se utiliza para las fuentes planas. Seguidamente, se demuestra que la noción de «poder de resolución en superficie» debe completarse con la de «poder de resolución en profundidad». Esta última se deduce del estudio de la imagen de un objeto de forma geométrica simple y establece las dimensiones límite por debajo de las cuales este objeto deja de ser perceptible. Las curvas que ilustran esta noción permiten comparar las ventajas de los diferentes colimadores perfectos.

En la cuarta parte se muestra cómo los resultados teóricos pueden aplicarse a los casos de la práctica al definir con precisión ciertas propiedades de los colimadores reales. Por último, se comparan los poderes de resolución que los diversos métodos de registro permiten alcanzar.

Le désir du praticien qui utilise la scintigraphie pour établir ou préciser son diagnostic est évidemment de pouvoir tirer le maximum d'informations d'un examen souvent très long et difficile, sinon impossible, à recommencer. Il souhaiterait donc pouvoir sélectionner a priori les valeurs des paramètres dont il dispose de façon à être certain d'obtenir la meilleure image possible dès le premier examen. Il souhaite également pouvoir exploiter avec sécurité le document qu'il a obtenu.

Pour reprendre une comparaison que nous avions faite il y a plusieurs années [1], ce praticien se trouve dans une situation analogue à celle du photographe qui a le souci de ne pas gâcher de pellicule et qui mesure la luminance de son sujet afin de déterminer des couples de valeurs du temps de pose T et de l'ouverture du diaphragme O compatibles avec une bonne reproduction. Il choisit entre ces valeurs selon l'effet artistique qu'il désire obtenir, en tenant compte des tables de profondeur de champ.

Malheureusement les lois qui régissent la scintigraphie sont beaucoup moins simples que celles de la photographie et, à notre connaissance, il n'existe pas encore de critères absolus qui permettent de déterminer avec un minimum d'ambiguïté la vitesse d'exploration et les constantes du collimateur. Chacun procède donc empiriquement. C'est là une tâche difficile et qui a peu de chances de conduire au résultat optimum car le nombre de paramètres indépendants est très élevé.

L'étude théorique qui pourrait résoudre ce problème se heurte à de très gros obstacles, en partie à cause des nombreux paramètres indépendants, mais surtout parce que la plupart des facteurs qui interviennent sont essentiellement qualitatifs ou subjectifs et s'introduisent difficilement dans une théorie mathématique.

L'objet de ce mémoire est précisément de montrer qu'en introduisant des facteurs objectifs pour caractériser l'image et en donnant une définition mathématique acceptable aux facteurs qualitatifs qui caractérisent le collimateur, on peut établir d'une façon semi-théorique des relations entre ces grandeurs et tirer d'intéressantes conclusions de l'étude de ces relations.

Il est évident que ces dernières feront intervenir également des grandeurs relatives à l'objet étudié et qu'elles seront d'autant plus simples, et, partant, plus facilement interprétables, que cet objet sera lui-même plus simple et défini par un plus petit nombre de paramètres.

Nous considérerons donc d'abord le cas d'un objet plan d'activité superficielle uniforme; nous verrons ensuite celui où l'objet à examiner correspond à une répartition uniforme de l'activité entre deux plans parallèles.

Ces deux cas extrêmes schématisent respectivement un organe mince (thyroïde) et un organe épais (foie).

Cependant, avant d'aborder l'étude de l'image scintigraphique, il est bon de préciser certaines définitions relatives aux collimateurs supposés parfaits, définitions dont nous ferons usage par la suite.

1. LE COLLIMATEUR PARFAIT

Nous appellerons collimateur parfait un collimateur formé d'une pupille d'entrée et d'une pupille de sortie percées dans deux écrans qui absorbent intégralement le rayonnement. Pour nous limiter aux collimateurs pratiquement utilisés, nous admettrons (mais ces conditions ne sont pas essentielles) que les deux écrans sont des plans parallèles séparés par une distance d et que les contours des deux pupilles sont des courbes convexes régulières (cercles ou polygones réguliers) qui se déduisent l'une de l'autre par projection cylindrique ou conique. Il est alors possible de parler de l'axe du collimateur: c'est l'axe du cône ou du cylindre; il peut être incliné. La figure 1 représente schématiquement deux collimateurs parfaits et précise les différents paramètres géométriques caractéristiques.

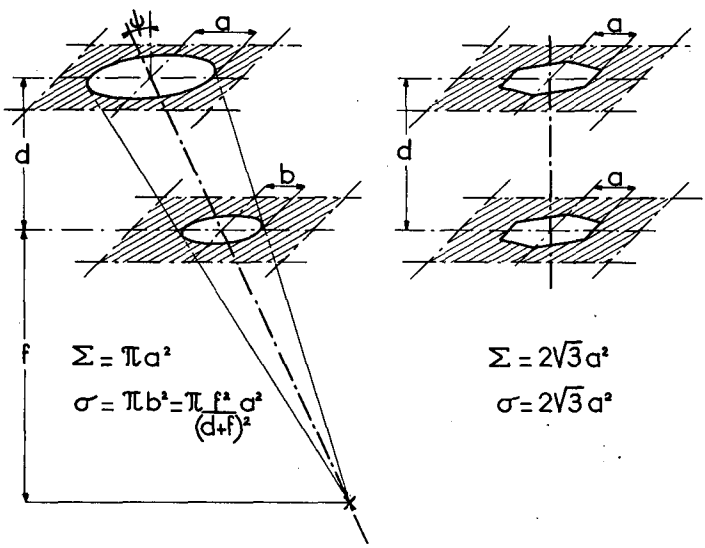

Figure 1

Collimateurs parfaits. La surface de la pupille d'entrée σ et celle de la pupille de sortie Σ s'expriment par des relations $\sigma = k\, b^2$ et $\Sigma = k\, a^2$.

Le collimateur est accouplé à un détecteur dont l'efficacité ϵ est égale au rapport entre le nombre n_s de signaux qu'il fournit et le nombre n_p de photons qui l'ont atteint:

$$\epsilon = n_s / n_p.$$

L'efficacité dépend en général de l'énergie $h\nu$ des photons.

1.1. Courbe de réponse

Pour tracer une «courbe de réponse» d'un collimateur, on déplace une source ponctuelle sur une droite parallèle aux plans des deux pupilles qui coupe l'axe du collimateur en un point P.

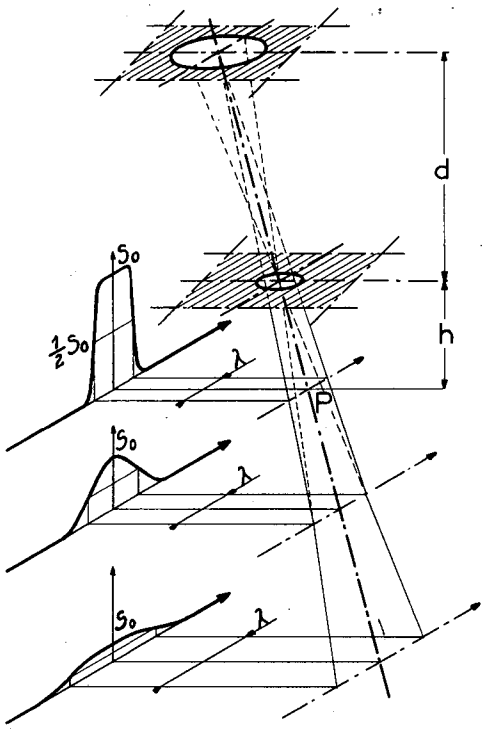

Figure 2

Diverses courbes de réponse d'un collimateur parfait.

On porte en ordonnées le rapport entre le nombre de photons transmis et le nombre de photons émis, en abscisses l'abscisse de la source, l'origine étant le point P (fig. 2).

Les courbes de réponse dépendent de la distance h qui sépare la source du plan de la pupille d'entrée. En se limitant aux cas où l'angle ψ que fait l'axe du collimateur avec la normale aux deux écrans est petit, et où la distance d entre ces deux écrans est grande par rapport aux dimensions linéaires des pupilles, ces courbes sont symétriques par rapport à l'origine et ont généralement un sommet plat (fig. 2). On peut alors les définir par leur largeur à mi-hauteur λ et par l'ordonnée S_0 de leur maximum, qui mesure la sensibilité géométrique du collimateur. Cette dernière dépend de h.

Il serait intéressant de pouvoir exprimer λ en fonction des paramètres du collimateur par une expression simple. Malheureusement les calculs conduisent généralement à des expressions compliquées et inutilisables. Cependant, lorsque les pupilles sont carrées et lorsque la source ponctuelle se déplace parallèlement aux côtés des carrés, les calculs sont faciles et les résultats simples. On trouve:

$$\lambda = 2b\,(h + d)/d = 2a\,f\,(h + d)/(f + d)\,d \qquad (1)$$

lorsque $h \leq f$, et

$$\lambda = 2a\, h/d = 2b\, (f + d)\, h/f\, d \qquad (1')$$

lorsque $h \geq f$, les côtés des pupilles étant respectivement égaux à 2a et 2b.

Les figures 3a et 3b indiquent, en tirets, les lieux des points pour lesquels la réponse est égale à 50% du maximum.

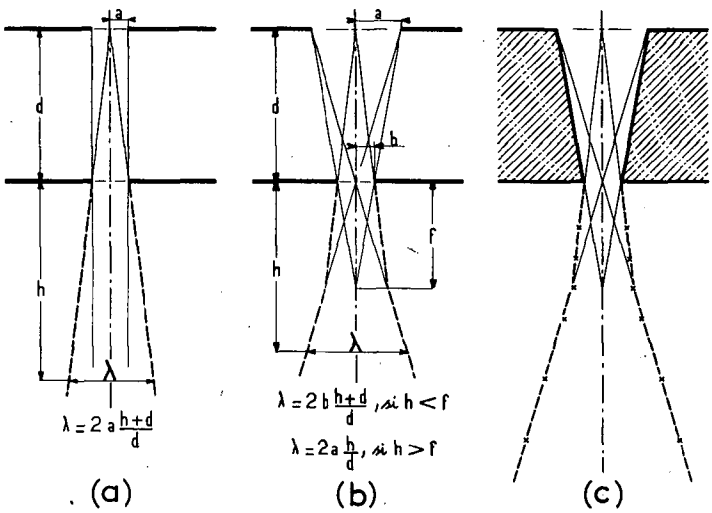

Figure 3

En a et b, construction géométrique des points pour lesquels la réponse est égale à 0,5 S_0, lorsque les pupilles sont des carrés de côtés 2a et 2b. En c, l'expérience montre que la même construction reste valable pour un collimateur réel à pupilles circulaires de rayons a et b.

On constate que, pour $h \leq f$, la courbe relative à un collimateur conique est identique à celle du collimateur cylindrique ayant même pupille de sortie.

Ce qui est remarquable c'est que l'expérience montre que les expressions (1) et (1') représentent encore λ avec une bonne précision pour un collimateur réel lorsque les pupilles sont circulaires, si a et b sont les rayons des pupilles. La figure 3c compare les résultats de mesures effectuées sur un collimateur conique de section circulaire, aux valeurs trouvées par les formules (1) et (1').

Nous adopterons donc ces formules dans la suite de cette note.

Notons que λ est indépendant du fait que le milieu qui entoure la source est absorbant ou non, à condition de ne considérer que les photons non diffusés.

1. 2. Collimateurs multicanaux

Pour en terminer avec les généralités sur le collimateur parfait, nous allons indiquer une expression donnant une valeur approchée de λ pour un collimateur multicanaux formé de m collimateurs coniques identiques ayant

même sommet et juxtaposés selon un réseau régulier ayant un axe de symétrie (des cloisons integralement absorbantes separent les divers canaux).

Un tel collimateur possède alors des propriétés focalisantes: sa sensibilité passe par un maximum pour un point de l'axe de symétrie voisin du sommet commun des cônes. En première approximation on peut admettre que le point de focalisation coïncide avec ce sommet.

Dans le «plan focal», c'est-à-dire le plan parallèle aux pupilles et passant par le sommet, la largeur à mi-hauteur λ_f de la courbe de réponse vaut

$$\lambda_f = 2b\,(f + d)/d = 2a\,f/d\,, \tag{2}$$

mais il est impossible de déterminer λ par le calcul, dans un plan situé à une distance h différente de f.

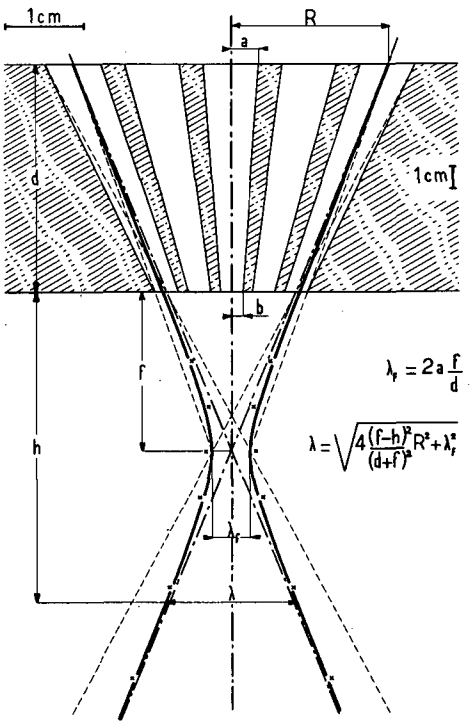

Figure 4

Détermination expérimentale du lieu des points pour lesquels la réponse est égale à 0,5 S_0 dans le cas d'un collimateur réel à 19 canaux.

Cependant la figure 4, qui représente les résultats de mesures effectuées sur un collimateur à 19 canaux à réseau hexagonal, montre que les points expérimentaux se placent assez bien sur une hyperbole ayant pour asymptotes les axes des canaux extrêmes. On obtient alors pour λ l'expression suivante:

$$\lambda = \left[\, 4\,(f - h)^2 R^2/(f + d)^2 + \lambda_f^2 \,\right]^{\frac{1}{2}}\,, \tag{3}$$

où R est le rayon du cercle sur lequel sont situés les centres des pupilles de sortie de la couronne extérieure.

Cette expression donne un ordre de grandeur suffisamment précis et sera utilisé par la suite.

2. SCINTIGRAPHIE DES SOURCES PLANES

2.1. Le collimateur

Connaissant l'ensemble des courbes de réponse pour toutes les directions possibles de déplacement de la source ponctuelle autour du point P, on peut, en principe, calculer le nombre de photons transmis par un collimateur situé au dessus d'une source plane donnée. La complexité analytique des courbes rend ce procédé impraticable, même en faisant des approximations simplificatrices. Il est donc préférable de caractériser le collimateur par de nouveaux paramètres; c'est ce que nous allons faire.

2.1.1. Sensibilité

Il est facile de montrer [2, 3] qu'un collimateur quelconque situé au dessus d'un plan infini, uniformément actif, parallèle aux plans des pupilles et dont l'activité superficielle est A (désintégrations/s par unité de surface)* transmet n_p photons par seconde; n_p étant donné par

$$n_p = A\Phi/4\pi.$$

Dans cette expression Φ, qui est «l'étendue» du faisceau de radiation délimité par les deux pupilles, ne dépend pas de la distance h qui sépare le plan actif de la pupille d'entrée et s'exprime par la relation:

$$\Phi = (\Sigma\sigma)/d^2 \cos^3 \psi \tag{4}$$

lorsque les surfaces Σ et σ sont petites devant d^2.

En pratique l'angle ψ est assez faible pour qu'on puisse faire $\cos^3\psi = 1$. Dans ces conditions nous pourrons exprimer la sensibilité du collimateur pour une source plane par la relation

$$S_2 = n_p/A = \Sigma\sigma/4\pi d^2. \tag{5}$$

Pour un collimateur multicanaux à m canaux la sensibilité est

$$S_2 = m\,\Sigma\sigma/4\pi d^2. \tag{6}$$

Cette dernière étant indépendante de h, le collimateur ne manifeste pas d'effet focalisant dans la direction de son axe.

---

* Nous admettrons, dans ce qui suit, qu'un seul photon détectable est émis par désintégration. S'il n'en est pas ainsi il s'introduit un terme correctif évident.

2.1.2. Finesse

Pour définir la finesse d'un collimateur, nous considérerons une source plane constituée de deux régions d'activités superficielles uniformes mais différentes A et A' séparées par une frontière rectiligne y y' (fig. 5).

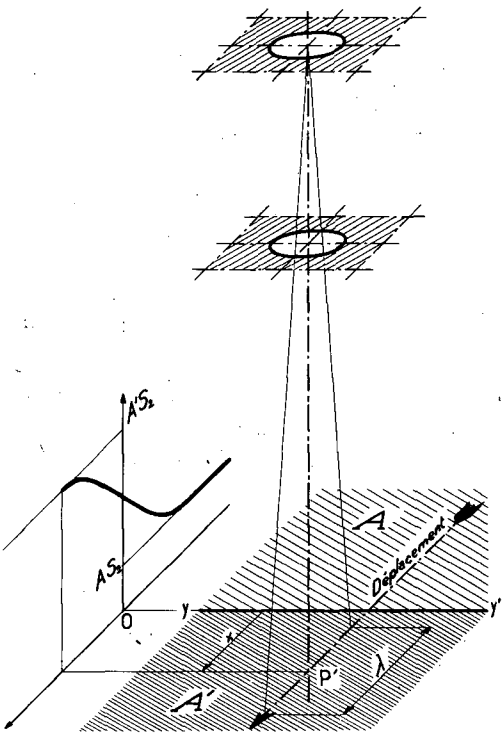

Figure 5

Tracé d'une «courbe de passage».

Nous tracerons une «courbe de passage» en déplaçant le collimateur parallèlement au plan de la source dans une direction perpendiculaire à y y'. Nous porterons en ordonnées le nombre de photons transmis par unité de temps, en abscisses la distance x du point P' (où l'axe du collimateur perce le plan de la source) à la frontière y y'.

Cette courbe a la forme indiquée sur la figure 5. Deux paliers d'ordonnées A S_2 et A'S_2 sont reliés par une partie monotone qui présente un point d'inflexion à l'origine. Sa forme analytique est très complexe et ne permet pas de définir par le calcul un paramètre utilisable pour caractériser le collimateur. Cependant, comme elle coïncide pratiquement avec sa tangente à l'origine sur la plus grande partie de sa variation (fig. 6), on peut l'assimiler à une fonction linéaire entre les abscisses $-\Lambda/2$ et $+\Lambda/2$, sans que cela risque d'entraîner une erreur prohibitive.

L'intervalle de variation Λ peut alors être utilisé comme mesure de la «finesse» du collimateur.

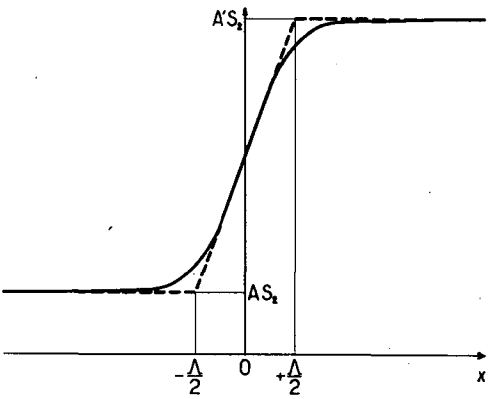

Figure 6

Approximation d'une « courbe de passage » par sa tangente à l'origine.

Seule l'expérience nous permet de déterminer Λ mais en comparant les valeurs trouvées à celles de λ, comme nous l'avons fait sur le tableau I, on constate qu'à 10% près ces deux longueurs coïncident.

Nous admettrons donc, dans la suite, que la «finesse» du collimateur est égale à λ et s'exprime à l'aide de l'une des expressions (1), (1') ou (3), selon le cas.

2.1.3. Relation entre la finesse et la sensibilité

Les diverses expressions que nous avons indiquées plus haut permettent d'établir, pour chaque catégorie de collimateurs, une relation entre la finesse et la sensibilité de la forme $S_2 = Q\,\lambda^4$. Ces relations sont rassemblées dans le tableau II.

Le facteur Q est fonction de la distance h et de divers paramètres indépendants de λ: d, f, etc... Lorsque ces paramètres auront mêmes valeurs pour divers collimateurs de même catégorie, nous dirons que ceux-ci sont de même type.

2.2. Image scintigraphique de la source plane

Les paramètres du collimateur que nous venons de définir vont nous permettre de déterminer certaines caractéristiques de l'image scintigraphique obtenue lorsque l'ensemble détecteur-collimateur se déplace avec la vitesse constante v à la distance h au-dessus d'une source plane.

2.2.1. Noircissement

Nous considérerons d'abord la source qui vient de nous servir pour définir la « courbe de passage», la direction de balayage étant perpendiculaire à la frontière y y' entre les deux plages.

Lorsque le collimateur est au-dessus de la région A, tant que son axe est à une distance de y y' supérieure à la distance $\lambda/2$ correspondant à la

TABLEAU I

VALEURS EXPÉRIMENTALES DE λ ET DE Λ POUR DIVERSES CIRCONSTANCES

Distance	Collimateur					
	Cylindrique		Conique		19 Canaux	
h	λ	Λ	λ	Λ	λ	Λ
3	1,22	1,11	1,57	1,47	1,04	1,01
5	1,42	1,35	1,71	1,71	0,61	0,60
7	1,62	1,52	2,10	2,10	0,67	0,67
9	1,80	1,66	2,62	2,58	0,84	0,80
13	2,14	2,02	3,86	3,82	1,64	1,60
17	2,50	2,38	5,08	4,82	2,52	2,46
h, λ et Λ sont exprimés en cm						

TABLEAU II

RELATIONS ENTRE LA FINESSE ET LA SENSIBILITÉ POUR TROIS CATÉGORIES DE COLLIMATEURS

Collimateur	Relations entre S_2 et λ	
	h quelconque	Valeurs particulières de h
Cylindrique	$S_2 = \frac{k^2}{64\pi} \frac{d^2}{(h+d)^4} \lambda^4$	$h = 0 \quad S_2 = \frac{k^2}{64\pi d^2} \lambda_0^4$
Conique	$S_2 = \frac{k^2}{64\pi} \frac{(f+d)^2 d^2}{f^2(h+d)^4} \lambda^4, \quad h \leq f$	$h = 0 \quad S_2 = \frac{k^2}{64\pi} \frac{(f+d)^2}{f^2 d^2} \lambda_0^4$
	$S_2 = \frac{k^2}{64\pi} \frac{f^2 d^2}{(f+d)^2 h^4} \lambda^4, \quad h \geq f$	$h = f \quad S_2 = \frac{k^2}{64\pi} \frac{d^2}{f^2(f+d)^2} \lambda_f^4$
Multicanaux	$S_2 = \frac{mk^2}{64\pi} \frac{\pi^2 f^2 (f+d)^2 d^2}{[(f-h)^2 d^2 k \nu + f^2 (f+d)^2 \pi]^2} \lambda^4$	$h = f \quad S_2 = \frac{mk^2}{64\pi} \frac{d^2}{f^2(f+d)^2} \lambda_f^4$
Dans ces formules: $k = \frac{\Sigma}{a^2} = \frac{\sigma}{b^2}$; $\nu = \frac{\pi R^2}{ka^2}$.		

hauteur h, le nombre d'impulsions fournies par le détecteur par unité de temps est en moyenne

$$K = \epsilon\, A S_2$$

et le dispositif d'enregistrement marquera

$$N = \epsilon\, A S_2 / v \tag{7}$$

traits par unité de longueur de l'image. Au-dessus de la plage A' et dans les mêmes conditions, on aura $K' = \epsilon\, A' S_2$ et

$$N' = \epsilon\, A' S_2 / v. \tag{7'}$$

Nous appellerons N ou N' le noircissement* probable de l'image de l'une ou l'autre plage [4].

Lorsque le collimateur franchira la frontière y y', le noircissement variera de N à N' suivant la même loi que la courbe de passage. Nous admettrons donc que cette variation est linéaire sur un intervalle de longueur λ.

Cependant, si l'on examine une longueur L de l'image de la plage d'activité A, par exemple, et si l'on compte le nombre $\mathscr{K}$ d'impulsions enregistrées, on peut déterminer un noircissement moyen observé

$$\mathscr{N} = \mathscr{K} / L$$

qui est généralement différent de N: c'est que les impulsions sont réparties au hasard selon une loi de Poisson dont on observe les fluctuations statistiques. L'image d'une source uniforme n'a donc pas une teinte homogène mais présente des modulations d'autant plus marquées que le noircissement probable N est plus faible.

2.2.2. Contraste

Nous appellerons contraste probable entre les deux plages de l'image l'expression $C = |N' - N| / N$, qui est nulle lorsque $N' = N$ et positive dans les autres cas.

Comme pour le noircissement, nous aurons un contraste moyen observé entre deux éléments de longueur L pris sur la même ligne ou sur deux lignes différentes qui s'exprimera par

$$\mathscr{C} = |\mathscr{N}' - \mathscr{N}| / \mathscr{N}.$$

L'existence des fluctuations statistiques se traduit par l'apparition de contrastes moyens $\mathscr{C}$ différents de zéro sur l'image d'une source uniforme pour laquelle le contraste probable C est nul.

Or l'examen visuel du document scintigraphique consiste précisément à comparer les contrastes moyens entre les différentes régions de l'image,

* Il ne faut pas confondre le noircissement probable ainsi défini avec le noircissement de l'image obtenue par photo-scintigraphie, bien qu'il existe une parenté entre ces deux grandeurs.

afin d'en tirer des informations concernant la répartition de l'activité de la source.

Nous rencontrons là une des difficultés essentielles de la méthode qui a été reconnue dès l'origine: les contrastes observés ne traduisent pas nécessairement des variations d'activité superficielle. L'interprétation de l'image repose généralement sur des bases empiriques et exige une grande expérience.

Une autre difficulté de la scintigraphie provient du fait que le procédé classique d'enregistrement donne des images où les contrastes probables doivent être importants pour être sensibles à l'examen visuel. Des améliorations considérables ont été apportées par des perfectionnements tels que l'amplification de contrastes, la photo-scintigraphie [5], la scintigraphie en couleurs [6, 7], etc... mais ces techniques ont l'inconvénient d'amplifier également les contrastes statistiques et, si elles permettent de «voir» des accidents que l'on ne verrait pas autrement, elles ne permettent pas de sélectionner à coup sûr les contrastes significatifs de ceux qui ne le sont pas.

2.3. Pouvoir de résolution

2.3.1. Pouvoir de résolution linéaire

Nous considérerons d'abord une source plane dont l'activité superficielle a la valeur uniforme A sauf sur une bande rectiligne de largeur L où elle vaut A'.

Le long d'une ligne de balayage perpendiculaire à la bande, le noircissement probable varie comme l'indiquent les différents schémas de la figure 7.

La courbe qui représente ses variations subit un accident sur un intervalle de longueur $L + \lambda$. Sur cet intervalle, le nombre probable d'impulsions enregistrées est donné par l'expression

$$K = (\epsilon S_2/v)(A\lambda + A'L). \tag{8}$$

Afin de simplifier l'exposé, nous supposerons $A > A'$ mais les résultats que nous obtiendrons seront indépendants de cette condition.

En fait le nombre $\mathscr{K}$ d'impulsions enregistrées diffère de K et a même une probabilité non nulle d'être supérieur au nombre $\mathscr{K}_0$ d'impulsions enregistrées sur un intervalle de même longueur pris sur l'image de la région d'activité uniforme A. Nous ne pouvons donc pas affirmer avec certitude que la dépression d'activité se manifestera sur l'image par un noircissement moyen plus faible que sur un élément de ligne pris au dessus de la région uniforme. Cependant, si la probabilité que $\mathscr{K}_0$ soit inférieur ou égal à $\mathscr{K}$ est extrêmement faible et vaut ϖ, nous dirons que nous avons la quasi certitude à ϖ près d'obtenir une image qui reflète l'inhomogénéité de la source. Nous admettrons que $\varpi = 0,025$ fournit une marge de confiance raisonnable.

La théorie des probabilités permet de montrer, par un calcul assez compliqué que nous ne reproduirons pas ici, que la quasi certitude à 25 millièmes près est pratiquement obtenue, dans le cas de la scintigraphie,

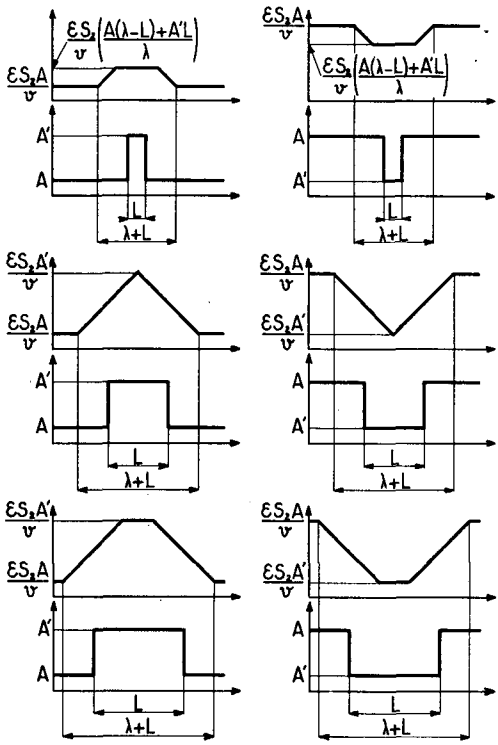

Figure 7

Variations du noircissement probable lorsque le collimateur de finesse λ franchit diverses bandes de largeurs L différentes, dont l'activité superficielle est A', et qui sont situées au sein d'un plan d'activité uniforme A.

lorsque l'inégalité suivante entre les nombres probables d'impulsions K et K_0 est vérifiée:

$$K_0 - K \geq 2,7\sqrt{K_0}\,, \tag{9}$$

inégalité qui se traduit d'une façon très générale par

$$|A - A'|\frac{\epsilon S_2}{v} L - 2,7\left[\frac{\epsilon S_2 A}{v}(L+\lambda)\right]^{\frac{1}{2}} \geqq 0 \tag{10}$$

en remplaçant K et K_0 par leurs expressions, et qui est vérifiée si L est supérieur à la valeur L_0 qui annule le premier membre

$$L_0 = \frac{1 + [1 + (\epsilon\, S_2/1,82\,v)\,(A' - A)^2\lambda/A]^{\frac{1}{2}}}{(\epsilon\, S_2/3,65\,v^2)\,(A' - A)^2/A} \tag{11}$$

Ceci signifie que la bande d'activité A' doit avoir une largeur au moins égale à L_0 pour que l'on ait la quasi certitude à 0,025 près de l'observer

sur une ligne de l'image. Inversement, si nous observons sur une ligne une longueur $L + \lambda$ sur laquelle le noircissement moyen est plus faible que celui observé sur tout autre élément de ligne de même longueur, nous ne pourrons affirmer (avec la probabilité de 0,975 de ne pas nous tromper) que cette variation de teinte est significative que si L est supérieur à la valeur L_0 donnée par l'équation (11). Cette valeur L_0 peut donc servir de définition au «pouvoir de résolution linéaire» de l'ensemble de scintigraphie.

Nous voyons que ce pouvoir de résolution ne dépend pas seulement du collimateur mais également de la vitesse de balayage v et de l'activité de la source. C'est pour cette raison que nous avons préféré employer le mot finesse pour qualifier le collimateur, contrairement à l'usage qui est d'appeler λ son pouvoir de résolution. Cet usage nous semble d'ailleurs particulièrement incorrect pour la raison suivante: si nous comparons des collimateurs de même type dans des conditions identiques, nous pouvons exprimer L_0 en fonction de λ seulement en remplaçant S_2 par la relation $S_2 = Q\,\lambda^4$ dans la formule (11). On obtient:

$$L_0 = \frac{1 + [1 + Q\epsilon\,(A' - A)^2\,\lambda^5/1,82\,v\,A]^{\frac{1}{2}}}{\epsilon Q\,(A' - A)^2\,\lambda^4/3,65\,v\,A}, \qquad (12)$$

relation qui montre (fig. 8) que L_0 croît lorsque λ décroît.

L'interprétation de ce résultat apparemment paradoxal est cependant extrêmement simple, comme le montre la figure 9 qui représente les courbes de variation du noircissement probable obtenues avec quatre collimateurs de finesses λ différentes, au-dessus de la même bande de largeur L: lorsque λ augmente, l'image de la bande d'activité A' devient plus floue mais la sensibilité croissant comme λ^4, le nombre d'impulsions enregistrées augmente très rapidement; ce qui améliore considérablement la statistique et rend de plus en plus improbable l'existence d'une variation accidentelle du noircissement ayant la même importance que celle que l'on observe.

Nous noterons sur cet exemple que le contraste probable diminue lorsque λ augmente; il passe de 1,25 à 0,91 lorsque λ passe de 0,6 à 1,2 L. Ce n'est donc pas nécessairement le contraste le plus élevé qui permet la meilleure interprétation de l'image, lorsqu'on considère le problème d'un point de vue non subjectif. Il n'en reste pas moins vrai que de deux bandes de même largeur, mais d'activités A' et A'' différentes, c'est celle qui donne le plus grand contraste probable qui a le plus de chances d'être détectée.

2.3.2. Pouvoir de résolution en surface

En fait, l'image scintigraphique ne se réduit pas à une seule ligne de balayage mais est formée d'un grand nombre de lignes juxtaposées. Ceci améliore l'aspect statistique du problème et rend significatifs des détails qu'il faudrait considérer comme des fluctuations si l'on n'examinait qu'une seule ligne à la fois.

Par contre, les accidents que l'on veut détecter ne sont pas des bandes infinies dans une direction mais des surfaces limitées, ce qui diminue le contraste probable si leurs dimensions sont comparables à la finesse du collimateur utilisé. Les grandes anomalies sont donc plus faciles à déceler

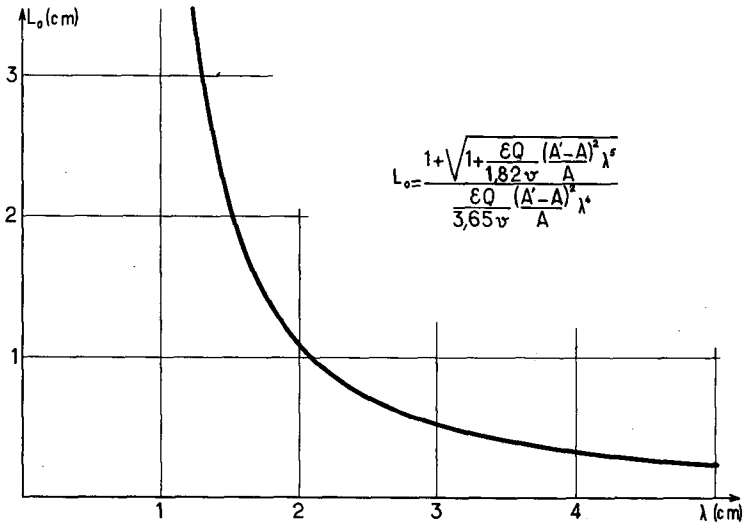

Figure 8

Variation du pouvoir de résolution linéaire en fonction de la finesse, pour une série de collimateurs cylindriques du même type utilisés dans les mêmes conditions. Valeurs numériques utilisées pour tracer cette courbe:

$S_2 = Q\,\lambda^4$, avec $Q = 2,4 \cdot 10^{-4}\,cm^{-2}$,

$A = 3,7 \cdot 10^4$ d.p.s./cm², $A' = A/2$,

$\epsilon = 0,36$, $v = 0,64$ cm/s.

que ne le laisse prévoir la théorie précédente mais les irrégularités d'activité de faible étendue ont plus de chances de passer inaperçues, ainsi que nous allons le montrer.

Considérons un objet constitué d'un plan d'activité superficielle uniforme A sauf sur un carré de côté c où l'activité vaut A'. Pour simplifier nous supposerons que ce carré est orienté de façon que deux de ses côtés soient parallèles à la direction du balayage. Dans ces conditions il donnera une image inscrite dans un carré de côté $\lambda + c$ formée de $(\lambda + c)/i$ lignes, i étant la largeur de l'interligne du balayage.

On pourra compter le nombre total $\mathcal{N}'$ d'impulsions sur cette image et le nombre $\mathcal{N}_0'$ d'impulsions qui se produisent sur un carré de mêmes dimensions pris sur l'image de la région uniformément active.

Moyennant certaines simplifications, on peut calculer la valeur probable K' de $\mathcal{N}'$. Cette valeur est donnée par l'expression

$$K' = (\epsilon S_2/3 v i)(A' - A)(3c^2 + \lambda^2) + K_0' \qquad (13)$$

lorsque $c > \lambda$, ou par

$$K' = (\epsilon S_2/3 v i)(A' - A)(c^2/\lambda^2)(c^2 + 3\lambda^2) + K_0' \qquad (13')$$

lorsque $c < \lambda$.

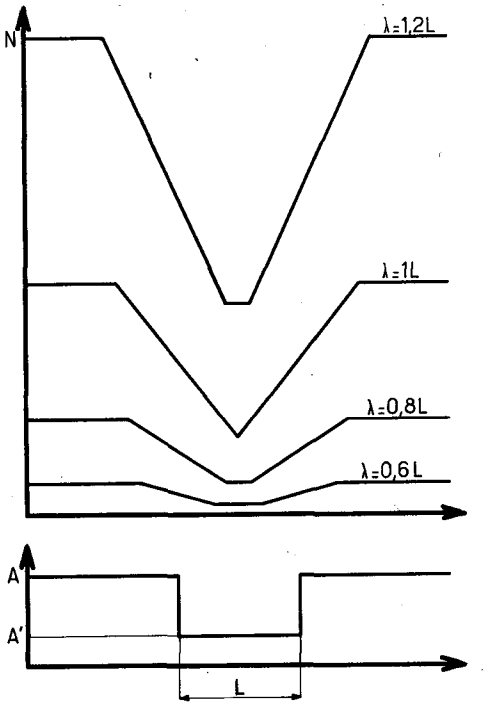

Figure 9

Noircissements probables obtenus avec quatre collimateurs de même type, mais de finesses λ différentes, au-dessus de la même dépression d'activité.

En répétant les raisonnements que nous avons faits plus haut au sujet du pouvoir de résolution linéaire, on arrive à la conclusion suivante: pour que le carré d'activité A' soit décelable sur l'image avec une quasi certitude à 0,025 près, il faut que c soit supérieur à r_0, la limite r_0 étant donnée par la formule

$$r_0 = [1 + (1 + 12\beta\lambda - 12\beta^2\lambda^2)^{\frac{1}{2}}] \,/\, 6\beta\,, \tag{14}$$

lorsque $\beta\lambda < \frac{1}{2}$, ou la formule approchée

$$r_0 = [1 + (1 + 16\beta\lambda)^{\frac{1}{2}}]/8\beta, \tag{14'}$$

lorsque $\beta\lambda > \frac{1}{2}$; expressions où

$$\beta = \frac{1}{8,1}\,(\epsilon\, S_2/v\, i)^{\frac{1}{2}}\, |A' - A| \,/\sqrt{A}\quad . \tag{15}$$

Il est tentant de généraliser ce résultat et de dire qu'une surface s d'activité superficielle A', au sein d'un plan d'activité uniforme A, donnera une image significative si $s \geq r_0^2$. Nous ne voudrions pas affirmer que cette généralisation est légitime dans tous les cas mais elle nous semble raison-

nable quand la plus petite dimension linéaire de s est de l'ordre de grandeur de λ, et au moins supérieure à l'interligne i.

Nous adopterons donc r_0 pour caractériser le « pouvoir de résolution en surface ».

2.3.3. Problèmes divers

Les différents problèmes qui se posent en scintigraphie peuvent être classés en deux catégories: ceux qui sont relatifs à la recherche des conditions opératoires optima et ceux qui ont trait à l'interprétation de l'image. Nous évoquerons un cas de chaque catégorie.

Soit, par exemple, la recherche, au sein d'un organe mince, d'une lésion caractérisée par une fixation anormale de l'indicateur radioactif qui se traduit par une activité superficielle $A' = q\,A$.

La question qui se pose peut être: pour quelles valeurs de q pourra-t-on détecter une lésion de surface s, A et les paramètres de l'appareil étant connus? Ou bien: quelle est la valeur minimum de A qui permettrait de déceler une lésion de surface s; q et les paramètres de l'appareil étant connus?

La réponse est fournie par les relations (14) ou (14'). Il suffit d'y remplacer A' par q A pour obtenir une fonction r_0 ($\epsilon\, S_2A/vi$, λ, q) dont on peut représenter les variations par un réseau de courbes comme nous l'avons fait sur la figure 10. Les limites cherchées se déterminent alors graphiquement.

L'autre type de problème se présente de la façon suivante.

L'image obtenue offre une région de surface s' qui a un contraste moyen $\mathscr{C}$ par rapport à la plage qui l'entoure, plage dont le noircissement moyen est $\mathscr{N}_0$. Doit-on conclure à l'existence d'une lésion?

Moyennant quelques approximations les équations (14), (14') et (15) vont nous fournir une réponse.

L'équation (15) s'écrit en effet:

$$\beta = \frac{1}{8,1\sqrt{i}} \left(\frac{\epsilon\, S_2A}{v}\right)^{\frac{1}{2}} \left[\frac{|\epsilon\, S_2A'/v - \epsilon\, S_2A/v|}{\epsilon\, S_2A/v}\right] .$$

L'expression entre crochets est égale au contraste probable C entre les images de deux plages de grande étendue d'activités A et A'.

En première approximation nous pouvons remplacer cette expression par le contraste moyen observé $\mathscr{C}$. En remplaçant de la même façon par $\mathscr{N}_0$ le terme $\epsilon\, S_2A/v$, il vient:

$$\beta = \frac{1}{8,1} \left(\mathscr{N}_0/i\right)^{\frac{1}{2}} \mathscr{C} . \qquad (16)$$

Lorsqu'on connaît les conditions opératoires, on connaît λ. Il suffit alors de comparer $\sqrt{s'}$ à la valeur $r_0 + \lambda$ donnée par celle des expressions (14) ou (14') qui est compatible avec la valeur de $\lambda\beta$ pour connaître le cause la plus probable de l'image observée.

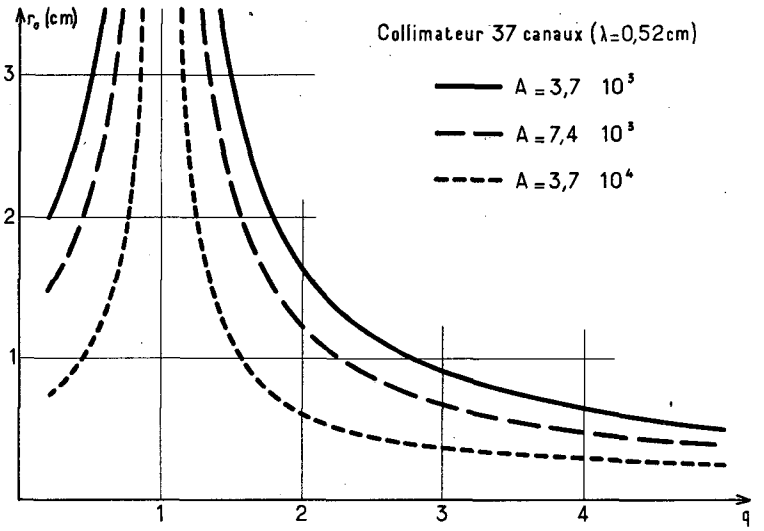

Figure 10

Variations de la fonction r_0 (ϵ AS_2/vi, λ, q).
On a tracé les variations de r_0 en fonction de q pour trois valeurs de ϵ AS_2/vi: 4,7, 9,4 et 47, correspondants aux trois valeurs de A indiquées sur la figure.

3. IMAGES DES SOURCES A TROIS DIMENSIONS

3. 1. Sensibilité du collimateur

La figure 11a représente un collimateur parfait quelconque placé au-dessus d'un milieu absorbant uniformément actif, d'activité volumique ρ (désintégrations/s par unité de volume), compris entre deux plans parallèles séparés par une distance E et infini dans deux directions.

Moyennant quelques hypothèses simplificatrices justifiées en pratique, le calcul de nombre de photons non diffusés qui traversent la pupille de sortie, donne [3] :

$$n_p = S_2 \rho (1 - \exp - \mu E)/\mu \qquad (17)$$

où μ est le coefficient d'absorption linéaire du milieu pour la radiation considérée. Ce nombre est indépendant de la distance h; c'est celui que donnerait un plan d'activité superficielle uniforme $A_e = \rho (1 - \exp - \mu E)/\mu$ situé à une distance h' quelconque.

La sensibilité du collimateur peut encore être exprimée par S_2.

3. 2. Caractéristiques de l'objet

La figure 11b représente le même collimateur situé au-dessus d'un milieu absorbant homogène compris entre deux plans parallèles mais cette fois l'activité n'est plus répartie uniformément dans tout le milieu: elle

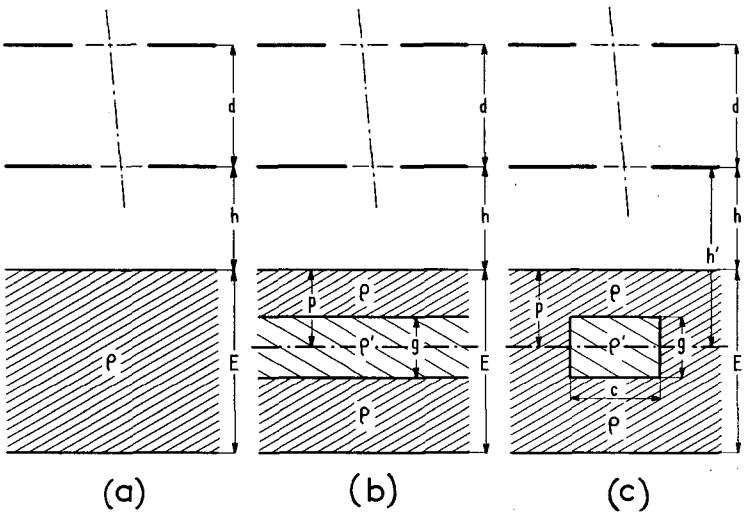

Figure 11

Objets à trois dimensions:

a) milieu infini suivant deux dimensions et uniformément actif,
b) répartition hétérogène de l'activité volumique dans une direction,
c) hétérogénéité localisée.

vaut ρ' dans une région comprise entre deux plans parallèles aux précédents et séparés par une distance g, elle vaut ρ dans le reste du milieu.

Le nombre de photons non diffusés qui traversent la pupille de sortie est alors donné par la relation

$$n'_p = S_2 \left[\rho \frac{1 - \exp{-\mu E}}{\mu} + (\rho' - \rho) \exp{-\mu(p - g/2)} \frac{1 - \exp{-\mu g}}{\mu} \right] \qquad (18)$$

où p est la profondeur du plan médian de la région d'activité ρ'.

Le volume actif est donc équivalent à un plan d'activité $A'_e = n'_p/S_2$ et dont la distance h' peut être quelconque.

Considérons enfin le même milieu absorbant homogène au sein duquel l'activité volumique a la valeur ρ sauf dans un cylindre de hauteur g et de section droite C^2 (fig. 11c).

Nous pouvons assimiler cet objet à un plan dont l'activité superficielle A_e est uniforme excepté sur une surface C^2 où elle vaut A'_e; mais nous ne pouvons plus choisir arbitrairement sa distance h' au collimateur. En effet la finesse du collimateur, nous l'avons vu plus haut, dépend de h'; l'aspect de l'image en dépend donc également.

L'expérience montre qu'en prenant h' = h + p l'image que l'on observe réellement coïncide d'une façon très satisfaisante avec celle que laisse prévoir la théorie.

3. 3. Pouvoir de résolution en profondeur

Lorsqu'on examine un objet plan situé à la distance h du collimateur, le pouvoir de résolution en surface est défini par une des relations (14) ou (14') et sa connaissance suffit pour interpréter l'image observée.

Ce n'est plus le cas lorsqu'on a affaire à un objet épais. En effet, si nous portons dans ces relations les valeurs A_e et A_e' du paragraphe 3. 2 et si nous y exprimons λ en fonction de h', nous constatons que r_0 est fonction de la profondeur p.

La relation $r_0 = f(p)$ traduira ce que nous appellerons le pouvoir de résolution en profondeur.

La fonction f (p) dépend également de l'épaisseur E du milieu actif, de celle g du «nodule» que l'on cherche à mettre en évidence, de la distance h entre le collimateur et la surface de l'objet, de l'énergie des photons émis (par l'intermédiaire de μ), des activités volumiques ρ et ρ' et, enfin, de la vitesse d'exploration v et de l'interligne i.

Etant donné le nombre impressionnant de variables indépendantes, la seule façon d'utiliser cette fonction consiste à tracer des réseaux de courbes sur chacune desquelles l'une de ces variables est considérée comme un paramètre dont la valeur change d'une courbe à l'autre.

C'est que nous avons fait sur la figure 12 où l'on suit les variations de r_0 en fonction de la profondeur p pour différentes valeurs de g.

Les courbes 12a se rapportent à un milieu de 10 cm d'épaisseur, celles de la figure 12b à un milieu de 5 cm.

La comparaison des familles de courbes tracées en traits pleins, et qui s'appliquent à un collimateur cylindrique, et des courbes en tirets, valables pour un collimateur multicanaux de même sensibilité, permet d'évaluer immédiatement les mérites relatifs des collimateurs.

4. CONSIDÉRATIONS PRATIQUES

Pour établir les résultats précédents, nous avons postulé l'existence de collimateurs parfaits, nous avons également admis implicitement que l'image était capable d'enregistrer et de restituer toutes les informations que lui fournissait le détecteur, nous avons enfin supposé que celui-ci pouvait distinguer les photons qui l'atteignaient directement de ceux qui avaient subi une diffusion.

Si cette dernière hypothèse ne soulève aucune difficulté, – un compteur à scintillation associé à un sélecteur d'amplitude réalise avec une très bonne approximation le détecteur idéal, – il n'en est pas de même pour les deux autres.

4. 1. Le collimateur réel

Le collimateur réel est un bloc d'un matériau dense percé d'un ou plusieurs trous: l'absorption du rayonnement n'est pas totale et la collimation du faisceau s'accompagne de diffusion. Pour tenir compte de ces phénomènes il va falloir modifier certaines des formules établies plus haut.

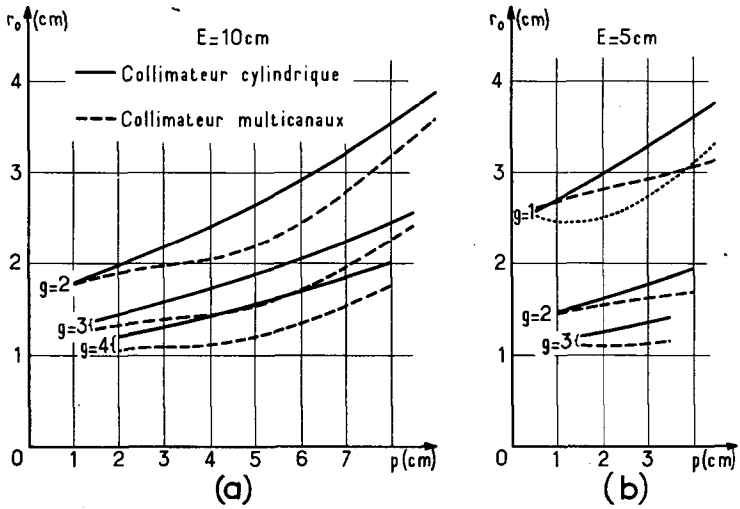

Figure 12

Pouvoir de résolution en profondeur.

Traits pleins: collimateur cylindrique (2a = 1,23 cm, d = 10 cm, $S_2 = 1,12 \cdot 10^{-3}$ cm², h = 2 cm)
Traits interrompus: collimateur 37 canaux (2a = 0,74 cm, d = 10 cm, f = 7 cm, $S_2 = 1,12 \cdot 10^{-3}$ cm², h = 2 cm)
Pointillés: le même collimateur mais h = 4,5 cm.
Pour l'ensemble: $\epsilon = 0,36$, v = 0,64 cm/s, i = 0,5 cm, $\mu = 0,1$ cm^{-1}, $\rho = 8 \cdot 10^3$ d.p.s./cm³, $\rho' = 0$.

4.1.1. Finesse

Les expressions (1) et (1') peuvent être considérées comme des lois expérimentales: c'est l'expérience qui nous a montré qu'elles étaient valables pour des collimateurs réels. Nous n'avons donc aucune modification à y apporter. Nous reviendrons plus loin sur la formule (3) relative aux collimateurs multicanaux.

4.1.2. Sensibilité

Pour un collimateur conique ou cylindrique, il a été montré [2] que la transparence du matériau dont il est constitué a pour effet de réduire l'épaisseur réelle d d'un «parcours moyen» $\delta = 1/\mu$, à chaque extrémité (μ' est le coefficient d'absorption linéaire du matériau). En fait l'expérience semble indiquer une valeur de δ légèrement différente de $1/\mu'$.

L'effet du rayonnement diffusé est plus difficile à interpréter théoriquement. Il semble toutefois qu'on puisse lui attribuer le fait que, lorsque la surface des pupilles augmente, la sensibilité varie un peu moins rapidement que ne l'indique la formule (5). Toutefois comme cette relation est vérifiée à 10% près pour une variation de S_2 de 1 à 600, il n'est pas nécessaire de tenir compte de cet effet.

En résumé, pour un collimateur réel simple, la formule (5) peut être remplacée par la suivante:

$$S_2 = (\sigma^2/4\pi)\ (f+d-\delta)^2\,(f+d)^2/f^4(d-2\,\delta)^2$$

où σ est la surface réelle de la pupille d'entrée et δ une longueur voisine de $1/\mu'$ que l'expérience permet de déterminer.

Pour un collimateur multicanaux, la transparence des cloisons qui séparent les divers canaux joue un rôle prépondérant et, au nombre de photons transmis au travers des pupilles, il y a lieu d'ajouter le nombre des photons transmis au travers des cloisons.

En nous inspirant d'un travail théorique publié à ce sujet [8], nous avons trouvé que l'expression

$$S_2 = \frac{m\sigma^2}{4\pi}\ \frac{(f+d-\delta)^2\,(f+d)^2}{f^4(d-2\,\delta)^2}\ (1+u\ \exp\text{-}wd),$$

dans laquelle u et w sont des paramètres déterminés expérimentalement, rendait très bien compte des variations de la sensibilité.

La transparence des canaux se traduit également par une détérioration de la finesse du collimateur, surtout dans le plan focal. On peut en tenir compte dans la formule (3) en attribuant à λ_f la valeur trouvée expérimentalement au lieu de celle que l'on tire de la formule 2.

4. 2. L'image

Les notions de pouvoir de résolution que nous avons adoptées reposent sur des considérations purement statistiques: nous avons fait implicitement l'hypothèse que l'image peut restituer intégralement les informations numériques qui lui ont été fournies. Examinons donc à ce point de vue les divers procédés d'enregistrement.

En imprimant sous forme d'un trait chaque impulsion fournie par le détecteur on arrive très rapidement à une saturation. Dès que le noircissement moyen atteint 15 traits au centimètre, de nombreux traits commencent à se chevaucher à cause de leur distribution statistique.

L'emploi d'un dispositif diviseur entre le détecteur et le système d'impression permet d'éviter cet inconvénient mais l'appréciation visuelle des contrastes devient difficile et il n'est pas possible de connaître la valeur du noircissement à 20% près; or une telle différence peut être significative.

Cette difficulté est partiellement levée par les systèmes de scintigraphie en couleurs mais l'exploitation numérique des images n'est pas améliorée. La photo-scintigraphie, qui effectue une conversion numérique-analogique, permet également d'augmenter la gamme des noircissements utilisables. Grâce à la possibilité de faire varier les contrastes d'une façon continue, elle facilite la recherche des faibles inhomogenéités de teintes. Notre absence d'expérience dans ce domaine ne nous autorise pas à juger de ses possibilités quant à la sécurité de l'interprétation des documents.

Cependant, du point de vue où nous nous sommes placés, la seule méthode qui semble parfaitement satisfaisante est l'enregistrement sur bande magnétique [9]. En effet, outre la reproduction sur oscilloscope d'images analogues à celles qui sont fournies par les autres procédés, cette méthode produit un document capable de restituer intégralement les infor-

mations numériques qui lui ont été fournies par le détecteur. Elle peut donc se prêter particulièrement bien à l'interprétation statistique des images.

Le support même de ces documents, la bande magnétique, suggère immédiatement l'utilisation d'une calculatrice numérique et d'une méthode de traitement de l'information pour le dépouillement des données. Cette idée a déjà donné lieu à une réalisation pratique [10] sur laquelle nous n'avons que des renseignements fragmentaires, mais nous sommes persuadés qu'elle peut apporter une solution parfaite, bien qu'onéreuse, aux problèmes de scintigraphie.

RÉFÉRENCES

[1] GANDY, A. et JAMMET, H., 2ème Conf. int. util. EAFP(ONU) 26 (1958) 242-251.
[2] MATHER, R.L., J. of appl. Phys. 28 (1957) 1200-1207.
[3] GANDY, A. et GONGORA, R., Simposio su le Applicazioni della Scintigrafia Roma (1963).
[4] FOLICHON, A. et GANDY, A., J. de Radiologie et d'Electrologie 37 (1956) 334-344.
[5] BENDER, M.A. and BLAU, M., Int. J. Appl. Rad. & Isotopes 4 (1959) 154-161.
[6] MALLARD, J.R. and PEACHEY, C.J., Brit. J. Radiol. 32 (1959) 652-657.
[7] BASCHIERI, I. and D'APUZZO, B., Nuclear Med. 2 (1962) 290-299.
[8] MYHILL, J., Int. J. Appl. Rad. & Isotopes 12 (1961) 10-19.
[9] BERNE, E. and JONSSON, V., Nuclear Med. 1 (1959) 80-90.
[10] KAWIN, B., J. of Nucl. Med. 4 (1963) 182.

DISCUSSION

A. DESGREZ: In connection with the safety margins that can reasonably be expected, I should have thought that an error of 2.5%, i.e. approximately 2σ, was insufficient. From the medical point of view the important thing is surely the question, not of how probable it is that a small elementary zone corresponds to a statistical artefact, but how probable it is that the scan contains a zone that might correspond to an artefact.

By way of example let us take the case of a liver 200 cm^2 in size – which is a plausible value. This area will be made up of 50 elementary zones of 4 cm^2, so that it is rather like playing a game of chance fifty times. Assuming 2% error, one must be prepared to be mistaken once in these fifty times. This means that on each occasion the scan will show a 4-cm^2 artefact which might be considered to be a pathological nodule. This is unsatisfactory, particularly when one considers that better safety margins can be obtained with modern high-efficiency multichannel collimators. The point is an especially important one when use is made of equipment employing artificial contrast enhancement.

A. GANDY: As I see it, the situation is as follows. You observe an abnormal region in your picture and the problem is to find out whether there is a real reason for the abnormality or whether it is statistical in origin. The reply to this question takes the form of the numerical value of a probability. The same question can be asked for another region of the picture and the two replies are independent of one another.

Our limit of 2.5% is certainly open to discussion. However, we thought it was reasonable, and furthermore some calculations we performed with a value of 0.1% led us to some very pessimistic conclusions.

A COMPARISON BETWEEN COLLIMATOR THEORY, EXTENDED TO ALLOW FOR THE EFFECT OF WALL PENETRATION, AND EXPERIMENT

H.A.B. SIMONS
ROYAL FREE HOSPITAL SCHOOL OF MEDICINE, LONDON, ENGLAND

Abstract — Résumé — Аннотация — Resumen

A COMPARISON BETWEEN COLLIMATOR THEORY, EXTENDED TO ALLOW FOR THE EFFECT OF WALL PENETRATION, AND EXPERIMENT. The response of a collimator to a point source of radiation moving on a line perpendicular to the axis of the collimator may be determined by calculating the variation of the solid angle subtended by the exit pupil of the collimating hole at the source. The experimental response curves so determined are always broader than the theoretical curves, principally because of the penetration effect of quanta through the material of the collimator wall. The magnitude of the penetration effect has been calculated for a cylindrical hole both for points lying within the umbra and within the penumbra of the hole. Numerical values are given for a point source on a plane perpendicular to the axis of the hole in terms of the dimensionless parameters d/r and μH where d is the perpendicular distance of the source from the axis of a hole of radius r, μ the linear absorption coefficient of the collimator material and H the perpendicular distance of the source from the exit pupil.

These calculations have been extended to the case of a hole in the form of a truncated cone where the source plane coincides with the focal plane of the cone. Experimental response curves have been measured for cylindrical and conical holes for sources of different quantum energy. These may be compared with theoretical curves obtained after allowing for the penetration effect. The magnitude of the ratio, f, of the number of quanta penetrating the collimator wall to those passing through the exit pupil of the hole has been measured for a point source on the axis of a cylindrical hole for different quantum energies and is in reasonable agreement with theoretical values.

The response curves for a point source, allowing for collimator penetration, are applied to the calculation of the figure of merit of Dewey and Sinclair of some simple collimator systems for plane sources of varying target diameter and quantum energy.

LES COLLIMATEURS: COMPARAISON ENTRE LA THÉORIE, ÉTENDUE POUR TENIR COMPTE DES EFFETS DE PÉNÉTRATION DANS LA PAROI, ET L'EXPÉRIENCE PRATIQUE. La réponse d'un collimateur pour une source ponctuelle de rayonnement se déplaçant perpendiculairement à l'axe du collimateur peut être déterminée en calculant la variation de l'angle solide ayant la source pour sommet et l'orifice du collimateur pour base. Les courbes de réponse expérimentales ainsi déterminées sont toujours plus larges que les courbes théoriques, notamment à cause de l'effet de pénétration de quanta dans la paroi du collimateur. La valeur de l'effet de pénétration a été calculée, pour une ouverture cylindrique, pour des points situés dans l'ombre et dans la pénombre de l'ouverture. L'auteur donne les valeurs numériques pour une source ponctuelle dans un plan perpendiculaire à l'axe de l'ouverture, en fonction des paramètres sans dimensions d/r et μH, où d est la distance entre la source et l'axe d'une ouverture de rayon r, μ le coefficient d'absorption linéaire de la substance du collimateur et H la distance entre la source et l'orifice du collimateur.

Ces calculs ont été étendus au cas d'une ouverture ayant la forme d'un tronc de cône, le plan de la source coïncidant avec le plan focal. On a mesuré les courbes de réponse expérimentales dans les cas d'ouvertures cylindriques et coniques pour des sources d'énergies quantiques différentes. Ces courbes peuvent être comparées aux courbes théoriques établies en tenant compte de l'effet de pénétration. D'autre part, on a calculé la valeur du rapport, f, entre le nombre de quanta pénétrant dans la paroi du collimateur et le nombre de quanta passant par l'orifice de sortie dans le cas d'une source ponctuelle située sur l'axe d'une ouverture cylindrique, avec différentes énergies quantiques; les valeurs calculées sont raisonnablement en accord avec les valeurs théoriques.

Les courbes de réponse pour une source ponctuelle, établies en tenant compte de l'effet de pénétration, sont appliquées au calcul du coefficient de qualité de Dewey et Sinclair pour quelques systèmes simples de collimateurs, en ce qui concerne des sources planes ayant des diamètres et des énergies quantiques variables.

СРАВНЕНИЕ ТЕОРИИ КОЛЛИМАТОРА, УЧИТЫВАЮЩЕЙ ЭФФЕКТ ПРОНИКНОВЕНИЯ ЧЕРЕЗ СТЕНКУ, С ЭКСПЕРИМЕНТОМ. Чувствительность коллиматора к точечному источнику радиации, перемещающемуся по линии, перпендикулярной к оси коллиматора, можно определить путем подсчета изменения телесного угла, стянутого выходным зрачком коллимирующего канала в излучателе. Определенные таким способом экспериментальные кривые чувствительности всегда шире, чем теоретические кривые, главным образом ввиду проникновения квантов через вещество стенки коллиматора. Величина эффекта проникновения подсчитана для цилиндрического отверстия как в отношении точек, лежащих в тени, так и в полутени отверстия. Численные значения даются для точечного источника на плоскости, перпендикулярной к оси отверстия, в виде безразмерных параметров d/r и μH, где d означает перпендикулярное расстояние источника от оси отверстия с радиусом r, μ — линейный коэффициент поглощения вещества коллиматора и H — перпендикулярное расстояние источника от выходного зрачка.

Эти расчеты применялись и в том случае, когда отверстие представляет собой усеченный конус, где плоскость источника совпадает с фокальной плоскостью конуса.

Экспериментальные кривые чувствительности измерены для цилиндрических и конусных отверстий с источниками различной энергии кванта. Эти кривые можно сравнить с теоретическими кривыми, полученными с учетом эффекта проникновения.

Величина соотношения (f) между числом квантов, проникающих через стенку коллиматора, и числом квантов, проходящих через выходной зрачок камеры, подсчитана для точечного источника на оси цилиндрического отверстия для различных энергий квантов и в приемлемой степени совпадает с теоретическими оценками.

Кривые чувствительности точечного источника, с учетом проникновения коллиматора, применяются при вычислении показателя качества (по Дьюи и Синклеру) некоторых простых систем коллиматоров для плоских источников с меняющимися диаметром мишени и энергии кванта.

EFECTO DE PENETRACIÓN EN LAS PAREDES DE LOS COLIMADORES: COMPARACIÓN ENTRE LOS RESULTADOS TEÓRICOS Y LOS RESULTADOS EXPERIMENTALES. La respuesta de un colimador a una fuente puntiforme de radiaciones que se mueve a lo largo de una línea perpendicular al eje del colimador puede determinarse calculando la variación del ángulo sólido subtendido por la pupila de salida del canal de colimación. Las curvas experimentales de respuesta así determinadas son siempre más anchas que las curvas teóricas como consecuencia sobre todo del efecto de penetración de los cuanta a través del material de la pared del colimador. El autor ha calculado la magnitud del efecto de penetración para puntos situados en la umbra y en la penumbra de un canal cilíndrico. En su memoria presenta valores numéricos para una fuente *puntiforme situada en un plano perpendicular al eje del canal en función de los parámetros adimensionales* d/r y μH, en los que d es la distancia entre la fuente y el eje de un canal cilíndrico de radio r, medida perpendicularmente, μ el coeficiente de absorción lineal del material del colimador y H la distancia, medida también perpendicularmente, entre la fuente y la pupila de salida.

Estos cálculos se han ampliado para tener en cuenta el caso de un canal en forma de cono truncado en el que el plano de la fuente coincide con el plano focal del cono. El autor ha medido para canales cilíndricos y cónicos las curvas experimentales de respuesta correspondientes a fuentes de diferente energía cuántica. Esas curvas pueden compararse con las curvas teóricas obtenidas teniendo en cuenta el efecto de penetración. Ha calculado la magnitud de la razón, f, entre el número de cuanta que atraviesan la pared del colimador y el de los que atraviesan la pupila de salida para una fuente puntiforme situada en el eje de un canal cilíndrico y para diferentes energías cuánticas; los datos obtenidos concuerdan razonablemente con los valores teóricos.

El autor ha aplicado las curvas de respuesta correspondientes a una fuente puntiforme, teniendo en cuenta el efecto de penetración en el colimador, al cálculo del factor de cualidad de Dewey y Sinclair correspondiente a algunos sistemas sencillos de colimador para fuentes planas de diámetro de blanco y de energía cuántica variables.

1. INTRODUCTION

The response of a collimated gamma-detecting system to a radioactive source of any known shape and activity may be theoretically deduced if the response of the system to a point source of the same quantum energy is

known. If degradation of the quantum energy occurs by scattering, the effect of the majority of such quanta may be neglected if the detecting system has some form of energy discrimination; and an allowance may be made for the effect of absorption.

The geometrical response of a collimator to a point source may be determined by a calculation of the variation of the solid angle that the exit pupil of the hole presents at the source. Such calculations are simple in principle and have been published by BROWNELL [1] and the results may be given either as isocount contours, i.e. lines on which the solid angle subtended by the exit pupil of the hole is a constant, or as shown in Fig. 1. Here

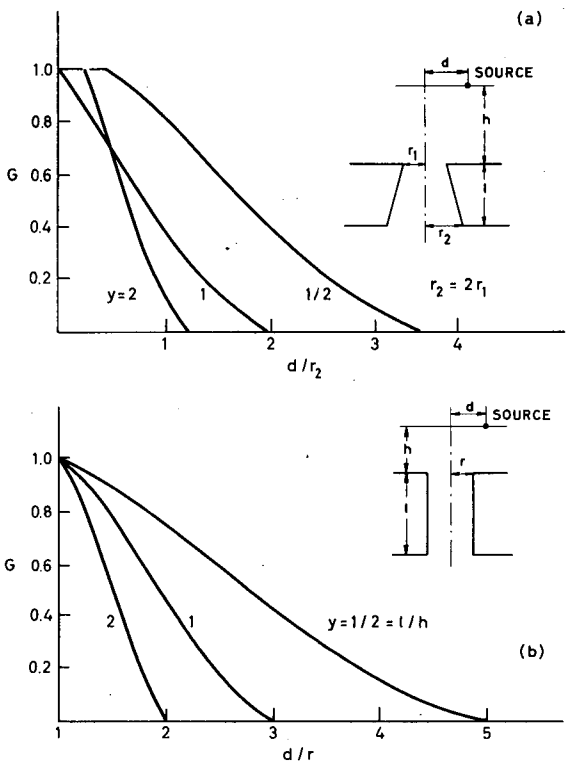

Fig. 1

(a) Geometrical response curve for a taper hole where $r_2 = 2r_1$ and $y = \frac{1}{2}$, 1 and 2
(b) Geometrical response curve for a cylindrical hole for $y = \frac{1}{2}$, 1 and 2.

the response curves are plotted in Fig. 1a for a focusing collimator in which the hole is a truncated cone and in Fig. 1b for a hole of cylindrical section. The ordinate G is the fraction of the maximum response (with the source on the axis) that is obtained for each value of d/r. Each curve applies to a particular source plane, and is normalized to unity on the axis. The abscissa is given in terms of the non-dimensional parameter d/r where r is some radius of the hole.

The resolution or resolving power of the system, that is the ability to distinguish between different sources, depends upon the shape of the source [2], but for convenience the point-source resolution can be defined from the curves in Fig. 1 as twice the width of the curve from G = 0, to G = 0.5, being given in terms of d/r.

The response of a complex multi-hole collimator system, such as a focusing collimator, may in theory be calculated by the summation of the response curves for each hole, allowance being made for their relative positions.

It is well known that the effects of penetration of quanta through the collimator wall and also scattering of quanta from the surface of the collimating hole into the exit pupil have the effect of decreasing the resolution of the system. This effect has been demonstrated experimentally [3] and calculations have been made of penetration effects [4, 5, 6], and of scattering effects [5]. The magnitude of the scattering effect is much smaller than that of the penetration effect and will not be treated further in this paper. In multi-hole collimators a further effect, which decreases the resolution, arises from the penetration of radiation through the septa between the holes so that a quantum may reach the detector after having passed through one or more septa and one or more collimating channels. A calculation of the magnitude of this effect is complex and has been given by MYHILL [7].

The penetration effect for a point source and a cylindrical hole has been given in [6] for points lying within the volume bound by the projection of the hole, and for a focusing collimator for axial points. This paper will show how these calculations may be extended to non-axial points and compare the theoretical and experimental effects of collimator penetration, and also show how the "figure of merit" [2] of a collimation system for plane targets may be obtained from the point response function.

2. CALCULATION OF THE PENETRATION FACTOR FOR A POINT SOURCE ON A PLANE PERPENDICULAR TO THE AXIS OF A CYLINDRICAL HOLE

*2.1. Points within the umbra**

The penetration factor f is defined as the ratio of the number of quanta penetrating the side wall to the number passing through the exit pupil of the hole when the source is on the axis. This has been calculated in [6] and shown to have the value: (refer to Fig. 2 for the symbols).

$$f = -(1+\mu H) + (H^2/h^2)(1+\mu h)\exp[-\mu(H-h)]$$
$$+\mu^2 H^2 \exp(-\mu H)[\mathrm{Ei}(\mu H) - \mathrm{Ei}(\mu h)] \qquad (1)$$

where $\mathrm{Ei}(\mu H)$ is the exponential integral. Using the asymptotic expansion of $\mathrm{Ei}(x)$ for large x and if

* See Appendix I for a Glossary of Symbols used in this paper.

$$(H^2/h^2)\exp[-\mu(H-h)] << 1$$

then

$$f = \frac{2!}{\mu H} + \frac{3!}{\mu^2 H^2} + \frac{4!}{\mu^3 H^3} + \ldots \frac{(n+1)!}{\mu^n H^n} . \qquad (2)$$

It is also shown in [6] that equations (1) and (2) are applicable to point sources within the umbra of the hole.

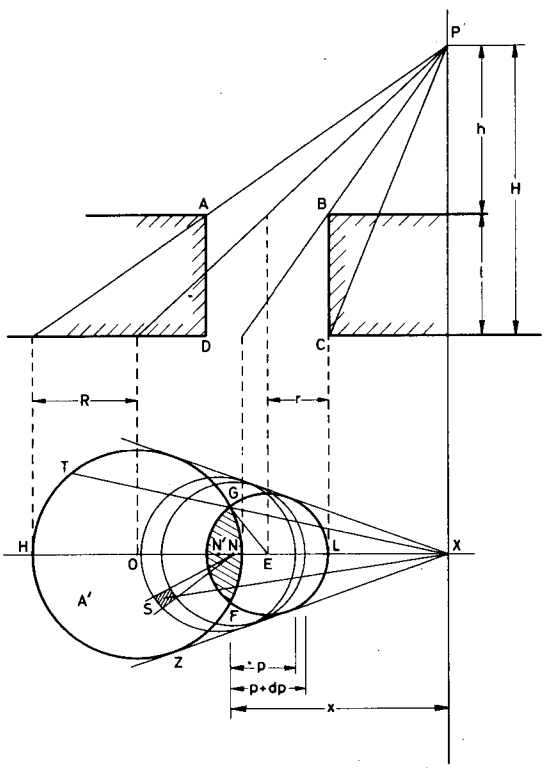

Fig. 2

Diagram showing geometry of quantum penetration for a cylindrical hole

2. 2. Points within the penumbra

In Fig. 2 ABCD is the section of a cylindrical hole and a point source at p lies within the penumbra of the hole. The lower part of the Figure shows the plane of the exit pupil so that the collimating hole is the circle with centre E and radius r, and the circle with centre O and radius R is the projection of the entrance pupil on this lower plane. The shaded area common to both circles is that part of the exit pupil which may be seen from the source. Radiation from P which enters the collimating hole and passes through the wall to reach the exit plane will pass through an area A_1 equal to the area

of the circle centre O less the shaded area. Radiation which passes through the upper face of the collimating block and then into the collimating hole will pass through a similar area equal to the area of the circle centre E less the shaded area. The effective penetration solid angle a_p is obtained by calculating the total solid angle subtended by these areas at P, each element of the solid angle being decreased by a multiplying factor to allow for the attenuation of radiation in passing through the collimating material.

Then the fraction f is equal to a_p divided by the solid angle that the exit pupil of the collimator subtends at the source when it is on the axis.

Calculation of a_p is performed in two parts by integration over each crescent area shown in Fig. 2, the values of the two integrals being called I_1 and I_2. Referring to the lower part of the Figure the common tangents to the two circles are drawn intersecting at X which is the orthogonal projection of P. Let the angle HXZ = α.

The area A_1 is subdivided by drawing circles of varying radii which touch the common tangents and with centres lying between E and O.

Two such circles are shown of radius p and p + dp with centres at N and N'. The elementary area at S is produced by the arcs of these two circles and radii of angular separation $d\psi$ at an angle $\psi = O\hat{N}S$. Let XN = x and NN' = dx then p = x sin α and the movement of the centre from N to N' contributes dx cos ψ to the length of the area at S. Thus the elemental area at S

$$ds = p(1 + \operatorname{cosec}\alpha \cos\psi)\, dp\, d\psi$$

If $H \gg p$ the inclination factor cos SPX may be neglected and SP $\approx$ H.

The penetration length in the collimator material for a line joining P to any point along the arc on which S lies may be shown to be equal to SP(p-r)/p and the attenuation factor is thus: $\exp -\mu H(p-r)/p$

Thus

$$I_1 = \int_{-\psi_1}^{\psi_1} \int_r^R \frac{P(1 + \operatorname{cosec}\alpha \cos\psi)\exp -\mu H(p-r)/p\, dp d\psi}{H^2}.$$

If integration over the whole crescent is made the limits of ψ are a function of p. To enable the integrals to be separated the limits of ψ are restricted to $\pm\psi'$ such that if a line is drawn from X to the intersection of the circles at G and produced to T then $H\hat{E}G = \psi^1$.

Similarly $H\hat{O}T = \psi^1$ and the integration within $\pm\psi^1$ covers that part of A_1 which lies within the lines TX and a similar line drawn from X to F and produced. The error made in the value of I_1 may be estimated and increases as the circles R and r separate where P is moved further from the collimator axis.

Writing $I_1 = [I_\psi][I_p]$.

Then if $u = r\mu H/p$

$$I_p = \frac{1}{H^2}\int_r^R p \exp[-\mu H(p-r)/p]dp = -\mu^2 r^2 \exp(-\mu H)\int_{\mu H}^{\mu Hr/R} \frac{e^u}{u^3} du$$

Now $\mu Hr/R = \mu h$, and using the asymptotic expansion for large x that

$$Ei(x) = \int_{-\infty}^{x} \frac{e^u}{u} du = \frac{e^x}{x}\left(1 + \frac{1!}{x} + \frac{2!}{x^n} + \cdots \frac{n!}{x^n}\right).$$

Then

$$I_p = \frac{\mu^2 r^2}{2}\left\{\left[\frac{2!}{\mu^3 H^3} + \frac{3!}{\mu^4 H^4} + \cdots\right] - \exp[-\mu H(1 - r/R)]\left[\frac{2!}{\mu^3 h^3} + \frac{3!}{\mu^4 H^4} + \cdots\right]\right\}.$$

Neglecting the exponential term

$$I_p = \frac{\mu^2 r^2}{2}\left(\frac{2!}{\mu^3 H^3} + \frac{3!}{\mu^4 H^4} + \cdots\right)$$

$$I_\psi = \int_{-\psi_1}^{\psi_1} (1 + \operatorname{cosec}\alpha \cos\psi)\, d\psi = 2(\psi_1 + \operatorname{cosec}\alpha \sin\psi_1)$$

where

$$\psi_1 = \cos^{-1}\left[\frac{r^2 + (R - r)^2 \operatorname{cosec}^2\alpha - R^2}{2r(R - r)\operatorname{cosec}}\right].$$

In calculating the value of I_ψ it is convenient to write the distance of P from the collimator axis, that is EX = d and then $\operatorname{cosec}\alpha = d/r$. Writing $y = \ell/h$ and $d/r = k$ then $R = r(1+y)$ and

$$\psi^1 = \cos^{-1}[y(k^2 - 1) - 2]/2k.$$

If d = r so that P lies on the projection of the collimator wall, the circle r lies inside the larger circle R and touches it at a point.

Thus generally

$$I_1 = (\psi_1 + k \sin\psi_1)\mu^2 r^2\left[\frac{2!}{\mu^3 H^3} + \frac{3!}{\mu^4 H^4} + \cdots \frac{(n-1)!}{\mu^n H^n}\right]. \tag{3}$$

The value of the second integral I_2 is obtained in a similar manner to I_1 (see Fig. 3).

The element of area at S is, as before, equal to

$$p(1 + \operatorname{cosec}\alpha \cos\psi)\, dp\, d\psi$$

and the penetration length for points on the arc RQ is approximately

$$(rH/p) - h$$

thus

$$I_2 = \frac{2}{H^2}\int_{\pi}^{\psi_2}\int_{r}^{R} p(1 + \operatorname{cosec}\alpha \cos\psi)\exp(\mu h - \mu r H/p)\, dp\, d\psi$$

where

$$\psi_2 = \widehat{HOF}.$$

Integration proceeds as before leading to

$$I_2 = [\psi_2 + \sin\psi_2 \operatorname{cosec}\alpha - \pi]\mu^2 r^2 \left[\frac{2!}{\mu^3 h^3} - \frac{3!}{\mu^4 h^4} + \frac{4!}{\mu^5 h^5} - \frac{5!}{\mu^6 h^6} \cdots \right] \tag{4}$$

where

$$\psi_2 = \cos^{-1}\left[\frac{-1(y+2) - yk^2}{2k(1+y)} \right].$$

Thus

$$f = (I_1 + I_2)/\pi r^2 H^{-2}$$

and adding (3) and (4)

$$= \frac{1}{\pi}[\psi_1 + k\sin\psi_1]\left(\frac{2!}{\mu H} + \frac{3!}{\mu^2 H^2} + \cdots \frac{(n+1)!}{\mu^n H^n}\right)$$

$$+ \frac{1}{\pi}[\psi_2 + k\sin\psi_2 - \pi]\left(\frac{H^2}{h^2}\right)\left(\frac{2!}{\mu h} - \frac{3!}{\mu^2 h^2} + \frac{4!}{\mu^3 h^3} \cdots \frac{(-)^{n+1}(n+1)!}{\mu^n h^n}\right) \tag{5}$$

where ψ_1 and ψ_2 are defined as above.

The value of the two multiplying factors in the above expression may be tabulated as a function of d/r for specific values of $y = \ell/h$.

Thus, if

$$\frac{1}{\pi}(\psi_1 + k\sin\psi_1) = A \text{ and } \frac{1}{\pi}(\psi_2 + k\sin\psi_2 - \pi) = B$$

Table I is obtained.

Values of the semiconvergent series

$$f(\mu H) = \frac{2!}{\mu H} + \frac{3!}{\mu^2 H^2} + \frac{4!}{\mu^3 H^3} + \cdots \frac{(n+1)!}{\mu^n H^n}$$

and

$$\phi(\mu h) = \frac{2!}{\mu h} - \frac{3!}{\mu^2 h^2} + \frac{4!}{\mu^3 h^3} \cdots \frac{(-)^{n+1}(n+1)!}{\mu^n h^n}$$

are given in Fig. 4 which have been calculated by adding the values of the terms of series down to the value of the smallest term.

The application of these results may be seen in Fig. 5 which, for a cylindrical collimator where $y = 1$ and $\mu H = 10$ the geometrical response G, the fraction f as a function of d/r, the curve $f + G$ which is the sum of the

TABLE I

FACTORS REQUIRED IN THE CALCULATION OF f FOR NON-AXIAL POINT SOURCES

d/r = k	$y=\frac{1}{2}$		d/r = k	y = 1		d/r = k	y = 2	
	A	B		A	B		A	B
1.0	1.000	0.000	1.0	1.000	0.000	1.0	1.000	0.000
1.5	1.048	0.0809	1.2	1.015	0.0209	1.2	1.018	0.0172
2.0	1.171	0.1908	1.4	1.034	0.0528	1.4	0.954	0.0402
2.5	1.249	0.2961	1.6	1.048	0.0872	1.6	0.863	0.0578
3.0	1.291	0.3850	1.8	1.093	0.120	1.8	0.674	0.0606
3.5	1.279	0.4379	2.0	1.038	0.147	2.0	0.000	0.000
4.0	1.184	0.4554	2.5	0.878	0.178			
4.5	0.939	0.3927	3.0	0.000	0.000			
5.0	0.000							

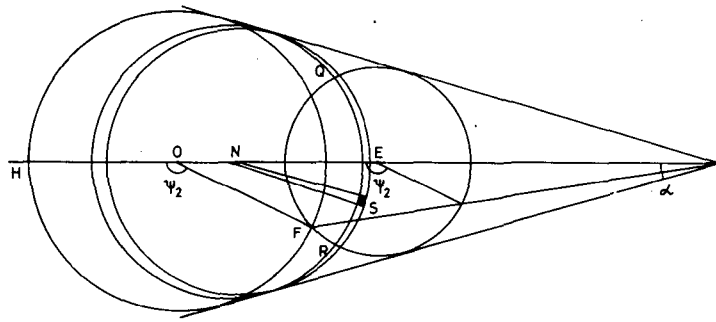

Fig. 3

The plane of the exit pupil of a cylindrical hole

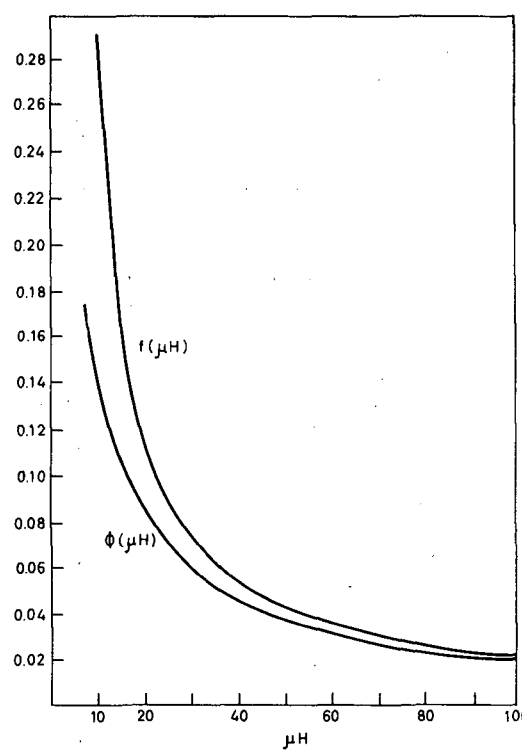

Fig. 4

$\phi(\mu H)$ and $f(\mu H)$ shown as a function of μH

curves f and G normalized to unity where $d/r = 0$. It is interesting to note that the contribution of penetrating quanta rises with increasing value of d/r until it is in fact equal to the contribution of the geometrical response at a value of d/r approximately equal to 2. Owing to the approximations made in

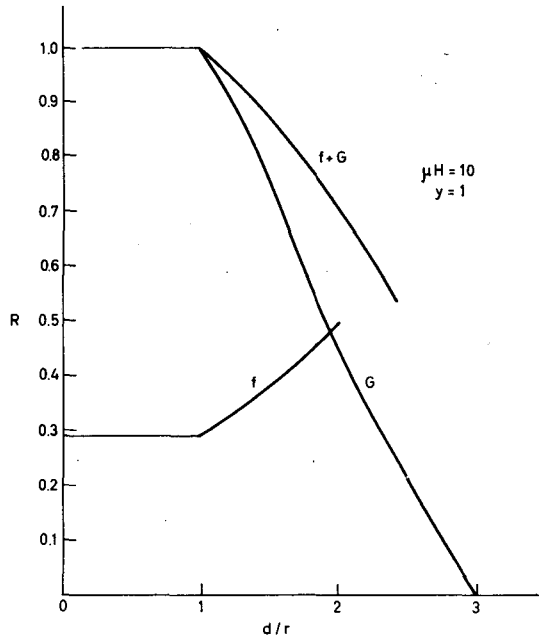

Fig. 5

Geometrical response and penetration fraction f as a function of d/r for a cylindrical hole where $\mu H = 10$

the determination of f the calculated values for d/r greater than 2 are inaccurate since f is underestimated, the error increasing with increasing d/r.

For the same collimator Fig. 6 shows the calculated curves for values of $\mu H = 10$, 20, 50 and ∞, the latter curve corresponding to the geometrical case only. As μH is decreased, i.e. for a given value of H, μ is decreased corresponding to the radiation of a greater penetrating power and the width of the response curve increases. It may be seen from Fig. 6 that the width of the curve is increased by about a third between the values of $\mu H = \infty$ and $\mu H = 10$.

Figure 7 shows a comparison between the experimental points obtained with lead collimators and the theoretical curves derived from equation (5) with appropriate values of μ for lead and the quantum energy concerned.

2. 3. Experimental determination of penetration factor f

The comparison between the point-source response curves obtained experimentally and theoretically is not a sensitive test of the adequacy of the calculations of penetration, since the shape of the normalized response curve does not vary rapidly with the variation of the contribution to it arising from penetrating radiation. Therefore, experiments were performed to determine the value of f corresponding to an axial point source. Three measurements of the counting rate from a scintillation counter with a NaI(Tl) crystal and a cylindrical collimator were made corresponding to the three situations

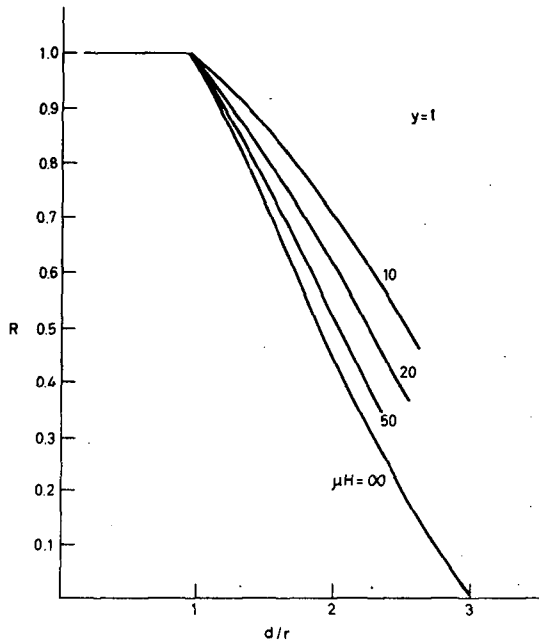

Fig. 6

The normalized response, including penetration, for a cylindrical hole as a function of μH and d/r

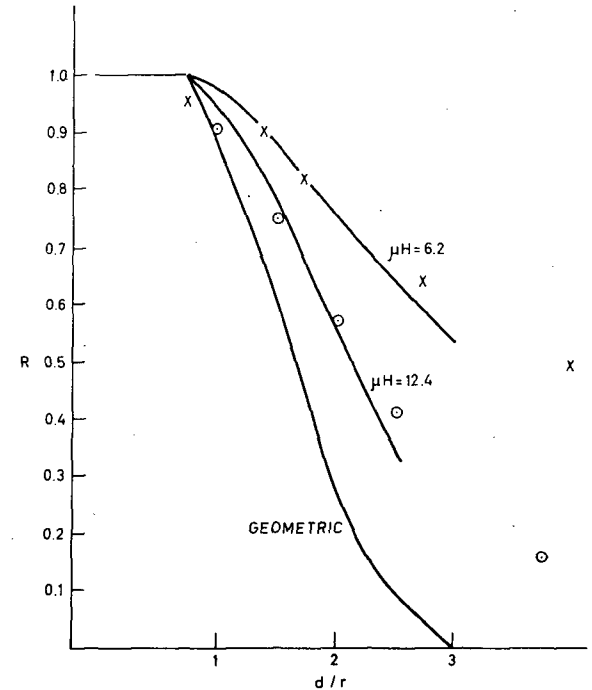

Fig. 7

A comparison between theoretical and experimental response curves for a cylindrical hole and different values of μH

⊙ Expt. $\mu H = 12.4$
X Expt. $\mu H = 6.2$

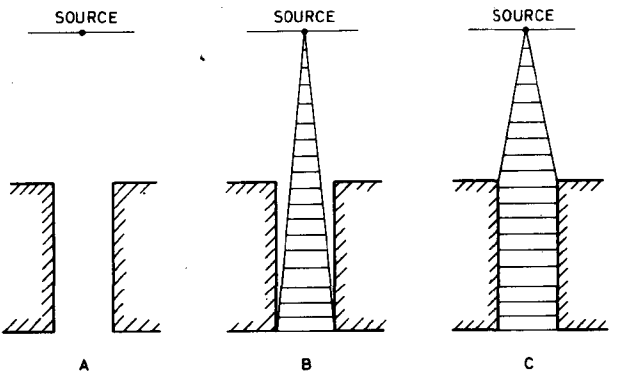

Fig. 8

The assembly of lead plugs used in the measurement of f for an axial source and a cylindrical hole

A, B, C, shown in Fig. 8. Measurement A includes radiation passing through the geometrical aperture, penetrating radiation and radiation which is scattered into the exit pupil. Measurement B with a lead cone records radiation

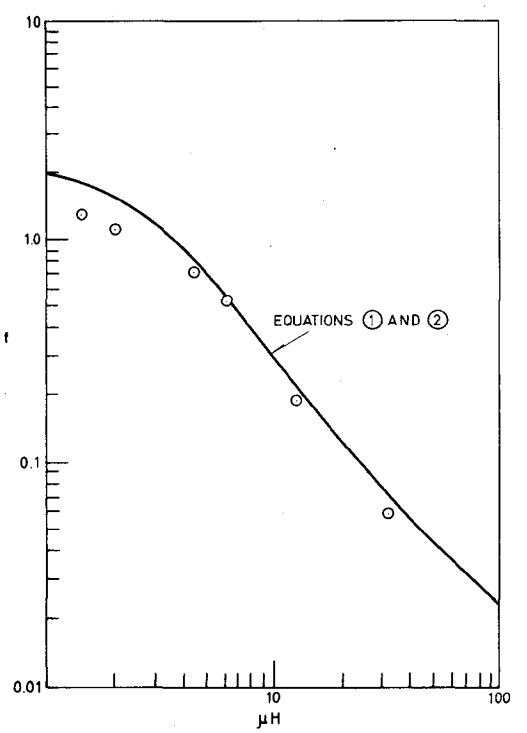

Fig. 9

f for an axial source as a function of μH showing a comparison with experimental points
⊙ Expt.

which penetrates the collimator wall, and measurement C, as shown with a lead plug, records background and radiation which penetrates the whole thickness of the collimator block: Thus, neglecting the contribution of scattered radiation,

$$f = (B - C)/(A - B). \tag{6}$$

If scattered radiation contributes appreciably to the measurement then the denominator in (6) will be too large and hence the value of f too small.

Experiments were done with both a lead collimator and an aluminium "collimator", the latter being used to obtain low values of μH and thus to extend the verification of the calculations. Measurements A, B and C were made with small sources of radiation using I^{131}, Au^{198}, Cs^{137}, Co^{60} and Na^{24} and lead cones were made of appropriate length for values of $y = 2$, 1, and $\frac{1}{2}$. The sources were kept as small as possible, less than a millimetre in diameter. The depth ℓ of the collimators was 5 cm and corrections were made where appropriate for the decay of the isotope during counting, and penetration of the lead cones by high energy quanta.

The results obtained for $y = 1$ are shown in Fig. 9 where it will be seen that the agreement with the curves from equations (1) and (2) is good for large values of μH becoming less as μH decreases. This is to be expected since a small value of μH corresponds either to a small H where geometrical approximations made in the derivation of 1 and 2 are invalid, or μ is small in which case Compton scattering of radiation through the exit pupil tends to decrease the value of f.

3. TAPER COLLIMATOR

The geometrical response of a taper collimator with a hole of circular cross-section is shown in Fig. 1a where the focal distance is equal to the collimator length. For a point source on the axis $f = 0$ at the focus, and as the source moves from the focus remaining on the axis, f increases, a theoretical value of f being given in [6].

To obtain the effect of penetration on the resolution in the focal plane it is necessary to obtain f as the point moves from the axis.

3.1. Penetration factor f for a taper hole

The calculation of f is similar to that given in section 2.

In Fig. 10 the source is at P in the focal plane at a distance d from the axis of a collimator of principal radii r_1 and r_2.

As previously, the two penetration regions are the crescent-shaped portions of the circles with centre O and centre E, these circles having r_2 radii.

If $EN = AD = x$, the element of area at $S = r_2 \cos\psi \, dx \, d\psi$ and the penetration length p for points on the arc with centre N and radius r_2 is

$$AP \cdot x/(d + x) \approx Hx/(d + x).$$

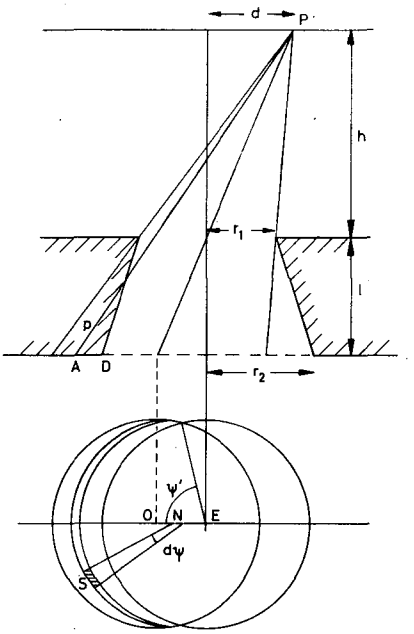

Fig.10

The geometry of quantum penetration for a taper hole

Thus,

$$d(ap) = \frac{1}{H^2} \cdot r_2 \cos\psi \exp[-\mu Hx/(d+x)]\,dx \cdot d\psi$$

and

$$I_1 = \frac{1}{H^2} \int_{-\psi_1}^{\psi_1} \int_0^{dy} r_2 \cos\psi \exp[-\mu Hx/(d+x)]\,dx \cdot d\psi .$$

Since $\exp[-\mu Hx/(x+d)]$ is large for $x \ll d$, it may be approximated by $\exp(-\mu Hx/d)$ and $I_1 = (2/H^2)\sin\psi_1 dr_2/\mu H$.

Similarly

$$I_2 = 1/H^2 \int_{-\psi_2}^{\psi_2} \int_0^{dy} r_2 \cos\psi \exp[-\mu hx/d(1+y)]\,dx \cdot d\psi = \frac{2r_2 \sin\psi_2\, d(1+y)}{H^2 \mu h}$$

Now if $\psi = \psi_1 = \psi_2 = \cos^{-1} dy/2r_2$ and $ap = I_1 + I_2$ we have

$$f = (I_1 + I_2)/\pi r_2^2 H^{-2} = \frac{2}{\pi} \cdot \frac{d}{r_2} \left[\frac{1}{\mu H} + \frac{(1+y)}{\mu H}\right] \sin\psi. \qquad (7)$$

The point-response function of a lead collimator where $\ell = h = 5$ cm, $r_1 = 0.375$ cm, $r_2 = 0.75$ cm has been investigated and the curves for Co^{60} radiation where $\mu H = 6.6$ and for Cs^{137} radiation where $\mu H = 12.4$ are shown in Fig. 11. The geometrical response curve for $\mu H = \infty$ is shown together with points calculated from equation (7) with the appropriate values of μH and d/r.

It will be seen that the agreement between theory and experiment is only fair. The fractional increase in width of the curves at one half the maximum ordinate is much greater for corresponding values of μH than in the case of the cylindrical hole, although the absolute values of the width of the curves in terms of d/r are slightly smaller for the taper hole. If r_2 for the taper hole is equal to r for the cylindrical hole the collimator sensitivities are equal and the resolving powers of the two types of collimator are then comparable.

4. APPLICATION OF THE RESPONSE CURVES TO THE DETERMINATION OF THE FIGURE OF MERIT OF A COLLIMATOR

It has been shown by DEWEY and SINCLAIR [2], using a statistical analysis, that if the criterion of detection of a plane target is that the increase in counting rate, when the collimator is over the target, must be n times the standard error of the non-target counting rate, then

$$C_{NT} = \frac{s_\infty}{s_t^2} \cdot \frac{n^2}{(1-f_a)^2} \frac{1}{T}$$

where s_t is the counting rate per unit time if the target has unit activity per unit area and the collimator axis is coincident with the centre of the target.

s_∞ is the counting rate if the collimator is placed over an infinite plane source of unit activity per unit area.

T is the time of observation.

f_a is the ratio of the target to the non-target activity, (assuming that the non-target is effectively infinite.)

If the values of f_a, T and n are fixed, then the value of the ratio s_t^2/s_∞ determines the smallest value of C_{NT} that can occur and hence the sensitivity of the system. The quantity s_t^2/s_∞ is fixed by collimator design only and must be made as large as possible for optimum conditions of detection.

The above equation does not include the resolution of the system and it will be seen below that it is inadequate to determine completely the merit of a collimating system.

s_t^2/s_∞ will be called the "figure of merit" of the system.

4.1. Calculation of the figure of merit of a cylindrical hole and circular plane targets

Suppose that the hole has a radius r and that the target lies in the plane $y = 1$.

Let the counting rate from unit source placed on the axis of the hole be C per unit time.

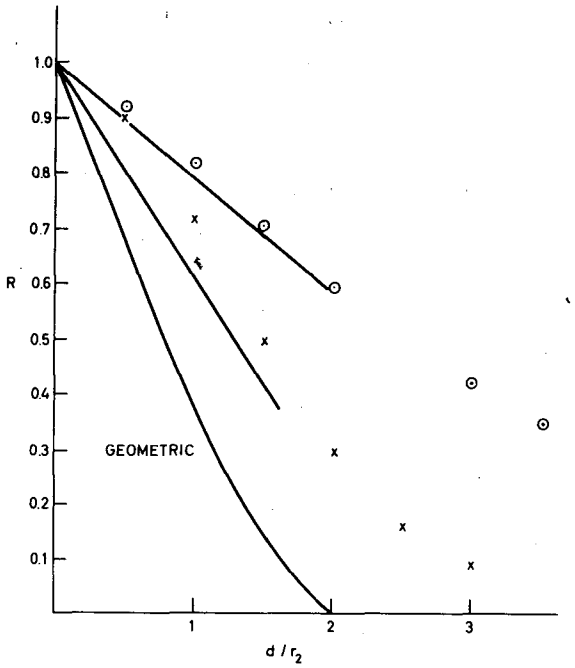

Fig. 11

A comparison between theoretical and experimental response curves for a taper hole and different values of μH

⊙ Expt. Co^{60} $\mu H = 6.6$
X Expt. Cs^{137} $\mu H = 12.4$
Lines from equation (7).

Then, as before writing $d/r = k$, the response curve of the collimator may be formalized to

$$f(k) = 0 \qquad \text{for } 0 \le k \le 1$$
$$f(k) = 3/2 - k/2 \quad \text{for } 1 \le k \le 3$$

Thus, for an infinite source of unit activity per unit area

$$s_\infty = 2\pi C r^2 \int_0^\infty k\, f(k)\, dk$$

$$= 2\pi C r^2 \left\{ \int_0^1 k dk + \int_1^3 [(3/2)k - k^2/2]\, dk \right\}.$$

Hence

$$s_\infty = \frac{13\pi}{3} C r^2.$$

Now, if a circular target has a radius r_t so that $r_t = k_t r$ then s_t is given by

$$2\pi C r^2 \int_0^{kt} kf(k)dk$$

and the value of s_t^2/s_∞ may be calculated as a function of k_t.

Table II gives the results of these calculations for source planes $y = \frac{1}{2}$, 1 and 2.

In each case a formalized response function has been used so that G = 1, where k = 1, and G = 0 where k = 5, 3 and 2 respectively.

The values of s_t^2/s_∞ in this Table are plotted in Fig. 12 as a function of k_t. The very rapid rise in this quantity as k_t increases may be seen. If the

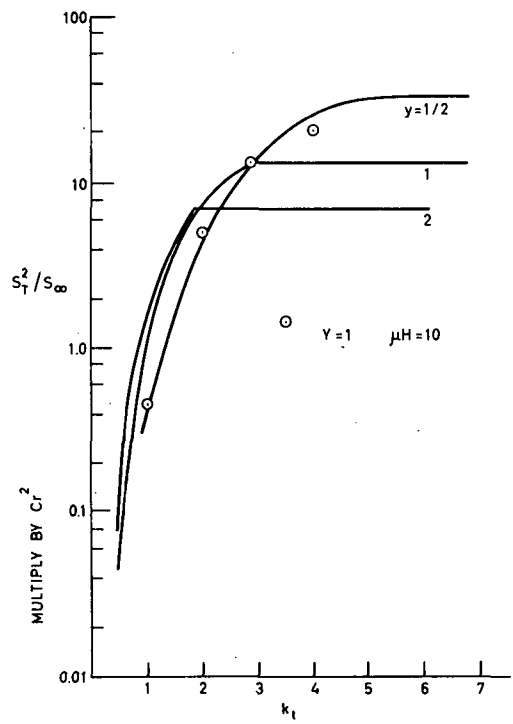

Fig. 12

s_t^2/s_∞ calculated for a cylindrical hole and $y = \frac{1}{2}$, 1 and 2, the plotted points showing the effect of quantum penetration.

figure of merit is compared for $y = \frac{1}{2}$, 1 and 2 it must be remembered that the appropriate value of C must be used since $C \alpha\ r^2/H^2$, thus $C_{(y=2)} = 16/9\ C_{(y=1)}$ and $C_{(y=\frac{1}{2})} = 4/9\ C_{(y=1)}$.

Thus, e.g. where $k_t = 1$, the corrected values of the figures of merit are 2.38, 0.725 and 0.135 (multiplied by r^2) for values of y = 2, 1 and $\frac{1}{2}$ respectively.

TABLE II

FIGURES OF MERIT FOR A CYLINDRICAL COLLIMATOR

$y = \frac{1}{2}$			$y = 1$			$y = 2$		
k_t	s_t $x\pi Cr^2$	s_t^2/s_∞ xCr^2	k_t	s_t $x\pi Cr^2$	s_t^2/s_∞ xCr^2	k_t	s_t $x\pi Cr^2$	s_t^2/s_∞ xCr^2
1	1.00	0.304	0.25	0.0625	0.00283	0.25	0.0625	0.00526
2	3.58	3.90	0.50	0.250	0.0453	0.50	0.25	0.0842
3	6.66	13.51	1.0	1.000	0.725	0.75	0.563	0.426
4	9.17	26.02	1.5	2.083	3.77	1	1.0	1.346
5	10.33	32.46	2	3.160	7.27	1.5	1.92	4.95
s_∞	10.33	32.46	3	4.33	13.62	2	2.33	7.32
			s_∞	4.33	13.62	s_∞	2.33	7.32

Hence, and perhaps not surprisingly, it appears that the best conditions for working are with the source plane as near to the end of the collimator as possible.

The values of s_t^2/s_∞ may be used to calculate the optimum collimator radius for a given target radius. This is shown in Table III for a target of 1-cm radius; a similar result being obtained for any other radius.

In Table III the value of Cr^2 has been put equal to unity for unit collimator radius and, since C to a first approximation is proportional to r^2, Cr^2 is proportional to r^4.

TABLE III

VARIATION OF THE FIGURE OF MERIT FOR A 1-cm RADIUS TARGET WITH VARIATION OF COLLIMATOR RADIUS FOR A CYLINDRICAL HOLE

y = 1				
Collimator radius (cm)	k_t	s_t^2/s_∞ x Cr^2	Cr^2	Figure of merit
$\frac{1}{3}$	3	13.62	1/81	0.168
$\frac{1}{2}$	2	7.27	1/16	0.454
1	1	0.725	1	0.725
2	$\frac{1}{2}$	0.0453	16	0.725
4	$\frac{1}{4}$	0.00283	256	0.725

It may be seen from this criterion that the optimum collimator radius is equal to the target radius and no further advantage accrues from a further increase in radius since this will be accompanied by a decrease in resolution.

A similar result is obtained if the figure of merit of a target of different radius is calculated, although the maximum figure of merit increases with increasing target radius.

The effect of collimator penetration on these results is twofold. Referring to Fig. 6 and taking the case of $\mu H = 10$ the curve may be formalized to

$$f(k) = 0 \qquad \text{for } 0 \leq k \leq 1$$
$$f(k) = 4/3 - k/4 \quad \text{for } 1 \leq k \leq 4$$

and from this the values of s_t^2/s_∞ may be determined. These have been calculated and are plotted on Fig. 12. It will be seen that for small k_t there is some decrease in "merit" but it must be remembered that the value of C for $\mu H = 10$ is about 30% larger than for the geometrical case. This factor, except for large k_t, nearly cancels the apparent difference between the curves for the geometrical case and that allowing for penetration. The effect of penetration is however, as shown in Fig. 6, always to decrease the resolving power of the system.

4.2. The figure of merit for a taper collimator and circular plane targets.

The method of analysis used in section 4.1. may be applied to the case of a single tapering hole.

Consider the case where ℓ equals h and the source moves where $y = \frac{1}{2}$, 1 and 2. From Fig. 1a it may be seen that the response curves for the geometric case may be formalized as follows:

$$
\begin{array}{lll}
y = \frac{1}{2} & f(k) = 1 & 0 \le k \le \frac{1}{2} \\
 & f(k) = 7/6 - k/3 & \frac{1}{2} \le k \le 7/2 \\
 & & \\
y = 1 & f(k) = (1 - k/2) & 0 \le k \le 2 \\
 & & \\
y = 2 & f(k) = 1 & 0 \le k \le 1/4 \\
 & f(k) = 5/4 - k & 1/4 \le k \le 5/4
\end{array}
$$

where $k = d/r_2$.

Hence Table IV may be obtained.

The values of s_t^2/s_∞ are plotted in Fig. 13. If r_2 for a focusing collimator is made equal to r for a cylindrical collimator, the respective figures of merit of the two may be compared since their sensitivities are equal.

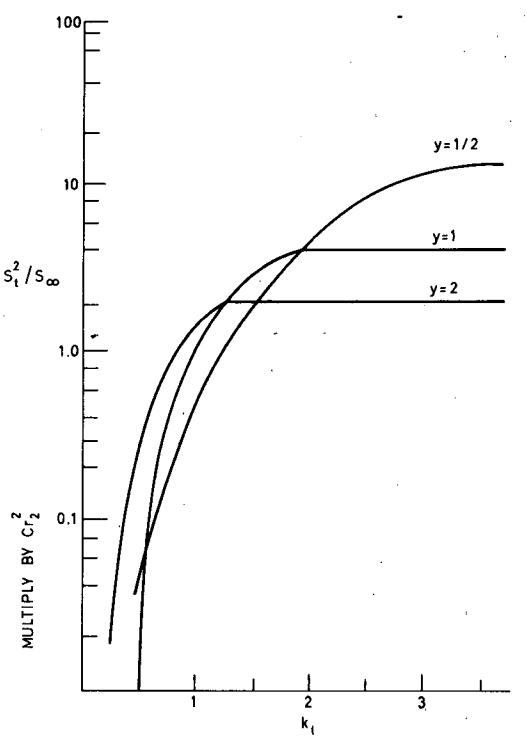

Fig. 13

s_t^2/s_∞ calculated for a taper hole where $r_2 = 2r_1$ and $y = \frac{1}{2}$, 1 and 2.

TABLE IV

FIGURES OF MERIT FOR A TAPER COLLIMATOR

$y = \frac{1}{2}$			$y = 1$			$y = 2$		
k_t	s_t $x\pi Cr_2^2$	s_t^2/s_∞ xCr_2^2	k_t	s_t $x\pi Cr_2^2$	s_t^2/s_∞ xCr_2^2	k_t	s_t $x\pi Cr_2^2$	s_t^2/s_∞ xCr_2^2
0.5	0.25	0.0413	0.25	0.0572	0.00775	0.25	0.0625	0.019
1	0.931	0.573	0.5	0.208	0.102	0.5	0.226	0.250
2	2.875	5.47	1.0	0.667	1.046	1.0	0.579	1.626
3.5	4.75	14.92	1.5	1.125	2.982	1.25	0.646	2.028
s_∞	4.75	14.92	2	1.333	4.188	s_∞	0.646	2.028
			s_∞	1.333	4.188			

TABLE V

FIGURE OF MERIT FOR A CYLINDRICAL AND A TAPER HOLE AS A FUNCTION OF COLLIMATOR RADIUS

Cylindrical hole					Taper hole				
Radius r	k_t	s_t^2/s_∞	Cr^2	Figure of merit	r_2	k_t	s_t^2/s_∞	Cr_2^2	Figure of merit
$\frac{1}{2}$	2	7.27	1/16	0.454	$\frac{1}{2}$	2	4.19	1/16	0.262
1	1	0.725	1	0.725	1	1	1.05	1	1.05
2	$\frac{1}{2}$	0.0453	16	0.725	2	$\frac{1}{2}$	0.102	16	1.63
4	$\frac{1}{4}$	0.00283	256	0.725	4	$\frac{1}{4}$	0.00775	256	1.98

Comparing the two types of collimator for the focal plane of the focusing type where $y = 1$, and $r_2 = 2r_1$, Table V is obtained for a 1-cm radius target.

The taper hole, neglecting penetration, has about twice the resolving power of the cylindrical hole for a value of r_2 equal to the radius of the cylindrical hole. From Table V it can be seen that the optimum radius of the cylindrical hole for the target detection is 1 cm where the figure of merit is 0.725. If the focusing collimator is used, then approximately the same resolving power will be obtainable with a collimator of $r_2 = 2$ cm. For this the figure of merit is 1.63 and it is seen that this offers a better chance for detecting the target than does the cylindrical hole.

The figure of merit will vary with the quantum energy of the incident radiation, if a scintillation detector is used, since the value of C depends upon the crystal efficiency. Thus, the figure of merit will decrease with increasing quantum energy.

In the case of a multi-hole collimator having n equal holes, the axes of which coincide in a point in the focal plane, the value of s_t^2/s_∞ is n times that for the single hole of which the collimator is made. Of course it is important that the detector sensitivity under each hole be equal for this to be true. In many practical cases, to economize in the size of the requisite scintillation crystal, the outer holes of the collimator have a lower sensitivity than those more central. This is the case in the work reported in [2] where the values of s_t^2/s_∞ reported for the different designs of collimator are not self-consistent.

If the criterion of equal sensitivity under each hole can be attained, or a weighting factor is allowed for those holes of lower sensitivity, the above discussion should enable an estimate to be made of the figure of merit of a collimator of known design.

ACKNOWLEDGEMENTS

I am indebted to Mr. R. Doe for the suggestion of the method of subdivision of the integrated area of the plane of the exit pupil in section 2.2. and for making some of the measurements in section 2.3. I wish to thank Mr. R. Dennis for the skill that he has shown in construction of the apparatus used in the work reported here.

APPENDIX I

Glossary of Symbols

C	The counting rate from a unit source on the axis.
C_{NT}	The counting rate from the non-target area.
d	The distance of the source from the collimator axis.
f	The ratio of the number of quanta from a source which penetrate the collimator walls to the number passing through the exit pupil when the source is on the axis.

f_a The ratio of target to non-target activity.

G The geometrical response, the ratio of the area of the exit pupil seen from the source to the area seen when the source is on the axis.

h The perpendicular distance from the source to the plane of the upper face of the collimator.

H The perpendicular distance from the source to the plane of the lower face of the collimator.

k The ratio d/r.

k_t The ratio of the target radius to the collimator radius.

ℓ The collimator length.

p The penetration length in the collimator material.

r Radius of the hole of a cylindrical collimator.

r_1 Radius of the smaller hole of a taper collimator.

r_2 Radius of the larger hole of a taper collimator.

R The radius of the projection from the source of the entrance pupil on the plane of the exit pupil.

s_t The counting rate from a circular plane target when the axis passes through the centre of the target.

s_∞ The counting rate from an infinite plane source of unit activity per unit arc.

T The time during which counts are recorded.

y The ratio ℓ/h.

μ Total linear absorption coefficient of the collimator material.

REFERENCES

[1] BROWNELL, G.L., Int.J.appl.Radiat. 3 (1958) 181 - 192.
[2] DEWEY, W.C. and SINCLAIR, W.K., Int.J.appl.Radiat. 10 (1961) 1 - 16.
[3] SIMONS, H.A.B. and CHOMET, S., Phys.in Med.Biol. 3 (1959) 233 - 254.
[4] KÖNIG, K., Phys.Z. 40 (1939) 46 - 65.
[5] MATHER, R.L., J.appl.Phys. 28 (1957) 1200 - 1207.
[6] SIMONS, H.A.B., Phys.in Med.Biol. 6 (1962) 561 - 576.
[7] MYHILL, J., Int.J.appl.Radiat. 12 (1961) 10 - 19.

STUDIES ON THE RELATIONSHIP OF ORGAN SIZE AND SCANNING PICTURE

R. WOLF AND J. FISCHER
INSTITUTE FOR CLINICAL RADIOLOGY
AND I. MEDICAL CLINIC AND POLICLINIC,
UNIVERSITY OF MAINZ,
FEDERAL REPUBLIC OF GERMANY

Abstract — Résumé — Аннотация — Resumen

STUDIES ON THE RELATIONSHIP OF ORGAN SIZE AND SCANNING PICTURE. The quantitative relationship between scintigram area and cross-section of the organ under investigation has, up to now, been studied only in connection with determinations of the volume of the thyroid gland. In such measurements the accuracy of depiction is in many ways dependent on the equipment used, collimator, background cut-off, scan speed etc. Yagan et al. have introduced a method for determining the size of the liver which utilizes a variable cut-off. For organs such as the thyroid gland and the kidney it is of interest to establish a clear correlation between the X-ray picture or the palpation findings and accumulating and non-accumulating tissue. It is important to know precisely the size relationships, for example, in scintigraphy of the cardio-vascular blood pools. With an organ such as the spleen which may rapidly be altered in size in various diseases the exactitude of the scintigraphic depiction is of decisive importance.

For this reason a series of phantom studies was made to determine the accuracy of the scintigraphic depiction under various conditions. The models used were made of plastic and could be filled with radioactive solutions. The investigations were carried out in air and in water and the effects of changes in concentration of the radioisotopes, as well as of various parameters such as collimator-object distance, cut-off, contrast enhancement, scanning speed, channel width of the spectrometer and the depth of the absorbing water mass over the organ, were studied. A Picker "Magnascanner" was used with two different collimators, 19-hole honeycomb collimator and a 31-hole honeycomb fine-focus collimator. The latter was used only for the thyroid gland.

The results show that the accuracy of the depiction when using the fine-focus collimator is very sensitive to changes in the distance from collimator to object. When using a 19-hole collimator on the other hand the distance is not of great importance. It is advantageous to work with the same maximal pulse rate as far as possible when comparing sizes.

By retaining the same fixed relationships between channel width of the spectrometer, cut-off, pulse rate and scanning speed, a faithful depiction is obtained for large organs such as the spleen.

ÉTUDES SUR LA RELATION ENTRE LES DIMENSIONS DE L'ORGANE ET LE SCINTIGRAMME. On n'a étudié jusqu'à présent la relation quantitative entre la surface du scintigramme et la coupe de l'organe examiné qu'à l'occasion de déterminations du volume de la thyroïde. Dans des mesures de ce genre, la précision de la description dépend à de nombreux égards du matériel utilisé: collimateur, écran contre le bruit de fond, vitesse d'exploration, etc. Pour déterminer les dimensions du foie, Yagan et d'autres ont introduit une méthode utilisant un écran variable. Pour des organes tels que la thyroïde et les reins, il y a interêt a etablir une correlation nette entre l'image formée par les rayons X ou les données de la palpation et le tissu qui fixe ou ne fixe pas le radioisotope. Il importe de connaître de façon précise les rapports de dimensions, par exemple, dans la scintigraphie des réservoirs de sang cardio-vasculaire. Dans le cas d'un organe comme la rate, dont les dimensions peuvent changer rapidement dans diverses maladies, l'exactitude du scintigramme a une importance décisive.

Pour cette raison, on a procédé à une série d'études sur des fantômes pour déterminer l'exactitude du scintigramme dans diverses conditions. Les fantômes utilisés étaient en matière plastique et pouvaient contenir des solutions radioactives. Les expériences ont été faites dans l'air et dans l'eau; on a étudié les effets des variations de la concentration des radioisotopes, ainsi que les effets de divers paramètres: distance du collimateur au sujet, écran, renforcement du contraste, vitesse d'exploration, largeur du canal du spectromètre et épaisseur de la masse d'eau absorbante au-dessus de l'organe. On a utilisé un «Magnascanner» de la société

Picker, avec deux collimateurs différents: un collimateur alvéolaire à 19 trous et un collimateur alvéolaire à 31 trous ayant une faible distance focale. Ce dernier n'a servi que pour la thyroïde.

Les résultats montrent que l'exactitude du scintigramme dépend fortement de la distance du collimateur au sujet lorsqu'on utilise le collimateur à faible distance focale. En revanche, cette distance ne présente pas une grande importance avec le collimateur à 19 trous. Lorsqu'on compare les dimensions, il y a avantage à opérer avec le même nombre maximum d'impulsions.

En maintenant les mêmes rapports fixes entre la largeur du canal du spectromètre, l'écran, le nombre d'impulsions et la vitesse d'exploration, on obtient un scintigramme fidèle pour de gros organes tels que la rate.

ИЗУЧЕНИЕ СООТВЕТСТВИЯ РАЗМЕРА ОРГАНА И ИЗОБРАЖЕНИЯ ЕГО НА СКЕННОГРАММЕ. Количественная взаимосвязь между областью сцинтиграммы и поперечным сечением исследуемого органа до настоящего времени изучалась только в связи с определениями объема щитовидной железы. При таких измерениях точность определения во многих случаях зависит от используемого оборудования, коллиматора, устранения фона, скорости развертки и т.д. Яган с сотрудниками разработал новый метод определения размера печени с использованием различных порогов пропускания. Для таких органов, как щитовидная железа и почки, представляет интерес установить четкое соответствие с рентгеновским снимком или результатами пальпации и аккумулирующей и неаккумулирующей тканью. Важно точно установить размер этого соотношения, например, при сцинтиграфии кровяных депо сердечно-сосудистой системы. Что касается такого органа, как селезенка, размеры которой могут быстро меняться при различных заболеваниях, то точность сцинтиграфического изображения имеет решающее значение.

С этой целью была проведена целая серия исследований на фантоме для определения точности сцинтиграфического изображения при различных условиях. Использовавшиеся модели были изготовлены из пластика и могли заполняться радиоактивными растворами. Исследования проводились на открытом воздухе и под водой; изучались результаты измерения концентрации радиоизотопов, а также такие параметры, как расстояние от объекта до коллиматора, граница пропускания, контрастное увеличение, скорость развертки, пролет каналов спектрометра и глубина водной абсорбирующей массы вокруг органа. Использовался "Магнаскеннер" фирмы Пиккер с двумя различными коллиматорами, коллиматор с 19 ячейками и коллиматор с тонкой фокусировкой, имеющей 31 ячейку. Последний использовался только для щитовидной железы.

Результаты показали, что точность изображения при использовании коллиматора с точной фокусировкой зависит от изменений расстояния от коллиматора до объекта. С другой стороны, при использовании коллиматора с 19 ячейками расстояние не имеет большого значения. Когда сверяются размеры, лучше всего работать при одной и той же максимальной частоте повторения импульсов, насколько это возможно.

При соблюдении фиксированного соотношения между шириной канала спектрометра, порогом пропускания, частотой импульсов и скоростью развертки получают точное изображение таких крупных органов, как селезенка.

ESTUDIOS SOBRE LA RELACIÓN ENTRE LAS DIMENSIONES DE UN ÓRGANO Y EL CENTELLEOGRAMA. Hasta la fecha la relación cuantitativa entre el área del centelleograma y la sección transversal del órgano investigado sólo ha sido estudiada al determinar el volumen de la tiroides. En esas mediciones la exactitud de la representación depende de diversos factores relacionados con el equipo y el colimador utilizados, la supresión de la actividad de fondo, la velocidad de exploración, etc. Para determinar el tamaño del hígado, Yagan y sus colaboradores han ideado un método en el que se recurre a una supresión variable de la actividad de fondo. Para ciertos órganos como la tiroides y los riñones, conviene establecer una neta correlación entre la radiografía o los resultados obtenidos por palpación y la masa de tejido que ha fijado radioisótopos. Es importante conocer exactamente las relaciones de tamaño al efectuar, por ejemplo, la centelleografía de la masa sanguínea del corazón y de los grandes vasos. Cuando se trata de un órgano como el bazo cuyo tamaño puede modificarse rápidamente como consecuencia de distintas enfermedades, la exactitud de la representación centelleográfica es de importancia capital.

Por esta razón, los autores han efectuado una serie de estudios con órganos simulados para determinar la exactitud de dicha representación en diversas condiciones. Para ello han utilizado modelos de material plástico que pueden llenarse de soluciones radiactivas. Las investigaciones se han realizado en el aire y en el

agua, y se han estudiado los efectos que ejercen sobre el órgano los cambios de concentración de los radioisótopos, así como varios parámetros, por ejemplo: la distancia entre el colimador y el objeto, la supresión de la actividad de fondo, el aumento del contraste, la velocidad de exploración, la amplitud del canal del espectrómetro y la profundidad de la masa de agua absorbente situada encima del órgano. Para esas investigaciones se ha empleado un «Magnascanner» Picker con dos colimadores diferentes: un colimador alveolar de 19 canales, y otro de 31 canales de elevado poder de resolución. Este último sólo se ha utilizado para estudios de la tiroides.

Los resultados obtenidos demuestran que la exactitud de la representación centelleográfica cuando se utiliza un colimador de elevado poder de resolución depende mucho de las variaciones de la distancia entre el colimador y el objeto. En cambio, cuando se utiliza un colimador de 19 canales la distancia no es un factor muy importante. En la medida de lo posible, al comparar los tamaños conviene trabajar con el mismo índice máximo de recuento.

Si se mantienen las mismas relaciones fijadas entre la amplitud del canal del espectrómetro, el grado de supresión de la actividad de fondo, el índice de recuento y la velocidad de exploración, se obtienen centelleogramas fieles de órganos de grandes dimensiones como el bazo.

1. INTRODUCTION

A scintigram is intended to furnish information about the position, shape and size of the organ in question and, moreover, on the distribution of the radioisotope within the organ. The information obtained depends to a great extent on the scanning equipment used, and in particular on such factors as the crystal size, the characteristics of the collimator, the possibility of contrast enhancement or reduction of background disturbance etc. In addition a decisive factor, which is inherently coupled with the method, is the statistical variation in the decay of the radioactive material. The error hereby involved can only be decreased in scintigraphy by reducing the scanning speed or increasing the tracer dose. Finally, certain anatomical features may alter the quality of the scintigram in a manner difficult to control. Thus, as a result of the position of the organ, the distance between collimator and the organ may be rarely held constant, and the depth of the absorbing tissue over the organ under investigation varies.

2. FACTORS INFLUENCING THE SIZE OF THE SCINTIGRAM

It must be clearly understood that the fulfilment of all the conditions for obtaining the most faithful picture with respect to shape, size and a high contrast depiction of the radioactivity distribution, may be realized only with great difficulty in one scanning procedure. Attempts to improve the quality of the scintigram by use of the cut-off technique show that it is impossible with only one given level to bring into view the size, shape and any possible accumulation defects. For example, in order to bring out defects in an organ such as the liver a very high cut-off threshold must be selected which, however, leads to reduction in size of the entire scintigram [1, 2, 3]. Therefore, several scannings must be made with different cut-offs, or a magnetic storage equipment must be used and the scintigram made with different background suppressions. Also, by the use of contrast enhancement, a diminution of the picture may result, since in such cases a certain threshold is prescribed. These problems have already been discussed, particularly in connection with scintigraphy of the liver, even though the discussions have been mainly qualitative. It is nevertheless often desirable,

in addition to information on the activity distribution, to obtain definite information about the cross-section of the organ and its relationship to palpable nodes or tumours, or to the radiological findings. In addition, repeated examinations should provide exact information about changes in size.

The possibility of determining the area of a scintigram by planimetry depends on several factors. First, a good outline contrast is essential in order to determine the exact limits from the background. Outline contrast is improved by the use of background suppression. Nevertheless, in order to obtain a proper cut-off setting, the difference in pulse rate between the background and the thinnest parts of the organ must be sufficiently great. In other words, the difference must be such, that for a given scanning speed the statistical variation is not so large that a definite limitation between organ activity and background activity is no longer possible. Moreover, the inevitably limited resolution power of the collimator does not permit a sufficiently rapid increase in count-rate when passing over a sharply defined activity edge but, instead, only allows a continuous transition. Moreover, the equipment controlling the contrast enhancement is regulated mostly by the output voltage of a ratemeter. Thus, the damping of the ratemeter is an important factor. According to the extent of damping and the scanning speed, a certain displacement in the registered lines results since a certain time elapses before the threshold value is reached (Fig. 1). The extent of the line displacement is not constant but is dependent on the difference in pulse rate. The equilibrium time of a ratemeter is given by the formula

$$T = \tau\,(1/2\ \ln 2n\tau + 0.394),$$

where

τ = time constant
n = count-rate.

Therefore, the extent of line displacement increases with increasing difference in pulse rate. For a good outline contrast, however, a sufficiently large difference in count-rates is desirable. Since the damping of the rate is inevitable, the only possibility left for reducing line displacement is the reduction in scanning speed in conjunction with a small time constant. However, in the interest of the patient, especially in examining a large organ, there are certain sharp limits imposed. Some extent of line displacement must therefore be tolerated. In a meander form of scanning, this line displacement occurs in opposite directions for each second line. Thus, a certain compensation is afforded in the entire picture. In planimetry the mid-distance of the ends of two lines may be taken as the edge or outline of the organ. Systems have been described by means of which the contrast may be enhanced without lag in registration and so this difficulty may be avoided [4, 5], but most of the commercially available scanners employ the ratemeter.

A further question is that of reduction of dot frequency. It would be desirable to have in the maximal count region just as many dots or dashes printed per centimetre as may be resolved by the eye. In this way the activity differences may best be recognized. On the other hand, this leads

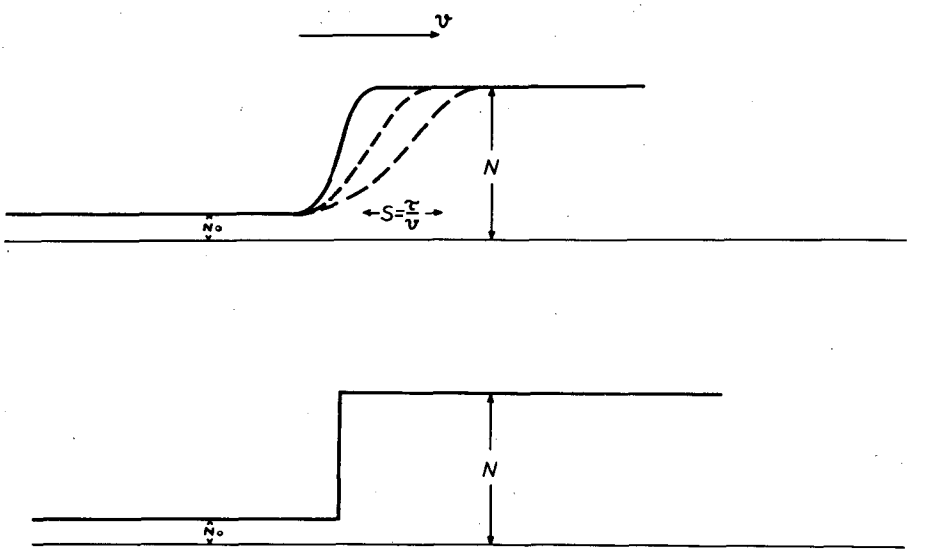

Fig. 1

Increase of count-rate during the transition of a sharp activity margin

——— Influence of the finite degree of resolution of the collimator
------ Influence of various extent of damping of the ratemeter

to a great reduction in the number of dots in the thinnest marginal region of the organ, and so to an increase in outline fluctuations. In determining the size of an organ, it would be useful to select the conditions for the dot registration in such a way that separation of the dots is no longer possible in the maximum activity area when, by doing so, the outline contrast is increased. This can be done particularly when two separate systems are available for registration, such as a stylus system and a photoregistration, whereby the one may be used for determining the size of the organ and the other with contrast enhancement for determining differences in the accumulation of radioactivity in the organ.

Apart from the factors discussed above, the characteristics of the collimator used is a decisive factor in determining the organ size by scintigraphy. On the one hand, the degree of resolution of the collimator together with the damping of the ratemeter and the scanning speed determine the outline sharpness. On the other hand, in cases where the distance between object and detector varies considerably because of anatomical conditions, the depth of focus is important. In our investigations we used a Picker-Magnascanner, which is equipped with two different collimators. The focus-collimator distance for both is about 6 cm in water. The 31-hole fine-focus collimator has a depth range of about 2 cm at the 100% isoresponse level and the 19-hole honeycomb collimator a depth range of about 4 cm at the 80% isoresponse level. The degree of resolution of the fine-focus collimator is, of course, correspondingly greater.

3. EXPERIMENTAL PROCEDURE

Our investigations were carried out on phantoms. There was a number of thyroid gland, spleen and liver models available. The phantoms were made from moulds prepared from organs of human corpses. They are made of plastic, are hollow and may be filled with radioactive fluid. Details of studies on the thyroid gland will not be given here, since they have been fully treated elsewhere [6]. The cross-section of the organ models were determined from X-ray pictures, taken at great FSD (focus-skin distance), in which the surface area was measured with a planimeter. The scintigrams were measured in the same manner with proper consideration of the above-mentioned criteria. Measurements were made on the phantoms in air and in water. Under these conditions, variations of cut-off, contrast enhancement, distance collimator-object, maximal count-rate, the relationship of maximal count-rate to background etc., were investigated. For our experiments, the isotopes Cr^{51}, I^{131} and Au^{198} were used.

4. RESULTS

4.1. Influence of the collimator-object distance

Apart from the characteristics of the equipment the results of the scintigraphy are dependent on the existing count-rate distribution over the organ. For a given activity distribution the pattern varies with the distance of the collimator from the object. By varying this distance a corresponding change in count-rate does not occur over each separate point to the same extent. The reason for this lies in the nature of the isoresponse curve of the collimator. By increasing the collimator-object distance over the middle of the object (in air) the count-rate at first increases somewhat and then hardly decreases since, with increasing distance, greater portions of the organ come within the focal angle of the collimator. On the other hand, over a marginal area a corresponding decrease in count-rate with increasing distance appears (Fig. 2). If the phantom is submerged in water, a count-rate decrease is observed over both central and marginal areas with increasing object-collimator distance, but the decrease occurs later in the central area than in the marginal one. Therefore, the count-rate pattern varies with collimator-object distance and with the depth of the absorbing layer over the organ.

With an organ such as the thyroid gland, the absorption over the organ is practically insignificant, but changes in object-collimator distance produce considerable changes in the size of the scintigram (Fig. 3). With increasing distances these variations are more noticeable when using the 31-hole fine-focus collimator than with the 19-hole collimator.

Alterations in object-collimator distance are of little significance for large organs. In air, an increase in the distance produces little change in scintigram area (Fig. 4). In water, the absorption by the layer over the organ produces a reduction in scintigram area, but this reduction may be avoided when an increased dose of radioisotope compensates for the absorption loss, and in each case the same maximal count-rate is used.

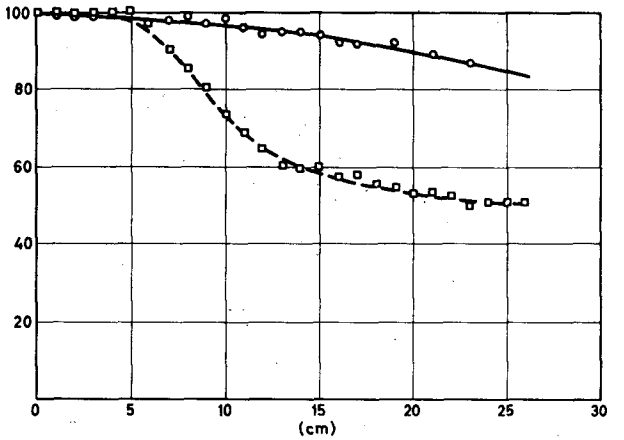

Fig. 2

Variations of the count-rate with collimator-object distance over a broad object (in air)

——— over the centre of the phantom
------ over the marginal region

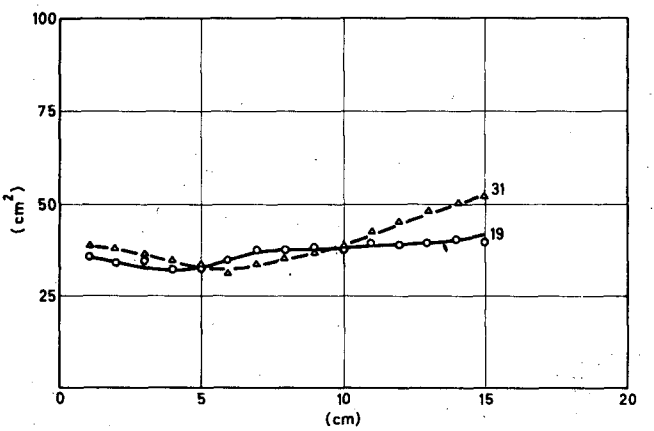

Fig. 3

Variations of the scintigram area of a thyroid gland model in changes of collimator-object distance

——— 19-hole honeycomb collimator
-------- 31-hole honeycomb collimator

With a change in object-collimator distance of 5 to 10 cm as occurs in practice, one can in this way achieve reproduceable results.

4.2. Influence of cut-off

It may be readily seen that, in the case of an organ such as the thyroid gland that is subject to a number of morphological changes which are re-

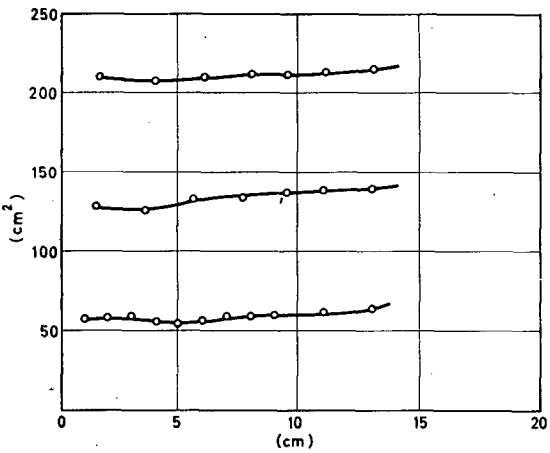

Fig. 4

Dependence of scintigram area on collimator-object distance for various spleen models (Volume: 115, 435 and 1065 cm³)
Corresponding areas of the X-ray pictures: 51, 133 and 208 cm².

flected in the scintigram, the use of the background cut-off may produce a reduction in area which is difficult to control. A size estimation is only possible when sufficiently high activity accumulation is present in all parts of the gland and a low cut-off is selected.

These relationships also apply accordingly for other organs such as the liver. The difference in thickness between the two lobes as well as the possible variations in form also increase the difficulty of size estimation when using the cut-off [1, 2, 3]. Figure 5 shows the relationship of scintigram area to selected cut-off for three different models and in comparison with the corresponding areas of X-ray pictures. With increasing cut-off there is a corresponding reduction in the scintigram area. With low cut-off the scintigram area is somewhat larger than the X-ray picture. On the other hand the spleen offers an advantage in so far as the general form remains practically unchanged even when there is a great alteration in size. Changes in cut-off therefore do not lead to such great differences in scintigram area as is the case with other organs. With increasing activity accumulation in the organ, i.e. with increasing maximal count-rates, there is an increasing enlargement of the scintigram area for a low cut-off (Fig. 6). The area of the scintigram is also dependent on the relationship of the maximal count-rate over the organ and to the pulse rate of the background for a low cut-off since, with increasing background, the distinction of the object from the background becomes more difficult and in extreme cases may ultimately be impossible (Fig. 7).

4.3. Choice of channel width

The selected channel width of the spectrometer has a certain influence on the scintigram area. The isoresponse curves, and therefore the degree

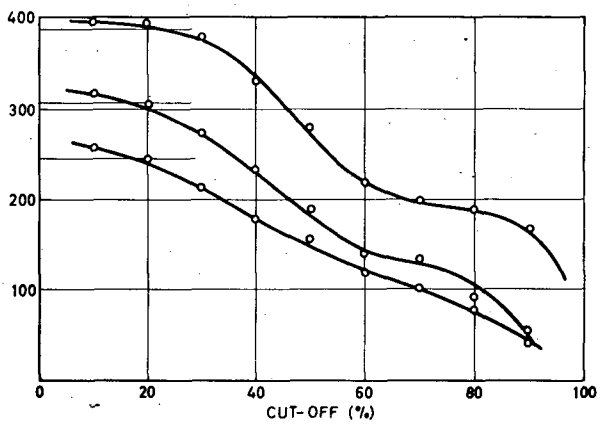

Fig. 5

Variations of scinitgram area with cut-off for three different liver phantoms (1265, 1980, 2530 cm³)
Horizontal lines: Area of the X-ray picture.

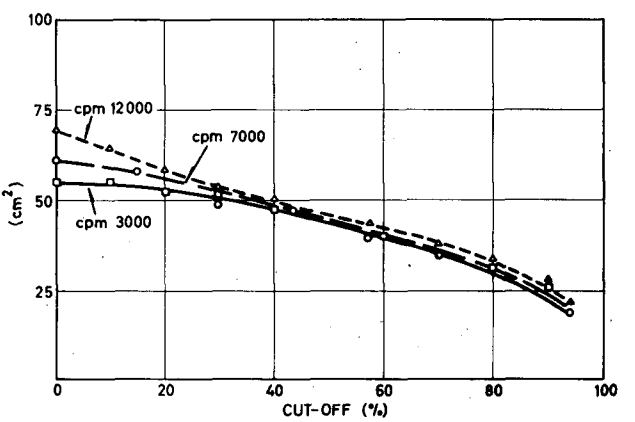

Fig. 6

Variations of scintigram area with extent of cut-off on a spleen model with different activity concentrations

of resolution of the collimator, are dependent on the window width of the pulse-height analyser as has already been pointed out by TUBIANA and ALBAREDE [7].

Moreover the radiation over the organ and the stray radiation near the organ possess completely different spectra (Fig. 8) so that the relationship of effective rays and background rays changes with the channel width, which is again reflected in the scintigram.

By varying the discriminator range, while holding other conditions constant, an increase in scintigram area results from a reduction in the lower discriminator threshold (Fig. 9).

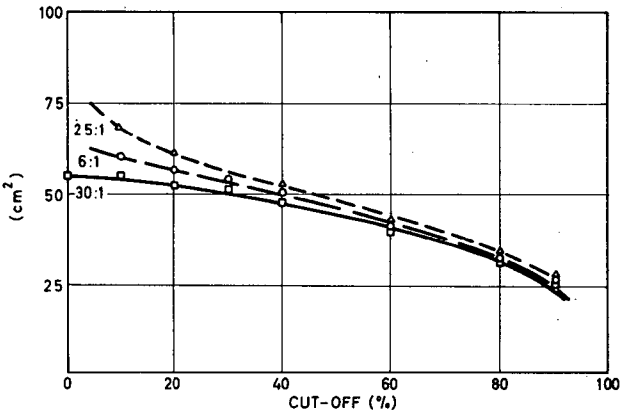

Fig. 7

Variations of scintigram area for variable ratio between organ and background activities

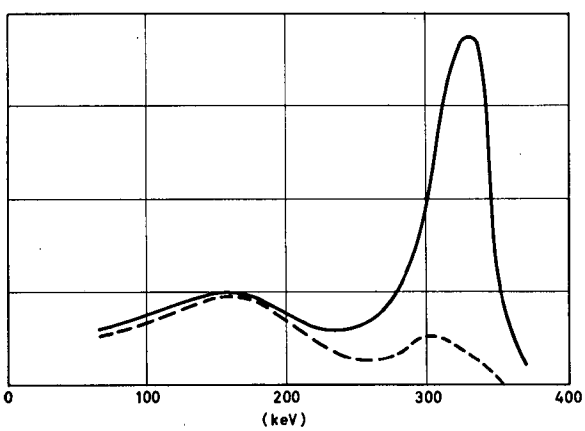

Fig. 8

Chromium (Cr^{51}) spectrum over the organ (——) and the spectrum of the stray radiation measured in the immediate vicinity of the organ (---), normalized on the same level of the Compton peak

4.4. Scanning speed and damping of the ratemeter

No change in scintigram area results from changes in scanning speed, since the line displacement occurs in both directions and so is compensated for. The same holds for damping the ratemeter as long as extremely high damping settings are not chosen.

5. CONCLUSIONS

In summary the following may be said:

(1) When using contrast enhancing systems the area of the scintigram depends on the selected cut-off and the extent of contrast enhancement.

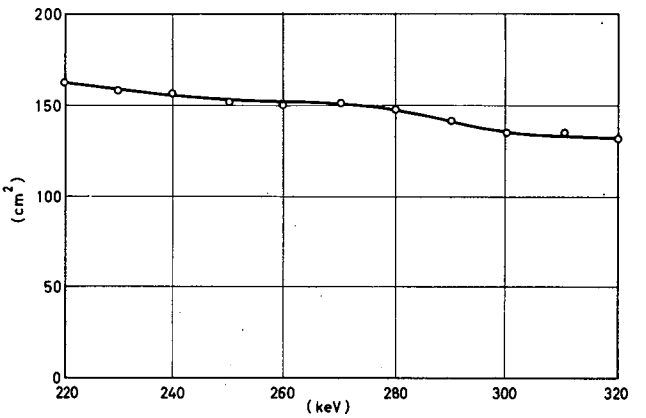

Fig. 9

Changes in scintigram area by variations of the lower discriminator threshold (using Cr^{51})

(2) For the most precise determination of size as well as the detection of defects, a sufficiently high concentration of the radioisotope must be present in the organ, i.e. the count-rate difference between the organ, including its peripheral region and the background, must be sufficiently great with respect to the statistical fluctuations possible under the given scanning conditions, in order to permit a clear distinction of the organ from its surroundings when using a low cut-off.

(3) Changes in distance between collimator and organ produce no appreciable effect in the scintigram for large organs.

(4) Size estimation should be carried out under the same conditions as far as possible, including the same maximal count-rate.

(5) Under these conditions a reliable comparison of the size of organs with a regular shape, such as the spleen, is possible.

REFERENCES

[1] CHRISTIE, J.H., MACINTYRE, W.J., GOMEZ CRESPO, G. and KOCHWESER, D., Radiology 81 (1963) 455.

[2] YAGAN, R., MACINTYRE, W.J., CHAMBERLAIN, W.B. and CHRISTIE, J.H., J. nucl. Med. 2 (1961) 151.

[3] YAGAN, R., MACINTYRE, W.J. and CHRISTIE, J.H., Amer. J. Roentgenol. 88 (1962) 289.

[4] HAWLIZEK, F. and ZITA, R., Nukl.-Med. 3 (1963) 315.

[5] PRAEG, R., Strahlentherapie 119 (1962) 569.

[6] TICHBI, E., Diss. Mainz (1964).

[7] TUBIANA, M. et ALBAREDE, P., Ann. Radiol. 5 (1962) 173.

BIBLIOGRAPHY

ALLEN, H.C. and GOODWIN, W.E., Radiology 38 (1952) 68.

BAUER, F.K., GOODWIN, W.F., LIBBY, R.L. and CASSEN, B., J. Lab. clin. Med. 39 (1952) 153.

BENDER, M.A. and BLAU, M., Int. J. appl. Rad. 4 (1959) 154.

BROWNELL, G.L., Int. J. appl. Rad. 3 (1958) 181.
BROWNELL, G.L., Medical Radioisotope Scanning, IAEA, Vienna (1959) 1.
CHRISTIE, J.H. and MACINTYRE, W.J., Radiology 79 (1962) 472.
DEWEY, W.C. and SINCLAIR, W.K., Int. J. appl. Rad. 10 (1961) 1.
DOERING, P. and KRAMER, K., Strahlentherapie 105 (1958) 245.
ENDLICH, H.L., Amer. J. Roentgenol. 87 (1962) 156.
FISCHER, J. and WOLF, R., Dtsch. med. Wschr. 88 (1963) 305.
FISCHER, J. and WOLF, R., Acta Hepato-Splenol. 10 (1963) 209.
FISCHER, J. and WOLF, R., Dtsch. med. Wschr. 88 (1963) 1430.
FISCHER, J., SEVERIN, G. and WOLF, R., Acta radiol. (Stockh.) (In press).
FOLICHON, A. et GANDY, A., J. Radiol. Electrol. 37 (1956) 334.
GOMEZ CRESPO, G., MACINTYRE, W.J. and CHRISTIE, J.H., Amer. J. Roentgenol. 88 (1962) 296.
GOODWIN, W.E., CASSEN, B. and BAUER, F.K., Radiology 61 (1953) 88.
GROS, C.M., KEILING, R. et BURGY, P., Ann. Radiol. 5 (1962) 1.
GROS, C.M. et KEILING, R., J. Radiol. Electrol. 42 (1961) 297.
HERRING, C.E., J. nucl. Med. 1 (1960) 83.
HOLZBACH, R.Th., CLARK, R.E., SHIPLEY, R.A., KENT, W.B. and LINDSAY, G.E., J. Lab. clin. Med. 60 (1962) 902.
HORST, W., THIEMANN, K.J. and TRALAU, G., Fortschr. Roentgenst. 93 (1960) 343.
JOHNS, H.E. and CEDERLUND, J.F., Medical Radioisotope Scanning, IAEA, Vienna (1959) 41.
KAKEHI, H., Medical Radioisotope Scanning, IAEA, Vienna (1959) 13.
KAUFMANN, G. and ERNST, H., Strahlentherapie 107 (1958) 493.
KELLY, F.J., J. clin. Endocr. Metab. 14 (1954) 326.
KROHMER, J.S. and BONTE, F.J., Amer. J. Roentgenol. 88 (1962) 269.
KUHL, D.E., CHAMBERLAIN, R.H., HALE, J. and GORSON, R.O., Radiology 66 (1956) 730.
LIBBY, R.L., J. Clin. Endocrin. Metab. 14 (1954) 1265.
MACINTYRE, W.J. and HOUSER, T.S., Amer. J. Roentgenol. 77 (1957) 471.
MACINTYRE, W.J., FRIEDELL, H.L., GOMEZ CRESPO, G. and REJALL, A.M., Radiology 73 (1959) 329.
MACINTYRE, W.J., GOMEZ CRESPO, G. and CHRISTIE, J.H., J. Nucl. Med. 1 (1960) 262.
MACINTYRE, W.J., REJALL, A.M., CHRISTIE, J.H., GOZZ, F.S. and HOUSER, T.S., Int. J. appl. Rad. 3 (1958) 193.
PICCHIO, C., Minerva nucleare (Torino) 5 (1961) 339.
PRAEG, R., Strahlentherapie 110 (1962) 3.
WEBER, M.M., Int. J. appl. Rad. 5 (1959) 71.
WINKLER, C., Fortschr. Roentgenstr. 90 (1959) 387.
WINKLER, C. and SCHEPERS, H., Nukl.-Med. 2 (1961) 67.
WOLF, R., Tag. Sudwestd. u. Hess. Roentgenol. Pforzheim, (October 1962).
WOLF, R., Dtsch. Krebskongress Mainz, (September 1963).
WOLF, R. and FISCHER, J., Fortschr. Roentgenstr. (In press).

THE EVALUATION OF STRAIGHT-BORE, TAPERED AND FOCUSING COLLIMATORS AS A FUNCTION OF GAMMA-RAY ENERGY

W. J. MacINTYRE, J.H. CHRISTIE AND I. TATSUNO
HIGHLAND VIEW HOSPITAL, CLEVELAND, OHIO,
UNITED STATES OF AMERICA

Abstract — Résumé — Аннотация — Resumen

THE EVALUATION OF STRAIGHT-BORE, TAPERED AND FOCUSING COLLIMATORS AS A FUNCTION OF GAMMA-RAY ENERGY. In the choice of one collimator or type of collimator over another for scanning purposes, either isoresponse curves or the geometric response to a point source has been previously utilized as a basis of evaluation. While this technique is helpful in a comparison of resolution between focusing collimators, extrapolation of the results to the extended sources that are of interest in scanning is extremely difficult.

For this reason, comparison of various collimators has been made with a phantom consisting of a series of flat, cylindrical discs which can be filled with radioactive material alone or displaced by a defect of specific size. This phantom has made it possible to measure the counting-rate contribution from each segment of an extended source as well as the drop due to the defect placed at various distances from the collimator. Summation of any number of such contributions then reflects the response of any desired focus of interest in the midst of any desired environment.

By this system, comparisons have been made of both counting rates and spatial resolution of straight-bore, tapered and focusing collimators. For example, a seven-hole focusing collimator of 3-in-length holes tapering from ½ in at the top to ¼ in at the bottom exhibits the same counting rate from these extended sources as a 3-in long 0.54-in diam. straight-bore collimator.

Varying the gamma-ray energy has demonstrated what fraction of the counting rate is due to intraseptal penetration of the focusing collimators in addition to the self-absorption and scatter of the phantom. The study has indicated that no one collimator is necessarily optimal for all purposes but that whereas one collimator may be superior to another in the detection of one type of defect at one energy, the converse may be true for another type at another energy.

ÉVALUATION DE COLLIMATEURS A OUVERTURE CYLINDRIQUE, A OUVERTURE CONIQUE ET A FOCALISATION EN FONCTION DE L'ÉNERGIE DU RAYONNEMENT GAMMA. Dans le choix d'un collimateur ou d'un type de collimateur, on s'est fondé jusqu'à présent sur les courbes d'isoréponse ou sur la réponse géométrique à une source ponctuelle. Bien que cette méthode soit très utile pour comparer la résolution de collimateurs à focalisation, il est extrêmement difficile de faire une extrapolation des résultats pour les sources en volume auxquelles on a affaire dans la pratique.

C'est pourquoi les auteurs ont comparé divers collimateurs au moyen d'un fantôme formé d'une série de disques plats et cylindriques qui peuvent être remplis uniquement de matière radioactive ou contenir une «défectuosité» de grandeur connue. Ce fantôme a permis de mesurer la contribution au taux de comptage de chaque segment d'une source non ponctuelle, de même que la diminution de ce taux due à une défectuosité placée à diverses distances du collimateur. La somme d'un nombre quelconque de contributions reflète la réponse pour le foyer considéré dans le milieu ainsi déterminé.

De cette façon, les auteurs ont comparé à la fois les taux de comptage et la résolution spatiale de collimateurs à ouverture cylindrique, à ouverture conique et à focalisation. Par exemple, un collimateur à focalisation à sept canaux d'une longueur de 7,5 cm et ayant une ouverture de 0,63 cm à la base et de 1,25 cm à l'extrémité accuse le même taux de comptage pour une source en volume qu'un collimateur à ouverture cylindrique de même longueur et ayant un diamètre de 1,33 cm.

En faisant varier l'énergie du rayonnement gamma, les auteurs ont déterminé la fraction du taux de comptage qui est due à la pénétration à travers les parois des collimateurs à focalisation, ainsi qu'à l'auto-absorption et à la dispersion dans le fantôme. L'étude a montré qu'aucun collimateur n'est optimum pour

tous les besoins; de plus, si un collimateur peut être supérieur à un autre pour la détection d'une défectuosité à une certaine énergie, l'inverse peut être vrai pour une autre défectuosité à une autre énergie.

ОЦЕНКА ЦИЛИНДРИЧЕСКИХ, КОНИЧЕСКИХ И ФОКУСИРУЮЩИХ КОЛЛИМАТОРОВ В ЗАВИСИМОСТИ ОТ ЭНЕРГИИ ГАММА-ЛУЧЕЙ. При выборе коллиматора или типа коллиматоров из ряда других для целей сканнирования до сих пор в качестве базы для оценки использовались или кривые равных ответных реакций или геометрические ответные реакции. Хотя этот метод и полезен для сравнения разрешающей способности разных фокусирующих коллиматоров, экстраполяция этих результатов на используемые для сканнирования протяженные источники чрезвычайно затруднительна.

Поэтому сравнение различных коллиматоров было произведено на фантоме, состоящем из ряда плоских цилиндрических дисков, которые могут заполняться либо только радиоактивным материалом, либо меняться в результате дефекта определенного размера. Такой фантом дает возможность измерять долю скорости счета от каждого участка протяженного источника, а также спад, вызываемый дефектом, помещаемым на различные расстояния от коллиматора. В таком случае сложение любого числа таких долевых скоростей счета отражает ответную реакцию в любой точке изучаемого места в любой желательной среде.

Этот метод был использован для сопоставления как скоростей счета, так и пространственной разрешающей способности цилиндрических, конических и фокусирующих коллиматоров. Так, например, фокусирующий коллиматор с семью каналами длиной 7,5 см и диаметром, сходящим с 1,25 см в верхней части на 0,6 см в нижней части, дает такую же самую скорость счета излучения этих протяженных источников как цилиндрический коллиматор длиною 7,5 см и с внутренним диаметром 1,3 см.

Изменение энергии гамма-лучей показало, какая доля скорости счета приходится на проникновение фокусирующих коллиматоров во внутрь в дополнение к самопоглощению и к рассеянию в фантоме. Это исследование показало, что ни один из коллиматоров не может быть оптимальным для всех надобностей, но что один коллиматор может превосходить другой при обнаружении дефекта определенного вида при одном уровне энергий, тогда как обратное может быть справедливым для другого типа коллиматоров и при другом уровне энергий.

EVALUACIÓN DE COLIMADORES ENFOCADOS DE CANALES CILÍNDRICOS O CÓNICOS EN FUNCIÓN DE LA ENERGÍA DE LOS RAYOS GAMMA. Para la exploración centelleográfica la selección del colimador o del tipo de colimador se había efectuado hasta ahora utilizando como base de evaluación las curvas de isorrespuesta o la respuesta geométrica a una fuente puntiforme. Esta técnica es útil para comparar el poder de resolución de los colimadores enfocados, pero resulta muy difícil extrapolar sus resultados a las fuentes extensas que se presentan en la práctica.

Por este motivo, los autores han comparado diversos colimadores utilizando un simulador constituído por una serie de discos planos, cilíndricos, que pueden llenarse de material radiactivo exclusivamente o incorporando a dicho material "defectos" de un tamaño determinado. Este simulador ha permitido medir la contribución al índice de recuento de cada segmento de una fuente extensa, así como la disminución debida a la presencia de un defecto a diversas distancias del colimador. La suma de estas contribuciones refleja entonces la respuesta a la fuente de que se trate, rodeada de un material que se puede escoger libremente.

Por este sistema se han comparado los índices de recuento y la resolución espacial de colimadores enfocados con canales cilíndricos o cónicos. Por ejemplo, un colimador enfocado de 7 canales cónicos de 3 pulg de longitud, ½ pulg de diámetro en la parte superior y ¼ pulg en la inferior, da con estas fuentes extensas el mismo índice de recuento que un colimador de 3 pulg con canales cilíndricos de 0,54 pulg de diámetro.

La penetración a través de los tabiques del colimador enfocado, así como la autoabsorción y la dispersión en el simulador son factores que influyen en el índice de recuento; variando la energía de los rayos gamma se ha podido evaluar la contribución del primero de estos factores. El estudio ha indicado que ningún colimador es necesariamente óptimo para todos los fines; un colimador puede ser superior a otro para la detección de un tipo de defecto a una energía determinada, pero para otro tipo de defecto y para otra energía puede muy bien ocurrir lo contrario.

In the selection of a collimator for radioisotope scanning, the primary objective is to obtain the maximum differential between the site of interest and its surrounding environment while maintaining a total counting rate suf-

ficient to permit a statistically accurate portrayal of this differential. It would be ideal to select a collimator whose visual field subtended the smallest solid angle or, in other words, which had the finest possible spatial resolution. Such a collimator would then be equally useful for the visualization of both small and large areas of counting-rate change. Unfortunately, spatial resolution is only a part of detection ability in radioisotope scanning. The other parameter is counting rate, which ultimately must represent the limiting factor in visualization. Counting rate is, of course, dependent upon patient dose limitations which control the total number of counts introduced for any particular radioisotope procedure. From patient considerations scanning time is likewise limited.

Counting rate is controlled primarily by the size of the visual field of the collimator. Unfortunately, as this visual field is made smaller in order to detect small regions of non-homogeneity, there is a drastic reduction in counting rate. Because of counting rate or statistical limitations, in the visualization of counting rate variation it is quite possible for a collimator with a finer spatial resolution to be much inferior with respect to detection ability in comparison with a collimator of coarser spatial resolution.

In the evaluation of collimators for radioisotope scanning it has been customary to measure the response of a collimator to a point source, i.e., to obtain isoresponse curves. This method of evaluation, while useful in the laboratory, has two major disadvantages in the evaluation of collimators for clinical scanning. First, scanning is always concerned with the differentiation of counting rates of extended sources, thus, isoresponse curves must be integrated over the volume of interest to be meaningful. Second, these curves are difficult to extrapolate information as to the counting rate efficiency of the collimator over a volume source.

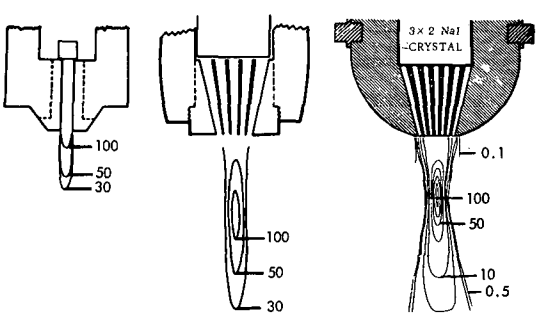

Fig. 1

Isoresponse curves of ½-in straight bore, a 19-hole lead collimator (Picker X-ray Model 2107), and the 37-hole ORNL gold-tungsten collimator. Radiology 79 (1962) 472-482, and Progress in Medical Radioisotope Scanning, TID 7673 (1963) 52.

For example, in Fig. 1, vastly different isoresponse curves are shown for a ½-in straight-bore lead collimator [1], and the Oak Ridge National Laboratory 37-hole gold-tungsten [2] collimator of the same length. While the isoresponse curves show easily recognizable differences, it is not at all obvious as to what variation clinical scans would exhibit.

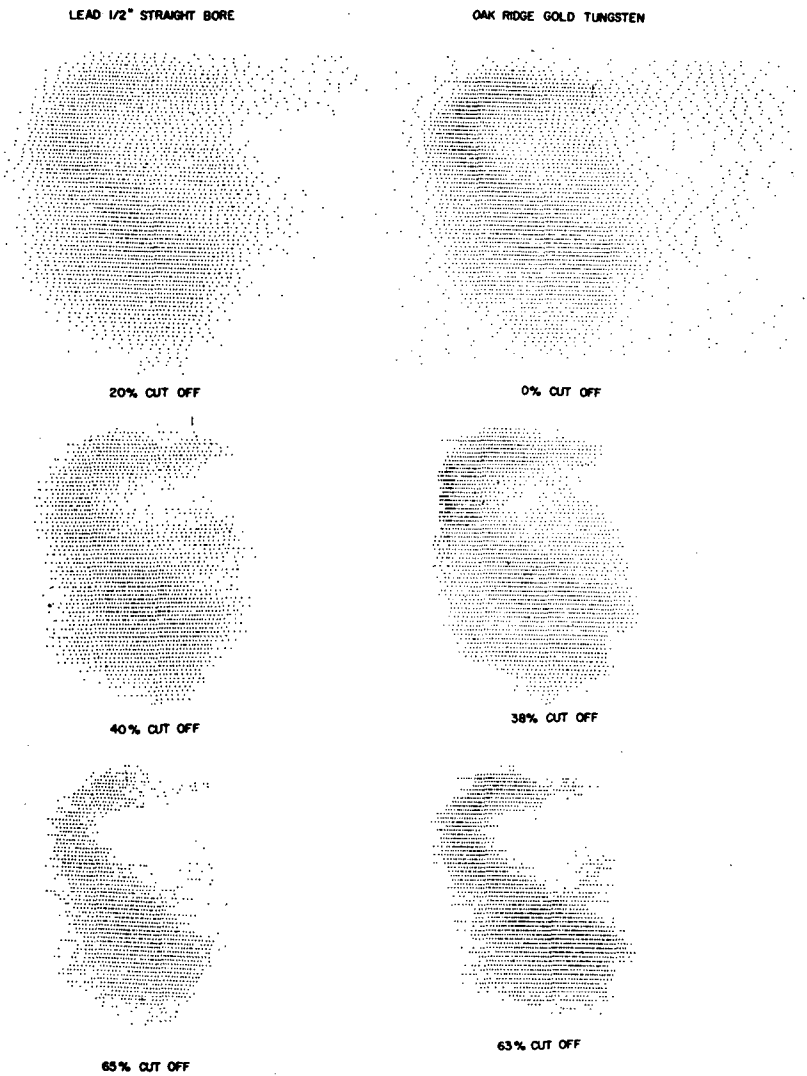

Fig. 2

Liver scans of a patient with metastatic carcinoma scanned with 0.3 mc of colloidal Au^{198} administered to the patient. Comparison of ½-in straight-bore lead and 37-hole gold-tungsten collimator. Radiology 79 (1962) 472.

In Fig. 2, liver scans of the same patient are shown as recorded from these two collimators [1]. It is seen that there is very little difference between the scans except at the lower cut-off level where it was necessary to use a 20% cut-off with the straight-bore collimator in order to reduce the effect of lateral penetration due to inadequate shielding.

Quantitative evaluation of the collimators by such clinical scans is, of course, not feasible. In fact, evaluation of collimators by any type of scan

is inherently difficult because of the problems of the quantification of scan records as well as the non-linearity of response of any accentuation factor that might be used.

As a first approach to an examination of why greater differences were not perceived between the two radically different collimators, measurements were made with the rather simple phantom shown in Fig. 3. This phantom

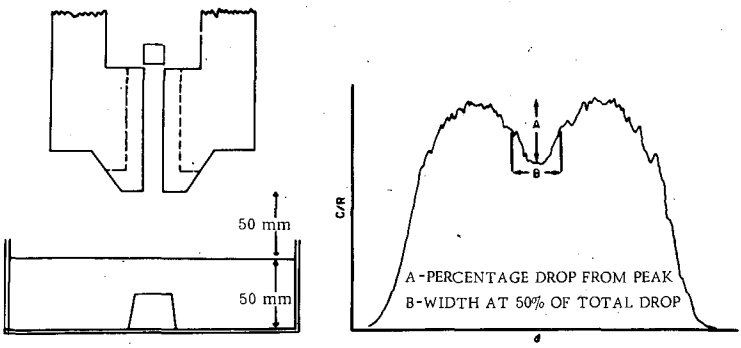

Fig. 3

Schema of simple phantom used to evaluate the straight-bore and 37-hole focusing collimator
On profile on right, line A shows percentage decrease used.
Radiology 79 (1962) 472.

was devised to show the change in counting rate by means of a profile recording over a volume source in which had been placed a 1-in-diam. displacement. The profile on the right is an example of the profile obtained by passing the detector laterally across the phantom. (A) refers to the maximum percentage drop and (B) refers to the width at half maximum. Figure 4 shows the comparative profiles of the two different collimators used in the clinical comparison. It is apparent that the differences in the profiles more nearly reflect the modest improvement in clinical scans than do the iso-response curves.

Since the decrease over the defect is so small in such a phantom, it is difficult to obtain quantitative measurements over larger phantoms of dimensions comparable to the organs of interest. While an appreciable decrease is attained for a 1-in defect in a 2-in-deep phantom, more challenging examples are much more difficult. For example, a 1-cm-thick defect in a 15-cm phantom will displace no more than 6.7% of the volume and consequently, assuming uniform response, no more than 6.7% of the counting rate. This is far beyond the identification of most counting-rate differentials in clinical scanning. This is not to say that such defects cannot be visualized in phantom scanning. Indeed, a 1% change may be visualized with proper cut-off or film accentuation techniques and with adequate counting rates. There is no organ homogeneity in clinical scanning that would make such identification practical, however. Nevertheless, measurements of such accuracy can be important for the accurate comparison of collimators with reference to their response to various sized areas of counting-rate changes at various depths within an extended source and with widely varying radioisotope energies.

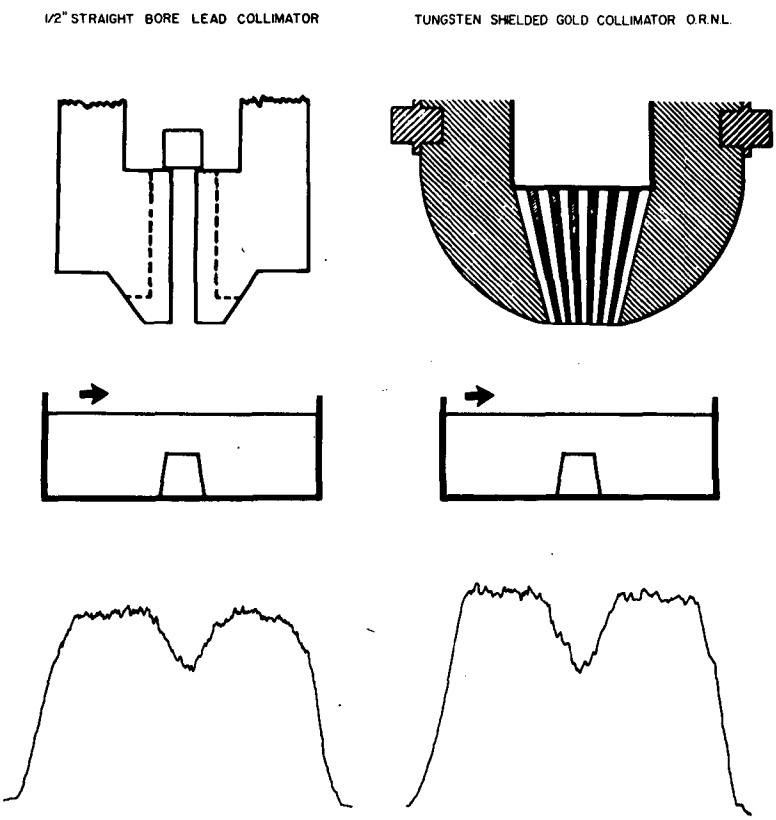

Fig. 4

Comparative profiles of straight-bore and 37-hole collimator over phantom of Fig. 3. The counting-rate of the straight bore dropped 31% while that from the focusing collimator dropped 37%. Actual volume displacement is approximately 50%.

To obtain such measurements with the greatest possible accuracy it was decided to evaluate the contribution of individual sections of an extended source by separating these contributions into 1-cm-thick segments. Only one of these segments contains radioactive material. Within it was placed a volume of varying size containing either no radioactivity or increased radioactivity. The other segments contain water or a tissue equivalent material.

Using this phantom accurate overall counting-rate changes of 6.7%, as used in the previous example, are quite possible to measure and, while admittedly such accuracy is not practical in clinical scanning, the comparison with other collimators of equal counting-rate efficiency, or with another radioisotope of different energy which shows only a 3% change may be important.

The primary reason for using a segmented phantom is to determine not only how many counts are received but specifically from what region they are being received. In a volume or large organ phantom only the sum-

mation from all thicknesses is known. In the segmented phantom the same total is recorded by summating the counts from the radioactive segment placed in each position. In addition, exact knowledge of the contribution from each segment is obtained. The selection of a 1-cm thickness, while somewhat arbitrary, represents a compromise segment that is thick enough to be practical while thin enough not to cause uncertainty as to the origin of the counts. By filling only one disc with radioactivity and the rest with water or a tissue equivalent material, the site of interest may be measured with optimal accuracy while still maintaining extended source conditions of absorption and scattering.

While the measurement of discs at all levels gives exact information as to what fraction of the total counting rate is derived from each level, it does not reveal whether the counting rate obtained is desirable; that is, received through the collimator; or undesirable, received through the septa, side shielding, or from an adjacent area through Compton scattering. To answer this question a defect or void is placed in the segment containing the radioactivity. The counting rate over the radioactivity is then compared with that obtained with the collimator centred over the void. For a collimator whose projected solid angle is no greater than the defect size the counting rate should drop to zero. Any counting rate greater than zero indicates that either some of the counts are received through the shielding, are the result of Compton scattering, or that the solid angle subtended by the collimator is not perfectly matched and is indeed larger than the defect size.

It is obvious that the same information could be obtained by filling the central volume of the segment with increased radioactivity rather than a void. In this case, with a similarly matched collimator, the counting rate over the central volume would be increased and should be in the exact ratio of the radioactive concentrations of the two regions. With the discs containing the voids, the counting rates due to a region of increased activity may be easily calculated by merely subtracting the counting rate with the collimator over the void from the counting rate over the periphery. Whichever system is used, either voids or regions of increased radioactivity, is a matter of personal choice and is immaterial. The importance of these measurements is to ascertain both the counting rate that is received from each segment of an extended volume source and to determine whether it is from the site of interest or from elsewhere. By obtaining this information through a summation of segments, not only can the contributions of each segment be known with high accuracy but the origin of the differences of counting rates and differentials may be derived.

A photograph of a phantom designed to obtain these data is shown in Fig. 5. The discs are 15 cm in diam. and 1 cm thick. One of the discs is filled with a solution of radioactive material and is placed at various levels with the additional discs filled with water to act as absorbing and scattering media. The additional disc seen on the left may contain either central solid or hollow inserts of various sizes.

The use of this phantom is illustrated by the schematic drawing in Fig.6. Nine of the discs contain water with the tenth containing an inactive void in a radioactive solution. The scanner head is passed over the mid portion of the phantom with the profile of the counting rate recorded on an X-Y recorder. While the phantom is scanned at all ten levels the profiles shown

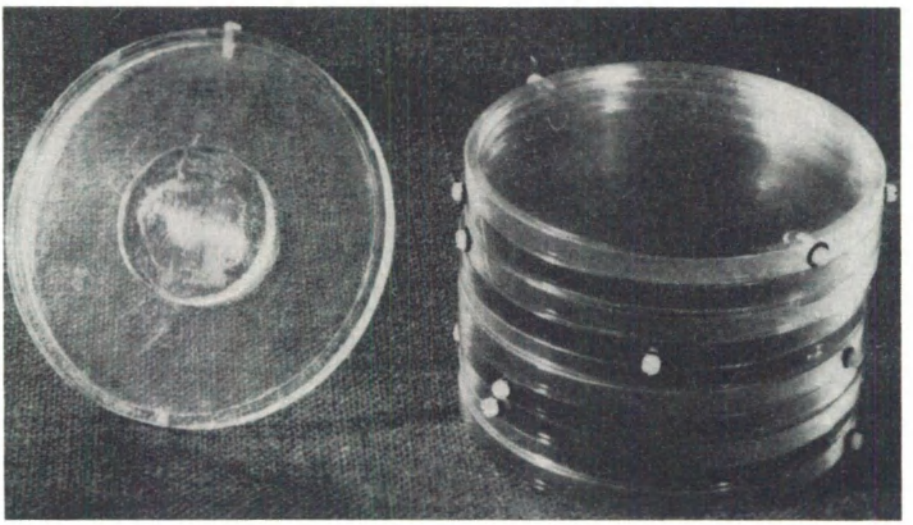

Fig. 5

Segmented phantom used in following studies
Defect placed in centre included those of 1 cm, 2 cm, 4 cm, and 6 cm diam.
Hollow inserts used were 2 cm, 4 cm, and 6 cm diam.

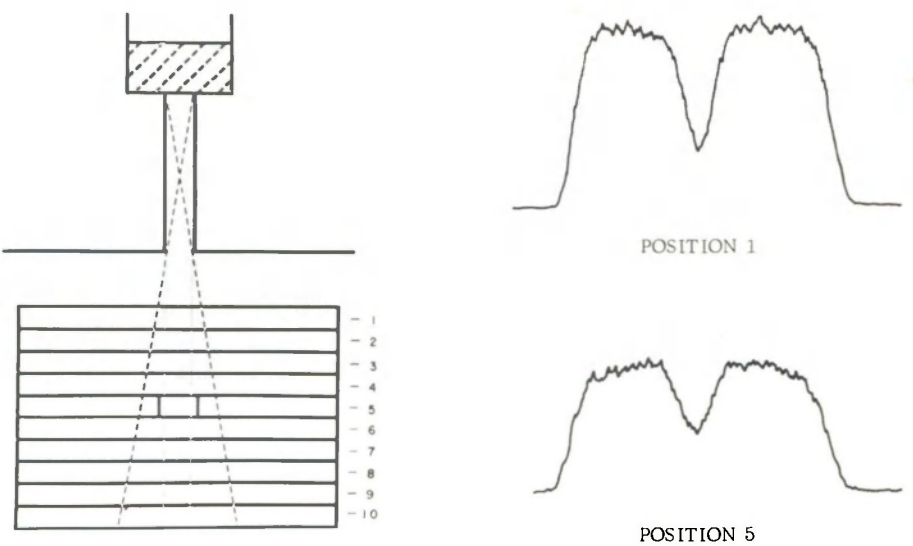

Fig. 6

Schema of measurement on segmented phantom. Note decrease in both peak reading and percentage drop with defect in position 5 as compared with position 1.

in this Figure are from positions one and five. The profile recording is obtained to show the limitations of the primary information to be displayed by the scanning system. This application of profiles to scan recording was pointed out by BRUCER [3] and used by HARPER et al. [4] as well as others [5]. This technique with its linear recordings of counting-rate change eliminates the errors in the interpretation of these changes when recordings are made with data accentuation techniques which usually depart from linear representation. Profile recording is subject to the usual problems of rate recording, thus the speed of the scanner head must be kept reasonably short in comparison with the rate-meter time constant. At present a digital count-rate meter (Atomium) has been quite useful. Incremental movements with scaler recording would be equally valid.

Initially, the information determined from these curves is the maximum counting rate, which is the counting rate observed when the defect is entirely out of the field of view of the detector so that the detector sees only a uniform extended source of radioactivity. Comparing the maximum counting rate of the profile from position 5 with the profile from position 1 shows a drop in counting rate. This difference in height of the curve represents a summation of counts lost by inverse square and absorption and the amount gained by the increase in the visual field of the penumbra. In the comparison of radioisotopes of various energies any change in this percentage decrease is due primarily to absorption, since the loss by inverse square and the gain by the increased visual field of the penumbra are essentially unchanged.

Secondly, the percentage drop over the defect will reflect the solid angle subtended by the collimator at this level as well as the effect of scattering. This percentage drop will depend on the size of the umbra, to some extent the penumbra, and on the amount of gamma-ray penetration through the shielding and septa.

By means of these techniques, families of curves were recorded from various collimators, various sized defects, and various gamma ray energies. Such a set recorded from Au^{198} is shown in Fig. 7. The highest counting rate and the largest percentage drop is recorded from position 1. As the defect is placed in lower positions the maximum counting rate falls and there is a concomitant smaller percentage drop over the defect.

While the curves themselves are not meaningful, they contain all the data necessary to calculate the percentage drop from any thickness defect at any level in the phantom. The calculations to obtain this percentage drop are simply

$$\% \text{ drop} = \sum_{1,n} \frac{(c_{max} - c_{min})}{\sum_{1,n} c_{max}} \times 100 .$$

As an example, Fig. 8 shows the calculation of a percentage drop of a 2 × 2-cm defect in a 4-cm thick phantom. In this case there is no defect in positions 1 or 4, therefore, the maximum and minimum counting rates are the same. Thus, the net percentage drop is due entirely to the drop observed in positions 2 and 3 but this drop must be calculated in reference to the summation of the total counting rates at all four levels.

It is with respect to these two parameters that the comparison data will be presented. For example, in Fig. 9 is illustrated the effect of gamma-ray

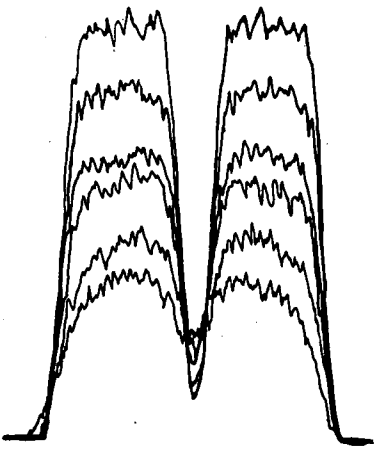

Fig. 7

Composite photograph of family of profiles from a 4-cm defect in phantom disc filled with Au^{198}. Depths of 1, 3, 5, 7, 9 cm shown.

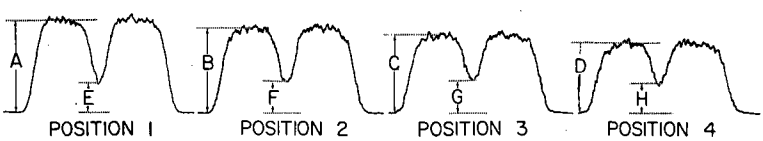

$$\frac{(A + B + C + D) - (A + F + G + D)}{A + B + C + D} \times 100 = \text{PERCENT DROP}$$

Fig. 8

Sample calculation of the percentage drop obtained from a 2 × 2-cm defect in the middle of a 4-cm-thick phantom

energy on the percentage drop of a 2-cm-diam. and 2-cm-thick void in a 10-cm phantom. It is apparent that as the energy is lowered to the 122-keV gamma-ray of Co^{57} a greater difference is noted between the counting rate over the defect and the counting rate over the extended source.

This moderate improvement is primarily due to the decrease in contributions from the lower levels because of increased absorption, and secondarily to a reduction of gamma-ray penetration of the septa at the lower energies. It is noted that when the defect is placed in the lower position, the increase of percentage drop is of less magnitude since the variation in level contribution is not so great. This was illustrated in Fig. 7, where it was shown that with Au^{198} the lower level contributes only one-third as much to the total counting rate as the upper level. With Co^{57}, the absorption is, of course, even greater.

It is further seen from the data obtained from the measurements of the gamma rays of Au^{199} and Hg^{197} that the experimental points did not fall on the extrapolated section of the curve. This decrease is due to scatter from

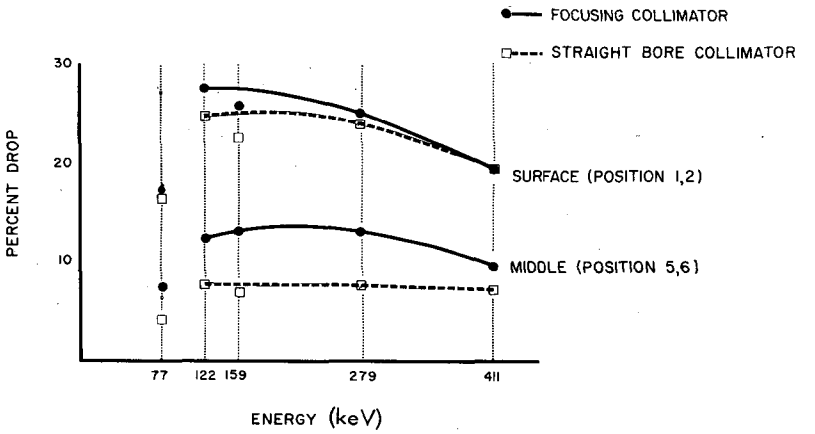

Fig. 9

Effect of gamma-ray energy on percentage drop of a defect displacing 20% of subtended volume 2×2-cm defect in 10-cm-thick phantom. Note inconsistency of Au^{199} and Hg^{197} points due to complex spectra and resultant high Compton scattering.

the higher energy gamma-rays of the complex spectra of the isotopes which, as has been shown by ROSS and HARRIS [6], can be difficult to remove without appreciable loss of counting rate. It should be remembered that identical curves would be obtained if, instead of a defect, a volume of similar dimensions to the void but containing twice the concentration of the surrounding environment was used. In this case the only difference would be the term percentage increase used for the ordinate.

Also, illustrated in this Figure is the indication that there is relatively little difference between the percentage drop from the defect on the surface as obtained from a $\frac{1}{2}$-in-diam., 3-in straight-bore collimator and the inner seven holes of the 19-hole Picker X-ray focusing collimator shown in Fig. 1. This is not too surprising since at the surface the 2-cm-diam. defect is sufficiently large to block the umbras of both collimators. With the defect in the lower position a greater variation is seen between the two collimators.

More complete data for Co^{57} is shown in Table I. This Table shows the absolute percentage decrease from a 2-cm-diam., 2-cm-thick void in a range of phantom thicknesses from 2 cm to 10 cm.

As would be expected the percentage decrease is greatest in the thin phantom and becomes progressively smaller both as the phantom is enlarged and as the void becomes more deeply placed in the phantom.

Comparative results with similar measurements made with Au^{198} are shown in Table II.

In general, the percentage decreases are lower than the same levels with Co^{57}. This reduction is primarily a result of the higher contributions from the lower segments of Au^{198}, while the Co^{57} absorption reduces the contribution from the deep levels.

The Tables merely show what percentage drop may be obtained from voids of these dimensions. They do not tell whether these voids could be visualized by scanning procedures. To determine the latter, knowledge of

TABLE I

PERCENTAGE DECREASE FOR 2 × 2-cm DEFECT (SEVEN-HOLE FOCUSING COLLIMATOR)

		Phantom thickness (cm)								
		2	3	4	5	6	7	8	9	10
Co^{57} Centimeter of phantom above defect	0	87.9	61.9	48.8	41.5	36.6	33.2	30.6	28.9	28.2
	1		50.4	41.5	35.1	31.0	27.1	26.0	24.5	23.3
	2			34.4	29.1	25.7	23.3	21.6	20.3	19.3
	3				23.5	20.7	18.7	17.5	16.5	15.6
	4					16.3	14.8	13.7	12.8	12.2
	5						11.3	10.5	9.9	9.4
	6							8.2	7.7	7.3
	7								6.3	5.9
	8									5.3

the counting rate statistics of the scanning parameters selected must be known. This is illustrated by the nomogram of Fig. 10 in which scanning speed and counting rate are shown together with the relationship to standard deviation. In the example cited, a counting rate of 5000 cpm and a speed of 10 in/min will exhibit for a $\frac{1}{2}$-in resolution a standard deviation of ± 6.3%, or a total variation of 25.2% for two standard deviations. While the partial rescanning of the same area will afford us somewhat better accuracy it is still doubtful that any percentage decrease of less than 15% would be reliably identified with such scanning parameters. Reference to Table I and Table II will now let us specify what size void in what size phantom may be visualized with these parameters.

It is obvious that selection of any collimator must be a compromise between obtaining the largest possible percentage drop (or percentage increase) and attaining the highest counting rate. In fact the same compromise must often be made in the settings of the pulse height analyser, since it has been shown that the greatest percentage differences are obtained with narrow window settings, but at the expense of reduced counting rate [6]. This relationship is illustrated by Fig. 11 in which both the variation of percentage

TABLE II

PERCENTAGE DECREASE FOR 2 × 2-cm DEFECT
(SEVEN-HOLE FOCUSING COLLIMATOR)

		Phantom thickness (cm)								
		2	3	4	5	6	7	8	9	10
Au^{198} Centimeter of phantom above defect	0	66.8	46.4	36.0	30.1	26.0	23.1	20.9	19.3	18.1
	1		40.0	31.1	25.9	22.4	19.9	18.1	16.7	15.6
	2			27.9	23.2	19.6	17.9	16.3	15.0	14.0
	3				20.7	17.9	15.9	14.4	13.3	12.5
	4					14.8	13.2	11.9	11.0	10.3
	5						10.8	9.8	9.0	8.4
	6							8.0	7.3	6.9
	7								6.0	5.6
	8									5.0

drop and counting rate are shown by a variation of setting of the threshold discriminator for Hg^{203}.

In view of this compromise between percentage drop and counting rate, it is only reasonable to compare the percentage drops between collimators that exhibit similar counting rates to an extended source. It must be recognized that collimators may exhibit vastly different counting rates to "point sources" while showing identical responses to volume sources of a size greater than their umbra. In fact, one collimator may show a lower maximum count to a "point source" as compared to a second collimator and at the same time exhibit a many fold increase in counting rate to a volume source. As a standard to compare the various focusing collimators, the relative counting rates of various straight bore collimators exposed to an extended volume source is shown in Table III.

It is seen here that as the collimator diameter is increased by a factor of two, the counting rate increases by a factor of 16 or 2^4. This measurement is reasonably consistent with the calculated prediction based on the analysis that the counting rate is proportional to the product of the solid angle or area of the collimator entrance multiplied by the solid angle or area of the collimator exit. In terms of tapered collimators the same counting rate

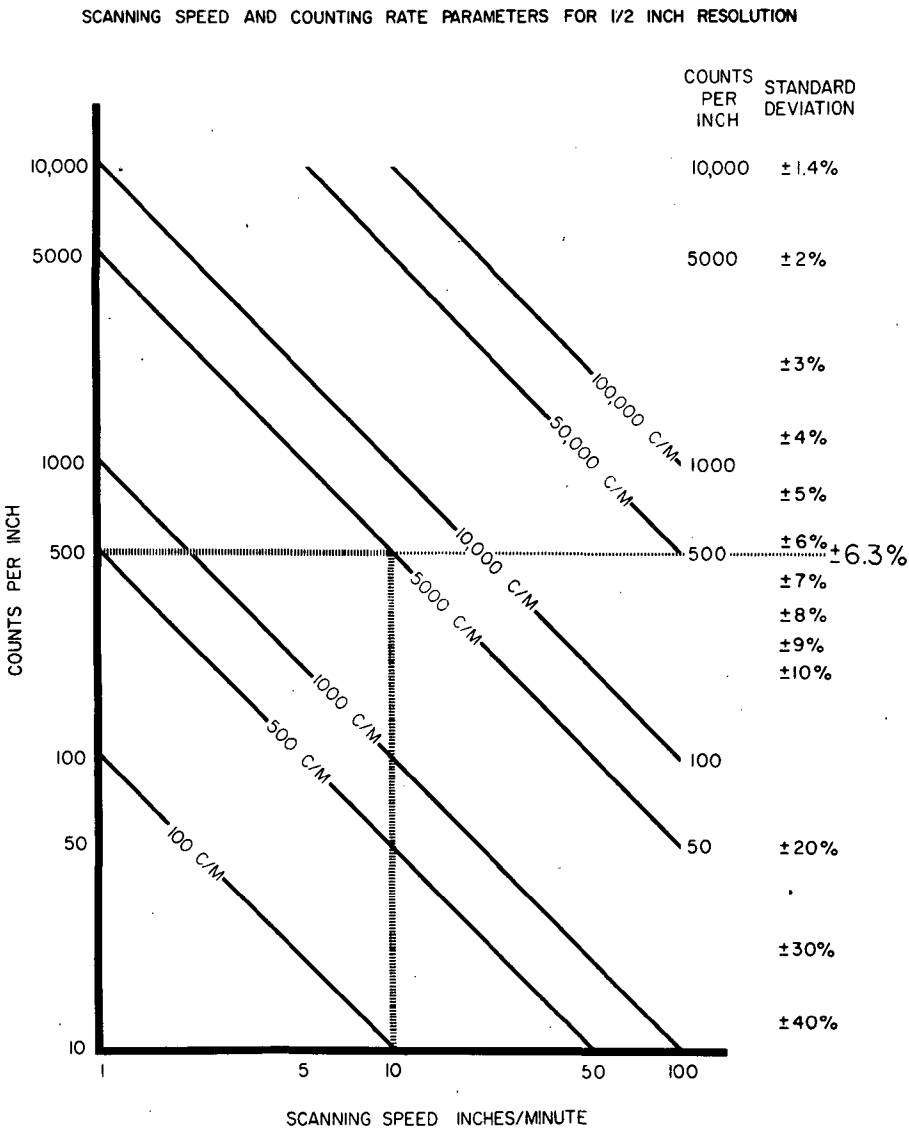

Fig. 10

Nomogram of scanning parameters showing expected standard deviations with respect to total counts collected over a ½-in distance

should be expected from any taper where the products of the area of the entrance and exit are equivalent. This is seen in Table IV.

From this analysis it is apparent that a tapered collimator will exhibit the same counting rate from an extended source regardless whether the large or small end is facing the source.

Once the counting rate is normalized it is possible to evaluate the per-

[6]

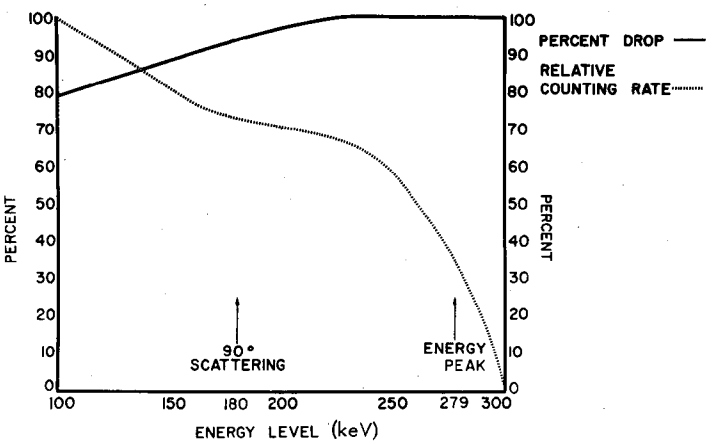

Fig. 11

Effect of discrimination setting on counting rate and percentage drop of 4-cm defect with Hg^{203}
Note as the lower energy gamma-rays are accepted the counting rate increases but the percentage drop is poorer because of Compton scattering.

TABLE III

RELATIVE COUNTING RATES OF VARIOUS 3-in STRAIGHT-BORE COLLIMATORS TO THE SAME EXTENDED SOURCE

(1-cm-thick disc, 15-cm diam. at 1 in from collimator aperture - Co^{57})		
(in)	Measured (cpm)	Calculated (cpm)
0.250	1125	1050
0.375	5285	5200
0.500	16900	16500
0.540	23975	22500
0.580	28975	30000
0.620	38175	39500
0.660	47375	49000
0.700	60975	62000
19-hole focusing collimator*	3725	3971
7-hole focusing collimator**	27415	24000

* Inner 19 holes of a lead model of the 37-hole ORNL gold-tungsten collimator shown in Fig. 1.

** Inner 7 holes of the lead 19-hole Picker X-ray collimator shown in Fig. 1.

TABLE IV

RELATIVE COUNTING RATES OF A HALF-INCH STRAIGHT-BORE COLLIMATOR AND EQUIVALENT TAPERS TO VOLUME SOURCE Co^{57}

	Small diameter down (cpm)	Small diameter up (cpm)
½-in Straight bore	14 000	14 000
1.000/0.250-in Taper	13 400	13 400
0.667/0.375-in Taper	13 200	13 600
0.572/0.438-in Taper	13 800	14 000

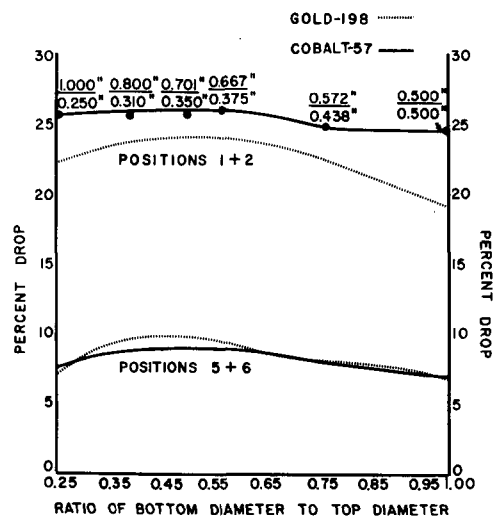

Fig. 12

Percentage drop of a 2-cm defect in a 10-cm phantom as recorded from various tapers all exhibiting the same counting rate to an extended source. Ratio 1 refers to same diameter of upper and lower apertures (straight bore of ½-in diam.). Smallest ratio tested was 0.25, derived from a 1-in aperture at the crystal and a ¼-in aperture facing the source.

centage decrease between collimators of various tapers with their straight-bore equivalent. This comparison is shown in Figs. 12 and 13. While only minor differences are seen with the large defect of Fig. 12, a much greater dependence of the taper with the smaller defect size is noted in the latter Figure.

Using the solid angle relationship the equivalence in counting rate of any tapered collimator to a straight-bore collimator may be calculated by the nomogram of Fig. 14. The upper example shows one of the comparative collimators of Table IV, where a collimator with a 0.7-in upper diameter

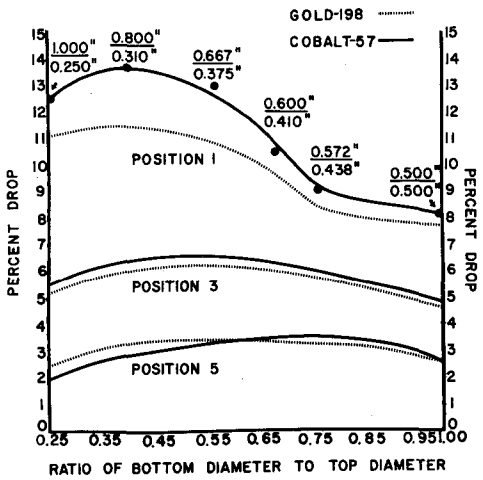

Fig. 13

Similar measurements as preceding figure except with a 1×1-cm defect in a 5-cm phantom. Note the variation with lower ratios reaching a maximum at about 0.45.

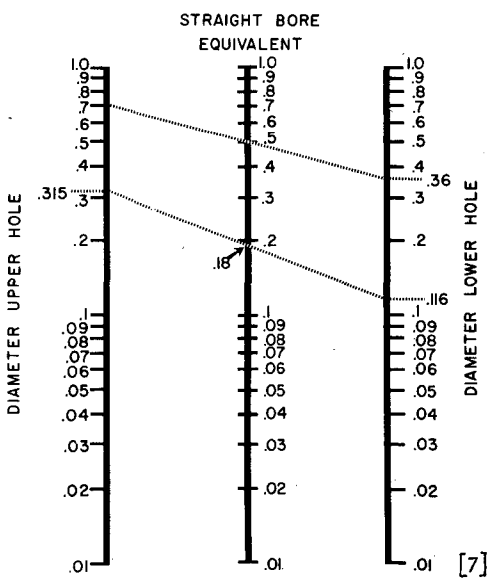

Fig. 14

Nomogram showing straight-bore equivalence of any tapered collimator obtained by connecting lines between upper and lower aperture diameters.

and a 0.36-in lower diameter aperture is equivalent to a 0.5-in straight-bore collimator.

The lower line in Fig. 14 shows this calculation for a 19-hole lead focusing collimator (or more properly, a convergent channel collimator) of the same dimensions as the inner 19 holes of the 37-hole ORNL gold-tungsten

collimator. The example shows that one taper of upper aperture 0.315-in diam. and lower aperture 0.116-in diam. is equivalent to a straight bore of 0.180-in diam. This straight-bore collimator based on the relationship of counting rate to bore size as established in Table III for 3-in collimators would predict a 240-cpm response for one taper. The actual focusing collimator is 3⅜ in, however, which reduces this value to 190 cpm for a one taper hole and 3610 cpm for the entire nineteen. Adding a 10.4% increased efficiency [7] because hex holes instead of round holes were used gives a predicted value of 3971 cpm.

The actual measurement with the same extended source shown in Table III gives a value of 3725 cpm. This value would indicate an equivalence to a 0.350-in diam. straight-bore collimator.

The percentage drops obtained from a 1-cm-diam. void in a 10-cm thick phantom obtained with this collimator are shown in Fig. 15, compared with

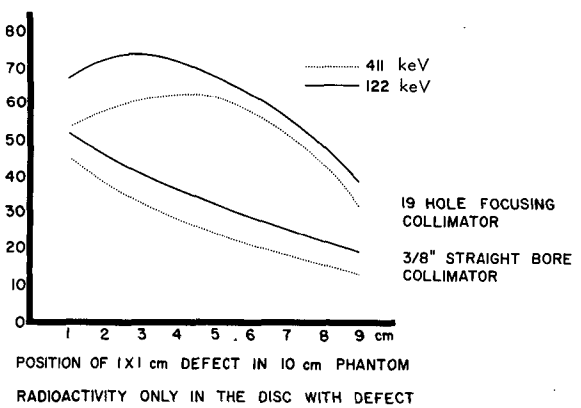

Fig. 15

Comparison of percentage drop over a 1×1-cm defect for the 19-hole focusing collimator with straight-bore collimator of similar counting rate characteristics. Co^{57} and Au^{198} used.

similar decreases from a 0.375-in straight-bore collimator. The improvement of the focusing collimator with the lower energy where septal penetration is minimized is moderate but significant at all levels.

A similar comparison of this collimator with a 2-cm void showed little difference. If the umbra of the collimator is very much smaller than the defect, the percentage drop (or increase) is very close to the ideal case. It is only when the defect becomes comparable in size to the umbra that an appreciable departure is seen. In Fig. 16, it is seen that with the defect in the surface position of the phantom the ideal case (100% drop) is maintained as long as the defect is twice the size of the umbra. At a 1.5 ratio the percentage decrease has dropped 90% and when the defect and umbra are equal the drop is 50%.

This relationship shows that the choice of a collimator should be made with reference to what is the smallest lesion that the counting-rate relationship indicates can be detected. For example, if a 2-cm lesion in the liver is a reasonable expectation of minimum detection, a straight-bore or a con-

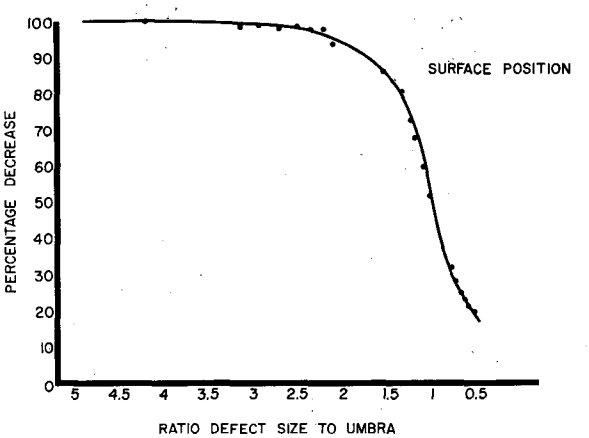

Fig. 16

Relationship of percentage decrease to the ratio of the defect to umbra. Seven different sized straight-bore collimators and three different sized defects were used to delineate the curve.

vergent channel collimator of straight-bore equivalence of no less than 1.33 cm diam. should be selected.

In summary, it has been the attempt of this evaluation to present a quantitative basis for the selection of collimators or the selection of various energy gamma emitters. It is somewhat meaningless to classify one energy as better or worse for scanning. For such an evaluation to be useful it is necessary to specify what phantom conditions are used and what is the degree of improvement. As seen here, while the detection ability of a scanner system is generally improved with the lower energies, in many cases this improvement is less than can be visualized in the scan record itself.

Lastly, the importance of counting rate on collimator selection cannot be over-emphasized. It makes little sense to develop a collimator of fine resolution if by so doing the counting rate is so reduced that statistical accuracy is so low as to preclude its very use. It is here that the evaluation of spatial resolution without counting-rate information can be deceptive. It is not enough to prove with phantom measurements that a specific size region can be visualized. To be clinically useful it must be shown that this visualization is statistically reliable before an interpretation can be made as to whether a counting rate variation represents a change in radioactive deposition or not.

In retrospect, the explanation of the comparative scans of Fig. 2 can be interpreted. While the focusing collimator possesses greatly superior spatial resolution and finer isoresponse curves, visualization of lesions of the magnitude in this clinical example as seen with both collimators shows relatively the same percentage drop. This is illustrated by the similarity at the higher cut-off levels. The main superiority of this focusing or convergent channel collimator for such gross scanning applications is the vastly improved side shielding, which is indicated in the fact that the zero cut-off

of the focusing collimator compares favourably with the 20% cut-off of the straight bore..

ACKNOWLEDGEMENTS

The authors gratefully acknowledge the efforts of Saar Porrath, M.D. and Elaine Roth for their assistance in collecting this data, and to Sharon Sladek, Mrs. Carol Hino, and Mr. Warren Strauss in the preparation of the manuscript.

We should also like to express our appreciation to David Weir, M.D., Medical Director of Highland View Hospital, for his long continued support of this investigation.

REFERENCES

[1] CHRISTIE, J.H. and MacINTYRE, W.J., Radiology 79 (1962) 472-482.
[2] FRANCIS, J.E., Jr., HARRIS, C.C. and BELL, P.R., J. nucl. Med. 3 (1962) 10-17.
[3] BRUCER, M., Symposium on Radioisotope Scanning, Naval Medical School, Bethesda (1959) 1-30.
[4] ENDLICH, H., HARPER, P., BECK, R., SIEMENS, W. and LATHROP, K., Amer. J. Roentgenol. 87 (1962) 148-155.
[5] MacINTYRE, W.J., CRESPO, G.G. and CHRISTIE, J.H., J. nucl. Med. (1960) 262-272.
[6] ROSS, D.A., SATTERFIELD, M.M., JORDAN, J.C., HARRIS, C.C. and BELL, P.R., Low-Energy Gamma Emitters in Scanning and Other Clinical Applications, Abstracts of 6th Int. Symp., Bad Gastein, Austria (1964).
[7] HARRIS, C.C., BELL, P.R., FRANCIS, J.E., Jr, SATTERFIELD, M.M., JORDAN, J.C. and MURRAY, J.P., Jr., in Progress in Medical Radioisotope Scanning (Knisely, R.M., Andrews, G.A. and Harris, C.C.) Oak Ridge Institute of Nuclear Studies, Oak Ridge (1963) 25-65.

DISCUSSION

H. A. B. SIMONS: In connection with your method for finding the percentage drop due to a large defect, there is surely a physical difference between a 2-cm void and a void of twice 1 cm. The scattering conditions at the interface are physically different in the two cases. How accurate is your process of addition?

W. J. MacINTYRE: There is a difference because of the interface of lucite above and below the defect. However, the difference in the case of a 2-cm-thick defect as compared to two 1-cm-thick defects is minimal (under 1%, which is below our degree of accuracy). At 4-cm the difference might be perceptible but here again it would only be of the order of 1%.

H. A. B. SIMONS: What thickness of void would you allow?

W. J. MacINTYRE: Since the plastic differs little from tissue in absorbing properties, the full 10 cm can be used.

STATEMENT BY W. J. MacINTYRE ON THE ICRU TASK GROUP ON SCANNING

The Task Group on Scanning of the International Commission on Radiological Units and Measurements has been asked to consider the use of a

phantom or phantoms for the evaluation or standardization of scanning procedures. Any suggestions for such a phantom would be most helpful, and should be sent to:

W. J. MacIntyre,
Chairman, ICRU Task Group,
Highland View Hospital,
Ireland Drive,
Cleveland 22, Ohio
United States of America.

COLLIMATOR EVALUATION WITH THE IAEA SCANNING PHANTOM

M. A. BENDER AND M. BLAU
ROSWELL PARK MEMORIAL INSTITUTE, BUFFALO, N.Y., UNITED STATES OF AMERICA

Abstract — Résumé — Аннотация — Resumen

COLLIMATOR EVALUATION WITH THE IAEA SCANNING PHANTOM. The IAEA Scanning Phantom was designed at the Symposium on Medical Radioisotope Scanning in 1959. This phantom was designed to provide an easily reproducible large organ phantom that could be used as a standard to compare more accurately different scanning systems. A unique feature of the phantom is that when all four sides are scanned, the four "tumours" (1, 1.5, 2 and 3 cm in diam.) are each viewed at depths of 0, 5, 10 and 15 cm. This report covers the use of the IAEA phantom for the evaluation of four commonly used 3-in focusing collimators: 19, 37 and 61 channel lead collimators and a 37 channel tungsten collimator.

The experiments were designed to determine the optimum collimator configuration for a variety of gamma-ray energies, "tumour"-pool concentrations and "tumour" sizes and depths. Each collimator was used with eight different isotopes emitting photons ranging in energy from 0.027 MeV to 1.3 MeV. Each isotope-collimator combination was evaluated with four "tumour"-pool concentration ratios: voids, X2, X5 and X10. The activity in the pool was at a level consistent with that encountered clinically. Using photorecording, four sides of the phantom were scanned for every combination of collimator, isotope, and "tumour"-pool concentration ratio, a total of 512 scans. The scans were interpreted independently by three experienced observers. These data provide a basis for the rational choice between these collimators for various scanning situations. They also provide information on the minimum gamma-ray energy suitable for large organ scanning and the effect of septal cross-over by high-energy gamma-rays on the target: non-target ratio.

ÉVALUATION DES COLLIMATEURS AVEC LE FANTÔME DE L'AIEA. Lors du Colloque sur l'exploration médicale au moyen des radioisotopes organisé par l'AIEA en 1959, on a mis au point un fantôme destiné aux études scintigraphiques. Il s'agissait de représenter matériellement un organe de grandes dimensions facile à reproduire afin de pouvoir utiliser ce fantôme pour comparer avec la plus grande précision possible différents systèmes de scintigraphie. Le fantôme présente la particularité suivante: lorsqu'on l'explore sur les quatre faces, chacune des quatre «tumeurs» (ayant respectivement un diamètre de 1, 1,5, 2 et 3 cm) est vue à des profondeurs de 0, 5, 10 et 15 cm. Le mémoire est consacré à l'emploi du fantôme de l'AIEA pour l'évaluation de quatre collimateurs à focalisation de 7,6 cm couramment utilisés: les collimateurs en plomb à 19, 37 et 61 canaux et un collimateur en tungstène à 37 canaux.

Les expériences avaient pour but de déterminer la configuration optimum du collimateur pour diverses énergies de rayons gamma, divers rapports de concentrations du radioisotope entre la «tumeur» et le reste du fantôme et diverses dimensions et profondeurs de la tumeur. On a utilisé chaque collimateur avec huit radioisotopes différents émettant des photons d'une énergie allant de 0,027 MeV à 1,3 MeV. On a évalué chaque combinaison d'un collimateur avec un radioisotope pour quatre rapports de concentrations entre la «tumeur» et le reste du fantôme: zéro, 2, 5 et 10. L'activité dans le reste du fantôme était comparable à celle que l'on rencontre en clinique. On a exploré les 4 faces du fantôme pour chaque combinaison d'un collimateur avec un radioisotope et un rapport de concentrations; on a donc obtenu 512 scintigrammes. Ces scintigrammes ont été interprétés indépendamment par trois observateurs expérimentés. Ces données fournissent une base lorsqu'il s'agit de choisir rationnellement lequel de ces collimateurs convient le mieux dans chaque cas d'exploration. Elles indiquent également quelle est l'énergie gamma minimum appropriée pour l'exploration des gros organes et quel est l'effet du franchissement des parois par les rayons gamma de haute énergie sur le rapport cible-tissus avoisinants.

ОЦЕНКА КОЛЛИМАТОРА С ПОМОЩЬЮ ФАНТОМА МАГАТЭ ДЛЯ СКЕННИРОВАНИЯ. В 1959 году на симпозиуме МАГАТЭ по медицинскому радиоизотопному скенниро-

ванию было запланировано создание фантома для сканнирования. Этот фантом был сконструирован таким образом, чтобы обеспечить наличие легко воспроизводимого фантома крупного органа, который мог бы использоваться в качестве стандарта для более точного сравнения различных систем сканнирования. Уникальной особенностью данного фантома является то, что при сканнировании всех четырех сторон, каждая из четырех "опухолей" (диаметром 1; 1,5; 2 и 3 см) просматривается на глубине 0,5; 10; 15 см. В данном докладе рассматривается использование фантома МАГАТЭ для оценки четырех обычно используемых фокусирующих 3-дюймовых коллиматоров: свинцовые коллиматоры с 19, 37 и 61 каналом и вольфрамового коллиматора на 37 каналов.

Целью экспериментов являлось определение оптимальной конфигурации коллиматора для различных энергий гамма-лучей, различной концентрации в районе "опухоли" и "опухолей" различных размеров и глубин залегания. Каждый коллиматор исследовался с 8 различными изотопами, излучающими фотоны с энергией в диапазоне от 0,027 до 1,3 Мэв. Каждая комбинация коллиматора с изотопами оценивалась при четырех уровнях концентраций в районе "опухоли" при следующем соотношении: пустота, X 2, X 5 и X 10. Активность в месте нахождения "опухоли" соответствовала уровням, встречающимся в клинических условиях. Сканнирование производилось с четырех сторон фантома для каждой комбинации коллиматора, изотопов и уровня концентрации в районе "опухолей"; использовалась фотозапись, в общем получено 512 сканнограмм. Интерпретация сканнограмм проводилась независимо тремя опытными специалистами. Эти данные составляют основу для рационального выбора между такими коллиматорами при сканнировании в различных ситуациях. Они также предоставляют информацию по минимальной энергии гамма-лучей, пригодной для сканнирования крупного органа и влияют на септальный кроссовер с помощью гамма-лучей высокой энергии, действующих на мишени при соотношении мишень—объект.

EVALUACIÓN DE COLIMADORES CON EL ÓRGANO SIMULADO DISEÑADO POR EL OIEA. En el Simposio sobre exploración médica mediante radioisótopos, organizado por el OIEA en 1959, se diseñó un órgano simulado destinado a los estudios centelleográficos. Se trataba de representar materialmente un órgano de grandes dimensiones, fácil de reproducir, a fin de poder emplearlo para comparar con la mayor precisión posible diversos sistemas de exploración gammagráfica. Una característica peculiar de este órgano simulado es que cuando se exploran sus cuatro lados, cada uno de los cuatro «tumores»(de 1, 1, 5, 2 y 3 cm de diámetro) es visto a profundidades de 0, 5, 10 y 15 cm. La memoria trata del empleo de este órgano simulado para la evaluación de cuatro colimadores enfocados de 3 pulg corrientemente utilizados: los colimadores de plomo de 19, 37 y 61 canales y el colimador de wolframio de 37 canales.

La finalidad de los experimentos era determinar la configuración óptima del colimador para diversas energías de rayos gamma, diversas relaciones de concentración del radioisótopo entre el «tumor»y el resto del órgano y diversas dimensiones y profundidades del «tumor». Cada colimador se empleó con ocho isótopos diferentes que emitían fotones de energía comprendidas entre 0,027 y 1,3 MeV. Se evaluó cada combinación de un colimador con un radioisótopo para cuatro relaciones de concentración entre el «tumor» y el resto del órgano simulado: cero, 2, 5 y 10. La actividad en el resto del órgano simulado era análoga a la que se encuentra en los estudios clínicos. En total se exploraron los cuatro lados del órgano simulado para cada combinación de un colimador con un radioisótopo y una relación de concentraciones; se obtuvieron, pues, 512 centelleogramas, que fueron interpretados independientemente por tres observadores experimentados. Los datos obtenidos sirven de base para elegir racionalmente el colimador más conveniente para cada caso de exploración. Indican también cuál es la energía gamma mínima apropiada para la exploración de órganos de grandes dimensiones y el efecto que ejercen sobre el cociente blanco/tejido circundante los rayos gamma de alta energía que atraviesan los tabiques del colimador.

INTRODUCTION

The choice of an optimum collimator for large-organ radioisotope scanning depends partly on: (1) The gamma-ray energy of the radioisotope; (2) the size and depth of the target tissue; (3) the target: non-target concentration ratio; and (4) the amount of the radioisotope in the region to be scanned. Scanning collimators have been evaluated on a theoretical basis by BECK [1]

and have been assessed by means of the profile counting of suitable phantoms by CHRISTIE and MacINTYRE [2]. Both of these approaches to collimator analysis neglect the role of target-tissue configuration in scan interpretation. The interpretation of scans of the IAEA Standard Scanning Phantom can be a basis for a collimator evaluation study in which this important parameter is included. This phantom provides the opportunity to scan a quasi-clinical situation with controlled conditions of target: non-target ratio, target depth, size and concentration of radioisotope. The information is presented and interpreted in the same manner as in a clinical study.

The present report is an evaluation of four commonly used 3-in focusing collimators. Each collimator was tested with 7 radionuclides having gamma-ray energies ranging from 0.027 MeV to 1.3 MeV. Each collimator, radionuclide combination was evaluated with four different target: non-target ratios and with four different "tumour" sizes each at four different depths. Specific questions to be answered included: (1) At what gamma-ray energy is a tungsten collimator superior to a lead collimator? (2) At what tumour size is a high-resolution, low-efficiency collimator superior to a low-resolution, high-efficiency collimator? (3) How does gamma-ray attenuation affect the ability to detect tumours at a depth within a large organ? (4) What tumour volumes and concentration ratios are required to accurately visualize a lesion in the clinical situation?

PROCEDURE

Phantom

The phantom is the same as that designed at the Medical Radioisotope Scanning Symposium held in Vienna in 1959 [3]. It is in the form of a truncated pyramid constructed of $\frac{1}{4}$-in-thick plexiglas. The height is 15 cm and the outside dimensions of the ends are 15×15 cm and 12×12 cm respectively. The volume is 2200 ml. Four spherical "tumours" with internal diameters of 3.0 cm (14.2 ml), 2.0 cm (4.2 ml), 1.5 cm (1.7 ml), and 1.0 cm (0.5 ml) are mounted within the phantom. The only alteration from the original design was the substitution of the 1.5-cm diameter sphere for a recommended 0.5-cm diameter sphere. The 0.5-cm diameter sphere with a volume of only 0.07 ml, was felt to be too small to contribute any significant information with our current instrumentation and clinically available target: non-target ratios. The 1.5-cm diameter sphere provided critical information for a source volume which was marginal for most collimators currently in use. The four spheres are so arranged that if the four sides of the phantom are scanned, each sphere is visualized at depths of 0, 5, 10, and 15 cm. All scans were performed with the 12-cm end of the phantom elevated 1.5 cm above the scanning bed with the collimator as close as possible to the phantom at the 15-cm end.

Scanner and collimators

The Baird-Atomic CS-500 Medical Scanner was used throughout this study. The detector has a 3-in diameter, 2-in-thick sodium iodide (Tl)

crystal and the side shielding is 1.25 in of lead and 0.75 in of tungsten. The four focusing collimators are three inches in height and have a point focus three inches from the collimator face. Three lead collimators (61 channel, 37 channel, and 19 channel) and one tungsten collimator (37 channel) were evaluated. The lead collimators have hexagonal apertures in cross-section and the tungsten collimator circular apertures in cross-section. The percentage of the crystal surface exposed for the four collimators is given in Table I.

TABLE I

% CRYSTAL SURFACE EXPOSED

Collimator	Crystal surface exposed (%)
61 lead	44
37 lead	47
37 tungsten	43
19 lead	57

Photorecording with a 40% cut-off was used for all scans. The 40% cut-off presented the full dynamic range of the film over the top 60% of the maximum count-rate. When voids were scanned, the gain was adjusted so that the non-target count-rate would provide 70 - 80% of the maximum film density. When "hot" tumours were scanned, the non-target count-rate provided 50% of the maximum film density. The scan speed was 6 in/min with unidirectional recording and the scan spacing was $\frac{3}{16}$ in. A 2-s time constant was used on the photorecording count-rate meter. Total scanning time for each view was 25 min. The window of the pulse-height analyser was set at 20% of the photopeak energy and in all cases the window was centred over the photopeak.

Radionuclides

The radionuclides used in this study were I^{125} (0.027 MeV), Hg^{197} (0.068, 0.077 MeV), Hg^{203} (0.28 MeV), I^{131} (0.36 MeV), Sr^{85} (0.51 MeV), Cs^{137} (0.66 MeV) and Fe^{59} (1.1, 1.3 MeV).

A concentration of 0.01 μc/ml Hg^{203} in the phantom was chosen as the standard. The concentration of the other radioisotopes was adjusted to obtain the same count-rate in the photopeak from the uncollimated crystal. For some isotopes (e.g. I^{125}, Hg^{197}, and Fe^{59}) this required concentrations substantially more than 0.01 μc/ml. The concentration of 0.01 μc/ml Hg^{203} was chosen as it approximates the concentration in a patient following the injection of a brain-tumour localization dose. Four concentration ratios were used with each isotope. The spheres were filled with water (voids) and two, five and ten times the concentration in the phantom.

Scan interpretation

The appearance of each sphere in every position was scored using a scale of 0 - 10. A score of 0 indicated that there was no evidence of the sphere on the scan. A score over 4 would be interpreted as positive if it were seen on a clinical scan and the higher scores of 8 and above were reserved for an excellent reproduction of the size and configuration of the sphere. The results of the interpretations of the scans are itemized in Table II.

DISCUSSION

The scores achieved for a given combination of gamma-ray energy and collimator configuration were summed for all tumours and concentrations and are presented in Fig. 1. For the sake of clarity, the gamma-ray energies

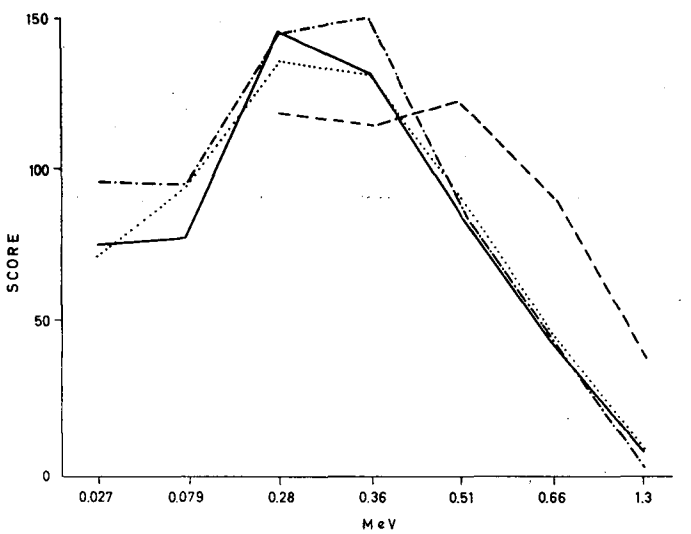

Fig. 1

Total score - all spheres

—— 61 lead
..... 37 lead
—·— 19 lead
----- 37 tungsten

are plotted at uniform intervals across the horizontal axis. These data reveal that there is very little difference in the overall scores for the three lead collimators. The 37-channel tungsten collimator gave a 20% lower score than the lead collimators in the medium energy range. However, at 0.51 MeV the tungsten gave a 30% higher score, presumably because the tungsten maintains its resolution while the lead collimators lose resolution due to septal crossover. The superiority of the tungsten collimator in-

TABLE II

SCORES FOR SPHERE VISUALIZATION

Isotope	Collimator	.....	61 lead				37 lead				19 lead				37 tungsten			
	Depth (cm)	.....	0	5	10	15	0	5	10	15	0	5	10	15	0	5	10	15
		Sphere diameter																
I^{125}	Voids*	1.0	3	0	0	0	0	0	0	0	1	2	0	0	-	-	-	-
		1.5	0	0	0	0	0	0	0	0	4	0	0	0	-	-	-	-
		2.0	1	0	0	0	1	2	0	0	4	2	0	0	-	-	-	-
		3.0	4	1	0	0	4	1	0	0	8	3	0	1	-	-	-	-
	X2	1.0	0	0	0	0	0	0	0	0	0	0	0	0	-	-	-	-
		1.5	0	0	1	0	0	0	0	0	0	0	0	0	-	-	-	-
		2.0	1	2	0	0	0	0	0	0	0	0	0	0	-	-	-	-
		3.0	1	2	0	0	0	1	0	0	1	0	0	0	-	-	-	-
	X5	1.0	0	1	0	0	0	0	0	0	0	0	0	0	-	-	-	-
		1.5	0	0	0	0	4	0	0	0	4	0	0	0	-	-	-	-
		2.0	5	0	0	0	5	2	0	0	6	3	0	0	-	-	-	-
		3.0	7	6	0	1	7	7	0	1	8	6	0	0	-	-	-	-
	X10	1.0	0	0	0	0	0	0	0	0	0	0	0	0	-	-	-	-
		1.5	4	2	0	0	4	2	0	0	5	5	0	0	-	-	-	-

		2.0	6	5	1	0	7	5	1	0	9	5	0	0	-	-	-	-
		3.0	9	8	3	0	9	8	0	0	9	9	2	0	-	-	-	-
Hg^{197}	Voids*	1.0	0	0	0	0	0	0	0	0	0	0	0	0	-	-	-	-
		1.5	0	2	0	0	1	0	0	0	0	0	0	0	-	-	-	-
		2.0	0	0	0	0	3	0	1	0	4	0	0	0	-	-	-	-
		3.0	5	2	2	1	4	2	0	0	5	3	0	0	-	-	-	-
	X2	1.0	0	0	0	0	3	0	0	0	0	0	0	0	-	-	-	-
		1.5	0	0	0	0	0	0	0	0	0	1	0	0	-	-	-	-
		2.0	0	0	0	0	0	0	0	0	0	0	0	0	-	-	-	-
		3.0	1	1	0	0	1	0	1	0	0	0	0	0	-	-	-	-
	X5	1.0	0	0	0	0	2	0	0	0	0	0	0	0	-	-	-	-
		1.5	3	0	0	0	2	3	0	1	4	0	0	0	-	-	-	-
		2.0	3	3	0	0	5	2	0	0	6	5	0	0	-	-	-	-
		3.0	4	4	2	0	6	5	2	0	7	7	2	0	-	-	-	-
	X10	1.0	0	0	0	0	1	0	0	0	0	0	0	0	-	-	-	-
		1.5	2	5	0	0	3	5	0	0	3	6	0	0	-	-	-	-
		2.0	7	6	4	0	7	6	1	3	7	7	2	0	-	-	-	-
		3.0	8	8	5	1	8	8	6	4	9	8	4	4	-	-	-	-
Hg^{203}	Voids*	1.0	0	1	2	2	3	3	0	0	2	0	0	0	0	1	0	0
		1.5	3	1	1	0	0	0	2	2	1	0	0	0	0	0	0	0
		2.0	4	3	1	0	3	2	0	0	2	0	1	0	2	5	0	0
		3.0	5	5	2	1	5	4	2	0	6	4	0	1	6	3	1	1

TABLE II (cont.)

Isotope	Collimator	.....	61 lead				37 lead				19 lead				37 tungsten			
	Depth (cm)	.....	0	5	10	15	0	5	10	15	0	5	10	15	0	5	10	15
		Sphere diameter																
Hg^{203} (cont.)	X2	1.0	0	0	0	0	0	0	0	0	0	0	0	0	0	0	0	0
		1.5	0	1	1	1	0	0	0	0	0	0	1	0	1	0	0	1
		2.0	0	2	0	0	0	0	0	0	0	1	0	0	1	0	0	0
		3.0	2	3	0	0	2	0	0	0	2	3	2	0	1	2	1	1
	X5	1.0	1	0	0	0	2	0	1	0	2	0	0	0	0	0	0	1
		1.5	2	2	0	0	3	4	0	0	3	2	1	1	4	2	0	1
		2.0	5	4	2	0	6	4	0	3	6	5	2	1	4	5	1	0
		3.0	7	8	4	5	8	8	5	4	7	7	5	3	7	7	2	1
	X10	1.0	5	2	2	0	1	0	0	1	2	0	0	0	1	0	1	1
		1.5	4	5	2	0	6	3	0	1	6	6	0	2	4	4	0	0
		2.0	8	7	5	1	8	7	2	3	8	7	3	3	5	8	5	1
		3.0	8	9	5	4	9	9	6	6	9	10	7	5	7	9	5	5
I^{131}	Voids*	1.0	2	1	0	0	0	0	1	1	0	1	0	0	0	0	1	0
		1.5	1	0	1	0	1	1	0	0	0	0	0	1	2	0	1	0
		2.0	3	1	3	1	4	3	1	0	2	0	0	0	1	0	0	1
		3.0	5	6	1	2	2	5	2	1	3	5	1	1	1	4	2	2

	X2	1.0	0	0	0	0	0	1	0	0	0	0	0	0	0	0	0	0
		1.5	0	0	0	0	0	0	2	0	0	0	0	0	2	0	0	0
		2.0	0	2	0	0	0	0	2	1	2	0	0	2	1	0	0	1
		3.0	2	1	2	1	1	3	1	0	1	1	1	1	0	1	1	0
	X5	1.0	1	0	0	1	1	3	0	0	0	0	0	0	1	0	0	0
		1.5	1	5	3	1	3	4	0	1	3	5	3	0	3	0	0	1
		2.0	5	2	2	2	4	4	2	0	5	3	2	2	3	4	3	1
		3.0	6	5	5	1	6	7	3	2	8	7	7	4	5	5	5	1
	X10	1.0	0	0	5	1	1	0	0	0	5	0	0	0	0	0	0	0
		1.5	5	2	0	3	4	5	0	2	7	6	1	0	6	1	2	0
		2.0	5	6	1	2	4	6	5	2	8	7	5	5	7	7	5	4
		3.0	7	8	5	5	9	8	7	4	9	10	8	7	8	8	7	5
Sr^{85}	Voids*	1.0	0	0	0	0	0	0	0	0	0	0	0	0	1	0	1	0
		1.5	1	1	0	0	0	0	0	0	0	1	0	0	1	4	0	0
		2.0	2	3	0	0	0	0	1	0	0	1	0	0	2	1	2	0
		3.0	2	5	2	0	2	0	0	0	3	2	1	0	2	6	0	2
	X2	1.0	0	0	0	0	0	0	0	0	0	0	0	0	0	0	0	0
		1.5	0	0	0	0	0	0	0	0	0	0	0	0	0	0	0	0
		2.0	0	0	0	0	0	0	0	0	0	0	0	0	1	0	0	0
		3.0	0	1	1	1	0	1	0	0	1	2	0	0	1	0	1	0

TABLE II (cont.)

Isotope	Collimator Depth (cm)	....	61 lead				37 lead				19 lead				37 tungsten			
			0	5	10	15	0	5	10	15	0	5	10	15	0	5	10	15
		Sphere diameter																
Sr^{85} (cont.)	X5	1.0	0	0	0	0	0	0	1	0	0	0	0	0	0	0	0	1
		1.5	1	0	0	0	1	1	0	0	2	0	0	0	1	1	1	0
		2.0	3	1	1	1	2	3	1	0	2	2	1	2	2	3	3	2
		3.0	6	5	2	1	6	5	4	1	6	4	3	1	7	6	4	1
	X10	1.0	0	0	0	0	0	3	0	0	0	0	0	0	1	1	1	0
		1.5	3	3	0	0	4	2	1	0	4	3	0	0	4	4	5	0
		2.0	5	5	0	3	6	4	4	0	5	3	1	2	8	4	5	2
		3.0	8	8	6	3	8	8	6	4	8	8	5	4	8	8	6	5
Cs^{137}	Voids*	1.0	0	0	0	0	0	0	0	0	0	0	0	0	1	0	0	0
		1.5	0	0	0	0	0	0	0	0	0	0	0	0	0	0	0	0
		2.0	0	0	0	0	0	2	0	0	0	0	0	0	4	0	0	0
		3.0	3	3	0	0	0	2	0	0	0	3	0	0	4	3	2	0
	X2	1.0	-	-	-	-	-	-	-	-	-	-	-	-	-	-	-	-
		1.5	-	-	-	-	-	-	-	-	-	-	-	-	-	-	-	-
		2.0	-	-	-	-	-	-	-	-	-	-	-	-	-	-	-	-
		3.0	-	-	-	-	-	-	-	-	-	-	-	-	-	-	-	-

	X5	1.0	0	0	0	0	0	0	0	0	0	0	0	0	0	0	0	0	0	1
		1.5	0	1	0	0	0	0	0	0	2	0	0	0	4	2	0	1
		2.0	0	0	0	0	0	0	0	0	2	0	0	2	3	1	1	1
		3.0	3	3	0	0	2	2	1	0	3	2	1	0	5	5	1	2
	X10	1.0	2	0	0	0	0	0	0	0	0	0	0	0	1	0	0	0
		1.5	1	3	0	0	3	2	0	0	0	0	0	1	3	1	2	0
		2.0	3	0	0	1	3	3	0	1	3	3	0	0	7	6	2	1
		3.0	7	7	2	4	8	7	4	4	6	6	4	4	7	7	6	5
Fe^{59}	X5	1.0	0	0	0	0	0	0	0	0	0	0	0	0	0	0	0	0
		1.5	0	0	0	0	0	0	0	0	1	0	0	0	0	0	0	0
		2.0	0	0	0	0	0	0	0	0	0	0	1	1	0	0	0	0
		3.0	0	0	0	0	0	0	0	0	3	4	2	0	0	0	0	0
	X10	1.0	0	0	0	0	0	0	0	0	0	0	0	0	0	0	0	0
		1.5	0	0	0	0	0	0	0	0	0	0	0	0	0	0	0	0
		2.0	1	0	0	0	1	0	0	0	5	1	2	0	0	0	0	0
		3.0	3	2	0	0	2	2	1	0	7	7	3	1	1	2	0	0

* The score for voids is significantly higher than X2 although they are theoretically equivalent. However, the effective volume of the void includes the 1 to 2-mm-thick plexiglas of the sphere walls.

creases at 0.66 MeV and it is still useful at 1.3 MeV. Presumably the 20% lower scores of the tungsten collimator for Hg^{203} and I^{131} are the result of the poor geometric efficiency due to round rather than hexagonal apertures.

The scores for I^{125} and Hg^{197} are 60% of those for Hg^{203} and I^{131}. These low scores reflect the attenuation, absorption, and low angle scatter of the low-energy gamma-rays within the large volume of the phantom. It is surprising to note that the poor-resolution 19-channel collimator gives a higher score than the high-resolution 61-channel collimator for the gamma-ray energies of 0.027 and 0.077 MeV. At low-energy levels, septal crossover is not a problem and the higher intrinsic resolution of the 61-hole collimator should result in an equal or higher score. The anomalous low score is due to the fact that most of the radiation detected by any collimator at these energy levels arises primarily from the upper portion of the phantom. All the collimators have the same poor resolution 2 in from the focus point. The advantage of the 19-hole collimator over the 61-hole collimator for I^{125} and Hg^{197} results from the increased count-rate obtained with the coarser collimator.

The similarity of scores for the high-, medium- and low-resolution collimators is due to the balancing effect of the increased count-rate obtained with decreased resolution. The data presented in Fig. 1 strongly suggest that a high score for the visualization of the tumours is much more dependent upon gamma-ray energy than collimator configuration. This is clearly demonstrated in Figs. 2 and 3. Figure 2 presents the scores for

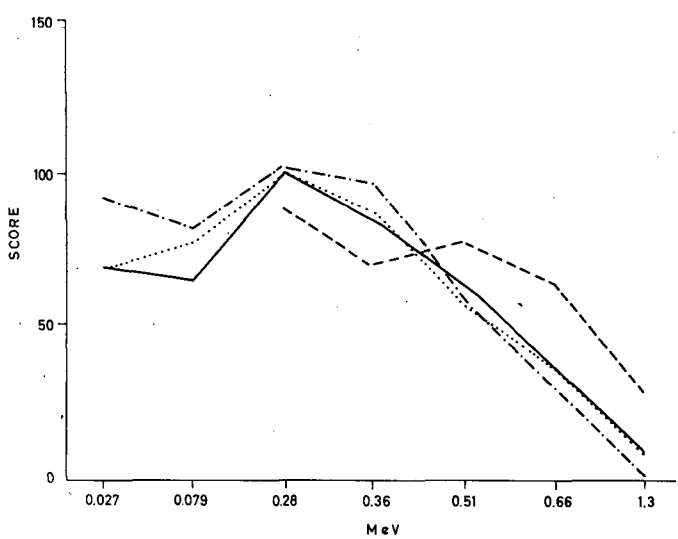

Fig. 2

Superficial spheres

—— 61 lead
..... 37 lead
—·— 19 lead
----- 37 tungsten

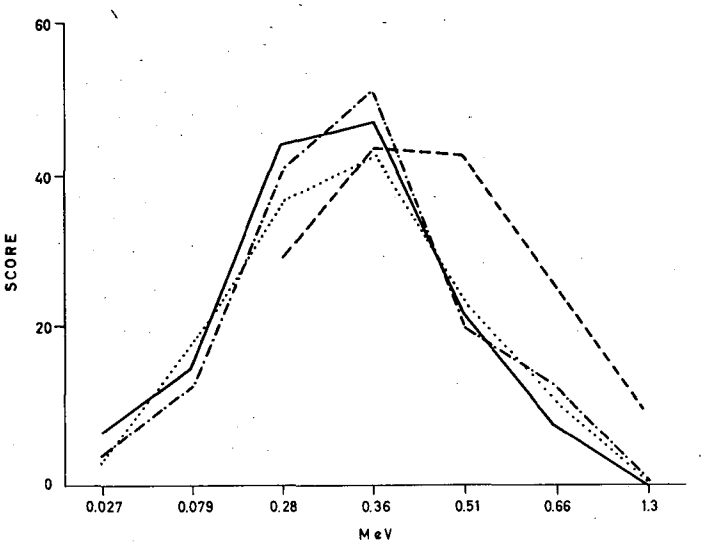

Fig. 3

Deep spheres

—— 61 lead
..... 37 lead
—·— 19 lead
----- 37 tungsten

visualizing the spheres in the superficial positions of 0 and 5 cm. Figure 3 presents the scores for the deep positions when the spheres are at depths of 10 and 15 cm. In the superficial positions, collimator configuration and gamma-ray energy do not appear to affect the score materially. However, even for these positions the scores for I^{125} and Hg^{197} do not equal those for Hg^{203} and I^{131}. Septal crossover with the higher gamma-ray energies lowers the scores for all collimators. For the deep positions there is even less difference between collimator configurations, but the score is much more dependent upon gamma-ray energy. The scores achieved with I^{125} and Hg^{197} are less than one-third those obtained with Hg^{203} and I^{131}. Above the apparent optimum energies of Hg^{203} and I^{131}, septal crossover and penetration of shielding again result in decreased target: non-target ratios resulting in lower scores.

If differences in collimator resolution are to be detected by this test system, the differences should be apparent if the scores for detecting small spheres are compared with the scores for detecting large spheres. Figures 4 and 5 present these data. As expected, the 61-channel collimator has a higher score for detecting the 1- and 1.5-cm spheres and the 19-channel collimator is superior for detecting the 2- and 3-cm-diam. spheres.

It is important to note that these conclusions are only applicable to the conditions under which these experiments were performed. Changes in the concentration of the radioisotopes and scanning speed could markedly alter the results.

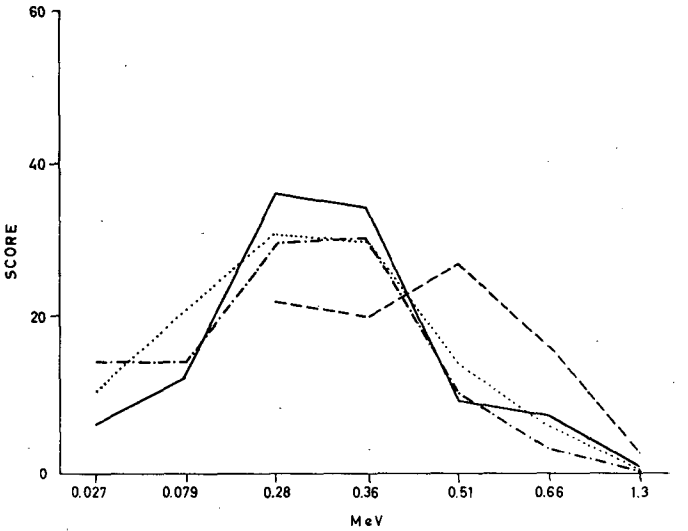

Fig.4

Small spheres

—— 61 lead
..... 37 lead
—·— 19 lead
----- 37 tungsten

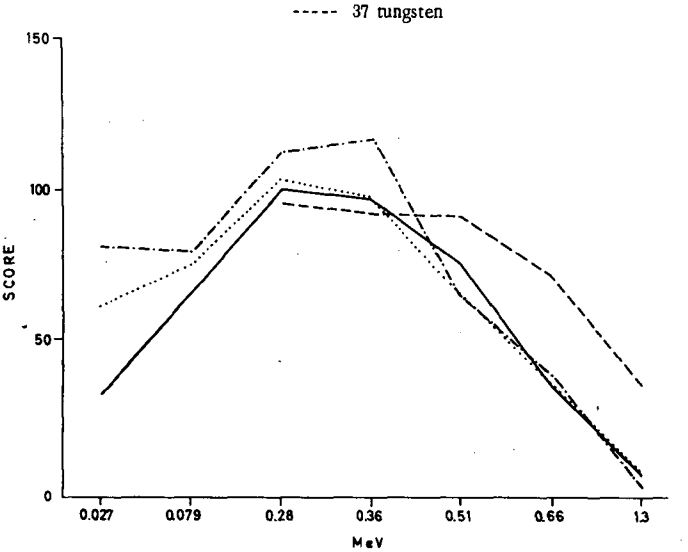

Fig.5

Big spheres

—— 61 lead
..... 37 lead
—·— 19 lead
----- 37 tungsten

SUMMARY

Four 3-in focusing collimators were evaluated with the IAEA Scanning Phantom using seven radionuclides having gamma-ray energies from 0.027 MeV to 1.3 MeV. Under conditions of low isotope concentration and slow scan speed, the following conclusions were reached:

(1) Collimator resolution is not an important factor in obtaining a high score for visualizing the spheres within the IAEA phantom. Apparently the increased count-rate obtained with coarse collimators balances the loss of resolution. The net effect is neither a gain nor a loss in ability to detect the "tumours".

(2) Gamma-ray energy is the single most important factor in obtaining a high score for visualizing the spheres. Maximum scores with the lead collimators were obtained with Hg^{203} (0.279 MeV) and I^{131} (0.364 MeV). The scores for Hg^{197} and I^{125} were 60% of the maximum achieved with Hg^{203} and I^{131}.

(3) The 61-channel collimator is superior to the others for visualizing the 1- and 1.5-cm-diam. spheres. The 19-channel collimator is superior for the visualization of the 2- and 3-cm-diam. spheres.

(4) The tungsten collimator has a 50% higher score than the lead collimators at 0.51 MeV and this advantage increases with increasing gamma-ray energy.

REFERENCES

[1] BECK, R.W., A Theoretical Evaluation of Brain Scanning Systems, J. nucl. Med. 2 (1961) 313-324.

[2] CHRISTIE, J.H. and MacINTYRE, W.J., Liver Scanning, Progress in Medical Radioisotope Scanning, ORINS, Oak Ridge, Tenn. (1962) 405-431.

[3] "Discussion on Design of Standard Phantom", Medical Radioisotope Scanning, IAEA, Vienna (1959) 251-253.

DISCUSSION

C. KELLERSHOHN: The curves which show score versus radiation energy do not go below 0.28 MeV for the tungsten collimators. Why?

M. BENDER: We assume that the tungsten collimator would show to advantage only at the higher energies where septal crossover was the important factor in degrading the information. At 0.5 MeV the scores for the tungsten were roughly twice what they were for any of the leads, but since the process tends to be a very tedious one we decided not to try to do the same thing at the lower values.

C. HARRIS: Would you agree that the transmissions of most collimators are too low at 280 keV and below? At < 160 keV the septa can hardly be made thin enough . And would you also agree that collimator properties are scatter-dominated below 160 keV and penetration-dominated above that value?

M. BENDER: Yes.

C. HARRIS: Then don't you think that the low-energy scores might have been improved if you had used asymmetrical window settings?

M. BENDER: In my opinion, a 20% window centred over 0.079 MeV comes fairly close to the "asymmetrical" window which you recommend for Hg^{197}.

P. HARPER: Did you attempt to correlate the results with whether or not the spheres covered the entire field of view of the collimators?

M. BENDER: No, but the data are in the tables and this information could be obtained easily.

W. PAUL: Can you tell me what the resolution diameters were for the collimators with 19, 37 and 61 holes?

M. BENDER: No, but these are standard Oak Ridge National Laboratory designs. The relevant data can be found in the literature.

J. MALLARD: Can you tell me whether the collimators which did best for the deep tumours showed isocount lines which were higher at the lower depths, i.e. which were more "depth independent"?

M. BENDER: All the collimators were 3-in point-focus collimators.

J. MALLARD: So the effect you describe is purely an energy effect?

M. BENDER: Yes.

D. KUHL: Since photon energy affects crystal efficiency and attenuation in the phantom as well as septal penetration, would it not be better to normalize the photon density in the phantom for each radio-nuclide rather than normalize the count rate over the phantom with a bare crystal?

M. BENDER: With the "clinical" concentration used in this study the statistics of each scanning situation probably affect the quality of the resulting image more than any other single factor. Since the primary purpose of the study was to evaluate collimator configuration as a function of gamma-ray energy it was felt that the statistics should be kept the same for every isotope. Because of this we had to use ten times as much I^{125} as we did Hg^{203}, five times as much Hg^{197} and three times as much Ce^{141}.

C. M. E. MATTHEWS: If the aim is to compare different isotopes rather than different gamma energies, it seems to me that it would be better to normalize to the dose in rads delivered to the critical organ rather than to gamma-ray density, since this dose will depend on the beta rather than the gamma emission. I have done this in calculating the statistical probability of detection. Using this calculation and the experimentally measured figure of merit which I mentioned in the discussion on Dr. Brownell's paper *, I found very similar results and there was little difference for different collimators. I am interested to see that you obtained the same results experimentally.

D. KUHL: I have two further comments. Firstly, the difficulty of normalizing the radiation dose to the patient lies in the fact that this frequently depends more on the beta component and the biochemistry of the labelled compound than on the physics of the photons associated. Secondly, it would be surprising if collimators sufficiently thick in septa for higher-energy photons would be of advantage below 270 keV. Collimators designed to take advantage of energies of less than 270 keV would have thinner septa and be shorter, and would probably be more efficient. As far as I can see no collimators of this sort were studied by you.

M. BENDER: I agree, but these four collimators are the ones most

* BROWNELL, G.L., "Theory of radioisotope scanning" (SM-51/58), these Proceedings I.

commonly used nowadays. Perhaps one should not use isotopes emitting exceptionally low - or high-energy gamma rays unless the detector is optimized for that particular energy. Even with optimum detector design I believe that gamma attenuation for energies below 150 keV will be prohibitive for the visualization of small deep lesions.

A. M. BAPTISTA: Can you give me some background information on this phantom?

M. BENDER: I would refer you to Reference [3] in our paper. In my opinion the phantom provides an ideal means of answering such basic questions as how large, how superficial or how "hot" a lesion must be if it is to be visualized with a particular scanning system.

THE DESIGN AND PERFORMANCE OF A LARGE HIGH-RESOLUTION FOCUSING COLLIMATOR*

C.C. HARRIS, P.R. BELL, M.M. SATTERFIELD, D.A. ROSS AND J.C. JORDAN
OAK RIDGE NATIONAL LABORATORY, TENN.,
UNITED STATES OF AMERICA

Abstract — Résumé — Аннотация — Resumen

THE DESIGN AND PERFORMANCE OF A LARGE HIGH-RESOLUTION FOCUSING COLLIMATOR. The primary reason for use of a "focusing collimator" is to permit the use of a large detector giving increased counting rate without loss of spatial resolving power. Since many apertures aimed at a common point are used, a sort of "focusing" effect is achieved. Because the septa between the apertures are necessarily thin, penetration of these walls by gamma rays causes a loss of spatial resolution. Tungsten and gold have been used (for 3-in-diam. detectors) to reduce this penetration as compared with lead. Reducing penetration by using a longer lead collimator damages the main design objective, that of increased counting rate, unless a larger detector is also used.

We have designed and constructed a 91-hole lead collimator for use with a 5.25-in (13.5 cm) by 3-in (7.5 cm) NaI(Tl) detector. The focal point is 9.5 in (24 cm) from the detector, and the solid angle of acceptance is the same as focusing collimators in common use with 3-in detectors. The maximum length is 6.5 in (16.5 cm); normal design length is 5.5 in (14 cm). At these lengths, the optical "circles of resolution" are 0.476 in (1.2 cm) and 0.304 in (0.77 cm) respectively.

The designs achieved the following: (1) A longer focal distance with an increase of counting efficiency due to the larger phosphor; (2) a lead collimator with a resolving power comparable with shorter gold collimators (a scan of a point source of $Cs\text{-}Ba^{137}$ appears only 7 mm in diam.); (3) a high-resolution collimator for human and small animal scanning; (4) a basic assembly design for use with larger-solid-angle collimators for increased counting efficiency.

Total-body scans have been made with Au^{198} and I^{131}. The scans indicate the increased efficiency and resolution of the 5.5-in collimator. A scan (Au^{198}) of a dog with the 6.5-in collimator showed well a concentration of activity apparently less than ¼ in (6 mm) in diam.; the activity was only five times "body background" but was clearly separated by ¼ in from a ¾-in diam. source about 50 times more intense.

ÉTUDE D'UN GRAND COLLIMATEUR A FOCALISATION ET FORT POUVOIR DE RÉSOLUTION: RÉSULTATS. Le collimateur à focalisation a pour principal avantage de permettre l'emploi d'un grand détecteur pour augmenter le taux de comptage sans diminuer la résolution dans l'espace. Un grand nombre d'orifices étant orientés vers un point unique, on obtient une sorte d'effet «de focalisation» Etant donné que les parois entre les orifices sont obligatoirement minces, la pénétration de ces parois par les rayons gamma provoque une diminution de la résolution dans l'espace. Afin d'atténuer cette pénétration, on a utilisé, au lieu de plomb, le tungstène et l'or pour les détecteurs de 7,5 cm de diamètre. A moins d'utiliser aussi un plus grand détecteur, le fait d'utiliser un collimateur en plomb plus long pour réduire la pénétration compromet l'objectif essentiel de l'étude de l'appareil, qui est d'augmenter le taux de comptage.

Les auteurs ont étudié et construit un collimateur en plomb, à 91 orifices, destiné à être utilisé avec un détecteur à NaI(Tl) de 13,5 cm sur 7,5 cm. Le foyer est à 24 cm détecteur, et l'angle solide d'acceptation est le même que pour les collimateurs à focalisation utilisés couramment avec des détecteurs de 7,5 cm. La longueur maximum est de 16,5 cm; la longueur normale de l'appareil étudié est de 14 cm. A ces longueurs, les «cercles de résolution» optiques sont de 1,2 cm et 0,77 cm, respectivement.

Les résultats de l'étude sont les suivants: a) distance focale plus longue et augmentation de l'efficacité de comptage, grâce à l'emploi d'un scintillateur de plus grandes dimensions; b) collimateur en plomb, avec résolution comparable à celle de collimateurs en or, plus courts (sur le scintigramme, l'image d'une source

* Research sponsored by United States Atomic Energy Commission under Contract with the Union Carbide Corporation

ponctuelle de Cs-^{137}Ba ne mesure que 7 mm de diamètre); c) collimateur à fort pouvoir de résolution, pour la scintigraphie de l'homme et des petits animaux; d) ensemble standard destiné à être utilisé avec des collimateurs à plus grand angle solide, en vue d'augmenter l'efficacité de comptage.

Des scintigrammes de l'organisme entier ont été obtenus au moyen de ^{198}Au et de ^{131}I. Ces scintigrammes montrent que le collimateur de 14 cm a une plus grande efficacité et une plus grande résolution. Sur un scintigramme (^{198}Au) de chien obtenu au moyen du collimateur de 16,5 cm, on a discerné nettement une zone active d'un diamètre apparent inférieur à 6 mm; l'activité n'était que cinq fois supérieure au bruit de fond dû aux tissus, mais la zone active était nettement séparée par un espace d 0,6 cm d'une source environ cinquante fois plus intense ayant un diamètre de 1,8 cm.

КОНСТРУКЦИЯ И ХАРАКТЕРИСТИКА КРУПНОГО ФОКУСИРУЮЩЕГО КОЛЛИМАТОРА С ВЫСОКОЙ СТЕПЕНЬЮ РАЗРЕШЕНИЯ. Основная причина использования "фокусирующего коллиматора" сводится к тому, чтобы позволить использовать крупный детектор, дающий повышенную скорость счета без потери пространственной разрешающей способности. Поскольку используется несколько апертур, направленных на одну общую точку, достигается хороший "фокусирующий" эффект. Ввиду необходимости иметь тонкую перегородку между апертурами, проникновение сквозь эти стенки гамма-лучей вызывает потерю пространственного разрешения. Были использованы вольфрам и золото (для детекторов диаметром 7,5 см) для того, чтобы уменьшить это, что дало возможность провести проникновение по сравнению с тем, когда применяется свинец. Уменьшение проникновения за счет применения удлиненного свинцового коллиматора наносит ущерб основным конструкционным целям из-за увеличения скорости счета, если не используется также крупный детектор.

Авторы спроектировали и создали свинцовый коллиматор с 91 отверстием для использования с детектором NaJ (Tl) размером 13,5 × 7,5 см. Фокус находится на расстоянии 24 см от детектора, а пространственный угол восприятия аналогичен углам фокусирующих коллиматоров при одновременном использовании их с детекторами на 7,5 см. Максимальная длина составляет 16,5 см; обычная длина конструкции составляет 14 см. При данных величинах длины оптические "окружности разрешения" составляют соответственно 1,2 и 0,77 см.

Эти конструкции дают следующее: 1. Более длинное фокусное расстояние с одновременным увеличением эффективности счета благодаря более крупному люминофору. 2. Свинцовый коллиматор с разрешающей способностью, которую можно сравнить с более короткими коллиматорами из золота (сценнограмма точечного источника Cs—Ba^{137} имеет диаметр всего 7 мм). 3. Коллиматор с высокой степенью разрешения для сценнирования человеческого организма и мелких животных. 4. Основная конструкция сборки для использования коллиматоров с более крупным пространственным углом для увеличения эффективности счета.

Получены сценнограммы всего организма с применением золота-198 и йода-131. Обнаружена возросшая эффективность и разрешение 14-см коллиматора. На сценнограмме собаки с 16,5 см коллиматором хорошо видна концентрация активности, имеющая, очевидно, в диаметре менее 6 мм; активность, лишь в 5 раз превышающая "фон организма", все же была четко отделена расстоянием 6 мм от источника диаметром 1,8 см с более высоким (в 50 раз) уровнем активности.

DISEÑO Y FUNCIONAMIENTO DE UN GRAN COLIMADOR ENFOCADO DE ALTO PODER DE RESOLUCIÓN. Los «colimadores enfocados» permiten utilizar detectores de grandes dimensiones que dan un índice de recuento mayor sin pérdida del poder de resolución espacial. Como estos colimadores tienen muchos canales dirigidos hacia un mismo punto se obtiene con ellos una especie de efecto «de enfoque». Los tabiques de esos canales son necesariamente delgados y, por consiguiente, los rayos gamma los atraviesan en detrimento de la resolución espacial. A fin de reducir esa penetración se han empleado, para detectores de 3 pulg de diámetro, colimadores de wolframio y oro, de preferencia a los de plomo. Si se reduce la penetración empleando un colimador de plomo más largo se malogra la finalidad perseguida ya que el índice de recuento disminuye, a no ser que se emplee también un detector de mayores dimensiones.

Los autores han diseñado y construido un colimador de plomo de 91 canales para emplearlo con un detector de NaI(Tl) de 5,25 pulg (13,5 cm) por 3 pulg (7,5 cm). El foco está situado a 9,5 pulg (24 cm) del detector, y el ángulo sólido de admisión es igual al de los colimadores enfocados que se emplean corrientemente con detectores de 3 pulg. La longitud máxima es de 6,5 pulg (16,5 cm); la normal es de 5,5 pulg (14 cm). Para estas longitudes, los «círculos de resolución» ópticos son, respectivamente, de 0,476 pulg (1,2 cm) y 0,304 pulg (0,77 cm).

Se han logrado las siguientes mejoras: a) un incremento de la distancia focal con un aumento de la eficacia de recuento debida al empleo de un cristal de mayores dimensiones; b) un colimador de plomo con un poder de resolución comparable al de los colimadores de oro más cortos (la imagen de una fuente puntiforme de $Cs^{-137}Ba$ tiene sólo 7 mm de diámetro); c) un colimador de alto poder de resolución para la exploración en seres humanos y animales pequeños; d) una estructura básica diseñada de modo que permite emplear colimadores de ángulo sólido mayor para incrementar la eficacia de recuento.

Se han efectuado exploraciones del organismo entero con oro-198 y yodo-131. Las imágenes indican una mejora de la eficacia y del poder de resolución del colimador de 5,5 pulg. La imagen de un perro obtenida con el colimador de 6,5 pulg en una exploración efectuada con oro-198 mostró muy bien una concentración de actividad de un diámetro aparentemente de menos de 0,25 pulg (6 mm); la actividad era sólo cinco veces mayor que el «fondo corporal», pero quedaba claramente separada por 0,25 pulg de una fuente de 0,75 pulg de diámetro unas 50 veces más intensa.

The purpose of the "focusing" collimators (more properly called convergent multiple channel collimators) used in scanning is to obtain high efficiency through the use of a large detecting crystal. At the same time, good spatial resolution is provided. The focusing effect results simply from the presence of many holes, aimed at a common point. Since gamma rays penetrate all materials, and particularly the rather thin partitions between the collimator holes, leakage always causes some loss of spatial resolution. In the absence of penetration – a condition approached at low gamma energies – the response of a collimator can be predicted entirely on optical considerations. The discussion will start on this basis.

Consider a collimator consisting of a single, tapered, hexagonal hole, as shown in Fig. 1, with walls aimed at the focal point. Let the length of the collimator be half the distance from crystal to focus. The plane passing through the focal point, and perpendicular to the axis of the hole, is the focal plane. Given this arrangement, an eye placed at the focus will see the outer and inner apertures of the hole one exactly behind the other, and thus none of the inner aperture is out of sight. As the eye is moved away from the focal point, however (always remaining in the focal plane), its view of the inner aperture (and therefore of the crystal) is gradually reduced, until finally, at displacement R, it is completely cut off. When the collimator length is half the distance from crystal to focal point, the radius of the "circle of resolution", R, is equal to the diameter of the collimator's inner aperture. For other collimator lengths, R is calculable from similar triangles. For the general case, $R = D/L\ d_i$; D is the distance from the external end of the collimator to the focal point, L is the length of the collimator, and d_i is the diameter of the inner aperture.

Note also, from Fig. 1, that the diameter of the "50% contour" holds no magic. The half-maximum width, or the width at any other level for that matter, is always a predictable fraction of R.

Simple geometry can be used to calculate the area of the inner aperture in view at each stage of the cutting-off process, and thus we can plot the response of the detector, as percentage of maximum, in terms of the displacement of a very small, low-energy source away from the on-centre position. See Fig. 1. To make the treatment valid for any collimator length, the displacement is in terms of X/R, the fraction of the displacement required for complete cut-off. Two cases will arise, depending on whether the direction of motion corresponds with the greater or the lesser diameter

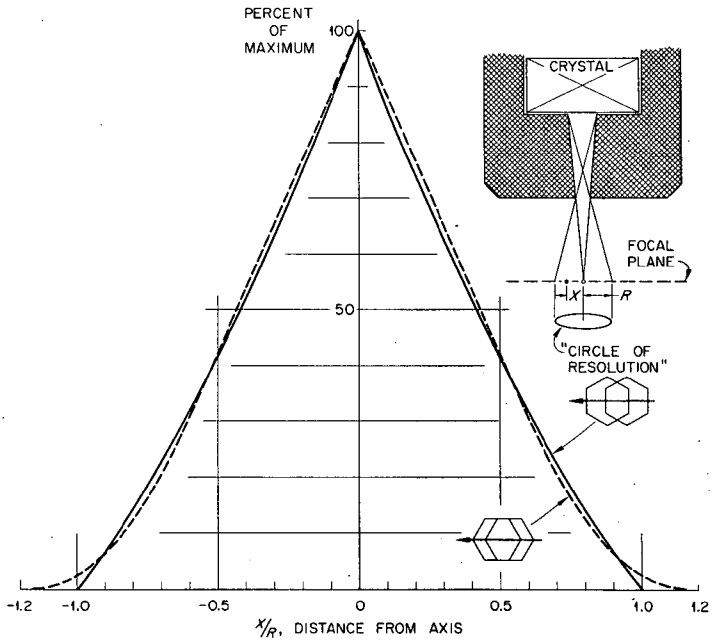

Fig. 1

Diagram to show the derivation of the "optical response" that visible light would give, with a hexagonal collimator hole. There will be two curves, since there are two ways of crossing the image of the hexagon (see small inserts). Both responses are nearly triangular.

of the hexagon; hence two curves are shown. They are not strikingly different, and both are nearly triangular; when the hexagon is traversed along its major diameter, the cut-off point is only about 15% farther out.

Figure 2 shows these curves replotted with a logarithmic response scale; here the slope of a curve will indicate how fast the collimator is cutting off. The differences between the two cases are brought out more clearly here. With both modes, however, the response starts falling at a fair rate, and is soon falling steeply.

This is the calculated response for a single collimator hole. A number of holes can be designed to look at the same point, but because of manufacturing errors they will not do so perfectly, and the response will therefore be smudged a little. Moreover, the geometry shows that for the slanting holes R will be a little greater than for the vertical one, which adds to the smudging. With careful fabrication, the performance can be gratifying.

So far we have assumed no leakage through the septa, and have calculated the "optical response" that would hold for visible light. The right-hand side of Fig. 2 shows how the actual, measured response departs from the optical curve when mildly penetrating gamma-rays are used (323 keV). The Cr^{51} source is very small, $\frac{1}{4}$ mm for the axial region of the picture where there was no need for the activity to be high. The collimator was the $5\frac{1}{2}$-in lead one shown in Fig. 3. Here 323-keV gamma-rays and visible photons behave similarly from the 100% level down to 1 or 2%, except that the

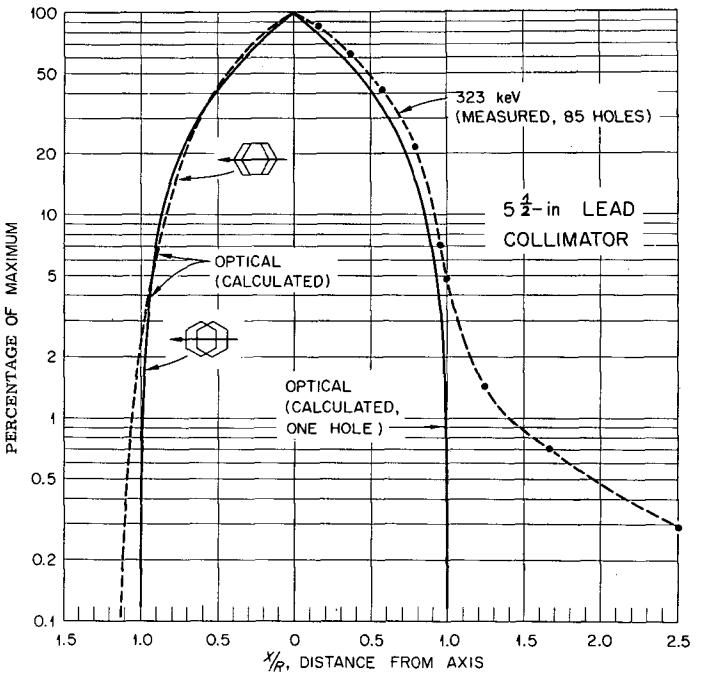

Fig.2

Left-hand side: log plot of the two "optical" curves of Fig.1, to bring out the small differences.
Right-hand side: the "optical" response again, compared with the gamma-ray response (323 keV) of the 85-hole, 5½-in lead collimator shown in Fig.3. Cut-off is incomplete, due to leakage through the partitions.

presence of 85 holes widens the focal area slightly. In the low percentage region the curve spreads rapidly, and this is clearly due to leakage. At the Cr^{51} energy the leakage is rarely serious, but with higher-energy radiation the spreading becomes more prominent.

It would seem, then, that a good focusing collimator is simply one that provides a gamma-ray response closely approaching a chosen optical response. It also appears that an approach to collimator design can be made using rather simple steps. First the size of the crystal is selected; then one must choose the distance from crystal to focal point. This fixes the "gross solid angle", the entire solid angle subtended by the crystal at the focal point. The net solid angle is the sum of the solid angles of all the holes, and is less than the gross solid angle because of the lead partitions. The ratio of net angle to gross is termed the transmission factor; it roughly defines the fraction of the crystal face that looks into the collimator holes – or, the fraction of the crystal face that is "used". Naturally, one would like to make this ratio high, but it can approach unity only at the expense of partition thickness, so there must always be a compromise between good transmission (bringing improved count-rate) and septal leakage. Experience shows that it is a mistake to use transmissions much above 50%, unless the collimator's service will definitely be restricted to the low-energy emitters.

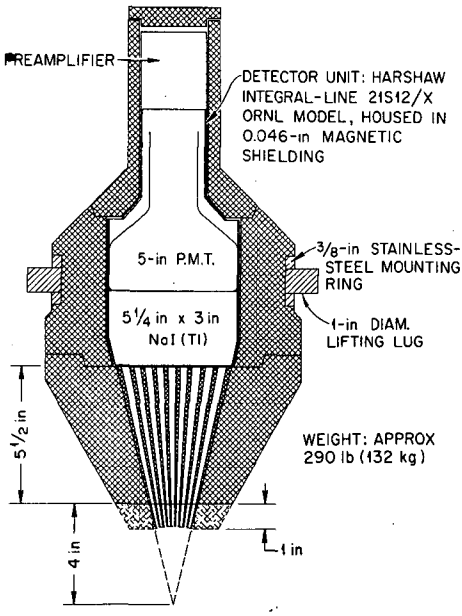

Fig.3

Longitudinal section through the new, lead-shielded detector, showing the components. The collimator insert is cast 6½-in long, to provide for special, high-resolution work. Normally the outer inch is machined off.

Transmission factor is related to the number of collimator holes; with few holes, the septa can be thick, giving low leakage but poor transmission.

The distance from crystal to focal point can now be divided, tentatively, into collimator length and working clearance. Considering the future uses of the collimator, one then chooses the radius of the optical circle of resolution. To specify "50% diameter", simply calculate R by direct proportion - see Fig.1. When collimator length, working clearance, and R have been chosen, the diameter of the inner aperture follows by simple geometry (see collimator diagram in Fig. 1). This diameter, together with the transmission, fixes the number of holes: one knows the area of the crystal face; multiply by the transmission to get "used" area; the inner-aperture size determines its area; divide this into the "used" crystal area to get the number of holes. A bit of minor juggling will be needed to fit the number of holes into the hexagonal pattern.

Before the design is frozen, however, a check should be made to see whether enough septal material has been allowed. BECK [1] has calculated the approximate, effective path length, L', presented by the septa to an off-target ray, as $L' = L(1 - T)$. L is collimator length and T is transmission factor. Assuming an energy of interest, one can calculate the attenuation from the effective path length and the absorption coefficient of the material. The number of holes, the transmission factor, and the collimator length can now be juggled against one another until a practical hexagonal design, with tolerable leakage, emerges.

Using this approach, we have constructed a lead collimator for a $5\frac{1}{4}$-in diam. by 3-in-thick sodium iodide crystal. The front face of the crystal was reduced in diameter to $4\frac{3}{4}$ in by bevelling the front corner, since the sodium iodide in this corner contributes little to crystal function, whereas lead, occupying the same space, significantly improves the lateral shielding. For this first collimator a gross solid angle of $\pi/16$ was chosen, this being the same as in many of the current commercial collimators. The resulting focal-point distance of $9\frac{1}{2}$ in was tentatively divided into $5\frac{1}{2}$ in for collimator length and 4 in for clearance.

The value desired for R was 0.25 in, or about 6 mm, making the diameter of the inner aperture about 0.34 in. The transmission selected was 50% (net solid angle $\pi/32$); this is a compromise, based on prior experience, between geometrical efficiency and adequate septal thickness.

The final design required only a slight adjustment to be acceptable and practical, with 91 holes, R = 0.24 in, and inner aperture = 0.33 in. The other quantities were the same as originally chosen. When off-axis leakage was calculated, it indicated that this lead collimator would confine its response to the optical acceptance region as well as a 3-in, 61-hole gold collimator shielded in tungsten.

A mould was made and several collimators were cast. (The half-pins at the six corners became damaged and were thereafter omitted, leaving 85 holes). The collimator as cast was actually $6\frac{1}{2}$ in long; thus, if it remained untrimmed at the small end it would make R = 0.152 in, which would perhaps provide unusually high resolution (although at reduced clearance) for use with human patients and small animals.

Figure 3 shows a section drawing of the detector assembly. The outer shield was designed for the minimum weight consistent with adequate lateral protection against the patient's body background. An energy of 511 keV was used for the leakage calculations. Total detector weight is about 132 kg, or 290 lb.

The properties of this new $5\frac{1}{2}$-in, 85-hole collimator were measured by moving point sources through the focal point, perpendicular to the axis of the central hole. Counting rate as a function of source position was obtained at enough points to define a "transverse response profile" at each of three energies: 1114 keV (Zn^{65}), 662 keV (Cs^{137}), 323 keV (Cr^{51}), and "zero" (calculated optical curve). Figure 4 compares this collimator's responses with those of an earlier, 3-in, gold-tungsten collimator with 61 holes. Since any complete response profile is symmetrical about the axis, only half of each curve is shown, with the gold collimator family on the left-hand side and the $5\frac{1}{2}$-in lead at the right.

The lead collimator should provide a counting rate at least 10% higher than in the 61-hole gold, for in the lead design the transmission factor is 10% higher; also, the larger crystal has greater inherent efficiency. The curves of Fig. 4 show that for comparable energies the leakages in the two collimators are remarkably similar. This suggests that the $5\frac{1}{2}$-in lead detector might be preferable to the smaller but more expensive gold-tungsten one. The large shield assembly, incidentally, can be used for other collimators where a large solid angle is needed.

Figure 5 provides a similar comparison between the normal $5\frac{1}{2}$-in collimator and the extra-long $6\frac{1}{2}$-in one. The primary reason for the extra length

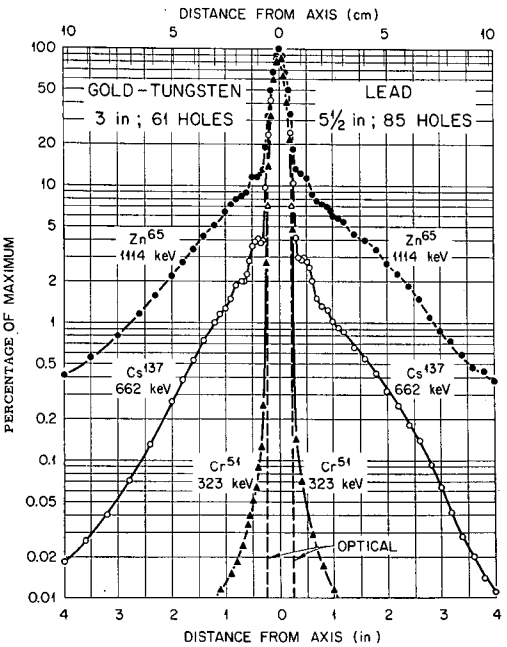

Fig. 4

Measured response curves (plus calculated, one-hole optical) for two collimators, using 3 source energies, as indicated. Left: 61-hole, 3-in long, gold-tungsten. Right: 85-hole, $5\frac{1}{2}$-in long, lead (Fig. 3). The performances are remarkably similar.

was to achieve a smaller optical circle of resolution, and to make the response more nearly optical. Figure 5 shows that this was accomplished. Since the leakage shown by the $5\frac{1}{2}$-in collimator is not distressing (especially below 662 keV) we are planning a further design in which the high resolution of the $6\frac{1}{2}$-in collimator (say R = 0.15 in) will be combined with a focal distance shortened to $8\frac{1}{2}$-in, thus achieving increased gross and net solid angles and a better counting rate. The 3-in working clearance of our current $6\frac{1}{2}$-in collimator will be used in the impending design, since it is adequate for most purposes; in fact, this is the clearance in many contemporary collimators using 3-in crystals.

The measurements that led to Figs. 4 and 5 also include axial or "Z-axis" data, and these show that the 3-in 61-hole gold and the $5\frac{1}{2}$-in lead collimators are about equal in this respect also. For example, at 323 keV the lengths of the contours of 50% and 30% of maximum response for the gold collimators are 1.4 and 2.3 in respectively. For the $5\frac{1}{2}$-in lead collimator these same lengths are 1.5 and 2.2 in respectively. The length of the sensitive region always increases with rising energy, but less with the long lead than with the shorter gold – an advantage inherent in a long collimator. In the extra-long version ($6\frac{1}{2}$-in), the 50% contour is 1.0 in long at 323 keV, and the 30% is 1.4 in long.

These numbers, together with Figs. 4 and 5, describe these large collimators to anyone generally familiar with point-source isoresponse plots of

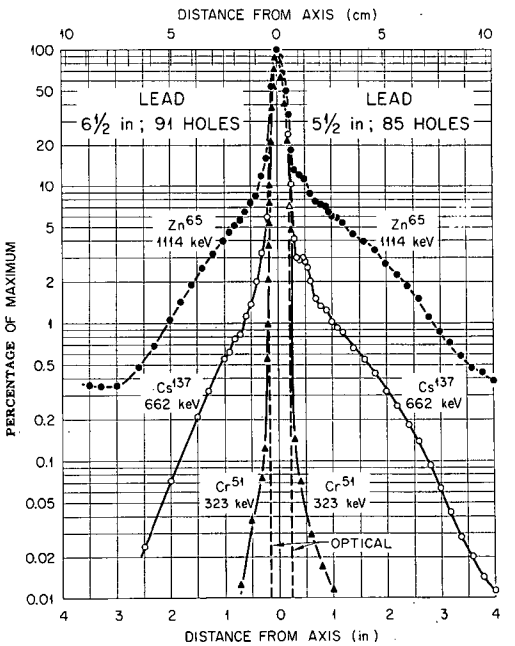

Fig. 5

Comparison, as in Fig. 4, between the long ($5\frac{1}{2}$-in) and extra-long ($6\frac{1}{2}$-in) lead collimators of Fig. 3. As anticipated, the $6\frac{1}{2}$-in version focuses more sharply, and permits less leakage.

multi-apertured collimators [2]. Such plots have similar appearances from collimator to collimator, differing mostly in the details shown in Figs. 4 and 5.

It is customary to demonstrate the performance of a collimator on some sort of phantom containing volume sources. There seems to be little agreement as to the best, or even a proper, phantom for such measurements. Perhaps this is because the usual spherical or cylindrical volume source or void is seen best if the collimator's circle of resolution is about the size of the source, and the size of the targets in the various phantoms have been wholly arbitrary. For this reason we do not particularly like this kind of test object. However, we do need some measure of practical worth for our new collimator, and since there is still almost no clinical experience with it, we have chosen three phantoms on which to try it out. Two of them were selected simply because they have appeared in the literature: these are the box phantom proposed at the IAEA conference in Vienna in 1959 [3], and the dish-and-stopper phantom of CHRISTIE and MacINTYRE [4], although we did not feel that either will tell us very much. The third phantom represents also only a beginning, but it contains sufficient structure to tax a collimator's performance. It will be described after discussion of the other two.

We made a series of measurements on the Vienna, 1959, "proposed standard phantom". The box was filled with a solution of I^{131}, and the

"tumours" contained 10 times as much activity per centimeter. For defect measurements, the tumours contained clean water. The phantom was scanned very slowly (0.01 in/s) and counting-rate profiles were obtained with a new

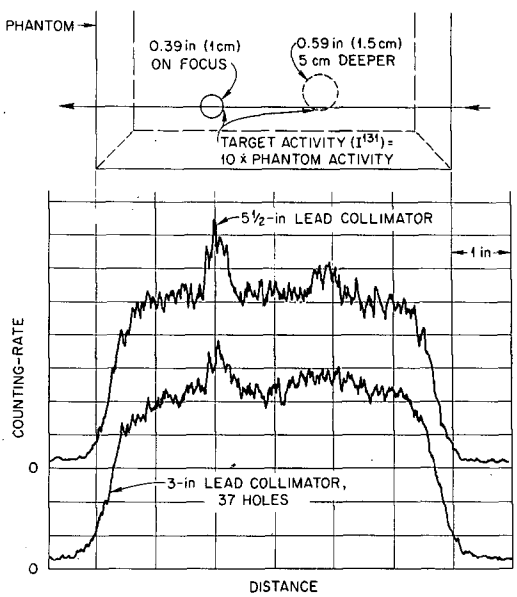

Fig. 6

Count-rate profiles for the "1959 Vienna standard phantom", with test spheres containing 10 times the $\mu c/cm^3$ of the surrounding water (I^{131}). The two collimators are lead: 85-hole $5\frac{1}{2}$-in, and 37-hole 3 in. Base lines are offset; count-rates not comparable (see text). The long collimator does a better job.

square-memory rate-recorder that does not suffer from exponential memory effects. Figure 6 shows the path traced by two collimators over the phantom; both collimators were moved so that their focal points passed through the 1-cm source. The collimator chosen to compare with the $5\frac{1}{2}$-in collimator is one in wide-spread use – a 3-in long, 37-hole lead collimator for a 3-in diam. crystal – focusing 3 in in front of the lead. Figure 6 shows the profiles obtained from the two collimators (note the base-line displacement), with the sources containing 10 times the box concentration. The profile for the long collimator looks better. The off-target counting-rates, incidentally, are not the same (the scales are different); the long collimator delivers only half the count-rate of the shorter one, in spite of having the same net solid angle. This is because the short collimator sees a larger volume of water, partly due to leakage from beside the sensitive volume, and from above and below. The extra counts, therefore, are spurious ones. The other profiles, including those run with non-radioactive tumours, show about the same contrast in performance. The energy band used was 324 to 404 keV.

Figure 7 shows a section view of a simple phantom, one of many used by Christie and MacIntyre. Several collimators were tested on this phantom,

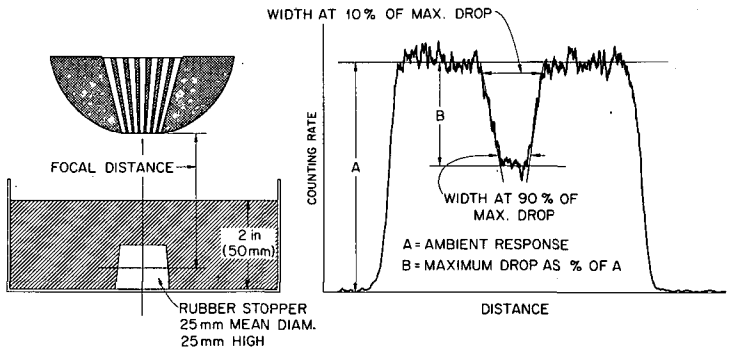

Fig. 7

The "stopper phantom" of Christie and MacIntyre. Response over stopper ideally should be 45.1% of that elsewhere. The widths of the trough where depression is 10% and 90% of maximum depression "B" indicate fidelity of response.

both by profile plotting and by scaler counts over the stopper and over the full depth of liquid (I^{131}, 324-404 keV). Figure 7 also shows the parameters used to describe the performance of several collimators. The counting-rates denoted as A (for the surrounding fluid) and B (looking at the stopper) were determined with a scaler. The depth of the drop in counting-rate over the stopper was determined and recorded as a percentage of A. The width of the profile is measured where the count-rate depression is 10% of the total drop, and again where it is 90%. This approach was chosen for two reasons. First, the often-used 50% width is uninformative, for it is always the same as the width of the stopper. Second, the profiles show a flat bottom to the drop over the stopper, something that has not previously appeared in published curves from this phantom. The "10% width" and the "90% width" show the shape of the drop. The width at 10% tells how sharp the break at the top is, and should be only a little over 1 in. The width at 90% gives some indication of the flatness of the bottom of the depression; the larger this is, the better the resolution. The profile shown in Fig. 7 came from a 37-hole, gold-tungsten collimator [5], with a 3-in crystal. The magnitude of the drop over the stopper is 42.4%, greater than the 37.5% reported by Christie for this same collimator. The shape of this profile leads us to believe that the older value is in error chiefly because of memory effects in the count-rate meter used for the older measurement.

Table I shows a comparison of several collimators, using the parameters defined in Fig. 7. We present this Table with some hesitation, realizing that it tempts a reader simply to choose the detector with the highest counting rate as supposedly best for his particular job. This would be a mistake. Compare the 37-hole gold and lead collimators: since they are optically identical, the higher count-rate with the lead can only be due to leakage, and thus the extra counts provide not information, but misinformation. There is further evidence for this in the size and shape of the count-rate depression as the detector passes over the stopper: with the lead collimator the 10% width is too large, the 90% width too narrow, and the dip is not deep enough (theoretical drop = 45%). We find similar signs of leakiness in comparing the 61-hole lead collimator with the 61-hole gold; the lead has

TABLE I

TABULATIONS OF THE RESULTS OF TESTING VARIOUS COLLIMATORS ON THE DISH-AND-STOPPER PHANTOM OF CHRISTIE AND MacINTYRE (1-in STOPPER)

Collimator	Counting rate (A) relative to 61-hole gold collimator	Percentage drop (B) over stopper Max. = 45.1%	Shape of Drop	
			10% width (in)	90% width (in)
3-in, 37-hole Pb	2.52	35.9	1.4	0.55
3-in, 61-hole Pb	1.52	35.5	1.25	0.75
3-in, 37-hole Au	1.36	42.4	1.26	0.7
3-in, 61-hole Au	1.00	42.6	1.17	0.65
$5\frac{1}{2}$-in, 85-hole Pb	1.23	42.9	1.19	0.72
$6\frac{1}{2}$-in, 91-hole Pb	0.5	44.8	1.16	0.75

(3-in-diam, 2-in thick crystal used with 3-in collimators, $5\frac{1}{4}$-in, 3-in-thick crystal used with large collimators.)

a higher count-rate and a smaller percentage drop over the stopper. Thus the short lead collimators get a poor rating, and the lower four look better. The progressively falling count-rate in these four is the price one pays for improving resolution; the other figures are quite comparable.

In short, a high count-rate may be desirable, but it is not in itself a guarantee of quality, and other characteristics must be considered along with it. We feel that other tests, with more demanding phantoms, will provide better guides.

The effect of target (or void) size is shown in an additional experiment. The test conditions were modified by raising the detector until its focalplane lay 1 in deep, at the middle of the water mass; then the large stopper was exchanged for a small, rubber cylinder, 0.5 × 0.5 in, suspended with its axis vertical and its centre at a depth of 1 in. A test run was made with each collimator, and the results are summarized in Table II. It confirms in general the earlier observations and conclusions, although here the percentage drop in count-rate ("B") comes surprisingly close to what it should be, for the 3-in gold, $5\frac{1}{2}$-in lead and $6\frac{1}{2}$-in lead collimators.

The unsuitability of these test objects for the prediction of general scanning performance – each concentrating on a narrow part of the overall picture – has recently led us to construct a crude sort of head phantom, which we have named "Alasper Yorick" for ease of reference [6]. It is basically a hollow, 6-in sphere of acrylic plastic containing radioactive background fluid, plus a number of "vascular" structures, two "tumours", and an insert containing higher activity to represent the background in the facial region. It is sketched at the right-hand side of Fig. 8. The numbers "14 ×" etc. refer to the radioactivity/cm^3 in the indicated component, relative to that of the background water in the head. This factor of 14 was culled from the published literature, but actually it should be higher because the

TABLE II

TABULATION OF THE RESULTS OF TESTING VARIOUS COLLIMATORS ON THE DISH-AND-STOPPER PHANTOM OF CHRISTIE AND MacINTYRE ($\frac{1}{2}$-in STOPPER AT MID-DEPTH OF LIQUID)

Collimator	Counting rate (A) relative to 61-hole gold collimator	Percentage drop (B) over stopper	Shape of drop	
			10% width (in)	90% width (in)
3-in, 37-hole Pb	2.52	14.5	0.78	0.23
3-in, 61-hole Pb	1.52	17.3	0.7	0.22
3-in, 37-hole Au	1.36	22.9	0.71	0.22
3-in, 61-hole Au	1.00	24.1	0.67	0.28
$5\frac{1}{2}$-in, 85-hole Pb	1.23	24.6	0.62	0.28
$6\frac{1}{2}$-in, 91-hole Pb	0.5	25.1	0.6	0.35

(Maximum theoretical drop is about 28% since the stopper is actually 0.55 in tall.)

walls of our "vascular" tubes contain no activity, whereas in the head vessels they would. It is clear, at any rate, that the normal vessels are much easier to see in a real head scan than in our phantom, and to this extent

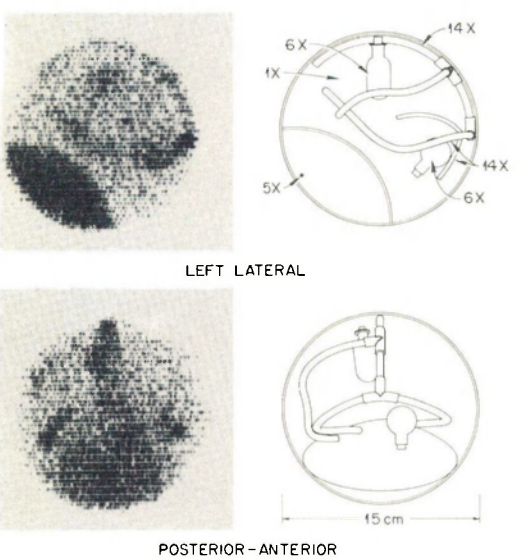

Fig. 8

Scans of head phantom containing I^{131}. Collimator: lead, $5\frac{1}{2}$-in, 85-holes. Top: Left lateral scan with drawing at right to show structures in the phantom. The numbers refer to the net loading/cm^3 relative to the surrounding fluid. Bottom: Postero-anterior scan with corresponding drawing at right.

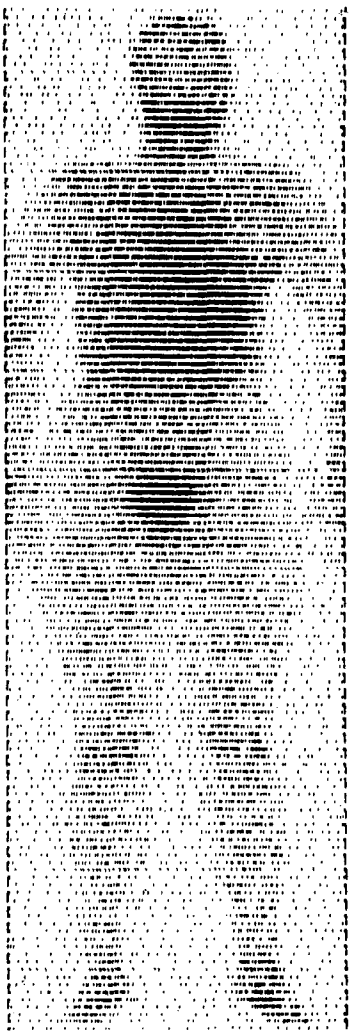

Fig. 9

Whole-body scan with $5\frac{1}{2}$-in lead collimator. Thyroid cancer patient, thyroid previously removed, no known metastases (ORINS No. 810874). 5 mc NaI^{131} by mouth, 5 h before scan. (Courtesy of Medical Division, Oak Ridge Institute of Nuclear Studies, Inc., under contract with the USAEC).

Alasper represents an unrealistically demanding test target. Studies with this phantom are still in the early stage, but in time it should provide all the information obtained from the other phantoms. In addition, we may well obtain minimum detectability criteria for physically realistic targets.

A $5\frac{1}{2}$-in, 91-hole lead collimator in a shield somewhat thicker than the one shown in Fig. 3 was installed on an Ohio-Nuclear total-body scanner at the Medical Division of the Oak Ridge Institute of Nuclear Studies. The detector assembly was essentially the same as that of Fig. 3. During early

experimentation with the device a whole-body scan of a thyroid cancer patient was performed. The resulting record is shown in Fig. 9. It is felt that this record shows the expected excellent resolution of the collimator.

In collaboration with Dr. Takashi Honda of Kanazawa University – then with the Medical Division of the Oak Ridge Institute of Nuclear Studies – the $6\frac{1}{2}$-in, 91-hole collimator was used to scan a dog that had received an intralymphatic injection of colloidal gold-198. Figure 10 shows a ventrodorsal scan of the dog's pelvic region, taken 3 d after the injection. The intense activity at the lower left of the record is in the right popliteal lymph nodes. The sensitivity and resolution of the $6\frac{1}{2}$-in collimator are demonstrated in the portrayal of the activity in the iliac lymph node, near the centre of the record. A weak concentration, activity and size unknown, is shown just to

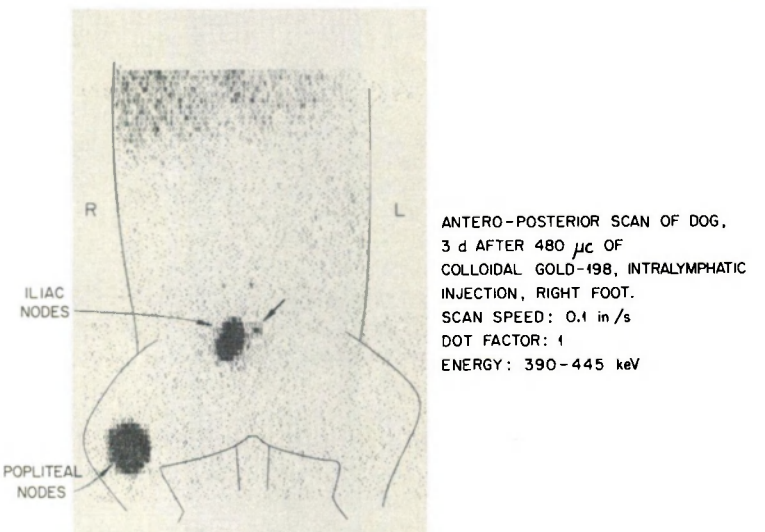

Fig. 10

Scan looking at stomach side of dog, using $6\frac{1}{2}$-in lead collimator. Note prominent popliteal and iliac nodes. The collimator demonstrates the space between iliac node and a small, weak spot just to its left. (In collaboration with pre-clinical section, ORINS Medical Division).

the right of the intense activity of the iliac node. Even though the activity in the iliac node is at least 50 times that in the spot beside it, the separation between the two – no larger than the small spot – is clean. This is a pretty clear indication that this collimator's small optical circle of resolution (R = 0.152 in) gives it highly useful properties.

In summary, this development provides the following: (1) A high-resolution, collimated detector with long working clearance, useful in human and small-animal scanning; (2) a detecting crystal having increased inherent efficiency; (3) a detector-collimator assembly made of lead, functionally equal to the earlier, gold-tungsten collimator yet only about half as expensive; (4) a detector-shield assembly that can be used for collimators for increased solid angle.

ACKNOWLEDGEMENTS

The authors gratefully acknowledge the tireless efforts of Ann Miller, Oak Ridge National Laboratory, in preparing this material for publication. We thank Brena Stevens and Ray Cockreham for their expert help in reproducing copies for use at the symposium. The work of W.C. Colwell, W.N. Tillery and their groups in preparing the illustrations is also gratefully acknowledged.

REFERENCES

[1] HARPER, P.V., BECK, R., CHARLESTON, D. and LATHROP, K.A., Nucleonics 22:1 (1964) 50-54.
[2] HARRIS, C.C., BELL, P.R., FRANCIS, J.E., Jr., SATTERFIELD, M.M., JORDAN, J.C. and MURRAY, J.P., Jr., Progress in Medical Radioisotope Scanning, United States Atomic Energy Commission TID 7673 (1963) 47-60.
[3] JOHNS, H.E., BENDER, M.A. et al., Medical Radioisotope Scanning, IAEA, Vienna (1959) 252-253.
[4] CHRISTIE, J.H. and MacINTYRE, W.J., Progress in Medical Radioisotope Scanning, USAEC, TID 7673 (1963) 420-423.
[5] FRANCIS, J.E., Jr., HARRIS, C.C. and BELL, P.R., J. nucl. Med. 3 (1962) 10-17.
[6] SHAKESPEARE, W., Hamlet, "Alas, poor Yorick; I knew him, Horatio; ..." Act 5, Scene I.

DISCUSSION

P. KENNY: Do you have any figures on the effect of the crystal bevel on the efficiency of the detector?

C. HARRIS: Pulse-height spectra show that the outer corners are very effective, even at 1114 keV; there is little or no degradation of resolution even for the outside holes. We are inclined to think that the bevel improves light collection from the corner region. We get a line width (FWHM) of 8.2% at 662 keV, both on the crystal in the Medical Division of the Oak Ridge Institute of Nuclear Studies and on the one in our laboratory.

A. GANDY: In your paper you make use of a concept which is very similar to our "transit-curve" concept. In your case however you consider the variation interval from 10 to 90% whereas we use the interval Λ, which is defined by the tangent at the point of inflexion.

Employing the concept of "rise time" (current in electronics), we first of all worked with the 10 to 90% interval and then found that the interval Λ was almost always equivalent to it. Whenever there was a difference we found that the interval Λ was nearer to the half-height width of the response curve; the values of this width can easily be expressed as a function of the parameters. We seem therefore to be expressing the same idea in two different ways.

C. HARRIS: I agree.

III

MOVING DETECTORS AND COLLIMATORS
(cont.)

COLLIMATORS FOR RADIOISOTOPE SCANNING SYSTEMS

R. N. BECK
ARGONNE CANCER RESEARCH HOSPITAL*,
CHICAGO, ILL., UNITED STATES OF AMERICA

Abstract — Résumé — Аннотация — Resumen

COLLIMATORS FOR RADIOISOTOPE SCANNING SYSTEMS. The total response of a collimator viewing a large distributed gamma-ray source consists of three components produced by gamma rays which enter the collimator (1) "geometrically" or properly, (2) by penetrating the collimator septa, and (3) by scattering in the source or collimator. This paper describes procedures for the design, construction and testing of focused collimators based on equations for these components. Since no single design procedure is appropriate for the entire range of gamma energies, the problem is considered in three parts.

(1) Below approximately 0.150 MeV, few gamma-rays can penetrate the thinnest lead septa which can be conveniently cast. Here the design procedure maximizes geometrical response for specified focal length, radius of view, septum thickness, and crystal diameter (or "shape factor", which determines the divergence of the collimator field of view, and can be used as an independent variable in place of crystal diameter).

(2) In the energy range from approximately 0.150 to 1 MeV, the response to gamma-rays which penetrate the collimator septa is not negligible and must be controlled. In this case, geometrical response is maximized for specified gamma energy, collimator material, focal length, radius of view, penetration fraction and crystal diameter (or shape factor).

(3) Above approximately 1 MeV, it is not always possible to design a multi-channel collimator having acceptably small penetration. In this case, a single hole having a taper which maximizes geometrical response is used.

In general, the pulse-amplitude spectrum from a collimated scintillation detector viewing a distributed source contains geometrical, penetration and scatter components. By a suitable choice of source configurations, these components can be separated experimentally for comparison with theoretical values.

Following modern practice in optics, a procedure is described for measuring collimator resolution in terms of "sine wave response" using a "sunburst" test pattern. It is suggested that this pattern be adopted as a standard for measuring over-all system resolution for distributed sources.

Techniques for casting and "facing off" multi-channel collimators having very thin septa (approximately 0.007 in) are briefly described.

COLLIMATEURS POUR SCINTIGRAPHES. La réponse totale d'un collimateur dirigé sur une source en volume de rayons gamma est la somme de trois composantes dues aux rayons gamma qui pénètrent dans le collimateur: a) «géométriquement» ou de façon normale; b) à travers les parois du collimateur; 3) par dispersion dans la source ou le collimateur. Le mémoire décrit des méthodes d'études, de réalisation et d'essai de collimateurs à focalisation, fondées sur les équations de ces trois composantes. Etant donné qu'aucune méthode d'études ne convient à toute la gamma des énergies gamma, l'auteur distingue trois cas:

1. Au-dessous d'environ 150 keV, peu de rayons gamma peuvent traverser les parois de plomb les plus minces qu'il est possible de mouler aisément. Dans ce cas, on cherche à obtenir la réponse «géométrique» optimum pour des valeurs données de la distance focale, du rayon du champ, de l'épaisseur des parois et du diamètre du cristal (ou du «facteur de forme», qui détermine la divergence du champ du collimateur et peut être utilisé comme variable indépendante à la place du diamètre du cristal).

2. Entre 150 keV et 1 MeV, la réponse aux rayons gamma qui traversent les parois du collimateur n'est pas négligeable et doit être contrôlée. Dans ce cas, on cherche à obtenir la réponse «géométrique» optimum pour des valeurs données de l'énergie gamma, du matériau du collimateur, de la distance focale, du rayon du champ, de la pénétration par les parois et du diamètre du cristal (ou du facteur de forme).

* Operated by the University of Chicago for the United States Atomic Energy Commission.

3. Au-dessus de 1 MeV, il n'est pas toujours possible de réaliser un collimateur à plusieurs canaux où la pénétration par les parois soit suffisamment petite pour être acceptable. Dans ce cas, on obtiendra la réponse «géométrique» optimum en utilisant un collimateur à une seule ouverture conique.

D'une manière générale, le spectre des amplitudes d'impulsion donné par un détecteur à scintillation collimaté, dirigé sur une source en volume, a trois composantes: «géométrie», pénétration et dispersion. Par un choix judicieux des configurations de la source, on peut séparer ces composantes par voie expérimentale, de manière à permettre une comparaison avec les valeurs théoriques.

S'inspirant de la pratique moderne en optique, l'auteur décrit une méthode qui permet de mesurer la résolution du collimateur en fonction de la «réponse à une onde sinusoïdale» provoquée au moyen d'une décharge violente. Il suggère d'adopter cette méthode pour mesurer la résolution de l'ensemble du dispositif pour les sources en volume.

Le mémoire décrit brièvement les techniques de moulage et de finissage de collimateurs à canaux multiples ayant des parois très minces (environ 0,2 mm).

КОЛЛИМАТОРЫ ДЛЯ СИСТЕМ РАДИОИЗОТОПНОГО СКЕННИРОВАНИЯ. Общая характеристика коллиматора для наблюдения за крупным распределенным источником гамма-лучей состоит из трех компонентов, образуемых гамма-лучами, которые попадают в коллиматор: 1) "геометрически" или правильно, 2) проникая через перегородки коллиматора и 3) рассеиваясь в источнике или коллиматоре. В этом докладе описываются процедуры, связанные с конструкцией, построением и испытанием сфокусированных коллиматоров, основанные на уравнениях для этих компонентов. Поскольку нет подходящей единой конструкционной процедуры для всего диапазона гамма-энергий, эта проблема рассматривается в трех разделах.

1. Некоторые гамма-лучи с энергией приблизительно ниже 0,150 Мэв могут проникать через тончайшие свинцовые перегородки, которые можно легко изготовить. В таком случае конструкционная процедура максимально увеличивает геометрическую характеристику для установленной длины фокусного расстояния, радиуса наблюдения, толщины перегородки и диаметра кристалла (или "коэффициент формы", который определяет дивергенцию сектора наблюдения коллиматора и может использоваться как независимая переменная вместо диаметра кристалла).

2. В диапазоне энергий приблизительно 0,150–1 Мэв характеристика для гамма-лучей, которые проникают через перегородки коллиматора, не является незначительной, и должна контролироваться. В этом случае геометрическая характеристика доводится до максимума для конкретного вида гамма-энергии, материала коллиматора, фокусного расстояния, радиуса наблюдения, проникающей фракции и диаметра кристалла (или коэффициент формы).

3. При энергиях примерно выше 1 Мэв не всегда возможно сконструировать многоканальный коллиматор, имеющий небольшую приемлемую степень проникновения. В этом случае используется единственное отверстие, имеющее крышку, которое доводит до максимума геометрическую характеристику.

В общем спектр амплитуды импульсов при наблюдении за распределенным источником с помощью сцинтилляционного детектора, снабженного коллиматором, содержит геометрические компоненты и компоненты проникновения и рассеяния. При соответствующем выборе конфигураций источника эти компоненты могут быть экспериментально разделены для сравнения с теоретическими величинами.

В соответствии с современной практикой в оптике описывается процедура для измерения разрешения коллиматора при условии "синусоидной волновой характеристики" с использованием экспериментального образца типа "солнечная вспышка". Предполагается, что этот образец будет принят в качестве стандарта при измерении разрешения всей системы для распределенных источников.

Кратко описываются методы изготовления и полировки многоканальных коллиматоров, имеющих очень тонкие перегородки (примерно 0,2 мм).

COLIMADORES PARA DISPOSITIVOS DE EXPLORACIÓN GAMMAGRÁFICA. La respuesta total de un colimador dirigido hacia una fuente muy extensa de rayos gamma es la suma de tres componentes, debidos a los rayos gamma que penetran en el colimador: a) «geométricamente» o de manera normal; b) atravesando los tabiques del colimador; c) por dispersión en la fuente o en el colimador. En la memoria se describen métodos de estudio, de fabricación y de ensayo de colimadores enfocados basados en las ecuaciones

de estos tres componentes. Como no existe un método único de estudio apropiado para todo el intervalo de energías gamma, el autor distingue tres casos.

1. Por debajo de 0,150 MeV aproximadamente, poco rayos gamma atraviesan los tabiques de plomo más delgados que pueden obtenerse fácilmente por colada. En este caso se trata de conseguir la respuesta geométrica óptima para valores dados de la distancia focal, del radio del campo, del espesor de los tabiques y del diámetro del cristal (o del «factor de forma», que determina la divergencia del campo del colimador y puede utilizarse como variable independiente en lugar del diámetro del cristal).

2. Entre 0,150 y 1 MeV aproximadamente, la respuesta a los rayos gamma que atraviesan los tabiques del colimador no es despreciable y debe ser controlada. En este caso se trata de obtener la respuesta geométrica óptima para valores dados de la energía gamma, del material del colimador, de la distancia focal, del radio del campo, de la penetración por los tabiques y del diámetro del cristal (o del factor de forma).

3. Por encima de 1 MeV no siempre es posible construir un colimador multicanal en el que la penetración por los tabiques sea suficientemente reducida. En este caso se obtendrá la respuesta geométrica óptima utilizando un colimador con un solo canal cónico.

Por lo general, el espectro de las amplitudes de impulso dado por un detector de centelleo colimado dirigido hacia una fuente extensa tiene tres componentes: geometría, penetración y dispersión. Si se elige bien la configuración de la fuente, estos componentes pueden separarse experimentalmente para compararlos con los valores teóricos.

Inspirándose en la prática actualmente seguida en óptica, el autor describe un método que permite medir el poder de resolución del colimador en función de la «respuesta a una onda sinusoidal» provocada mediante una descarga violenta. Sugiere que se adopte este método para medir el poder de resolución del conjunto del dispositivo para las fuentes extensas.

En la memoria se describen brevemente las técnicas de colado y pulido de colimadores multicanales con tabiques muy delgados (de 0,007 pulg aproximadamente).

1. INTRODUCTION

The successful use of scanning systems in diagnostic procedures depends upon the preferential uptake of the administered isotope in certain tissues and the detailed mapping of the distribution of radioactivity by means of a collimated gamma-ray detector (see Fig. 1). These procedures become useful clinical tests only if the radiation dosage to the patient is low, the time required is short, the statistical reliability is high and the spatial resolution of the distribution of radioactivity is good. These factors are determined by the sensitivity and field of view of the collimated detector. Making use of equations derived elsewhere [1] for collimator response to distributed sources, this paper deals with the design of single and multichannel collimators, such as those shown in Figs. 1 and 2.

2. DETECTOR RESPONSE

The total response of a scintillation detector is the sum of responses to gammas which have entered the collimator (a) properly (geometrical efficiency); (b) after being scattered in the source or collimator; and (c) by penetrating the collimator septa or surrounding shielding. The total response can be written as:

$$C\,(\text{counts/s}) = E_T\,\eta\sigma = E\,(1 + P + S)\,\eta\sigma,$$

where E_T (cm^2) = the total collimator efficiency, E (cm^2) = the geometrical

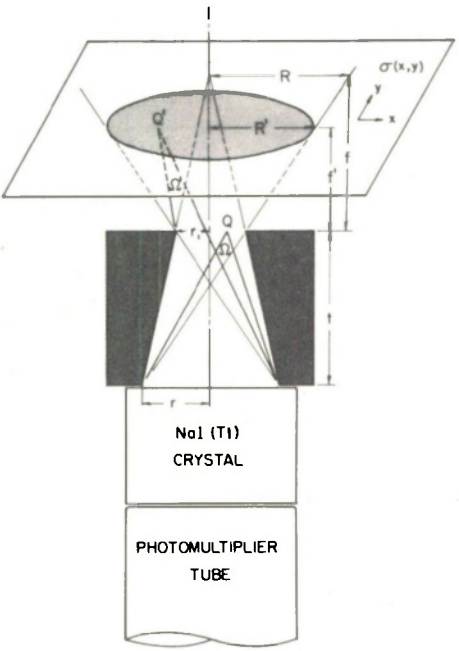
I
R
σ(x,y)
y
x
Q'
R'
f
f'
Ω₁
r₁
Q
Ω
t
r
NaI (Tl)
CRYSTAL
PHOTOMULTIPLIER
TUBE

Fig. 1

Scintillation detector with a single-hole collimator which defines a circular field of view with radius R' at distance f' The response to a uniform sheet distribution σ(γ's emitted/cm²s), is independent of the distance f' to the sheet.

efficiency for distributed sources, P = penetration fraction, or the penetration efficiency relative to the geometrical efficiency, S = scatter fraction, η = photopeak crystal efficiency, and σ(γ's emitted/cm² s) = source strength or the concentration of activity on a uniform sheet distribution*.

In any particular application σ is limited by the radiation dosage that can be permitted, and the response is determined by the detector efficiency (or sensitivity), $E_T\eta = E(1 + P + S)\eta$. To maximize sensitivity, the scintillation crystal should be large enough for η to be near 1; larger crystals simply increase the background count rate and require heavy shields. The total collimator efficiency E_T cannot be simply maximized, because the penetration and scatter components of response (EP and ES) degrade the spatial resolution. The aim of collimator design is then to maximize the geometrical efficiency E for a given set of conditions, while keeping P + S small compared to 1.

The scatter fraction is the sum of two components from scattering events which take place in the source and in the collimator. The source scatter fraction has been discussed elsewhere [1] and is not relevant to col-

* If the actual source is a uniform volume distribution having concentration ρ(γ's emitted/cm³ s), thickn ss H and attenuation coefficient μ, then the same response to unattenuated gammas would be observed if this source were replaced an "equivalent" sheet distribution $\sigma = \rho(1 - \exp - \mu H)/\mu$. Similar expressions apply when the volume distribution has a concentration which varies with depth.

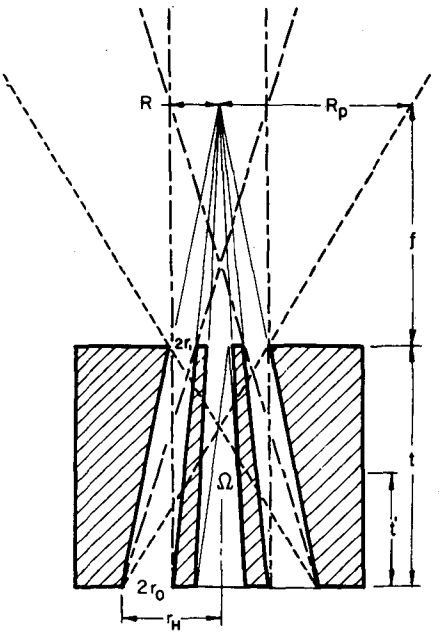

Fig. 2

Focussed collimator cross-section
Gamma rays arising anywhere within the fields of view of the small holes may enter the collimator properly or "geometrically".
In addition, gammas arising within the region defined by R_p may enter the detector by penetrating the collimator septa which must be made thick enough to limit the penetration to a negligible fraction of the geometrical response.

limator design. MATHER [2] has shown that the collimator scatter fraction is a monotonic increasing function of gamma energy and is less than 0.07 for energies below 1 MeV for a collimator with $t/r = 32$. This fraction is considered negligible and the problem of collimator design is reduced to a consideration of the geometrical and penetration responses.

3. COLLIMATOR DESIGN

Since no single design procedure is appropriate for the entire range of gamma energies, the problem is considered in three parts.

(1) Below approximately 150 keV, few gammas can penetrate the thinnest lead septa that can be conveniently cast. Here the design procedure maximizes geometrical response for specified focal length, radius of view, septum thickness and crystal diameter (or "shape factor", to be introduced later).

(2) In the energy range from approximately 150 keV to 1 MeV the response to gammas which penetrate the collimator septa is not negligible and must be controlled. In this case, geometrical response is maximized

for specified gamma energy, collimator material, focal length, radius of view, penetration fraction and crystal diameter (or shape factor).

(3) Above approximately 1 MeV it is not always possible to design a multichannel collimator having an acceptably low penetration fraction. In this case, a single hole having a taper that maximizes geometrical response is used.

3. 1. Specification of parameters

In all cases the design procedure requires the specification of a certain radius of view R' at a certain distance f' from the collimator face, where f' may not be equal to f, the "focal" distance (see Fig. 1). The choice of R' may be based on any one of several considerations.

(1) First, we may have in mind the smallest tumour that we hope to detect, and a range of depths at which it might exist. For example, we may wish to design a collimator for detecting brain lesions that are at least 2 cm in diameter and that might exist anywhere between the surface of the brain and the midline. NEWELL [3] has concluded that any choice of 2R' between 0.9 and 2 times the tumour diameter is within 20% of optimum. Here, "optimum" is determined by a statistical criterion based on the time required to detect the tumour. If, in addition to detection time, some significance is attached to the sharpness with which the tumour is outlined (this is important if the tumour is to be detected by a visual inspection of the scan picture), then the optimum diameter of view is probably closer to the small end of the range specified by Newell. Thus, a choice of 2R' equal to the tumour diameter should not be far from optimum.

(2) An alternative, but similar, basis for choosing R' is as follows: A suitable detector figure of merit Q is maximized by some value of R' for detecting structures of a specified size. The procedure for finding this R' is facilitated by expressing Q in terms of the "modulation transfer function" M which can be conveniently measured as a function of R'. The quantities Q and M are discussed in section 5. 2.

(3) Finally, for a given source concentration σ in an area A to be scanned in time T, the value of R' which maximizes the "information content" I in the scan picture can be computed [1].

3. 2. Single-hole collimators

In the case of single-hole collimators (which may be the only possibility for relatively high energy gammas), MATHER [2] has shown that the effective radius of view is larger than R' because of edge penetration. If a slab equal in thickness to one mean free path length in lead were removed from each face of the collimator, then the R' would equal the effective radius of view with edge penetration.

With the choice of R' determined by this and the above considerations and f' set approximately equal to the deepest structure that we wish to detect, it remains only to maximize the geometrical efficiency, which can be expressed in a very general form applicable to straight and tapered holes:

$$E = \frac{\pi r^2}{4t^2}\left(\frac{tR' - f'r}{f' + t}\right)^2 \tag{1}$$

The simplest collimator is a single straight hole, for which Eq. (1) can be put in the form:

$$E = \frac{\pi r^2}{16f'^2}(R' - r)^2 .$$

For specified values of R' and f', E is maximum when 2r = R' and t = 2f'; thus

$$E_{max} = \pi R'^4/256f'^2.$$

The most efficient straight hole requires a crystal with diameter $D \geqslant 2r = R'$. For the same crystal diameter, R' and f', a tapered hole can be found (with t = 1.37f') which is 15% more efficient. In general, for tapered holes with specified values of R', f' and r (where r is given its maximum convenient value) E is maximum when $t = (rf'/R')[1 + (1 + R'/r)^{1/2}]$. In this case f' is not equal to f (see Fig. 1).

For tapered holes with specified values of R', f' and t (where t is given its maximum convenient value), E is maximum when $r = tR'/2f'$. This relation implies that f' = f (and consequently R' = R); thus r = tR/2f and Eq. (1) can be written:

$$E = \frac{\pi r^4}{4t^2(1 + t/f)^2} = \frac{\pi R^4}{16f^2(2 + R/r)^2} . \tag{2}$$

Using this formulation, a tapered hole can be found which is 78% more efficient than a straight hole having the same R', f' and t. However, the required crystal diameter is twice as large. Thus it is always possible to find a tapered hole that is more efficient than a straight hole for the same values of R', f' and t or r.

For multichannel focussed collimators, f' = f provides the most convenient taper; thus the relation 2rf = Rt and Eq. (2) will be used in all focussed collimator design.

3.3. Focussed collimators for low-energy gamma rays

By using N holes tapered to a single point, the collimator efficiency given by Eq. (2) is multiplied by N, without altering the radius of view R at the focal distance f. Fig. 2 shows in cross-section the overlapping fields of view of three such tapered holes which are part of a seven-hole hexagonal array. Gammas emitted at points outside the geometrical field of view but within the region denoted by R_P may enter the scintillation crystal by penetrating the collimator septa. This degrades the spatial resolution. However, for gamma energies below approximately 150 keV, lead is sufficiently opaque for the probability of septum penetration to be small even for quite thin septa.

In this case, the goal of collimator design is to maximize

$$E = \frac{N\pi R^4}{16f^2(2 + R/r)^2} \tag{2a}$$

for specified R, f and s, the thinnest septa which can be conveniently cast. Two special cases are discussed.

3.3.1. Collimators for specified R, f, s and D

If the collimator is to be designed for a given crystal, we begin by expressing E in terms of R, f, s and D, where D is the diagonal of the hexagonal array of N round tapered holes, and is usually set equal to the crystal diameter. The septum thickness s is measured at the crystal face. If n is the number of holes on a diagonal of the array, then

$$D = 2rn + s(n - 1). \tag{3}$$

The total number of holes in the array is

$$N = \frac{3n^2 + 1}{4} \simeq \frac{3D^2}{4(2r + s)^2}, \tag{4}$$

where n = 1, 3, 5, 7, . . . give N = 1, 7, 19, 37, . . . Under most circumstances, $D \gg s$ and $N \gg 1$.

In this case, the approximation for N in Eq. (4) is valid, and Eq. (2a) can be written:

$$E = \frac{3\pi R^4 D^2}{64f^2(2 + R/r)^2 (2r + s)^2}. \tag{5}$$

3.3.1.1. Solution for maximum E. For specified values of R, f, s, and D, E is maximum when $2r = \sqrt{Rs}$. This relation can then be used to find the values of t, N and E_{max} :

$$t = f\sqrt{\frac{s}{R}}, \tag{6}$$

$$N \simeq \frac{3D^2}{4(\sqrt{Rs} + s)^2}, \tag{7}$$

$$E_{max} = \frac{3\pi R^4 D^2}{256f^2(\sqrt{R} + \sqrt{s})^4}. \tag{8}$$

For example, if we specify R = 5/32 in, f = 2.5 in, s = 0.012 in and D = 1.75 in, then E is maximum when 2r = 0.043 in, t = 0.69 in, $N \simeq 750$ and $E_{max} = 1.66 \times 10^{-4}$ in^2 $= 1.07 \times 10^{-3}$ cm^2.

3.3.1.2. Solution for near maximum E. The above example raises the serious practical problem of constructing collimators consisting of large numbers of small holes. Before undertaking the construction of such a collimator, it is advisable to determine how much less efficient are collimators with fewer holes (but the same R, f, s, D). For this purpose, if we substitute Eqs.(3) and (4) in Eq. (2a), we get:

$$E = \frac{\pi R^4}{256 f^2} \frac{3n^2 + 1}{(Rn/[D - s(n-1)] + 1)^2}. \tag{9}$$

Then E can be computed for each value of n (1, 3, 5, 7, . . .), and the procedure terminated when E is "close enough" to E_{max}.

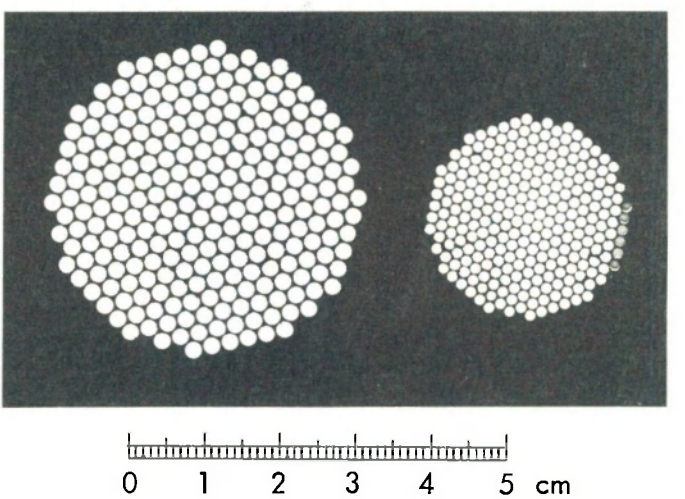

Fig. 3

For low-energy gammas, the penetration fraction is negligible and the septa are made as thin as possible to maximize the geometrical response Here the septa are 0.012 in at the large end and 0.008 in at the small end of the collimator.

The collimator shown in Figs. 3 and 4 (IX) was designed in this way for the values of R, f, s and D specified in the above example. It consists of 253 holes (an incomplete 271-hole array) having base diameter 2r = 0.085 in, t = 1.36 in and $E = 1 \times 10^{-3}$ cm^2, which is very close to $E_{max} = 1.07 \times 10^{-3}$ cm^2. The other collimators shown in Fig. 4 were formed by cutting off the basic mould to double and quadruple the efficiency.

3.3.2. Collimators for specified R, f, s and K

The above procedure is probably satisfactory whenever the source is not very thick, when a small crystal is used, or when good resolution is required only near the focal distance, (This set has been used primarily for thyroid and liver scanning with I^{125} (~30 keV) and Tc^{99m} (140 keV).) How-

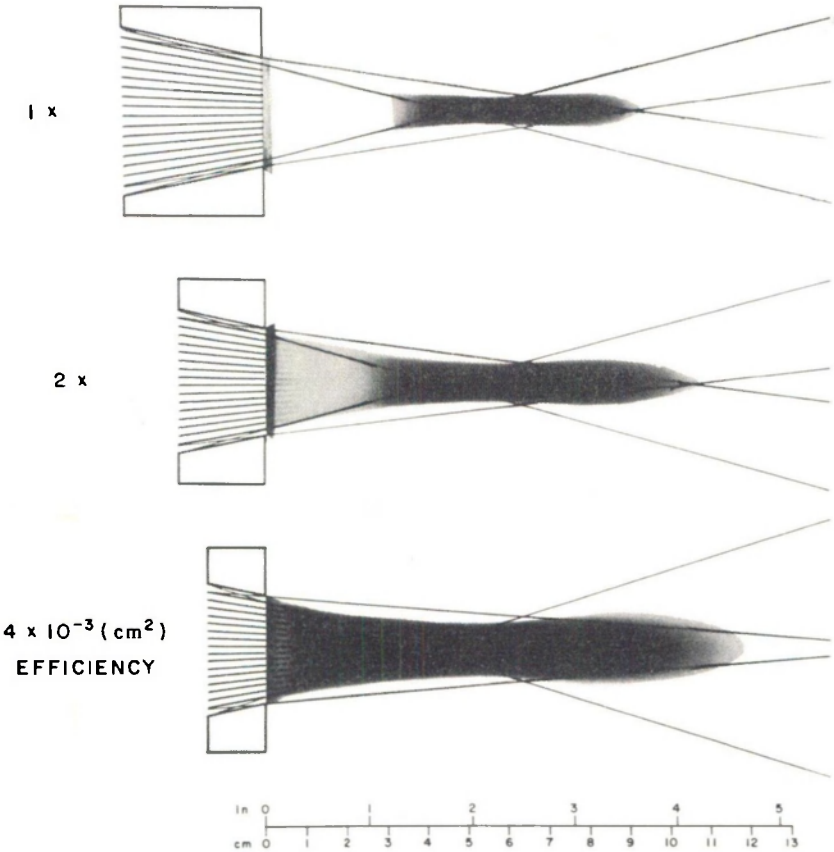

Fig. 4

Response patterns for a set of collimators for low-energy gammas having the hole layout shown in Fig. 3
The centre and lower collimators were formed by cutting down the original casting to double and quadruple the geometrical response to distributed sources, with some loss in resolution.

ever, for large crystals, this procedure leads to collimators having very "divergent" fields of view, i. e. the width of the field of view increases rapidly with distance from the focal point. This can be described by a "shape factor", K, which is defined by the equation:

$$\frac{3\sqrt{3}D^2}{8}\left(\frac{R}{R+2r}\right)^2 = \pi R^2 K, \tag{10}$$

which simply says that the cross-sectional area of the field of view at the collimator face is K times the area of view at the focal distance. For K = 1, the field of view has a cross-sectional area which is essentially constant from the collimator face to the focal distance. Beyond this point, the field

of view diverges. Eq. (10) can be solved for D^2 which reduces Eq. (5) to

$$E = \frac{\pi^2 R^4 K}{8\sqrt{3}\, f^2 (2 + s/r)^2}. \tag{11}$$

In this case, for specified R, f, s, and K, E is maximum when r is maximum. Using Eqs. (3) and (10), r can be expressed as

$$r = \frac{kR - s(n-1)}{2(n-k)}, \tag{12}$$

where $k = (8\pi K/3\sqrt{3})^{1/2} = 2.2\sqrt{K}$. It is clear from Eq. (12) that r is maximum when (n - k) takes on its minimum positive value. This occurs for the smallest value of n satisfying $n \geqslant 2.2\sqrt{K}$, where n = 1, 3, 5, . . .

It is interesting to note that, in this case, where K is specified in place of D, the most efficient collimators consist of a small number of large holes and tend to be quite thick and to require large diameter crystals. In practical cases, it is usually necessary to sacrifice some efficiency by using larger values of n.

3.4. Focussed collimators for the 150 keV to 1 MeV energy range

For gamma energies above approximately 150 keV, lead is not so opaque that septum penetration is negligible when s is less than approximately 0.020 in. In order to limit the penetration response ($PE\sigma$) to some small fraction of the geometrical response ($E\sigma$), it is necessary to have an equation which estimates the penetration fraction P in terms of the collimator parameters, R, f, D, λ, N and r, where λ is the attenuation coefficient of the collimator material (lead, gold, tungsten, etc.) for the particular gamma energy under consideration. For example, the septum thickness required to reduce the penetration fraction to 0.01 is not as great for Hg^{203} (279 keV) as it is for I^{131} (364 keV). Since some geometrical efficiency (E) is wasted if the septa are unnecessarily thick, an equation which estimates P is needed to enable one to design collimators having a specified penetration fraction. This problem has been discussed elsewhere [1]. Briefly,

$$P = \frac{E_H - E}{E} M, \tag{13}$$

where M is the mean probability of septum penetration for gammas emitted from a uniform sheet distribution σ which is at least large enough to cover the region denoted by R_P in Fig. 2. Here E_H is the geometrical efficiency of the large hexagonal hole which would be formed if all the septum material were removed (or were transparent to gamma rays). An estimate* of M which is probably adequate under most conditions [1] is

* It should be noted that this estimate of M is insensitive to the distribution of path lengths through the septa. For a given transmission ratio τ, an array of hexagonal holes provides fewer short paths through the septa than does an array of round holes; therefore, M and P are somewhat smaller for hexagonal holes than for round holes. For an alternative formulation based on a path length distribution function see [1].

$$M = e^{-\lambda t(1-\tau)}, \tag{14}$$

where τ is called the transmission ratio and is defined by

$$\tau = \frac{8N\pi r^2}{3\sqrt{3}D^2} = \frac{\text{total base area of the N small holes}}{\text{base area of the large hexagonal hole}}. \tag{15}$$

To complete the formulation, E_H is estimated by the geometrical efficiency of a round tapered hole with the same base area. Here we make use of an expression for E which is slightly different from Eq. (2) and which has been derived elsewhere [1]:

$$E = \frac{\pi r^4}{2(2t^2 + r^2)(1 + t/f)^2} = \frac{\pi R^4}{2(8f^2 + R^2)(2 + R/r)^2}. \tag{16}$$

This equation is more accurate than Eq. (2) when r is not negligible compared to t, as in the case of E_H for the large hexagonal hole. Here, the equivalent hole radius, r_H, is found by solving $\pi r_H^2 = 3\sqrt{3}D^2/8$; the equivalent radius of view is $R_P = (3\sqrt{3}/2\pi)^{1/2}(fD/t)$. Using these relations for r_H and R_P in Eq. (16) for E_H, and N times Eq. (16) for the geometrical efficiency of the collimator, the penetration fraction can be expressed in terms of the collimator parameters:

$$P = \left[\frac{27D^4(1 + R^2/8f^2)}{64\pi^2 r^4 N(1 + 3\sqrt{3}D^2R^2/64\pi r^2 f^2)} - 1\right] \exp\left[-\frac{2rf}{R}\lambda\left(1 - \frac{8N\pi r^2}{3\sqrt{3}D^2}\right)\right]. \tag{17}$$

This equation is used in two procedures for collimator design.

3.4.1. Collimators for specified R, f, P, λ and D

In this case, we wish to design a collimator with specified R and f for a particular gamma energy and collimator material which together determine λ, for a crystal having a diameter at least equal to D, and for P equal to some small fraction, say 0.1 or 0.01. It will become apparent later that the exact value specified for P is not very critical. When these quantities are introduced into Eq. (17), only N and r are undetermined. Then the problem is first to find those pairs of values of N and r which satisfy this equation, and then to find that pair which maximizes E as given in Eq. (2a). If we restrict the design to hexagonal arrays of holes, N can take on only discrete values: 7, 19, 37... This leaves only r to be determined for each value of N. However, Eq. (17) is transcendental in r and cannot be solved explicitly in closed form. The simplest procedure from this point is the graphical method illustrated in Fig. 5, where a lead collimator is to be designed for Hg^{203} (279 keV) and having D = 2 in, R = 0.5 in, f = 4 in, and P = 0.1. Here P is plotted as a function of r for several values of N. For N = 7, 19, 37 and 61, there exist values of r which make P = 0.1. For each set of values of N and r satisfying P = 0.1 the geometrical efficiency E is computed. In this particular case, E is maximum when N = 37 and r = 0.130 in. For this hole size, t = 2.08 in. For values of N larger than 61, there are no so-

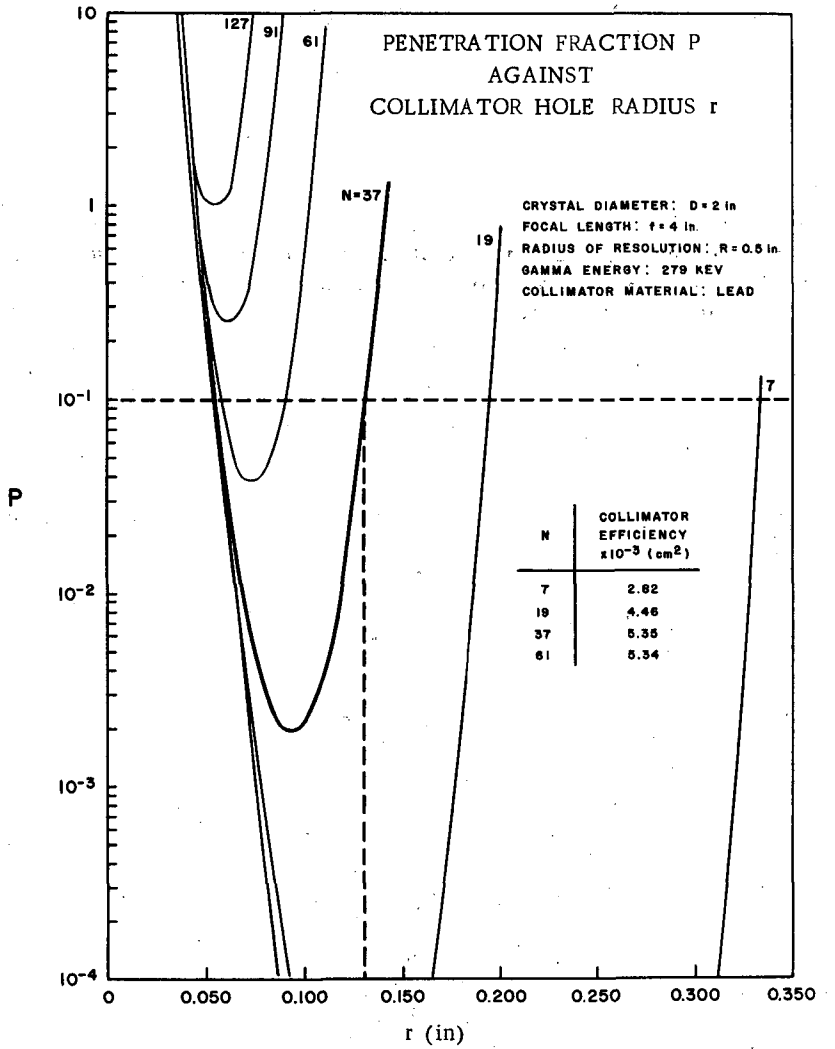

Fig. 5

Example of the graphical method for finding the most efficient collimator satisfying the values specified for R, f, P, D and λ
Here the "optimum" collimator has 37 holes with radius r = 0.130 in.

lutions for P = 0.1. Had we specified P = 0.01, it is apparent from Fig. 5 that no solution exists when N is greater than 37, although solutions do exist for N = 7, 19, 37. In this case, the most efficient collimator again has 37 holes; however, these holes are somewhat smaller (r = 0.120 in) and the geometrical efficiency is reduced about 12%. Thus, in this example, when P was reduced by a factor of 10, E was reduced by approximately 0.12. This suggests that little is lost in geometrical efficiency even when quite conservative values are specified for the penetration fraction. The practical value

of this comes from the fact that we will probably never know the accuracy of estimates of P such as Eq. (17) for all combinations of R, f, λ, and D, even when each parameter has only a finite range. However, by specifying a quite small value for P, say 0.01, little absolute accuracy is required of the equation estimating P, yet little loss in E is incurred.

It is of interest to note in Fig. 5 that for N = 7, 19, 37, and 61, a second value of r satisfying P = 0.1 exists at approximately r = 0.050 in for all N's. These solutions have no practical significance, because in each case, E is greater for the larger value of r. Solutions tend to exist for larger values of N if f, D, P or λ is increased or R is decreased. On the other hand, if λ is small (as it is for high-energy gammas), it may happen that no solution exists, even for N = 7. In that case, the single-hole collimator is the only choice.

3.4.1.1. The effect of collimator material on E. While it is intuitively evident that more efficient collimators can be constructed from gold than from lead, for the same values of R, f, P, D and gamma energy (since λ is larger for gold than for lead), it is of interest to know how much E can be increased, since the cost of gold collimators is substantial. This can be found by direct calculation or by plotting E against λ for a set of lead collimators designed for different gamma energies; then the corresponding values of E for gold collimators can be estimated by interpolation. In the example used to illustrate the interpolation procedure (see Fig. 6) D = 2 in, f = 4 in, P = 0.01. For 511 keV photons, the gold collimators are about 50% more efficient than their lead counterparts, for the three values of R considered. For 279 keV (Hg^{203}), the increase in E is only about 25%, and continues to decrease with decreasing gamma energy. While the efficiency to be expected from gold collimators can be estimated in this way, the number and size of the holes can be found only by the design procedure outlined above.

3.4.2. Collimators for specified R, f, P, λ and K

The procedure in 3.4.1 is analogous to the low-energy case discussed in 3.3.1 and, similarly, leads to collimators having "divergent" fields of view for large values of D, etc. An alternative procedure, analogous to that discussed in 3.3.2, makes use of the "shape factor" defined by Eq. (10) and is useful when the source is thick, etc. Clearly, Eq. (10) can be solved for D^2 which can then be used to express P as a function of R, f, λ, K, N and r. From this point, a design procedure that is virtually identical to that described in section 3.4.1 can be used.

A slight, but interesting, variation on this procedure makes use of a simplified equation for P. In this case it is assumed that $E \ll E_H$ (see Eq. (13)) and that Eq. (2) provides an adequate basis for estimating E_H. Then P can be put in the form:

$$P \simeq \left[\frac{27D^4}{64\pi^2 r^4 N}\right] \exp\left[-\frac{2rf\lambda}{R}\left(1-\frac{8N\pi r^2}{3\sqrt{3}D^2}\right)\right]. \tag{18}$$

Substituting for D^2 from Eq. (10) and rearranging the terms, we get

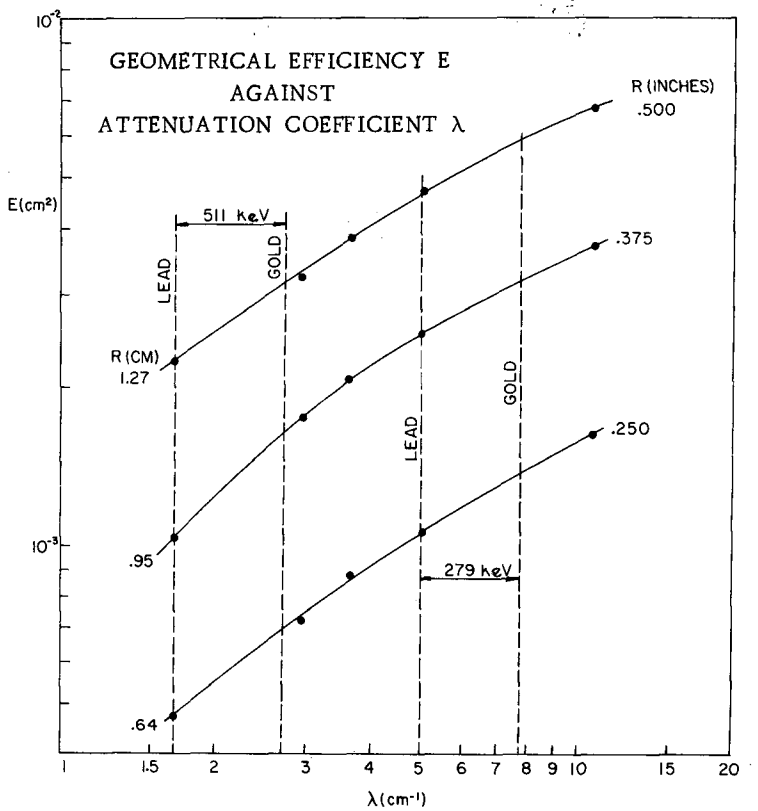

Fig. 6

Comparison of geometrical efficiencies of lead and gold collimators designed for the same R, f, P, D and λ
At 511 keV, gold collimators are about 50% more efficient than corresponding lead collimators
This advantage decreases with gamma energy and is about 25% at 279 keV.

$$f\lambda = \frac{R}{2r}\left[\log_e \frac{(2+R/r)^4 K^2}{PN}\right]\left[1 - \frac{N}{(2+R/r)^2 K}\right]^{-1}. \tag{19}$$

A convenient design procedure which retains a degree of generality can be used if only P and K are specified at the outset. For example, we may wish to design a set of collimators having different values of R, f and λ but having the same values of P and K. The procedure is illustrated in Fig. 7 for P = 0.01 and K = 1; in this case, the area of view at the focal distance is equal to the area of the hexagonal array at the collimator face. In Fig. 7 fλ is plotted as a function of R/r for several values of N using Eq. (19) and as a function of f for several gamma energies. In addition, $E/(\pi R^4/16f^2) = N/(2+R/r)^2 = K\tau$ is plotted as a function of R/r. Suppose we wish to design a collimator for Hg^{203} (279 keV) having f = 4 in and R = 0.5 in. Starting at a in Fig. 7 with f = 4 in, fλ for 279 keV is found to be 51 at b. This value of fλ occurs for N = 7 and N = 19 at c and d. For N = 7, fλ = 51 when R/r = 2f/t = 0.71;

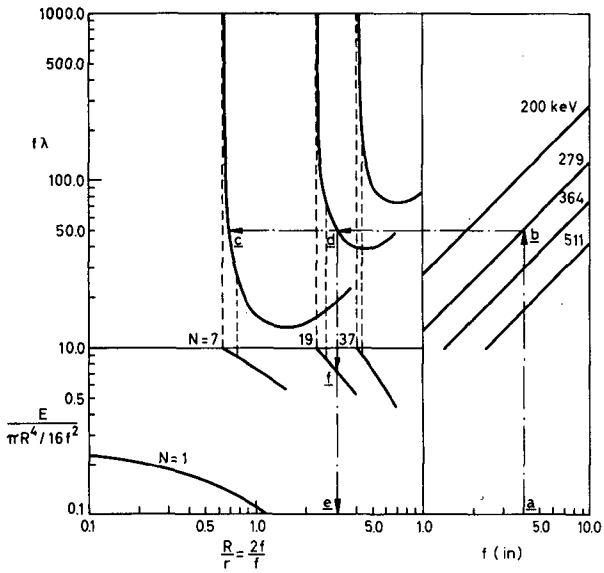

Fig. 7

Graphical procedure for designing collimators having P= 0.01 and "shape factor" K= 1. Letters a through f indicate the design of the collimator shown in Fig. 9b.

however, the septum thickness is zero when $R/r = 0.78$, and smaller values have no significance unless hexagonal holes are used. Even in that case, the seven-hole collimator would be more than 11 in thick and would require a crystal with a diameter at least 4.25 in. For $N = 19$, $f\lambda = 51$ when $R/r = 2f/t = 3$ (see e, Fig. 7). This implies that $r = 0.166$ in, $t = 2.66$ in and $D = 1.83$ in. Also, for this value of R/r, $E = \pi R^4(0.75)/16f^2$ (see f, Fig. 7). The seven-hole collimator described above, with hexagonal holes, is more efficient, with $E = \pi R^4/16f^2(0.95)$; however, the 19-hole collimator shown in Fig. 9b is much easier to construct. This situation is analogous to that described in section 3.3.2, where it was noted that when K is specified instead of D, the most efficient collimator has the smallest number of holes satisfying the relevant equations. Again, practical considerations may dictate the construction of less efficient collimators having more holes. For larger values of K, significant solutions may not exist for small values of N; for example, for $K = 2$, no significant solutions exist for $N = 7$. In this case, the most efficient collimators tend to have 19 holes, while the 37-hole collimators tend to have more practical dimensions of thickness and required crystal diameter.

4. CONSTRUCTION OF FOCUSSED COLLIMATORS

The method of construction naturally depends upon the collimator material used and the shape of the individual channels. The casting technique described here is used for constructing lead collimators consisting of round tapered holes. The mould consists of round tapered steel rods held in place

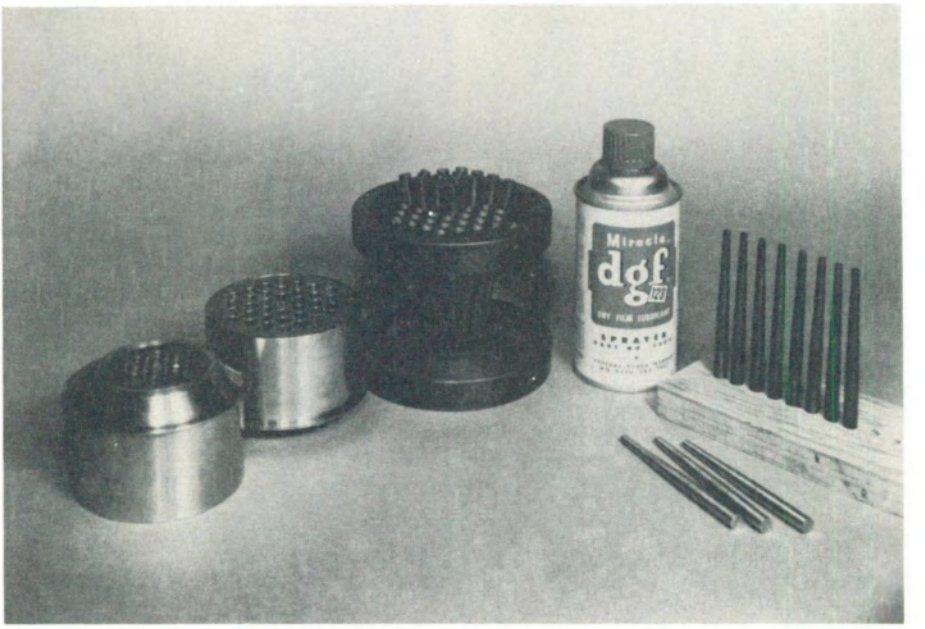

Fig. 8

Centre - mould for casting lead collimators shown on the left
Stainless steel jacket was removed to show the lower guide plate for the tapered rods.

by upper and lower guide plates as shown in Fig. 8 and surrounded by a thin stainless steel cylinder that serves as a protective jacket for the finished collimator. If the holes are few and fairly large, the rods can be tapered on a lathe; for many small holes, the tapered rods can be formed on a centreless grinder. Before assembling the mould, each rod is coated with a spray graphite lubricant (such as dgf 123, a product of Miracle Power Products Co.) which forms a thin protective film to prevent wetting of the steel rods by hot lead, and assures easy extraction of the rods from the completed casting. This is especially important if the septa are thin and fragile. The assembled mould is preheated in a furnace to about 500°C, and the lead is heated to approximately 375°C. Just before the casting is made, the surface layer of lead oxide is carefully removed to prevent its clogging the septa. For casting, a ladle large enough to fill the mould in a single pouring is used to prevent oxide interfaces. On cooling, lead shrinks appreciably and this tends to produce voids in the septa. These voids can be prevented by keeping the top of the casting melted with a torch as the lead solidifies from the bottom up, and adding more lead if necessary. The upper surface of the solidified casting (this fits against the crystal face) is not flat and must be "faced off". (Our practice is to design the mould so that the casting is somewhat thicker than the finished collimator is to be; this excess is then "faced off".) If the septa are fairly thick, this operation presents no problem; however, if the septum thickness is less than ~0.02 in, special precautions must be taken. In this case, the collimator holes are

filled with a molten mixture of approximately equal parts of graphite and sulphur, which has a melting point well below that of lead. On cooling, this forms a solid machinable mass which protects the fragile septa while the collimator is faced off in a lathe. The collimator holes are then opened by gradual heating in an oven until the sulphur-graphite mixture melts and runs off. The collimator is finally cleaned in an ultrasonic bath to remove any residual scale.

5. TESTING COLLIMATORS

Tests for collimators can be divided, somewhat arbitrarily, into two categories: (1) those designed to determine the accuracy of equations for the theoretical response components: and (2) those designed to determine the "effectiveness" of the collimator for detecting non-uniformities in the source distribution.

The best known and most widely used test of collimator performance is the measurement of the response to a point source. These measurements are usually summarized in the form of isoresponse contour lines. Geometrical response can be determined by using a low-energy point source, while penetration and scatter responses can be studied using sources of higher energy gammas. Measured responses have been compared with theoretical values by a number of writers [4, 5].

Analogous tests using uniform disc sources have been devised and are in some ways more easily interpreted. Some of these tests are illustrated in Fig. 9 for the "constant area" (K = 1) collimator discussed in section 3.4.2.

A detailed qualitative picture (see Fig. 9b) of the point source response function can be produced by placing a uniform sheet distribution of I^{125} (27.4 keV X-rays) against the crystal side of the collimator and a sheet of film on the collimator axis in what is normally the source field. Photons passing "backwards" through the collimator expose the film. By reciprocity, this interchange of source and detector (film in this case) reproduces the geometrical response pattern provided that the film is <u>not</u> exposed by: (a) scattered radiation, and (b) photons which have penetrated the collimator septa. These conditions are approximately satisfied by I^{125} .

Making use of the fact that the geometrical response to a uniform sheet distribution that covers the field of view is independent of the distance from the collimator, any decrease in response with distance is attributable to the effects of penetration or scatter. This is shown in Fig. 9a, where response to a small disc source is plotted for several gamma energies. The effects of septum penetration and small-angle scatter are not readily separated experimentally. Taking MATHER's [2] theoretical values of collimator scatter to be exact, the penetration response can be estimated. For example, on the basis of an 8% decrease in count rate as the disc of Hg^{203} (279 keV) is moved to the focal distance, the combined penetration and scatter fractions can be estimated to be less than 10%. For an omni-directional source of this energy, the scatter fraction is approximately 3% so that $P \leq .\%$ experimentally. The theoretical value of P is approximately 1%. In general, "order of magnitude" or better agreement with Eq. (17) has been observed.

An interesting exception has occurred in the case of the set of low-

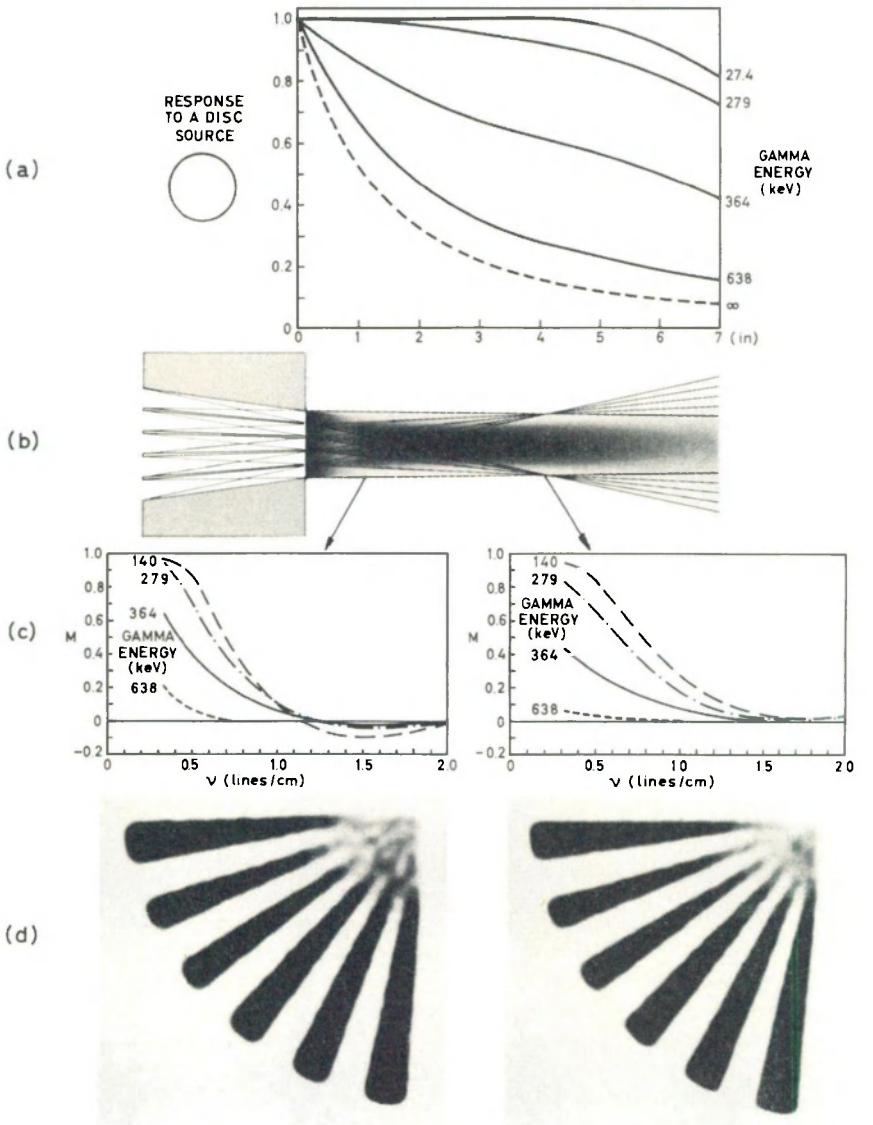

Fig. 9

Four tests of a collimator for brain scanning with Hg^{203} (279 keV)
Collimator was designed by the method illustrated in Fig. 7.
(a) Collimator response to disc sources just large enough to cover the field of view to the focal point.
(b) Point source response pattern.
(c) The modulation transfer function, M, at 1 in and 4 in from the collimator face.
(d) Scans of radioactive sunburst pattern at 1 in and 4 in. This test pattern was used to measure M.

energy collimators shown in Fig. 4. Using a uniform disc of I^{125} covering the collimator face, the relative geometrical efficiencies of these colli-

mators agree with theoretical values to within less than 2%. However, for Tc^{99m} (140 keV) the response of the thinnest collimator (with efficiency 4×10^{-3} cm^2) is about 30% higher than would be expected. While the theoretical penetration fraction is highest for this collimator, at 140 keV P is only 2.5%. Differences in scatter from the septa for the three collimators are believed to be negligible at this energy. Thus, the accuracy of Eq. (17) for P appears to be somewhat less than "order of magnitude" in this case. It would appear that, when the septum thickness is much smaller than $t(1 - \tau)$, the estimate of M given in section 3.4 may not be adequate. The estimate of M based on a distribution of path lengths, referred to in the footnote of section 3.4, leads to a penetration equation:

$$P = \frac{6N}{\lambda^3 t^3 (2 + \tau)(1 - \tau)^2 \tau^2}. \tag{20}$$

It is interesting to note that for this equation, P is approximately 34% for the above collimator, in close agreement with the observed 30% excess over geometrical response. The general behaviour of this alternative estimate of P has not been fully explored. Should it become important to estimate P more accurately, it may be necessary to develop several equations, each quite accurate in a limited energy range.

The problem of determining the "effectiveness" of a collimator for detecting lesions has two aspects. The choice of a suitable model or "phantom" and the choice of a suitable criterion for "effectiveness" are both somewhat arbitrary. The excellent work of different writers is sometimes difficult to compare because different models and criteria are used.

It appears that much of this work (both theoretical and experimental) could be discussed in terms of a concept which has been referred [6] to as "sine wave response", "space frequency response", "modulation transfer function", "contrast transmission", etc. This function describes the detector response to objects of different sizes; more precisely, it describes the response to sinusoidal variations in the distribution of activity as a function of the space frequence expressed in lines per centimetre. This function can be determined approximately from the detector response to a "square wave" test pattern such as the Siemen's star* in Fig. 9d, consisting of alternate wedges of activity and no-activity. This pattern can be easily constructed from Lucite sheets, and conveniently emptied and refilled with radioactive solutions through screw-sealed access ports. In this case, the modulation transfer function, M, is defined by

$$M = \frac{C_t - C_0}{C_t + C_0}, \tag{21}$$

where C_t and C_0 are the maximum responses to source and no-source wedges respectively. A plot of M against space frequency ν (see Fig. 9c) indicates the detector response to structures of decreasing size as ν increases. This function is quite sensitive to the shape of the point source response function, septum penetration and scattered radiation, as indicated in Fig. 9c (for penetration).

* This test pattern is used in optics to measure M for lenses.

The "effectiveness" of a collimator for detecting lesions is dependent not only on this count rate "contrast" but also on the sensitivity; thus, a large change in count rate (or large M) over a lesion does not assure its detection if the overall count rate is very low due to an inefficient collimator. These factors of sensitivity (as measured by $C = E\eta\sigma$) and contrast (as measured by M, which serves as a generalization of collimator resolution) can be combined [1] in a measure of effectiveness or figure of merit Q where

$$Q = \frac{C_0(C_t/C_0 - 1)^2}{4(C_t/C_0 + 1)} = \frac{C_0 M^2}{2(1 - M)} = \frac{C_t M^2}{2(1 + M)}. \tag{22}$$

This quantity can be determined for any collimated detector and used as a criterion for comparing different systems. Clearly, the value of any such criterion (and others, equally plausible, can be formulated) must be determined by its usefulness in establishing improved scanning procedures.

ACKNOWLEDGEMENTS

The author is indebted to D. B. Charleston, P. V. Harper, M. D. and P. Eidelberg for many suggestions and constant assistance, and to J. J. Stupka, C. R. Brebach and B. W. Fromes for their complete co-operation in the construction of collimators and related equipment.

REFERENCES

[1] BECK, R. N., A theory of radioisotope scanning systems, these Proceedings I.
[2] MATHER, R. L., Research and development technical report, Rpt USNRDL-TR-174 NS 081-001 (20 May 1957).
[3] NEWELL, R. R., SAUNDERS, W. and MILLER, E., Nucleonics 10 (1952) 36.
[4] MYHILL, J., Int. J. appl. Rad. Isotopes 12 (1961) 10-19.
[5] HEFFERLIN, R. A. and KREGER, W. E., Research and development technical report, Rpt. USNRDL-TR-202 NS 081-001 (12 Mar. 1958).
[6] PERRIN, F. H., J. Soc. Motion Picture Television Engrs 69 (1960) 151-156, 239-249.

DISCUSSION

J. MALLARD: The pictures showing the response to the star pattern were obviously obtained with a good collimator of high resolution. If you had a collimator of low resolution, would you be able to measure C_0 between the wedges accurately?

R. BECK: The response to the star pattern is defined by the modulation transfer function, $M = (C_t - C_0)/(C_t + C_0)$, where C_t and C_0 are the count rates over the centre of the source and no-source wedges respectively. When the collimator resolution is relatively poor, that is, when the collimator field of view is large as compared with the wedge width, C_0 may be as large as C_t, in which case M is near zero. This does not present any special

problem in measuring C_0, once the collimator is positioned over the centre of the wedge. An alternative procedure is to record the count rate on a strip recorder as the test pattern is rotated round its mid-point, the maximum count rate then corresponding to C_t and the minimum to C_0.

CONSTRUCTION OF A HIGH-EFFICIENCY, LOW-ENERGY COLLIMATOR *

R. HÖFER AND A. ROSZUCZKY
SECOND MEDICAL UNIVERSITY CLINIC, VIENNA, AUSTRIA

Abstract — Résumé — Аннотация — Resumen

CONSTRUCTION OF A HIGH-EFFICIENCY, LOW-ENERGY COLLIMATOR. The advent of I^{125} makes it necessary to revise the conventional measuring equipment constructed for use with isotopes emitting gamma rays of a comparatively high energy.

The most important modification of scanning equipment, made possible by the low gamma energy of I^{125}, lies in reducing the thickness of the septa of the collimator. This increases counting efficiency without loss in the resolving power of the collimating device.

A focusing multichannel lead collimator with septa less than 1 mm thick has been designed. The construction of such a collimator is shown in some detail and some results of studies of its efficiency and resolving power with I^{125} presented.

CONSTRUCTION D'UN COLLIMATEUR A GRANDE EFFICACITÉ POUR LES FAIBLES ÉNERGIES. L'utilisation de ^{125}I rend nécessaire une revision des appareils de mesure classiques, conçus pour des radioisotopes émettant des rayons gamma d'une énergie relativement élevée.

La modification la plus importante des appareils d'exploration pour tenir compte de la faible énergie gamma de ^{125}I consiste en une réduction de l'épaisseur des cloisons du collimateur. On augmente ainsi l'efficacité du comptage sans diminuer le pouvoir de résolution du collimateur.

Les auteurs ont conçu un collimateur en plomb à canaux multiples et à focalisation, dont les cloisons ont moins de 1 mm d'épaisseur. Ils donnent des indications assez détaillées sur la construction de ce collimateur et mentionnent quelques résultats d'études portant sur son efficacité et son pouvoir de résolution pour ^{125}I.

КОНСТРУКЦИЯ ВЫСОКОЭФФЕКТИВНОГО КОЛЛИМАТОРА НИЗКОЙ ЭНЕРГИИ. Получение йода-125 сделало необходимым пересмотреть обычную измерительную аппаратуру, сконструированную для измерения изотопов, излучающих гамма-лучи сравнительно высокой энергии.

Наиболее важное изменение в сканнирующем оборудовании, ставшее возможным благодаря низкой энергии гамма-излучения йода-125, состоит в уменьшении толщины перегородок коллиматора. Это уменьшение толщины увеличивает эффективность счета без потери разрешающей способности коллимирующего устройства.

Был разработан свинцовый многокальный фокусирующий коллиматор с перегородкой толщиной менее 1 мм. Сообщаются некоторые подробности конструкции этого коллиматора и приводятся некоторые результаты исследований его эффективности и разрешающей способности при использовании йода-125.

CONSTRUCCIÓN DE UN COLIMADOR DE GRAN EFICACIA PARA BAJAS ENERGÍAS. La posibilidad de recurrir al ^{125}I obliga a modificar el equipo clásico de medición construido para emisores gamma de energía relativamente elevada.

El cambio más importante que la baja energía gamma del ^{125}I permite introducir en el equipo de exploración centelleográfica consiste en reducir el espesor de los tabiques del colimador. Con ello se incrementa la eficacia de recuento sin que disminuya el poder de resolución.

Los autores han diseñado un colimador multicanal de plomo enfocado, cuyos tabiques tienen menos de 1 mm de espesor. En la memoria se describe con bastante detalle la construcción de este colimador y se presentan algunos resultados de los estudios de su eficacia y poder de resolución efectuados mediante ^{125}I.

* This work was supported by an IAEA Research Contract (NO 190 B)

INTRODUCTION

A collimator's increasing resolution eventually leads to a loss of counting efficiency; thus, a compromise must be reached between resolution and counting efficiency for any collimator-detector system. For isotopes with a relatively high gamma energy a higher resolution and a higher counting efficiency may be obtained by only increasing the crystal size and by using, for example, gold instead of lead for the collimator. However, the use of low-energy gamma emitters in radioisotope scanning is another means of increasing both resolution and counting efficiency, because leakage through the septa of the collimator is minimized and a reduction of the septa size is possible, depending on the gamma energy of the isotope used.

From the beginning, the introduction into thyroid scintillation scanning of the low-energy gamma emitter I^{125} (MEYERS [1] and FELLINGER et al. [2]) focused the investigators' interest on adjusting collimation to the physical characteristics of the isotope. Obviously a focused multichannel collimator, specially constructed for I^{125}, could have very thin septa without any loss of resolution due to the septum penetration, since the half-value layer for the photons of this isotope in lead is about 0.00152 cm. Such a collimator, specially designed to be used with I^{125}, could have a higher resolution and a higher counting efficiency than usual with equipment designed for scanning with I^{131} or other "high-energy" radioisotopes.

Since it is desirable to build individual collimators for each low-energy radioisotope to benefit fully from its physical properties for scanning purposes, we looked for a simple and cheap way of constructing a low-energy, high-efficiency and high-resolution collimator.

METHOD

The type of collimator built is a multichannel focusing collimator consisting of a series of truncated hollow cones, all focused at the same point (Fig. 1). The space between the cones is subdivided by radiating septa (Fig. 2). Septa and cones must be milled exactly.

In order to assemble the individual parts correctly, the following procedure was adopted: the cones were mounted on a base of plexiglas which was cut to hold the base of the cones and the septa, and another series of plexiglas disks was cut to serve as a counterpart for the base at the top of the collimator (Fig. 3). A central bolt keeps base and top-holders in place (Fig. 4). When the collimator is assembled, the smallest cone is first put into place between base and top-holder and the first series of septa is inserted as shown in Fig. 5. The septa are glued on the cones with Araldit; the second, larger cone is put in place and left alone some hours to allow the Araldit to dry. The top-holder is then removed and replaced by the next, larger one and the next row of septa is inserted and fixed. This procedure is repeated as often as necessary. Within limits a collimator with any desired number of holes and with any possible dimensions of septa and cones could be constructed by using this procedure.

Fig. 1

A series of focused truncated lead cones to be used for making a 43-hole collimator

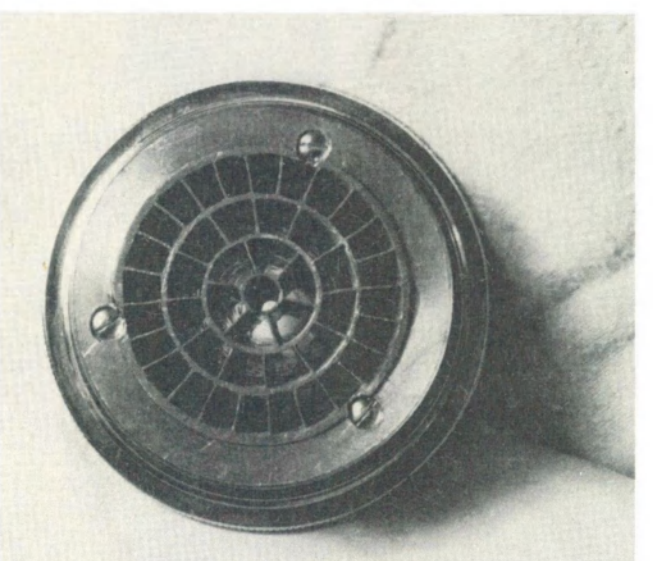

Fig. 2

The 43-hole collimator seen from the crystal face,
showing the radiating septa subdividing the space between the cones

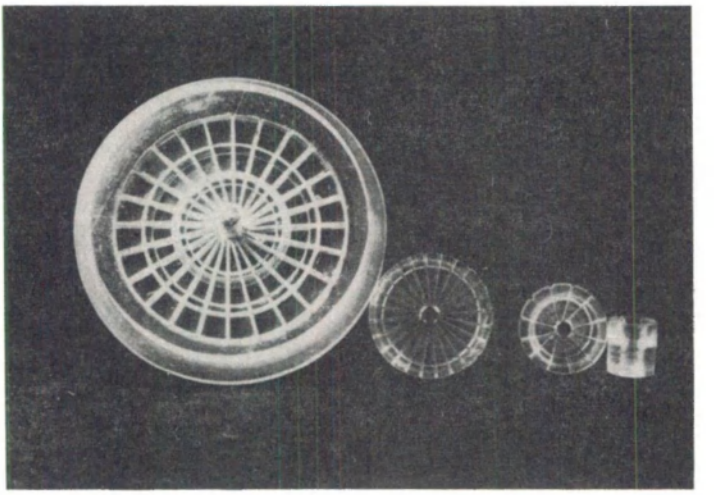

Fig. 3

Plexiglas base (left) and three plexiglas top-holders
(note incisions for cones and septa)

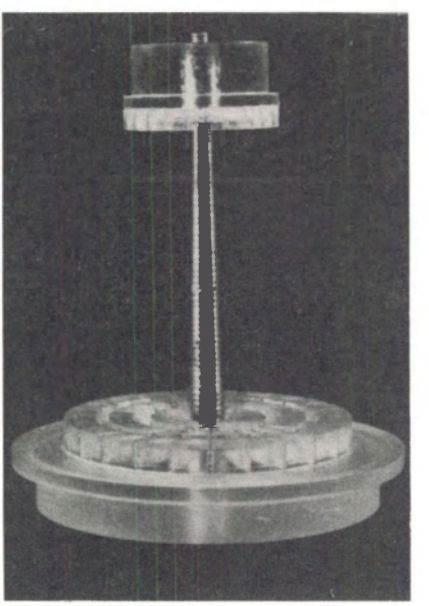

Fig. 4

Plexiglas base and top-holder mounted with central bolt

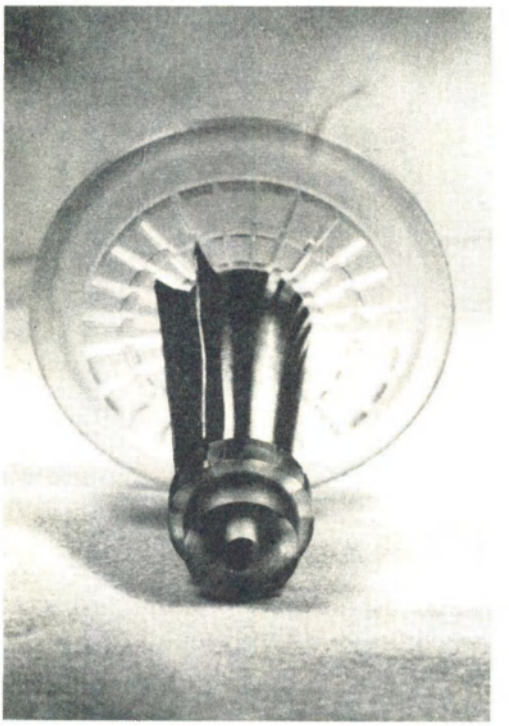

Fig. 5

Assembling of collimator: base and top-holders with truncated cone and two septa inserted

PRACTICAL APPLICATION

A 43-hole focusing collimator to be used for I^{125}, together with a 2× 2-in crystal, was constructed. In theory lead septa and lead cones 0.15 mm thick (10 times the half-value layer) would have been sufficient. However, the mechanical strength of pure lead enabled us to go down to only about 0.5 mm for the time being. Thus, only 15%, or 287 mm^2, of the crystal surface is covered with lead, while 85%, or 1674 mm^2, of the crystal remains open. The collimator is 50 mm long and, at the face of the collimator, the relation of open to lead-covered surface is 484 : 132 mm^2, or 78.5% : 21.5%. The largest width of the holes amounts to 8 mm at the crystal and to 4 mm at the face of the collimator and the geometrical penumbra at focal distance has a 14-mm diam.

We used some of the criteria of DEWEY and SINCLAIR [3] for evaluating our collimator. All measurements were done at focal distance using the collimator together with a 2× 2-in crystal and a one-channel pulse-height analyser setting a 6-V window at the 27 + 35.4-keV sum peak. The plane sources used were cut out from agar plates about 2 mm thick containing known amounts of I^{125}.

The quantities used for the calculations were the same as those used by Dewey and Sinclair:

K = sensitivity (cpm/μc/cm^2) to radiation emitted from a whole-body plane source when the collimator is over the centre of the source. In place of the whole-body source used by Dewey and Sinclair we used a source only 80 mm in diam. because no counting-rate change was observed when sources larger than 52-mm diam. were measured.

k = sensitivity (cpm/μc/cm^2) to radiation emitted from the target area when the collimator is directly over the target.

S(k/K) = relative counting rate – the ratio of target sensitivity to non-target sensitivity.

In plotting the relative sensitivity versus the radius of a plane source (Fig. 6), it can be seen that a value of 1 is already obtained with a source

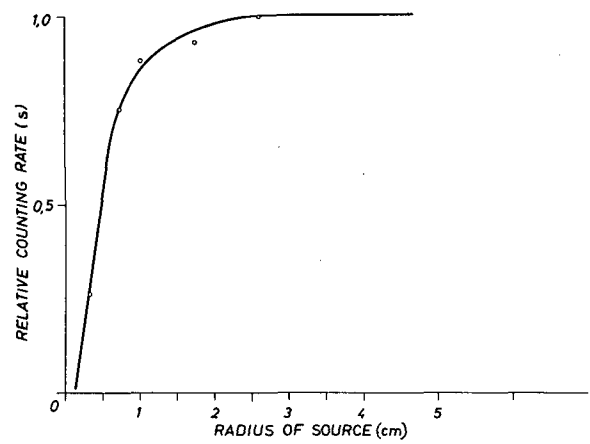

Fig. 6

Relative sensitivity versus size of I^{125} plane source measured at focal distance

26 mm in radius. The shielding parameter, that is the relative counting rate when the source has the radius of the geometrical penumbra, is 0.76. This means there is almost no septum penetration. The small collimation insufficiency shown by the curve in this Figure may be due to the peculiar scatter phenomenon of low-energy gamma rays as pointed out by ROSS [4], and not to septum penetration.

Resolution for a point source in the focal plane is 6 mm. By definition this is twice the lateral distance that one must move the axis of the collimator away from the point source in order to decrease the response to half-maximum.

Resolution for a plane source of the size of the penumbra is shown in Fig. 7 and it can be seen that the response decreases to half-maximum before the axis of the collimator has moved over the edge of the source.

To evaluate resolution versus sensitivity the figure of merit $(1/KS^2)\times 10^3$, for our collimator was calculated and Fig. 8 shows the results for our collimator together with the data given by Dewey and Sinclair. It is quite

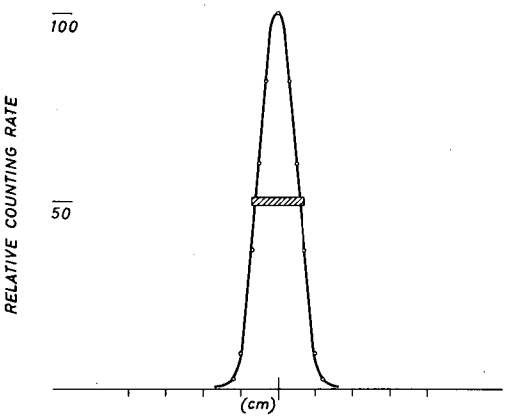

Fig. 7

Relative counting rate versus lateral displacement of circular plane source from the collimator axis

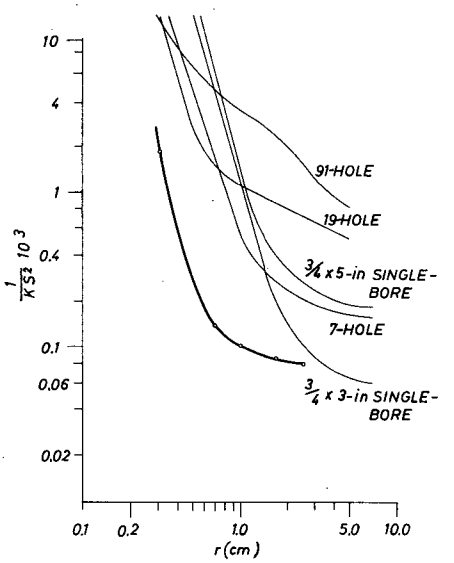

Fig. 8

Figure of merit versus target size. The thick line corresponds to the measurements performed with the 43-hole collimator presented in this paper and a plane source of I^{125} as described in the text. The measurements for the figure of merit versus target size indicated by the thin lines (91-hole, 19-hole, 3/4 x 5-in single bore, 7-hole, 3/4 x 3-in single bore) were taken from the paper of Dewey and Sinclair.

obvious that, with the exception of results obtained with a single-bore collimator for very large sources, our collimator gives the best figure of merit.

Finally, Fig.9 shows an agar phantom scan. The activity of the phantom was 1.7 μc of I^{125}/cm^2 and the agar layer was 2 mm thick. Five holes were cut out of the agar plate in a row. The size of the holes was 4, 6.2, 8.1, 9.4

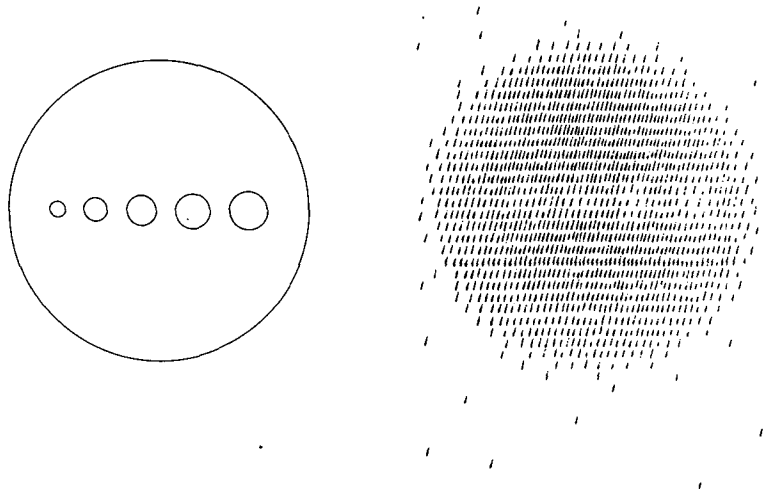

Fig. 9

Diagram and scan of an agar phantom 2 mm thick, containing 5 holes with diameters of 4, 6.2, 8.1, 9.4 and 10.2 mm. The distance from hole to hole amounts to 5 mm. The agar contains 1.7 $\mu c/cm^2$.

and 10.2 mm in diam. and the distance between the holes was 5 mm. The three largest holes are distinctly shown on the scan, the smallest cannot be detected at all and the 6.2-mm hole can just be seen.

In conclusion we would like to state that the collimator, presented as a practical example of the construction principle described, is certainly not the optimal collimator for I^{125}. However, it serves well to demonstrate that ours is an adequate method for constructing collimators and that it is worth while trying to adapt collimation if low-energy gamma emitters are used.

REFERENCES

[1] MEYERS, W.G. and VANDERLEEDEN, J.C., Radioiodine-125, J. nucl. Med. 1 (1960) 149.

[2] FELLINGER, K., HÖFER, R. and VETTER, H., Szintigraphie der Schilddrüse mit Jod-125, Nucl. Med. 3 (1962) 20.

[3] DEWEY, W.C. and SINCLAIR, W.K., Criteria for Evaluating Collimators used in In Vivo Distribution Studies with Radioisotopes, Int. J. of appl. Radiat. Isotopes 10 (1961) 1.

[4] ROSS, D.A., SATTERFIELD, M.M., JORDAN, J.C., HARRIS, C.C. and BELL, P.R., Low-energy gamma emitters in scanning and other clinical applications, Suppl. J. Strahlentherapie 6 (in press).

DISCUSSION

P. CZERNIAK: Your value of 1.7 μc per cm^2 would correspond to 1.5 mc of I^{125} for a liver scan and about 50 μc for a thyroid scan. These values are rather large. Have you also experimented with smaller doses and what are the results?

R. HÖFER: The activity of 1.7 μc of I^{125} per cm^2 for our plane sources was chosen because Dewey and Sinclair carried out their measurements with about the same activity. There is no reason why an equally good phantom scan should not be performed with a lower dose; it would merely be necessary to adjust the other factors, for example scaling factor and scanning speed, to the lower activity of the source. We have not done phantom scans with lower activities, but we have obtained excellent scans of thyroid glands with activities of 3-5 μc of I^{125} per gland.

W. G. MYERS: Dr. Höfer, you said you were able to make good scans of the thyroid with 3-5 μc of I^{125} when you used your collimator with a NaI(Tl) crystal that was 50 mm thick. If you had used your collimator in conjunction with a crystal only a few millimetres thick, would you not have been able to make comparable scans with less than 1 μc of I^{125}?

R. HÖFER: We have only recently started to use our collimator in conjunction with a $2 \times \frac{1}{4}$-in crystal having a beryllium window and a phototube of low dark current and we have the impression that we shall be able further to reduce the tracer dose, as you suggest.

D. FOLLETT: When phantoms were used, were measurements made with tissue-equivalent material between the collimator and the phantom? I should also like to ask if the effect of absorption on the collimator response was allowed for in the design? We are also working on the problem of iodine-125 thyroid scanning and have found that absorption has a considerable influence on the isocount curves, effectively compressing them towards the collimator. This must be allowed for in design.

P. CZERNIAK: May I also ask Dr. Höfer, at this point, whether he has investigated the detection of deeper space-occupying lesions by means of phantoms?

R. HÖFER: I am aware of the need for further measurements with sources of different volumes and with varying layers of tissue-equivalent material between the collimator and the source. However, since the collimator described was finished only very recently, we have not been able to make these additional experiments in time to present the results here.

H. A. B. SIMONS: I should like to congratulate Dr. Höfer on the very interesting way he constructs collimators. May I point out that his figures of merit are not comparable with those of Dewey and Sinclair because of the higher gamma-detection efficiency of I^{125}.

A DEPTH-FOCUSSING COLLIMATOR FOR THE INVESTIGATION OF THE BRAIN CORTEX

H. I. GLASS *
WESTERN REGIONAL HOSPITAL BOARD, GLASGOW, SCOTLAND

Abstract — Résumé — Аннотация — Resumen

A DEPTH-FOCUSING COLLIMATOR FOR THE INVESTIGATION OF THE BRAIN CORTEX. A detector is described which consists of a 5-in diam. by ¼-in thick sodium iodide crystal and a depth-focusing collimator. The collimator was designed initially for use in brain cortical blood-flow investigations using Xe^{133}, but may be used with other soft gamma-emitting isotopes such as I^{125}.

The collimator, which is constructed of lead, is ¼-in thick and is of multichannel design. The focus is at 1.75 cm from the face of the collimator. The response in air to a point source on the central axis of the collimator falls to 10% of the maximum at ±0.75 cm from the focus. The far field response in tissue is considerably better than in air due to high tissue attenuation of the soft gamma radiation. The response of the collimator to a point source in air and inside a skull is presented.

The collimator has been used to measure local cortical blood flow in the brain using Xe^{133}. However, using I^{125}-tagged chemicals, the detection of cortical tumours and haemorrhages is possible using this apparatus.

COLLIMATEUR A FOCALISATION PROFONDE POUR L'EXPLORATION DE LA SUBSTANCE CORTICALE DU CERVEAU. L'auteur décrit un détecteur constitué par un cristal de NaI (125 mm de diamètre et 6 mm d'épaisseur) et un collimateur à focalisation profonde. Ce collimateur a été conçu pour étudier le flux sanguin dans la substance corticale du cerveau à l'aide de ^{133}Xe, mais il peut aussi être utilisé avec d'autres émetteurs de rayons gamma mous, tels que ^{125}I.

Le collimateur, à canaux multiples, est en plomb; il a une épaisseur de 6 mm. Son foyer est à 17,5 mm de la face du collimateur. La réponse dans l'air pour une source ponctuelle placée sur l'axe central du collimateur tombe à 10% de la valeur maximum à ± 7,5 mm du foyer. La réponse pour un champ éloigné est sensiblement meilleure dans les tissus que dans l'air, du fait de la forte atténuation des rayons gamma mous. Le mémoire indique la réponse du collimateur pour une source ponctuelle dans l'air et à l'intérieur de la boîte crânienne.

Ce collimateur a été utilisé pour mesurer, à l'aide de ^{133}Xe, des flux sanguins localisés dans la substance corticale du cerveau. Toutefois, l'appareil permet aussi de détecter, avec des produits chimiques marqués par ^{125}I, des tumeurs et des hémorragies de la substance corticale.

КОЛЛИМАТОР С ГЛУБИННОЙ ФОКУСИРОВКОЙ ДЛЯ ИССЛЕДОВАНИЯ КОРЫ ГОЛОВНОГО МОЗГА. Описывается детектор, состоящий из кристалла иодистого натрия диметром 12,5 см и толщиной 6,2 мм коллиматора с глубинной фокусировкой. Коллиматор первоначально предназначался для исследования кровообращения в коре головного мозга с помощью ксенона-133, но можно также использовать и другие мягкие гамма-излучающие изотопы, например йод-125.

Коллиматор со свинцовым корпусом толщиной 6 мм является многоканальным. Фокус находится на расстоянии 1,75 см от поверхности коллиматора. Чувствительность в воздухе к точечному источнику по главной оси коллиматора падает до 10% максимальной величины на расстоянии ±0,75 см от фокуса. Чувствительность дальнего поля значительно лучше в ткани, чем в воздухе ввиду большого ослабления в ткани потока мягких гамма-лучей. Приводятся данные о чувствительности коллиматора к точечному источнику в воздухе и внутри черепа.

Коллиматор использовался для измерения местного кровотока в коре головного мозга с помощью ксенона-133. Однако этот аппарат позволяет с помощью меченных йодом-125 препаратов обнаруживать кровоизлияния и опухоли коры головного мозга.

* Present adress: Department of Medical Physics, King's College Hospital, Denmark Hill, London, England.

COLIMADOR DE ENFOQUE PROFUNDO PARA ESTUDIOS DE LA CORTEZA CEREBRAL. El autor describe un detector que consiste en un cristal de yoduro de sodio, de 5 pulg de diámetro y ¼ de pulg de espesor, y un colimador de enfoque profundo. En principio, el colimador fue diseñado para el estudio de la circulación sanguínea en la corteza cerebral mediante el ^{133}Xe, pero puede utilizarse también con otros emisores de rayos gamma blandos, por ejemplo, el ^{125}I.

El colimador, de plomo, tiene ¼ de pulg de espesor y es de tipo multicanal. El foco está situado a 1,75 cm de la cara anterior. La respuesta en aire a una fuente puntiforme que se mueva a lo largo del eje central del colimador decrece hasta el 10% del valor máximo a ± 0,75 cm del foco. La respuesta en tejidos para campos alejados es considerablemente mejor que en aire debido a que los tejidos atenúan mucho la radiación gamma blanda. El autor describe la respuesta del colimador a una fuente puntiforme situada en el aire y dentro de un cráneo.

El colimador se ha empleado para medir, con ayuda de ^{133}Xe, la circulación sanguínea en la corteza cerebral; pero mediante productos químicos marcados con ^{125}I, permite también detectar hemorragias y tumores corticales.

1. INTRODUCTION

1.1. Local blood flow in the brain cortex of animals and humans has been measured using the inert radioactive gases krypton-85 and xenon-133 [1-8]. The principal disadvantage of using the krypton-85 method of LASSEN and INGVAR [1] lies in the necessity of exposing the brain cortex, since krypton-85 emits mainly beta particles. It does, however, also emit 0.4% of a 0.51-MeV gamma-ray and this has been utilized in order to estimate blood flow without exposing the brain cortex [4]. Although this gamma-ray may be readily detected by using a scintillation counter it is difficult to localize in depth by a collimator due to the comparatively high energy. Xenon-133, however, is particularly well suited for measuring local cerebral blood flow because it emits principally a low-energy gamma-ray which therefore eliminates the necessity of exposing the brain surface. The low-energy (81 keV) radiation is readily absorbed in a small thickness of lead, and it also suffers appreciable absorption in the thickness of tissue associated with the human brain. These properties have facilitated the construction of a collimator which has a fine focus in depth and adequate sensitivity. This collimator permits a local area of the upper region of the brain, the brain cortex, to be studied. Local blood flow in the cortex of the human brain has been estimated by using the collimator described below [7, 8].

2. DESCRIPTION OF COLLIMATOR

2.1. The basic design of the collimator is shown in Fig. 1. It consists of two segmented tapered circular annuli cut in a ½-in-thick lead disc. Within the central cross-over region, a maximum volume of the sodium iodide crystal, situated behind the collimator, is viewed. The response falls off rapidly outside this region. The collimator is shown in Fig. 2 and the mechanical dimensions are shown in Figs. 3 and 4. The detector consists of a 5-in-diam. by ¼-in-thick sodium iodide crystal and a 5-in-diam. photomultiplier tube. The background count of this detector, when used in association with a pulse-height analyser is 8 counts/s. The maximum count-rate following a continuous injection over two minutes of approximately 1 mc of xenon is

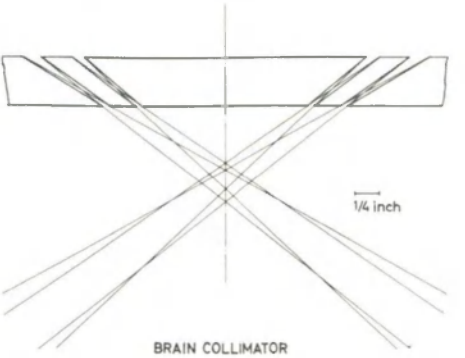

Fig. 1

Diagrammatic representation of basic design of collimator

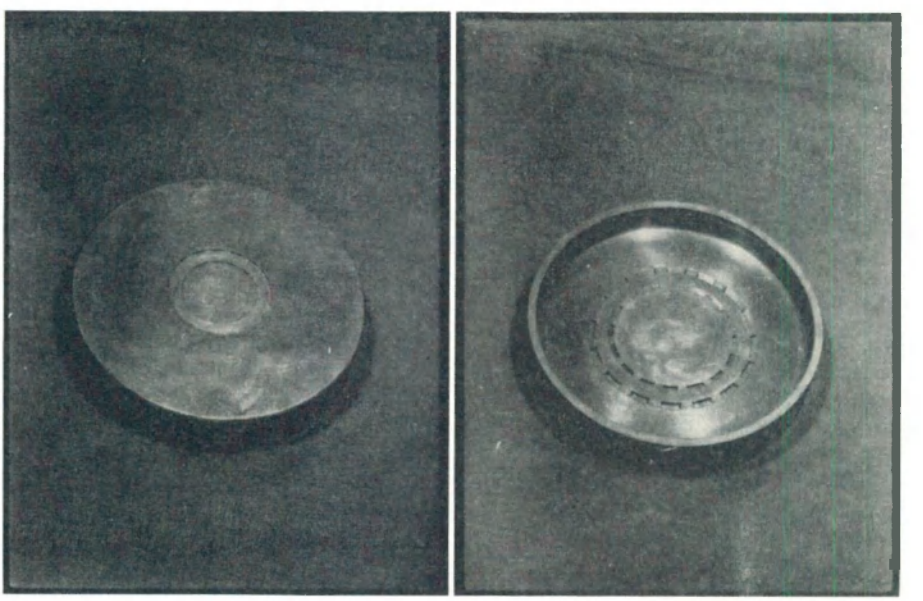

Fig. 2

The collimator viewed from the front (left) and rear

about 200 counts/s. The exposed area of the crystal is equivalent to the unobstructed area of an 0.85-in-diam. crystal. A plastic scintillator assembly with the excess scintillator removed was also built but this detector was not sufficiently sensitive.

2.2. The design of the collimator was governed largely by the size of the crystal, anatomical and mechanical considerations, and the attenuation characteristics of the lead shield for xenon. It is necessary to use a mini-

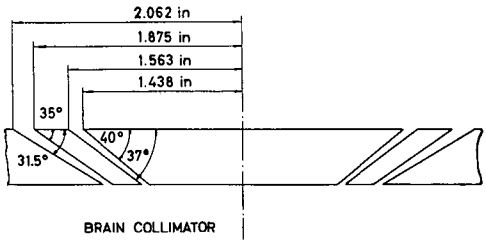

Fig. 3

Mechanical dimensions of section through collimator

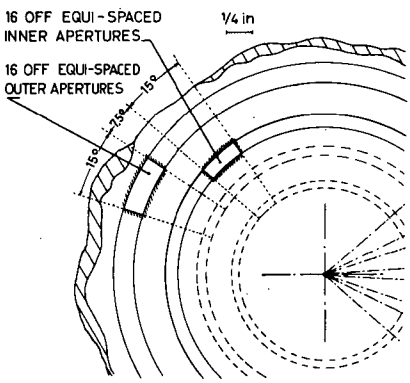

Fig. 4

Mechanical dimensions of plane of collimator

mum thickness of lead consistent with adequate shielding, since the depth response will be improved by keeping the angle of the conical apertures as large as possible. From this point of view lead is not the optimum shielding material as the attenuation coefficient of tin exceeds that of lead at 81 keV, tungsten is better than lead by a factor of 7 and gold by a factor of 10. In order to improve the area localizing properties, a segmented geometry was adopted, the segments shielding approximately one third of the crystal exposed by the annuli.

3. COLLIMATOR CHARACTERISTICS

3.1. The response of the detector to a point source of xenon in air is shown in Fig. 5. The maximum response occurs 1.75 cm from the collimator face on the central axis. This is approximately the depth of the lower edge of the human brain cortex. The width of the central axis response curve at 10% and 1% of the maximum response is 1.4 cm and 2 cm respectively. The maximum response at 2 cm and 3 cm off the central axis is 10% and 5%. Figure 6 shows the response of the same collimator to a point source of xenon

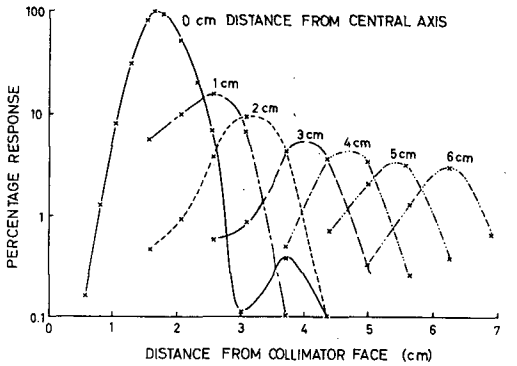

Fig. 5

Response of collimator to a point source of xenon in air

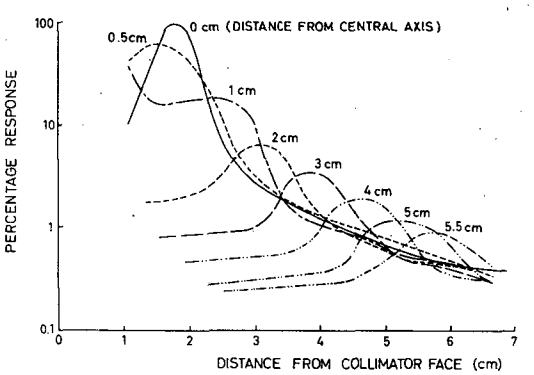

Fig. 6

Response of collimator to a point source of xenon within a water-filled skull

within a water-filled skull. The width of the central axis response at 10% and 1% of the maximum is now 1.4 cm and 3.5 cm. However, due to absorption of the xenon in tissue, the off-axis response is now reduced, yielding a maximum of 6.5% and 3.5% at 2 cm and 3 cm respectively from the central axis.

4. THEORY OF BLOOD-FLOW ESTIMATION

4.1. List of symbols

C_t = average concentration of inert gas;
C_{i0} = initial concentration of inert gas in i^{th} tissue at onset of desaturation;
w_i = weight of ith tissue (g);

f_i = flow in i^{th} tissue in ml/g/min;
p_i = partition coefficient between tissue and blood of ith tissue;
N_t = observed count-rate;
N_0 = observed initial count-rate;
k_i = detector sensitivity factor for i^{th} tissue;
N_{c0} = initial count-rate due to small volume of cortical tissue;
N_{g0} = initial count-rate due to grey matter in whole brain;
N_{w0} = initial count-rate due to white matter in whole brain;
B = concentration of inert gas in blood during continuous injection;
T = injection time;
C_{g0} = initial concentration in grey matter of inert gas;
C_{w0} = initial concentration in white matter of inert gas;
f_g = average flow in grey matter ml/g/min;
f_w = average flow in white matter ml/g/min;
k_g = detector sensitivity factor for all grey matter;
k_w = detector sensitivity factor for all white matter;
p_c = partition coefficient between cortical tissue and blood;
p_g = partition coefficient between grey matter and blood;
p_w = partition coefficient between white matter and blood;
S_0 = initial slope of clearance curve.

4.2. The desaturation curve following the injection of an inert gas and assuming no arterial re-circulation can be shown [9] to be the summation of n monoexponential functions, n being the number of different tissues and i signifying each individual tissue.

$$C_t = \sum_{i=1}^{n} (w_i/\Sigma w_i)\, C_{i0}\, e^{-(f_i/p_i)t} \quad . \tag{1}$$

The observed count-rate can be expressed as

$$N_t = \sum_{i=1}^{n} k_i\, (w_i/\Sigma w_i)\, C_{i0}\, e^{-(f_i/p_i)t} \, . \tag{2}$$

The initial count-rate is given by

$$N_0 = \sum_{i=1}^{n} k_i\, (w_i/\Sigma w_i)\, C_{i0} . \tag{3}$$

Consider three regions of the brain, (a) a small volume composed almost entirely of cortical tissue, (b) the grey matter of the whole brain and (c) the white matter of the whole brain. Let

$$N_0 = N_{c0} + N_{g0} + N_{w0} . \tag{4}$$

The initial concentration of tissue i can be expressed [4] by the formula

$$C_{i0} = B\, p_i\, (1 - e^{-(f_i/p_i)t})\, T \doteqdot B\, f_i T . \tag{5}$$

From (5)

$$C_{g0}/C_{w0} = f_g/f_w. \tag{6}$$

If we assume that $f_g \doteqdot 5 f_w$, $k_g \doteqdot k_w$, and also 60% of the brain is composed of grey matter, then

$$N_{g0}/N_{w0} = 0.46/0.04 . \tag{7}$$

If we assume that 50% of the total response is due to local cortical radioactivity and that the initial concentration of the cortex is approximately equal to that of grey matter then from (2), (3) and (7)

$$N_t/N_0 = 0.5\ e^{-(f_c/p_c)t} + 0.46\ e^{-(f_g/p_g)t} + 0.04\ e^{-(f_w/p_w)t}. \tag{8}$$

Therefore, if we further assume $p_g \doteqdot p_c$, then

$$p_g \frac{d}{dt}\left[\frac{N_t}{N_0}\right]_{t=0} = 0.5\ f_c + 0.46\ f_g + 0.04\ f_w \frac{p_g}{p_w}, \tag{9}$$

and if $f_c \doteqdot f_g$ then

$$f_c = (p_g/0.95)\ S_0 . \tag{10}$$

5. DISCUSSION

5.1. Equation (9) indicates that the effect of the clearance of xenon-133 from the white matter on the initial slope of the clearance curve will be approximately 5% to 10%. If, however, the local cortical flow were to reduce substantially, this would produce a marked decrease in the value of the first term in the right-hand side of equation (8), and in the case of complete reduction of flow in that region the initial slope might be expected to change by up to 50%.

5.2. Animal investigations have indicated that the effect of re-circulation on the initial slope of the clearance curve following a 2-min continuous injection of xenon dissolved in saline into the carotid artery may reduce the numerical value obtained for the flow by approximately 5%.

5.3. If one assumes a uniform distribution of activity throughout one half of the brain, the total response of the detector may be calculated by volume integration of the point source response. Figure 7 shows that in such an idealized case, 50% of the total response would be due to a cylinder with a 2-cm radius and 1.5-cm depth from the top of the brain surface. Since the response from the small volume of tissue will play such a dominant role during the initial part of the clearance curve, local changes of blood flow within this region will be readily detected.

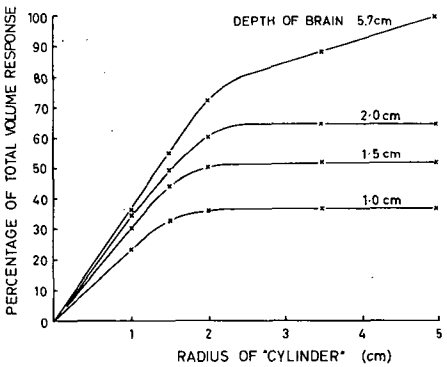

Fig. 7

Calculated response of collimator to brain containing a uniform distribution of radioactivity

6. CONCLUSION

6.1. There may be some advantage in using such a collimator to locate tumours or haemorrhage in the cortical region of the brain by using substances which would not normally traverse the blood-brain barrier tagged with a low-energy emitter, such as iodine-125. This device, however, was intended for use in the measurement of local blood flow when the remainder of the brain contains varying amounts of xenon. The problem is therefore one of following the rate of change of activity level from a small part of a larger volume whose activity level is also changing.

6.2. For absolute measurement of blood flow the field of view of the present collimator is not considered sufficiently fine to enable the various geometrical corrections to be estimated with an accuracy of better than plus or minus 15%. By doing bilateral observations, or repeated observations on the same site, after some change in the conditions of the investigation, geometrical factors may be effectively eliminated and regions of change of local blood flow would be readily determined. In view of the unfavourable volume-response characteristics of open cylindrical collimators, it is felt that the method described represents an advance in the search for a technique for measuring the local cortical blood flow in the intact human skull, and the device may well have useful clinical applications.

ACKNOWLEDGEMENTS

The author gratefully acknowledges the support and encouragement of Dr. J. M. A. Lenihan and Professor W. A. Mackey throughout this work. The invaluable co-operation of Dr. A. M. Harper and the technical assistance of Mr. John Waller was greatly appreciated in developing the collimator described in this paper. I also wish to thank Mr. E. Fahey and Mr. John Drysdale for their skill in constructing this collimator.

REFERENCES

[1] LASSEN, N. A. and INGVAR, D. H., Experentia 17 (1961) 42.
[2] INGVAR, D. H. and LASSEN, N. A., Acta physiol. scand. 54 (1962) 325.
[3] INGVAR, D. H. and LASSEN, N. A., Lancet II (1961) 806.
[4] LASSEN, N. A., HOEDT-RASMUSSEN, K., SORENSEN, S. C., SKINHOJ, E., CRONQUIST, S., BODFORSS, B. and INGVAR, D. H., Neurology 13 (1963) 719.
[5] HARPER, A. M., GLASS, H. I. and GLOVER, M. M., Scot. med. J. 6 (1961) 1.
[6] GLASS, H. I., HARPER, A. M. and GLOVER, M. M., Phys. Med. Biol. 6 (1961) 65.
[7] GLASS, H. I. and HARPER, A. M., Brit. med. J. 1 (1963) 593.
[8] HARPER, A. M., GLASS, H. I., STEVEN, J. L. and GRANAT, A. H., J. Neurol. Neurosurg. Psychiat. (1964), In press.
[9] KETY, S. S., Pharmacol. Rev. 3 (1951) 1.

DISCUSSION

P. CZERNIAK: Is it possible to apply your theoretical data to clinical work? If so, what are the smallest space-occupying lesions that could be detected in the human body and what is the maximum depth at which they could be detected?

H. GLASS: The collimator described is designed for a highly specialized application, namely the detection of a rate of change of activity near the surface of the head. It is not possible to extend this technique to investigate changes in deep-lying regions.

P. HARPER: Is it not true that the total response of the collimator is the sum of that from all tissues occupying the field of view and that the limitation of the response to the superficial structures is only caused by attenuation of the gamma radiation from the deeper tissues?

H. GLASS: You are quite right, and it is for this reason that lower-energy, more highly attenuated radiation would be desirable. However, it is necessary, when designing the collimator, to ensure that maximum response is associated with the region of interest, bearing the tissue-attenuation factor in mind.

W. G. MYERS: Do you not think that Xe^{131m} would have yielded better results than Xe^{133}? The former is the radioactive daughter of I^{131}. It is generated in about 0.5 - 1% of the disintegrations and has a half-life of 12 d. It could thus be readily produced in most medical radioisotope laboratories by means of a simple vacuum system with which Xe^{131m} could be milked as needed from a stock of I^{131}.

The greater penetration of the Xe^{131m} 164-keV gamma ray might be advantageous, particularly for some applications within the skull. Moreover, the internal conversion of this Xe^{131m} gamma ray is several times greater than that of the Xe^{133} 81-keV gamma ray. The resultant X-ray/gamma ray ratio, which is much higher, should permit the X-ray peak to rise well above the Compton continuum of the gamma ray spectrum. Consequently, the great differences in absorption of the X-rays and the gamma rays in tissues might be used to assess the depth of a radioactive source in terms of the value of this ratio, by an alternative method to the one you used.

It is even possible that the outputs of two discriminators, one adjusted to the energy of the X-ray and one to that of the gamma ray, could be fed into a suitable circuit to indicate changes in the value of this ratio, and thus changes in depth, directly. The much smaller X-ray/gamma ray ratio of Xe^{133} might not provide the opportunity referred to here, especially within the skull. Preliminary findings in my laboratory with I^{123}, which gives X-rays and gamma rays having energies almost the same as those of Xe^{131m}, but with an X-ray/gamma ray ratio near unity, indicate that the X-ray peak is "buried" too deeply in the Compton continuum to allow depth to be assessed by this method.

H. GLASS: A method of estimating local blood flow deep in the brain is urgently needed in clinical neurology. I very much appreciate Dr. Myers' remarks regarding the possible use of Xe^{131m} in the study of regions well below the surface of the brain.

P. C. R. TURNER: Xe^{133} is widely used for lung function studies and we have found that the X-ray peak can easily be distinguished from the 81-keV gamma peak. If I am not mistaken, the 81-keV gamma ray from Xe^{133} is about 65% converted.

H. GLASS: The relative height of the lower-energy X-ray peak certainly exceeds that of the 81-keV gamma ray. However, with our pulse-height analyser we were unable to utilize the lower-energy emission alone, although this would have been greatly to our advantage.

LOCALIZATION AND TOTAL BODY HIGH-ENERGY GAMMA-RAY SCANNING STUDIES IN CANCER PATIENTS

J.S. LAUGHLIN, P.J. KENNY, K.R. COREY, E. GREENBERG AND D.A. WEBER
DIVISIONS OF BIOPHYSICS AND CLINICAL INVESTIGATION,
SLOAN-KETTERING INSTITUTE FOR CANCER RESEARCH, NEW YORK,
UNITED STATES OF AMERICA

Abstract — Résumé — Аннотация — Resumen

LOCALIZATION AND TOTAL BODY HIGH-ENERGY GAMMA-RAY SCANNING STUDIES IN CANCER PATIENTS. A scanning system has been developed for use with energetic gamma-ray-emitting nuclides, which scans either the total body or specific portions of it and which presents the data quantitatively with a dynamic range of six orders of magnitude. This system has been applied over the past few years for studies with Ca^{47} and other radionuclides in cancer patients. The system includes two large crystal detectors mounted in 600-lb tungsten and lead-shielded heads whose motion, either continuous or discontinuous, above and below a patients' couch, can be programmed with great flexibility. A tungsten focusing collimator is used for "fine" scanning. Digital presentation provides exact data and permits statistical analysis of counting variations over body sites. Quantitative comparison has been made with analogue film presentation, which has a much more limited dynamic range and decreased sensitivity for detecting variations.

The system has been successful in the early detection and definition of bone lesions, and has permitted precise metabolic and kinetic studies of bone-seeking nuclides over long periods of time. A further feature of this system is the measurement of total activity independently of concentration or redistribution in out-patient kinetic studies. New results are presented.

SCINTIGRAPHIE, AU MOYEN DE RAYONS GAMMA DE HAUTE ÉNERGIE, D'ORGANES ET DU CORPS ENTIER DE CANCÉREUX. Les auteurs ont mis au point un dispositif de scintigraphie devant être utilisé avec des émetteurs gamma de haute énergie, qui explore le corps entier ou des organes déterminés et présente des données quantitatives dans une gamme de six ordres de grandeur. On utilise ce dispositif depuis quelques années pour des examens de cancéreux au moyen de ^{47}Ca et d'autres radionucléides. Le dispositif comprend deux détecteurs à grands cristaux, montés sur des têtes de 300 kg avec écran en tungstène et en plomb, dont on peut facilement régler à l'avance le mouvement, continu ou discontinu, au-dessus et au-dessous du lit du patient. On utilise un collimateur à focalisation en tungstène pour le balayage «fin». Une présentation numérique fournit des données exactes et permet l'analyse statistique des variations de comptage sur divers points du corps. Les auteurs ont fait des comparaisons quantitatives avec une présentation analogique sur film, qui a une gamme plus limitée et une moins grande sensibilité pour la détection des variations.

Ce dispositif a été utilisé avec succès pour la détection et la détermination d'une lésion osseuse au cours de ses premières phases et il a permis de faire, pendant de longues périodes, des études métaboliques et cinétiques précises de nucléides ostéophiles. Il permet en outre de mesurer l'activité totale, indépendamment de la concentration ou de la redistribution, au cours d'études cinétiques sur des patients non hospitalisés. Les auteurs présentent les nouveaux résultats obtenus.

ОПРЕДЕЛЕНИЕ ЛОКАЛИЗАЦИИ ОПУХОЛИ И СКЕННИРОВАНИЕ ВСЕГО ОРГАНИЗМА ПО ГАММА-ИЗЛУЧЕНИЮ ВЫСОКОЙ ЭНЕРГИИ У РАКОВЫХ БОЛЬНЫХ. Была разработана сканнирующая система для использования гамма-излучающих изотопов высокой энергии, дающая возможность получать сканнограммы всего организма, либо отдельных его частей и предоставляющая количественные данные в динамическом пределе шести порядков величины. Эта система в течение последних нескольких лет применялась для исследований с помощью кальция-47 и других радиоизотопов больных, страдающих раковыми заболевания-

ми. В систему включены два крупных кристаллических детектора, вмонтированных в головки с экраном из вольфрама и свинца весом 600 фунтов, которые передвигаются либо плавно, либо прерывисто как сверху, так и снизу койки больного, и могут быть программированы с большой гибкостью. Фокусирующий вольфрамовый коллиматор используется для "тонкого" сканирования. Цифровые показатели дают точные данные и позволяют проводить статистический анализ различных вариаций счета во всех частях тела. Было проведено количественное сравнение с показаниями снимков, которые имеют более ограниченный динамический предел и пониженную чувствительность к обнаружению вариаций. Система оказалась успешной при ранней диагностике и обнаружении костных повреждений и дала возможность провести точные метаболические и кинетические исследования изотопов, отлагающихся в костях в течение длительного времени. Другой характерной особенностью этой системы является возможность проводить измерение активности всего организма независимо от концентрации или перераспределения при кинетических исследованиях у амбулаторных больных. Приводятся новые результаты.

EXPLORACIÓN DEL ORGANISMO ENTERO MEDIANTE RAYOS GAMMA DE ALTA ENERGÍA PARA LOCALIZAR TUMORES CANCEROSOS. Los autores han ideado un dispositivo que se emplea con núclidos emisores de rayos gamma de alta energía para explorar el organismo entero, o partes de él, y que presenta los datos cuantitativamente con un intervalo dinámico de seis órdenes de magnitud. Durante los últimos años este dispositivo ha sido utilizado con ^{47}Ca y otros radionúclidos para estudiar casos de cáncer. Consta de dos grandes cristales detectores montados en blindajes de wolframio y plomo de 600 libras cuyo desplazamiento continuo o discontinuo por encima y por debajo del paciente puede programarse con gran flexibilidad. Para la exploración «fina» se emplea un colimador enfocado de wolframio. La presentación numérica facilita datos exactos y permite un análisis estadístico de las variaciones del recuento sobre distintas partes del cuerpo. Se han efectuado comparaciones cuantitativas con una presentación análoga en película de intervalo dinámico mucho más limitado y de menor sensibilidad para la detección de variaciones.

Este dispositivo se ha empleado con éxito para la detección precoz y la delimitación de lesiones óseas, y ha permitido realizar estudios metabólicos y cinéticos exactos de los núclidos osteófilos durante períodos de larga duración. Otra característica de este dispositivo es que permite realizar estudios cinéticos en pacientes ambulantes midiendo la actividad total independientemente de la concentración o de la redistribución. En la memoria se presentan nuevos resultados.

BACKGROUND AND APPLICATIONS

The scanning system here described was designed and built at Memorial-Sloan Kettering Cancer Center and has been in operation there since April 1960 [1]. It was designed to facilitate studies of calcium metabolism in the human skeleton by providing quantitative data on the uptake, distribution and retention of injected tracer doses of calcium-47 or strontium-85.

These measurements, made at different times following administration of the tracer, together with measurements of the variation of the serum specific activity, have provided basic information on the metabolism of calcium in the skeleton as a whole in a large number of studies and have also served to delineate local areas of increased or decreased turnover of calcium corresponding to bone lesions of various kinds [2, 3, 4]. The accretion rate and the size of the exchangeable calcium pool [5, 6] have been calculated in many studies for correlation with the patient's clinical status, and to help evaluate the effect of various types of therapy such as chemotherapy, radiation therapy or surgical procedures, on the skeletal metabolism [2, 3]. In addition to its application in this work, the scanner has also been used for heart, brain, liver and kidney scanning, and for

measurements of the retention of tracer doses of iodine-131 before cancer therapy with this isotope.

DESIGN CONSIDERATIONS

Some preliminary work on the distribution of injected tracer doses of calcium-47 was done with an iodine-131 uptake counter to which additional shielding had been added. The results of these pilot studies provided data for the design of the high-energy gamma-ray scanner (HEG scanner). Four considerations appeared to be of prime importance:

(1) The injected calcium-47 tracer is removed rapidly from the circulation and is taken up throughout the normal skeleton. It thus creates a general body background against which one must work when scanning for localized lesions.

(2) The main gamma-ray emission of calcium-47 is at 1.3 MeV in approximately 70% of disintegrations. The half-value thickness of lead for this radiation is approximately 1.1 cm so that massive shielding and collimation is necessary to achieve directional response and low background.

(3) In scanning for early lesions, such as metastases from a known primary cancer, one is looking for small variations in uptakes which are themselves very small – less than 1% of the injected dose. With tracer doses of the order of 50 μc it is therefore necessary to use crystals of sufficiently large size to achieve adequate counting efficiency.

(4) During the first few hours following injection, the tracer dose is rapidly redistributed in the body. Hence, in order to be able to measure retention reliably by scanning it was necessary to design the system so that for a given amount of radioactive material in the patient the counts recorded at the end of a total body scan should be independent of the distribution of the isotope in the body.

With the considerations outlined above in mind, the scanner was designed having two identical, opposed detectors track mounted above and below a light lucite platform on which the patient lies. The design allowed for easy removal of the platform and decoupling of the lower detector when a bed or stretcher patient had to be studied. Electric motors control the movements of the detectors in three mutually orthogonal directions. The maximum area of scan in the horizontal plane is 68 in by 28 in; in the vertical plane, the upper detector can be moved through a distance of 20 in and the lower detector through 7 in.

Two alternative types of motion are provided: (1) continuous, with line spacing adjustable at $\frac{3}{16}$, $\frac{3}{8}$, $\frac{3}{4}$, $1\frac{1}{8}$, $1\frac{1}{2}$, $2\frac{1}{4}$, or 3 in and speed continuously adjustable to a maximum of 83 in/min, and (2) discontinuous, with the same choice of spacing in both directions. In the discontinuous mode, the detectors stop for a preset time – adjustable between 1 and 60 s – at each counting position and transfer their accumulated counts at the end of this time to the read-out system before moving on to the next counting position.

The dimensions of the detector heads are shown in Fig. 1. The 19-hole tungsten focusing collimator shown here is easily removable and may be replaced by any one of a variety of other available collimators. The weight of each complete detector head is 600 lb. The upper detector is mounted

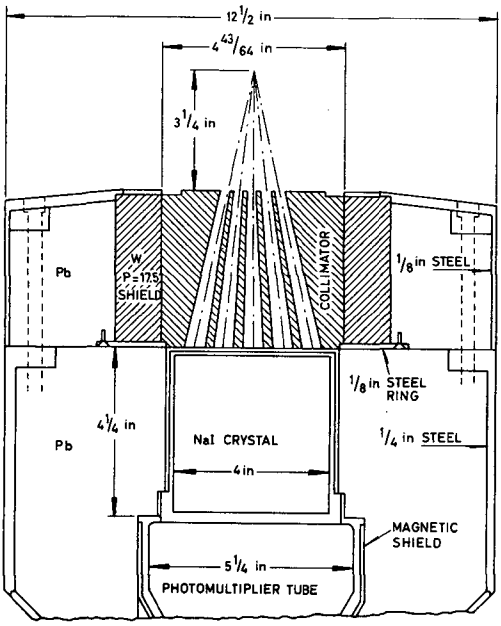

Fig. 1

Cross-section of a detector on high-energy gamma-ray scanner, with 19-hole tungsten focusing collimator in place

and balanced so that its axis may be easily angled over a hemisphere to facilitate stationary counting over various parts of the body. A manual switch is provided to position the detector for this application. Light sources, scales and protractors are mounted to permit precise reproduction of counting geometries.

Each detector is equipped with its own preamplifier, single-channel pulse-height analyser, scaler and high voltage supply. Auxiliary ratemeters, scalers and pulse-height analysers are available for special functions, such as background erase, contrast enhancement, or double tracer studies.

Figure 2 shows a block diagram of the electronics.

READ-OUTS

Two forms of read-out are currently used with the scanner for the display of localization scans:

(1) A true digital display is provided by an electric typewriter equipped with a 28-in wide carriage which is servo-driven in a one-to-one synchronism with the scanner detectors. This type of read-out is used with the discontinuous scanning mode and the first three significant digits of the counts accumulated at each stationary position are printed out on a roll of paper. The maximum count capacity of this system at any position is $10^6 - 1$. A two-colour ribbon shift on the typewriter from black to red indicates the order of magnitude of any count [9].

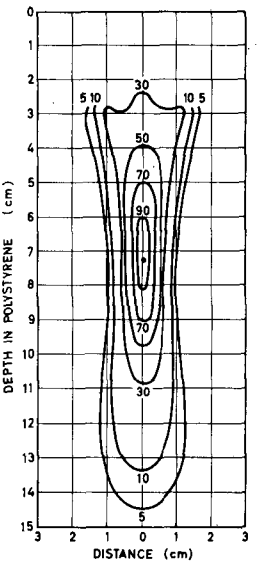

Fig. 2

Isocount contours of tungsten focusing collimator for iodine-131 point source in polystyrene

Spatial resolution of 19-hole tungsten collimator
Isocount contours in axial plane
I^{131} point source in polystyrene; Channel width: 40-keV at 0.364 MeV
Width of 50% contour in focal plane: 1.05 cm

(2) A black and white photographic record is provided by an intensity modulated cathode-ray tube which is moved over a photographic film by servomotors in one-to-one synchronism with the movement of the scanner detectors. The voltage applied to the cathode-ray tube is taken from the output of a ratemeter in series with one of the detectors. The parameters which may be preset are: (i) The "on time" of the tube for each count; (ii) The intensity of the light from the tube; (iii) The time constant of the ratemeter; (iv) An adjustable scaling factor may be introduced between the output of the detector and the input to the ratemeter; (v) The voltage change on the cathode-ray tube corresponding to a given percentage change in output from the ratemeter may be preset thus allowing for contrast enhancement; and (vi) background subtraction may be preset at any level. The flexibility of these controls has permitted a sensitive evaluation of the capabilities of the photographic read-out in displaying small significant variations in the count-rate. This evaluation will be discussed more fully later.

RESOLUTION AND SENSITIVITY

The isocount contours of one of the detectors with the focusing collimator in place are shown in Figs. 3 and 4 for point sources of iodine-131 and calcium-47 respectively. The sensitivity of the detector for a point

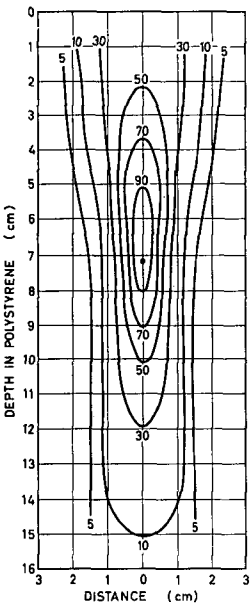

Fig. 3

Isocount contours of tungsten focusing collimator for calcium-47-point source in polystyrene

Spatial resolution of 19-hole tungsten collimator
Isocount contours in axial plane
Ca^{47} point source in polystyrene; Channel width: 120 keV at 1.31 MeV
Width of 50% contour in focal plane: 1.1 cm

source of calcium-47 at the focal point is approximately 1800 cpm/μc when used with this collimator and a 120-keV channel centred at 1.3 MeV.

The corresponding figure for a strontium-85 source is approximately 5000 cpm/μc with a 100-keV channel centred at 0.51 MeV.

The ability of the detector to locate small volumes of strontium-85 of higher specific activity than the surrounding medium was determined by observing the count-rates from two cylindrical sources, with active dimensions of 0.4 cm diam. by 0.4 cm height and 1.9 cm diam. by 0.4 cm height respectively placed in a lower specific activity scattering medium. The sources were placed, in turn, coaxially with the detector, at the focal distance, in a water phantom of dimensions 36.2 × 28.6 × 12.5 cm. The source holders, which were constructed of polystyrene, had a wall thickness of 1 mm and the gap between the front of the collimator and the water surface was 5 mm. Counting with a 100-keV channel centred at 0.51 MeV, the smaller source registered 2300 cpm/μc and the larger source registered 1530 cpm/μc. The count-rate due to background solution only was 5.76×10^4 cpm/μc with a uniform specific activity of 1 μc/cm^3 throughout the volume. From these values, the probability of detecting sources of these dimensions in the focal plane of the detector for any combination of source specific activity, background specific activity, and counting time may be calculated for this particular phantom. Table I presents results

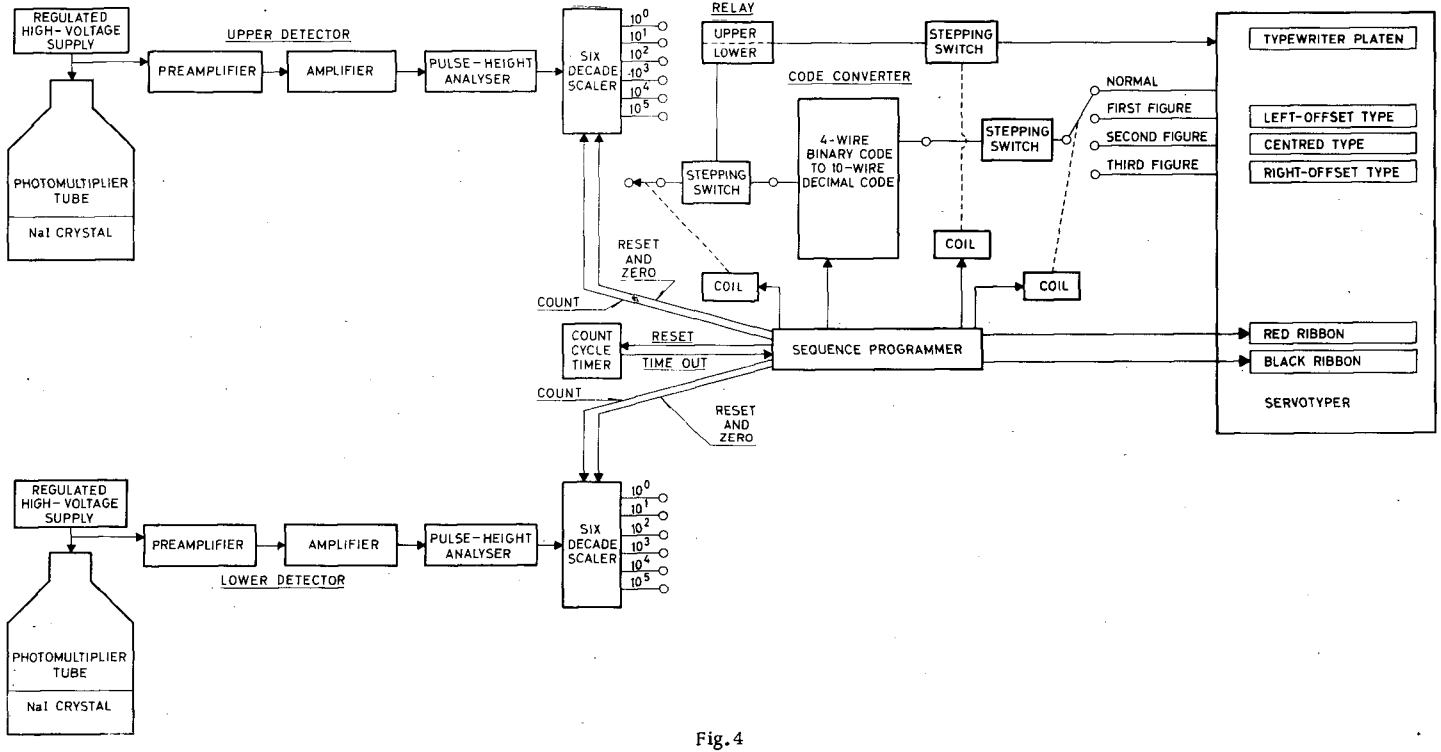

Fig. 4

Block diagram of electronics and read-out system of high-energy gamma-ray scanner

TABLE I

COUNTING TIMES REQUIRED TO DETECT DIFFERENCE BETWEEN SOURCE AND BACKGROUND WITH 95% CONFIDENCE LEVEL (1.96 STANDARD DEVIATIONS)

Source size: 0.4 cm diam. by 0.4 cm height Background solution specific activity: 1 μc/cm³		
Specific activity ratio (source to background)	Counting time (s)	Percentage difference between mean background and mean of background plus source
3	57	0.9
10	5.1	2.9
20	1.4	5.7
As above, but with background solution specific activity 0.1 μc/cm³		
3	570	0.9
10	51	2.9
20	14	5.7
Source size: 1.9 cm diam. by 0.4 cm height Background solution specific activity 0.1 μc/cm³		
3	4.3	9.8
10	0.2	33

of some calculations to illustrate the detection capabilities in different situations. Two levels of background solution specific activity (1.0 μc/cm³ and 0.1 μc/cm³) and three different values of the ratio of source to background solution specific activity (3, 10 and 20) are considered, and the counting times required to establish a 95% confidence level difference (corresponding to 1.96 standard deviations) between the source and background are listed.

These figures indicate the practical limits of sensitivity of a single detector with the tungsten focusing collimator when used for strontium-85 search scans. It should be emphasized that these limits of detectability apply only if the read-out system used can distinguish the differences between the mean background count-rate and the mean background plus source count-rate. It is clear that the ultimate sensitivity of a scanner to detect small variations in activity cannot be greater than the ability of its read-out system to represent these variations in a clearly distinguishable way.

LOCALIZATION SCANNING

The tracer doses used in these studies varied between 40 and 100 μc of calcium-47 (carbonate) or strontium-85 (chloride). The specific activity

of the calcium-47 injected was approximately 200 μc/mg calcium and that of the strontium-85 approximately 8 mc/mg strontium.

The total amount of calcium in the serum is approximately 400 mg, so that an injection of 100 μc does not effectively alter the amount of this circulation, and the specific activity of the circulating isotope in the serum immediately following the injection is around 0.25 μc/mg calcium. The observed accretion rates of calcium in normal subjects are around 500 mg/d, and in patients with widespread active bone lesions are generally elevated above this level, reflecting the increased local turnover rates of calcium around the lesions. Hence, with a detector having a sensitivity of a few thousand counts per minute per microcurie it should be possible to detect very small changes in local turnover rates — approaching values of the order of 1 mg/d. Furthermore, since the net uptake of the isotope in any localized area is the difference between accretion and resorption in that area, measurement of the tracer uptake will give an indication of local turnover rates within a day following injection. The sensitivity of radiographic techniques to detect such changes depends on detecting a net change in mineralization, which requires a much longer period of observation [7, 8]. The energy discriminations routinely used when scanning are a 100-keV channel at the 1.3-MeV peak of calcium-47 or at the 0.51-MeV peak of strontium-85. Background count-rates at these settings are approximately 35 and 70 cpm respectively.

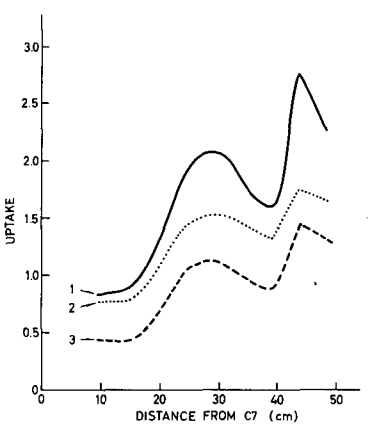

Fig. 5

Patterns of uptake of calcium-47 and strontium-85 in spine of patient M.S. Distances are measured from seventh cervical vertebra.

M.S. ♀ Breast cancer, activity profile in spine: 2-in collimator
1 : 6 d following 100 μc Ca^{47} I.V.
2 : 7 d following 80 μc Sr^{85} I.V.
3 : 8 d following 80 μc Sr^{85} I.V.

Figure 5 is a comparison of the activity profiles in the spine of a patient following injections of calcium-47 and strontium-85. It was obtained using a 2-in diam. straight-bore collimator in the upper detector and illustrates the general similarity of the distribution of these isotopes in the spine. The

uptake is expressed relative to the counting rate of the total injected amount measured in the same standard geometry for both isotopes. The calcium-47 injection in this case was made two days following the strontium-85 injection. In this patient the whole spine, from approximately 10 cm below the seventh cervical vertebra, was involved by metastatic disease from a primary breast carcinoma and elevated values of uptake are seen throughout this area. It is apparent that there is some suggestion of greater specificity of calcium-47 in certain areas of the spine, as indicated by its sharper profile.

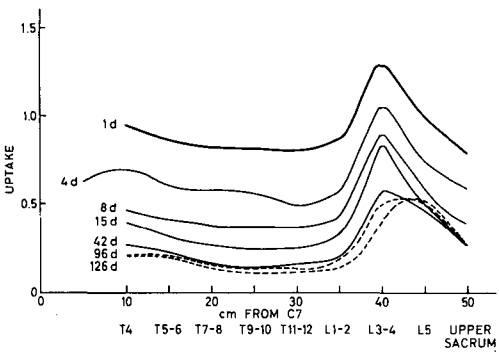

Fig. 6

Variation of uptake of strontium-85 with time in spine of patient H.G., from 1 to 126 d following injection
Re-distribution of the isotope in the area around the
fifth lumbar vertebra is indicated in the latter part of the study.

H.G. ♀ Breast cancer 97.4 μc Sr^{85} I.V.

Figure 6 is a plot of a similar activity profile in the spine of a patient with primary breast carcinoma. The activity peak seen at the third and fourth lumbar vertebrae corresponds to a metastatic lesion which was given radiation therapy (2000 rad) between the 8th and 15th days of the tracer study. The measurements made on days 96 and 126 show a redistribution of the tracer in the area around the third, fourth and fifth lumbar vertebrae with an increase in uptake developing in the fifth lumbar vertebrae. This kind of redistribution has been observed in another study of a patient who had received radiation therapy to a lesion in the spine and will be described in detail in a separate publication.

Figure 7 shows the result of a double tracer scan of two femurs. This scan was made 5 d after intravenous injection of 58 μc of calcium-47 and 6 d after intravenous injection of 52 μc of strontium-85. The upper read-out represents the counts accumulated in a 20-s preset time from strontium-85 and the lower read-out the counts accumulated in the same time from calcium-47. The tungsten focusing collimator shown in Fig. 1 was used in this scan and the spacing was $\frac{3}{8}$ in. The area of higher uptake over the left edge of the left femur was later identified as a metastatic lesion from a primary breast carcinoma.

Figure 8 illustrates a scan of the right elbow of a patient with primary breast cancer who had received a tracer dose of strontium-85. The high uptake corresponds to a metastatic deposit. The figure illustrates one of

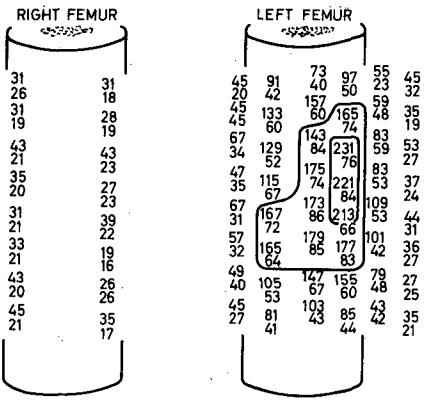

Fig. 7

Result of double tracer scan on midshafts of femurs of patient S.K.
Upper read-out represents counts accumulated per 20 s from strontium-85.
Lower read-out represents counts accumulated per 20 s from calcium-47.
Corresponding backgrounds 26 and 13 counts respectively. Focusing collimator used.

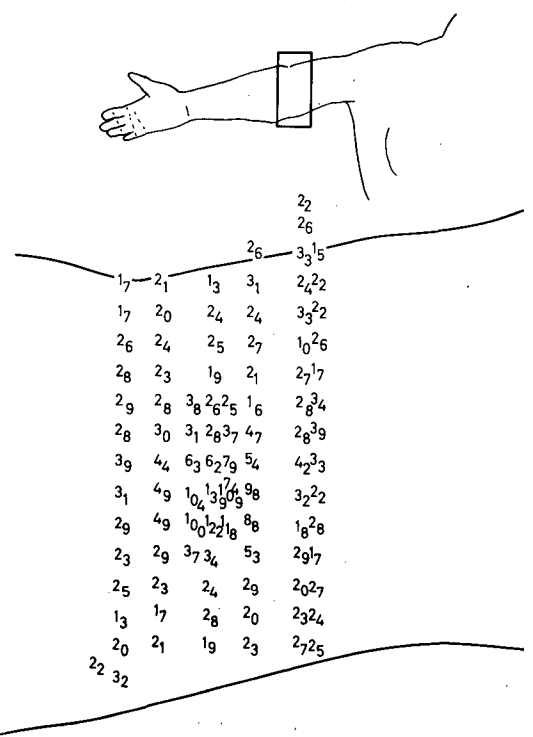

Fig. 8

Result of scan of elbow on patient E.K. following tracer injection of strontium-85
This scan illustrates the ability to interpolate extra lines or point readings
to further delineate areas of increased uptake.

the features of the digital read-out system and its controls. The digital record of the scan is immediately available to the correct scale and when further detail is required to delineate particular areas, extra lines may be automatically interpolated at the required position and spacing.

RETENTION SCANNING

The possibility of measuring the retention of an administered tracer dose by scanning the entire body and totalizing the counts accumulated by each detector was first investigated with the aid of a water-filled polyethylene phantom in which various arrangements of sources could be placed. Twenty small sources of iodine-131, strontium-85 and calcium-47 were used successively for this work. Values of the scan parameters were determined for which the total accumulated counts (from upper plus lower detector) at the end of each scan remained essentially constant for any rearrangement of the sources. It was found that this condition could be satisfied by scanning the entire 68 × 28-in area with a 23-in separation between the upper and lower collimator fronts. Cylindrical 4.7-in-diam. collimators were used and a 1.5-in line spacing in the continuous scan mode. The energy discriminations used were the same as those for search scans. The time required for this scan is approximately 15 min. The sensitivity for calcium-47 is approximately 1800 total counts (upper plus lower) per microcurie retained in the body and the total background is 1000 counts. For strontium-85 the corresponding figures are 5000 and 4000 respectively. Figs. 9 and 10 show a comparison of the retention of calcium-47 in a patient,

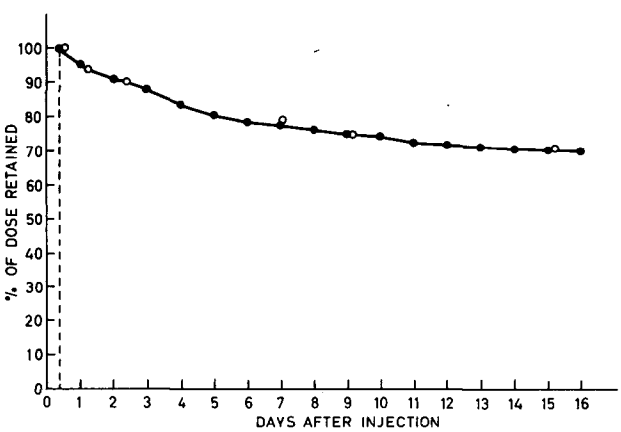

Fig. 9

Comparison of the retention of calcium-47 for patient M.D. as measured by scanning and by collection and assay of excretions. First study.

M.D. ♀ Breast cancer
Study 1: 50.6 μc Ca^{47} I.V.
○ Percent retention from scan measurements
● Percent retention from assay of collected excretions

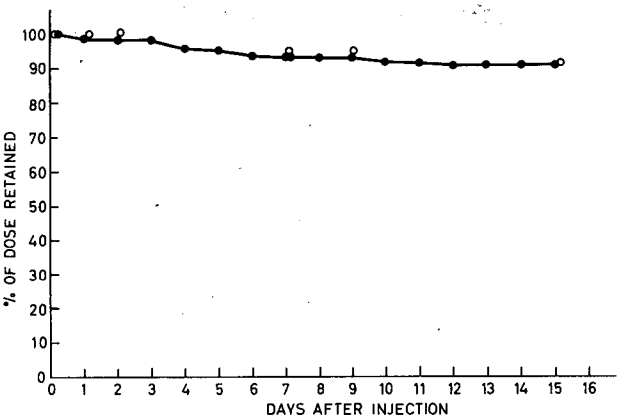

Fig.10

Comparison of the retention of calcium-47 for patient M.D. as measured by scanning and by collection and assay of excretions. Second study.

M.D. ♀ Breast cancer
Study 2: 51.1 μc Ca^{47} I.V.
○ Percent retention from scan measurements
● Percent retention from assay of collected excretions

as measured by scanning and by collection and assay of excretions in two studies about one month apart. Good agreement is demonstrated here between the two methods of measuring retention. In a number of comparisons of retention as measured by scanning and by collection and assay of excretions the scanning measurement has indicated a lower retention. The difference between the two measurements increased slightly with time and has amounted to approximately 5% after 8 d. It was theorized that some of this difference might be due to loss of isotope from the body by perspiration. This possibility was confirmed in the case of an iodine-131 therapy patient who had received 330 mc orally. Measurements of the bed linen used during the first six days following therapy indicated a perspiration loss of approximately 2% of the dose. The loss of calcium by this route has been investigated by CONSOLAZIO et al. [10], who report that perspiration may contain as much as 33% of the total calcium excreted, under extreme sweating conditions. While the corresponding percentage in the case of patients maintained on a metabolic ward is not likely to approach this figure, it is of interest to note that in over 20 comparisons of retention measured by scanning and by collection of excretions, any differences after the third day were all in the direction of a lower retention on the scanning measurement.

In summary, measurement of retention by scanning has the advantage that it is a convenient, direct measurement which is not subject to errors of incomplete or inaccurate collections and does not require the time-consuming laboratory procedures associated with preparation and assay of many samples. It has the further advantage that it may be done on an out-patient basis.

READ-OUT SYSTEMS

The information which the read-out system of a scanner must present is digital in form. It is the number of gamma rays which deposit a specified amount of energy in the crystal at each position of the detector within the scan limits. Ideally, this information would provide a map of the activity variations in the organ scanned. Up to the present this has not been possible because it is a three-dimensional problem and because the spatial resolution of scintillation detectors in three dimensions is not sufficiently sharp. However, even accepting this limitation, there is still the problem of displaying the counts registered by the detector at each position of its movement. The most common forms of read-out used to date have been analogue in form, either dot tappers or photographic, in black and white or colour. The main shortcomings of these systems is that they are not quantitative, have a limited dynamic range, are subject to saturation and distortion and depend on subjective evaluation. There is the further disadvantage with the photographic read-outs that they cannot be inspected during the scan. The dot tapper representation may be converted into a digital record by counting the numbers of dots in adjoining equal areas and writing in the totals. In practice this is seldom if ever done and this type of read-out must, therefore, also be classified as analogue. The advantages of the digital read-out are:

(1) It is quantitative and may be related to the amount of tracer administered or retained in the body or to the clinical category of the subject.
(2) It presents all the original information in an unmodified form and thus does not act as a limitation on the ultimate sensitivity of the detector.
(3) It has a practically infinite dynamic range and does not saturate or distort at any level of count-rate.
(4) It allows immediate inspection during the scan and indicates the statistical significance of any variations.

The main objection to this form of read-out has been the difficulty of interpretation. However, this is a matter of practice only. In the case of liver scans, covering an area of 24 × 24 cm, and containing approximately 600 point readings spaced 1 cm apart, it is routinely possible to plot the isocount contours manually in 15 min, which is less than the time required for processing a film. Each contour is labelled in multiples of:

$$\frac{\text{Number of counts at each point}}{\text{Number of microcuries injected} \times e^{\lambda t}}$$

where λ is the decay constant and t the time elapsed since the injection. The resulting activity map is both easily interpretable and quantitative in terms of administered dose for intercomparison with normal levels and patterns. It is proposed that this is the most complete and useful way at present for presenting scan data.

The digital and photographic read-outs on the HEG scanner have been used simultaneously to display the results of a number of test scans over

sources of different sizes with different values of the adjustable parameters on the photographic read-out. Apart from the limitation of a short dynamic range which, at most, is two orders of magnitude, the photographic representation suffers from the further drawback that the sensitivity of the human eye to detect small variations in optical density is not constant over the usable optical density range of 0.2 to 2.0. Tests on 15 individuals to determine their abilities to detect density differences from 0.01 to 0.2 over the range of absolute densities from 0.30 to 1.8 showed that there is a marked decrease in sensitivity with increasing absolute density, and indicated that even in the range of 0.3 to 1.0 the density variations would have to exceed 0.10 (or 10%) for reliable detection. It is clear that this response phenomenon places an additional and unnecessary limitation on the ultimate sensitivity of scanning. From Table I it can be seen that a 0.4 × 0.4-cm cylindrical source in the focal plane, with a 20 to 1 specific activity ratio above a background of 1 $\mu c/cm^3$, can be detected with 95% confidence with counting times of 1.4 s at each position. The difference here between the mean background count and the mean source plus background count is 5.7% which would be masked completely on a photographic display.

SUMMARY

A scanning system is described which has the capability of making localization and total body retention measurements on patients who have received tracer doses of isotopes emitting gamma rays with energies up to 1.3 MeV. Figures on resolution and sensitivity are presented and the merits and shortcomings of analogue and digital read-out systems are discussed. An easily interpretable, quantitative method of presenting scanning data is described.

REFERENCES

[1] LAUGHLIN, J.S., BEATTIE, J.W., COREY, K., ISAACSON, A. and KENNY, P., Radiology 74 (1960) 108.

[2] COREY, K.R., KENNY, P., GREENBERG, E., PAZIANOS, A., PEARSON, O.H. and LAUGHLIN, J.S., Amer. J. Roentgenol., Rad. Therapy and nucl. Med. 85 (1961) 955-975.

[3] GREENBERG, E., PAZIANOS, A., COREY, K.R., KENNY, P., LAUGHLIN, J.S. and PEARSON, O.H., Proc. Conf. on Research on the Radiotherapy of Cancer, University of Wisconsin, June 16-18, 1960. American Cancer Society, New York (1961) 158-172.

[4] COREY, K.R., KENNY, P., GREENBERG, E. and LAUGHLIN, J.S., J. nucl. Med. 3 (1962) 454-471.

[5] BAUER, G.C.H., CARLSSON, A. and LINDQUIST, B., Kungl. Fysiogr. Sallskap. Lund Forhandl. 25 (1955) 1-16.

[6] BAUER, G.C.H. and RAY, R.D., J. Bone and Joint Surg. 40-A (1958) 171-186.

[7] LACHMAN, E. and WHELAN, M., Radiology 26 (1936) 165.

[8] LACHMAN, E., Amer. J. Roentgenology, Rad. Therapy and nucl. Med. 74 (1955) 712.

[9] BEATTIE, J.W. and BRADT, G., IRE Trans. Bio-Medical Electronics 8 (1961) 24-28.

[10] CONSOLAZIO, C.F., MATOUSH, L.O., NELSON, R.A., HACKLER, L.R. and PRESTON, E.E., J. of Nutrition 1 (1962) 78.

[11] KENNY, P.J., LAUGHLIN, J.S., WEBER, D.A., COREY, K.R. and GREENBERG, E., Progress in Medical Radioisotope Scanning (KNISELEY, R.M. et al., Eds.) Oak Ridge Institute of Nuclear Studies, Oak Ridge, Tenn. (1963) 236-249.

DISCUSSION

R. BECK: How do you draw the contour lines from the numerical data? Do you use an interpolation procedure?

P. KENNY: When drawing these contours it is necessary to bear in mind the inherent statistical variations in the pattern and some smoothing of the data is performed. This is possible because the numerical read-out allows one to estimate the standard deviation of any count printed. We are at present working on a computer programme which will control the processing of our paper tape record so that the smoothing and plotting of the isocount contours can be performed automatically.

M. BLAU: Is not most of the deposition of the isotope in bone lesions due to exchange rather than accretion?

P. KENNY: The early uptake, i.e. within the first few hours, is mainly due to rapid equilibration of the tracer within the exchangeable calcium pool, part of which is in bone. Later the rate of uptake in or around the tumour is slower and has been taken as a measure of accretion rate.

M. BLAU: Would you agree that, in the ordinary hospital possessing no large tungsten collimators, F^{18} and Sr^{87m} can be more conveniently and effectively used for the detection of bone lesions than Ca^{47}?

P. KENNY: For localization purposes only, where one is not concerned with kinetic studies, it is probable that Sr^{87m} would be a very convenient tracer to use.

H. GLASS: I believe you said that you can detect changes in bone formation rate of the order of a few milligrams per day. Is this correct?

P. KENNY: Yes. Since normal accretion rates are of the order of 500 mg per day and since, in the presence of widespread active lesions, these rates are observed to be significantly elevated as a result of the contributions of individual lesions, it is reasonable to expect that such changes could be observed with a detector recording a few thousand counts per minute.

E. LUBIN: In Fig. 6 of your paper you showed what you called evidence of increased accretion during localized radiotherapy at the site of a bone metastasis. Have you seen similar pictures during chemotherapy? I should also like to ask whether you have done experimental work in which you irradiated normal bone.

P. KENNY: In Fig. 6 there was a suggestion of redistribution of the isotope in the region around the fifth lumbar vertebra. This happened to be on the edge of an area which was receiving radiation therapy. It also corresponded to a newly developing lytic lesion. We cannot as yet be sure of the reason for this redistribution. A similar phenomenon was observed in one other case and is the subject of further study. We have not seen such changes during chemotherapy and we have not tried irradiating normal bone.

A. BAPTISTA: I should like to describe the system of quantitative gammagraphy I developed with D. Gomes and F. Bilé (Laboratório de Isótopos, Instituto Português de Oncologia, and Centro de Estudos de Energia Nuclear, Instituto de Alta Cultura, Lisbon), with the support of the Calouste Gulbenkian Foundation. This is a very simple system in which the isocount contour can be obtained directly and thus help in the interpretation of the

scans. It has been in routine operation since 1960 and about 1500 scans have been obtained.

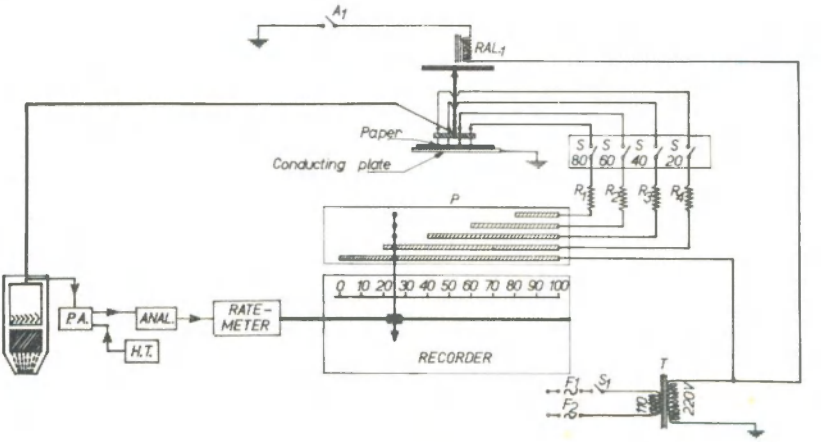

Fig. 1

Diagram of a quantitative gammagraphy system

After pre-amplification, pulses from the detector go to a single-channel pulse-height analyser and to a ratemeter (Fig. 1). The ratemeter, which can provide an output of 0-100 mV, drives a 10-mV recorder; thus, full-

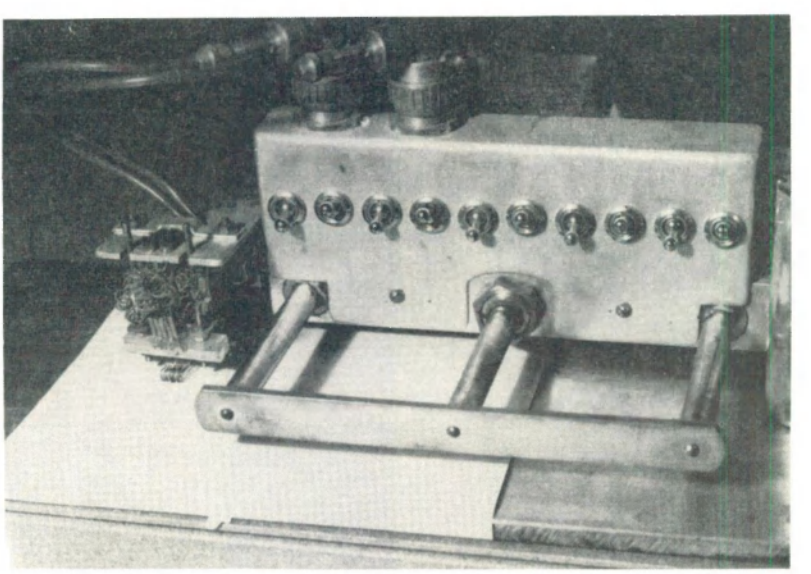

Fig. 2

Photograph of a quantitative gammagraphy system

Left: ten pens, each corresponding to the different percentages.
Right: ten switches corresponding to each channel.

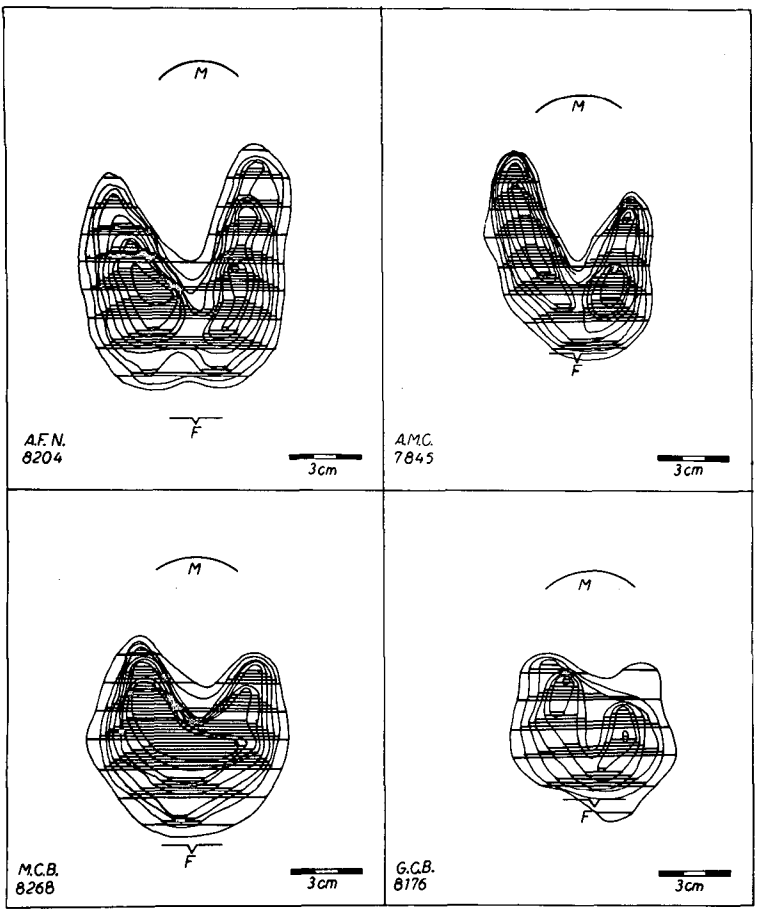

Fig.3a

Quantitative thyroid scan gammagraphies

scale deviation of the recorder can be obtained with any counting rate above 10% of full scale. Coupled to the "carriage" of the recorder are 11 insulated metallic springs with wheels at the extremities (in Fig. 1 only 5 are shown). The wheels travel over a bakelite support on which 11 metallic slides are spaced out vertically; the lowest one has a length equal to the full scale of the recorder; the next one goes from the 10% position to the end of the recorder scale; the following one starts from the 20% position, and so on.

Before scanning, we search the area of interest for the region of maximum radioactivity; the ratemeter output is then adjusted to give full-scale (100%) deflection of the recorder.

If, during scanning when the recorder pen moves to the 10% position, the corresponding wheel contacts the second slide and an electric circuit is closed between the lowest and the 10% slide, a line is then traced on paper for as long as the counting rate exceeds 10% of the maximum. If the

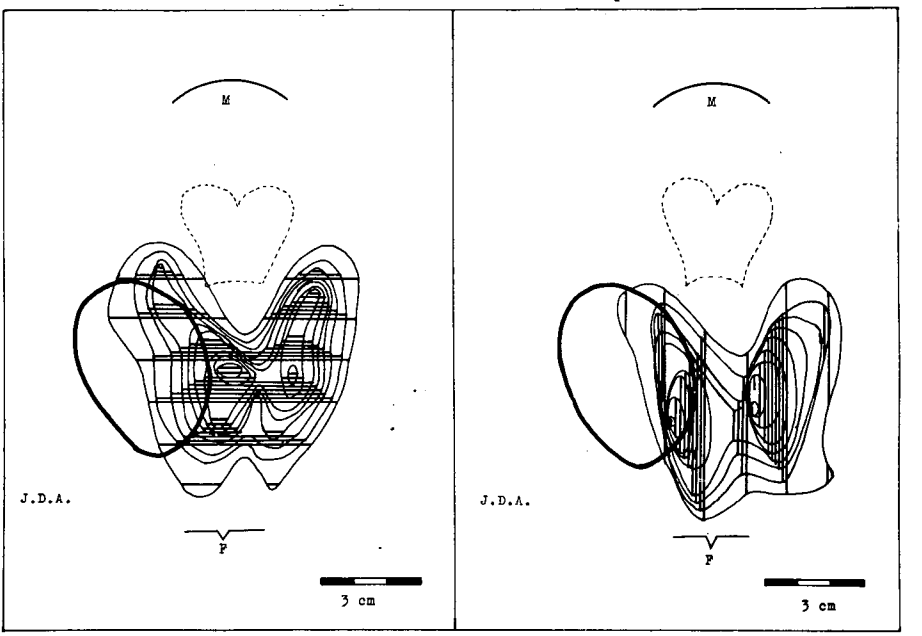

Fig.3b

Quantitative scans of the same thyroid gland with a cold nodule in the right lobe
(2 perpendicular scanning directions)

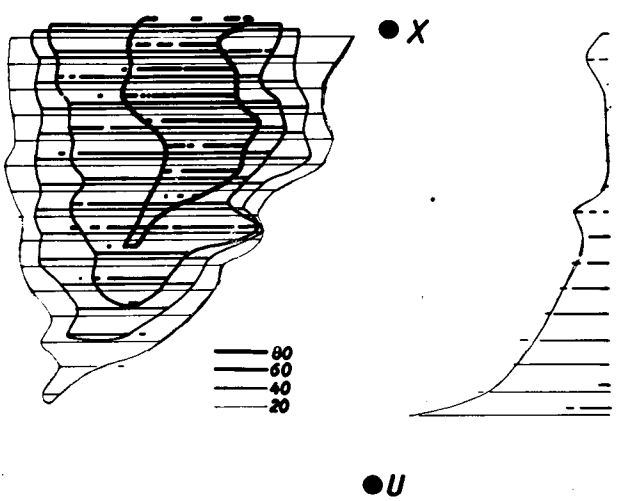

Fig.4

Quantitative liver scan with hydatid cyst
(4 channels only used)

counting rate further increases so that a contact corresponding to the 20% position is established, a second line is traced parallel to the first one, and so on. We thus obtain a series of parallel lines, each corresponding to a given percentage of the maximum radioactivity. From these lines, the isocount contours may readily be obtained.

Figure 2 shows the 10-channel system just described. We can, if we desire, switch off any channel; for example, to erase background we can switch off the lower channels.

We have been using this system to investigate various organs, including thyroid, liver, spleen and lungs. Figures 3a and 3b show thyroid scans obtained with a 61-channel focused collimator, and Fig. 4 shows a liver scan obtained with a 7-channel focused collimator. A hydatid cyst was present in the liver and the corresponding abnormality is quite noticeable in the scan.

We have found this technique to have been very helpful in many difficult situations and we shall in due course publish our clinical results. The data could also be presented in colour, but this would not yield appreciably better results. The advantages of the system I have described are that it is cheap and easy to operate and that the isocount data can be plotted directly on the scan.

A CLINICAL RADIOISOTOPE SCANNER FOR CYLINDRICAL AND SECTION SCANNING*

D.E. KUHL
DEPARTMENT OF RADIOLOGY, UNIVERSITY OF PENNSYLVANIA,
PHILADELPHIA, Pa., UNITED STATES OF AMERICA

Abstract — Résumé — Аннотация — Resumen

A CLINICAL RADIOISOTOPE SCANNER FOR CYLINDRICAL AND SECTION SCANNING. The scanner described was built to explore potential advantages of modifying the motion of the radiation detector over the patient. In the study of a round organ, such as the liver, a cylindrical scanning motion is used to expose more of the organ to survey. Another modification is section scanning which permits the separation of images of radioactive structures according to specific planes in body depth. This mode of scanning can be of particular use when images of body structures overlap in the recording and are confusing.

During scanning the patient is supported on a cantilever platform between two opposed scintillation detectors mounted at the extremities of a yoke. The yoke is powered to provide three motions of the detectors about the patient: longitudinal, transverse, and rotary. Particular attention has been paid to the precise control of detector position and speed by incorporating servo-mechanical control mechanisms. The recording system includes: (1) Non-destructive data storage on punched paper tape; (2) provision for rapid regeneration of scanning images on a cathode-ray oscilloscope; and (3) facility for electronic operations on the image signal.

Examples of the clinical applications of this instrument are described, with particular emphasis on cylindrical scanning of the liver and section scanning of the brain.

DISPOSITIF DE SCINTIGRAPHIE POUR L'EXPLORATION EN SPIRALE ET DANS PLUSIEURS PLANS. Le dispositif décrit dans le mémoire a été construit en vue d'étudier les avantages qui pourraient résulter de la modification du déplacement du détecteur de rayonnement au-dessus du patient. Dans l'étude d'un organe à peu près rond tel que le foie, on procède à l'exploration par un mouvement en spirale afin d'examiner une plus grande portion de l'organe. On peut également faire une exploration par «tranches», qui permet de séparer les images des structures radioactives dans des plans déterminés en profondeur. Ce mode d'exploration peut se révéler particulièrement utile lorsque les images des diverses structures se superposent sur le scintigramme, qui est alors difficile à interpréter.

Au cours de l'exploration, le patient est installé sur un lit cantilever entre deux détecteurs à scintillation montés aux extrémités d'un support qui se déplace de manière à permettre le mouvement des détecteurs en trois sens: longitudinal, transversal et rotatoire. On a veillé tout particulièrement à assurer un contrôle précis de la position et de la vitesse des détecteurs par l'incorporation de servo-mécanismes. Le système d'enregistrement comprend: a) un stockage permanent des données sur bandes de papier perforé; b) un moyen de reproduction rapide des images scintigraphiques sur un oscilloscope à rayons cathodiques; c) un dispositif électronique d'exploitation des signaux.

L'auteur donne des exemples des applications cliniques de cet appareil, notamment de l'exploration en spirale du foie et de l'exploration dans plusieurs plans du cerveau.

ЦИЛИНДРИЧЕСКИЙ РАДИОИЗОТОПНЫЙ СКЕННЕР ДЛЯ ЦИЛИНДРИЧЕСКОГО И СЕКЦИОННОГО СКЕННИРОВАНИЯ. Описываемый сканнер был построен для изучения потенциальных преимуществ видоизменения движения детектора излучения над пациентом. При исследовании такого округлого органа как печень используется цилиндрическая форма движения при сканнировании для наблюдения болшей части исследуемого органа. Другим видоизменением является секционное сканнирование, которое позволяет провести разделение изображений радиоактивных структур в соответствии с конкретными плоскостями внутри орга-

* This work was supported by USPHS Research Grant No. C-4456, USPHS Research Career Development Award CA-14,020, and USAEC Contract No. AT (30-1)-3175.

низма. Этот вид сканнирования может представлять определенную пользу, если изображения структур организма будут перекрываться при регистрации и получаться неотчетливыми.

Во время сканнирования пациент находится на платформе, установленной на кронштейне между двумя противоположно расположенными сцинтилляционными детекторами, смонтированными на крайних концах крестовины. Эта крестовина снабжена силовым двигателем, чтобы обеспечить три вида движения детекторов вокруг пациента: продольное, поперечное и вращательное. Особое внимание уделено точному контролю за положением детектора и скоростью, определяемую сервомеханическими контрольными механизмами. Регистрирующая система включает: 1) безразрушительное хранение данных на перфорированной бумажной ленте; 2) обеспечение быстрого воспроизведения изображений сканнограммы на катодно-лучевом осциллоскопе и 3) установку для электронных операций на изобразительном сигнале.

Описываются примеры клинического использования этого прибора, с уделением особого внимания цилиндрическому сканнированию печени и секционному сканнированию мозга.

APARATO GAMMAGRÁFICO PARA EXPLORACIONES CILÍNDRICAS Y POR SECCIONES. El aparato descrito en la memoria se construyó para estudiar las ventajas que puede ofrecer el empleo de un detector de radiaciones que se desplace sobre el enfermo de manera distinta de la habitual. Al estudiar un órgano aproximadamente redondo, como el hígado, el aparato es animado de un movimiento cilíndrico a fin de poder explorar una parte mayor del órgano. Otra modificación consiste en la exploración por secciones, que permite separar imágenes de estructuras radiativas en planos situados a diversas profundidades del organismo. Este procedimiento tiene particular interés cuando las imágenes de las diversas estructuras corporales se superponen en el registro dando resultados difíciles de interpretar.

Durante la exploración, el paciente se encuentra sobre una camilla sujeta por uno de sus extremos y situada entre dos detectores de centelleo montados en las extremidades de una pieza en forma de yugo capaz de desplazarse en dirección longitudinal y transversal y de describir un movimiento giratorio. Se ha prestado particular atención a la posibilidad de regular exactamente la posición y la velocidad del detector y, para ello, se han instalado servomecanismos de control. El sistema de registro comprende: a) almacenamiento no destructivo de datos sobre cinta de papel perforada, b) posibilidad de regenerar rápidamente las imágenes de exploración en un osciloscopio de rayos catódicos y c) un dispositivo para analizar electrónicamente las imágenes.

En la memoria se describen algunos ejemplos de aplicaciones clínicas de este aparato y, en particular, la exploración cilíndrica del hígado y la exploración del cerebro por secciones.

Rectilinear scanning produces a record that is a summation of overlapping images of radioactivity at many different depths in the body. At times, this overlapping may conceal important information. For instance, the image of a tumour may not be recognized if it is obscured by other superimposed images. Similar problems are encountered when radiographic techniques are used, and here much attention has already been directed to ways of separating these overlapping images. Multiple view examinations, stereoradiography, and tomography are well established methods of improving the diagnostic accuracy in radiography. These same image separation techniques can be of advantage in radioisotope scanning. For example, we have explored steroscopic scanning [1, 2] and LEVY and OKEZIE have applied it clinically [3]. Other laboratory experiments in image separation have led us to predict an advantage to scanning the liver in a semicylindrical pattern [4] and have demonstrated that tomographic scanning is possible [1, 2]. This report describes an instrument we have constructed for cylindrical and section radioisotope scanning, as well as our first experiences in applying these modes to study of the liver and brain [5].

INSTRUMENTATION

Scanning system

The scanner mechanism includes a yoke, a rotation arm, and a pedestal mounted on tracks by flanged wheels (Figs. 1 and 2). The patient is supported on a cantilever platform between the two opposed scintillation de-

Fig. 1

Radioisotope scanner and associated electronics. The patient is cantilevered between the two detectors.

tectors mounted at the extremities of the scanner yoke. Each detector has a 3-in-diam. by 2-in-thick sodium iodide crystal with a minimum of 2 in of lead side-wall shielding and a set of focusing collimators having designs appropriate for different photon energies [6]. The detectors have a full range of motion in their mountings and may be locked in required positions.

The three basic motions of the scanner are rotary, transverse, and longitudinal. For detector rotation, power is applied to the central axle of the rotation arm (Fig. 3A). For a "straight-line" detector motion transverse to the patient, the central axle turns the rotation arm, while synchronized counter-rotation is applied to the yoke axle to fix the angle of the detector with respect to the line of travel (Fig. 3B). This transverse excursion is a shallow arc of 2 cm rise for a 30-cm chord length. The transverse scan line can be oriented at any angle about the patient by appropriate

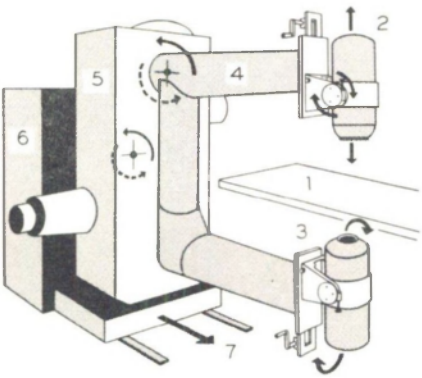

Fig. 2

Scanner mechanism. (1) patient platform. (2). (3) detectors. (4) detector yoke. (5) rotation arm. (6) pedestal, and (7) floor track.

positioning of the rotation arm before the excursion. For line spacing, the entire scanner can be moved step-wise with the powered wheels through a maximum longitudinal distance of 125 cm. (Fig. 3C).

The machine is programmed for operation by adjusting calibrated front panel controls for the scanning geometry desired. A servo-mechanism is used to maintain speed regulation in spite of changes in loading as the detector positions change.

Data recording

The original counting and positional data are collected and stored without loss or distortion on perforated paper tape at the time of the scanning procedure. Time compression play-back with contrast processing is under the control of the operator.

At the time of scanning, the two channels of counting data from the detector are processed in pulse-height analysers and counted in a dual-channel cyclic counter with adjustable time interval. A binary code representing the counts detected during each time interval is alternately recorded on the perforated tape along with a channel identification code. The counting data punch is activated only during the true traverse portion of the raster. The positions of the detectors during scanning are sensed as electrical signals and the beginning of each scan line is recorded on the tape in code.

An average 30-min scan with dual detectors produced approximately 30 ft of perforated paper tape. This length of paper tape is processed in approximately 12 s by a tape reader operating at a speed of 300 characters/s. The output of the reader is introduced into a raster control and count-decoding unit.

The raster control unit decodes the positional data and regenerates the rectilinear raster of the scan on the face of an oscilloscope. At the same time, the binary characters representing counts in a single channel are translated to analogue voltages in the count decoder and are introduced to the

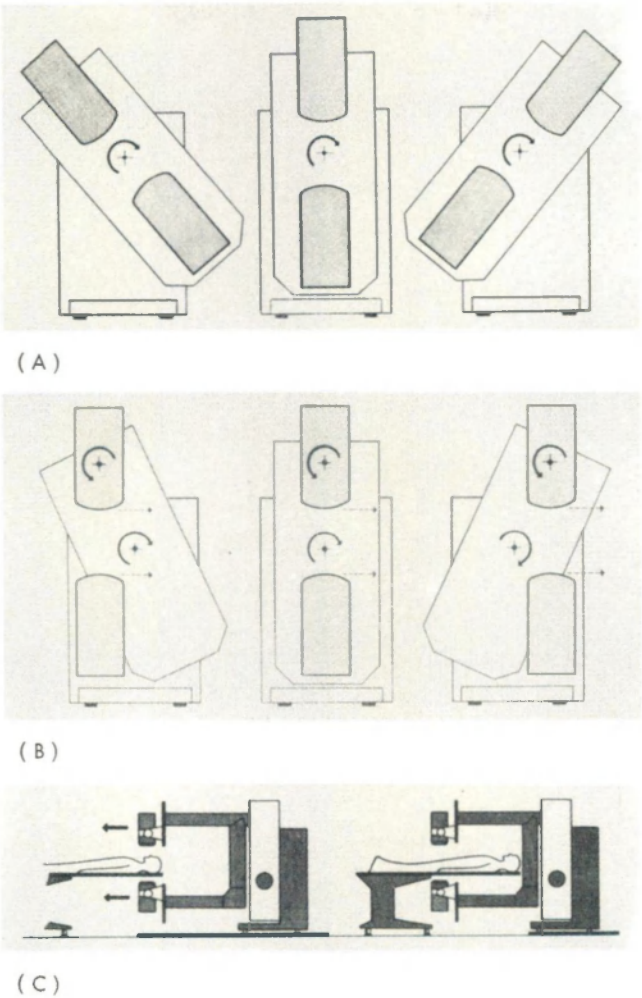

Fig.3

Basic motions of scanner. (A) rotary, (B) transverse, and (C) longitudinal. (From Ref. [5]).

Z axis of the oscilloscope to control the beam brightness. A contrast control permits the operator to choose the image contrast desired. The final image is recorded on the film of an open shutter oscilloscope camera during the 12 s required to read the paper tape of an average scan.

SCANNING MODES

This instrument permits three distinct scanning modes. These are rectilinear scanning, cylindrical scanning, and section scanning for eight longitudinal or transverse slices.

Rectilinear scanning

Rectilinear scanning is the mode in most common use today. It consists of a combination of transverse lines of motion with uniform longitudinal spacing at the end of each scan line. A field size 35 cm wide and 115 cm long can be scanned simultaneously over both sides of the patient's body, and on any plane parallel to the patient's long axis (Fig. 4).

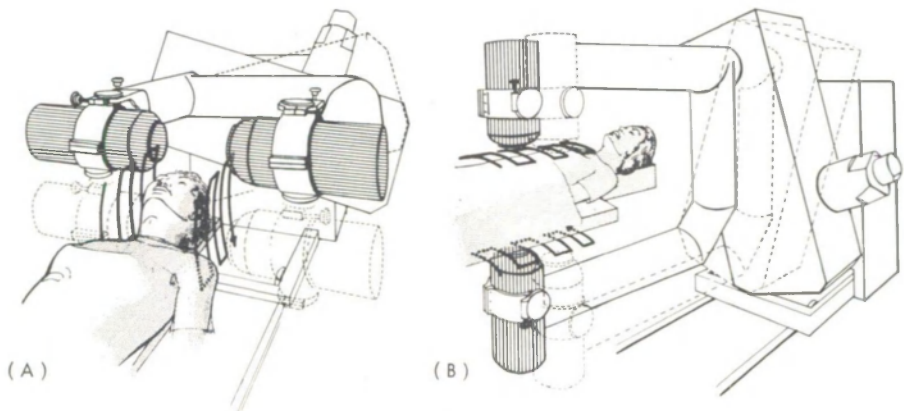

Fig. 4

Rectilinear scanning in (A) vertical and (B) horizontal planes.

Cylindrical scanning

The effectiveness of a liver scan is influenced by the anatomy of the liver. Because of its location and its semi-globular shape, at least half of the liver volume is curved beneath the right lateral rib cage. It is difficult to detect a small tumour void if it is deeper than a few inches within the radioactive liver. Because of this, tumours posterior in the right liver lobe are usually missed when a liver scan is performed with the patient supine using a flat rectilinear raster (Fig. 5A). Yet, this is presently the most commonly used method of liver scanning.

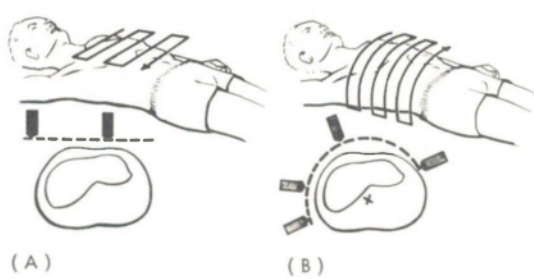

Fig. 5

Liver scanning geometry with (A) rectilinear and (B) cylindrical modes. Cylindrical scanning keeps the detector close to the entire outer surface of the liver.

Cylindrical scanning can be used to reduce this obscuring effect of the overlying radioactive right lobe [4]. For cylindrical liver scanning, only one detector is counting and its transverse motion is in a semi-circular path designed to keep the detector as close as possible to the entire outer surface of the liver (Fig. 5B). The central axle of the rotation arm revolves the detector back and forth in an arc of 180° around the liver, from the left anterior axillary line to the right posterior axillary line. This method of scanning is just as effective for detecting tumors anterior in the left lobe as is rectilinear scanning (Fig. 6). But, the semi-cylindrical scan over the

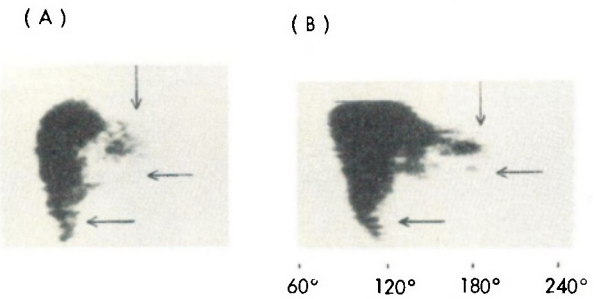

Fig. 6

Liver metastases, predominantly in left lobe, are seen equally well in (A) anterior rectilinear scan and (B) cylindrical scan.

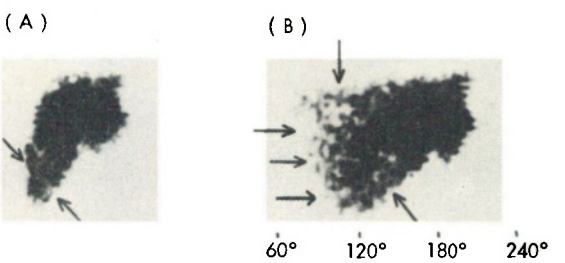

Fig. 7

Liver matastases, predominantly in right lobe, are seen to better advantage in cylindrical scan (B) than in anterior rectilinear scan (A). (From Ref. [5]).

liver surface "unrolls" the curved liver and permits a more adequate survey of the otherwise hidden posterior right lobe (Fig. 7). We have found that a single cylindrical scan of the liver is more easily interpreted than three rectilinear scans covering the same area in the anterior, oblique, and lateral projections.

Section scanning

Section radioisotope scanning depends on the same principles as body-section radiography and produces images of radioisotope distributions according to their depths in the body [1, 2, 5]. Longitudinal section scanning

is analogous to conventional tomography [7] and demonstrates the radioactivity of selected body layers parallel to the patient's long axis. Transverse section scanning is analogous to the more rarely used axial transverse tomography and represents the radioactivity in a body cross-section.

Longitudinal section scanning

In longitudinal section scanning, several rectilinear scans of the same volume are made at different projections. The recordings are then superimposed so that only the images from one specific depth at a time coincide.

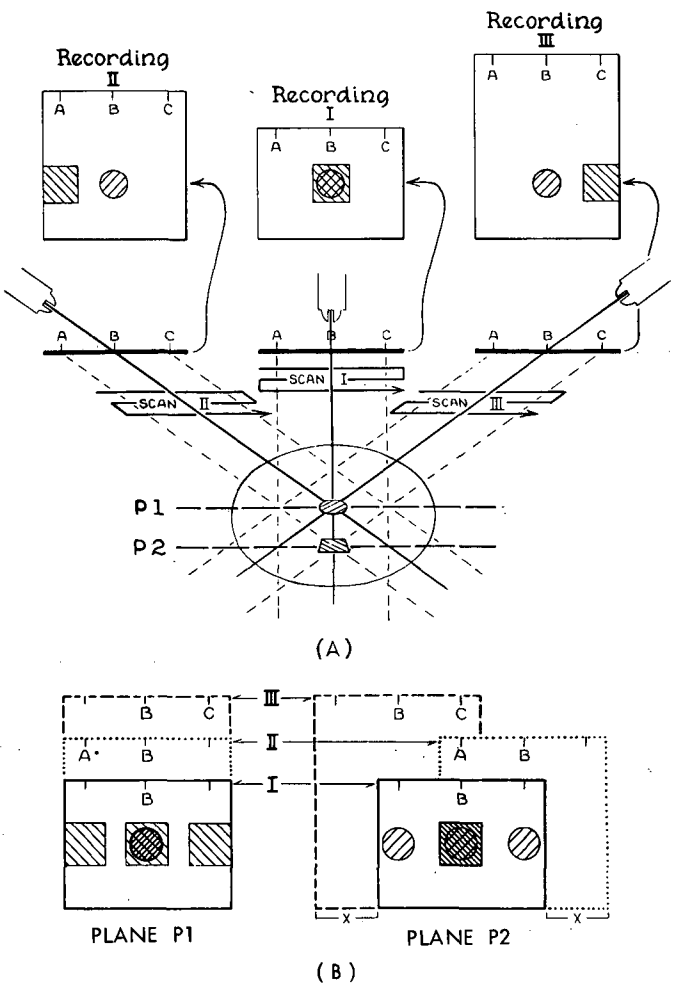

Fig. 8

(A) Longitudinal section scanning. Several rectilinear scans of a body are made at different projections. (From Ref. [1]).

(B) The recordings of Fig. 8A may be superimposed so that only images from one specific depth coincide and reinforce. (From Ref. [1]).

The principles of longitudinal section scanning can be understood by examination of Fig. 8. In this example, three scan recordings are made of a body which contains two radioactive sources, a round source above a square source. In scan I the detector is held vertical, while the detector is inclined in the other two scans. Three recordings are produced. The images are superimposed in recording I and separated in the other two recordings. If the three transparent recordings are superimposed so that the co-ordinates BI, BII, BIII are aligned, only the images of the round source on plane P1 will overlap, while the images from the other planes will be spread from each other and will not reinforce (Fig. 8B). However, if the recordings are shifted to align coordinates BI, AII, CIII, the square images of plane P2 will overlap and now the round images of the more superficial plane will fail to reinforce. By appropriate shifting of the various recordings, it is possible to demonstrate the images associated with any desired level in the scanned body, since only these images will coincidence and reinforce each other.

Our present longitudinal section technique is to make five separate rectilinear scans of the area under study, one with the detector vertical, and the others with the detector inclined 30° in different directions (Fig. 9). The transparent film recordings are then superimposed in a calibrated holder, trans-illuminated, and viewed with a closed circuit television system for

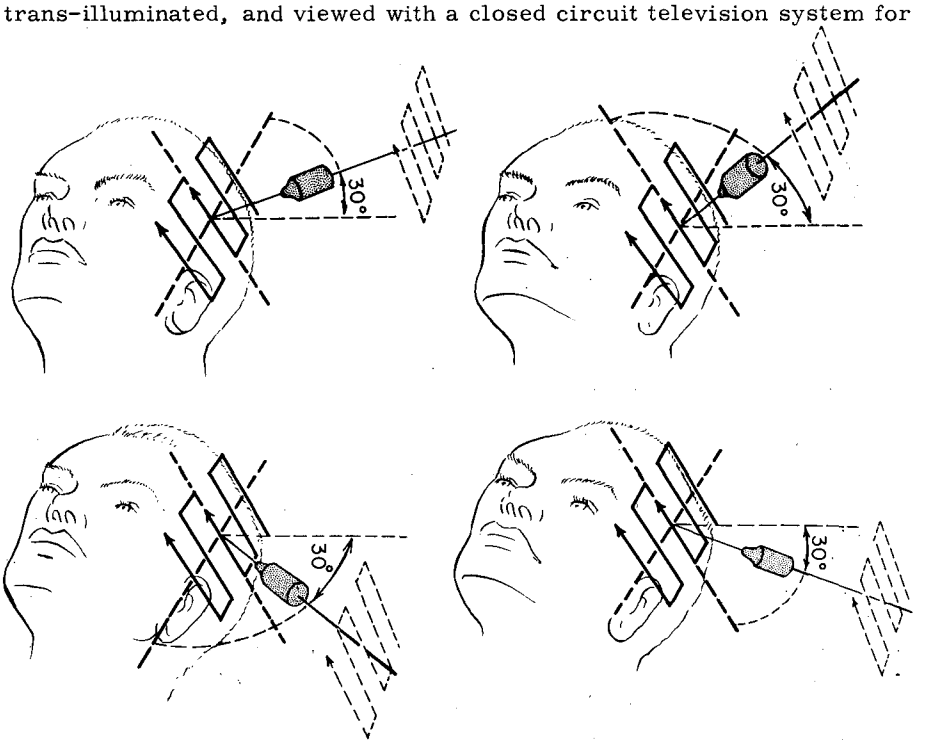

Fig. 9

Longitudinal section scanning technique. Five separate rectilinear scans are recorded, with the detector vertical and the others with the detector inclined 30° in different directions.

contrast control. By a simple adjustment of the relative positions of the films in the trans-illuminated sandwich, the operator can bring into view a succession of images of radioactivity associated with one body layer after another in depth.

Longitudinal section scanning is useful in improving the detail of a structure that would otherwise be obscured by other images of overlying or underlying structures. For example, in the following case, longitudinal section scanning was useful in separating the image of a brain tumour from the confusing image of underlying radioactive blood [5].

In September 1963, a 55-yr-old patient with generalized motor seizures was referred to us for brain scanning after no significant abnormalities had been found in roentgen examination of the skull, bilateral carotid arteriography, and pneumoencephalography. The neurologic signs suggested a left motor lesion, but an abnormal electroencephalogram focus was demonstrated on the right side.

Brain scanning was performed using a 2.5-mc intravenous dose of clormerodrin Hg^{197}, a 127-hole collimator with a $\frac{1}{2}$-in resolution distance at a focal length of 3 in, and a scan speed of 0.5 cm/s. The brain scanning views obtained (Fig. 10) were normal, except for the left lateral view where

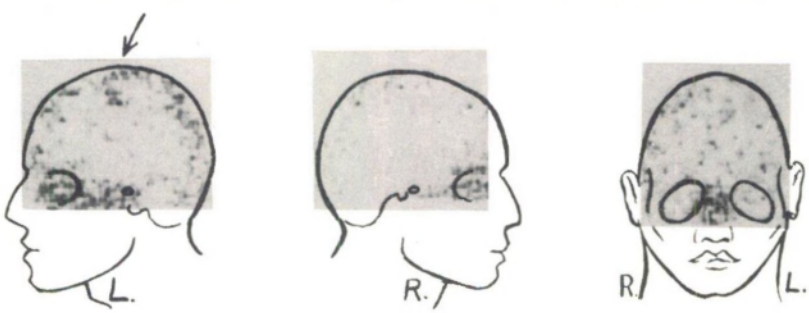

Fig. 10

Left lateral rectilinear brain scan in September 1963 suggested abnormal concentration in posterior left frontal lobe (arrow), but definition was obscured by underlying radioactive sinus. (From Ref. [5]).

an abnormal radioisotope concentration was suspected in the posterior left frontal lobe. However, definition in this region was unclear because the suspected tumour image was superimposed on the image of the underlying radioactive sagittal sinus.

To separate these images, a 10-cm square longitudinal section scan was obtained through the left fronto-parietal area. Using the same collimation and scan speed, an additional hour of scanning time was required to complete the study. The sagittal sections demonstrated an abnormal round image of radioactivity in the middle of the left motor strip which was clearly separate from the normal underlying midline sagittal sinus (Fig. 11).

In November 1963, the patient's motor seizures reappeared and the survey brain scans were repeated using the same scanning factors as in the September study (Fig. 12). The tumour was now definitely apparent in the left motor strip, as predicted two months earlier with the section study. Craniotomy revealed the tumour to be a Grade IV astrocytoma.

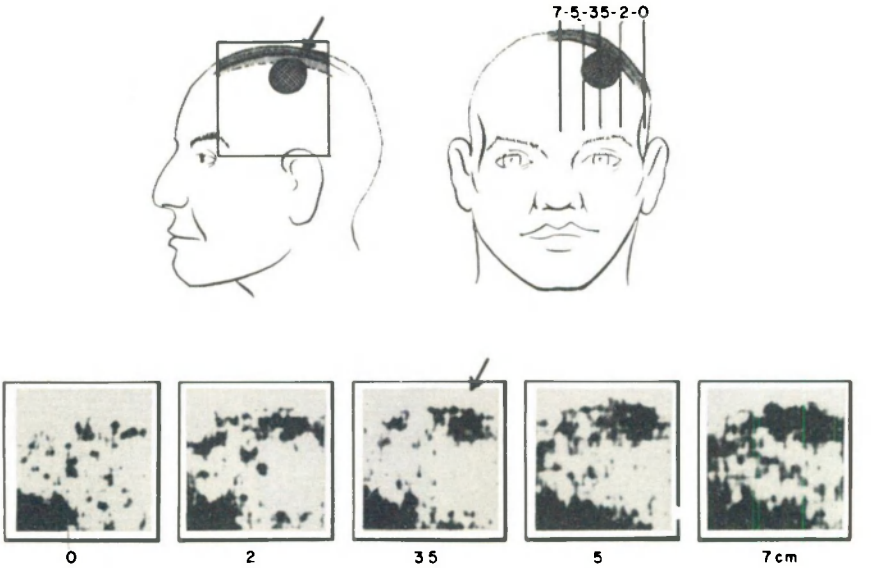

Fig. 11

After study in Fig. 10, sagittal section scans distinguish radioactive tumour image (arrow) separate from underlying sinus. (From Ref. [5]). Scanning time was one hour.

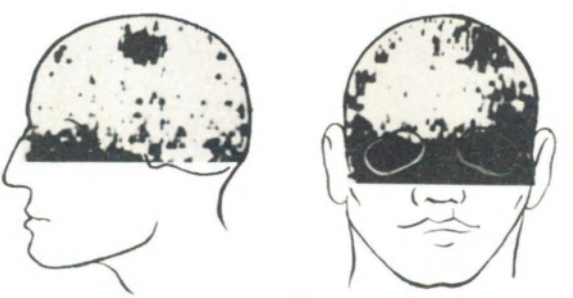

Fig. 12

Rectilinear brain scans in November 1963 confirm left motor area tumour identified earlier in section study. Compare with Fig. 11. (From Ref. [5]).

Transverse section scanning

In transverse section scanning, a cross-section image is made of the distribution of radioactivity in the patient [1, 2, 5]. In this method, the pair of detectors makes a sequence of tangential scans at 15° angular intervals around the patient at the level of the cross-section desired (Fig. 13). At the same time, the detector axis is represented on an oscilloscope face by a thin line of light which is moved across the screen to duplicate the motion of the detectors. At the end of each tangential detector scan, the film holder is rotated to correspond to the angle of the detectors. The brightness of

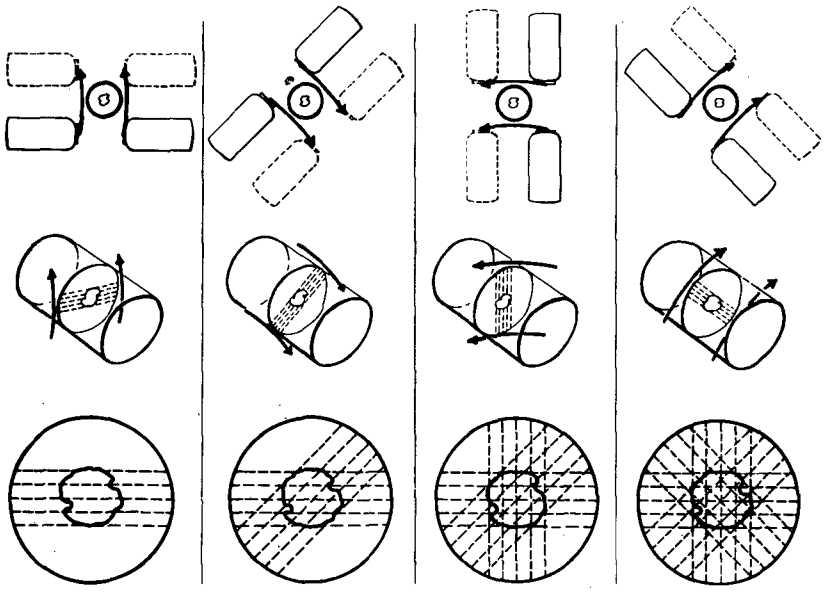

Fig. 13

Transverse section scanning. The detectors make a sequence of tangential scans about one cross-section of the patient. The formation of the section image on the oscilloscope camera film is diagrammed at the bottom of this Figure.

the line varies with the sum of the counting rates from the two detectors. An adjustable limiter is included in the beam brightness control to prevent over saturation of the film from any single scan line. During scanning, the open shutter oscilloscope camera records the bands of increased film density which converge and overlap on the film to represent an image of the radioactive structures in transverse section.

When an analogue recording is made simultaneous with the scanning procedure, as described above, the final section image is obtained by viewing the film record with closed circuit television for optimum contrast control. When the perforated paper tape recording is made, the contrast is adjusted by the operator during the time compression readout of the tape.

Our present technique for transverse section scanning of the liver is to use an intravenous dose of 500 μc of Au^{198}, a pair of 127-hole collimators with $\frac{1}{2}$-in resolution distance at a focal length of $4\frac{1}{2}$ in, a scan speed of 0.5 cm/s, and 15° interval angle. A transverse section of the liver can be completed in 18 min of scanning time with these factors.

The transverse section image obtained from scanning a liver phantom is shown in Figure 14. In this phantom, 400 μc of Au^{198} are distributed in 1500 ml of water divided in three compartments and surrounded by masonite to represent the abdomen. Three voids present in the largest vessel measure 1 in, $1\frac{1}{2}$ in, and 2 in in diam. with heights equal to their diameters. All three voids, as well as the three separate radioactive containers can be distinguished on the scan.

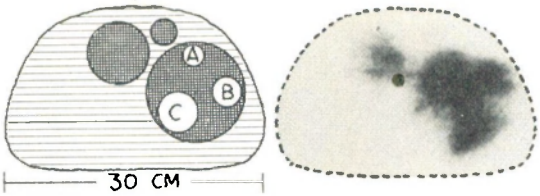

Fig. 14

Transverse section scan of phantom showing three containers of radioactive water and three voids measuring (A) 1 in × 1 in, (B) $1\frac{1}{2}$ in × $1\frac{1}{2}$ in, and (C) 2 in × 2 in. Scanning time was 18 min.

Transverse section scans were made at two different levels through the liver of a patient whose anterior rectilinear scan demonstrated metastatic disease (Fig. 15). The sections show the contour of the liver as well as the presence of the metastases (Fig. 16).

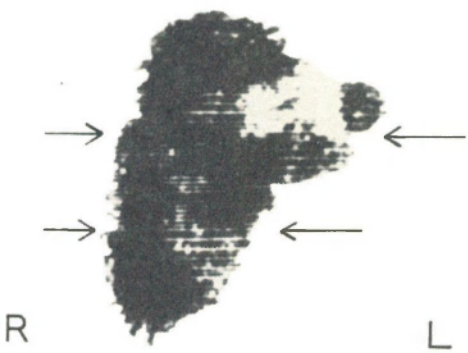

Fig. 15

Metastatic liver disease shown by rectilinear scan. Transverse section scans were then performed at levels indicated by arrows.

Transverse section scanning of the brain is now usually done following our routine four view rectilinear survey. At the present time we are using chlormerodrin Hg^{197} in doses of 20 μc/lb of body weight. A pair of 217-hole collimators with $\frac{1}{2}$ in resolution distances at focal lengths of $4\frac{1}{2}$ in are used with a scan speed of 0.5 cm/s and a 15° interval angle. Approximately 12 min is required to complete a transverse section of the brain.

The survey rectilinear scans of the patient shown in Fig. 17 demonstrate a left occipital-parietal metastasis from carcinoma of the lung. The lesion is accurately shown in the transverse section image of Fig. 18.

The survey rectilinear scans of another patient shown in Fig. 19 demonstrate an olfactory groove meningioma measuring about 4 cm in diam. The transverse section scan (Fig. 20) shows that the lesion is predominantly to the right side, a feature not appreciated in the survey scan. The location was verified by subsequent arteriography and craniotomy.

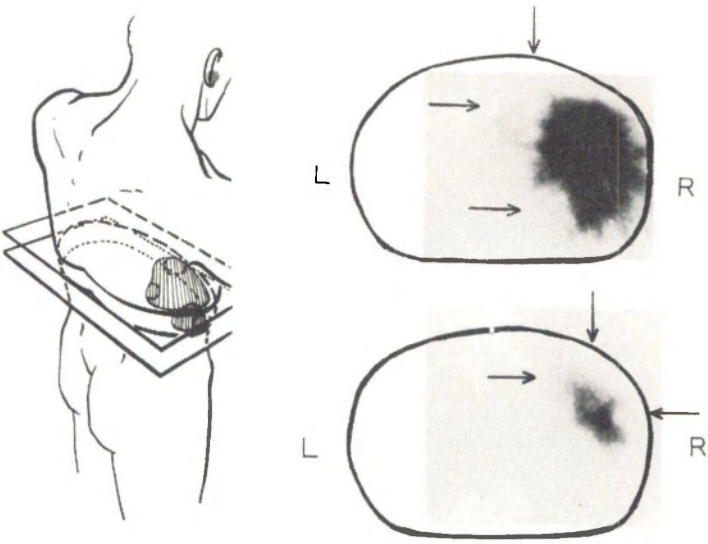

Fig. 16

Transverse sections of liver at two levels show contours of organ and metastatic disease. Compare with Fig. 15. Scanning time was 18 min for each section.

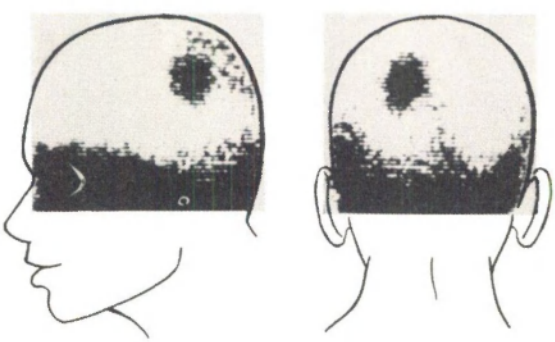

Fig. 17

Rectilinear scans of left occipital-parietal brain metastasis. Made with a commercial scanner.

DISCUSSION

With cylindrical and section scanning, the limitations of representing a three-dimensional body structure on a flat two-dimensional recording are reduced. In some instances, section scanning has demonstrated the extent of disease in the liver and brain, which has not been possible with any other diagnostic technique. These same techniques can probably be applied with equal advantage to radioisotope scanning of other body structures such as thyroid, spleen, pancreas and heart.

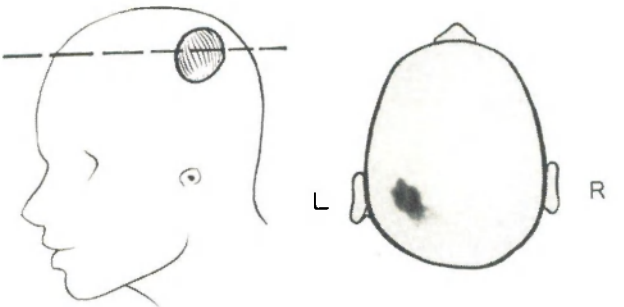

Fig. 18

Transverse section image through metastasis shown in Fig. 17. Scanning time was 12 min.

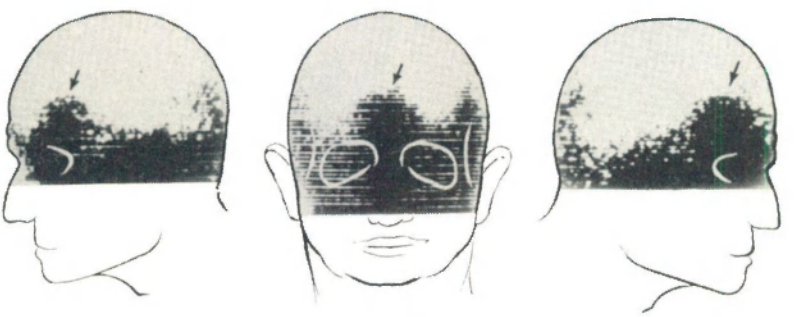

Fig. 19

Rectilinear scans of olfactory groove meningioma. Made with a commercial scanner.

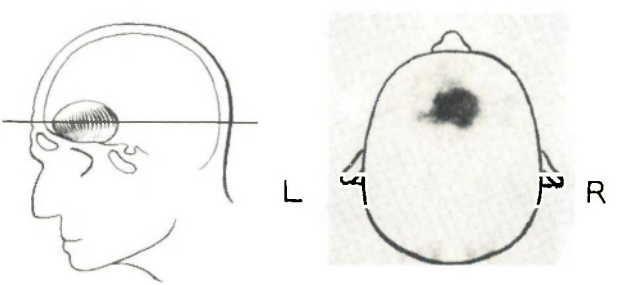

Fig. 20

Transverse section image through meningioma shown in Fig. 19. Note the right sided location of the meningioma, not recognized on the rectilinear scans, but verified by subsequent arteriography and craniotomy. Scanning time was 12 min.

For the widest possible acceptance of the new methods, it would be advantageous to reduce the complexity of the present research scanning system. This complexity is in part due to the use of large heavily shielded detectors adaptable to a wide range of photon energies. One way of simpli-

fying the instrumentation would be to limit its scanning capabilities to photon energies of less than 200 kEV and to use the very light detectors suggested by HARPER, BECK, CHARLESTON and LATHROP [8].

The recent introduction of Tc^{99m} (140 keV) labelled compounds by HARPER and RICHARDS [9] for high photon flux brain and liver scanning [8] should have an additional important influence on the future clinical application of section scanning. The short physical half-life of Tc^{99m} permits use of large millicurie doses without excessive radiation exposure to the patient. Because of this, very fast scanning speeds can be used to reduce the scanning time markedly. With shorter scanning time, longitudinal section scanning of large areas should become more practical. Also, it should be possible to perform multiple layer transverse section scanning at narrow separation intervals in reasonable scanning times for a true three-dimensional representation of the radioactivity in entire structures such as the brain or abdomen.

SUMMARY

A radioisotope scanning instrument is described which includes a dual detector system, a punch-paper tape-recorder with time-compression read-out, and a wide range of operations including large area rectilinear, cylindrical, and body section scanning.

In cylindrical scanning, the curved liver is "unrolled" to improve the accuracy of detecting tumours in the posterior right lobe.

Section scanning can be used to obtain images of thin layers of the body in either longitudinal or transverse planes. Longitudinal section scanning has been used to separate a partially obscured brain tumour image from the superimposed image of underlying radioactive blood. Transverse section scanning has been used to demonstrate brain and liver tumours in cross-section for a more accurate assessment of their distributions.

REFERENCES

[1] KUHL, D.E. and EDWARDS, R.Q., "Image Separation Radioisotope Scanning", Radiology 80 (1963) 653-662.

[2] KUHL, D.E., "Section Scanning for Image Separation," Progress in Medical Radioisotope Scanning, 171-189, ORINS, Oak Ridge, Tennessee (1963).

[3] LEVY, L.M. and OKEZIE, O., "Three-Dimensional Scintiscanning," J. nucl. Med. 4 (May 1963) 181.

[4] KUHL, D.E., "Rotational Scanning of the Liver", Radiology 71 (1958) 875-876.

[5] KUHL, D.E. and EDWARDS, R.Q., "Cylindrical and Section Radioisotope Scanning of the Liver and Brain," Radiology (In press).

[6] KUHL, D.E., "Effect of Collimator Design and Photon Energy on Detection Efficiency in Liver Scanning", Physics in Med. and Biol. (In press).

[7] ANDREWS, J.R., "Roentgenography: Body-section", Med. Physics I. Ed. O. Glasser, Chicago, Year Book Publishers (1955).

[8] HARPER, P.V., BECK, R., CHARLESTON, D., and LATHROP, K.A., "Optimization of a Scanning Method Using Tc^{99m}", Nucleonics 22 (1964) 50-54.

[9] RICHARDS, P., Brookhaven National Laboratory, Private communication.

DISCUSSION

P. CZERNIAK: What new findings can be obtained by means of cylindrical and sectional liver and brain scans?

D. KUHL: We have not compared the relative usefulness of conventional scanning and cylindrical or section scanning using large numbers of randomly selected cases. Our technique has been evolving so rapidly that such a comparison would serve no useful purpose. For example, in the past month (since I submitted my paper) we have followed the example of Dr. Harper of the University of Chicago and now use Tc^{99m} – pertechnetate rather than Hg^{197} – chlormerodrin for brain scanning. Because the physical half-life of Tc^{99m} is only 6 hours, we administer millicurie amounts (200 μc/kg body weight) and obtain count rates as high as 200 - 300 counts/s. This has changed all our brain scanning parameters. We now scan at 2 cm/s, with a line-spacing of 0.25 cm, sample the counts eight times per second, and complete four rectilinear views of the head in about 40 min. A transverse section scan of the head could be completed in several minutes, if it were necessary. When we are satisfied that either the brain or liver scanning technique should be standardized in our laboratory, we shall study a randomly selected group of cases for comparison with conventional scanning.

I. BASCHIERI: I should like to congratulate you on the extremely interesting apparatus you constructed. I wish, however, to point out that at the Rome University Institute of Medical Pathology a somewhat less complicated and expensive device was constructed, consisting of two detectors facing each other (Bull. schweiz. Akad. med. Wiss., 18 (1962) 414). This device increases the counting efficiency and also indicates the depth at which a radioactive concentration or defect is located.

With regard to rotary scanning of organs such as the liver, would you not agree that two scans, one anterior and one posterior, taken simultaneously, are better than one cylindrical scan? Lesions situated on the side of the liver still appear on our scintigrams, provided they are sufficiently thick, a proviso which applies even when the rotation technique is used.

D. KUHL: A cylindrical liver scan should give more information than two scans, one anterior and one posterior. On the other hand, the resultant advantage would tend to decrease as the number of different rectilinear views of the liver increased.

CLINICAL PHOTOSCINTILLOGRAPHY: TECHNIQUE AND APPLICATIONS

K.H. EPHRAIM
ROTTERDAMSCH RADIO-THERAPEUTISCH INSTITUUT,
ROTTERDAM, THE NETHERLANDS

Abstract — Résumé — Аннотация — Resumen

CLINICAL PHOTOSCINTILLOGRAPHY: TECHNIQUE AND APPLICATIONS. For clinical applications of photoscintillography, collimation, contrast-amplification and data storing are of great importance. For the detection of space-occupying lesions in thick organs such as liver and brain, a special 36-channel multifocus collimator was developed. The isoresponse lines of this collimator are shown. Its response hardly changes from the surface to a depth equal to the thickest part of the liver.

A special contrast-amplifier was built: a small incandescent "primary" bulb, triggered via a pulse-amplifier by the output of a single-channel analyser, is monitored by a light dependent resistor (L.D.R.). The resistance of the L.D.R. varies with the count rate. In series with the L.D.R. is a scanning "secondary" incandescent bulb. The brightness as well as the frequency of the flashes of the latter vary with the count rate and thus a non-linear response is obtained without the introduction of the inertia of a ratemeter circuit. The "secondary" flashes are recorded on film.

To prevent loss of information by registering in the saturation region of the film-sensitivity curve, a moderate contrast-amplification is used and the film is viewed on a closed-circuit television system. The necessity is stressed of adapting the collimation to the clinical problem to be solved.

Clinical applications of the above technique in the study of diseases of the thyroid, kidneys, liver and the skeleton are discussed.

PHOTOSCINTIGRAPHIE CLINIQUE: MÉTHODE ET APPLICATIONS. La collimation, le renforcement du contraste et le stockage des données jouent un rôle très important dans les applications cliniques de la photoscintigraphie. On a mis au point un collimateur spécial à focalisation, à 36 canaux, pour détecter les lésions en volume dans de grands organes comme le foie et le cerveau. L'auteur présente les courbes d'isoréponse de ce collimateur. La réponse varie très peu entre la partie superficielle et la partie la plus profonde du foie.

On a construit un amplificateur spécial de contraste: une petite lampe à incandescence «primaire», reliée par un amplificateur d'impulsions au signal de sortie d'un analyseur à canal unique, est contrôlée par une photorésistance qui varie en fonction du taux de comptage. Une lampe à incandescence «secondaire» d'exploration est montée en série avec la photorésistance. L'intensité et la fréquence des éclairs émis par la lampe «secondaire» varient avec le taux de comptage, ce qui permet d'obtenir une réponse non linéaire tout en évitant les inconvénients dus à l'inertie du circuit d'un intensimètre. Les éclairs émis par la lampe «secondaire» sont enregistrés sur un film.

Afin d'éviter une perte d'informations du fait de l'enregistrement dans la région de saturation de la courbe de sensibilité du film, on utilise une amplification du contraste modérée et on projette le film sur un écran de télévision en circuit fermé. L'auteur insiste sur la nécessité d'adapter la collimation au problème clinique qui se pose.

Il examine les applications cliniques de la méthode ci-dessus dans l'étude des troubles de la thyroïde, des reins, du foie et des os.

КЛИНИЧЕСКАЯ ФОТОСЦИНТИЛЛОГРАФИЯ: МЕТОДИКА И ПРИМЕНЕНИЕ. При применении фотосцинтиллографии в клинике огромное значение имеют коллимация, усиление контрастности и накопление данных. Для обнаружения ограниченных участков поражения в таких плотных органах, как печень и мозг, был разработан специальный 36-канальный многофокусный коллиматор. Демонстрируются изочувствительные линии этого коллиматора. Его чувствительность мало меняется от поверхности до глубины, равной наибольшей толщине печени.

Был построен специальный усилитель контрастности: небольшая "первичная" лампа накаливания, соединенная через импульсный усилитель на выходе одноканального анализатора, управляется с помощью зависимого от света реостата (3 СР). Сопротовление 3 СР изменяется в зависимости от скорости. Последовательно по отношению к 3 СР соединена скеннирующая "вторичная" лампа накаливания. Яркость, а также частота вспышек последней зависит от скорости счета и тем самым нелинейная чувствителтность достигается без введения инерционного контура. "Вторичные" вспышки регистрируются на пленке.

С целью предотвращения потери информации при регистрации в области насыщения кривой чувствительности пленки применяется умеренный усилитель контрастности, и пленка просматривается в телевизионной системе с закрытым контуром. Подчеркивается необходимость адаптирования коллимации к решаемой клинической проблеме.

Обсуждаются результаты применения в клинике вышеупомянутой методики для изучения заболеваний щитовидной железы, почек, печени и скелета.

FOTOCENTELLEOGRAFÍA CLÍNICA: TÉCNICAS Y APLICACIONES. Para las aplicaciones clínicas de la fotocentelleografía son de gran importancia la colimación, el aumento del contraste y el almacenamiento de datos. Con objeto de detectar lesiones extensas en órganos de gran tamaño, como el hígado y el cerebro, el autor construyó un colimador especial enfocado de 36 canales. En la memoria se presentan las curvas de isorrespuesta de este colimador. La respuesta permanece prácticamente constante desde la superficie del órgano hasta la parte más profunda.

El autor construyó un amplificador especial de contraste en el que la salida de un analizador monocanal enciende a través de un amplificador de impulsos una pequeña lámpara incandescente «primaria», cuya luz modula una fotorresistencia. Esta resistencia varía en función del índice de recuento. En serie con dicha resistencia se ha conectado una lámpara incandescente «secundariã» de exploración. La intensidad luminosa y la frecuencia de los destellos de esta última varían con el índice de recuento, obteniéndose así una respuesta no lineal sin introducir la inercia de un circuito integrador. Los destellos «secundarios» se registran sobre película.

Para impedir la pérdida de datos debido a su registro en la región de saturación de la curva de sensibilidad de la película, se utiliza una amplificación de contraste moderada y la película se examina en un circuito de televisión industrial. El autor subraya la necesidad de adaptar las condiciones de colimación al problema clínico que haya de resolverse.

En la memoria se examinan las aplicaciones clínicas de esta técnica al estudio de enfermedades tiroideas, renales, hepáticas y óseas.

1. INTRODUCTION

Four points are of great importance for photoscintillography:

(1) Detection and how to get the most information out of the smallest radioactive dose;
(2) The problem of collimation;
(3) Registration; and
(4) Interpretation.

2. DETECTION

Gamma rays may interact with matter:

(1) By the photoelectric effect. All the energy of the photon goes to overcoming the binding energy of the orbital electron and to accelerating it.
(2) By the Compton effect; only part of the energy of the photon is used for knocking an orbital electron from its position. The photon is scattered and it proceeds with less energy in its new direction.

(3) By forming of a positron-electron pair. This last way of interaction with matter is of no importance for the gamma-ray energies currently used for photoscintillography.

When a NaI(Tl) crystal is hit by gamma-rays, scintillations are produced. Their intensity is proportional to the energy absorbed by the crystal from the impinging radiation. When these scintillations reach the photocathode of a photomultiplier tube they liberate electrons from its coating and are thus transformed to electronic impulses and these are amplified via the dynodes of the photomultiplier tube. The amplitude of the pulses from the photomultiplier tube is directly proportional to the brightness of the scintillations in the crystal. The spectrum of the pulses from the photomultiplier tube maybe considered as an electronic display of the energy transfer in the crystal and it reflects, therefore, photoelectric collisions and Compton collisions.

In gamma-ray spectrometry the pulses from the photomultiplier tube are amplified in a linear amplifier and then fed to a single-channel analyser. Thus the pulses entering the single-channel analyser are still directly proportional to the brightness of the different scintillations in the crystal. The energy distribution of these pulses is examined in the single-channel analyser. Pulses can get through the channel to a ratemeter, to a scaler or, as in our data presentation system, to a contrast amplifier only when they satisfy two conditions: they must surpass the lower energy level of the channel, but may not exceed the upper level.

In our laboratory we have tried to find the optimal way of applying gamma-spectrometry to scanning techniques and we have found that a rise in sensitivity of a factor of three and more can in most cases be achieved easily.

We have examined experimentally the influence on the gamma spectrum and on the sensitivity of the detection system of three parameters:

(1) The setting of the high tension on the photomultiplier tube;

(2) The gain of the linear amplifier; and

(3) The width of the channel.

Figure 1 shows the influence of varying the setting of the high tension. These spectra are made with a 6 cm×6-cm NaI(Tl) crystal. In this experiment the channel width and the gain of the linear amplifier were held constant. Fig. 1 shows that decrease in high voltage shifts the photopeak to the left, i.e. to a lower setting of the lower level of the discriminator. In addition the shift to the left is accompanied by an increase in the count rate.

In a second series of experiments only the gain of the linear amplifier was varied while the other parameters were held constant. Fig. 2 shows that an increase in the gain of the linear amplifier shifts the photopeak to the right, i.e. to a higher setting of the lower level of the single-channel analyser. But again more happens than merely this shift in the position of the photopeak. A movement of the photopeak to the left is accompanied by an increase in count rate. The photopeak becomes higher and narrower when moving to the left. This phenomenon is caused by elongation of the spectrum. Suppose that with a gain of 1000 on the linear amplifier the range of the single-channel analyser represents gamma energies from 200 keV to 1 MeV. Changing the gain of the linear amplifier to 2000 one gets a dif-

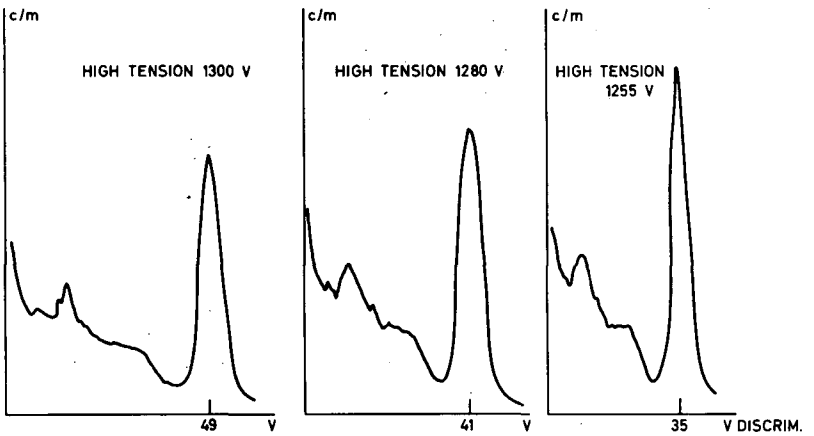

Fig. 1

The influence of high voltage setting on position and height of the photopeak in gamma-spectrometry

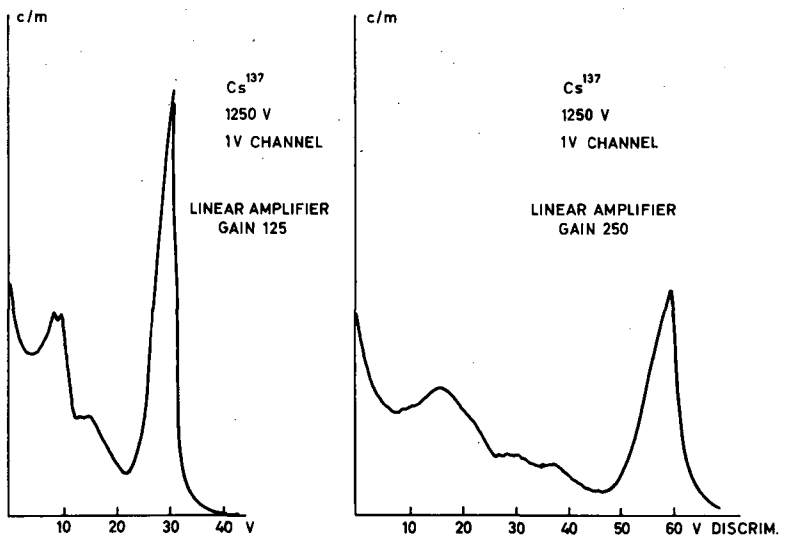

Fig. 2

The influence of gain of the linear amplifier on the position and height of the photopeak in gamma-spectrometry

ferent response from the single-channel analyser: now 100 keV pulses already pass the lowest setting of the lower level and now the upper level of the single-channel analyser represents approximately 500 keV. With a gain of 1000 on the linear amplifier the single-channel analyser in our example represents an energy range of 800 keV (from 200 keV to 1 MeV). A gain of 2000 reduces this energy range to 400 keV (from 100 to 500 keV). The energy range that is selected by the single-channel analyser is inversely

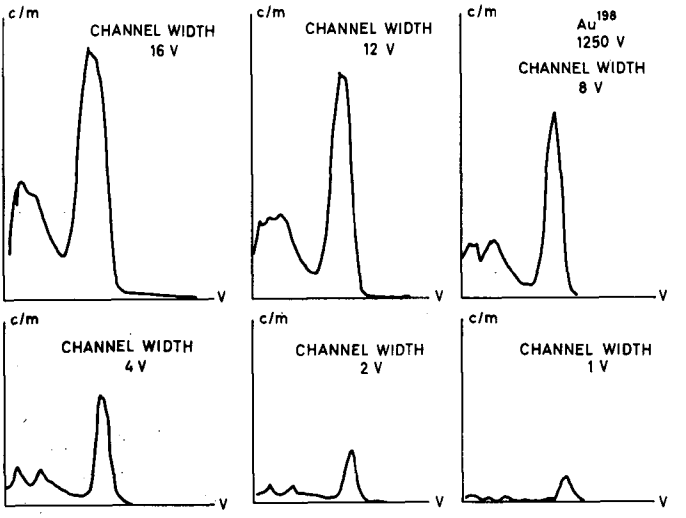

Fig.3

The influence of channel width on height and position of the photopeak in gamma-spectromety

proportional to the amplification. This phenomenon shows in our diagrams as an elongation of the spectrum.

In a third series of experiments the influence of the channel width was examined. Fig. 3 shows the effect of variation of the channel width on the gamma spectrum: widening of the window of the single-channel analyser causes a shift of the photopeak to the left and an increase in count rate. This shift to the left is partly caused by the way we indicate the position of the channel. When we say the photopeak is found at 26 V on the single-channel analyser and in one case gamma-spectrometry is performed with a channel width of 2 V and in a second case with a channel width of 10 V, the indication of the position of a photopeak in both cases is the same but its significance is quite different. In the first case the maximum count rate is found in a channel from 26 to 28 V and with its centre at 27 V. In the second case the window stretches from 26 to 36 V and has its centre-line at 31 V. In the second case the indication of the position of the photopeak is the same as in the first case, nevertheless the photopeak lies at a higher level.

Thus widening of the channel apparently causes the photopeak to move to the left. When the indication on the single-channel analyser is such that not the lower level but the midline is indicated so that the lower and upper levels are always situated symmetrically relative to this midline, then this shifting effect disappears almost totally. Fig. 4 shows the increase in the efficiency of the detecting system with the widening of the window. Of course, in these experiments the position of the window relative to the photopeak was adjusted for every channel width following the principles outlined above.

The conclusions of all these experiments are obvious:

(1) An increase of the high tension on the photomultiplier has the same effect as increasing the gain of the linear amplifier;

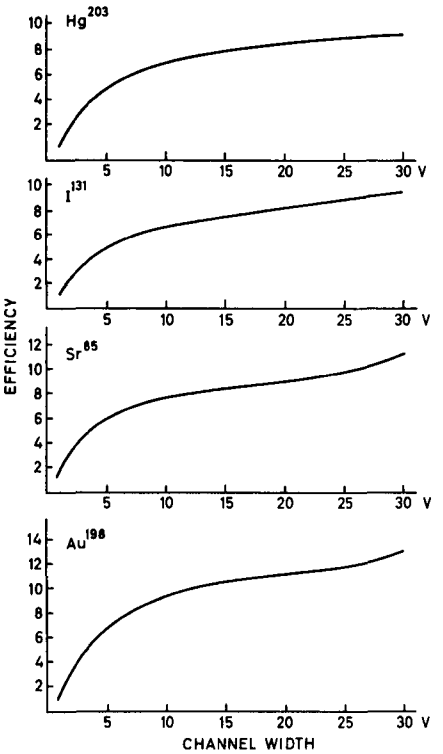

Fig. 4

The influence of channel width on detection efficiency for Hg^{203}, I^{131}, Sr^{85} and Au^{198}

(2) An increase in gain of the linear amplifier shifts the photopeak to the right in our diagrams, i.e. to higher settings on the single-channel analyser, and lowers the count rate;

(3) A widening of the channel shifts the photopeak to the left and increases the count rate.

On searching the medical literature one wonders that the channel width and other parameters of the detection techniques are mentioned so very seldom. Most of the time there is no indication at all of the technique of detection. Sometimes one finds that the window width was equal to 10% of the total scale of the single-channel analyser. This, of course, does not give very much information, as the spectrum can be stretched almost at will by raising either the gain of the linear amplifier or the high tension or both. An expression like "the width of the window was 5 V over a 36-V centre" is much more valuable. The "36-V centre" gives information about the total amplification and the 5-V width has now significance. When an author puts it like that, the reader gets a rather good impression of the way the possibilities of gamma-spectrometry were used. Still better would be if the indication of the channel width were expressed as an energy range.

As in almost all cases this is not in accordance with daily practice, I would like to suggest that in future publications we all use a simple uniform

and informative formula like "a window 12-V wide and stretching from 36 to 48 V".

3. COLLIMATION

Directional sensitivity of the detecting system is an essential condition in scintillography. The simplest collimator for this purpose has a cylindrical aperture through which gamma rays can enter the detector without any interference. The tissue block out of which gamma rays can enter the detector has approximately the form of the frustum of a cone.

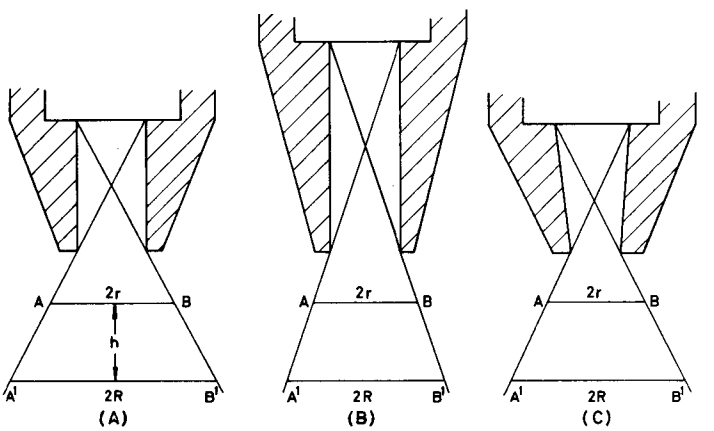

Fig. 5

Some principles of collimation (ABA'B': tissue block under examination)
(A) Cylindrical aperture
(B) Cylindrical aperture with the same diameter but greater height
(C) Single-hole tapered collimator with the same height as (A).

In Fig. 5, AB represents the surface of the body. For the sake of the argument we assume that gamma rays from tissue deeper than A'B' can be neglected. The volume of tissue overlooked by this collimator is

$$V = 1/3\, h\, \pi (R^2 + r^2 + rR).$$

Figure 5(B) shows an obvious way of improving the spatial resolution. The cylindrical aperture has the same diameter as in Fig. 5(A), but it is higher. The volume of the tissue block is smaller than in (A) as r_A and R_A and larger than r_B and R_B. In regard to spatial resolution collimator (B) is better than (A). However the efficiency of (B) is less than (A) because of the inverse square law.

Figure 5 (C) shows how in principle the spatial resolution of (B) and the efficiency of (A) can be combined by tapering the collimator. Now the tissue block (C) has about the same dimensions as tissue block (B) and the distance between detector and radioactive material is the same in both (A) and (C).

All these three collimators are, however, strongly sensitive to distance and are therefore only of any use if two conditions are satisfied:

(1) The organ under examination is rather thin; and

(2) Between this organ and the collimator there is not any tissue that contains more than a negligible amount of the nuclide.

In practice this means that collimation of the types mentioned above can only be used for scanning of the thyroid. But even for this purpose they are all but ideal. Collimation necessarily lowers the efficiency of the detecting system. One should try to achieve a combination of good spatial resolution and high sensitivity. This can be achieved by arraying many channels towards one focus.

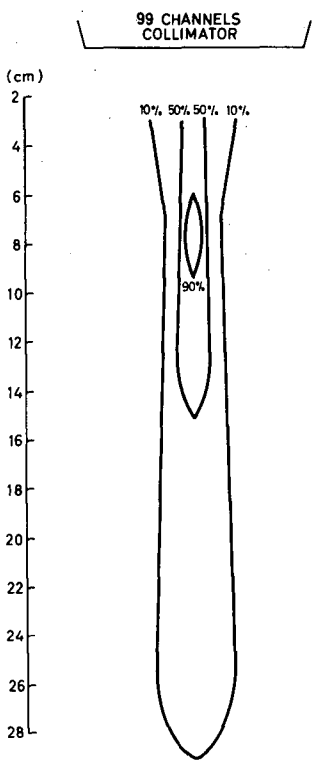

Fig. 6

Isoresponse lines of a 99-channel, single-focus collimator
The measurements were done in air, using pulse height selection.

Figure 6 shows the isoresponse lines of a 99-channel, single-focus collimator. This collimator is mainly used in our institute for scanning the thyroid. The dimensions of the crystal are 6 cm × 6 cm.

For scanning thick organs like the liver still other conditions have to be fulfilled. One would like for this purpose:

(1) The detector, when not moving in relation to the liver, to "see" a cylindrical block of tissue;

(2) This cylinder to be perpendicular to the plane of scanning;
(3) The response of the detector to be unchanged by any movement of a radioactive source in this cylinder;
(4) The diameter of this cylinder to be as small as the smallest lesion one can detect; and
(5) The efficiency to be large.

Point (3) is in direct contradiction to the inverse square law. Points (1) and (2) formulate the directional sensitivity. Point (4) considers the spatial resolution and point (5) needs all these requirements to be combined with a great sensitivity. All this appears to be a collection of contradictory wishes. However, it is possible to construct a collimator that fulfils these demands almost entirely.

Desiderata	Possible solution
Great sensitivity.	Use many channels
Directional sensitivity.	Focus these channels.
The detector should "see" a cylinder perpendicular to the plane of scanning.	Construct more than one focus on the central axis.
No sensitivity for distance.	Counteract the inverse square law by varying the diameter of the channel with the distance of the focus they are centred upon.

The results of the consideration of these wishes and possible solutions was a collimator with 36 channels in groups of twelve, focussed at three foci at 15 cm, 18 cm, and 21 cm from the surface of the crystal or 7 cm, 10 cm and 13 cm from the lower surface of the collimator respectively.

The diagram (Fig. 7) shows three planes. On each plane one focus is situated at the central axis. Twelve channels are focussed at each focus. The extensions of the walls of any channel in each group do not intersect at the focus of that group but a point on a plane 3 cm lower than the focal plane. So the focal distance of a single channel is larger than the focal distance of the group it is part of. Fig. 7 also shows the top view of this collimator. The isoresponse lines of this collimator are shown in Fig. 8. The necessary measurements were made with I^{131} and Au^{198}. The isoresponse lines do not differ for these two isotopes. This of course means that the septa are thicker than they need to be for a 360 keV gamma ray. These isoresponse lines are not constructed from measurements with point sources. We believe that using point sources – though probably better from the physical viewpoint – does not make much sense for the appraisal of the performance of a collimator of this kind. As far as we know, we never have to look for point sources of radioactivity in the human body when applying scanning techniques. Therefore we used instead of point sources glass spheres with diameters of one, two and three centimetres. The diagrams show that the performance of this collimator satisfies almost all our demands.

The influence of variation in the distance between the source and the detector is very small: the 80%-sensitivity region extends, for a 1-cm radius

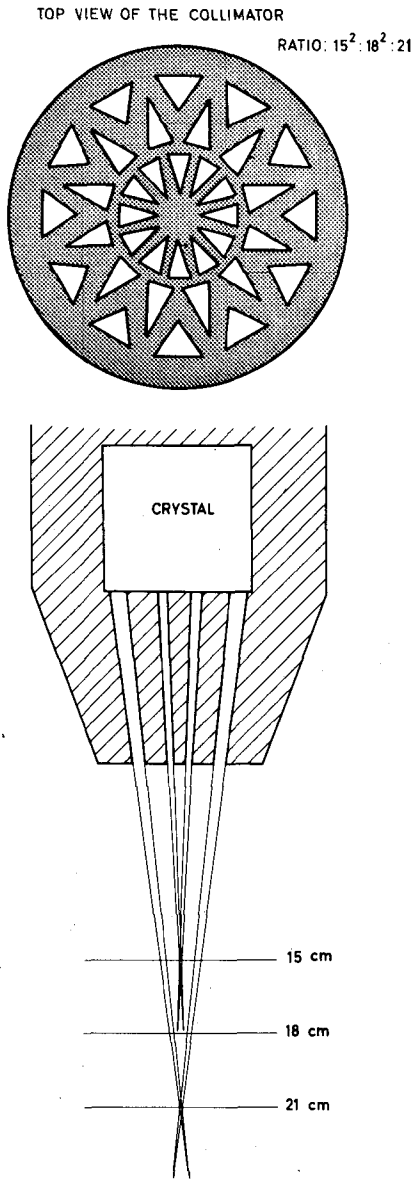

Fig. 7

Diagram of the 36-channel, three-focus collimator
Only two types of channel are shown in the diagram

sphere, 3 to 15 cm from the collimator. The spatial resolution is good: there is a steep fall from the 80% to the 50% isoresponse line. For $1\frac{1}{2}$-cm radius sphere the 80% sensitivity region is even longer, i.e. 3 to 24 cm from

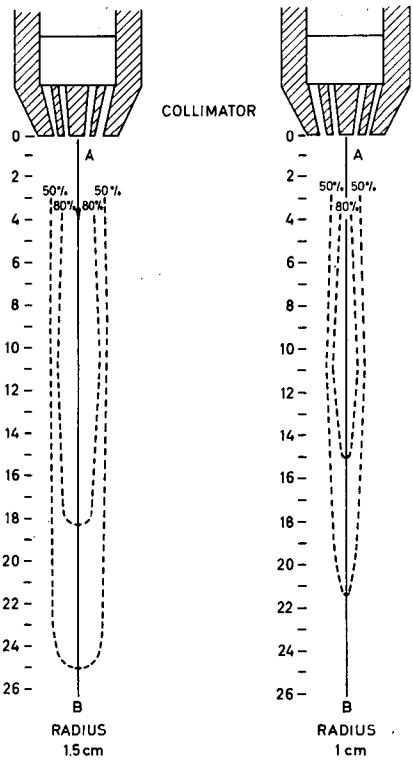

Fig. 8

Isoresponse lines of the 36-channel, three-focus collimator for spheres of radius 1 cm and 1.5 cm

the collimator. The width of the cylinder between the 80% isoresponse lines is in agreement with the diameter of the sphere used.

What is the smallest space-occupying lesion one can detect with this system? This question is obviously of paramount clinical importance. To answer this question, experiments with phantoms were performed. Spheres filled with water were placed in $2\frac{1}{2}$ l of water, in which 200 μc of Au^{198} were equally distributed. In the scintigram of these phantoms the spheres with a radius of 1 and $1\frac{1}{2}$ cm could easily be visualized. The spheres with a diameter of 1 cm could be made visible only with some difficulty.

This, however, does not answer the question of the size of the smallest solitary lesion one can detect in the liver of a patient. As the liver moves with respiration, the spatial resolution is not as good in the examination in vivo as in experiments with phantoms. It seems probable that in vivo the smallest solitary space-occupying lesion we can detect in the liver has a diameter of ~ 2 cm. This, of course, applies to solitary lesions and not to lesions that are far apart in x- and y-co-ordinates. When two space-occupying lesions in the liver differ much in z-co-ordinate, but are very near to each other in the x- or y-co-ordinate, then a cumulative effect occurs and smaller lesions may be visualized in the scintigram.

4. DATA STORING AND PRESENTATION

One gets the impression from the literature that the slit collimator for profile scanning or profile counting is not used very much. We find it a very good method for looking for functioning metastases of a thyroid carcinoma. It is a simple and little time-consuming method. We store the impulses on one track of a stereo-taperecorder and indicate simultaneously the position of the detector in relation to the body of the patient on the other track. The tape is played back and the impulses from the first track are fed via a ratemeter to an ink-writing recorder. The playback is done with a time expansion to facilitate the localization of the functioning metastases. The distance between the patient's sternum and the front of the crystal is 50 cm. The characteristics of the slit collimator were determined (Fig. 9)

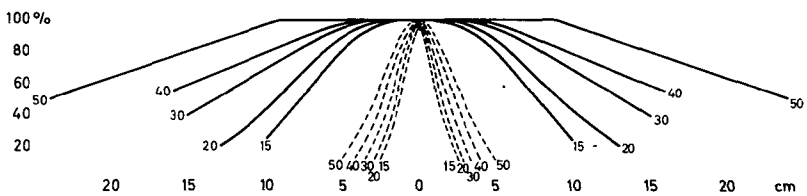

Fig. 9

Isoresponse lines of a slit collimator for different distances between radioactive source and crystal
——— parallel to the long axis of the slit
– – – – perpendicular to the long axis of the slit

under similar circumstances: the distance between one side of the crystal and the radioactive source was 50 cm.

In our institute we have abstained from any mechanical form of registration when data storing in two-dimensional scanning because of the inertia, the blocking of the mechanism that may occur with higher frequencies and because of the contrast decrease resulting from a scaling factor applied to prevent this blocking.

These drawbacks do not arise in photographic registration. In principle, one might change every pulse coming from the single-channel analyser to a flash from a neon bulb, which describes the same movements in relation to a photographic film as the detector does over the patient. In this way a theoretically ideal data-storing method would be achieved: the distribution of the radioactivity is represented without any distortion in frequency, without suppression of data and without any loss of information. Contrast amplification, however, is a necessity in daily practice because of the logarithmic reaction of the photographic film and the need for clearly interpretable scintigrams. All this was pointed out at the 1959 symposium in Vienna on medical radioisotope scanning [1].

Several methods are possible for contrast amplification. The pulses from a single-channel analyser may be fed into a ratemeter and the excursions of the ratemeter can be made to vary the voltage on an incandescent registering bulb. As the brightness of the filament varies with a power of the voltage, a strong contrast amplification is achieved. The use of a ratemeter circuit, however, introduces a RC-time and the danger of a lag in

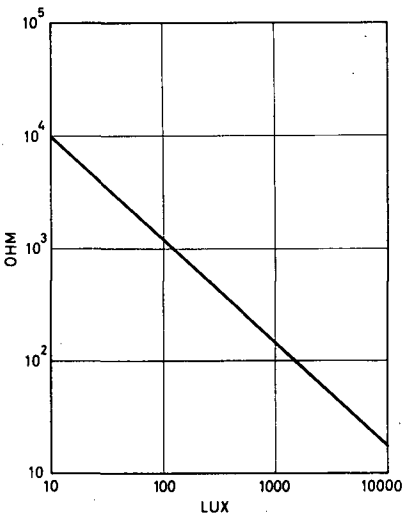

Fig. 10

Reaction of cadmium sulphide to light

data storing, compared to the actual position of the radioactivity. As long as this lag occurs in one direction only it is of no importance, but it may cause a disturbing distortion when scanning to and fro. A very simple method of contrast enhancement has been developed in our institute. Its basis is the reaction of cadmium sulphide to light (Fig. 10). Cadmium sulphide has a strong resistivity in the dark. When light falls on it the resistivity decreases. We have experimented with different commercially-available types of light-dependent resistors and with some that were still in a developmental stage*.

We found that the ORP 30 light-dependent resistor, manufactured by Philips, complied with our wishes. It has a very large resistivity (10–20 MΩ) in darkness.

Pulses from the single-channel analyser are fed to a scaler that has a connection for an external register. The pulses from this socket are fed to a variable pulse amplifier and they cause three small incandescent bulbs (e.g. 24 V, 80 mA) in parallel to flash synchronously with the impulses from the single-channel analyser. Each of these bulbs is monitored by a light-dependent resistor ORP 30 (Fig. 11).

When the radioactivity increases, the single-channel analyser feeds more impulses to the pulse amplifier and this makes the primary incandescent bulbs flash more frequently. With an increase in radioactivity more light falls on every light-dependent resistor, the resistivity is lowered and the voltage on the secondary bulb increases. The secondary bulbs flash synchronously with the primary ones but with contrast-amplification, because as the count rate increases the flashes from the secondary bulbs become both brighter and more frequent.

* These were kindly given to us by the Philips Physics Laboratory, Eindhoven.

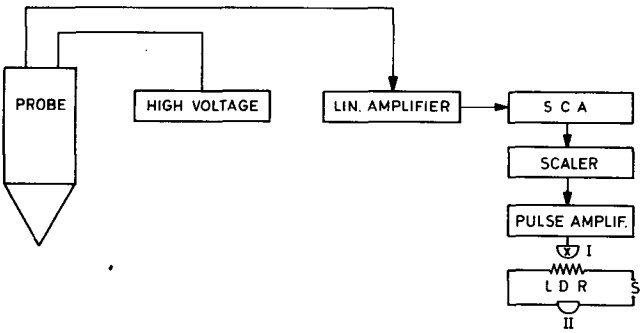

Fig. 11

Block diagram of detection and contrast amplification system
SCA = single-channel analyser
LDR = light-dependent resistor
I = primary incandescent bulb
II = secondary (scanning) incandescent bulb

The contrast amplification may be chosen at will by varying the gain of the pulse amplifier, by varying the voltage in the secondary circuit or by adjusting both.

Every pulse from the single-channel analyser in this system causes flashes in three scanning secondary bulbs. For each examination three simultaneous registrations are made, each with a different contrast enhancement. If necessary, these scintigrams are viewed on a closed television circuit. In our experience the best scintigrams are those which need no television techniques for their analysis. The only time we really need this closed television technique is for scanning the skeleton for metastases and for brain scanning, i.e. for examinations with a small differential absorption of the nuclide.

When the idea of the use of light-dependent resistors for contrast enhancement first arose, it was checked experimentally.

Number 1 of Fig. 12 is a scintigram of the thyroid gland. This scintigram was made without any contrast amplification. This "primary" scintigram was positioned on a view box and scanned by a small light-dependent resistor* attached for this purpose to our scanning machine and part of a secondary circuit, as shown above. No. 2 shows the result of such a scanning. For this "secondary" scintigram the illumination of the view-box was very low. Comparing No. 1 with No. 2 one notices that No. 1 shows a "differentiated" picture and that No. 2 might be called a more "integrated" picture. Radioactivity is shown as black in No. 1 and as white in No. 2. The action of the light-dependent resistor is comparable to the effect of a low-level energy discrimination: only when enough light is transmitted for a certain threshold to be passed is the resistance lowered sufficiently to make the bulb blacken the film.

Rather more illumination of the view-box was used for No. 3. One sees that now the discriminating level is passed more often. The viewbox was still brighter for the scanning of the scintigram in No. 4. Now the isthmus

* Philips, Type B8 73103

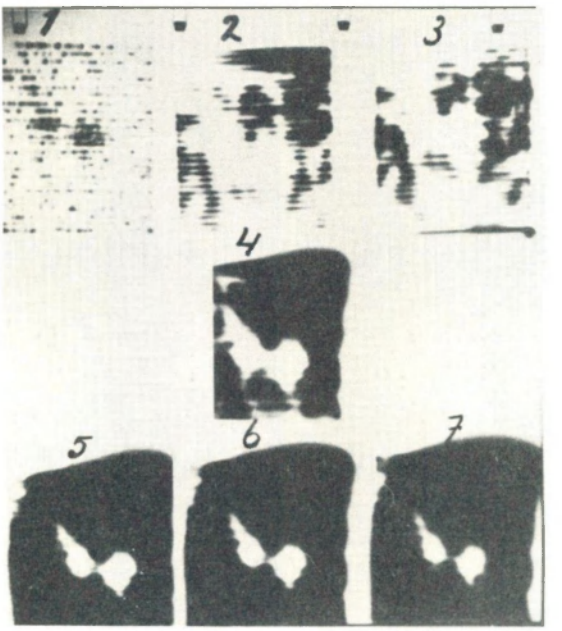

Fig. 12

Re-scans of a scan
1. Scintigram of a thyroid gland
2-7. Secondary scans of the same scintigram.

is clearly visible and a defect in the upper part of the left lobe is obvious. In Nos. 5, 6 and 7, for which still more illumination was applied, a defect in the lower part of the right lobe is seen.

What we have done in this experiment of scanning the scanning is an analysis of the registered data by applying a kind of clipping. Every time a new secondary scanning was done the threshold was lowered one step. These and similar experiments showed that the idea of a light-dependent resistor for contrast amplification is basically sound.

A closed television circuit works in essentially the same way: by varying the brightness or the contrast or by varying the incoming signal (i.e. the illumination of the view-box or the diameter of the optical diaphragm) all minor variations of blackness of the film can be detected.

5. CLINICAL APPLICATION

5.1. Scintillography of the thyroid

The questions that can be answered after scintillography of the thyroid are:

(1) What is the form and size of the thyroid;

(2) How is it situated relative to certain anatomical landmarks;

(3) Is there any ectopic thyroid tissue;
(4) Are there iodine-collecting metastases of a carcinoma of the thyroid; and
(5) How is the iodine distributed in the thyroid gland?

The techniques of the examination should be in accordance with the problem to be solved. If the question is to verify whether a shadow in the anterior mediastinum on an X-ray picture is caused by an intrathoracic struma, then it is obvious that the sharpest spatial resolution is not needed and that a collimator with less resolution but larger efficiency is best for this patient. If the problem is the detection of iodine-collecting metastases of a thyroid carcinoma, one should not in the first place make a scintigram but a profile scan, as this is a fast, reliable and easy method. We feed the pulses from the single-channel analyser to a scaler and take out the pulses from the amplifier of the scaler. These pulses are put on one track of a stereotape and on the other track the position of the detector relative to the body of the patient is indicated by speaking through a microphone. With this method one can play back the profile scan and make a graph with an ink-writing recorder while applying time expansion without any difficulty correlating between diagram and anatomy. One should not, however, be content with only one profile scan.

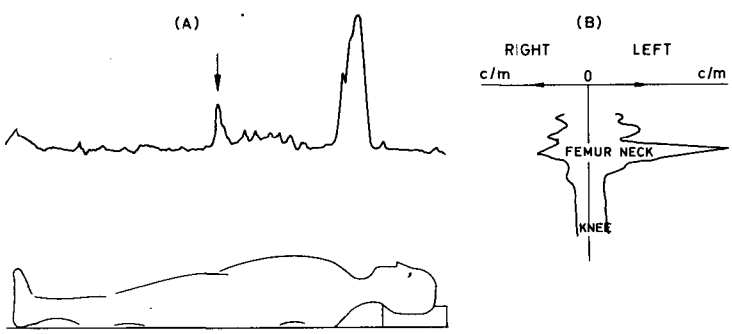

Fig. 13

Profile scan of metastatic thyroid carcinoma
(A) At a distance of 50 cm
(B) At a small distance above right and left femur.

Figure 13(a) shows the result of a profile scan made of a patient before an operation of the thyroid. She had a fracture of the left collum femoris. During operation the tumour was found to be the cause of the fracture. Histological examination showed it to be a metastasis of a thyroid carcinoma. The distance between sternum and crystal was 50 cm and from the isoresponse lines of the slit collimator we know that the detector "sees" slices of tissue at least as broad as the patient and about 3 centimetres high. The peak marked with an arrow might be ascribed to urine in the bladder.

We did more profile scans on this patient, but at a smaller distance above the right and left femur. In this way we obtained separate profile scans of the two femora and hips. Fig. 13(b) shows the result of this examination. A large difference between right and left can be seen.

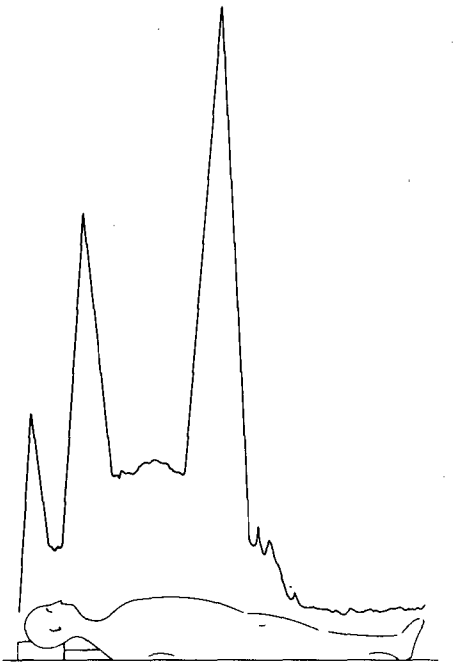

Fig. 14

Profile scan of metastatic thyroid carcinoma
The diagnosis of a tumour in the sacral bone was already established. The profile scan also shows the accumulation of I^{131} in the skull.

Figure 14 shows the profile scan of a 60-year-old woman. A tumour was found in the sacrum and histologically it had the appearance of normal thyroid tissue. It is obvious that we had every reason to suspect here the clinical entity formerly called "benign metastasing adenoma" of the thyroid. In reality this is so well-differentiated a carcinoma of the thyroid that the primary tumour and its metastases do not yield to normal thyroid tissue in functional capacity. A profile scan of this patient indicated clearly that the region of the head should be examined in more detail. Fig. 15 shows the scintigram of the head of this patient.

We have found profile scans to be of great value in detecting radioiodine concentrations in tumour metastases and we think that the comparison of profile scans of symmetrical parts of the body has real advantages.

One should always keep in mind that only the distribution of radioiodine is visualized. This means that even a nomenclature as vaue as "a space-occupying lesion" can be too suggestive to describe a "defect" in the scintigram. Fig. 16 shows several scans of thyroids. They all show a "defect", but the cause of this "defect" is in every case a different one. Fig. 16(A) is the scan of a thyroid with a carcinoma; (B) is of a patient with thyroiditis lymphomatosa (Hashimoto). The "defect" in scan (C) is caused by haemorrhage in the thyroid and (D) is caused by a toxic adenoma of the thyroid.

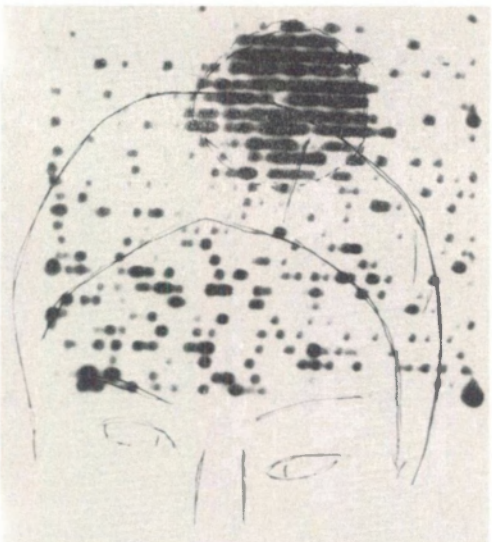

Fig. 15

Scintigram of the head of the patient in Fig. 14

Figure 17 shows the scintigram of case (D) after the administration of ten international units of TSH every day for three days.

In these scintigrams one sees "defects" that show no essential difference in their outlook. If one does not bear in mind that only the distribution of radioiodine is examined, the term "space-occupying lesion" easily appears. However, the only fact that has been shown in a scintigram with a "defect" is a local disturbance of function and this may be caused by:

(1) Resisting of normal thyroid tissue because of suppression of TSH production as a result of the increased thyroid hormone production by a toxic adenoma;

(2) An inflammatory process (thyroiditis);

(3) Replacement of thyroid tissue by another tissue and this may be blood, a benign tumour, a primary malignant thyroid tumour, a metastasis in the thyroid etc.

It is of great practical importance that one does not forget to spend a few minutes for every patient in looking for a lingual struma. If one finds radioiodine in the region of the tongue, then this should be visualized in an antero-posterior and a lateral scintigram; if not, one might take this for a metastasis. Fig. 18 shows a lingual struma. Fig. 19 shows a metastasis of a carcinoma of the thyroid that has the appearance of a lingual struma. However, it did not exist preoperatively and was found after thyroidectomy.

5. 2. Scintillography of the liver

The clinical problems to the solution of which scintillography of the liver can contribute concern:

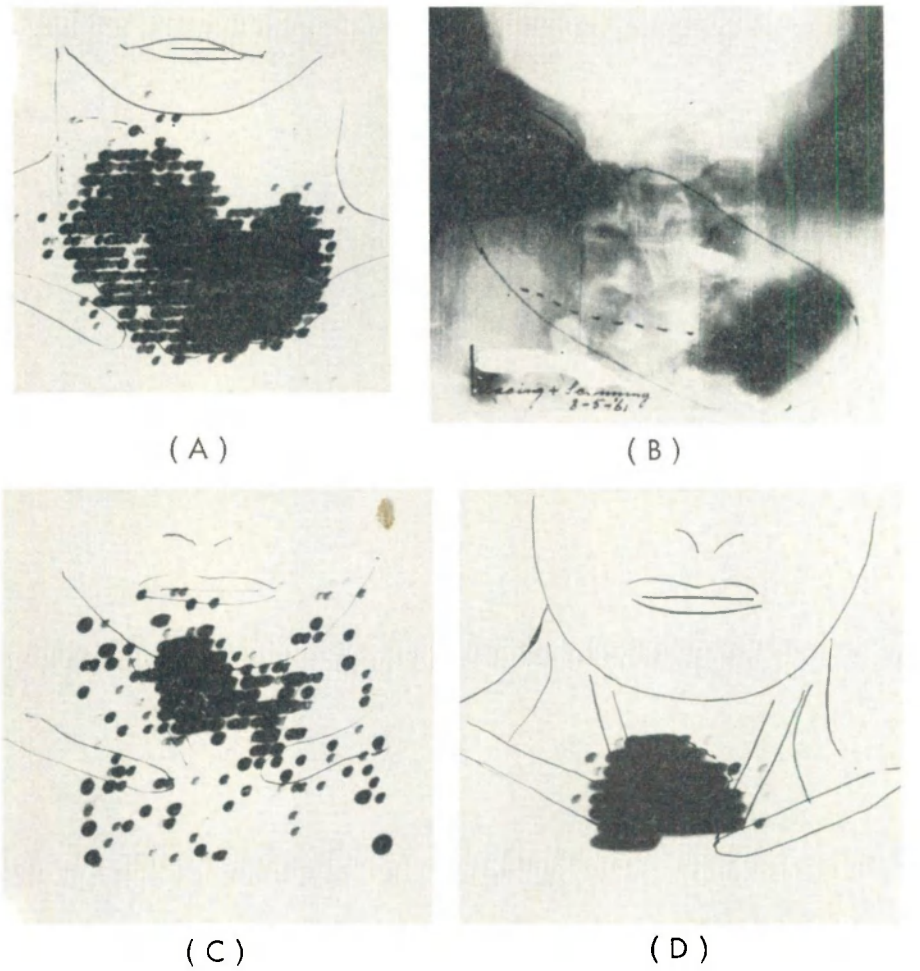

Fig. 16

"Space-occupying lesions" in thyroid scintigrams
(A) Carcinoma of the thyroid
(B) Thyroiditis lymphomatosa (Hashimoto)
(C) Haemorrhage in the thyroid
(D) Toxic adenoma of the thyroid.

(1) The size of the liver;
(2) The diagnosis of metastases;
(3) The diagnosis of primary carcinoma of the liver;
(4) The indication of the best spot for liver biopsy; and
(5) Diagnostic help in clinical puzzles.

We use colloidal Au^{198} (Philips-Duphar, Amsterdam). Initially our dose was 200-250 μc, but after the changes in detection techniques mentioned earlier in this paper 75 μc sufficed. Twenty to thirty minutes after the

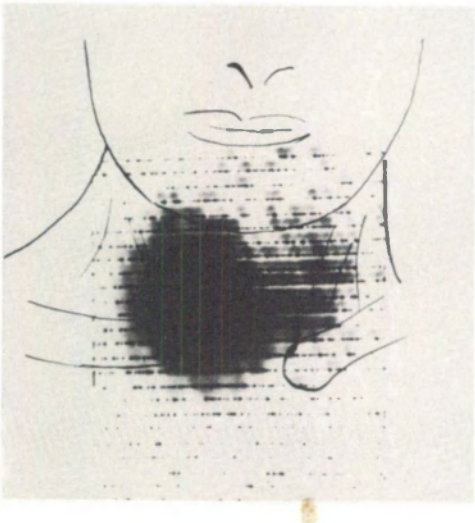

Fig. 17

Scintigram of case (D) of Fig. 16 after administration of thyroid stimulating hormone

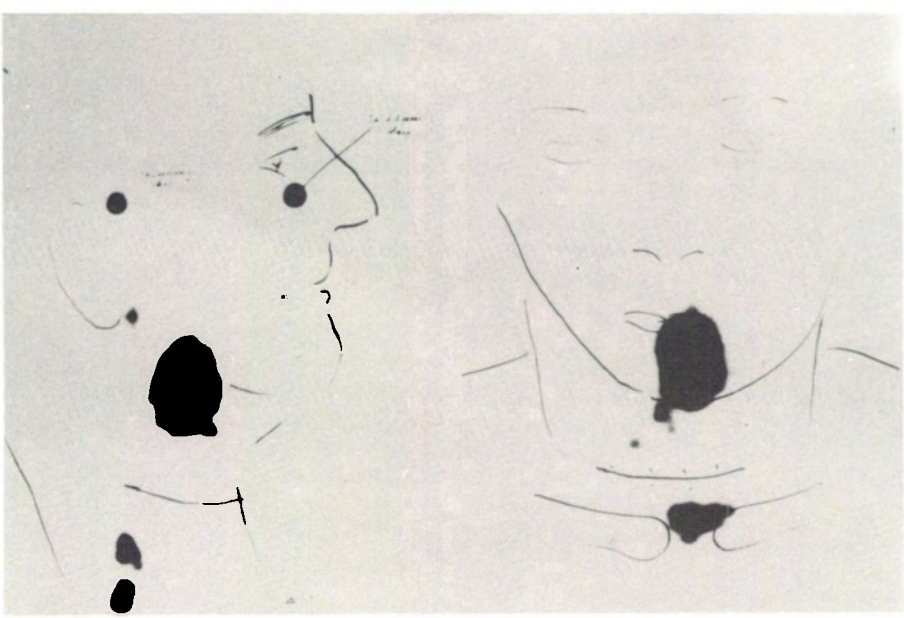

Fig. 18

Scintigrams of lingual struma

intravenous irjection of the colloid, scanning is started for this purpose; the 36-channel, multi-focus collimator, specially developed for the examination of thick organs, is used.

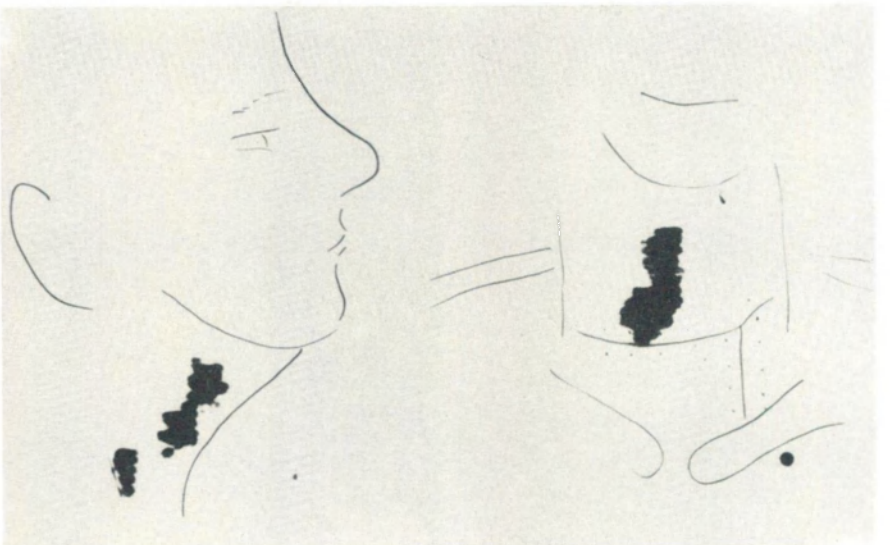

Fig. 19

Scintigrams of metastasis of a carcinoma of the thyroid, resembling lingual struma

Figure 20 shows the scintigram of the liver of a 35-year-old man. This very ill patient was sent for scintillography. No clinical diagnosis could be made. A large tender liver was found and the chemical liver functions were severely disturbed. In the scintigram we see a large liver with a poor uptake of the gold colloid. It shows a large "defect" and multiple rather diffuse "defects". This picture suggests a primary process in the liver with metastases in the liver. Combining this interpretation of the scintigram with the clinical findings (large, tender liver, high fever), the tentative diagnosis of "abscess of the liver" was made. A liver puncture was advised and point "A" was indicated as the best spot for it. This puncture was performed and a large amount of pus came out. Abscess of the liver is a very exceptional disease in the Netherlands, seen almost exclusively in patients repatriated from tropical or subtropical regions. This patient, however, had never left our country and the abscess was caused by an amoeba, that normally behaves more like a parasite than as a pathogenic agent. Fig. 21 shows a scintigram which we think is characteristic for a primary carcinoma of the liver. This scintigram does not differ essentially from the picture of Fig. 20. In both cases the interpretation of the distribution of Au^{198} is the same: "a large defect with multiple smaller ones". Only the combination of this interpretation with the clinical picture leads to a diagnosis. In the former patient this diagnosis was "abscess of the liver", in this last one the tentative diagnosis "primary carcinoma of the liver with metastases" was made. Liver biopsy and autopsy were not allowed, so we have no objective verification of this diagnosis. The reason we still give this picture is the fact that it shows best the characteristic large defect with smaller ones. The scintigrams of primary liver carcinoma verified by autopsy were made in rather late phases of the disease and are less suitable for reproduction.

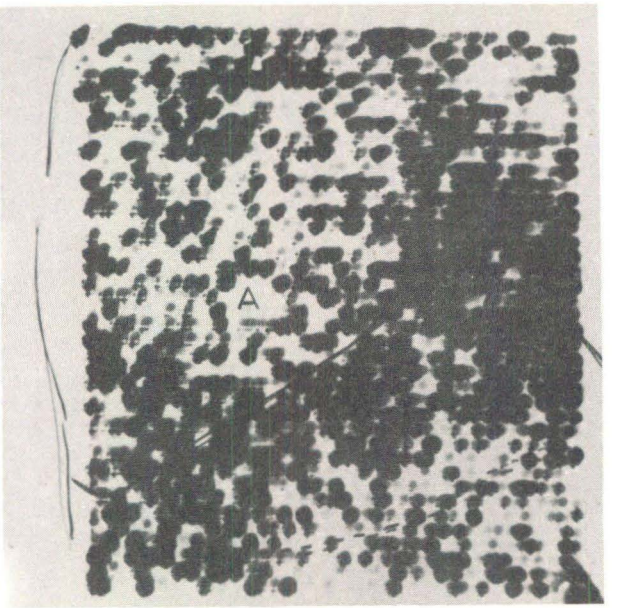

Fig. 20

Scintigram of an abcess of the liver
"A" was indicated as the best spot for liver biopsy.

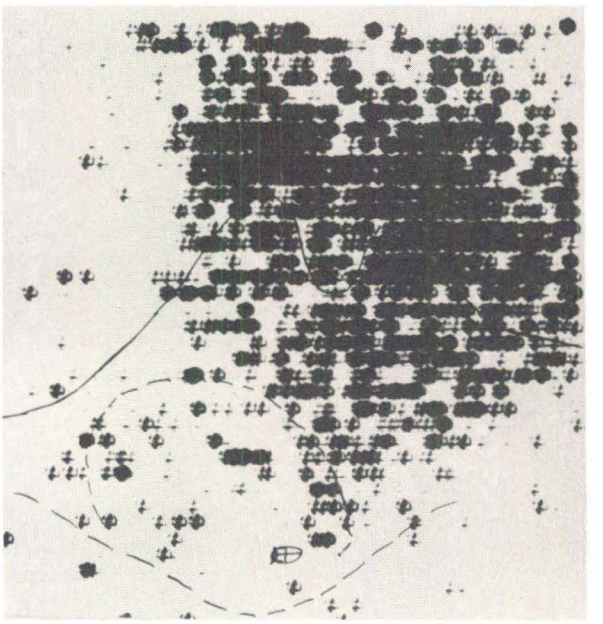

Fig. 21

Scintigram leading to the tentative diagnosis of primary carcinoma of the liver

Clinically the detection of metastases in the liver is of paramount importance, as in that circumstance it is our duty to refrain from extensive therapy in most cases. In this respect there are, however, difficulties. Some surgeons think it advisable to do a partial liver resection in case of a solitary metastasis. The supporter of this opinion must demand:

(1) That a space-occupying lesion diagnosed as solitary metastasis is, of course within the limit of normal clinical laboratory methods, really solitary; and

(2) That a solitary metastasis can be visualized in a state in which resection still is possible.

We have already shown (see section 3) that we cannot detect in vivo liver metastases with a diameter smaller than 2 cm. This proves that with our present technique we cannot guarantee with reasonable safety that a visualized metastasis is really solitary. Smaller ones might be present.

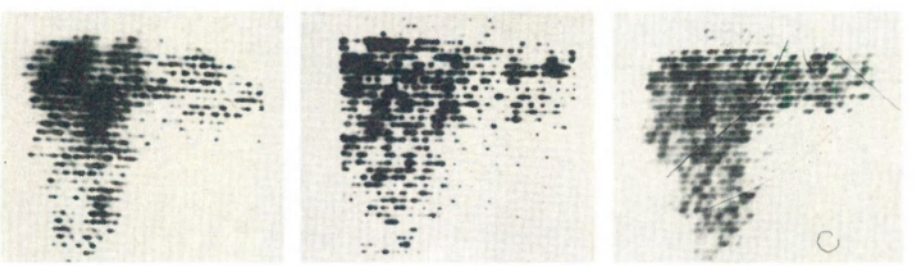

(A) (B) (C)

Fig. 22

Scintigrams of metastases of seminoma testis
(A) Original scintigram
(B) One year later
(C) After telecobalt therapy (1500 r midline dose).

The aspect of a scintigram of a liver with multiple metastases is shown in Fig. 22. This is of a 30-year-old man with seminoma testis. Hemicastration and irradiation of the lymphatics up to the diaphragm were performed. One year later supraclavicular lymph nodes and enlargment of the liver were found. The scintigram shows multiple defects in the liver. The supraclavicular lymph nodes and the thoracic lymphatics were irradiated. Six months later the scintigram of the liver showed marked progress. As a seminoma testis is very radiosensitive, radiotherapy of the liver was performed: 1500 r midline dose in three weeks were applied to the liver with telecobalt. This was well tolerated, the sedimentation of the erythrocytes went down from 35 to 6 mm in one hour. The scintigram of the liver three months after this telecobalt therapy shows a marked regression: only at the right lateral border and in the tip of the liver, where the irradiation field was rather restricted, we see "defects". The rest of the liver has a much more normal aspect than before this therapy. Fig. 23 shows that cirrhosis of the liver and tumour cannot be differentiated in a scintigram. This is the scintigram of a 46-year-old man with a cirrhosis of Laennec and portal hypertension.

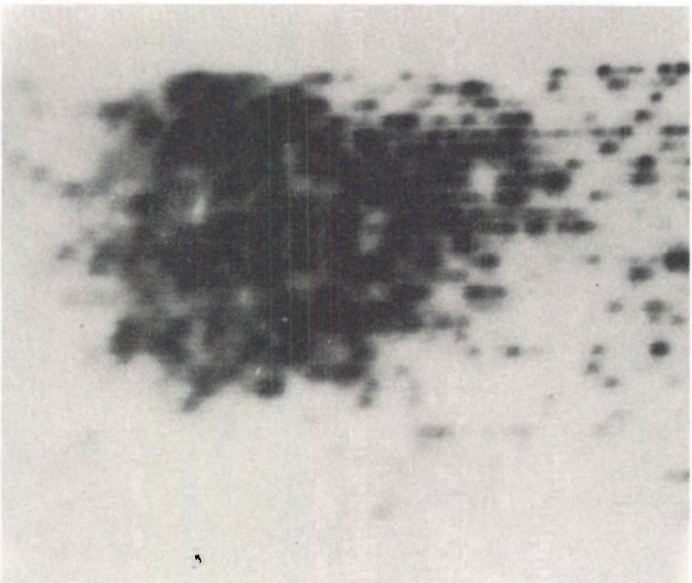

Fig. 23

Scintigram of cirrhosis of Laennec

It is our experience that very often we can visualize with photoscintillography metastases in the liver six to nine months before the chemical reactions give any indication of a disturbance. The earliest and most constant chemical sign is a rise in the serum alkaline phosphatase. A rise in level of the transaminase is in our opinion often a very cursory phenomenon.

5.3. Photoscintillography of the kidneys

The normal roentgen diagnostic methods like intravenous and ascendent pyelography give pictures of the calyces, pyelum and the rest of the urine-draining system. They do not visualize the parenchym of the kidneys; only X-ray pictures after aortography can give information of this. A simpler and less drastic diagnostic method would be an asset.

Photoscintillography of the kidneys after administration of Hg^{203} Neohydrin was considered for a short time as a possible substitute for aortography. The mercurial diuretics concentrate, however, only in the proximal tubules, i.e. almost exclusively in the cortex of the kidney. We must realize, when looking at a Hg^{203}-Neohydrin scintigram of the kidney, that we see only a shallow envelope projected on a plane. No direct information about the medulla of the kidney can be gained with our present kidney-scanning technique. The scanning is begun three to four hours after the administration (intramuscularly) of 200 μc of Hg^{203}-Neohydrin combined with hyaluronidase. The patient is in the supine position. The influence of the accumulation of Hg^{203} in the liver does not normally interfere with photoscintillography. The uptake in the liver is clearly raised in patients with

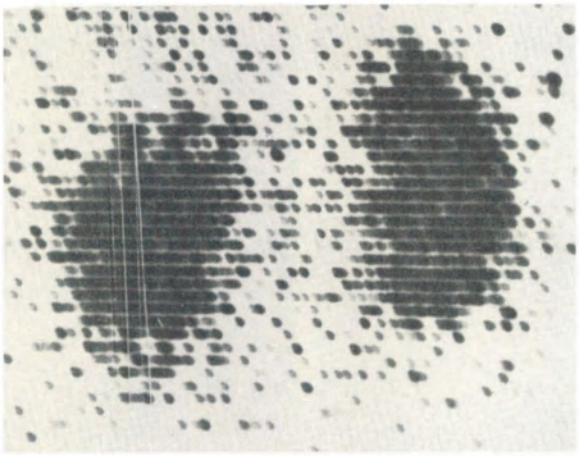

Fig. 24

Scintigram of normal kidneys

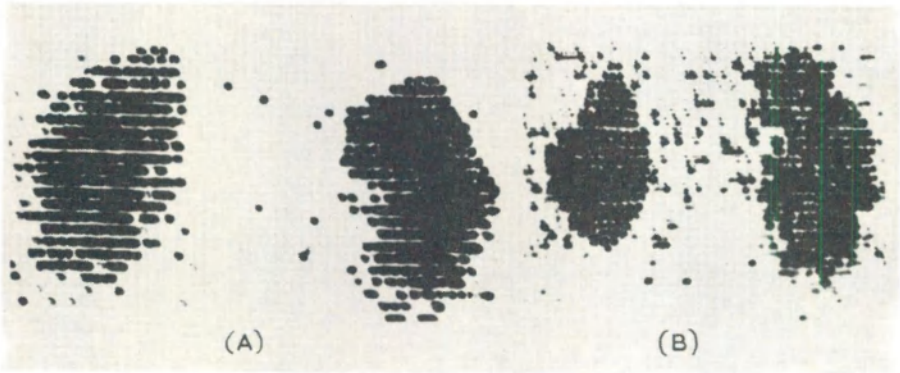

Fig. 25

Scintigrams of variants of normal kidneys
(A) Straight lateral border
(B) Arched protuberance
Both should be considered as remnants of foetal lobulation of the kidney

a bad functioning of one kidney. The normal scintigram of the kidneys is shown in Fig. 24. Variants of this normal form can be seen in Fig. 25. Fig. 25(A) shows a rather straight lateral border. This occurs more often in the left kidney, but may also occur on the right side. Fig. 25(B) shows an arched protuberance. This variant of normal anatomy also occurs more often on the left side than on the right. Both the straight border and the arched protuberance should be considered as remnants of foetal lobulation of the kidney. They are without pathological significance.

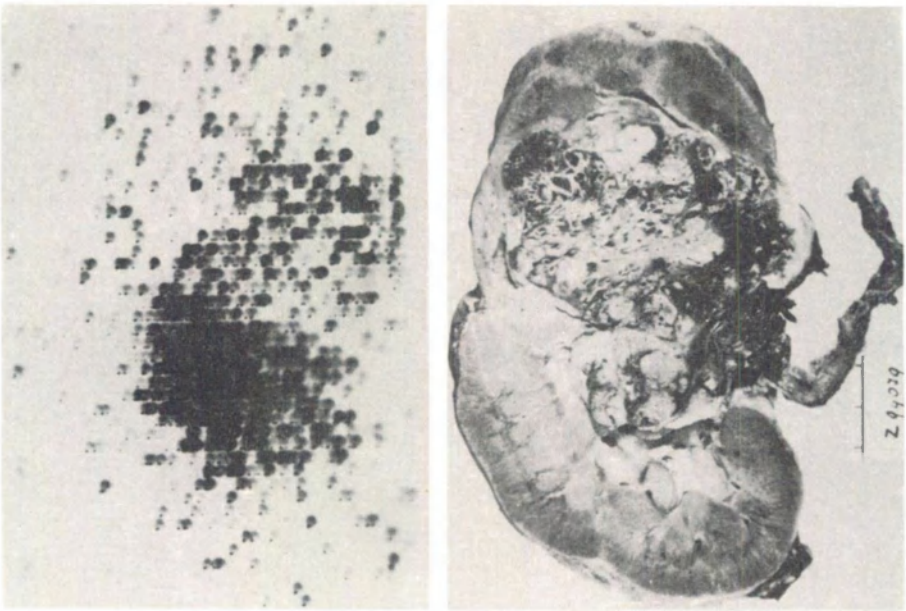

(A) (B)

Fig. 26

Adenocarcinoma of the kidney
(A) Pre-operative scintigram
(B) The extirpated kidney.

We had hoped that scintillography would contribute to the differential diagnosis between malignant tumour and cyst of the kidney. Fig. 26 shows the in vivo scintigram of a right kidney and the kidney itself after exstirpation. Histological examination showed it to be an adenocarcinoma of the kidney. Fig. 27 shows a lateral, well-delineated defect, while Fig. 28 shows well-delineated defects in both kidneys. The defects in the scintigrams of Figs. 27 and 28 are caused by cysts.

There is no essential difference between the detects caused by tumours or by cysts. We have noticed, however, one point that not infrequently gives a useful hint in differentiating between tumour and cyst. It is to be seen in Fig. 26: one gets the impression that around the tumour defect the function of the kidney tissue is diminished and the scintigram shows a rather diffuse accumulation of Hg^{203}-Neohydrin around the defect. Around the defects caused by a cyst the functional state of the surrounding tissue seems to be normal.

Photoscintillography can be valuable for the verification of the diagnosis of pyelonephritis. The X-ray picture often does not show much more than a rather hazily delineated calyx. However, the rather diffusely diminished functional state is clearly visible in a scintigram.

Figure 29 shows the scintigrams of two patients with horseshoe kidneys. In both cases the bridge between the lower poles of the kidneys consists of functioning renal tissue. This is, in the opinion of our urologist, a fact

Fig. 27

Scintigram of cyst in the right kidney

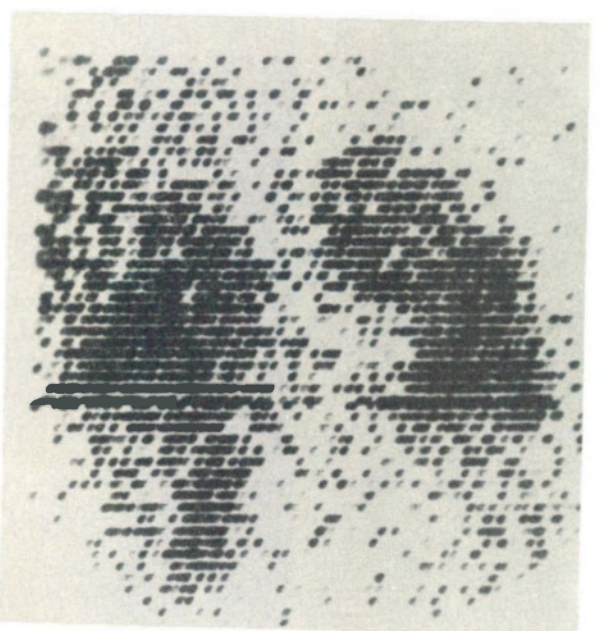

Fig. 28

Scintigram of polycystic kidneys

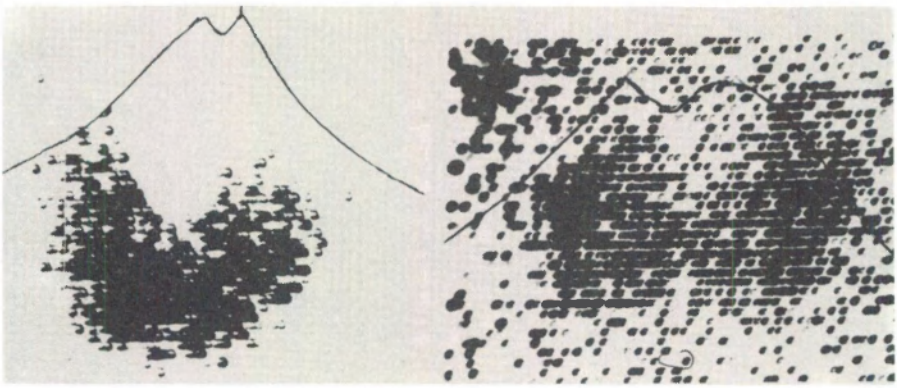

Fig. 29

Scintigrams of horseshoe kidneys

worth knowing before the operation, which sometimes seems to be necessary in such cases because of extrinsic pressure.

We are, however, rather disappointed in the clinical value of photoscintillography of the kidneys. Large cysts can pass undetected when they are located in the medulla and do not affect the cortex of the kidney. The same is true for tumours located in the medulla of the kidney.

We feel that photoscintillography of the kidneys will become of very great clinical importance as soon as we can devise a suitable radioactive compound that is accumulated both in the medulla and the cortex of the kidney. Once we possess such a compound, photoscintillography and routine X-ray diagnostic methods will complement each other: the renal parenchym is visualized by photoscintillography, the effluent urinary tract by the roentgenologist. The pharmacologists and the pharmaceutical industry must now take over and supply us with the tools we are waiting for.

5.4. Placentography

Placentography is a rather new branch of in vivo isotope techniques. Up to now the only question to be answered by this examination is the location of the placenta. Vaginal bleeding in the second half of pregnancy is a sign one cannot neglect, since it may be a symptom of placenta praevia. Often as a precaution these women are hospitalized for months. Placentography can be of great value in these cases as the location of the placenta can easily be assessed by this method. For this purpose we need a compound that does not pass the placenta and we label the erythrocytes of the mother with 50 μc of Cr^{51} and reinject the labelled blood into the mother. The technique is the same as described above for profile scanning.

We also make point-to-point measurements (Fig. 30). We made one mistake: it would have been better to centrifuge the blood after the labelling of the erythrocytes and wash several times with isotonic saline to remove the rest of the sodium chromate. This, however, was omitted and so we also find Cr^{51} in the bladder of the mother.

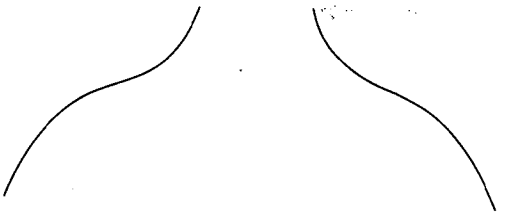

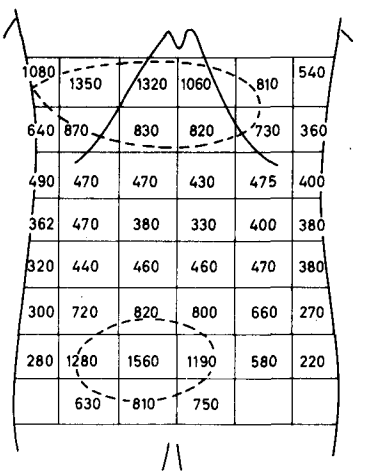

Fig. 30

Point to point count in placentography

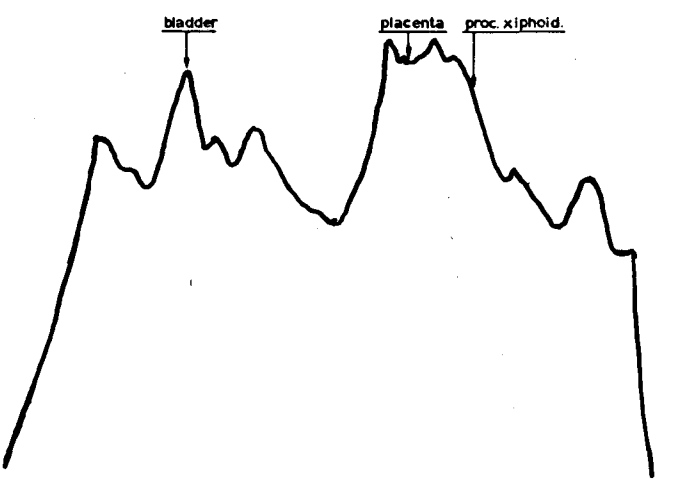

Fig. 31

Profile scans in placentography

Figure 31 shows profile scans in such a case. A was performed at a distance of 10 cm and B at a distance of 50 cm between abdomen and crystal. From the shift of the ratio placenta peak: bladder peak with variation of the distance, one can deduce that the placenta is nearer to the plane of

scanning that the bladder. Furthermore it is located in the fundus of the uterus. This is clearly a simple and fast way of placentography which, apart from the labelling, takes only eight minutes.

REFERENCE

[1] INTERNATIONAL ATOMIC ENERGY AGENCY, Medical Radioisotope Scanning, IAEA, Vienna (1959) 266 pp.

AN AUTOMATIC SCANNING SYSTEM, USING A TAPE PERFORATOR AND COMPUTER TECHNIQUES

H. SCHEPERS
INSTITUT FÜR STRAHLEN- UND KERNPHYSIK
AND
C. WINKLER
NUCLEARMEDIZINISCHE ABTEILUNG IN DER
CHIRURGISCHEN UNIVERSITÄTSKLINIK,
BONN, FEDERAL REPUBLIC OF GERMANY

Abstract — Résumé — Аннотация — Resumen

AN AUTOMATIC SCANNING SYSTEM, USING A TAPE PERFORATOR AND COMPUTER TECHNIQUES. The choice of scan velocity and spacing is purely a statistical problem, provided that the other parameters are determined. In the scanning devices commonly in use (detectors moving with constant velocity) optimum statistical conditions cannot, however, be predetermined. Therefore, the quantitative evaluation and the visualization of a non-uniform distribution of radioactivity can be improved.

In order to solve the problems mentioned above, a new scanning device has been developed. The object is scanned, with "preset count", point by point, and therefore the statistical error is determined. Thus, the degree of accuracy appropriate for each case can be chosen at the beginning of the scan. The scanning time is then exactly that which is determined by the selected degree of accuracy, no more and no less.

The data, including the co-ordinates of detector position and timing are recorded by a tape perforator and the paper tape is fed into a digital computer. The computer programme undertakes the following steps: calculation of the pulse rate for each point, subtraction of background and, if needed, correction for radioactive decay; least-squares approximation prevents statistical deviations of the single counts from influencing the evaluation of the final result. This is plotted by the computer in such a manner that any person not specially trained is easily able to plot a series of isocount curves. After evaluation of the plot, further quantitative calculations can be performed by the computer using an appropriate programme.

In a more sophisticated set-up, two probes with different collimators are used simultaneously, one with an aperture providing high resolution and the second one with poor resolution but high efficiency. The latter serves as an indicator giving a quick decision. The count rate is significantly increased when compared with the background. By using this equipment it is possible to reduce considerably the time necessary for the performance of the scan.

APPAREIL DE GAMMAGRAPHIE AUTOMATIQUE AVEC PERFORATEUR A BANDE ET CALCULATRICE ÉLECTRONIQUE. Le choix de la vitesse de balayage et de l'espacement des lignes pose un problème purement statistique, à condition que les autres paramètres soient connus. Or, pour les appareils de gammagraphie courants (détecteurs se déplaçant à une vitesse constante), il est impossible de déterminer à l'avance les conditions statistiques optima. En conséquence, l'évaluation quantitative et l'image d'une distribution non uniforme de la radioactivité sont susceptibles d'amélioration.

En vue de résoudre les problèmes susmentionnés, on a mis au point un nouveau dispositif de gammagraphie. Le sujet est exploré à l'aide d'un «appareil préréglé», point par point, et l'erreur statistique se trouve donc déterminée. Il devient ainsi possible de choisir le degré de précision approprié à chaque cas avant de procéder à l'exploration. La durée de l'exploration sera alors exactement égale à celle qui est fixée par le degré de précision choisi.

Les données, y compris les coordonnées indiquant la position du détecteur et la durée, sont enregistrées par un perforateur à bande et la bande de papier est introduite dans une calculatrice numérique. Le programme de la calculatrice comprend les opérations suivantes: calcul du nombre d'impulsions par point, soustraction du bruit de fond et, le cas échéant, correction du résultat pour tenir compte de la désintégration radioactive. Une approximation par la méthode des moindres carrés empêche que la dispersion statistique des différents coups n'affecte l'exploitation du résultat final. Ce dernier est représenté par la calculatrice de telle sorte

que toute personne, même si elle n'a reçu aucune formation spécialisée, peut facilement dresser une série de courbes isodoses. Après avoir exploité le diagramme, on peut utiliser la calculatrice pour d'autres calculs quantitatifs grâce à un programme approprié.

Dans un dispositif plus perfectionné, on emploie simultanément deux sondes munies de collimateurs différents: la première a un pouvoir de résolution élevé; la seconde a un pouvoir de résolution faible, mais une grande sensibilité; cette dernière est utilisée comme indicateur à réponse rapide, le taux de comptage se trouvant sensiblement accru par rapport au bruit de fond. Grâce à ce dispositif, il est possible de réduire considérablement le temps nécessaire à une exploration gammagraphique.

АВТОМАТИЧЕСКАЯ СИСТЕМА СКЕННИРОВАНИЯ ПРИ ПОМОЩИ ЛЕНТОЧНОГО ПЕРФОРАТОРА И ЭЛЕКТРОННОГО СЧЕТНОГО УСТРОИСТВА. Выбор скорости сканнирования и расстояния между строками является чисто статистической проблемой при условии, что остальные параметры уже определены. Однако при обычно используемых сканнирующих устройствах (движущиеся с постоянной скоростью детекторы) оптимальные статистические условия не могут быть определены заранее. Поэтому представляется возможным улучшить количественную оценку и изображение неравномерного распределения радиоактивности.

Для разрешения упомянутых выше проблем было разработано новое сканнирующее устройство. Изучаемый объект сканнируется по точкам с "заранее установленной скоростью счета", что позволяет определять статистическую погрешность. Таким образом представляется возможным в начале каждого сканнирования выбирать для каждого случая надлежащую степень точности. В таком случае время сканнирования совершенно точно определяется заранее выбранной степенью точности.

Данные, включающие координаты положения детектора в каждый момент и время, регистрируются на перфорированной ленте, и эта бумажная лента поступает в счетно-вычислительное электронное устройство. Программа вычислительного устройства выполняет следующие последовательные операции: подсчет скорости импульсов в каждой точке, вычитание фона и, в случае необходимости, поправку на радиоактивный распад; приближение по теории наименьших квадратов не допускает того, чтобы статистические отклонения отдельных подсчетов оказывали влияние на оценку конечного результата. Этот результат представляется счетным устройством в таком виде, что любой, даже без специальной подготовки, легко может построить сеть кривых с равной скоростью счета. По окончании расшифровки этой диаграммы счетное устройство может при помощи надлежащей программы, выполнять дальнейшие количественные вычисления.

В случае более сложного устройства два зонда с различными коллиматорами используются одновременно, причем один из них снабжен развертывающей апертурой с высоким разрешением, а второй со слабым разрешением, но с высокой эффективностью. Последний служит для принятия быстрого решения: скорость счета значительно повышается по сравнению с фоновой.

Использование этого оборудования позволяет значительно сократить время, необходимое для выполнения сканнирования.

SISTEMA AUTOMÁTICO DE EXPLORACIÓN CON REGISTRO EN CINTA PERFORADA Y ANÁLISIS DE DATOS EN UNA CALCULADORA. Una vez determinados los otros parámetros, la elección de la velocidad y de las intermitencias de la exploración constituye un problema puramente estadístico. No obstante, con los dispositivos de exploración generalmente empleados (detectores que se mueven a velocidad constante) no es posible determinar de antemano las condiciones estadísticas óptimas. La evaluación cuantitativa y la visualización de una distribución no uniforme de radiactividad pueden, por consiguiente, mejorarse.

Para resolver estos problemas se ha ideado un nuevo dispositivo de exploración. El órgano se explora por puntos con un "recuento preestablecido", con lo que se determina el error estadístico. Así, al comenzar la exploración se puede elegir el grado de exactitud adecuado para cada caso y este grado de exactitud determina a su vez el tiempo de exploración.

Los datos, incluidas las coordenadas de la posición del detector y de los tiempos, se registran en una cinta perforada que se pasa a una calculadora numérica. En virtud del programa de la calculadora se realizan las siguientes operaciones: cálculo del índice de recuento para cada punto, substracción del fondo y, de ser necesario, correcciones para tener en cuenta la desintegración radiactiva. Una aproximación por cuadrados

mínimos evita que las desviaciones estadísticas de los recuentos influyan en la evaluación del resultado final. La calculadora representa este resultado gráficamente de modo que cualquier persona, sin necesidad de preparación especial, puede trazar una serie de curvas de isorrespuesta. Partiendo de estas curvas la calculadora puede efectuar más cálculos cuantitativos siempre que se emplee un programa adecuado.

En una instalación más compleja se emplean simultáneamente dos detectores con colimadores diferentes; el primero con una apertura con la que se obtiene alta resolución y el segundo de baja resolución pero de alta eficiencia. Este último sirve como indicador y permite adoptar una decisión rápida cuando el índice de recuento aumenta marcadamente en comparación con el fondo. Con este equipo es posible reducir considerablemente el tiempo necesario para efectuar la exploración.

The increasing number of test substances for scanning purposes has led to more extreme requirements for the technical scanning equipment [1]. In using these devices a number of different parameters must be considered with the utmost accuracy. Provided that the resolution of the applied collimator is adapted to a special scanning problem [2], the possibility of detecting differences of the radioactivity within the body is essentially a function of the test dosage applied and of the time the detector is allowed to see the scanning area.

In conventional methods using moving detectors the line spacing must be adjusted to the resolution characteristics of the collimator. Furthermore, the scanning speed has to be adapted to the expected differences in the pulse-rates. This latter condition cannot be satisfied without compromises and requires adequate approximations. When scanning with constant velocity the statistical error varies as a function of the pulse-rate at each point, therefore records of optimum quality cannot be achieved. In low-activity regions the precision of counting is inadequate, whereas in regions of relative high intensities the selected speed is slower than necessary. A further problem arises from the fact that subjective factors cannot be eliminated in estimating the differences in density.

From earlier experiments [3] we came to the conclusion that these differences should have at least four times the value of the standard deviation δ. Taking into account that already a difference of 2δ is generally accepted as significant, it would be advantageous to use objective methods for quantitative evaluations. For calculations of this kind the scanning data have to be stored in a manner which allows statistical comparison of count numbers in different areas.

For routine diagnostic purposes we had developed previously a device that stores the pulses on a magnetic foil sheet [4]. To solve the more complex problems, however, an improvement in the recording and evaluation systems seemed to be desirable. This is the case, for example, if the uptake of radioactive tracers in tumours of the brain or other organs is very low. Similar problems arise when pulse-rates are reduced by minute differences because of small neoplasms or cysts in the parenchyma of glandular organs. In special cases it might be of interest to study tissues which are overlapped by organs with more or less similar uptake of radioactivity (liver + pancreas). For scanning of such difficult cases it is necessary for the experimental device to allow preselection of the statistical error in the essential parts of the picture. In addition the plotted graph of the scan should show directly the various exact levels of intensity.

To fulfil these requirements we considered that computer methods should be applied. This has the advantage that the processing of a large amount of data would be possible in a very short time, which is valuable for instance when employing several detectors in varying geometries.

These considerations led in the present conditions to the development of a scanning system diagrammatically shown in Fig. 1. As is usual the

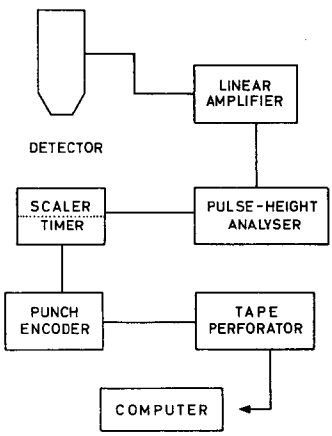

Fig. 1

Block diagram of a scanning system.

scintillation counts are fed into a linear amplifier, a pulse-height selector and a scaler-timer-system.

The area in the essential part of the picture is scanned point by point with "preset count", and consequently the statistical error is predetermined. Thus the degree of accuracy that is adequate for each case can be selected before beginning the scan and determines the scanning time.

If the background beyond the outlines of the organ is relatively low, it may be advantageous in addition to choose "preset maximum time". By this means the time consumption will be considerably reduced.

When one of the preset values is reached, the scaler-timer-system gives a signal and the detector moves to the next position. At the same time the data, including the co-ordinates of detector position and timing, are coded and recorded by the tape perforator.

Later the punched paper tape is fed into an electronic digital computer*.

The computer programme gives the following steps:

For each point, calculation of the pulse-rate, subtraction of background and, if needed, correction for radioactive decay. In addition a levelling calculation is performed by computing a weighted average at any point from 9 or 25 adjacent points, regardless of whether the distance between two points is small compared with the resolution of the collimator.

This smoothing improves the statistics at the single point. First we tried a least squares approximation, but discovered that the weighted average method is sufficiently accurate and less time-consuming.

* IBM 7090, Institut für Instrumentelle Mathematik der Universität Bonn.

The pulse-rate values between background and the maximum are divided into a definite number of levels, which must be calculated according to the "preset count", the difference between maximum pulse-rate and background and the size of the organ. For instance, the scans in the given figures had a "preset count" of 100, and we calculated 20 levels to be the most favourable division.

Figure 4 shows the computer output for a scan of a liver model. By drawing lines through equal symbols, representing the adequate levels, a graph is obtained showing lines of isointensity.

This new method of automatic recording and computing permits application of the well-known isointensity-lines-technique [5, 6, 7] with a large reduction in time consumption. The computing time is about 30 s and the lines can be drawn in a few minutes. The evaluation process can be simplified further by an X-Y-plotter which is available for the IBM 7090 and prints directly the isointensity lines in every desired scale.

In order to test the efficacy of our method for quantitative evaluation of scintigrams we performed examinations on definite phantoms. A model, considered to be extremely difficult, was based on the following biological principles:

Se^{75}-labelled methionine is enriched in the enzymes of the pancreas [8]. Simultaneously, however, liver tissue concentrates this amino acid as well. As in quite a number of cases the pancreas is overlapped by liver tissue the Se^{75}-methionine method is frequently insufficient for the demonstration of the pancreas by scintigram [9]. Therefore, the detection of small tumours in the organ by conventional scanning is completely out of the question.

If a tracer is applied which concentrates only in the liver, it is possible to obtain an exclusive liver scan. By means of the computer technique the data of the liver scan (multiplied by a correction factor) can be subtracted from the Se^{75}-liver + pancreas scan. This results in the distinct tracing of the pancreas, making defects within its tissue visible. This situation was imitated in our phantom (Fig. 2). In the overlapped area a tumour of 2-cm diam.

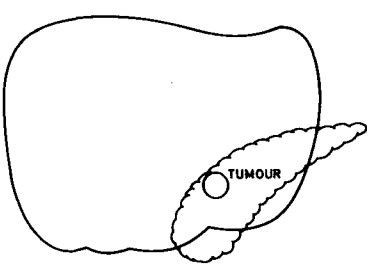

Fig. 2

Outlines of the model LP (liver + pancreas)

is located. The ratio in activity concentrations of liver and pancreas was 1 : 1.4. According to investigations by BLAU et al. this ratio in the living organism can amount to 1 : 8 [10].

Collimator and line spacing as well as the total scan time were identical in both conventional scintigrams (Fig. 3) and computer scans (Figs. 4, 5). As

(a)

(b)

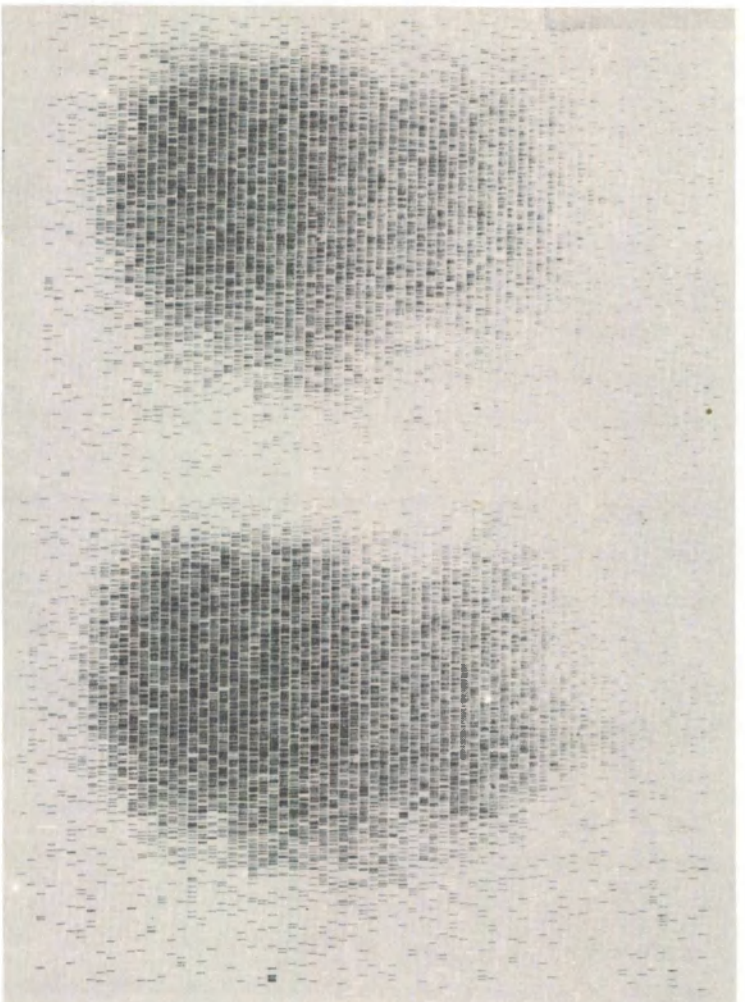

Fig. 3

Conventional scans of

(a) model L (liver)
(b) model LP (liver + pancreas)

Experimental conditions, including scanning time, analogue to Figs. 4 and 5

a result of the subtraction method Fig. 5 demonstrates the pancreas with the location of the tumour indicated by the indentation of the isointensity lines of the upper contour.

In our opinion the result of this experiment seems satisfying and promising, taking into account that actual biological conditions should be more favourable. In addition, as the original data are stored, nearly all the wanted numerical calculations may be programmed.

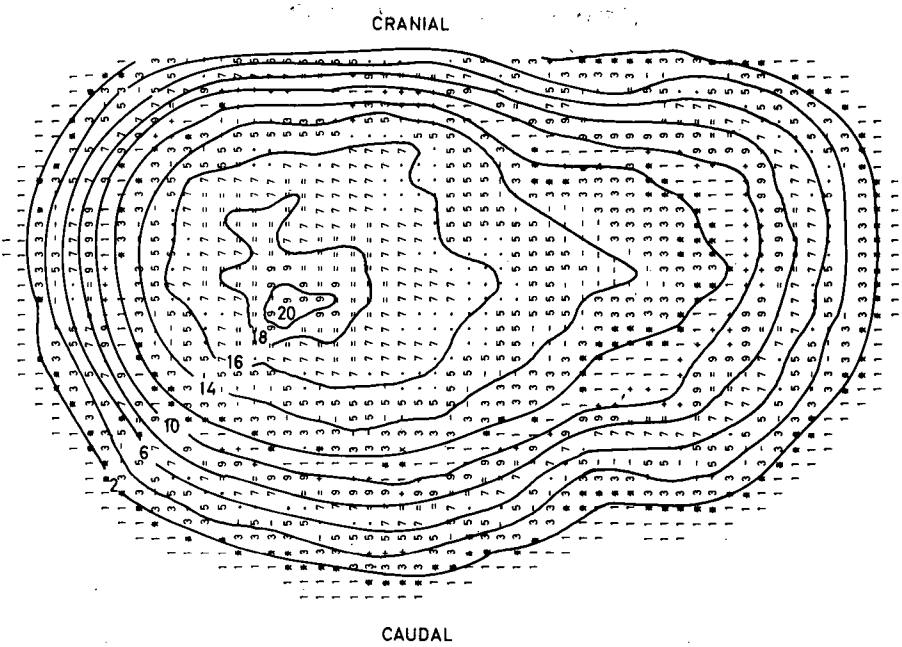

Fig. 4

Liver model scan
Evaluation of the computer output (isointensity lines, background subtracted)

The device and method described above represent the first stage of a research project which includes further improvements. Among them we plan to develop an arrangement which permits the continuous movement of the detector with varying speed geared by the scaler-timer-system. The application of a multichannel analyser or a magnetic tape recorder as buffer storage will practically eliminate the deadtime of the tape perforator.

In a special set-up two probes with different collimators are used simultaneously, one with an aperture providing high resolution and the second one with poor resolution but high efficiency. The latter serves as an indicator for a quick automatic decision on whether or not the count-rate is significantly increased when compared with the background. By using this equipment it is possible to reduce considerably the time necessary for the performance of the scan.

For technical reasons it is not possible at present to employ the computer method in routine diagnosis. At the moment its main importance lies in the possibility of investigating complicated cases and in the testing of new tracers for scintiscanning purposes.

SUMMARY

A new quantitative scan method is described in which the area of interest is scanned point by point with "preset count", and the data are stored by a

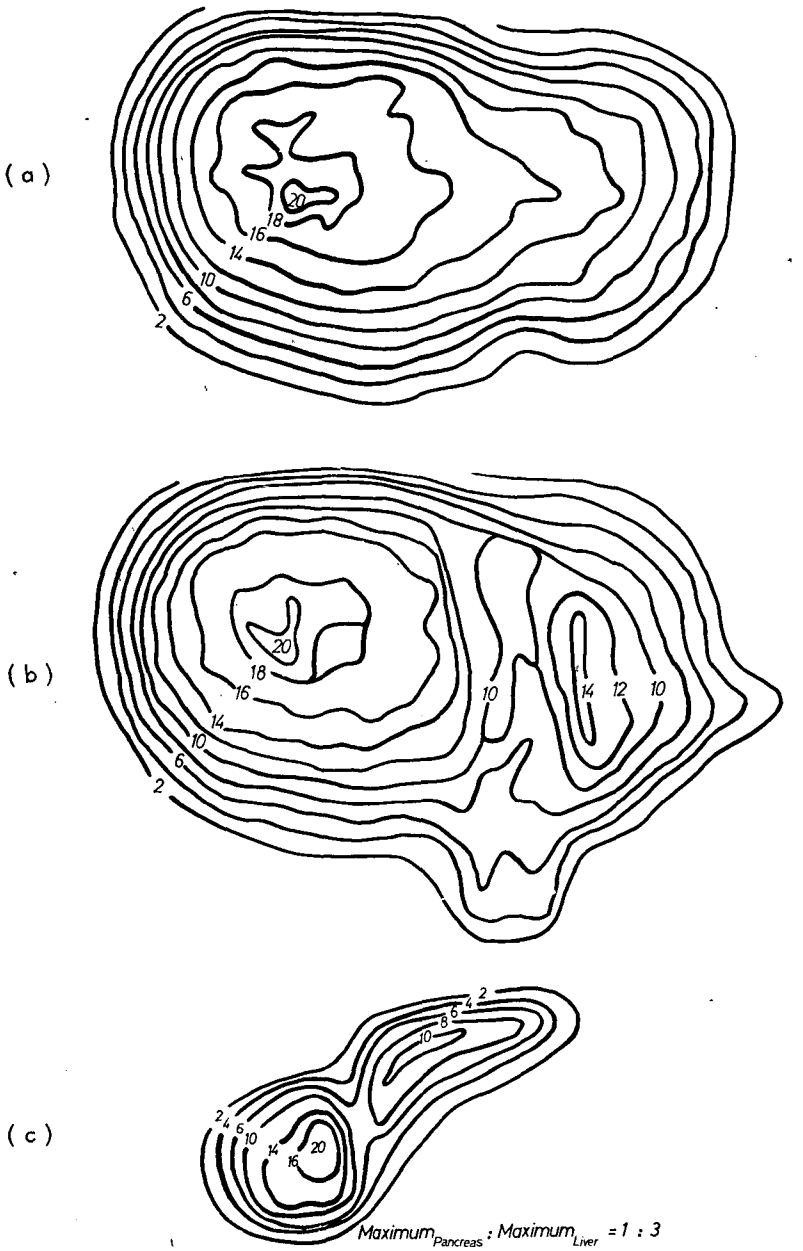

Fig. 5

Isointensity lines of

(a) model L (liver)
(b) model LP (liver + pancreas)
(c) visualization of the pancreas as a result of computing (LP - L)

tape perforator. The application of a digital computer permits different methods of analysis.

The scans are obtained as isointensity lines.

REFERENCES

[1] WINKLER, C., Fortschr. Gebiete Röntgenstrahlen u. Nucl.-Med. 90 (1959) 3.
[2] BROWNELL, G.L., "Theory of Isotope Scanning", Medical Radioisotope Scanning, IAEA and WHO, Vienna (1959) 1.
[3] WINKLER, C., Fortschr. Gebiete Röntgenstrahlen u. Nucl.-Med. 98 (1963) 134.
[4] WINKLER, C. and SCHEPERS, H., Nucl.-Med. 2 (1961) 67.
[5] ALLEN, H.C., Jr., LIBBY, R.L. and CASSEN, B., J. clin. Endocr. 11 (1951) 492.
[6] TAYLOR, S. and STEWARD, F.S., Lancet 11 (1951) 232.
[7] RAKOW, A. and ERNST, H., Strahlentherapie 114 (1961) 630.
[8] BLAU, M., MANSKE, R.F. and BENDER, M.A., J. nucl. Med. 3 (1962) 202.
[9] HAYNIE, T.P., SVOBODA, H.C. and ZUIDEMA, G.D., J. nucl. Med. 5 (1964) 90.
[10] BLAU, M. and MANSKE, R.F., J. nucl. Med. 2 (1961) 102.

DISCUSSION

P. KENNY: The authors are to be congratulated on this paper, which shows very clearly the potentialities of the quantitative read-out method. I have one question: what was the step spacing in the scans?

H. SCHEPERS: In the liver scans, 4 mm, and in the thyroid scans, 2 mm.

A. BAPTISTA: In actual clinical situations I think it would be very difficult indeed to use this subtraction method to obtain the pancreas contribution to the total liver and pancreas image. An image of the liver alone can, of course, be obtained with colloidal gold but nevertheless this would surely be a very difficult technique to use. Have you any experience of its clinical application?

H. SCHEPERS: In the example which I have described in the paper we took two scans, one with the liver model alone, the other with liver + pancreas. It might, however, be possible to run only one scan and use two different spectrometric channels to separate the contributions from two isotopes on the basis of their different gamma-energies. There would be some difficulty with scattered radiation, but we certainly intend to try this approach.

C. HARRIS: I would suggest that these excellent results, which represent a logical development predicted at the Oak Ridge Symposium on Progress in Medical Radioisotope Scanning in October 1962, could be improved even further if the contour plotting were performed on a cross-correlated record, in which each measurement was multiplied by the weighted sum of the surrounding measurements. This could be done fairly easily with a computer.

H. SCHEPERS: We have only used the weighted-average method for smoothing. Computing cross-correlations would certainly improve the results considerably, and this can be easily included in our computer programme. Thank you for a most useful suggestion.

H. WAGNER: What progress have you made in switching from a discontinuous to a continuous system?

H. SCHEPERS: In the system where the detector moves continuously, the scanning speed is controlled by the scaler-timer system and the number of counts recorded at each individual point is approximately equal to the preset-count number. At the moment this is only a mechanical problem.

R. HERBERT: If use is made of a preset-count system, the time spent in measuring background may be excessive. In routine sample counting it is customary to divide the total counting time between the sample and background in order to make the most economic use of the time available. Would it not be useful to do this in your case? Counting time could be controlled, for example, by a ratemeter.

H. SCHEPERS: Where it is not of interest to detect slight differences in pulse rates near the background, we use "preset-maximum time" in addition to "preset-count". This results in the most economic use of scanning time.

H. WAGNER: One advantage of computer techniques, of course, is that they make it possible for us to go over the organ systematically and then concentrate on areas where there are certain defects. It is not necessary to go back and forth over the organ. One can go over the organ in random fashion until a statistically significant amount of information is obtained; after that the scanning procedure can be stopped.

L. DONATO: You state that your system is bound to be of limited clinical interest in its present form, since it is dependent on the availability of a digital computer. I should have thought that a much simpler and cheaper way of producing numerical maps would be to use a digital ratemeter and a slightly modified electrical typewriter.

H. SCHEPERS: Yes, but there would be some disadvantages. For example, one would have to move at constant speed and the pre-selection of the statistical error would not be possible. If one has a computer, it is much more convenient to put the paper tape into it so that one has the map of the scans a minute later.

L. DONATO: The trouble is that not everyone has a digital computer on hand. I am merely suggesting this simpler instrument because numerical scans are so very important. Moreover, it is possible from a numerical map obtained in this way to derive conventional maps with the help of a tape puncher and reader.

IV

STATIONARY DETECTORS

DEUX NOUVEAUX TYPES DE DÉTECTEURS POUR CAMÉRA A RAYONS X OU γ

C. KELLERSHOHN ET A. DESGREZ
DÉPARTEMENT DE BIOLOGIE, SERVICE HOSPITALIER FRÉDÉRIC JOLIOT,
ET
A. LANSIART
DÉPARTEMENT D'ÉLECTRONIQUE,
CENTRE D'ÉTUDES NUCLÉAIRES DE SACLAY, FRANCE

Abstract — Résumé — Аннотация — Resumen

TWO NEW TYPES OF DETECTOR FOR X- OR GAMMA-RAY CAMERAS. X- or γ-ray cameras consist essentially of a hole-type or grid-type lens system together with a detector. The authors propose two kinds of detector quite different from the Anger device, which so far has been the only one in practical use.

The first consists of a self-triggering spark chamber. This chamber, about 20 cm in diam. and filled with a rare gas (argon or xenon), forms a cathode and two grids. The cathode and the second grid are subjected to a potential difference of several kilovolts, somewhat lower than the breakdown voltage. The first cathode-grid space serves as an electron source under the action of the low-energy X- or γ-ray photons. The cathode can also be plated with a metal of high Z, or a crystal scintillator connected to a photocathode can be used. After suitable amplification, the sudden burst of charges due to electron multiplication in the Townsend avalanche produces a well localized spark with a delay of a fraction of a microsecond. The image is obtained with the aid of a camera whose shutter is permanently open.

The second type of detector consists of a CsI (Tl) crystal connected to the photocathode of a Thomson tube, 20 cm in diam. and with electrostatic focusing. The image on the secondary screen of this tube is transferred by an optical device to the photocathode of a tube with parallel electric and magnetic field (manufactured by the English Electric Valve Company) and serving as shutter. Some of the light entering the optical device is received by a photomultiplier, which controls the opening of the shutter tube through an amplitude selector. This arrangement makes it possible to distinguish between the light due to the signal and that due to the noise of the Thomson tube. The shutter tube is opened only by the former. Since the shutter tube remains open for only an extremely short time, the signal-noise ratio of this detector arrangement is high enough to give an image on the end screen of the shutter tube using a permanently open camera.

The paper discusses the characteristics of these two types of detector and the preliminary results obtained.

DEUX NOUVEAUX TYPES DE DÉTECTEUR POUR CAMÉRA A RAYONS X OU γ. Les caméras à rayons X ou γ sont essentiellement constituées par une optique, sténopée ou grille, associée à un détecteur. Les auteurs proposent deux types de détecteur tout à fait différents du dispositif de Anger, jusqu'ici le seul à avoir été pratiquement utilisé.

Le premier est constitué par une chambre à étincelle auto-déclenchée. Cette chambre, d'une vingtaine de centimètres de diamètre et remplie d'un gaz rare (argon ou xénon), présente une cathode et deux grilles. La cathode et la deuxième grille sont soumises à une différence de potentiel de quelques kilovolts, un peu inférieure à la tension de claquage. Le premier espace cathode-grille sert de source d'électron sous l'action des photons X ou γ de faible énergie. On peut également utiliser un placage de la cathode par un métal de Z élevé ou un cristal scintillateur associé à une photocathode. La bouffée brusque de charges due à la multiplication des électrons dans l'avalanche de Townsend déclenche, après amplification convenable, une étincelle bien localisée avec un retard d'une fraction de μs. L'image est obtenue au moyen d'un appareil photographique dont l'obturateur est ouvert en permanence.

Le second type de détecteur est constitué par un cristal de CsI(Tl) associé à la photocathode d'un tube Thomson à focalisation électrostatique de 20 cm de diamètre. L'image sur l'écran secondaire de ce tube est transférée au moyen d'un dispositif optique sur la photocathode d'un tube à champ électrique et magnétique parallèle, de la compagnie English Electric Valve, jouant le rôle d'obturateur. Une partie de la lumière pénétrant dans le dispositif optique est reçue par un photomultiplicateur qui commande l'ouverture du tube

obturateur par l'intermédiaire d'un sélecteur d'amplitude. Cet artifice permet d'effectuer la sélection entre la lumière due au signal et celle due au bruit du tube Thomson. Seule la première déclenche l'ouverture du tube obturateur. Comme la durée de cette ouverture est extrêmement courte, le rapport signal/bruit de cet ensemble détecteur est assez élevé pour obtenir une image au moyen d'un appareil photographique ouvert en permanence sur l'écran terminal du tube obturateur.

Les caractéristiques de ces deux types de détecteur et les résultats préliminaires obtenus sont discutés.

О ДВУХ НОВЫХ ТИПОВ ДЕТЕКТОРОВ ДЛЯ РЕНТГЕНОВСКИХ ИЛИ ГАММА-КАМЕР. Камеры для рентгеновских или гамма-лучей создаются главным образом на основе совмещенного с детектором стенопированного или сетчатого оптического устройства. Авторы предлагают два типа детекторов, полностью отличающихся от прибора Ангера, который до последнего времени был единственным прибором такого рода.

Первый представляет собой камеру с самовозникающей сцинтилляцией. Эта камера, 20 см в диаметре и заполненная редким газом (аргоном или ксеноном), представляет собой катод и две сетки. Катод и вторая сетка находятся под разностью потенциала в несколько киловольт, немного ниже пробойного напряжения. Первое пространство между катодом и сеткой служит источником электронов, получаемых под воздействием рентгеновских или гамма-фотонов слабой энергии. Можно также использовать наклейку на катод из металла с повышенным числом Z, либо кристаллический сцинтиллятор, совмещенный с фотокатодом. Резкий выброс зарядов в результате размножения электронов в лавине Таунсенда приводит после соответствующего усиления к четко локализованной сцинтилляции с опозданием в какую-то долю мксек. Изображение получается с помощью фотоаппарата, затвор которого открыт постоянно.

Второй тип детектора представляет собой кристалл CsJ (Tl) присоединенный к фотокатоду трубкой Томсона диаметром 20 см с электростатической фокусировкой. Изображение на вторичном экране этой трубки передается оптическим устройством на фотокатод трубки с параллельным электрическим и магнитным полем, производимой компанией "Инглиш электрик вэлв" и играющей роль обтюратора. Часть света, проникающая в оптическое устройство, принимается фотоумножителем, который дает команду к открытию трубки обтюратора с помощью амплитудного селектора. Это приспособление позволяет отделять свет от сигнала и свет от шума в трубке Томсона. Лишь первый свет вызывает открытие трубки обтюратора. Поскольку продолжительность такого открытого состояния чрезвычайно коротка, соотношение сигнал/шум такого детектора весьма завышено в целях получения изображения с помощью фотоаппарата, постоянно открытого на конечный экран трубки обтюратора.

Обсуждаются характеристики этих двух типов детектора и полученные предварительные результаты.

DOS NUEVOS TIPOS DE DETECTOR PARA CÁMARAS DE RAYOS X O GAMMA. Las cámaras de rayos X o γ están constituidas esencialmente por un dispositivo óptico, consistente en un orificio o una rejilla, asociado a un detector. Los autores proponen dos tipos de detector completamente distintos del dispositivo de Anger, que hasta ahora es el único utilizado en la práctica.

El primero consiste en una cámara de chispa autodisparada, de unos 20 cm de diámetro, llena de un gas noble (argón o xenón). Contiene un cátodo y dos rejillas. Entre el cátodo y la segunda rejilla hay una diferencia de potencial de varios kilovoltios, algo inferior a la tensión de descarga. Bajo la acción de los fotones X o γ de poca energía, el primer espacio cátodo-rejilla sirve de fuente de electrones. Se puede también utilizar un cátodo contraplacado con un metal de elevado número atómico o un cristal centelleador asociado a un fotocátodo. Convenientemente amplificado, el incremento brusco de las cargas debido a la multiplicación de los electrones en la avalancha de Townsend provoca con un retardo de una fracción de microsegundo una chispa bien localizada. La imagen se obtiene por medio de un aparato fotográfico cuyo obturador permanece constantemente abierto.

El segundo tipo de detector consiste en un cristal de CsI (Tl) asociado al fotocátodo de un tubo de Thomson de enfoque electrostático, de 20 cm de diámetro. La imagen que aparece en la pantalla secundaria de este tubo es transferida por un dispositivo óptico al fotocátodo de un tubo de campos eléctrico y magnético paralelos, de la English Electric Valve, que actúa como obturador. Una parte de la luz que penetra en el dispositivo óptico es recibida por un fotomultiplicador que rige la apertura del tubo obturador por mediación de un selector de amplitudes. Este artificio permite efectuar la selección entre la luz debida a la señal y la debida al ruido

del tubo de Thomson. Sólo la primera ocasiona la apertura del tubo obturador. Como la duración de dicha apertura es sumamente corta, el cociente señal/ruido de este conjunto detector es suficientemente alto para obtener una imagen de la pantalla terminal del tubo obturador por medio de un aparato fotográfico abierto constantemente.

En la memoria se discuten las características de esos dos tipos de detector y los primeros resultados obtenidos.

INTRODUCTION

Depuis que, en 1951, CASSEN et al. [1] ainsi que MAYNEORD et al. [2] ont préconisé l'utilisation de détecteurs à scintillation convenablement collimés associés à un dispositif de balayage pour visualiser in vivo la distribution de la radioactivité dans un organe, cette technique a fait l'objet de développements considérables et, sous des vocables divers tels que «scintigraphie» ou «gammagraphie», est devenue d'usage courant pour l'investigation morphologique ou fonctionnelle de divers organes. Malgré cela elle est entachée d'un réel défaut: au cours de la constitution de l'«image» la majeure partie des informations utilisables données par l'«objet» est perdue [3]. En effet, les informations issues d'un point de l'objet ne sont reçues par le détecteur mobile que durant une faible fraction du «temps de pose», celle où le point considéré se trouve dans le champ du collimateur associé. D'autre part, les dispositifs à balayage ne permettent pas l'utilisation de radioisotopes de demi-vie petite par rapport au temps de pose. Aussi la réalisation de dispositifs stationnaires était elle désirable.

Deux voies furent suivies. L'une adoptée par ANGER [4] et dérivant d'une observation de Röntgen lui-même, consistait suivant le principe de la chambre noire, à réaliser, au moyen d'un sténopée dans une paroi en métal lourd, une image de l'objet sur un grand cristal plat d'iodure de sodium associé à un film photographique («pinhole camera»). Malgré son intérêt de principe, un tel dispositif était beaucoup trop peu sensible pour être utilisable in vivo. L'autre, adoptée par SKANSE et JOHANNSSON [5] KELLERSHOHN et PELLERIN [6, 7, 8] ainsi que FUCKS et KNIPPING [9] utilisait une dispositif multicollimateur constitué par une grille de plomb présentant une série de canaux cylindriques régulièrement espacés. Le détecteur était alors composé d'un film photographique associé soit à un grand cristal plat d'iodure de sodium [5], soit à un écran renforçateur pour rayons X à haut voltage [6], soit enfin à un réseau de petits cristaux d'iodure de sodium à raison de un cristal à l'extrémité de chaque canal collimateur [7, 8]. Dans un des travaux précités [9] le détecteur était constitué par une mosaïque de petits compteurs Geiger, un en bout de chaque canal de la grille et provoquant l'allumage d'une petite lampe faisant elle même partie d'une mosaïque homologue de celle des compteurs. Quoique plus «rapides» que la caméra sténopéique ces dispositifs à grille multicollimatrice ne permettaient pas encore des temps de pose assez courts pour l'usage in vivo, par suite de l'insuffisante sensibilité des détecteurs employés.

C'est le grand mérite de ANGER [10] d'avoir montré que l'association d'un nombre réduit de photomultiplicateurs couplés optiquement à un grand cristal d'iodure de sodium et d'un système électronique convenable permettait d'établir une correspondance spatiale entre la position d'un flash

lumineux dans le cristal dû à l'interaction d'un photon γ et la position du spot sur un écran d'oscillographe cathodique. Un tel dispositif représente un détecteur très sensible puisque à tout point de l'objet émettant un photon γ «effectif» il fait correspondre spatialement un point lumineux visible. Utilisé avec un sténopée ou une grille collimatrice, ce détecteur permet la réalisation de caméras pratiquement utilisables pour la visualisation d'un organe in vivo avec tous les avantages liés à un dispositif de détection stationnaire. Parallèlement aux derniers travaux américains [11], des caméras à scintillation ont également été réalisées en Angleterre par MALLARD et MYERS [12] et, en France, au Département d'électronique du Commissariat à l'énergie atomique par MORICHÈRE [13]. Malgré son ingéniosité le dispositif détecteur de ANGER n'est pas sans quelques inconvénients: complexité, nécessité de recalibrer fréquemment les nombreux photomultiplicateurs et défaut de linéarité dans la correspondance spatiale entre la position du spot sur l'écran d'oscillographe. BENDER et BLAU [14] ont résolu ce dernier problème en proposant comme détecteur une matrice de petits cristaux d'iodure de sodium, chacun correspondant à un canal d'une grille multicollimatrice [7, 8], et tels que ceux de chaque ligne et de chaque colonne de la matrice soient couplés par une optique fibrée à un photomultiplicateur distinct. Malgré son élégance cette solution doit rester assez encombrante et onéreuse par suite du prix élevé des optiques fibrées et du nombre de photomultiplicateurs utilisés (35 dans le dispositif cité, correspondant à 293 cristaux répartis en 20 lignes et 15 colonnes). D'autre part, si la correspondance spatiale entre la matrice de cristaux et l'écran de l'oscillographe est linéaire, elle est également, par structure, discontinue. Une alternative séduisante à la réalisation d'une correspondance linéaire entre le ou les cristaux d'iodure de sodium et le plan de l'image définitive est d'utiliser pour cela un tube amplificateur d'image. Un tel dispositif a été proposé il y a une dizaine d'années associé à un sténopée par ANGER et al. [15] et à une grille multicollimatrice par KELLERSHOHN et PELLERIN [16]. Malheureusement à cette époque les tubes amplificateurs d'image étaient affectés d'un bruit de fond beaucoup trop élevé pour permettre la réalisation d'«images» d'une collection radioactive in vivo chez l'homme. Par suite des progrès réalisés dans ce domaine, TER-POGOSSIAN et al. [17] ont montré récemment qu'en utilisant le rayonnement de faible énergie particulièrement favorable de l'iode 125 il était possible, en associant une grille d'argent à paroi mince et un amplificateur d'image commercial, d'obtenir des images de thyroïde de meilleure qualité et en un temps de pose plus court que celles données par un scintigraphe classique.

Le but du présent travail est d'exposer le principe de deux types très différents de détecteurs susceptibles d'être associés à un sténopée ou une grille multicollimatrice et les résultats préliminaires obtenus. Le premier consiste en un amplificateur électronique d'images dont le bruit de fond est réduit au moyen d'une technique de coïncidences. Le second, qui à notre connaissance, n'a jamais été employé pour la visualisation d'une collection radioactive in vivo est essentiellement constitué par une chambre à étincelle fonctionnant dans des conditions convenables.

DÉTECTION PAR AMPLIFICATEUR D'IMAGE

La réalisation de ce dispositif n'est pas encore assez avancée pour nous avoir permis de réaliser des images. Nous ne ferons donc ici que décrire son principe et donner certains résultats préliminaires qui laissent augurer favorablement de son fonctionnement effectif.

1. *Principe*

L'«optique» étant indifféremment une grille ou une sténopée, le détecteur est constitué par un cristal d'iodure de césium activé au thalium de 20 cm de diamètre et 3 mm d'épaisseur convenablement taillé pour être couplé optiquement à la photocathode d'un tube amplificateur d'image type TH 9421 de la Compagnie française Thomson-Houston dont l'écran primaire a été supprimé et remplacé par une simple photocathode. L'écran secondaire de ce tube amplificateur est optiquement conjugué, au moyen d'un objectif double ouvert à F/2,5 et de distance focale F = 100 mm, avec l'entrée d'un tube obturateur à champs électrique et magnétique parallèles de la Compagnie English Electric Valve. Une impulsion d'une durée de 100 ns suffit pour commander l'ouverture de ce tube qui peut ainsi être ouvert un grand nombre de fois par seconde. Ces impulsions de commande sont fournies par une électronique convenable associée à un sélecteur d'amplitude qui est lui-même déclenché par les impulsions d'un petit photomultiplicateur 152 AVP de la Radiotechnique dont la photocathode a 14 mm de diamètre et qui «voit» latéralement la lumière issue de l'écran secondaire du tube amplificateur. Si on admet que cette lumière est moins intense quand elle a pour origine le bruit de fond du tube amplificateur que lorsqu'elle est due à l'action des photons γ d'une source radioactive sur le cristal d'iodure de césium de la face d'entrée, il doit être possible par un réglage convenable du sélecteur d'amplitude de faire en sorte que le tube obturateur ne laisse essentiellement passer que la lumière engendrée par un photon issu de la source radioactive. Comme nous l'avons vu plus haut la largeur de l'impulsion nécessaire à l'ouverture du tube étant faible la majeure partie de la lumière engendrée par le bruit de fond du tube amplificateur peut être ainsi éliminée. L'entrée et la sortie du tube obturateur étant conjuguée, l'image définitive sera obtenue sur le film d'un appareil photographique dont l'obturateur est ouvert durant le temps de pose nécessaire et qui est mis au point sur l'image de sortie.

Nous espérons que ce dispositif à rapport signal/bruit de fond élevé, associé à un sténopée ou une grille multicollimatrice sera d'une grande sensibilité et permettra de réaliser l'image de la distribution d'une faible radioactivité dans un organe. Les résultats préliminaires autorisant un tel espoir portent sur les points suivants.

2. *Gain de lumière du tube amplificateur*

Un petit cristal d'iodure de césium activé au thalium de 30 mm de diamètre et 3 mm d'épaisseur, mis en contact optique avec la région centrale de la photocathode du tube est soumis à l'action d'une source radioactive (mélange de ^{197}Hg et ^{203}Hg, ou ^{137}Cs). Un spectre à scintillation est alors

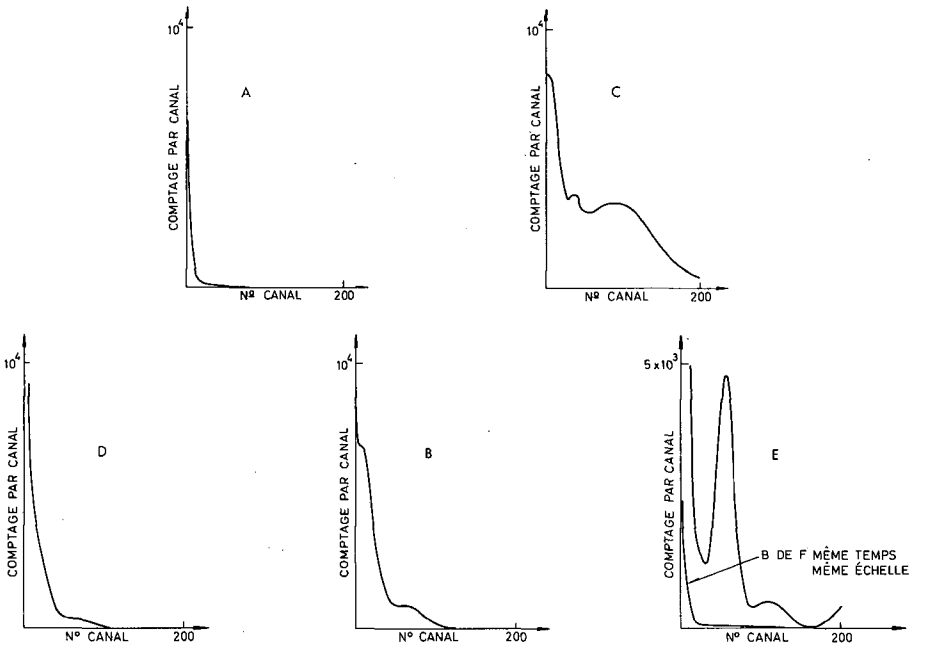

Figure 1

Répartition en amplitude des impulsions données par un photomultiplicateur situé derrière le tube amplificateur d'image sous différentes conditions (voir le texte et la figure 2).

Spectre A

Spectre obtenu avec les photomultiplicateurs PM_1 et PM_2 montés en coïncidence, mais sans source radioactive.

Tube alimenté avec scintillateur
(Bruit de fond du tube)
Tube: THT 25 kV
Scintillateur: CsI(Tl), $\phi = 30$ mm, $e = 3$ mm
PM: 150 AVP, HT = 1500 V, G = 100
PM: 152 AVP, HT = 1650 V, G = 400
Gamme: 4 V / 200 canaux
Rendement coïncidence: 75%.

Spectre B

Spectre obtenu avec les photomultiplicateurs PM_1 et PM_2 montés en coïncidence avec une source radioactive de ^{197}Hg.

Tube alimenté avec scintillateur
Temps de comptage: 6 min
Tube: THT kV
Scintillateur: CsI(Tl), $\phi = 30$ mm, $e = 3$ mm
PM: 150 AVP, HT = 1500 V, G = 400
Gamme 4V/200 canaux
Rendement coïncidence: 75%.

Spectre C

Spectre obtenu à partir du seul photomultiplicateur PM_1
avec une source de ^{197}Hg
(Vu par le PM situé de côté derrière l'écran du tube).

Tube: THT 25 kV
Scintillateur: CsI(Tl), $\phi = 30$ mm, e = 3 mm
PM 152 AVP : HT = 1650 V, G = 400
Gamme 4V/200 canaux.

Spectre D

Spectre obtenu à partir du seul photomultiplicateur PM_2
avec une source de ^{197}Hg
(PM derrière l'objectif F/2, 5, 100 mm).

Tube alimenté avec scintillateur
Tube: THT 25 kV
Scintillateur: Cs(Tl) $\phi = 30$ mm, e = 3 mm
PM 150 AVP : HT = 1500 V, G = 100
Gamme 4V/canaux.

Spectre E

Spectre obtenu sans optique avec le seul photomultiplicateur PM_2
dont la fenêtre est disposée au contact de la partie postérieure du tube amplificateur
en présence d'une source constituée par un mélange de ^{197}Hg et ^{205}Hg.

PM collé sur l'écran du tube
Tube alimenté avec scintillateur
Temps de comptage: 6 min
Tube THT 25 kV
Scintillateur: CsI(Tl), $\phi = 30$ mm, e = 3 mm
PM 150 AVP, HT = 1500 V, G = 62
Gamme 4V/200 canaux.

enregistré au moyen d'un photomultiplicateur type 150 AVP de La Radiotechnique dont la fenêtre (diamètre utile: 32 mm) est disposée au contact même de la partie postérieure du tube à la distance de l'écran secondaire la plus petite possible qui est de 6 mm. Le spectre E de la figure 1 montre le résultat obtenu pour un mélange de ^{197}Hg et ^{203}Hg où les pics photoélectriques du mercure 197 sont visibles ainsi que le début du pic photoélectrique à 279 keV du mercure 203.

Les rapports de la source et du petit cristal de CsI(Tl) étant inchangés, le tube amplificateur est enlevé et la fenêtre du photomultiplicateur est placée à 6 mm du cristal. Un deuxième spectre est enregistré. Le rapport des amplitudes d'impulsion correspondant au même photopic pour le premier et le deuxième spectre donne le rapport des quantités de lumière fournies par l'écran secondaire du tube amplificateur et par le cristal d'iodure de césium telles qu'elles sont mesurées par le même photomultiplicateur avec la même géométrie. Ce rapport peut donc être considéré comme une mesure du gain de lumière du tube amplificateur dû à la seule accélération des électrons dans le tube, à l'exclusion du gain en luminance dû à la réduction de l'image sur l'écran secondaire et qui n'intervient pas dans notre problème. En utilisant différents pics de ^{197}Hg, de ^{203}Hg et de ^{137}Cs, ce rapport est trouvé égal à 14.

3. *Transparence de l'optique*

Dans un premier temps, la moitié de l'optique de couplage est mise en contact par sa face de sortie avec la fenêtre d'un photomultiplicateur 150 AVP et son foyer objet disposé dans le plan de l'écran secondaire du tube amplificateur (fig. 2). Un spectre à scintillation de la source $^{197}Hg + ^{203}Hg$

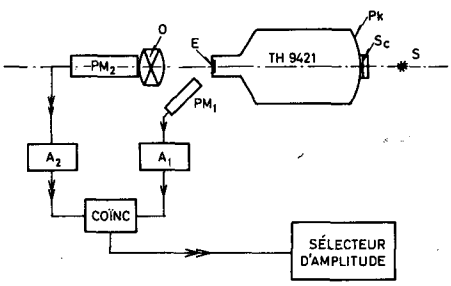

Figure 2

Schéma du montage destiné à vérifier la possibilité de discriminer les flashes lumineux de l'écran secondaire du tube amplificateur provenant du bruit de fond de ceux provenant d'une source radioactive.

S: source de ^{197}Hg
Sc: scintillateur CsI(Tl), $\phi = 30$ mm, $e = 3$ mm
TH 9421: tube amplificateur de brillance
Pk: photocathode S20
E: écran P16
O: objectif F/2,5, f: 100 mm
PM_1: photomultiplicateur 152 AVP, $\phi = 14$ mm
PM_2: photomultiplicateur 150 AVP, $\phi = 32$ mm
A_1 et A_2: amplificateurs
C: circuit de coïncidences
S: sélecteur d'amplitude.

est alors enregistré. Dans un deuxième temps l'optique est enlevée et la fenêtre du photomultiplicateur disposée à 100 mm de l'écran secondaire. Un deuxième spectre est enregistré. Le rapport des amplitudes d'impulsion correspondant à une même raie γ entre le premier et le deuxième spectre est considéré comme représentant la transparence de l'optique. Ce rapport est égal à 0.28.

L'absorption relativement importante s'explique par la répartition spectrale de l'énergie émise par les spots lumineux de l'écran secondaire P16 et la courbe de sensibilité du photomultiplicateur. Néanmoins cette valeur de la transparence reste suffisamment élevée pour que la perte de lumière soit acceptable et ne compromette pas les possibilités de fonctionnement du dispositif. Notons que la transparence de la deuxième moitié de l'optique est beaucoup plus élevée par suite du filtrage de la lumière dû à la première moitié.

4. Comparaison de l'intensité des flashes lumineux donnés par le tube amplificateur et dus respectivement à une source radioactive et au bruit de fond

Le montage utilisé pour cette étude est représenté schématiquement sur la figure 2 et photographiquement sur la figure 3. Le photomultiplicateur PM 1 (150 AVP) est disposé latéralement par rapport à l'écran secon-

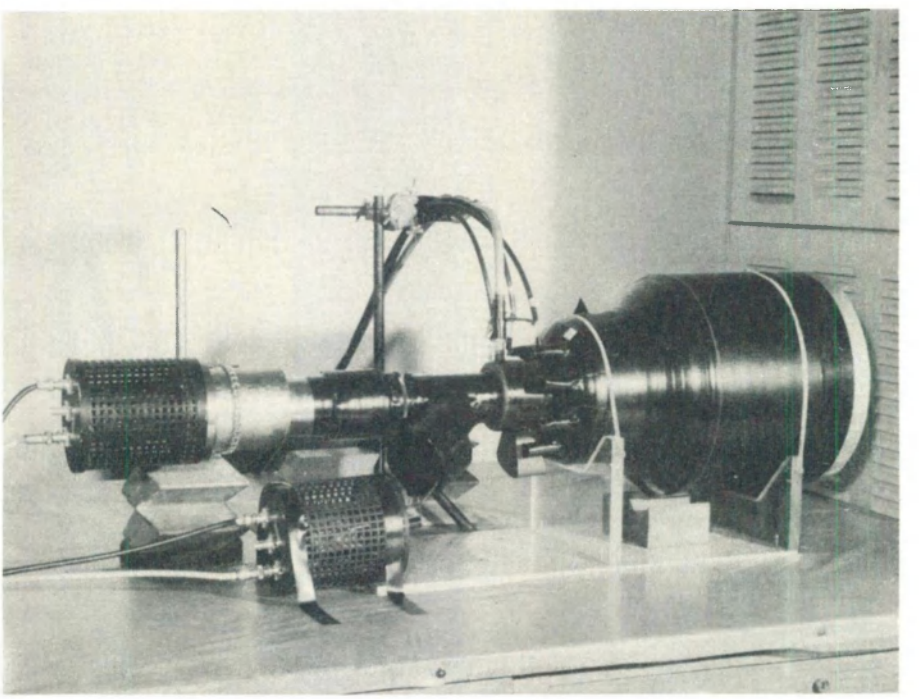

Figure 3

Photographie du montage correspondant au schéma de la figure 2.

daire du tube amplificateur comme cela a été décrit au premier paragraphe Son encombrement est suffisamment réduit pour qu'il ne porte pas ombre au faisceau lumineux principal défini par l'écran secondaire et la face antérieure de l'objectif. Les deux photomultiplicateurs sont associés à l'électronique d'un spectromètre à scintillation en coïncidence.

Le seuil des discriminateurs attenant à chacun des photomultiplicateurs étant réglé au niveau le plus bas, le spectre A de la figure 1 représente un enregistrement effectué sous la source radioactive S. Comme le bruit de fond propre du photomultiplicateur PM_2 est éliminé par le dispositif en coïncidence ce spectre représente la distribution des intensités lumineuses des flashes correspondant au bruit de fond du tube amplificateur. Le spectre E de la figure 1 est enregistré dans les mêmes conditions que le spectre A, à l'exception de la présence d'une source radioactive S de ^{197}Hg. La présence sur ce dernier spectre du pic photoélectrique correspondant à la raie

X à 68 keV de ^{197}Au et à la raie de transition γ à 77 keV de ^{197}Hg est manifeste. On peut obtenir de façon très précise ce pic en effectuant la différence des spectres B et A. Cette expérience montre que le principe sur lequel le dispositif détecteur envisagé est basé, à savoir: la discrimination des flashes lumineux donnés par le tube amplificateur et dus respectivement au bruit de fond et à une source radioactive émettrice de photons γ d'énergie relativement faible, est pratiquement applicable. La comparaison des spectres A et E montre qu'une élévation convenable du niveau de discrimination correspondant au photomultiplicateur PM_1 peut permettre une suppression quasi complète des flashes dus au bruit de fond en conservant la majeure partie de ceux dus à la source de ^{197}Hg, ce résultat étant obtenu par la commande de l'ouverture du tube obturateur par les impulsions de PM_1.

Le spectre C de la figure 1 correspond à la distribution des amplitudes d'impulsion du photomultiplicateur PM_1. Le spectre D de la même figure correspond à la distribution des amplitudes d'impulsion donnée par PM_2 en présence de la source de ^{197}Hg, mais sans mise en œuvre du dispositif de coïncidence avec PM_1. On voit que le spectre correspondant à la source est complètement noyé dans le bruit de fond propre du photomultiplicateur PM_2.

Les expériences mettant en jeu le tube obturateur sont en cours de réalisation, nous estimons que les résultats préliminaires que nous venons d'exposer sont suffisamment encourageants pour autoriser l'espoir de leur réussite.

DÉTECTION PAR CHAMBRE A ÉTINCELLE

La possibilité d'utiliser une chambre à étincelle comme détecteur pour la visualisation d'une source radioactive a été récemment envisagée par LANSIART et LELOUP [18]. Ces auteurs ont réalisé une chambre à étincelle autodéclenchée qui leur a permis d'obtenir les images de sources émettrices β en utilisant une grille multicollimatrice. Le but du présent travail est de décrire une chambre à étincelle dérivée de ce premier modèle, mais adaptée à la réalisation d'images au moyen de photons X ou γ, de présenter certains faits nouveaux intéressants concernant le déclenchement de l'étincelle et de donner les résultats obtenus ainsi que les perspectives d'avenir.

1. *Chambre à étincelle en régime autodéclenché*

a) Description et principe.

La figure 4 représente un schéma de la chambre réalisée, schéma dont l'échelle est donnée par la hauteur commune des rectangles symbolisant les différents matériaux employés qui correspond à 1 cm. Elle est constituée par un manchon cylindrique de verre fermé à son extrémité inférieure par une lame de mylar de 0,5 mm d'épaisseur et à son extrémité supérieure par une glace transparente de 1 cm d'épaisseur. La lame de mylar et la glace sont accolées au cylindre de verre par un joint d'indium. La rigidité

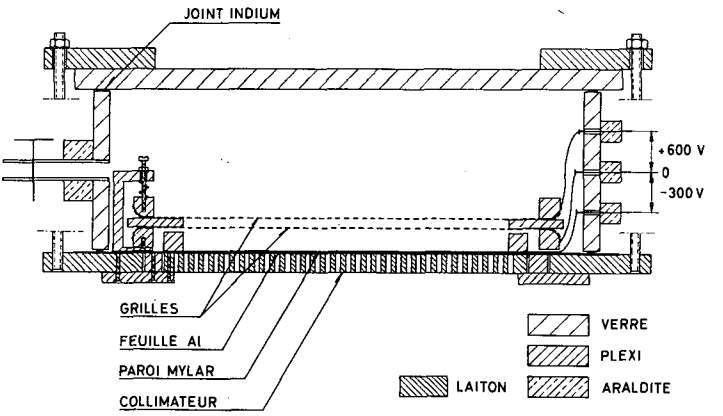

Figure 4

Schéma de la chambre à étincelle (légende dans le texte)

et l'étanchéité de l'ensemble sont assurées par deux rondelles de laiton reliées entre elles par des écrous de serrage permettant la compression de la glace et de la lame de mylar sur le cylindre. L'entrée et la sortie du gaz sont effectuées au moyen d'un robinet à joint d'araldite situé sur la face latérale du manchon. La liaison des électrodes avec l'extérieur est assurée par trois prises à joint d'araldite également disposées sur la face latérale du manchon. Tout cet ensemble est visible sur la photographie de la figure 5. Une grille collimatrice, de 1 cm d'épaisseur, solidaire de la chambre et constituée par un réseau régulier de canaux cylindriques de 2 mm de diamètre dont les axes sont distants de 4 mm est disposée immédiatement au dessous de la fenêtre de mylar.

Les électrodes sont au nombre de 3. Une cathode, constituée par une feuille d'aluminium de 20 μ d'épaisseur déposée sur la feuille de mylar. A une distance de 1 cm au dessus de cette cathode est disposée une grille réalisée au moyen de fils de bronze phosphoreux de 35 μ de diamètre délimitant un réseau de carrés de 40 μ de côté. Enfin, une anode constituée par une deuxième grille identique à la précédente est située à 5 mm au dessus de celle-ci. La rigidité et le parallélisme de ces trois électrodes sont assurés au moyen d'un bâti intérieur en plexiglas. L'espace situé entre la première grille et la grille anode où se produisent les étincelles est parfaitement défini au moyen d'une rondelle de plexiglas de 5 mm d'épaisseur et de 16 cm de diamètre intérieur. Cette dernière dimension représente donc le diamètre utile de la chambre. Celle-ci est remplie à la pression de 1 atm avec le mélange classique pour compteur, argon 90% - méthane 10%.

La cathode et l'anode sont reliées par l'intermédiaire d'une résistance de 100 MΩ à une haute tension continue telle qu'elles soient respectivement au potentiel -300 V et $+6000$ V quand la grille intermédiaire est au potentiel 0. Les électrons créés au niveau de la cathode et du gaz de l'espace cathode-grille par une partie des photons qui ont traversé le collimateur sont accélérés par la différence de potentiel de 300 V régnant entre ces électrodes, traversent en partie la grille et donnent naissance à une avalanche de

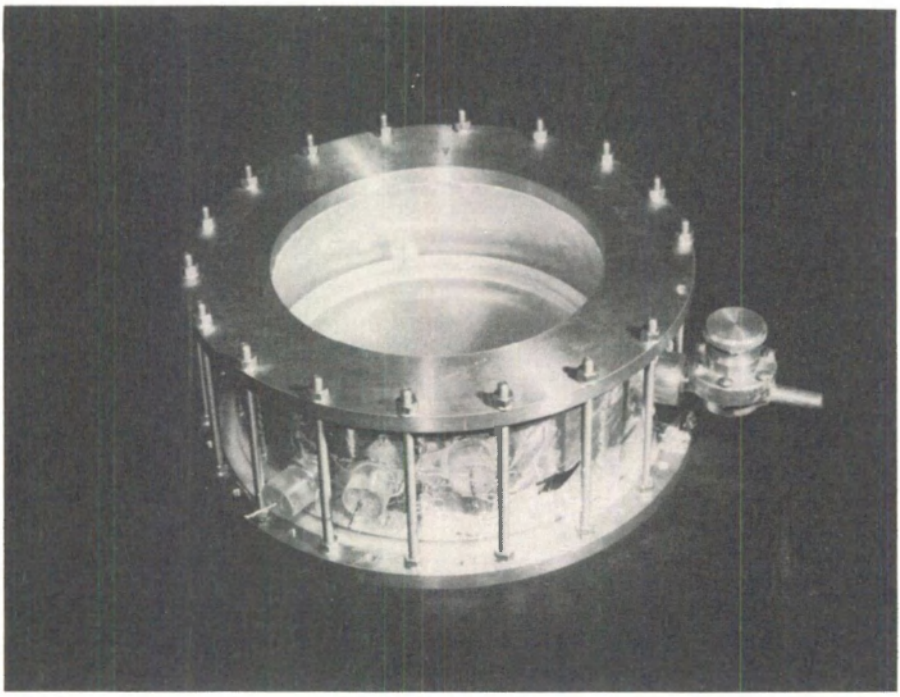

Figure 5

Photographie de la chambre à étincelle (légende dans le texte)

Townsend dans l'espace grille-anode sous l'action du champ électrique intense qui y règne. Eu égard à la géométrie des électrodes, la nature et la pression du gaz employé, la haute tension appliquée est inférieure de 100 à 150 V à la tension de claquage. Il ne se produit donc pas d'étincelle mais l'avalanche de Townsend provoque une impulsion négative sur l'anode dont l'amplitude minima correspond à une bouffée de charge de 85 000 charges élémentaires dans les conditions de fonctionnement décrites. Cette impulsion est amplifiée par un amplificateur à grand gain (10^4) puis traverse une porte après avoir déclenché un univibrateur qui bloque cette porte pendant la durée du temps mort de la chambre fonctionnant comme détecteur. Après avoir franchi la porte elle commande un générateur d'impulsion de haute tension qui délivre sur la grille une impulsion négative de 3 kV déclenchant l'étincelle dans l'espace grille-anode. Le temps qui sépare l'avalanche de Townsend de l'étincelle est inférieur à 0,5 ms et l'expérience montre alors qu'elle s'effectue au niveau de la trajectoire des ions créés par l'avalanche avec une bonne localisation par rapport à l'impact du photon initial.

b) Résultats

Eu égard au faible pouvoir absorbant pour les photons γ de l'ensemble cathode gaz dans le cas du montage que nous venons de décrire les expériences ont été effectuées avec le radioisotope le plus favorable qui soit

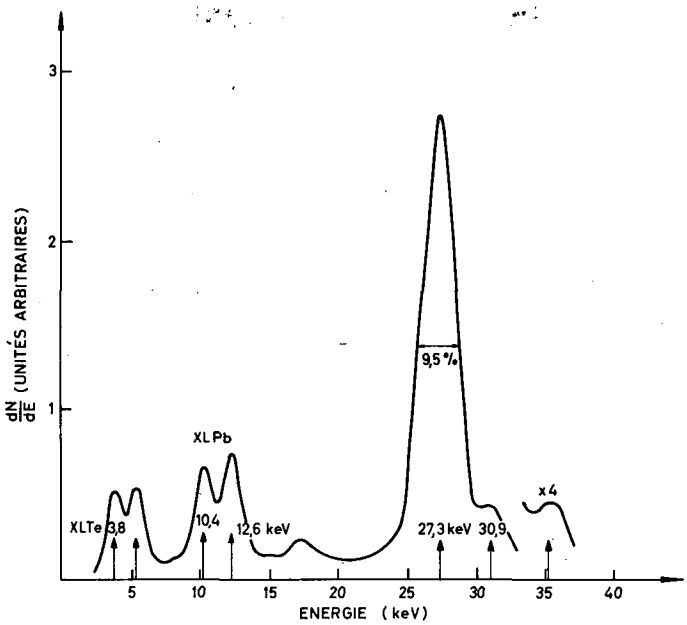

Figure 6

Spectre de l'iode 125 observé derrière la grille de collimation au moyen d'un compteur proportionnel de grand diamètre au xénon-méthane.

Gaz: xénon-méthane (850 mm Hg)
Fenêtre en béryllium de: 1 mm
Source: ^{125}I
Collimateur en Pb.

utilisé en pratique: l'iode 125. La figure 6 représente un spectre de ce radioélément obtenu avec un compteur proportionnel de grand diamètre au xénon-méthane. Ce spectre a été effectué dans les conditions même de réalisation d'une image en remplaçant la chambre à étincelle par le compteur proportionnel, afin d'avoir une idée précise du rayonnement réel que reçoit le détecteur. On distingue les raies L du tellure, les raies L du plomb dues à l'interaction des photons émis par la source avec la grille collimatrice, le mélange des raies $K\alpha_1$ et $K\alpha_2$ du tellure, d'énergie moyenne 27,3 keV, la raie $K\beta$ à 30,9 keV et ce qui reste après conversion de la raie de transition γ à 35 keV. On voit que le rayonnement émis est constitué en majeure partie par les photons XK du tellure à 27,3 keV, photons qui sont suffisamment pénétrants à travers les tissus pour permettre la réalisation d'une image de thyroïde in vivo et suffisamment mous pour subir une absorption appréciable dans le type de détecteur envisagé ici. L'image définitive s'effectue sur le film d'un appareil photographique mis au point sur le milieu de l'espace grille-anode (espace étincelle).

L'image d'une source plane ayant la forme d'un triangle équilatéral a été obtenue avec les caractéristiques suivantes:

Radioactivité totale de chaque source: 400 μc.
Densité radioactive superficielle: 100 $\mu c/cm^2$.

(a)

(b)

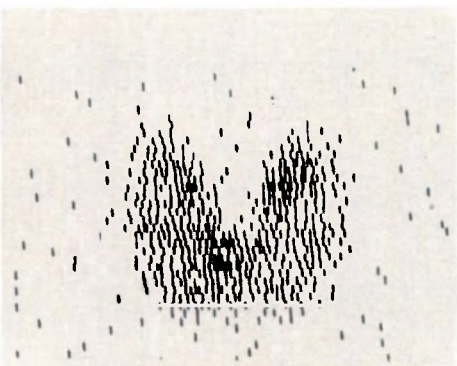

(c)

Figure 7

Comparaisons des images d'un fantôme plan de glande thyroïde données par la chambre à étincelles et par un scintigraphe.

a) Distance de la source à la grille collimatrice: 3 cm
Ouverture de l'objectif: f/16
Temps de pose. 15 min.

b) Distance de la source à la grille collimatrice: 3 cm
Ouverture de l'objectif: f/11
Temps de pose: 15 min.

c) Par suite de l'importance de la radioactivité de la source, le rayonnement a été atténué par 0.3 mm de Crysocal.
Vitesse de balayage: 400 mm/min
Précompte: 18
Collimateur cylindrique: diamètre: 1,2 cm
hauteur: 6,5 cm.
La largeur de la bande spectrométrique encadre le pic photoélectrique à 27,3 keV de ^{125}I.

Distance source-grille collimatrice: 1,4 cm.
Ouverture de l'objectif photographique: f/16.
Temps de pose: 5 min.

La définition des bords du triangle constituant la source était très bonne.

Les figures 7a, b et c correspondent à deux images données par la chambre à étincelle autodéclenchée et au scintigramme d'un même fantôme plan de thyroïde contenant 1800 μc de ^{125}I avec une densité superficielle de 100 μc/cm^2.

Les images de ce fantôme de thyroïde données par le dispositif décrit sont tout à fait encourageantes et peuvent même être qualifiées de bonnes. La comparaison des figures 7b et 7c est particulièrement frappante à cet égard. L'hétérogénéité du fantôme se retrouve de façon parfaitement homologue sur le scintigramme et l'image donné par la chambre à étincelle, la définition de cette dernière semblant d'ailleurs nettement meilleure. Ces premiers résultats très encourageants sont limités dans leur intérêt par la radioactivité beaucoup trop élevée de la source. La radioactivité du fantôme de thyroïde utilisé est 20 fois plus élevée que la radioactivité maxima permise chez un homme adulte pour un examen avec ^{125}I. Nous allons voir que de petites modifications de réglage nous ont amenés à découvrir un mode de fonctionnement tout à fait différent et inattendu de la chambre se traduisant par une sensibilité et simplicité du montage largement accrues.

2. *Chambre à étincelle en régime continu*

a) Fonctionnement

Les chambres à étincelle fonctionnent habituellement par application d'une impulsion de haute tension extérieure, que celle-ci soit provoquée par le passage des particules ionisantes dans la chambre comme dans l'exemple précédent où appliquée indépendamment comme dans le cas du fonctionnement d'une chambre à étincelle en régime pulsé. Or nous avons constaté, les autres conditions restant les mêmes, que en diminuant la tension cathode-grille de -300 à -100 V l'étincelle pouvait être déclenchée par la seule avalanche de Townsend sans l'intervention d'une impulsion de haute tension extérieure. Ce fait est remarquable car il permet d'envisager la réalisation d'images par la chambre sans l'intervention d'une électronique associée et de réaliser un appareillage d'une particulière simplicité. Nous avons accolé l'épithète de «continu» à ce régime de fonctionnement car en dehors des périodes de paralysie, la chambre est continuellement prête à donner une étincelle sous l'action d'un photon sans que celle-ci ait à coïncider avec l'application d'une impulsion de haute tension extérieure.

Nous n'avons pas d'idée précise sur le mécanisme de ce régime de fonctionnement. On peut admettre que l'étincelle est déclenchée par l'arrivée d'un nombre d'électrons dans l'espace étincelle (grille-anode) supérieure à une valeur minima. Quand une tension de - 300 V est appliquée à l'espace détecteur (grille-cathode) une part importante des électrons produits dans celui-ci est captée par la grille par suite du champ électrique élevé et le nombre d'électrons pénétrant dans l'espace étincelle est inférieur à la valeur minima: l'étincelle ne se produit pas. En abaissant la tension appliquée à l'espace détecteur de - 300 à - 100 V, la captation des électrons

par la grille diminue par suite de la diminution du champ et le nombre d'électrons pénétrant dans l'espace étincelle devient supérieure à la valeur minima: l'étincelle se produit. On peut donner un ordre de grandeur de cette valeur minima. Dans le cas des photons à 27,3 keV de ^{125}I chaque photoélectron produit dans le gaz considéré environ 1000 rayons δ. Eu égard à la valeur du champ électrique et à la géométrie des électrodes la dispersion de leur temps d'arrivée sur la grille est de l'ordre de 10 μs. D'autre part, le déclenchement de l'étincelle se produit environ 100 ns après le début de l'impulsion provoquée par le mouvement des charges. On déduit de ces données approximatives un ordre de grandeur d'une dizaine d'électrons comme valeur minima du nombre d'électrons qui doivent traverser la grille et pénétrer dans l'espace étincelle pour obtenir le déclenchement dans les conditions expérimentales décrites.

b) Rendement

Pour les photons à 27,3 keV de ^{125}I les rendements théoriques d'absorption dans les différentes régions de la chambre sont respectivement de l'ordre de 0,64% dans l'espace détecteur, de 0,2% au niveau de la cathode d'aluminium et de 0,2% dans l'espace étincelle. Le rendement théorique total est donc de l'ordre de 1%.

Le rapport entre le nombre d'étincelles déclenchées et le nombre de photons absorbés dépend bien entendu du temps mort de la chambre. Ce dernier dépend lui-même de la constante de temps du circuit de décharge, donc des résistances R d'anode et de cathode. Pour la valeur de 100 MΩ utilisée dans le dispositif autodéclenché, ce temps mort est de l'ordre de 200 ms. Le débit d'étincelles maximum est alors de 5/s. Ce taux n'est d'ailleurs atteint que pour des sources suffisamment actives par suite du caractère statistique de l'émission et de l'absorption des photons. Les résultats expérimentaux suivants obtenus avec la source triangulaire déjà décrite illustrent la variation du temps mort avec la résistance du circuit de décharge (fig. 8).

Dans le cas de la dernière expérience l'image obtenue était aussi bonne que celle de la figure 8 avec une radioactivité dix fois plus faible. D'autre part pour 5 = 20 MΩ le temps mort doit être très inférieur à 200 ms. Il s'ensuit que le nombre trouvé de 5 étincelles/s doit correspondre à un faible taux de perte dû au temps mort. Un calcul approximatif montre que pour cette source de 40 μc le nombre de photons incidant sur la chambre est d'environ 600 par seconde ce qui donne un rendement de $5/600 \simeq 1\%$ qui s'accorde bien avec les précisions théoriques précises plus haut.

En définitive en prenant une résistance de charge d'anode et de cathode la plus petite possible et en utilisant une source dont la radioactivité n'est pas trop élevée, le rendement pour les photons de l'iode 125 est de l'ordre de 1 étincelle pour 100 photons. Dans ces conditions il est possible d'obtenir une bonne image de thyroïde chargée à 50 μc de ^{125}I en quelques minutes de pose (fig. 9a et 9b).

Le dispositif paraît donc, sous sa forme actuelle, déjà supérieur au scintigraphe classique pour l'iode 125.

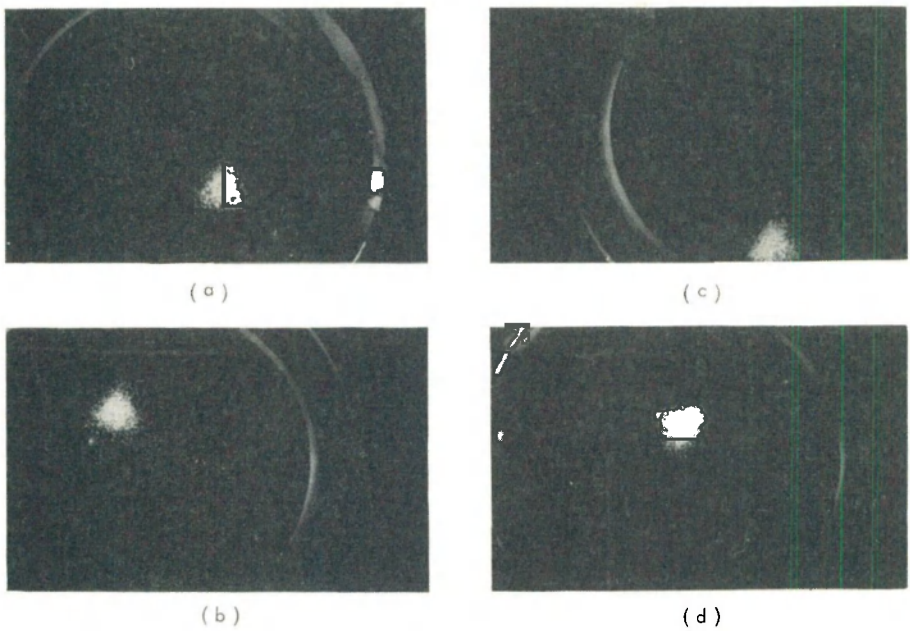

Figure 8

Influence de la résistance du circuit de décharge sur le temps mort de la chambre et le nombre maximum d'étincelles par unité de temps.

a) 1ère expérience:
Radioactivité: 400 μc
Résistance: 100 MΩ
Temps de pose: 5 min
Nombre d'étincelles/s: 5.

b) 2ème expérience:
Radioactivité: 400 μc
Résistance: 50 MΩ
Temps de pose: 2 min
Nombre d'étincelles/s: 12.

c) 3ème expérience:
Radioactivité: 400 μc
Résistance: 20 MΩ
Temps de pose: 3 min
Nombre d'étincelles/s: 20.

d) 4ème expérience:
Radioactivité: 40 μc
Résistance: 20 MΩ
Temps de pose: 3 min
Nombre d'étincelles/s: 5.

c) Bruit de fond

Dans un tel dispositif il semble principalement dû aux particules chargées du rayonnement cosmique, pour lesquelles le rendement est égal à

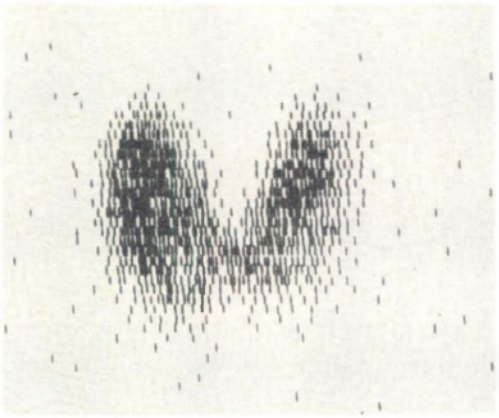

(a)

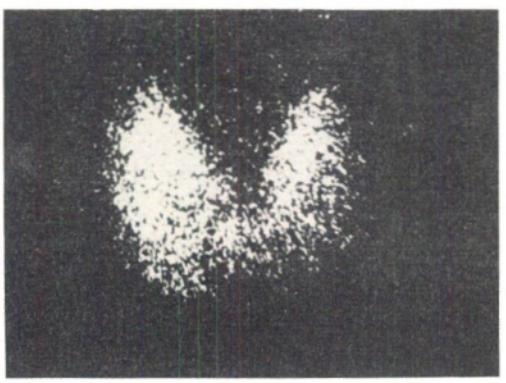

(b)

Figure 9

Image d'un fantôme de glande thyroïde.

a) Scintigraphe: vitesse de balayage, 400 mm/min
Précompte: 8
Collimateur cylindrique de diamètre 1,2 cm et hauteur 6,5 cm
La largeur de la bande spectrométrique encadre le pic photoélectrique à 27,3 keV de ^{125}I.

b) Chambre à étincelles: Radioactivité létale, 50 µc
Concentration radioactive superficielle, 2,5 µc/cm²
Distance de la source à la grille collimatrice: 3 cm
Ouverture de l'objectif photographique: f/16
Temps de pose: 10 min.

l'unité quand elles traversent la chambre en dehors de la période de temps mort. Le diamètre effectif est de 16 cm correspondant à une surface de l'ordre de 200 cm², ce qui pour le taux classique de une particule cosmique par cm² et par minute donne un bruit de fond d'environ 3 étincelles/s ré-

parties dans tout le volume de la chambre. C'est un ordre de grandeur qui correspond bien à l'observation.

PERSPECTIVES D'AVENIR

Des essais ont été effectués sur des fantômes de reins chargés en mercure 197 dont le rayonnement majeur est émis dans le domaine de 70 keV. Un exemple des résultats obtenus est donné par la figure 10. Celle-ci re-

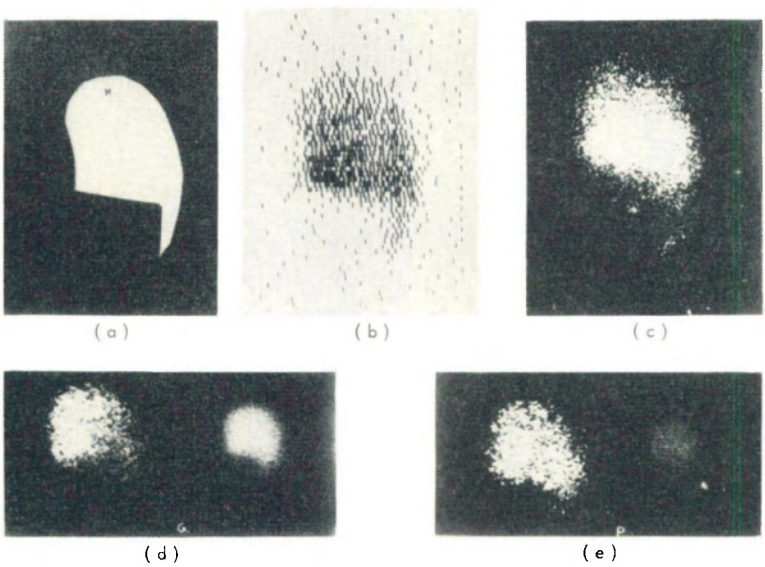

Figure 10

a) Fantôme plan de rein: Radioactivité totale: 800 μc
Concentration radioactive superficielle, 10 μc/cm²

b) Image scintigraphique: Précompte: 8. Vitesse, 280 m/min
Collimateur focalisé à 19 canaux dont le foyer est à 3 cm des orifices de sortie du collimateur
Distance de la source au collimateur: 7 cm.

c) Image donnée par la chambre à étincelles
Distance de la source à la grille collimatrice: 3 cm
Ouverture de l'objectif photographique: f/16
Temps de pose: 3 min.

d) Image donnée par la caméra à grille
Distance de la source à la grille: 2 cm
Temps de pose: inférieur à min
1. Image obtenue avec un tube oscillographique à mémoire.
2. Image obtenue avec un tube oscillographique ordinaire.

e) Image donnée par la «pinhole» caméra
Distance de la source au «pinhole», 14 cm
Temps de pose: 10 min
1. Image obtenue avec un tube oscillographique à mémoire.
2. Image obtenue avec un tube oscillographique ordinaire.

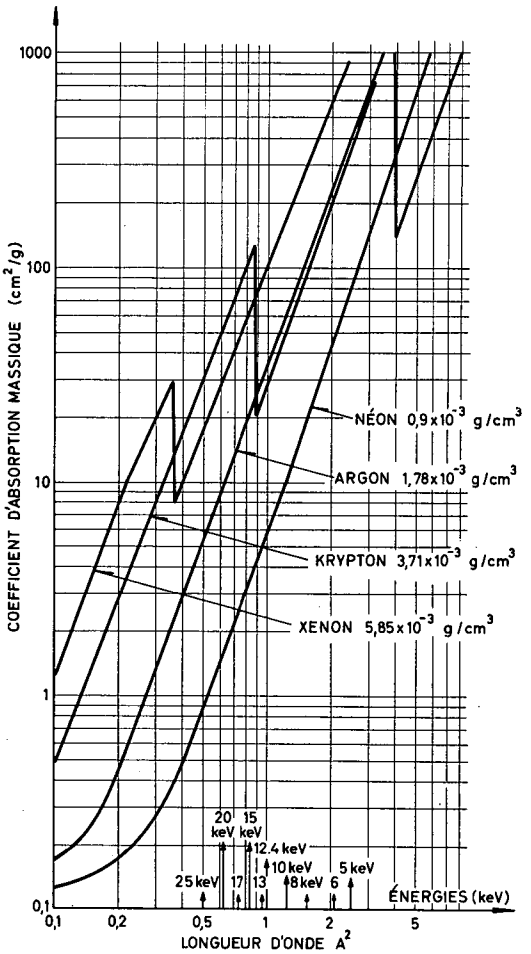

Figure 11

Variation en fonction de l'énergie et de la longueur d'onde du coefficient massique d'absorption de différents gazes rares.

présente une série d'images d'un même fantôme de rein obtenue avec différents dispositifs. Ce fantôme plan a été coupé en deux et seule une moitié présentant une encoche a été utilisée pour réaliser les images. L'encoche permet de se rendre compte du degré de finesse de l'image. On notera que des quatres dispositifs utilisés, scintigraphe, chambre à étincelles, caméra à grille et caméra du type «pinhole» celle donnée par la chambre à étincelles n'est pas la plus mauvaise. Quoique encourageante l'image obtenue est assez médiocre pour différentes raisons, Tout d'abord le parcours des photoélectrons étant beaucoup plus élevé dans les mêmes conditions de fonctionnement de la chambre qu'avec l'iode 125 la localisation de l'étincelle est beaucoup plus mauvaise. D'autre part,le rendement du gaz et de la cathode d'aluminium est très faible à cette énergie.

Nous comptons pallier à ces défauts en réalisant une chambre fonctionnant en régime continu avec du xénon. La figure 11 montrant la variation avec l'énergie du coefficient d'absorption massique des différents gaz rares, permet de prévoir que le gain de rendement devrait être important. L'utilisation d'une photocathode plus appropriée que l'aluminium (or par exemple) pour les photons d'énergie assez élevée doit également permettre d'améliorer le gain. Enfin nous envisageons de l'augmenter encore en utilisant le gaz sous pression.

Récemment, PETER, PISAREV et VAHLBRUCK [19] ont montré qu'il était possible de réaliser des photocathodes dont l'efficacité n'est que modérément réduite en atmosphère de gaz rares. Ceci permet d'envisager de remplacer le dispositif producteur d'électrons de la chambre décrite plus haut par l'association d'un cristal d'iodure de césium activé au thallium et d'une photocathode autorisant ainsi l'utilisation du dispositif avec des photons d'énergie élevée.

Nous nous proposons parallèlement de faire une recherche précise des conditions optima de résolution de ce type de dispositif. Quoi qu'il en soit les résultats obtenus sont très encourageants et montrent que pour certaines applications, ce type de dispositif peut être supérieur aux scintigraphes conventionnels et concurrencer les autres types de caméra. Une de ses caractéristiques les plus séduisantes est son extrême simplicité.

RÉFÉRENCES

[1] CASSEN, B., CURTIS, L., REED, C and LIBBY, R., Instrumentation for I^{131} use in medical studies, Nucleonics 9 2 (1951) 46.

[2] MAYNEORD, W. V., TURNER, R. C., NEWBERRY, S. P. and HODT, H J., Method of making visible distribution of activity in source of ionizing radiation, Nature, 168 (1951) 762.

[3] BROWNELL, G. L., Theory of isotope scanning, Medical Radioisotope Scanning, IAEA, Vienne (1959) 1

[4] ANGER, H. O., Use of a gamma ray pinhole camera for in vivo studies, Nature 170 (1952) 200.

[5] SKANSE, B. and JOHANNSON, J., A photographic method of determining the distribution of radioactive material in vivo, Acta Radiol. 39 (1953) 317.

[6] KELLERSHOHN, C. et PELLERIN, P., Sur la possibilité d'obtenir l'autoradiographie d'un organe in vivo, C.R. Acad. Sci. 239 (1954) 111.

[7] KELLERSHOHN, C. and PELLERIN, P., Scintillator grid localizes gamma emitters photographically, Nucleonics 13,12 (1957) 34.

[8] ANGER, H. O. and ROSENTHAL, O. J., Scintillation camera and positron camera, Medical Radioisotope Scanning, IAEA, Vienne (1959) 76.

[9] FUCKS, W. et KNIPPING, H. W., Eine γ-Retina zur Bestimmung der raum-zeitlichen Verteilung radioaktiver Substanzen, Die Naturwissenschaften 42 (1955) 93.

[10] ANGER, H. O., Scintillation Camera, Rev. Sci. Instr. 29 (1958) 27.

[11] ANGER, H. O., Gamma-ray and positron scintillation camera, Nucleonics 21, 10 (1963) 56.

[12] MALLARD, J. R. and MYERS, M. J., The performance of a gamma camera for the visualization of radioactive isotopes in vivo, Phys. Med. Biol. 8, (1963) 165.

[13] KELLERSHOHN, C., MORICHÈRE, J. et DESGREZ, A., Visualisation d'un organe in vivo au moyen de radioéléments artificiels (scintigraphie, caméra à scintillation), Onde Electrique, à paraître.

[14] BENDER, M. A. and BLAU, M., The Autofluoroscope, Nucleonics, 21 10 (1963) 52.

[15] MORTIMER, R. K., ANGER, H. O. and TOBIAS, C. A., The gamma-ray pinhole camera and image amplifier, University of California Radiation Laboratory Report No UCRL-2524 (1954).

[16] KELLERSHOHN, C. et PELLERIN, P., Sur la possibilité d'utiliser un tube amplificateur d'image pour mettre en évidence la localisation et la distribution d'un corps radioactif, C. R. Soc. Biol. 149 (1955) 533.

[17] TER-POGOSSIAN, M., KASTNER, J. and VEST, T. B., Autofluorography of the thyroid gland by means of image amplification, Radiology 81 (1963) 984.

[18] LANSIART, A. et LELOUP, J. Chambre à étincelle autodéclenchée, Comptes rendus du Colloque international sur l'électronique nucléaire, Paris 1963 (sous presse).

[19] PETER, G., PISAREV, A. F. and VAHLBRUCH, D. M., A photoelectronic image intensifier spark tube, Rapport P. 1063, Institut Unifié de Recherches Nucléaires, Dubna (1962).

ÉTUDE D'UNE CAMÉRA A SCINTILLATIONS: DESCRIPTION ET APPLICATIONS CLINIQUES

H. JAMMET ET R. GONGORA
FONDATION CURIE, PARIS
ET
J. MORICHÈRE ET P. DESNEIGES
CENTRE D'ÉTUDES NUCLÉAIRES DE SACLAY, FRANCE

Abstract — Résumé — Аннотация — Resumen

STUDY OF A SCINTILLATION CAMERA: DESCRIPTION AND CLINICAL APPLICATION. The spatial distribution of radioactivity within an organ is at present studied routinely with the aid of mobile detectors capable of examining different points in the organ one after the other by means of scanning. In recent years efforts have been made to construct fixed detectors which are able to explore all the points within an organ simultaneously. A detector of this sort is now being used by the authors of the paper.

The paper explains the functioning of the apparatus in which a single crystal is viewed by a number of photomultipliers. The main components of the apparatus are as follows:

(a) A detector head consisting of a crystal and 7 photomultipliers, plus a conical chamber fitted with a diaphragm or a grid;

(b) Devices for localizing scintillations in the crystal and for pulse selection, and

(c) Recording equipment consisting of two cathode-ray oscilloscopes fitted with a camera; one of these is equipped with a remanence memory tube.

The paper then describes the operating technique: approaching the organ; studying recording times; using the screen of the memory oscilloscope; producing the photograph.

Finally, the authors discuss the results obtained in exploring various organs, give some general information on the technique and adumbrate a number of novel applications.

ÉTUDE D'UNE CAMÉRA A SCINTILLATIONS: DESCRIPTION ET APPLICATION CLINIQUE. L'étude de la répartition spatiale de la radioactivité à l'intérieur d'un organe s'effectue couramment à l'aide de détecteurs mobiles dont le mouvement de balayage permet l'examen successif des différents points de l'organe. Depuis quelques années, les efforts ont porté sur la réalisation de détecteurs fixes qui permettent un examen simultané de tous les points de l'organe. Les auteurs utilisent un tel détecteur.

Après avoir exposé le principe de fonctionnement de l'appareil basé sur l'examen d'un cristal unique par plusieurs photomultiplicateurs, ils en décrivent les principaux éléments:

a) la tête de détection constituée essentiellement d'un cristal et de sept photomultiplicateurs et complétée soit par une chambre conique munie d'un diaphragme soit par une grille;

b) les dispositifs qui permettent la localisation des scintillations dans le cristal et la sélection des impulsions;

c) les dispositifs d'enregistrement constitués par deux oscilloscopes cathodiques équipés de caméra photographique, l'un d'eux étant muni d'un tube mémoire à rémanence.

Les auteurs décrivent ensuite la technique d'utilisation de l'appareil; ils envisagent successivement le mode d'abord de l'organe, l'étude des temps d'enregistrement, le mode d'utilisation de l'écran de l'oscilloscope mémoire, le problème de l'enregistrement photographique.

Ils présentent enfin les résultats d'explorations de différents organes, précisent les indications générales de cette technique et envisagent des applications originales.

СЦИНТИЛЛЯЦИОННАЯ КАМЕРА: ОПИСАНИЕ, МЕТОД ИСПОЛЬЗОВАНИЯ И РЕЗУЛЬТАТЫ. Изучение пространственного распределения радиоактивности внутри органа обычно производится с помощью передвижных детекторов, перемещение которых позволяет осуществлять успешное исследование в различных точках органа. В течение нескольких лет усилия

были направлены на создание стационарных детекторов, позволяющих одновременно исследовать различные точки органа. Авторы используют подобный детектор.

Излогается принцип действия прибора, основанный на изучении единственного кристалла с помощью нескольких фотоумножителей, дается описание основных элементов:

а) детектирующая головка, которая состоит в основном из кристалла и семи фотоумножителей и дополненная либо конической камерой, снабженной диафрагмой, либо решеткой;

б) приборы, позволяющие производить локализацию сцинтилляций в кристалле и отбор импульсов;

в) регистрирующие приборы в виде двух катодных осциллоскопов с фотокамерой, при этом на одном из них установлена запоминающая трубка с остаточным магнетизмом.

Дается описание метода использования прибора; последовательно излагается метод доступа к органу, изучение времени регистрации, метод использования экрана запоминающего осциллоскопа, проблема фоторегистрации.

В заключение приводятся результаты исследования различных органов, уточняются общие показатели этого метода и предлагается оригинальное использование прибора.

ESTUDIO DE UNA CÁMARA DE CENTELLEO: DESCRIPCIÓN Y APLICACIÓN CLÍNICA. El estudio de la distribución espacial de la radiactividad en el interior de un órgano suele efectuarse mediante detectores móviles cuyo movimiento de barrido permite examinar sucesivamente diferentes puntos del órgano. Desde hace algunos años se trata de construir detectores fijos que permitan examinar simultáneamente todos los puntos del órgano. Los autores utilizan un detector de este tipo.

Después de exponer el principio de funcionamiento del aparato basado en el examen de un solo cristal por varios fotomultiplicadores, los autores describen los elementos principales:

a) la cabeza detectora, constituida esencialmente por un cristal y siete fotomultiplicadores y completada por una cámara cónica provista de un diafragma o por una rejilla;

b) los dispositivos que permiten localizar centelleos en el cristal y seleccionar impulsos;

c) los dispositivos de registro constituidos por dos osciloscopios catódicos equipados con cámara fotográfica; uno de ellos está provisto de un tubo de memoria remanente.

A continuación los autores describen el modo de empleo del aparato, la manera de enfocar el órgano, el estudio de los tiempos de registro, el modo de empleo de la pantalla del osciloscopio de memoria y el problema del registro fotográfico.

Por último, presentan los resultados de la exploración de distintos órganos, precisan las indicaciones generales de esta técnica y sugieren algunas aplicaciones originales.

L'étude de la répartition spatiale de la radioactivité à l'intérieur d'un organe s'effectue couramment à l'aide de détecteurs mobiles, dont le mouvement de balayage permet l'examen successif des différents points de l'organe. Depuis quelques années les efforts ont porté sur la réalisation de détecteurs fixes qui permettent un examen simultané de tous les points de l'organe. La caméra à scintillations que nous utilisons à la Fondation Curie remplit ces conditions.

A. CARACTÉRISTIQUES GÉNÉRALES

1. *Formation de l'image (fig. 1)*

L'image est formée sur un scintillateur de NaI(Tl) de 200 mm de diamètre et de 6 mm d'épaisseur.

Les collimateurs, en alliage de tungstène, sont amovibles, leur densité est de 17,6 environ; la majeure partie des expériences a été effectuée avec un collimateur de 5 mm de diamètre.

Le champ de vision est de l'ordre de 60°.

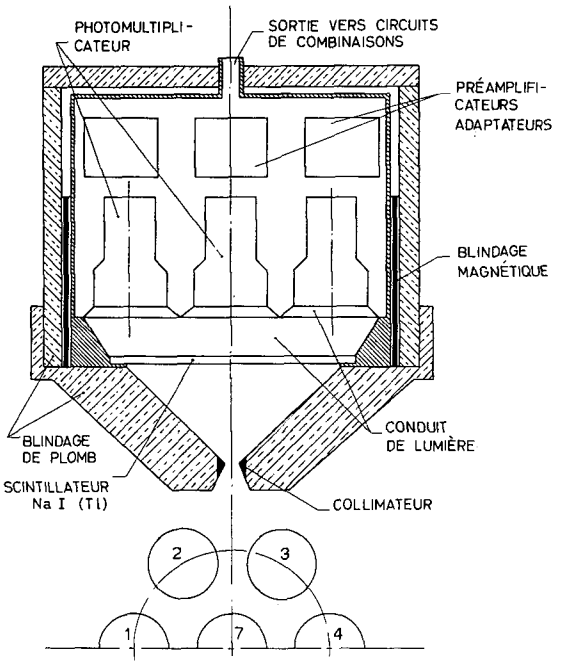

Figure 1

Coupe schématique de la caméra.

On a un rapport image/objet de 1, à une distance du collimateur de 12 cm.

2. *Localisation et reproduction des points constituant l'image*

Les éléments de localisation sont fournis par 7 photomultiplicateurs (diamètre utile: 65 mm), 6 PM périphériques et 1 PM central.

Le conduit de lumière est en plexiglass, les joints optiques étant assurés par de l'huile silicone.

La combinaison des impulsions est assurée au moyen d'un réseau de 17 transformateurs, dont le rapport de transformation correspond au coefficient attribué à chaque PM dans sa contribution aux impulsions, d'abscisse, d'ordonnée ou de sélection.

3. *Reproduction de l'image*

Dans la phase actuelle, deux oscilloscopes sont utilisés simultanément, les images obtenues avec chacun d'eux présentent un caractère particulier dû aux caractéristiques du tube cathodique qui l'équipe: a) tube à faible rémanence, b) tube à entretien d'image.

B. ÉTUDES D'IMAGE

1. *Surface utilisable*

La surface utilisable du scintillateur a été définie à partir des équations de reproduction des points. La figure 2 montre les déformations subies par des cercles concentriques; elle met en évidence: a) des déformations

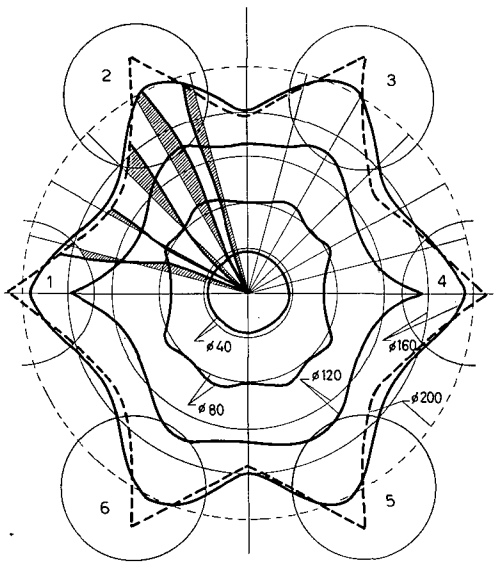

Figure 2

Distorsions systématiques apportées par le dispositif de localisation.

radiales, b) la superposition des zones extérieures qui sont ramenées à l'intérieur.

La surface utile a pour diamètre 70 à 80% du diamètre total du scintillateur.

L'expérience consistant à enregistrer l'image d'un liquide radioactif contenu dans un cristallisoir à une distance telle que le scintillateur soit largement recouvert par les rayons gammas émis, confirme les résultats du calcul.

2. *Homogénéité — contraste*

Tenant compte de la constatation précédente des essais ont été effectués de manière à ce que la surface du scintillateur utilisée ait 14 cm de diamètre.

La vue supérieure (fig. 3) est obtenue avec un cristallisoir de 150 mm de diamètre contenant une solution d'iode 131, d'activité spécifique 1 μc/cc.

Les vues suivantes sont obtenues au moyen de deux béchers de 60 mm de diamètre, placés dans le cristallisoir et dans lesquels on introduit suc-

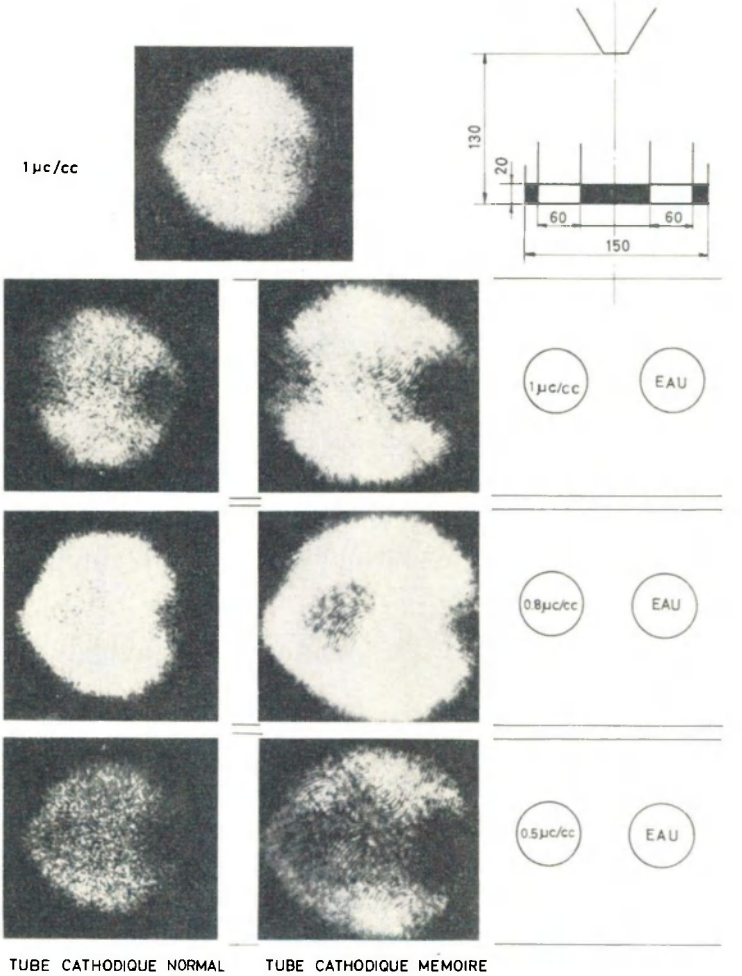

Figure 3

Homogénéité et contraste

cessivement de l'eau inactive et une solution d'iode 131 de différentes concentrations.

Dans chaque cas deux enregistrements ont été réalisés, sur les deux tubes cathodiques de l'installation.

La figure 4 illustre une étude de contraste effectuée à l'aide d'une cuve compartimentée par des cloisons de plexiglass de 1 millimètre d'épaisseur. Les compartiments sont remplis de solutions d'activités différentes, il est ainsi possible d'étudier, pour un compartiment donné, son contraste avec deux ou trois compartiments voisins.

Nous avons également effectué des essais de définition de séparation et de sensibilité, illustrés par les figures 5 et 6.

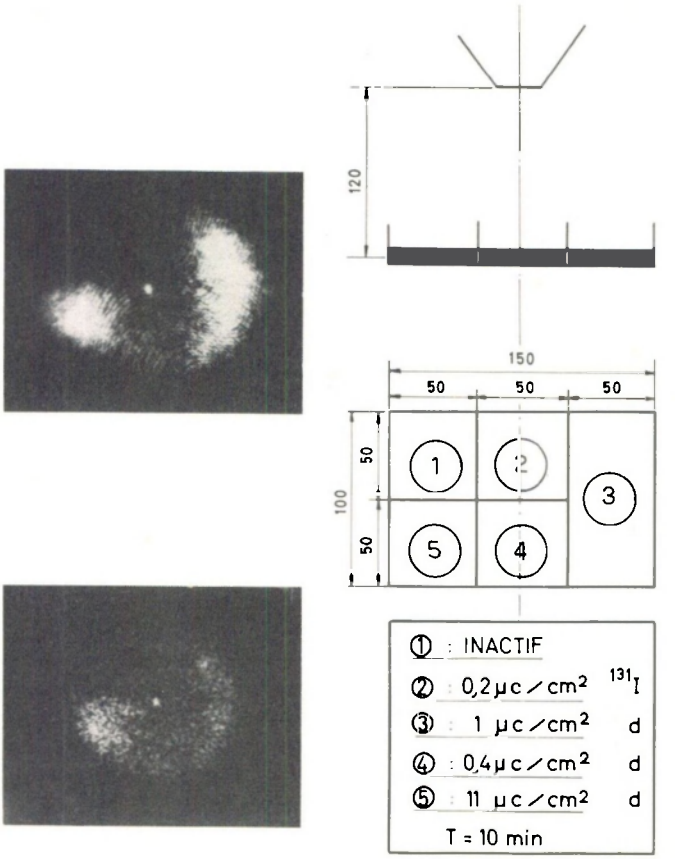

Figure 4

Homogénéité et contraste

APPLICATIONS CLINIQUES

Le temps nécessaire à l'obtention d'une image n'est plus lié à la surface de l'organe et est très inférieur à celui que nécessite la scintigraphie classique; le temps est de l'ordre de quelques minutes.

Cet avantage considérable permet de suivre, par de courts examens successifs, l'évolution de la répartition de la radioactivité d'un organe.

Le tube à entretien d'image permet le contrôle de la constitution de l'image en cours d'examen et la photographie de différentes étapes de sa constitution.

Par ailleurs l'oscilloscope, équipé du tube cathodique à entretien d'image offre la possibilité de faire varier de façon continue la brillance de l'image enregistrée. Le réglage continu de la brillance permet, en faisant apparaître ou disparaître les zones les moins denses de prendre successivement plusieurs vues correspondant à des contrastes différents. Ceci

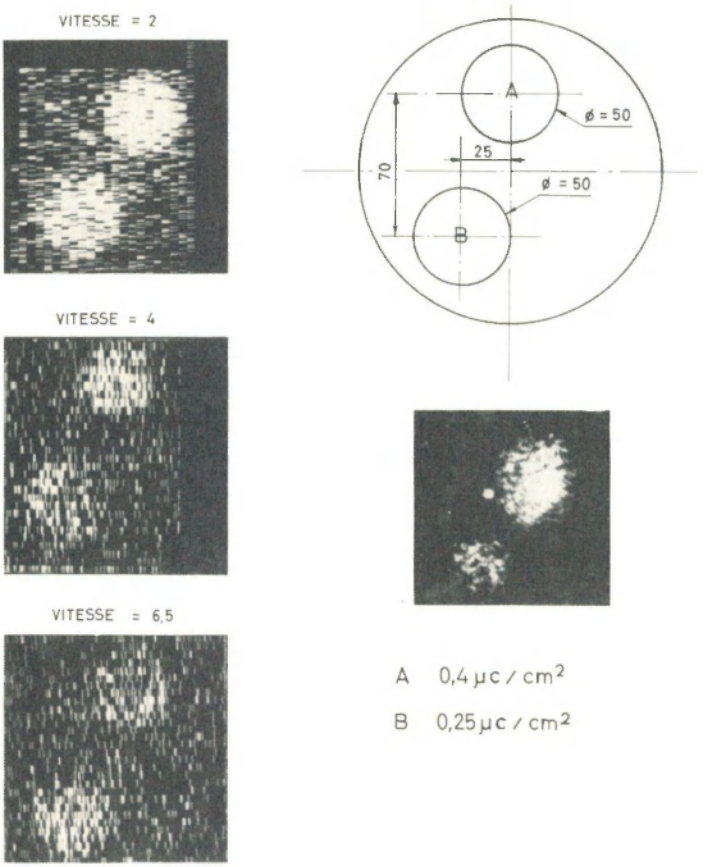

Figure 5

Sensibilité

facilite l'interprétation; en effet le réglage nécessaire à l'obtention de l'image complète de l'organe entraîne généralement la formation d'un halo autour des régions les plus denses.

Nous avons effectué à l'aide de la caméra à scintillations un certain nombre d'examens organo-fonctionnels de différents organes:

1. De par ses dimensions, le corps thyroïde se prête parfaitement à cet examen. Les images, pour une fixation normale, après administration de 50 μc de radio-iode, sont obtenues en 5 à 10 min (fig. 7).

Pour la majorité des examens effectués la caméra était munie d'un cône; cependant nous avons effectué quelques essais avec grille dans le but d'accroître la sensibilité et dont les résultats sont représentés (fig. 8); ces documents sont peu satisfaisants et nous poursuivons actuellement une étude dans ce domaine.

Nous avons répété les examens à 2 h, 6 h et 24 h après administration

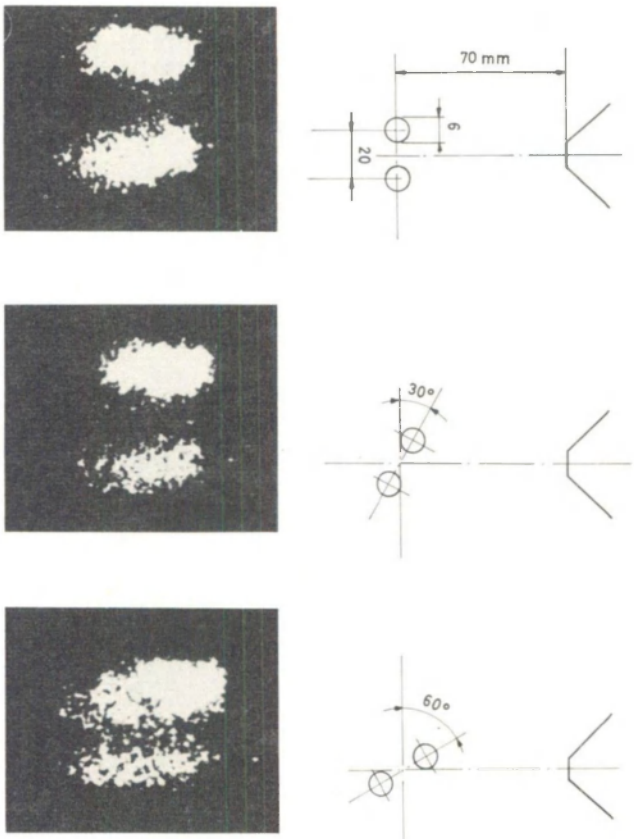

Figure 6

Séparation

Figure 7

Thyroide normale.

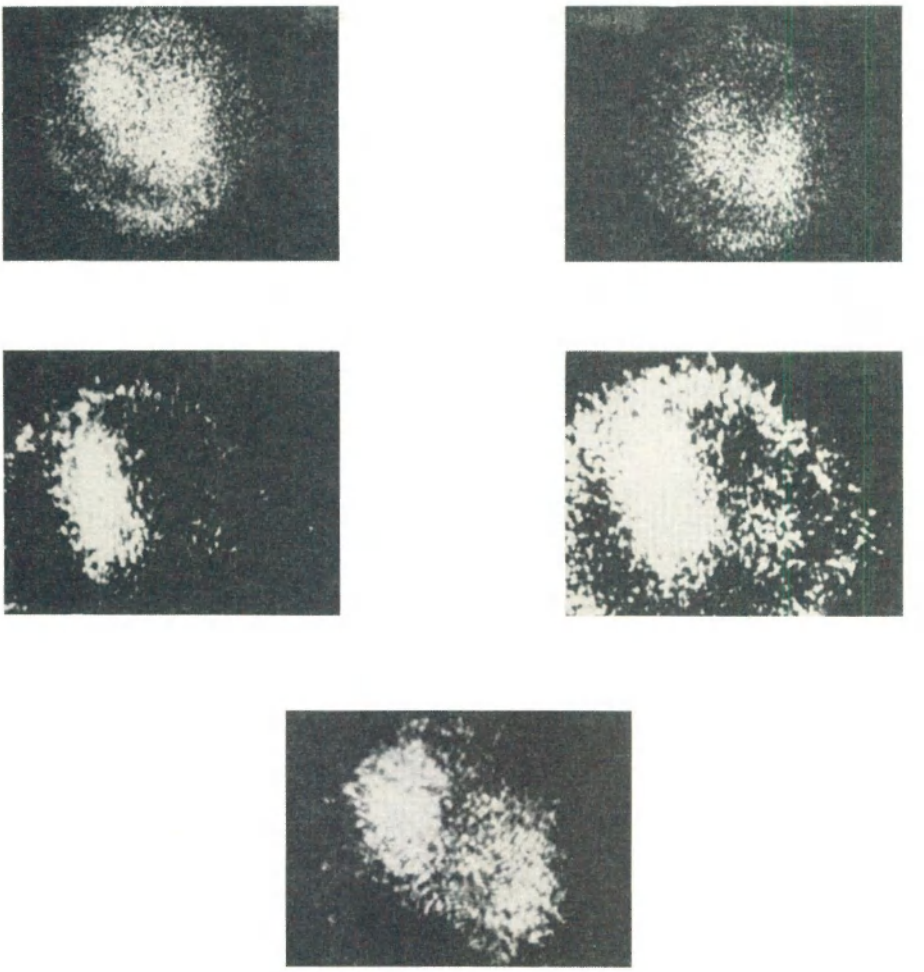

Figure 8

Thyroïdes effectuées avec grille.

du radio-iode et obtenu une série de documents qui rendent compte de la répartition de l'activité dans le temps (fig. 9).

Dans certains cas, le tube à entretien d'image a permis, par le jeu du seuil de lecture, de mieux explorer les images de tonalité fournies par la scintigraphie (la fig. 10 se rapporte à un kyste du lobe gauche).

2. La caméra à scintillations est particulièrement précieuse pour l'examen d'organes plus volumineux. Appliquée à l'étude fonctionnelle et morphologique du foie, elle nous a permis de suivre la fixation du radio-or dans les minutes qui ont suivi l'injection (fig. 11); l'écran du tube à entretien d'image a été photographié 5, 10, 20 et 30 min après injection du radio-or.

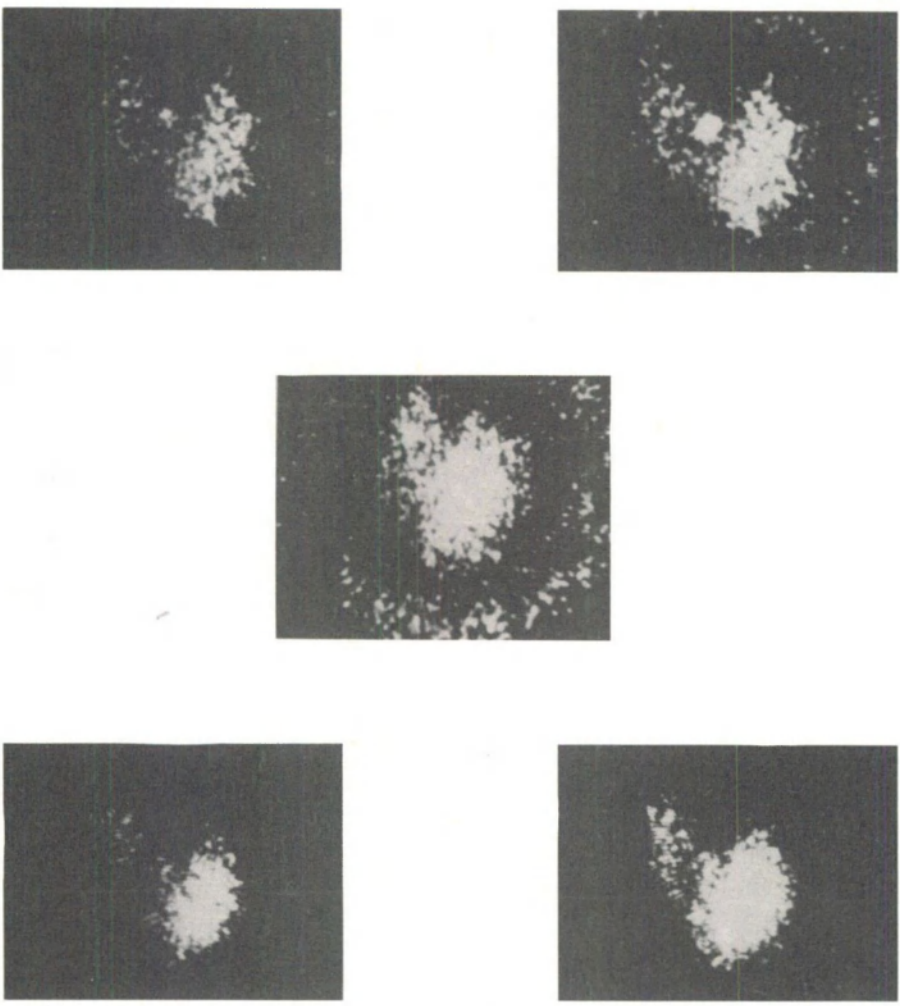

Figure 9

Examen thyroïdien: 2h; 6h et 24h après administration de radio-iode.

La constitution de l'image suivie sur l'écran du tube à entretien d'image et photographiée à intervalle de temps rapproché permet d'apprécier avec précision de faibles différences de densité entre différents points de l'organe. La figure 12 montre une série de documents obtenus pour des durées croissantes de temps d'enregistrement chez un malade présentant des métastases hépatiques.

Le tube à entretien d'image que nous utilisons accentue le contraste de façon importante (fig. 13).

Par ailleurs, les images lacunaires sont mieux appréciées à l'aide de multiples photographies de l'image réalisées avec des seuils de lecture différents (fig. 14, 15 et 16).

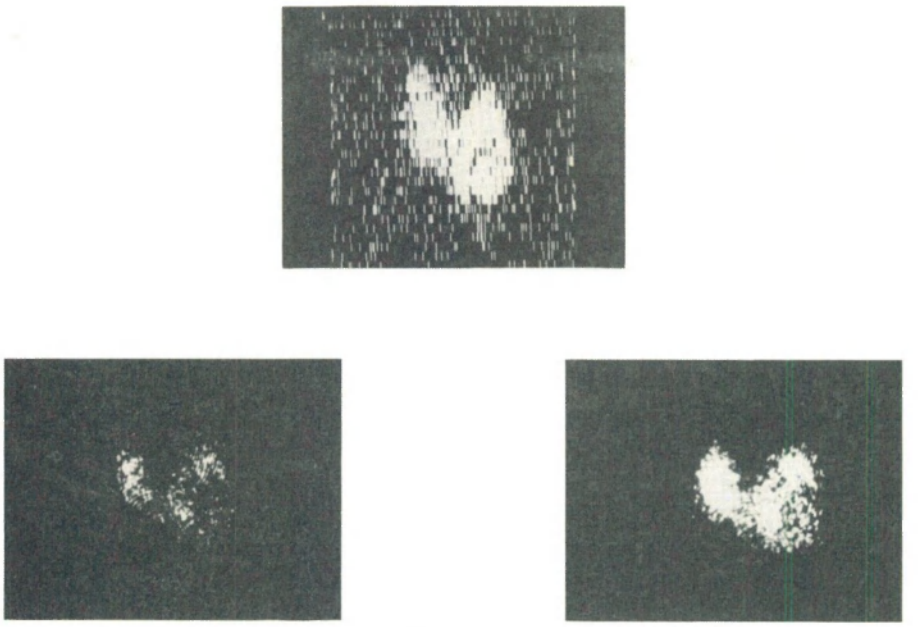

Figure 10

Kyste du lobe gauche du corps thyroïde pour différentes valeurs du seuil de lecture.

3. Nous avons également effectué des scintigraphies spléniques et rénales pour lesquelles l'intérêt réside essentiellement dans la vitesse d'exécution.

On observe sur la figure 17 une large encoche du bord antérieur de la rate qui répond à un kyste hydatique.

La figure 18 illustre un examen rénal et montre une encoche du bord externe du rein droit.

La figure 19 se rapporte à une polykystose rénale.

Nous avons enfin utilisé la caméra à scintillations pour contrôler rapidement la répartition dans l'organisme de radionuclides administrés à titre thérapeutique: a) radio-or 198 intra-pleural et intra péritonéal (fig. 20) et b) Lipiodol marqué à l'iode 131 endo-lymphatique. (La figure 21 montre que la répartition pulmonaire respecte le sommet droit, et que les chaînes lombo-aortiques iliaques externes et inguinales sont injectées.)

CONCLUSION

La caméra à scintillations par sa rapidité d'information permet de réaliser de multiples images sous diverses incidences, d'un même organe et ainsi d'approfondir l'étude de sa morphologie; elle présente un intérêt majeur pour l'étude de phénomènes biologiques dynamiques et dans ce domaine, l'adjonction d'une grille, semble devoir améliorer les résultats; enfin l'utilisation d'un oscilloscope muni d'un tube à entretien d'image confère à cet appareil une grande souplesse d'utilisation.

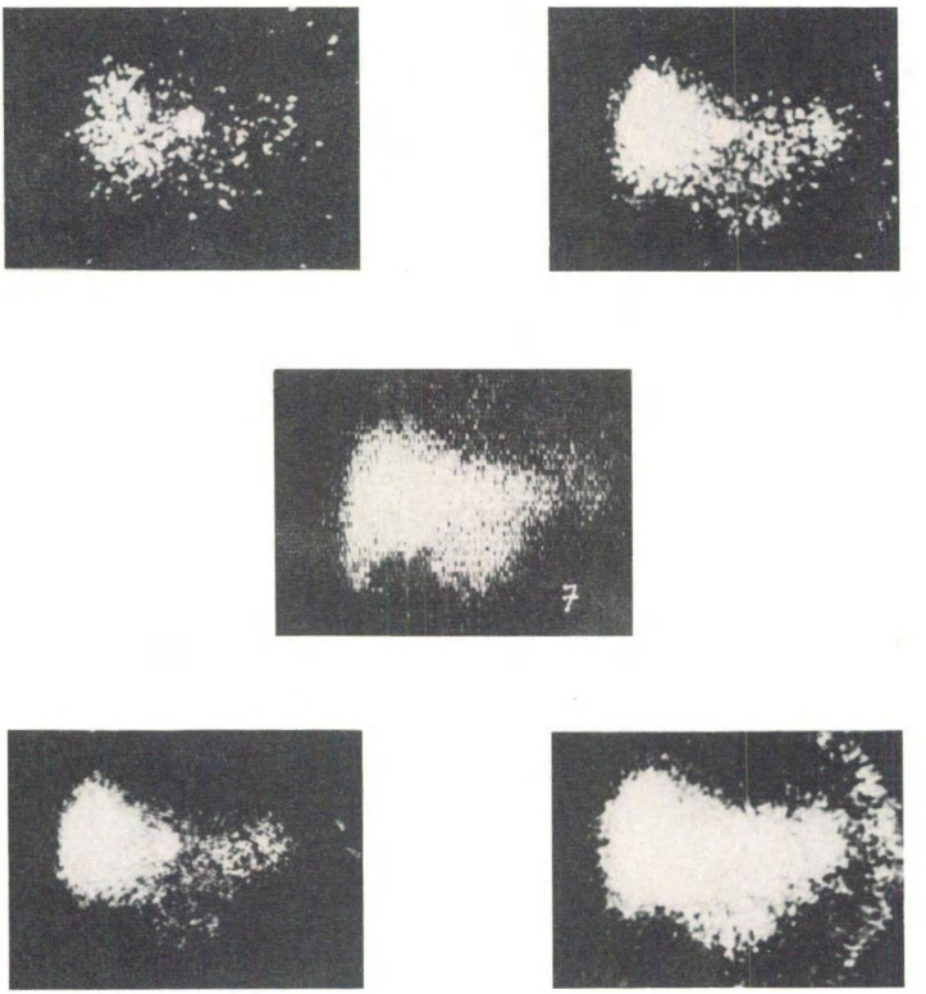

Figure 11

Constitution d'une image hépatique dans les minutes qui suivent l'injection de radio-or 198 réalisée 5, 10, 20 et 30 min après injection.

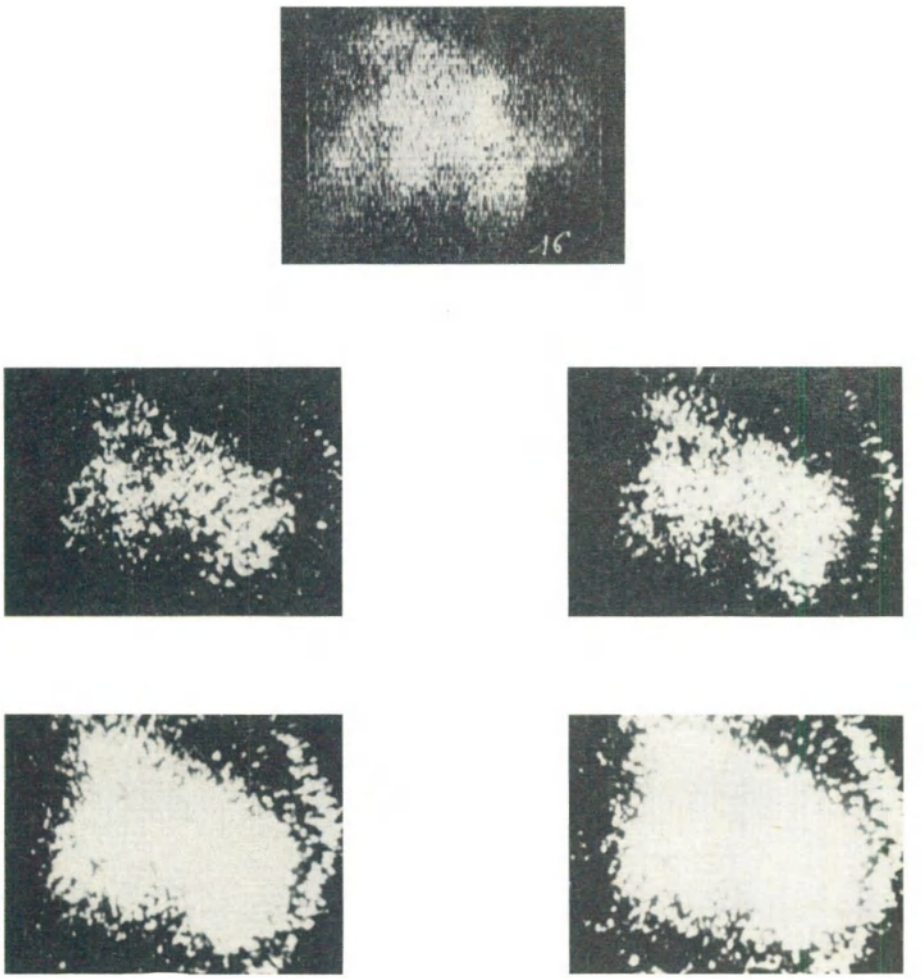

Figure 12

Images hépatiques réalisées avec des durées différentes du temps d'enregistrement: 5, 10, 15 et 20 min d'enregistrement.

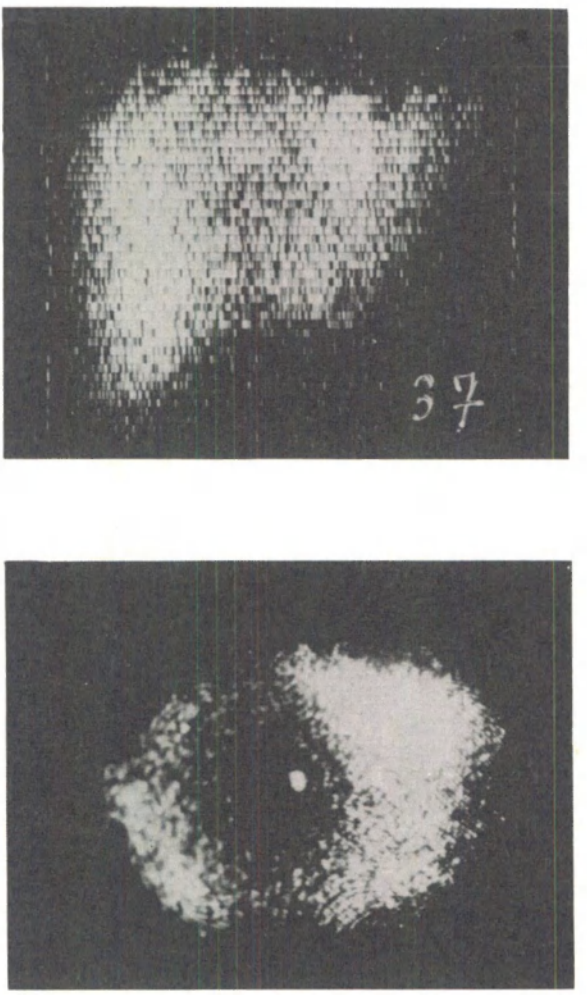

Figure 13

Accentuation du contraste à l'aide du tube à entretien d'image.
Abcès hépatique.

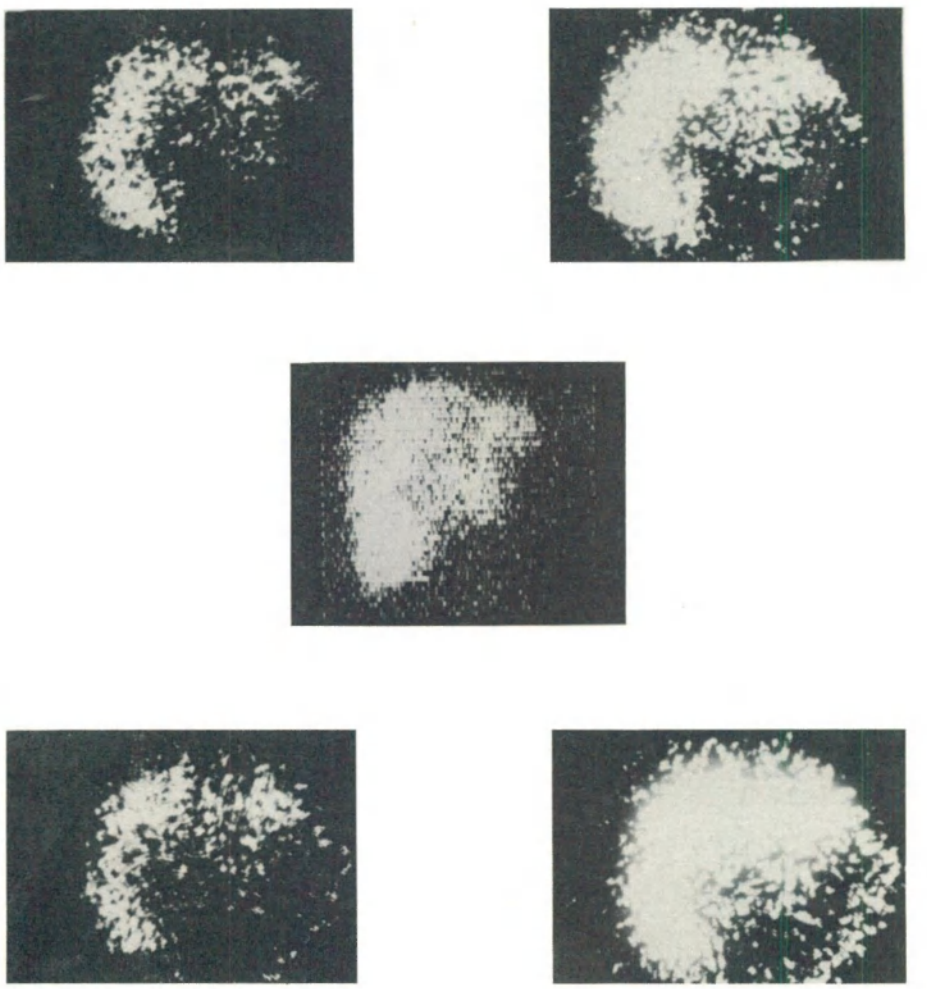

Figure 14

Même image de métastases hépatiques examinée avec des seuils de lecture différents.

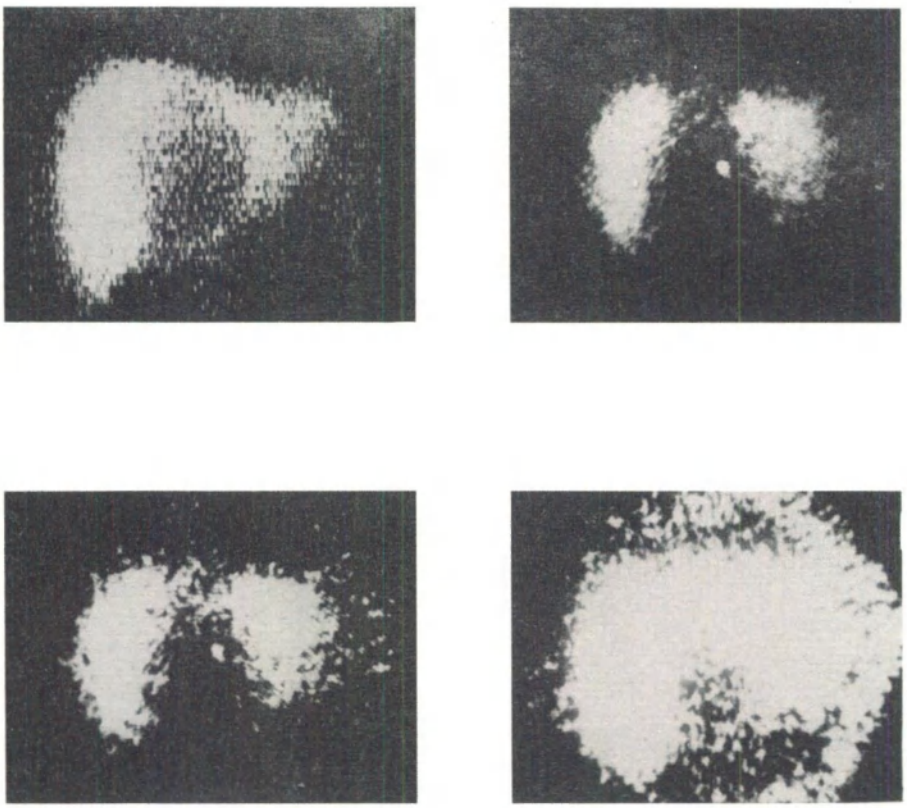

Figure 15

Même image d'un abcès hépatique examiné avec des seuils de lecture différents.

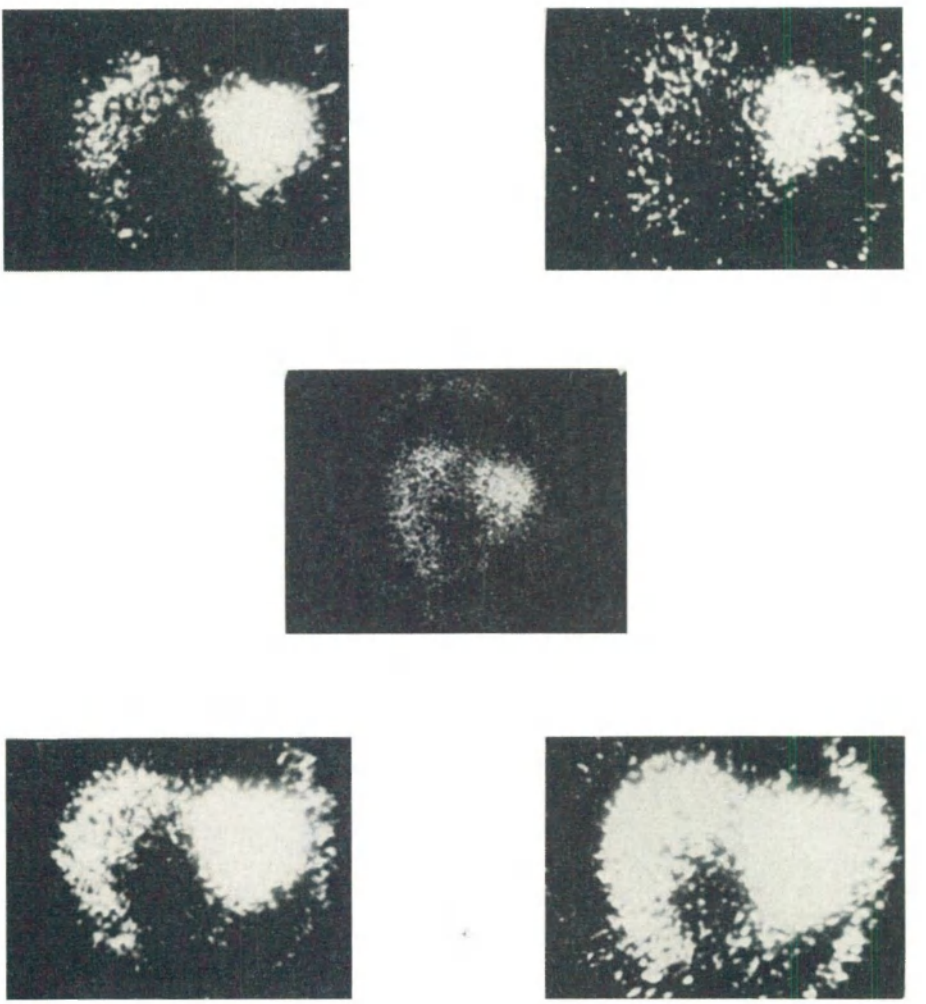

Figure 16

Même image de T. hépatique examinée avec des seuils de lecture différents.

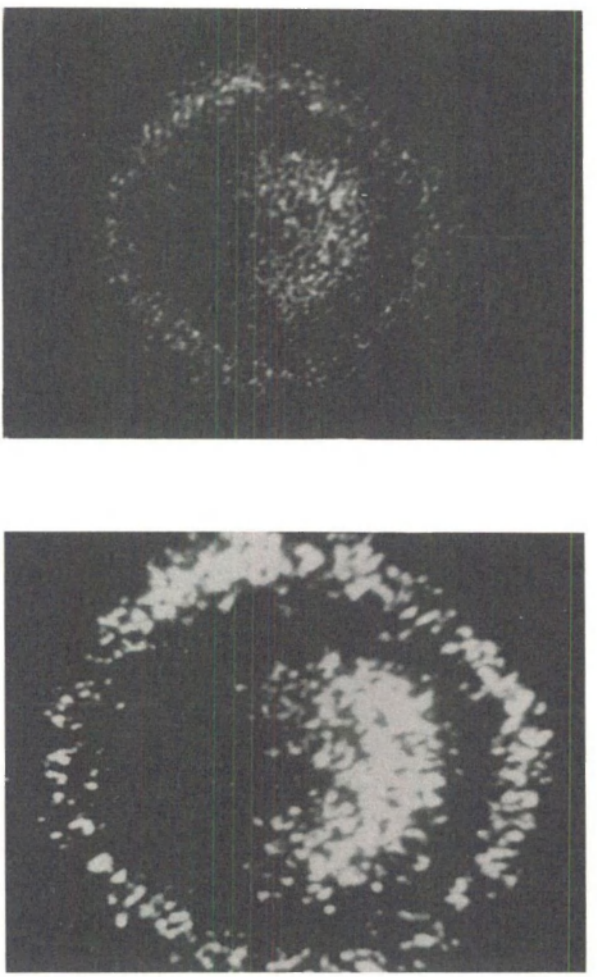

Figure 17

Kyste hydatique de la rate.

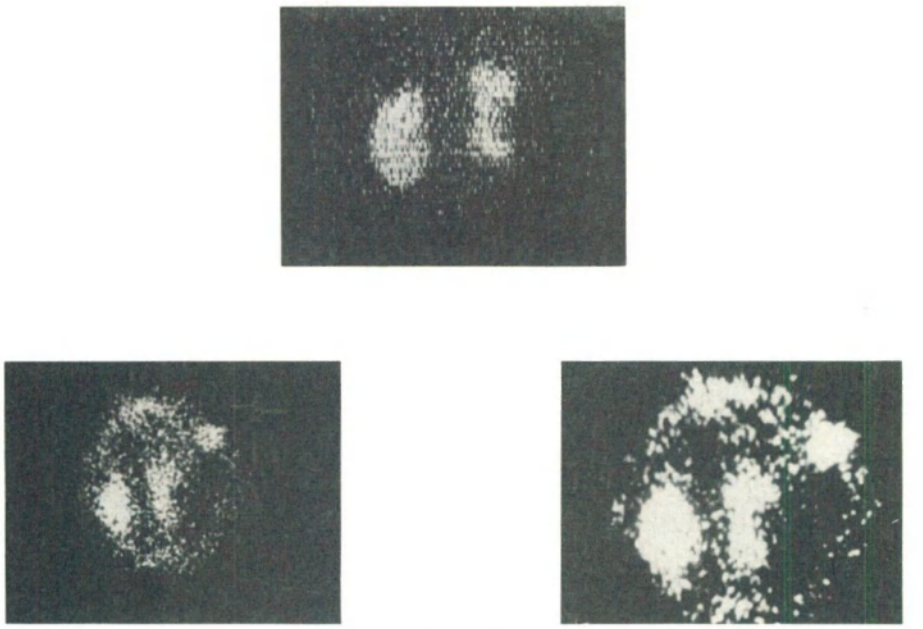

Figure 18

Tumeur du rein droit.

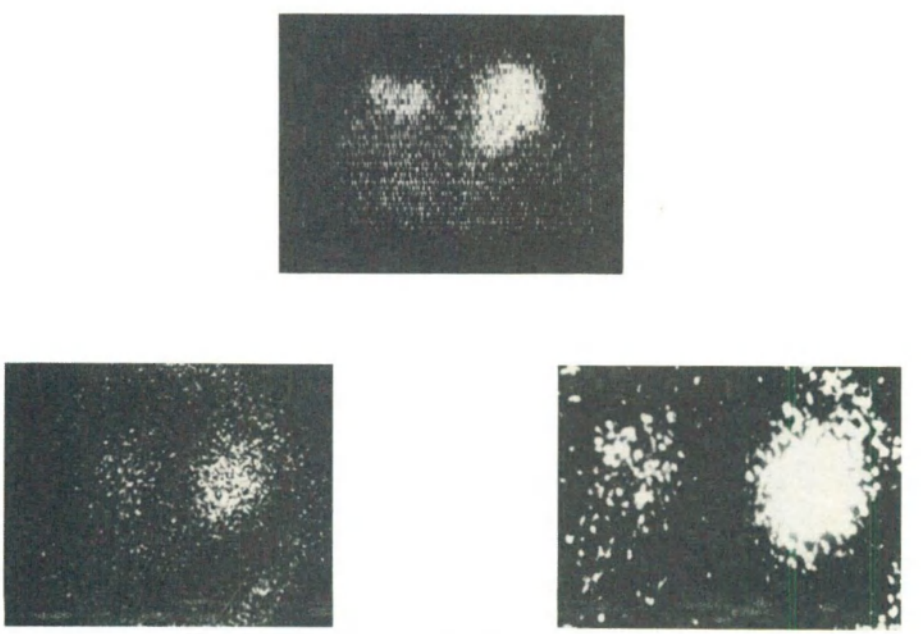

Figure 19

Polykystose rénale.

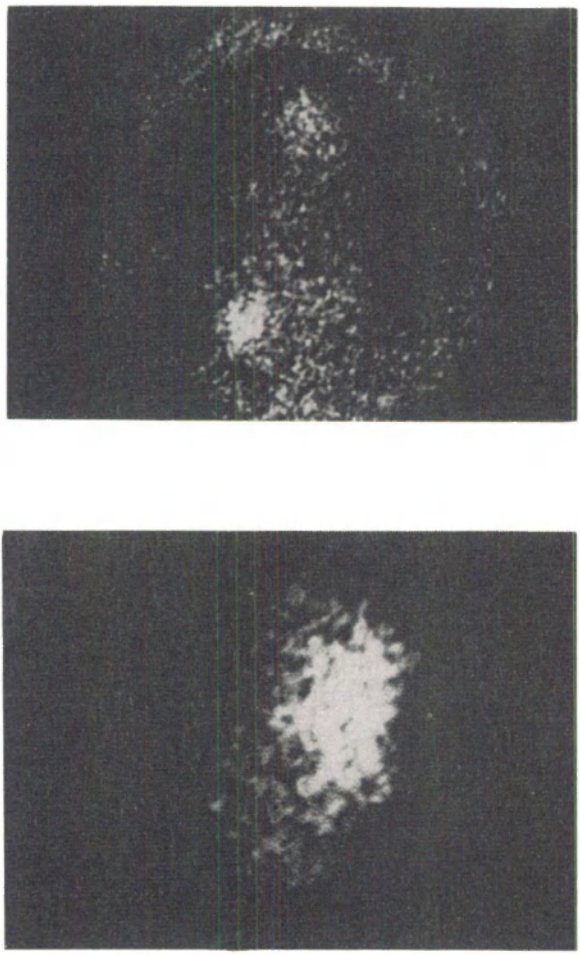

Figure 20

Répartition du radio-or dans des cavités pleurale et péritonéale.

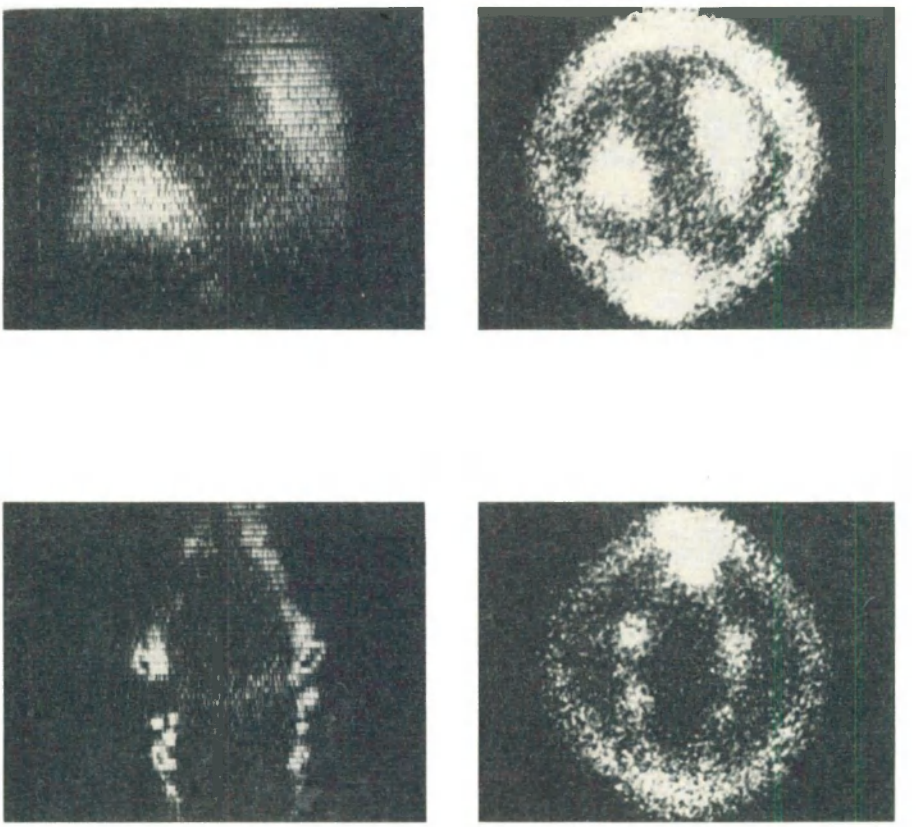

Figure 21

Répartition dans l'organisme de Lipiodol radioactif administré par voie endolymphatique.

DYNAMIC STUDIES WITH A GAMMA-RAY SCINTILLATION CAMERA

W.G. MYERS
THE OHIO STATE UNIVERSITY HEALTH CENTER, COLUMBUS, UNITED STATES OF AMERICA

Abstract — Résumé — Аннотация — Resumen

DYNAMIC STUDIES WITH A GAMMA-RAY SCINTILLATION CAMERA. A commercial model γ-ray scintillation camera of the type described by Anger has been used in this laboratory since October 1962 to study dynamic physiological and pharmacological processes in vivo. The 0.6 x 20-cm NaI crystal is viewed by 19 multiplier phototubes. Light flashes generated in this plate by γ-rays are caused electronically to appear as small coruscations in the same relative positions on an oscilloscope screen. A Polaroid camera focused on this screen gradually forms a picture, the spatial densities of which represent the spatial distribution of γ-rays projected from the biological object into the collimating system. Either a 5-mm diam. "pinhole" or a 771-hole multi-aperture lead collimator is used to view an area of ~16-cm maximal diameter. This ingenious instrument makes true "point-by-point" scans electronically. The pictures have no line structure to distort perception. No mechanical difficulties are possible.

The ability to view the entire area of interest continuously during a scanning seance is advantageous in reducing the dosage of radioactivity and the statistical errors. A unique feature is the opportunity provided by this camera to make pictures in fast sequence to record rapid changes in the distribution of γ-isotopes. A maximum rate of three pictures each minute has been achieved with 10-s Polaroid roll film. Motion-picture apparatus would provide even higher rates when required to record movements in extraordinarily fast processes.

After I^{131}-iodide was injected intravenously into a rat-fed Purina Labchow, a series of pictures, taken during the first 2 min of six successive 5-min intervals, revealed rapid disappearance of the radioiodine initially distributed throughout the whole body, and concentration in the stomach region within 30 min. Most of the radioactivity remained localized there during the remaining 7 h of the experiment, at which time only a modicum had accumulated in the thyroid. Similarly, after subcutaneous injection of I^{131}-orthoiodohippurate into a rat's supraclavicular region, the camera revealed migration into the kidneys within 3 min, into the bladder in 5 min, and complete clearance into the bladder in 90 min. Larger prototype scintillation cameras have been manufactured recently that incorporate 1.3 x 30-cm crystals.

ÉTUDES DE PROCESSUS DYNAMIQUES AVEC UNE CHAMBRE A SCINTILLATION GAMMA. Depuis octobre 1962, le laboratoire de l'auteur utilise une chambre à scintillation gamma classique, du type décrit par Anger, pour l'étude in vivo de processus physiologiques et pharmacologiques dynamiques. Le cristal de NaI de 0,6 x 20 cm est «vu» par 19 tubes photomultiplicateurs. Les éclairs provoqués par les rayons gamma sont projetés électroniquement sur l'écran d'un oscilloscope, sous forme de petites taches lumineuses occupant les mêmes positions relatives. Un appareil photographique «Polaroïd» réglé sur cet écran réalise progressivement une image dont les densités spatiales représentent la répartition spatiale des rayons gamma émanant de la matière biologique. On utilise soit un sténopé de 5 mm de diamètre, soit un collimateur en plomb à 771 canaux et plusieurs ouvertures pour explorer une surface d'un diamètre maximum de 16 cm environ. Ce dispositif ingénieux permet de faire électroniquement un véritable scintigramme point par point. Les images n'ont pas de structure linéaire pouvant provoquer une distorsion de la visualisation. Il ne se pose aucune difficulté mécanique.

La possibilité de «voir» continuellement la totalité de la surface intéressante pendant toute l'opération de scintigraphie est très avantageuse, car on peut ainsi réduire la dose de radioactivité reçue par le patient et diminuer l'erreur statistique. Une particularité intéressante est la possibilité de prendre des photographies en succession rapide pour enregistrer l'évolution de la répartition des émetteurs gamma. On a pu prendre jusqu'à trois photographies par minute avec la pellicule Polaroïd qui se développe en 10 s. Avec une caméra cinématographique, on pourrait faire des prises de vues encore plus rapides pour l'enregistrement de processus extrêmement rapides.

Après injection intraveineuse de radioiode à un chow-chow nourri de rats, une série de photographies, prises pendant les deux premières minutes de six intervalles de 5 min, a montré la disparition rapide de l'iode-131 réparti initialement dans l'ensemble du corps et sa concentration en moins de 30 min dans la région stomacale. La plus grande partie de la radioactivité restait localisée dans cette région pendant les 7 h suivantes; une faible quantité seulement s'était fixée dans la thyroïde. Après injection sous-cutanée d'orthoiodohippurate marqué avec ^{131}I dans la région supraclaviculaire d'un rat, l'appareil a permis de constater la migration dans les reins en 3 min, dans la vessie en 5 min et l'évacuation totale dans la vessie en 90 min. On a fabriqué des prototypes de chambres à scintillation plus grandes, avec des cristaux de 1,3 × 30 cm.

ДИНАМИЧЕСКИЕ ИССЛЕДОВАНИЯ С ПОМОЩЬЮ СЦИНТИЛЛЯЦИОННОЙ КАМЕРЫ ДЛЯ ГАММА-ИЗЛУЧЕНИЯ. Коммерческая модель сцинтилляционной камеры для гамма-излучения типа Ангера, используется в данной лаборатории с октября 1962 года для изучения динамики физиологических и фармакологических процессов in vivo. Кристалл NaJ размером 0,6 × 20 см проецируется двенадцатью фотоумножителями. Световые вспышки генерируются на этой пластинке с помощью гамма-лучей, возбуждаемых электронным способом, которые появляются на экране осциллоскопа в виде маленьких вспышек в симметричных участках. Камера "Полароид", сфокусированная на этот экран постепенно создает картину, пространственная плотность которой соответствует пространственному распределению гамма-лучей, проецируемых с биологического объекта на коллимирующую систему. Используется либо "булавочное отверстие" диаметром 5 мм, либо свинцовый многоканальный коллиматор с 771 отверстием, для наблюдения за областью с максимальным диаметром приблизительно 16 см.

Этот простой прибор дает точные "точка за точкой" электронные сценнограммы. Изображения не содержат линейных структур исказающих восприятие. Какие-либо механические трудности отсутствуют.

Возможность постоянного наблюдения внутренних органов, представляющих интерес во время сценнирования, позволяет уменьшить дозу радиоактивности и статистические ошибки. Уникальной особенностью является то, что эта камера обеспечивает возможность последовательно делать снимки, чтобы зафиксировать быстрые изменения в распределении гамма-изотопов. Максимальная скорость, 3 снимка в каждую минуту, была получена с помощью 10-секундной катушечной пленки "Полароид". Киноаппарат может обеспечить более высокие скорости, когда требуется зафиксировать изменения при чрезвычайно быстрых процессах.

После внутривенного введения йодо-131-йодида у крыс, получавших пуриновую диету, (Лабхоу), на серии снимков, сделанных в течение первых двух минут в течение последующих шести пятиминутных интервалов обнаружено быстрое исчезновение радиойода, первоначально распределившегося во всем организме, и концентрация в области желудка в течение 30 минут. Большая часть радиоактивности сосредоточилась в этом месте в течение последующих 7 часов эксперимента. За это время только очень небольшое количество аккумулировалось в щитовидной железе.

Подобно этому после подкожного введения меченой йодом-131 ортойодной производной гиппуровой кислоты в надключичное пространство крыс с помощью камеры установлено перемещение препарата в почки через 3 минуты, в мочевой пузырь — через 5 минут и полное очищение мочевого пузыря за 90 минут.

В последнее время были изготовлены более крупные прототипы сцинтилляционных камер, в которые вмонтированы кристаллы размером 1,3 × 30 см.

ESTUDIOS DINÁMICOS CON UNA CÁMARA DE CENTELLEO DE RAYOS GAMMA. En los laboratorios del Centro Médico de la Universidad del Estado de Ohío se emplea desde octubre de 1962 un modelo comercial de cámara de centelleo de rayos gamma, del tipo descrito por Anger, para estudiar in vivo procesos dinámicos fisiológicos y farmacológicos. Un cristal de NaI de 0,6 × 20 cm es analizado por 19 fotomultiplicadores. Los centelleos producidos en esta placa por los rayos γ se transforman electrónicamente y aparecen en la pantalla de un osciloscopio como pequeños destellos en las mismas posiciones relativas. Una cámara Polaroid enfocada sobre esta pantalla forma gradualmente una imagen cuyas densidades representan la distribución espacial de los rayos γ que penetran a través del sistema colimador. Para observar un área de unos 16 cm de diámetro máximo se emplea un orificio de 5 mm de diámetro o un colimador de plomo de 771 canales. Este ingenioso instrumento efectúa electrónicamente verdaderas exploraciones «por puntos». Las imágenes carecen de las estructuras lineales que obstaculizan la percepción. No es posible que surjan dificultades mecánicas.

El hecho de poder observar continuamente toda el área de interés durante una sesión de exploración tiene la ventaja de reducir la dosis de radiactividad y los errores estadísticos. Una de las características de esta cámara es que permite tomar imágenes a un ritmo acelerado para registrar cambios en la distribución de isótopos emisores γ. Con una película Polaroid de 10 s se ha logrado un máximo de tres fotografías por minuto. Una cámara cinematográfica permitiría trabajar con una frecuencia todavía mayor si ello fuese necesario para registrar movimientos en procesos estraordinariamente rápidos.

Después de inyectar por vía intravenosa yoduro marcado con ^{131}I en una rata alimentada con purina Labchow, se tomaron unas series de imágenes durante los dos minutos primeros de seis intervalos sucesivos de cinco minutos de duración; esas imágenes revelaron una rápida desaparición del radioyodo inicialmente distribuido por todo el organismo y, al cabo de 30 min, una concentración en la región del estómago. La mayor parte de la radiactividad siguió localizada en dicha región durante las siete horas restantes del experimento, después de las cuales sólo una pequeña cantidad se había acumulado en la tiroides. Análogamente, después de una inyección subcutánea de ortoyodohipurato-^{131}I en la región supraclavicular de una rata, la cámara reveló una migración hacia los riñones a los tres minutos, hacia la vejiga a los cinco minutos y la depuración completa en la vejiga al cabo de 90 min. Recientemente se han construido prototipos mayores de cámaras de centelleo con cristales de 1,3 × 30 cm.

1. OPERATION OF THE PINHOLE γ-RAY SCINTILLATION CAMERA

The theory and performance of the scintillation camera have been described previously [1-10]. The experimental prototype γ-ray scintillation camera* used in this laboratory since October 1962 is equipped with a 0.25-in-thick by 8-in-diam. NaI (Tl) crystal fluor plate that is "viewed" by 19 RCA 6199 1.5-in-diam. multiplier phototubes through about an inch of clear mineral oil. The lead housing collimator shield is 1.5 in thick. Of the three interchangeable dense metal "pinholes" of various apertures supplied with the instrument for insertion into the lower end of the lead shield, the one selected for this investigation has a 0.25-in-diam. aperture.

Light flashes generated in the crystal fluor by γ-rays that pass through the pinhole are caused "electronically" to appear as small coruscations in the same relative positions on the screen of an oscilloscope.

The read-out system included an oscilloscope camera which is referred to as the "recording camera" in this communication. It is equipped with a 75-mm f/1.9 lens that is focused on the screen. The shutter of this recording camera is locked open so the camera "sees" the oscilloscope screen continuously. This camera starts to record the individual coruscations as they appear on the oscilloscope screen whenever the circuit of the odometer-type timer is actuated, and it stops recording when the preset interval of the timer automatically ends and the oscilloscope beam is thereby interrupted. A Polaroid camera back is incorporated into the recording camera of the oscilloscope.

When one wishes to record tiny bright white dots, the lens is used at full f/1.9 aperture. The areal densities of these dots in the picture that gradually forms represent the relative spatial distributions of γ-rays projected from the biological object into the collimating system.

The diameters of the dots may be varied from less than 0.1 mm to about 1 mm simply by manipulating the intensity control dial of the oscilloscope. The "γ-icon" [11] pictures in Fig. 1 were made with the aperture of the

* Manufactured by Nuclear-Chicago Corporation, 333 East Howard Avenue, Des Plaines, Illinois.

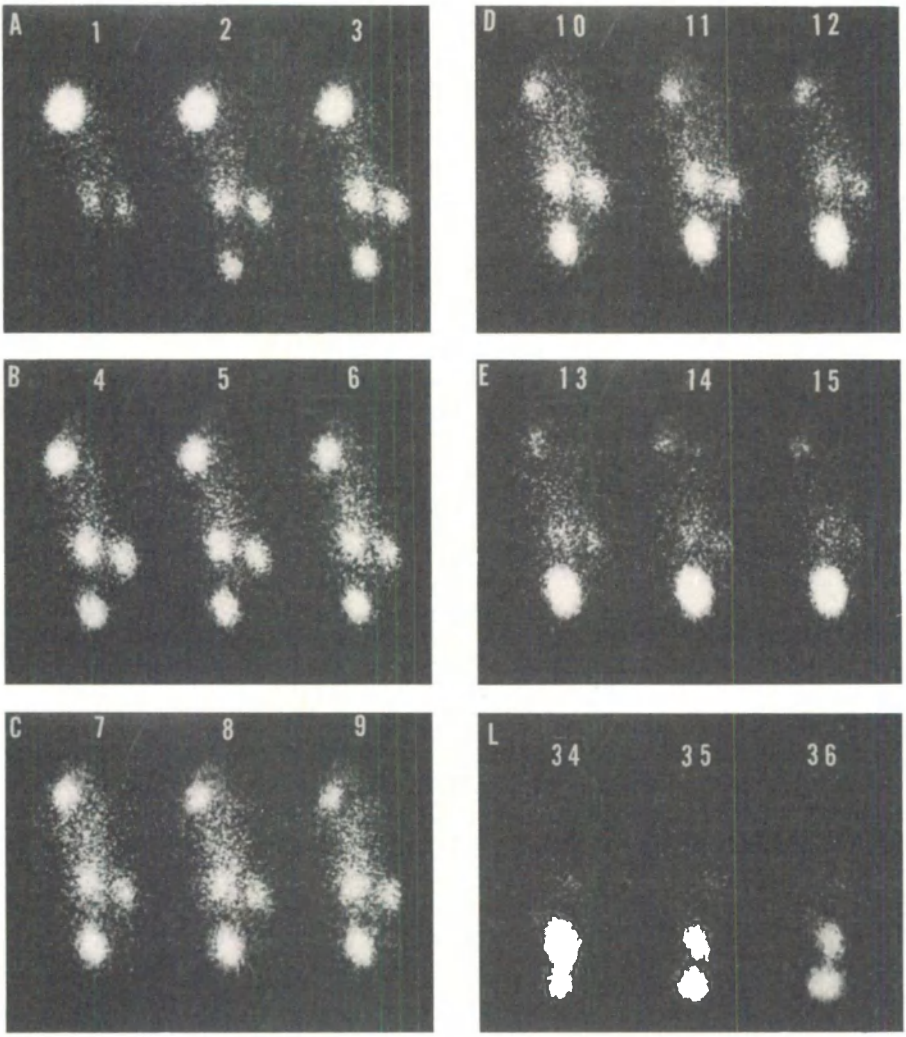

Fig. 1

"γ-icon" pictures made with the aperture of the recording camera decreased to f/4

recording camera lens decreased to f/4. This simple adjustment caused the individual white dots to be accompanied by a slightly elongated grey "halo" which overlapped and blended to build up pictures with a pleasing "halftone" gradation quality. The same effect resulted when the recording camera was thrown slightly out of focus, or a "defocusing" lens was placed over the camera lens.

Polaroid-type 47-speed 3000 roll film was used in the recording camera to accumulate the dots in the integrated patterns which constitute the individual pictures. The rectangular "frame" area is 7.4 × 9.8 cm. The scintillation camera is usually adjusted to make the diameter of a picture

of background about 5 cm. Because the camera was used to study the changing distribution in time of a "γ-ray carrier" [12-14] compound in rats that were 20-25 cm long from nose tip to tail base, the width of the "area of interest" was less than half of the length. Consequently, the movable carriage of the recording camera back was moved laterally along a grooved guide to register sets of 3 pictures each on a single frame, as shown in Fig. 1. Thus the 18 separate pictures in the figure were recorded on only 6 frames.

The "picture-period" intervals when dots were being registered were 3 min each. The "change-cycle" intervals between pictures were 2 min each, during which the recording camera carriage was re-positioned to register the 2nd or 3rd picture on the frame, or a frame bearing a set of 3 pictures was being developed within the camera, or both. The automatic picture-period odometer timer was also returned to zero during each change-cycle interval.

The Polaroid picture read-out system in the present scintillation camera is most convenient because a finished picture record may be processed and the data be ready for inspection and permanent storage within seconds after the circuitry automatically ends a preset picture-period interval. Development processing of the picture frame within the recording camera occurs during 10 s after the Polaroid reagent pod is broken by an external trigger manipulator and its contents are spread over the exposed sensitive surface during the manœuvre that advances the next frame into recording position. While development processing is occurring in these 10 s, the scintillation camera circuitry may be actuated again and a picture be recording on the next frame without loss of time.

Studies with a highly radioactive I^{131} phantom have demonstrated the feasibility of readily making pictures with the present read-out system at rates as high as 6/min, with 6-s picture-period intervals and intervening 4-s change-cycles. This means that very rapid dynamic processes might be recorded on 24 "stop-motion" pictures during only 4 min of "elapsed time" were they to be made in sets of 3 pictures on each of the 8 frames in a single roll of film.

The amount of the γ-ray carrier compound to be injected is adjusted in the syringe so that, when it is placed 20 cm below the pinhole, the counting-rate-meter in the circuitry indicates a range of about 1500-5000 cpm, depending on the anticipated duration and frequency of the pictures to be recorded.

A useful practical indication of the resolution is found in Fig. 1 where one sees that the kidneys of the rat are clearly distinguishable.

The background counting rate is 45-50 min when the usual energy discriminator "window" of the spectrometer includes the 364-keV I^{131} γ-ray peak symmetrically. For the 279-keV γ-ray of Hg^{203} the background rate is 75-80 cpm.

A useful practice is to record "background pictures" during the night and at other times when the scintillation camera is not otherwise in use. These monitor pictures of background serve to demonstrate the location and maximum diameter of the recording area, as well as the size and quality of the dots, and that other adjustments of the instrument are in operational readiness.

The scintillation camera circuitry is remarkably stable and little adjustment is required when it is left in operation continuously. Anticipated difficulties because of the sophisticated circuitry in this initial commercially-produced scintillation camera have not materialized. Field engineers have quickly restored the camera to the original operating order on two occasions when difficulties were encountered with the spectrometer and with the oscilloscope during the first year. Adjustment of the potentiometers to each of the multiplier phototubes to keep the picture field uniform has not been necessary in a year and a half of operation. No leakage of the mineral oil "light pipe" medium has occurred when the scintillation camera head has been operated with the pinhole pointed upward. Obviously, no mechanical difficulties could have been encountered.

Plans to improve the operation of the scintillation camera include the incorporation of an additional oscilloscope of the persistent-screen storage variety [8]. This should prove useful as a monitor for the present read-out system to help the camera operator decide quickly what the picture-period and the change-cycle intervals should be during the recording of the first few pictures, especially when a very rapid dynamic process is under study.

Another simple improvement, which will increase resolution and permit the pinhole version of the scintillation camera to be used with γ-rays of higher energy, would be the use of a pinhole insert made of "depleted" uranium. Rough experiments have indicated that the background will not thereby be increased significantly. Calculations reveal that the increased linear absorption coefficient of uranium will permit the pinhole camera to be used with the 511-keV γ-rays that accompany positronium annihilation and possibly with the 662-keV γ-rays of 2.6-min Ba^{137m} as well [6], especially when the thickness of the NaI(Tl) fluor plate is increased to 0.5 in [4, 8]. Marked improvements in these respects are anticipated when crystal fluor plates become available that have greater density and are composed of elements having higher atomic numbers.

2. EXPERIMENTAL

The first 12 "γ-icon" picture scans in Fig. 1 illustrate a principal advantage of scintillation cameras [1-10] over a mechanical scanning machine [11], for they were all made electronically in less than an hour. The study was designed to follow in vivo the rapidly changing distributions in time after subcutaneous injection of I^{131}-orthoiodohippurate * (OI* H). The objective was to establish a potential clinical applicability [10] of a "γ-ray carrier" [12-14] compound [15] for making "γ-icon" [11] pictures of the kidneys when administered in a manner to provide a usefully long transit time through them [16, 26].

A rat that was 20 cm long from the tip of the nose to the base of the tail was anaesthetized with diethyl ether. It was placed in the supine position 20 cm below the 0.25-in-diam. pinhole of the γ-ray scintillation camera. About 150 μc of OI*H in 0.7 ml of solution was injected rapidly subcutaneously into the right supraclavicular region at zero time.

* The I^{131}-orthoiodohippurate was donated for these studies by the Volk Radiochemical Company, 8260 Elmwood Ave., Skokie, Illinois.

The circuitry of the scintillation camera was actuated simultaneously to start accumulation of white dots as described in Section 1. The initial picture gradually built up during the first 3-min picture-period (Section 1). Then, in the 2-min change-cycle, the carriage of the Polaroid camera back was moved manually into the middle position in readiness to record the second 3-min picture in the 5 to 8-min elapsed-time interval after start of injection of OI*H at zero time. The third picture on the same frame A was made similarly during the 10 to 13 min elapsed-time interval. Then the Polaroid reagent pod within the camera was broken by the externally triggered mechanism and its contents were spread over the first frame A bearing pictures 1-3 to develop it, in the course of the manual advancement of the 2nd frame B into exposure position. Development processing of frame A was permitted to occur for 10-20 s before the first set of 3 pictures was removed from the back of the Polaroid camera. Then the camera carriage was returned to the initial position and the fourth picture was recorded for a 15 to 18-min elapsed-time interval at the left of the set of 3 pictures on the second frame B.

In Table I are listed 18 3-min elapsed-time intervals when the scintillation camera viewed the entire rat, together with the intervening 2-min change-cycles. Because of little change between pictures 15 and 33 during 75-163 min of elapsed time in the phenomena under study, frames F-K are not included in Fig. 1 and Table I.

3. RESULTS AND DISCUSSION

The first picture (see Fig. 1), which was recorded during only 3 min after an injection of the OI*H, shows that some of this "γ-ray carrier" compound [12-14] had already appeared in the kidneys [15, 16], although most of it remained at the site of subcutanous injection.* Picture 2 on frame A (Fig. 1) shows that some OI*H appeared in the bladder during the 5-8 min of elapsed time. It was possible to depict this rapid migration into the kidneys in 3 min, and into the bladder by 8 min, only because the scintillation camera scans point-by-point electronically and views an entire area of interest throughout a seance, however short this be made. Thus one may readily "stop" the motion of "atomic" pharmacological substances labelled with γ-isotopes [10] and demonstrate short "organ times" by iconography. This proved to be impossible previously with our conventional line-by-line mechanical scanning machine [11].

In Fig. 1 picture 5 (middle of frame B) demonstrates that there was almost the same amount of OI*H in the bladder and at the injection site during the 20 to 23-min elapsed-time interval. Thence the OI*H gradually "changed ends" as it faded from the injection site and most of it had reappeared in the bladder in about an hour (Fig. 1, picture 13, frame E). Pictures 1-15 of Fig. 1 clearly demonstrate that OI*H freely diffuses from a site of subcutaneous injection into the blood-stream of a rat, from which most of it is promptly cleared by the kidneys as first described by TUBIS et al. [15].

* It is tacitly assumed here that the I^{131} γ-isotope label remains firmly bound to the carrier compound so that it serves to "represent" the changing distribution of OI*H with time.

TABLE I

ELAPSED-TIME INTERVALS OF THE PICTURES

Serial picture number	Elapsed time (min)	Total gross counts	Serial picture number	Elapsed time (min)	Total gross counts
	Frame A			Frame D	
1	0-3	7424	10	45-48	6720
2	5-8	7040	11	50-53	6592
3	10-13	6816	12	55-58	6784
	Frame B			Frame E	
4	15-18	6688	13	60-63	6688
5	20-23	6560	14	65-68	6944
6	25-28	6560	15	70-73	6688
	Frame C			Frame L	
7	30-33	6688	34	165-168	6080
8	35-38	6592	35	170-173	4480
9	40-43	6624	36	175-178	4640

~150 μc of I^{131}-orthoiodohippurate (OI*H) in 0.7 ml of solution was injected subcutaneously at zero time into the right supraclavicular region of a female rat, 20 cm long from tip of nose to base of tail. She was anaesthetized with diethyl ether and laid in the supine position. Picture-periods were 3 min each, during which the listed numbers of dots were recorded; and change-cycles between pictures were 2 min each. Serial picture numbers and the elapsed-time intervals after the start of the injection correspond to the pictures in Fig. 1.

Note: A set of 3 pictures appears on each Polaroid frame.

Clearly the objective of this study was fulfilled and "γ-icon" pictures of the kidneys may be made soon (see below) after an OI*H subcutanous injection [16, 26]. The absorption rate from such an injection site into the blood stream of the rat is such as to result in the equivalent of a slow intravenous infusion. The grater convenience is manifest. Complete clearance of the OI*H into the bladder in less than 3 h is advantageous in comparison with the use of γ-ray carriers of mercury radioisotopes which have prolonged retention in the kidney, and which not only give unnecessary and therefore undesirable radiation exposures, but also preclude early repetition.

Pictures 34 and 35 on frame L (Fig. 1) were made between 165 and 173 min after the OI*H was injected subcutanously. The rat's vulva had been covered by a slightly dampened cotton pledget. And the pictures show that the bladder partially emptied the OI*H in it on to this pledget. The decreased counting-rate between the elapsed-time intervals 165-168 and 170-173 min in Table I indicate that absorption of I^{131} into the pledget obscured it somewhat from the pinhole.

The amount of OI*H present in each rat kidney appears to have been approximately the same in the first few pictures. But pictures 6-12 (Fig.1) demonstrate a lesser amount of the γ-isotope carrier compound in the left than in the right kidney. This phenomenon of differences in the quantity of OI*H in one or the other kidney at different times has been observed repeatedly [22] but no ready explanation comes to mind to account for it. Possibly the re-absorption of OI*H varies with time in a given kidney. Or, the blood supply to a kidney may occasionally lessen functionally. Either possibility raises the question of the interpretation of the relative sizes of the kidneys based on γ-icon scans made long after the subcutaneous injection of OI*H in rats. Our preliminary observations of this phenomenon justify much further work, especially in experiments designed to compare the γ-icon pictures made after the administration of OI*H, intravenously or otherwise, and in widely different specific activities.

TUBIS et al. [15] stated that OI*H does not complicate kidney function studies in man because of liver uptake. But DOLLERY and MATTHEWS [17] found an appreciable accumulation of OI*H by the livers of rats soon after intravenous injection. And picture 2 (Fig. 1) shows the beginning of a diffuse extrarenal accumulation of I^{131} label in what could well have been the liver, 5-8 min after a subcutanous injection. The relative proportion of the OI*H uptake in this extrarenal site reached a maximum in pictures 7-9 of frame C (Fig. 1) about 30-43 min after injection, and OI*H was still discernible in the same region in picture 13 an hour after injection.

Here one appreciates the unique features of the scintillation camera, first described by ANGER [1-4]. DOLLERY and MATTHEWS [17] used 30 rats and much time and effort to demonstrate that the same γ-ray carrier, I^{131} hippuran, accumulated in and disappeared from the liver of this species at rates which paralleled those found in the kidney. They stated, "No doubt other compounds will become available in time with advantages over hippuran. It may be valuable to examine their organ distributions in animals as a preliminary indication of their advantages and disadvantages for test procedures in man." A brief disclosure [10] recently indicated that the scintillation camera is proving to be especially useful for such studies in this laboratory.

A long search for γ-ray carrier compounds of potential clinical applicability has been under way here, and for 18 years several hundreds of them have been synthesized and studied in animals in this laboratory [12-14, 18,19]. Recent preliminary studies made by means of the scintillation camera have indicated that 2.6-diiodo-sulphanilate-I^{131} anion and EDTA-Cr^{51} chelate may have been proved to be useless in radioisotope renography [20, 21] because the pictures reveal little "hold-up" localization during rapid clearances of these γ-ray carriers from the blood through the kidneys of rats. Assuming these early studies can be confirmed, one is struck with the unique opportunity provided by the scintillation camera to pursue fundamental studies in vivo of times of hold-up in the kidney – possibly due to different degrees of re-absorption – of a wide variety of γ-isotope labelled compounds bearing acidic, or basic, or other functional chemical groups, as well as isomeric forms of them.

A particular advantage of the scintillation camera in studies of this nature is that a single animal serves as its own control throughout the experiment. This contrasts with the methods used by DOLLERY and

MATTHEWS [17] and with those used previously in this laboratory [18], where the dissection of several animals at each interval after injection of the labelled compounds is required. It seems probable that in many laboratories the savings realized in costs of animals and personnel time will soon offset the initial high cost of the instrument.

TUDDENHAM [23] presented concepts concerned with minification as an aid to perception in roentgenography, and SELTZER [24] recently advocated the use of a minifying lens as a simple means of contrast enhancement of the isotopic scintiscan. It will be noted that each γ-icon picture made in these experiments by means of the scintillation camera was automatically minified about 4 or 5 times. This intrinsic feature of the instrument is not only advantageous in the perception of details in the γ-icon picture, but it also provides for convenient storage and transportation.

4. CONCLUSIONS

The 18 pictures in Fig. 1, each taken within only 3 min, reveal, by "stop-motion" sequential iconography, the history of the movement of I^{131}-orthoiodohippurate from the site of a subcutaneous injection, through the kidneys, and into the bladder of a rat within about 3 h. They demonstrate the unique power of the scintillation camera, invented by Hal Anger, to provide an elegant method for study in vivo of the dynamicity of fundamental biological processes referred to by Professor HEVESY in his Faraday lecture in 1950 [25].

Because the instrument "examines point by point" electronically, there is no line structure to distort perception.

The entire "area of interest" is viewed throughout the seance, however short. This feature gives rise to superior statistics in comparison with line-by-line γ-icon pictures [11, 10, 7]. The decreased dose of radioisotope required [4] causes decreased radiation exposure. A particularly valuable feature is the opportunity provided by the camera for doing radioisotope iconography with short-lived photon emitters such as 2.6-min Ba^{137m} [6] and 2-min O^{15} [19] as well as 20-min C^{11}, a positron-emitter of tremendous potential.

Studies with phantoms containing large amounts of I^{131} reveal that as many as 6 pictures/min may be made with the present recording read-out system. This is in contrast with the minimal time of several minutes required to make a single picture with a mechanical line-by-line scanning machine [11].

The operation of the scintillation camera does not involve heavy moving mechanical parts that may malfunction; nor can a patient be annoyed or endangered in this respect by the camera.

5. SUMMARY

The operation of an experimental prototype pinhole γ-ray scintillation camera is described. It is equipped with a rapid read-out system that provides finished picture records 10 s after exposure. Sequential iconography at

rates as high as 6 pictures a minute has been illustrated. Automatic minification in the resultant γ-icon pictures is advantageous. The scintillation camera is shown to provide an elegant method for the study of dynamic processes in vivo that are not otherwise demonstrable.

REFERENCES

[1] ANGER, H.O., "Scintillation Camera", Rev. sci. Instrum. 29 (1958) 27-33.

[2] ANGER, H.O., "Scintillation Camera and Positron Camera", Medical Radioisotope Scanning, IAEA, Vienna (1959) 59-73.

[3] ANGER, H.O., "Radiation Image Device", United States Patent Office 3,011,057 (Nov.28, 1961).

[4] ANGER, H.O., "Gamma-Ray and Positron Scintillation Camera", Nucleonics 21, No.10 (1963) 56-59.

[5] ANGER, H.O. and GOTTSCHALK, A., "Localization of Brain Tumors with the Positron Scintillation Camera", J. nucl. Med. 4 (1963) 326-330.

[6] BENDER, M.A. and BLAU, M., "The Autofluoroscope," Nucleonics 21, No.10 (1963) 52-56.

[7] TER-POGOSSIAN, M., KASTNER, J. and VEST, T.G., "Autofluorography of the Thyroid Gland by Means of Image Amplification", Radiology 81 (1963) 984-988.

[8] MALLARD, J.R. and MYERS, M.J., "The Performance of a Gamma Camera for the Visualization of Radioactive Isotopes in vivo", Phys. Med. Biol. 8 (1963) 165-182.

[9] MALLARD, J.R. and MYERS, M.J., "Clinical Applications of a Gamma Camera", Phys. Med. Biol. 8 (1963) 183-192.

[10] MYERS, W.G., "Scintillation Camera for In Vivo Studies of Dynamic Processes", J. nucl. Med. 4 (1963) 182.

[11] MUELLER, G.E. and MYERS, W.G., "The Gammicon", News in Engineering 27, No.4 (1955) 3/6.

[12] MYERS, W.G., "A Gamma Ray Carrier Compound Useful for Clinical Physiologic Dynamic Studies", Int. J. appl. Rad. Isotopes 2 (1957) 158.

[13] MYERS, W.G. and DIENER, C.F., "EDTA-Cr^{51} γ-ray Carrier", J. nucl. Med. 1 (1960) 124.

[14] MYERS, W.G., "EDTA-Co^{*} γ-Ray Carrier", J. nucl. Med. 2 (1961) 137.

[15] TUBIS, M., POSNICK, E. and NORDYKE, R.A., "Preparation and Use of I^{131} Labeled Sodium Iodohippurate in Kidney Function Tests", Proc. Soc. Exper. Biol. Med. 103 (1960) 497-498.

[16] SCHEER, K.E., Personal Communication (7 August 1962).

[17] DOLLERY, C.T. and MATTHEWS, C.M.E., "Distribution of Hippuran Labelled with I^{131} in the Kidneys and Liver", Brit. J. exptl. Path. 43 (1962) 329-332.

[18] MYERS, W.G., "Localization of Radioactive Compounds in Tumours", Cancer Research 10 (1950) 234.

[19] MYERS, W.G., Discussion, pp 272-273 in Progress in Medical Radioisotope Scanning, Proc. of Symp. at The Medical Division of The Oak Ridge Institute of Nuclear Studies, 22-26 October 1962, (KNISELEY, R.M., ANDREWS, G.A. and HARRIS, C.C., Eds.), Office of Technical Services, U.S. Department of Commerce, Washington, D.C.

[20] WINTER, C.C. and MYERS, W.G., "Three New Test Agents for the Radioisotope Renogram: DISA-I^{131}; EDTA-Cr^{51}; and Hippuran-I^{125}", J. nucl. Med. 3 (1962) 273-281.

[21] WINTER, C.C., Radioisotope Renography, The Williams & Wilkins Company, Baltimore (1963).

[22] MYERS, W.G., Unpublished.

[23] TUDDENHAM, W.J., "The Visual Physiology of Roentgen Diagnosis", Amer. J. Roentgenol., Rad. Therapy nucl. Med. 78 (1957) 116-123.

[24] SELTZER, R.A., Letter to Editor, J. nucl. Med. 5 (1964) 76.

[25] HEVESY, G.C., "The Application of Radioactive Indicators in Biochemistry", J. chem. Soc. (1951) 1618-1639.

[26] WINKEL, K., Nierendiagnostik mit Radioisotopen, Georg Thieme Verlag Stuttgart (1964) 116-118.

DISCUSSION

(On the three foregoing papers)

A. BAPTISTA: I should like to ask Dr. Kellershohn if the main spark chamber works in the proportional region and if an image can be obtained by means of this chamber alone.

C. KELLERSHOHN: The chamber does not work in the proportional region. My colleague, Dr. Lansiart, will answer your second question.

A. LANSIART: In the continuous regime, an image cannot be obtained with two electrodes only. In the assembly with three electrodes the spark is generated by the secondary electrons which result from the interaction of gamma rays with the gas or the wall and which are highly ionizing at the end of their paths.

A. BAPTISTA: We have reported on the use of the spark chamber in conjunction with a photomultiplier tube. We also found that, if the operating voltage were increased up to the Geiger-Müller region, the intensity of light obtained from the spark chamber was in certain conditions sufficient to produce an image on photographic film with very short exposures.

H.P. JAMMET: I should like to comment on the problem of obtaining quantitative information with scintillation cameras. These cameras serve two main purposes. First, they provide morphological information which can be used in diagnosis. Secondly, they permit the study of dynamic phenomena as a function of time. This is important not only in clinical diagnostic applications but also in experimental work on radioactive contamination and the distribution of radionuclides in the organism. Quantitative interpretation of such data is difficult since it requires not only a knowledge of surface intensity but also an assessment of distribution of radioactivity in three dimensions and an estimation of the volume of the organ concerned.

A. DESGREZ: I should like to point out that, when the local activity varies as a function of time, it is possible to obtain an image by integrating the product of activity and time. Figure 1 shows a nephrogram obtained in the usual manner with I^{131}-Hippuran and a picture taken with a gamma camera during the recording of the nephrogram, the camera being placed between the two counters and moved slightly backwards. One can clearly distinguish on the gamma-camera picture the bladder and the two kidneys. The nephrogram indicates delayed drainage from the right kidney, which appears bigger and darker on the camera picture.

P.C.R. TURNER: I should like to comment on the possibility of obtaining a digital presentation of the data, using Anger-type cameras. The positioning information is presented as two analogue signals, the X and Y signal pulses, coinciding with an unblanking pulse. To present this information in digital form requires an analogue-to-digital conversion. To perform a complete analysis a two-dimensional analyser would be necessary; the information could then be stored in a ferrite store for later read-out. Such two-dimensional analysers are widely used in nuclear physics research but are usually more complex than we require. However, some 512-channel, one-dimensional, analysers have twin converters and can be used as two-dimensional analysers with a 16×32 matrix. Some modifications to the electronics of the camera are necessary to ensure that all positioning signals

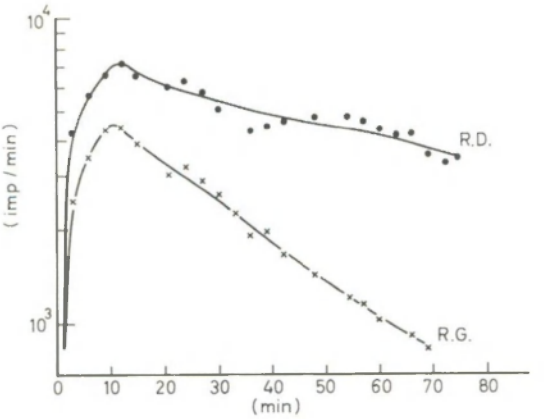

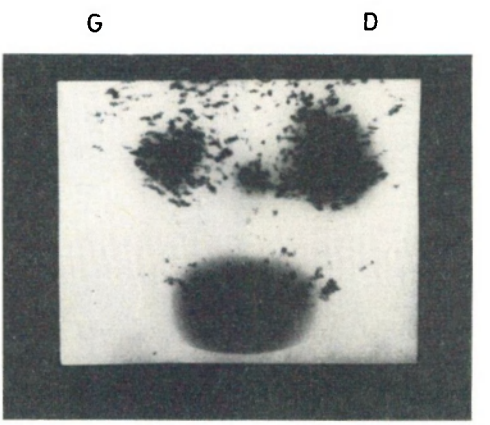

Fig. 1

Above: Nephrogram obtained with I^{131}-Hippuran
Below: Simultaneous gamma-camera picture showing kidneys and bladder

are of the same sense; this merely requires a shift of origin. This approach is rather cumbersome but it is necessary since the data are presented in an analogue form. An advantage of the elegant device described in a paper by Dr. Bender* is that the data are presented directly in digital form.

J. MALLARD: Two points arise from Professor Myers' paper. Firstly, Dr. Goolden has performed a series of colour scans at Hammersmith Hospital showing that it takes 24 hours for radioactive iodine to pass from the stomach to the thyroid in rats on iodide-free diet. I understand that the rat has an unusual iodine metabolism, but I do not know the details. Secondly, if one uses a storage tube instead of a cathode-ray oscilloscope, one can get any level of background suppression and contrast desired simply by turning a contrast-control knob, without losing the original picture stored on

* BENDER, M.A., "The clinical use of the autofluoroscope" (SM-51/70), these Proceedings I.

the storage mesh. This picture can be obtained again by turning the control knob in the opposite direction.

W.G. MYERS: As I suggested in my paper, I should like to incorporate a persistent-screen oscilloscope in my scintillation camera to serve as a monitor which would indicate how long the exposures should be when the polaroid read-out system is used.

P.C.R. TURNER: I should like to ask Dr. Jammet what type of image-storage tube he uses and if he could quote a figure for the writing rate.

H.P. JAMMET: The tube is made by the Compagnie Générale de Télégraphie Sans Fil (C.S.F.), 79 Boulevard Haussmann, Paris 8e. The tube has been used to record a sine curve of frequency 8 MHz with a peak-to-peak amplitude of 4 cm, corresponding to a speed of 1000 mm/μs. Brightness is then weak and contrast very mediocre.

THE DIGITAL AUTOFLUOROSCOPE

M. A. BENDER
ROSWELL PARK MEMORIAL INSTITUTE, BUFFALO, N. Y.
UNITED STATES OF AMERICA

Abstract — Résumé — Аннотация — Resumen

THE DIGITAL AUTOFLUOROSCOPE. The autofluoroscope is a stationary device designed to give a graphic representation of the distribution of gamma-emitting isotopes within the human body. The instrument incorporates the important features of modern scanners including collimation with a good depth response and adequate resolution, high efficiency and a high contrast data presentation system.

The detector consists of 300 2-in thick, $\frac{3}{8}$-inch diam. NaI (Tl) crystals packed in 20 files and 15 ranks in a 6 x 9-in array. Each of the 300 crystals is optically coupled to two Plexiglas light pipes with the 20 light pipes from a given rank going to one phototube and the 15 light pipes from a given file going to another phototube. Pulses occurring simultaneously in any pair of the 35 phototubes uniquely identify the crystal in which an interaction occurred. The position signal derived from the phototube array is independent of pulse height. Anticoincident circuits reject the simultaneous pulses arising from a Compton interaction followed by the absorption of the scattered radiation in an adjacent crystal. The digital nature of the light pipe system lends itself easily to magnetic core storage with subsequent non-destructive continuous read-out on a full-size CRT or numerical print-out for quantitative analysis.

The first advantage of the autofluoroscope over radioisotope scanners is a marked reduction in the time required to make an examination. Using the same dosage schedule, brain and liver tumours are localized in one tenth the time needed for conventional scanning.

The second advantage is related to the fact that information is collected from an entire organ at the same time. This permits the visualization of dynamic processes and the use of isotopes or labelled compounds having exceedingly short physical or biological half-lives. With decreasing half-life, there can be a commensurate increase in administered dose resulting in even shorter examination times. Exposure times can be so short that cinephotographic techniques are now used for the visualization and quantitation of the passage of I^{131}-labelled Hippuran through the kidneys and Ba^{137m} through the chambers of the heart.

L'AUTOFLUOROSCOPE NUMÉRIQUE. L'autofluoroscope est un appareil fixe destiné à donner une représentation graphique de la répartition des émetteurs gamma dans le corps humain. Cet instrument possède les caractéristiques principales des scintigraphes modernes: collimation donnant une bonne réponse en profondeur et une résolution suffisante, grande efficacité et fort contraste.

Le détecteur se compose de 300 cristaux de NaI(Tl) de 5 cm d'épaisseur et de 1 cm de diamètre, disposés en 15 rangées comportant chacune 20 cristaux; l'ensemble forme un rectangle de 24 cm de long sur 15 cm de large. Chacun des 300 cristaux est couplé à deux conduits optiques en plexiglas; les 20 conduits correspondant aux cristaux d'une même rangée conduisent à une cellule photoélectrique et les 15 conduits correspondant aux cristaux d'une même colonne conduisent à une autre cellule photoélectrique. Les impulsions produites simultanément dans deux quelconques des 35 cellules identifient le cristal qui a été le siège d'une interaction. Le signal de position donné par la batterie de cellules photoélectriques est indépendant de l'amplitude d'impulsion. Des circuits à anticoïncidence éliminent les impulsions simultanées dues à la diffusion Compton suivie de l'absorption du photon diffusé par le cristal voisin. Etant donné leur caractère numérique, les données fournies par l'ensemble des conduits optiques peuvent être facilement stockées dans un tore magnétique et ensuite lues continuellement, sans être détruites, sur un enregistrement échelle grandeur, TCR ou numérique, aux fins d'analyse quantitative.

Le premier avantage de l'autofluoroscope sur le scintigraphe réside dans la diminution considérable du temps nécessaire pour procéder à une exploration. Avec la même dose de radioisotopes, on localise des tumeurs du cerveau et du foie dix fois plus vite que par la scintigraphie classique.

Le deuxième avantage est que les données sont recueillies en même temps sur la totalité de l'organe. Cela permet d'observer des processus dynamiques et d'utiliser des radioisotopes ou des composés marqués ayant une période physique ou biologique extrêmement courte. Plus la période est courte, plus la dose administrée

peut être élevée, ce qui permet des temps d'exploration d'autant plus réduits. La durée de l'exposition peut devenir tellement brève qu'il est désormais possible d'exploiter les techniques cinéphotographiques pour l'observation quantitative du passage de l'Hippuran marqué à l'iode-131 dans le rein et du baryum-137m dans les cavités du cœur.

ЦИФРОВОЙ АВТОФЛУОРОСКОП. Автофлуороскоп является стационарным прибором, предназначенным для получения графического изображения распределения гамма-излучающих радиоизотопов в человеческом организме. Этот прибор сочетает важные черты современных сканнеров, включая коллимацию, с хорошей глубиной чувствительности и достаточной разрешающей способностью, высокой эффективностью и высококонтрастной системой представления данных.

Детектор состоит из 300 кристаллов NaJ (Tl) толщиной 5 см и диаметром 9 мм, упакованных в штабель размером 15 × 22,5 см, имеющий 20 рядов и 15 групп. Каждый из 300 кристаллов оптически соединен с двумя световыми плексигласовыми трубками, причем 20 световых трубок из данной группы подходят к одной фототрубке и 15 световых трубок из данного ряда подходят к другой фототрубке. Импульсы, возникающие одновременно в любой паре из 35 фототрубок, в равной мере достигают кристалла, в котором происходит взаимодействие. Позиционный сигнал, возникший в фототрубке, не зависит от высоты импульса. Контуры антисовпадения отводят одновременные импульсы, возникающие в результате взаимодействия Комптона, за которым следует абсорбция рассеянного излучения в соседнем кристалле. Цифровой характер системы световых трубок хорошо приспособлен к хранению на магнитном сердечнике с последующим непрерывным считыванием без разрушения показаний на полноразмерной катодно-лучевой трубке или к цифровому выписыванию для количественного анализа.

Первым преимуществом автофлуороскопа над радиоизотопными сканнерами является значительное сокращение времени, необходимого для исследования. При равной системе доз опухоли мозга и печени обнаруживаются в течение 0,1 времени, необходимого для обычного сканнирования.

Второе преимущество связано с тем, что предоставляется информация обо всем органе. Это дает возможность проследить динамические процессы визуально и использовать изотопы или меченые соединения, имеющие очень короткие периоды полураспада и полувыведения. С уменьшением периода полураспада может быть произведено соответствующее увеличение вводимой дозы, результатом чего является сокращение времени обследования. Время облучения может быть таким коротким, что в настоящее время стали использовать кинофотографические методы для визуального наблюдения и количественного определения прохождения гиппурана меченого, йодом-131, через почки и барием-137 через полости сердца.

AUTOFLUOROSCOPIO NUMÉRICO. El autofluoroscopio es un dispositivo fijo que sirve para representar gráficamente la distribución de los isótopos emisores gamma en el cuerpo humano. Como los aparatos modernos de exploración, ese instrumento dispone de un colimador sensible a fuentes profundas, con un poder de resolución suficiente, y de un sistema de alta eficacia para la presentación de datos con un contraste satisfactorio.

El detector consiste en 300 cristales de NaI(Tl) de 2 pulg de espesor y $\frac{3}{8}$ pulg de diámetro dispuestos en 20 columnas y 15 hileras que forman un cuerpo de 6 × 9 pulg. Cada uno de los 300 cristales está acoplado ópticamente a dos conductores de luz de plexiglás; los 20 conductores de cada columna van unidos a un fotomultiplicador y los 15 de cada hilera a otro. Los impulsos que se producen simultáneamente en cualquier par de los 35 fotomultiplicadores permiten identificar el cristal en que ha ocurrido una interacción. La señal localizadora determinada por el conjunto de los fotomultiplicadores es independiente de la amplitud del impulso. Los circuitos de anticoincidencia rechazan los impulsos simultáneos debidos a una interacción de Compton seguida por la absorción de la radiación dispersa en un cristal adyacente. El carácter numérico del sistema de los conductores de luz permite almacenar los datos en núcleos magnéticos y analizarlos cuantitativamente por representación continua no destructiva en un osciloscopio en escala 1 a 1 por impresión de datos numéricos.

La primera ventaja que el autofluoroscopio tiene sobre los aparatos corrientes de exploración radioisotópica consiste en reducir notablemente el tiempo necesario para efectuar el examen. Utilizando el mismo plan de dosificación, los tumores del cerebro o del hígado se localizan con la décima parte del tiempo que requiere una exploración corriente.

La segunda ventaja estriba en que se reúnen simultáneamente datos para todo el órgano. Ello permite visualizar procesos dinámicos y emplear isótopos o compuestos marcados de período físico o biológico extremadamente corto. Al disminuir el período se puede aumentar la dosis administrada y reducir aún más el tiempo

necesario para el examen. Los tiempos de exposición pueden ser tan cortos que actualmente se emplean técnicas cinematográficas para visualizar y determinar cuantitativamente el paso del Hipuran marcado con yodo-131 por los riñones, o el paso del bario-137m por las cavidades del corazón.

Recent advances in instrumentation have extended the usefulness of scanning but they have not greatly affected two major drawbacks of this type of study: (1) The distribution of the radioactive agent must be essentially static for the duration of the scan (up to one hour): and (2) ill patients are frequently unable to lie motionless for such extended periods.

One approach to the solution of these two problems has been the development of scintillation cameras. Scintillation cameras are fixed devices that view an entire organ or area of interest and concurrently receive and record the gamma radiation arising from the field of view. The basic components of a scintillation camera are the detector, the data transfer system and the data-recording system. The detectors are large diameter NaI crystals or a mosaic of small diameter crystals with suitable collimators. The data-transfer system is a phototube array which detects the location of a photoelectric interaction and translates this into a positioning signal which can be displayed as a point of light in a corresponding position on the face of an oscilloscope or other imaging tube. The data recording system of film, a magnetic core memory, or an image storage tube can then integrate these flashes of light with a resulting build-up of a picture of the distribution of the isotope in the patient.

Scintillation cameras can reduce the examination time by a factor of ten and can easily follow rapid dynamic processes. To take full advantage of the cameras, however, it is necessary to incorporate in these instruments those features that were found to be important in radioisotope scanners, i.e. high efficiency, optimum resolution, and when necessary, a high-contrast data-presentation system.

The scintillation cameras presently in operation fall into three main groups: The gamma-ray camera developed by ANGER [1], the positron cameras developed by ANGER [2] and BROWNELL [3] and the autofluoroscope developed by BENDER and BLAU [4].

DETECTORS

Crystal assemblies

Gamma-ray and positron cameras have a single sodium-iodide imaging crystal. These vary from 5 to 11 1/2 in in diam. and from 1/4 - 1/2 in in thickness. The autofluoroscope detector is composed of a mosaic of 260 sodium-iodide crystals, 3/8 in in diam. and 2 in thick. These are packed in an array 6 × 9 in in size with 1 cm on centre separation. This configuration was designed for the visualization of small tumours in large organs.

With a single crystal, resolution can be varied at will, either by changing the collimator on a gamma camera or by changing the electronic resolution or crystal distances in a positron camera. The principal disadvantages of a single crystal are the necessary limitations in crystal size. Crystal

thickness cannot be greater than 1/2 in or there is a significant loss of resolution due to the increased probability in thicker crystals of a single gamma-ray undergoing multiple interactions. When these interactions result in total absorption the pulse will pass the pulse-height analyser and the data-transfer system will display one scintillation situated somewhere between the two events. MALLARD et al. [5] estimate that although a 1-in thick crystal would double the efficiency for the photoelectric absorption of the 365-kV gammas of I^{131}, 40% of the recorded signals would be displaced with an average positioning error of 1/2 in. The necessity of using a thin crystal results in decreased efficiency. This is especially important when detecting gamma-rays having an energy above 300 kV. Another problem arising from the use of a single crystal is the limitation on size and configuration imposed by available manufacturing techniques. Lastly there is a loss of information at the periphery of a single crystal due to edge effects which reduce the usable area.

It is possible to overcome some of the resolution problems associated with efficient, thick crystals by the use of crystal matrices or mosaics. The positioning errors which arise when a single gamma-ray interacts with more than one crystal can be eliminated by anticoincidence circuitry. In addition, the light output from the individually canned crystal elements is highly collimated. This provides freedom from edge effects, high photon collection efficiency, and permits the use of light pipe techniques for data positioning. Mosaics can be produced in any desired size and configuration. A disadvantage of crystal matrices is that crystal element diameters must be varied to provide different resolutions to match the clinical requirements. The resolution of the system can be no better than the on-centre separation of the individual crystal elements.

Collimation

The positron cameras rely on the coincidence detection of annihilation radiation for "collimation". The gamma-ray camera and autofluoroscope rely upon the interposition of a high-density collimator between the detector and the object under study. The original Anger gamma-ray camera utilizes a single pinhole aperture in a lead collimator. The optics are those of a conventional pinhole camera and this system has the advantage that the size of the field of view can be varied by varying the distance between the end of the collimator and the subject. The disadvantage of the pinhole approach is the problem of conical aberration in which a source moved along an axis parallel to the central axis of the collimator appears to have a different lateral displacement when the source is at different depths. This distortion is not a problem when examining the thyroid where the detector is viewing a thin, superficial organ, but accurate localization of brain and liver tumours at depths within the body is extremely difficult.

Multiple-channel collimators have been used with the gamma-ray camera and of necessity are used with the autofluoroscope. These collimators are constructed of lead, with cylindrical or conical apertures having parallel axes. The autofluoroscope collimator is composed of three 1-in thick slabs of lead which, when super-imposed, provide a single collimator aperture for each crystal. This aperture is 3 in long with a 1/4-in diam. opening

at the crystal side and a 1/8-in diam. opening at the patient side. The resolution obtained with these collimators and the 1 cm on-centre separation of crystals provides the minimal overall resolution necessary to effectively visualize 1.5 - 2 cm diam. tumours in large organs. This is generally satisfactory as most clinically significant tumours are of this size when the patients are referred for initial examination. If decreased resolution with an increase in efficiency is desirable, one or two of the lead slabs can be removed.

Data-transfer systems

Early scintillation cameras attempted to obtain the image of the distribution of an isotope by directly exposing a photographic plate to the light emitted from a sodium-iodide crystal [1, 6]. The sensitivity was low and such devices could be used clinically only with therapeutic amounts of radioactive materials. The next step was an attempt to use image amplifiers faced with sodium-iodide crystals to improve sensitivity [1, 7]. Early image amplifiers however had insufficient gain and excessive dark current levels so that these too could not be used with tracer doses. Recently BROWNELL [8] has investigated the use of currently available image amplifiers and he reports that, with recent developments and the use of pulsing techniques, it is now feasible to obtain the necessary gain without prohibitive dark current levels.

The major advance in gamma-ray camera design came with ANGER's development [1] of a data-transfer system composed of a matrix of multiplier phototubes viewing the sodium iodide crystal. The position of an interaction in the crystal is determined by the relative pulse heights from the phototubes in the array, phototubes located close to the point of interaction receiving more light than those at a distance. Mixing circuits translate the phototube pulses into vertical and horizontal positioning signals which are applied to an oscilloscope. To exclude the recording of scattered radiation, pulse-height analysis is used. The summed output of all the phototubes is fed to a pulse-height analyser, the output of which serves as an unblanking pulse for the oscilloscope. The unblanking occurs simultaneously with the positioning signals. The result is a flash of light appearing on the oscilloscope face corresponding in position to a photoelectric event occurring within the crystal. Anger's system of data transfer has been used successfully in the gamma-ray camera, the positron camera and the early version of the autofluoroscope.

A major disadvantage of the Anger system of data transfer is that the size of the positioning signals, and therefore the location of the flash on the oscilloscope, depends upon the absolute magnitude of the phototube pulse. Therefore, the validity of the positioning signal is directly related to the analyser window width employed. To minimize positioning errors of this type, it is necessary to restrict recorded pulses to a narrow pulse-height range, generally less than 10%. In scanning, a 20-30% window is used routinely and this provides effective discrimination against scattered events occurring within the patient's body, septal cross-over, or penetration of shielding. It would be desirable to construct a more efficient camera in

which the positioning signals are not dependent upon pulse height so that all photoelectric events could be used.

With a crystal matrix, as in the autofluoroscope, a totally different approach to data transfer is possible. The data-transfer system in the digital autofluoroscope identifies the crystal undergoing an interaction by direct light piping to a rank and file phototube system [9]. The crystal matrix and the collimator apertures have a rank and file pattern containing 20 rows and 13 files. Each of the 260 crystals is optically coupled to two plexiglas light pipes with 20 light pipes from a given rank going to a phototube and 13 light pipes from a given file going to another phototube. Pulses occurring simultaneously in any pair of phototubes uniquely identifies the crystal in which the interaction occurred. Each phototube has an individual amplifier-discriminator and the output of each amplifier is of fixed height and is not dependent upon the height of the incoming pulse if it exceeds the noise level. Anticoincidence circuits eliminate all pulses arising simultaneously in more than one rank or more than one file amplifier. Such pulses are the result of single gamma-rays undergoing a Compton interaction in one crystal followed by total absorption of the scattered photon in another crystal. Unless eliminated these events would give pulses of a proper pulse height but would result in inaccurate position information. Using the crystal matrix described above, 22% of 365-keV gamma-rays were found to cause this type of multiple interaction.

In the digital autofluoroscope, the elimination of the pulse-height dependence of the position signals and the rejection of multiple interaction events results in unambiguous position information. The resolution achievable with this type of device is limited only by the diameter of the crystal mosaic elements. Currently a high resolution mosaic is under construction (0.25-in on-centre separation).

The digital nature of light pipe transfer systems lends itself easily to magnetic core storage with subsequent non-destructive continuous read-out on a full-size CRT and numerical print-out for quantitative analysis.

Data recording

The original method of recording the image of the distribution of radioactive material was to place a Polaroid camera over the face of the oscilloscope and, using time exposures, integrate the information on film. The recording of each point of light can be compared with the dot recording originally used in radioisotope scanning. The disadvantage of this type of data presentation lies in the fact that small differences in detected count-rate are not readily visible. It is for example almost impossible to distinguish the difference between 100 and 120 dots/cm^2 without a very careful analysis of the data. Photorecording with subsequent closed circuit television contrast enhancement was developed for scanners so that the small difference in count-rate could be more easily visualized [10].

A similar but direct viewing system is used with the autofluoroscope. The closed-circuit television camera views the oscilloscope face. A Westinghouse No. WL 7383 Permacon image tube is used in the camera and is able to retain images for periods up to 30 min. The system has proved extremely useful for tumour localization as the image can be built up on the

face of the television monitor in true size. Contrast enhancement can also be applied non-destructively as needed.

CLINICAL APPLICATIONS OF THE AUTOFLUOROSCOPE

Tumour localization

With the exception of thyroid visualization, the autofluoroscope has been used for all the clinical studies which ordinarily require the use of a radioisotope scanner. To establish its diagnostic accuracy, patients were examined with the autofluoroscope immediately following scanning. Although the number of patients that have been studied in this fashion is still small, no lesions have been missed by the autofluoroscope that were successfully visualized by the scanner. In all cases the time of examination with the autofluoroscope was about one-tenth that required for the equivalent conventional scan. The reduction in time permits the examination of more patients and extends tumour localization techniques to a significant number of critically ill patients who cannot lie still for extended periods of time.

Dynamic processes

Scintillation cameras, unlike scanners, are able to visualize fast dynamic processes. It is possible to quantitatively follow the transport of tracer agents having short physical or biological half-lives through anatomical compartments with organs [11]. With the digital autofluoroscope it is possible to record the number of events that have occurred in each crystal. If desired, groups of crystals corresponding to designated anatomic configurations can be automatically summed.

The flow of I^{131} Hippuran through the renal cortex, medulla and pelvis has been evaluated with this technique in a number of patients having a variety of renal problems. These "compartmental renograms" were then compared with conventional renograms. Abnormalities in the latter could then be related to an abnormality in a specific region within the kidney.

Radioisotopes having very short physical half-lives can be administered to patients in large quantities without delivering an appreciable radiation dose. Ba^{137m}, the 2.6-min half-life daughter of Cs^{137}, delivers approximately 1 mr total body radiation for every millicurie injected. Ba^{137m}, milked from the patent Cs^{137}, has been used for the cinegraphic visualization of the chambers of the heart. The resolution obtained does not compare with that obtained with radio-opaque materials and cinefluoroscopy. However, quantitative information which cannot easily be derived from cinefluoroscopy is available with the radioisotope technique.

REFERENCES

[1] ANGER, H.O., "Scintillation Camera", Rev. sci. Instrum. 29 (1958) 27-33.

[2] ANGER, H.O. and ROSENTHAL, D.J., "Scintillation Camera and Positron Camera", Medical Radioisotope Scanning, IAEA, Vienna (1959) 59-75.

[3] BROWNELL, G., Discussion in Medical Radioisotope Scanning, IAEA, Vienna (1959) 79.
[4] BENDER, M.A. and BLAU, M., "Autofluoroscopy: The Use of a Non-Scanning Device for Tumor Localization with Radioisotopes", J. nucl. Med. 1 (1960) 105.
[5] MALLARD, J.R. and MYERS, M.J., "The Performance of a Gamma Camera for the Visualization of Radioactive Isotopes In Vivo," Phy. Med. Biol. 8 (1963) 165-182.
[6] KELLERSHOHN, C., Discussion in Medical Radioisotope Scanning, IAEA, Vienna (1959) 76.
[7] KELLERSHOHN, C. and PELLERIN, F., Sur la possibilité d'utiliser un tube amplificateur d'image, C.R. Acad. Sci., Paris 149 (1955) 533.
[8] BROWNELL, G., Personal Communication.
[9] BENDER, M.A. and BLAU, M., "The Autofluoroscope", Nucleonics 21 (1963) 52.
[10] BENDER, M.A. and BLAU, M., "Detection of Liver Tumours with I^{131} Rose Bengal", Medical Radioisotope Scanning. IAEA, Vienna (1959) 83-6.
[11] BENDER, M.A. and BLAU, M., "Evaluation of Renal and Cardiac Dynamics with the Autofluoroscope," J. nucl. Med. 4 (1963) 186.

DISCUSSION

L. Van STEKELENBURG: The autofluoroscope produces a picture in one-tenth of the time taken by a normal scanner but, if the field were slightly larger than 6×9 in, it would have to be used two or three times. Thus, the time gained would be reduced.

M. BENDER: I agree. With the autofluoroscope, however, examinations could still be carried out five times faster.

I should like to take this opportunity to point out that in the digital autofluoroscope the information from the crystals around a given crystal, which is stored in the memory, can be used to make a better statistical analysis of what is going on in the crystal of interest.

C. KELLERSHOHN: Following your suggestions, we have started to use Ba^{137} in radiocardiography. I should like to know the amount of Cs^{137} contamination you find when you use the "cow" to produce Ba^{137}.

M. BENDER: The "cow" deteriorates with time. Thus, in the initial "milkings", we get fewer than one part per 10^9 of Cs^{137} but, as time goes on, we get up to a few parts per 10^6. However, we are permitted to administer at least 10 μc of Cs^{137}, and we never approach that amount.

R. HERBERT: How is the very short-lived Ba^{137m} sterilized? Could Tc^{99m} be similarly used in your investigation?

M. BENDER: Since the "cow" and the materials that go into it are sterile, the problem of sterilization of Ba^{137m} after it has been "milked" does not arise. As to your second question, I am sure that Tc^{99m} could be used. Of course, it has a somewhat longer half-life and the dose would therefore have to be reduced.

J. MALLARD: What is the cost of the digital autofluoroscope? I should like to mention that we are trying another method to overcome the energy dependence of the positioning signals of the Anger system which you have described. Instead of using linear amplifiers after the photomultipliers, we are trying to use logarithmic amplifiers. The difference signal from two photomultipliers (which is the positioning signal) then becomes a quotient independent of energy. We hope thus to be able to open out the window width so as to improve sensitivity for a given crystal size.

M. BENDER: The digital autofluoroscope costs $32 000. As to your comment, I should like to point out that we also, at one time, contemplated the use of logarithmic amplifiers. Such devices would not, however, help in the elimination of pulses arising simultaneously in more than one crystal as a result of single gamma rays undergoing a Compton interaction.

J. MORICHÈRE: The second autofluoroscope you showed is fitted with a matrix of scintillators, each of which is connected by two light pipes to two photomultipliers corresponding to a row and a file. A point of light from a scintillator can thus be reproduced as soon as a row and a file event coincide. An attempt is probably made by pulse-height analysis to "accept" only those pulses which are caused by the radioisotope under observation. Assuming this and assuming that one takes as a basis the pulse produced by a photoelectric absorption event in the scintillator, how wide is the pulse acceptance band used in the case of I^{131} as a percentage of the abscissa corresponding to the photoelectric peak?

M. BENDER: You can use any window width you wish. The positioning signals are not dependent on pulse-height analysis, which consequently is not really necessary. We prefer to use a 30% window because we feel that, as in scanning, some window should be used. You could get perfectly good results by using every single interaction that occurs in a crystal, as long as it occurs in that crystal alone.

A SCINTILLATION CAMERA FOR KINETIC STUDIES OF THE DISTRIBUTION OF RADIOACTIVE NUCLIDES IN THE BRAIN*

W. GROSS**, E. B. SCHLESINGER AND S. DE BOVES
DEPARTMENT OF NEUROLOGICAL SURGERY, COLUMBIA UNIVERSITY,
NEW YORK, N. Y., UNITED STATES OF AMERICA

Abstract — Résumé — Аннотация — Resumen

A SCINTILLATION CAMERA FOR KINETIC STUDIES OF THE DISTRIBUTION OF RADIOACTIVE NUCLIDES IN THE BRAIN. A scintillation camera specifically designed for the study of the kinetics of the distribution of radioactive nuclides in the brain has been developed. This device employs two banks of ¾ in × 1 in sodium iodide-thallium activated crystals, 63 crystals per bank arranged in a 7 × 9 close-packed array on 1-in centres. These banks can be placed so that both lateral views or one lateral and one P-A or A-P view can be obtained simultaneously. The field of view of each crystal is limited by a collimator consisting of nineteen tapered holes whose axes are all parallel. This design gives a response of nearly equal full-width at half height to a simulated tumour source at all distances up to 4 in from the front of the collimator. This response is sufficiently wide to avoid significant "dead" areas and yet narrow enough to permit accurate observation of the activity distribution within a very few minutes using normal tracer doses of iodine-131. Each crystal is optically coupled to its own photomultiplier in an integral package.

The output pulses of the photomultipliers are analysed by discriminators and the information stored in digital form in a quarter of the memory of a 512-channel pulse-height analyser. Time coincident pulses from the various detectors can be accepted by this equipment so that losses are negligible. Read-out in several forms is available. In digital form either a typewritten record or punched paper tape can be obtained. The latter may be read back into the equipment for review. Analogue read-out is made on a large screen oscilloscope. The scope beam is defocused and two 63 point display rasters generated to correspond to the spatial location of the scintillation counters. Intensity modulation of the oscilloscope beam as well as background erasure is used to assist in visualizing the activity distribution.

CHAMBRE A SCINTILLATION POUR DES ÉTUDES SUR LA CINÉTIQUE DE LA RÉPARTITION DES RADIONUCLÉIDES DANS LE CERVEAU. Les auteurs ont mis au point une chambre à scintillation spécialement conçue pour des études sur la cinétique de la répartition des radionucléides dans le cerveau. Ce dispositif utilise deux séries de cristaux NaI(Tl) de 1,8 cm sur 2,5 cm, chaque série comprenant 63 cristaux disposés sur 7 rangs de 9 cristaux selon un quadrillage de 2,5 cm de côté. Il est possible de placer les deux séries de manière à pouvoir obtenir simultanément, soit les vues sur les deux côtés, soit une vue latérale et une vue postéro-antérieure (ou antéro-postérieure). Le champ de vision de chaque cristal est limité par un collimateur à 19 orifices coniques dont les axes sont tous parallèles. Ce montage donne une réponse à une source continue dans une tumeur simulée, dont la largeur complète à mi-amplitude est presque égale pour toutes les distances jusqu'à 10 cm à partir de la face antérieure du collimateur. Cette réponse est suffisamment large pour éviter des zones «mortes» significatives, tout en étant assez étroite pour permettre de faire une observation précise de la répartition de l'activité en quelques minutes, si l'on emploie des doses normales d'iode-131. Chaque cristal est optiquement couplé à son propre photomultiplicateur.

Les impulsions des photomultiplicateurs à la sortie sont analysées au moyen de discriminateurs; l'information est emmagasinée sous forme numérique dans un quart de la mémoire d'un analyseur d'amplitude à 512 canaux. Cet ensemble peut accepter des impulsions coïncidant dans le temps et provenant des divers détecteurs; les pertes sont donc négligeables. La lecture peut se faire sous plusieurs formes. Sous une forme numérique, on peut obtenir, soit une feuille dactylographiée, soit une bande perforée en papier. Celle-ci peut être repassée dans l'appareil aux fins de contrôle. Sous forme analogique, la lecture se fait sur un oscillos-

* Supported in part by the American Cancer Society and the John A. Hartford Foundation, Inc.

** Radiological Research Laboratory, Department of Radiology.

cope à grand écran. On défocalise le faisceau de l'oscilloscope et on produit deux séries de 63 images dont chacune correspond à un cristal. La modulation de l'intensité du faisceau de l'oscilloscope et l'élimination du bruit de fond facilitent la visualisation de la répartition de l'activité.

СЦИНТИЛЛЯЦИОННАЯ КАМЕРА ДЛЯ КИНЕТИЧЕСКОГО ИССЛЕДОВАНИЯ РАСПРЕДЕЛЕНИЯ РАДИОАКТИВНЫХ ИЗОТОПОВ В ТКАНИ МОЗГА. Разработана сцинтилляционная камера, специально предназначенная для изучения кинетики распределения радиоактивных изотопов в ткани мозга. Этот прибор состоит из двух групп, активированных таллием кристаллов NaJ размером 1,8 × 2,5 см, причем 63 кристалла каждой группы собраны в порядок 7 × 9 на 2,5-см центрах. Эти группы могут быть расположены таким образом, чтобы одновременно получать обе боковые проекции или одну боковую и одну задне-переднюю или передне-заднюю проекцию. Поле зрения каждого кристалла ограничено коллиматором, состоящим из 19 суживающихся каналов с параллельными осями. Эта конструкция имеет чувствительность почти равную полной широте на половине расстояния до условного источника опухоли по всем расстояниям до 10 см от передней части коллиматора. Эта чувствительность достаточно широка, чтобы избежать нерадиоактивных зон, и в то же время достаточно узка, чтобы позволить точное наблюдение распределения активности в течение нескольких минут, при использовании нормальных индикаторных доз йода-131. Каждый кристалл оптически соединен со своим фотоумножителем в общей упаковке.

Выходные импульсы фотоумножителей анализируются с помощью дискриминаторов и информация хранится в цифровой форме в четверти запоминающего устройства 512-канального анализатора высоких импульсов. Совпадающие по времени импульсы из различных детекторов могут приниматься в этой установке с незначительными потерями. Считывание данных возможно в нескольких формах. Можно получить данные в цифровой форме, в машинописной форме или в виде перфокарт. Последние можно ввести обратно в прибор для повторного изучения. Аналогичное считывание производится на осциллоскопе с большим экраном. Пучок на этом приборе дефокусируется, и возникают две индикаторные сетки с 63 точками, соответствующими пространственному расположению сцинтилляционных счетчиков. Модулирование плотности пучка осциллоскопа, а также стирание фона используются для того, чтобы облегчить визуальное наблюдение распределения активности.

CÁMARA DE CENTELLEO PARA ESTUDIAR LA CINÉTICA DE LA DISTRIBUCIÓN DE RADIONÚCLIDOS EN EL CEREBRO. Los autores han construido una cámara de centelleo especialmente concebida para el estudio de la cinética de la distribución de radionúclidos en el cerebro. Este dispositivo contiene dos series de cristales de yoduro de sodio activados por talio, de $\frac{3}{4} \times 1$ pulg; cada serie comprende 63 cristales dispuestos en 7 filas de 9 cristales con una distancia de 1 pulg entre los centros. Las dos series pueden colocarse de modo que sea posible obtener vistas simultáneas de dos caras laterales, o de una cara lateral y una posteroanterior (anteroposterior). El campo de visión de cada cristal está limitado por un colimador de 19 canales cónicos cuyos ejes son paralelos entre sí. Este montaje da una respuesta prácticamente uniforme a todas las distancias hasta 4 pulg desde el frente del colimador, para una fuente contenida en un tumor simulado. Esta respuesta es suficientemente amplia para evitar zonas «muertas» significativas y, al mismo tiempo, bastante estrecha para poder observar con exactitud la distribución de la actividad en unos pocos minutos si se emplean dosis normales de yodo-131 como indicador. Cada cristal está acoplado ópticamente a su propio fotomultiplicador, constituyendo una unidad.

Los impulsos de salida de los fotomultiplicadores son analizados mediante discriminadores; la información se almacena en forma numérica en una cuarta parte de la memoria de un analizador de amplitud de impulsos de 512 canales. Como este aparato puede aceptar impulsos coincidentes en el tiempo o procedentes de varios detectores, las pérdidas son despreciables. La lectura puede efectuarse de distintas maneras. En forma numérica puede obtenerse ya sea un registro dactilografiado o una cinta de papel perforado. Esta última puede introducirse en el aparato para una nueva lectura. En forma analógica, la lectura se hace en un osciloscopio de gran pantalla. Se desenfoca el haz del osciloscopio y se producen dos reticulados de 63 puntos para corresponder a la situación espacial de los contadores de centelleo. La modulación de la intensidad del haz del osciloscopio y la supresión de la actividad de fondo facilitan la visualización de la distribución de actividad.

INTRODUCTION

Mapping of the distribution of radioactive nuclides in the brain by using collimated scintillation detectors mechanically moved over the surface of the head has been employed as a diagnostic technique for many years. The length of time needed to obtain statistically significant information by this method requires that the distribution of the nuclide in the brain be quasi-static if the results are to be easily interpreted. This requirement precludes the use of this type of scintillation mapping when the radionuclide distribution is changing rapidly or when the nuclide half-life is comparable to the time of the scan. Additionally, the prolonged scanning time (usually 45-60 min) during which the patient must be held stationary may result in discomfort and restlessness.

The limitations of a mechanical scanning system are inherent in the device as they are in any device which wastes most of the information available to it. In a mechanical scanner the detector views only a small portion of the head at any instant and obtains its information from this portion only. Radioactive disintegrations from other regions are not registered. A mapping device capable of viewing all the areas of interest simultaneously would overcome these limitations by utilizing far more of the available information. The time required to obtain statistically significant information would thereby be shortened markedly. Thus, it would be possible not only to scan rapidly and eliminate the time variable, but also to study the kinetics of nuclide movement.

To develop such an instrument a programme was begun in 1959 at the Neurological Institute of the Columbia Presbyterian Medical Center. This paper concerns the design principles and construction of the instrument. Clinical usage and evaluation reports shall be given at a later time.

Other scintillation cameras have been described [1] using techniques not fundamentally different from the ones employed here. Particular advantage is gained here by information storage in digital form with provision for review at any later date.

PRINCIPLE OF OPERATION

This scintillation camera determines the radioactive nuclide distribution by means of a set of discrete individually collimated scintillation detectors in a fixed spatial array. They all operate simultaneously and the data from each detector are separately and digitally recorded. Every detector views one portion of the area to be scanned and the collimators are arranged so that all the area is viewed but there is minimal overlap between detectors. Two separate banks of detectors (detector heads) are used to obtain two different, but simultaneous, views of the activity distribution.

Each detector must view an appreciable area if only a reasonable number are to be used and the entire region of interest is to be scanned. Thus, the design criteria of a collimator for this system are quite different from those for a conventional scanner. Here, the desire is to obtain a collimator with a lateral response curve which is constant over a distance equal to the centre-to-centre spacing between detectors. Beyond this distance the re-

sponse ideally should be zero. Further, as the source to collimator distance is varied (out to the maximum desired) response should remain constant. This latter criterion applies equally to the collimator for a conventional scanner. Of course, this desired response can only be approximated in practice.

It is important to note that the spatial resolution obtainable with this device is limited by the spacing between detectors. This in turn is determined from the area to be viewed and the number of detectors used. If an area A is to be scanned with n detectors then the area of resolution can be no better than A/n. As this scintillation camera is designed primarily for the localization of brain tumours where very detailed information is not required, this resolution limitation is acceptable. The resolution must only be fine enough to detect the tumour. The requirement used in the design was a statistically significant increase in a one minute count with a 3:1 uptake in a 0.8-in-diam. spherical tumour with normal patient doses of iodine-131 (5 μc/kg body weight).

DETAILED DESCRIPTION

Scintillation heads

The scintillation camera utilizes 126 individual crystal-photomultiplier counter units. Each unit contains a NaI (Tl) crystal $\frac{3}{4}$ in in diam. by 1 in thick, viewed by a photomultiplier (Amperex No. 152 AVP) having an outside diameter of $\frac{3}{4}$ in and a photocathode $\frac{1}{2}$ in in diam. The crystal and tube are packaged as an integral unit which contains a magnetic shield and plugs into a socket containing the dynode resistors and by-pass capacitors. Carbon film resistors are used to assure stability. Electrical connection is made through a single coaxial cable at the rear of the unit. The overall dimensions of the unit (not including the cable) are $\frac{15}{16}$ in diam. and 8 in long.

A total of 63 units are mounted in each of two separate heads. The units are arranged in nine rows and seven columns staggered to achieve a close-packed array with the counters on 1-in centres. Positioning is achieved by a honeycomb of tubes of 1 in outside diam., nested together, which serve as holders for the counter units. Each unit is spring loaded along its axis by a sponge rubber washer which fits over the coaxial cable and presses against the back plate of the detector portion of the heads. Holes in this plate are provided to pass the coaxial cable into the preamplifier section of the head.

At the front of the detector section is a steel-cased lead door $2\frac{1}{4}$ in thick. The door has $63\frac{1}{8}$-in holes drilled to line up with counter units and covered on the front by a thin aluminium sheet. The collimators fit into these holes. The sides and back of the head contain $1\frac{1}{2}$ in of lead in a steel casing, the back being a door to give access to the preamplifier section. Both front and back door openings have staggered lips to avoid radiation entry through cracks.

Two collimator designs are currently being clinically evaluated. One, for high sensitivity, is a single tapered hole whose diameter is $\frac{3}{4}$ in at the crystal and which comes to its focus 4 in from the front of the collimator.

The other is a 19 tapered hole design where again each hole comes to its focus 4 in from the front. However, the axis of each hole is parallel to the axis of the collimator. Both types of collimator are fabricated from lead in a thin outer brass protective sleeve.

Response curves of the multihole collimator to a point source of iodine-131 in a water phantom are shown in Fig. 1. As expected, the re-

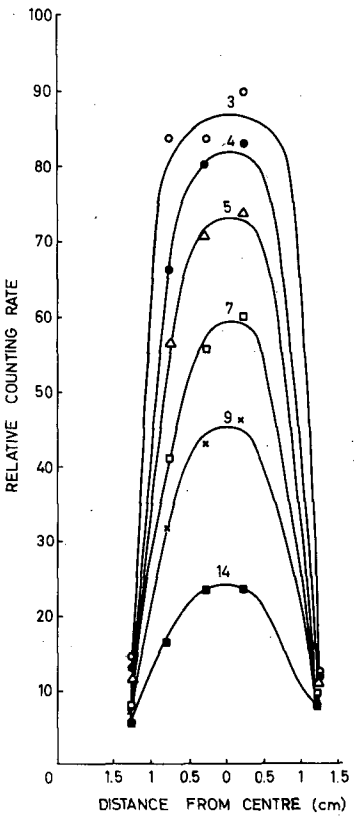

Fig. 1

Lateral response curves to a point source of iodine-131 for the 19-hole collimators. Numbers adjacent to the curves indicate the distance in centimetres from the source to the face of the collimator.

sponse curve is not ideal as the count-rate is not constant either with lateral displacement or with distance from the face of the collimator. However, the lateral response is broad and the full-width at half height is nearly constant for all distances out to the 4 in from the face of the collimator (the focal length of the holes). Also, the central axis fall-off is not extreme. The major drawback of this design lies in its relatively low sensitivity when compared to the single-hole design. However, the collimator does satisfy the criterion for tumour detection stated above.

The two heads are mounted on an inverted U frame as is shown in Fig. 2. The head on the right side of the Figure is movable in two directions in the

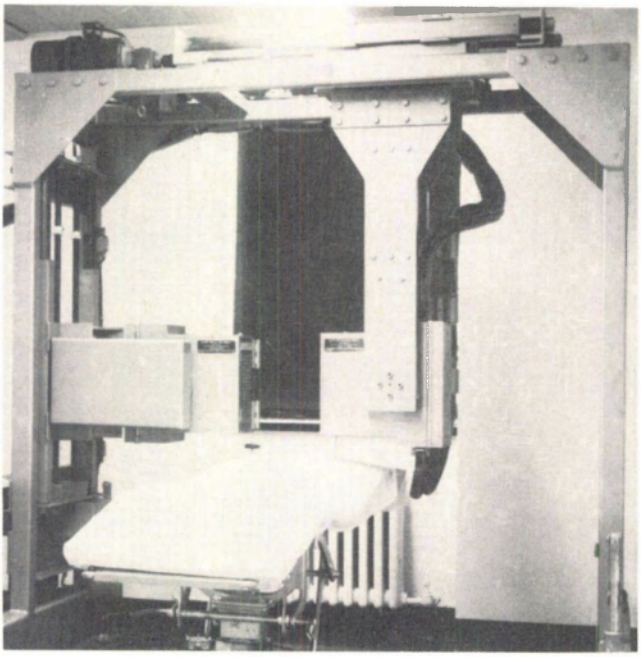

Fig. 2

Photograph of the scintillation detector unit

horizontal plane. It can be separated any distance up to 14 in from the other head by means of an electric motor controlled by a cabled handswitch. The right head can also be moved up to 2 in at right angles to this motion by means of a hand crank. The left head is movable up to 14 in in a vertical direction. The lowest position of this motion puts the two heads in the same vertical plane. This motion is also achieved by means of a motor controlled by the same handswitch. The left head is also rotatable up to 90° about a horizontal axis at right angles to the direction of view of the collimated scintillation counters. Rotation is achieved by means of a hand crank.

These various motions permit different views of the patient to be obtained. The patient is normally placed in a supine position on a stretcher between the two heads so that both left and right lateral views are obtained. The individual counters in the two heads can be placed exactly in line or with any degree of stagger between them. If an A-P view is desired the left head is raised and rotated and the patient placed beneath. Simultaneously, a laterial view is obtained with the right head. To obtain a P-A view it is merely necessary to turn the patient to a prone position.

Electronics

All information obtained from the scintillation counters is recorded in digital fashion. The system is shown in the block diagram (Fig. 3). The cable from each detector unit is connected through a selected resistor to

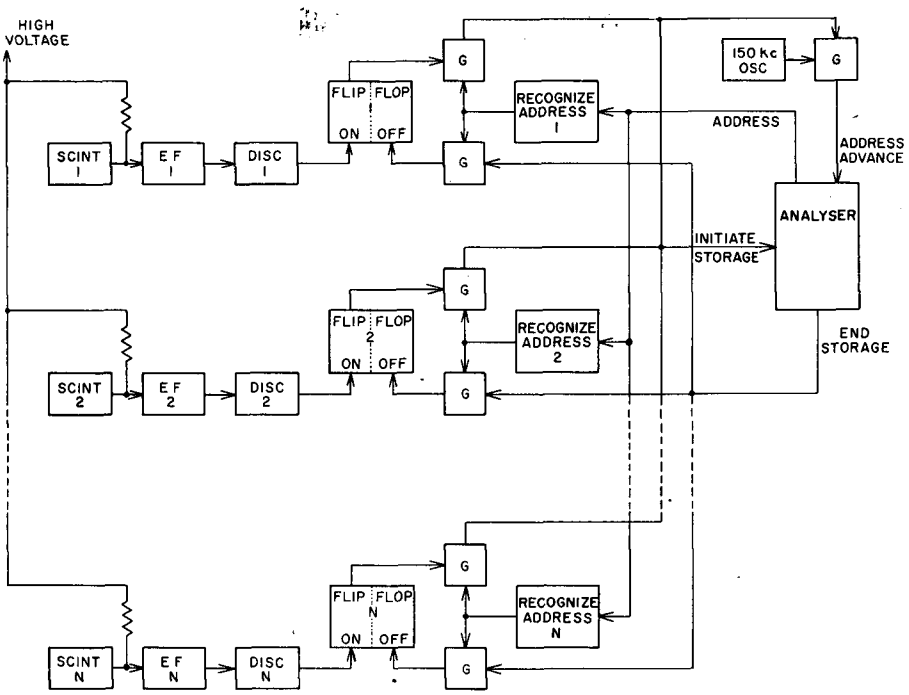

Fig. 3

Block diagram of the electronic system used for data recording

the high voltage supply which is common for all units within a head. The resistors are chosen such that the output pulse height for given energy deposition in each crystal is approximately the same in all units. The output pulse is then fed through an emitter follower located at the rear of the head and by way of a coaxial cable to the electronics console.

In the console the signals from the 126 emitter followers are analysed by means of an equal number of simple discriminators. These discriminators are set to the centre of the trough below the photopeak of the gamma-ray of interest. In our case this is the 364-keV iodine-131 gamma-ray. The discriminator output is used to set a flip-flop tied to the memory system of a conventional multichannel analyser. The analyser has been modified so that any quarter of its 512-channel memory system can be used as a storage unit for the data.

The memory system is used in a modified multichannel scaler mode with each channel of the memory quadrant used for data storage from one of the scintillation units. (Since there are 128 channels in the memory quadrant and only 126 scintillation units, 2 channels are unused.) During data acquisition the address scaler of the memory is continuously cycled at an approximately 150-kc rate. At each memory position the flip-flop connected to the detector discriminator is examined for state. If it has been set by an acceptable detector pulse a memory cycle occurs which results in an increase of one in the number stored at that memory position and the resetting of the flip-flop.

The use of this method of data storage allows the total number of counts from all detectors to be very large without interference among channels. The maximum count acquisition rate per channel is limited by the time required for one complete cycle through all addresses. This period is less than 1 ms. The requirement for no count loss is that in this time no detector may receive more than one pulse. This corresponds to more than 1000 cps for uniformly spaced pulses. Thus, for the detector receiving the highest count-rate, losses will be much less than 1% at counting-rates of 6000 mm. This figure is several times the maximum rate actually obtained.

Data presentation can be obtained in three forms of which two are digital and the third analogue. The digital methods are a typewritten record and a punched-paper tape. The typewritten output is extremely useful as it permits evaluation of the statistical significance of the data. The punched tape can be used to return the information into the memory for review at any time.

The analogue read-out is performed on an oscilloscope. Two 63-point rasters (one for each head of the unit) are generated with each point placed on the scope at a position which is geometrically equivalent to the spatial location of one of the scintillation counters in the head (Fig. 4). The scope beam is defocused to simulate the spatial response sensitivity of the collimated scintillation counters. As the memory is scanned for this type of

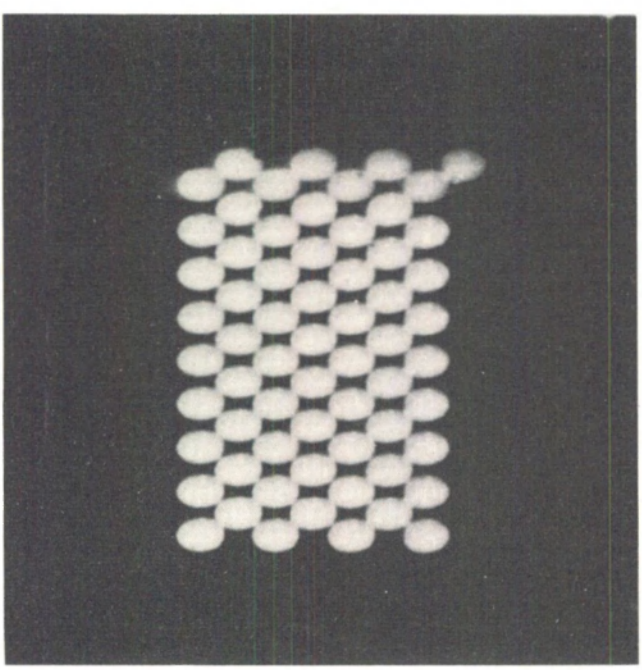

Fig. 4

Photograph of the oscilloscope raster.
The position of the circles is a replica of the positions of the scintillation detectors.
The circle at the extreme upper right of the photograph is not part of the data raster.

read-out the analogue voltage corresponding to the number of counts stored is compared to another voltage, the contour level. If the analogue voltage is the greater the defocused beam appears on the scope. If the contour level is greater then the beam is diverted so that it does not appear. Thus, only points corresponding to detectors having a stored count greater than the contour level will appear. Manual adjustment of the contour level then serves for background erasure. Additionally the contour level can be modulated so that the length of time the beam remains at any given point in the raster is a direct function of the number of counts received from the detector corresponding to that position. Thus, intensity modulation proportional to the counts is achieved and the proportionality can be linear or non-linear as desired to assist the visualization of the activity distribution. Figure 5

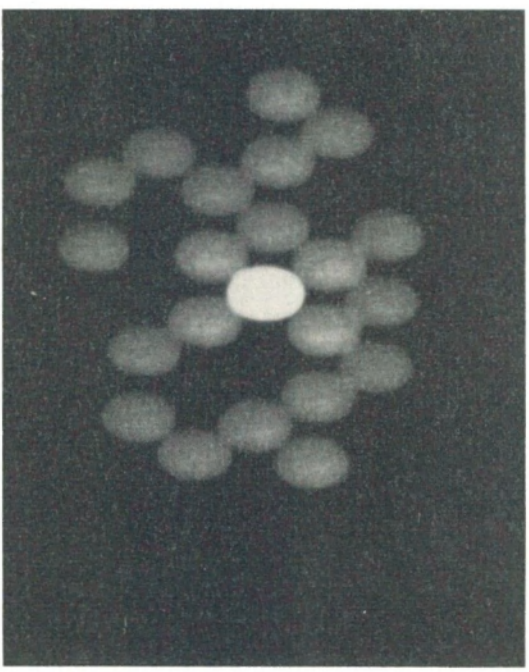

Fig. 5

Photograph of the oscilloscope raster obtained using background erasure and intensity modulation on data from a human head phantom with a cylindrical "tumour".

shows a view of the raster for a phantom of a human head and a cylindrical "tumour" 1 in high by $1\frac{1}{4}$ in in diam., with the latter having 8 times the iodine-131 activity of the phantom. Both background erasure and intensity modulation have been used.

ACKNOWLEDGEMENTS

The authors wish to express their gratitude to several individuals and corporations who have given unstintingly of their ingenuity and time in order

to translate a nebulous idea into a practical reality. These include Dr. Arthur Robinson and the Kollsman Instrument Company, Mr. Robert Schumann and Mr. Harry Ryan and the Nuclear Data Corporation. Especial thanks are due to Mr. Samuel Stempler of the Kollsman Instrument Company who has given of himself far beyond any reasonable expectation. We appreciate the help of Dr. H. H. Rossi in providing valuable consultative assistance over the years.

BIBLIOGRAPHY

For a discussion and bibliography on other scintillation cameras see Nucleonics 21, No. 10 (1963).

DISCUSSION

C.M.E. MATTHEWS: What was the concentration of I^{131} (in μc per ml) in the phantom?

W. GROSS: I cannot say exactly, but I think it would correspond to about three times the concentration with normal patient dosage.

W. PAUL: Did you make any attempt to connect opposite pairs of detectors in coincidence?

W. GROSS: No, because it seemed that the associated electronics would create difficulties.

AUTOFLUOROGRAPHY WITH AN X-RAY IMAGE AMPLIFIER

M.M. TER-POGOSSIAN AND J.O. EICHLING
WASHINGTON UNIVERSITY SCHOOL OF MEDICINE,
ST. LOUIS, MO., UNITED STATES OF AMERICA

Abstract — Résumé — Аннотация — Resumen

AUTOFLUOROGRAPHY WITH AN X-RAY IMAGE AMPLIFIER. The visualization of organs containing radioactive isotopes emitting X- or gamma-ray photons with energies between 20 and about 100 keV can be achieved by converting the radiation emerging from the organ into light by means of an X-ray image amplifier of conventional design. The apparatus designed for this purpose consists of the following elements:

(1) A collimator, the specifications of which are determined by the resolution and by the operating distance desired.

(2) An electrostatic focusing X-ray image amplifier, which converts the collimated X- or gamma-ray photons into an optical image of high brightness.

(3) A large aperture lens system which projects the image into:

(4) A "Polaroid" camera loaded with fast (10 000 ASA), high-contrast film.

The performance of this apparatus for low-energy photons is superior to that of conventional scintiscanners.

The usefulness of this apparatus for the visualization of brain tumours and kidneys and the thyroid gland is discussed.

AUTOFLUOROGRAPHIE A L'AIDE D'UN AMPLIFICATEUR D'IMAGES A RAYONS X. Pour permettre la visualisation d'organes contenant des radioisotopes émetteurs de rayons X ou gamma ayant une énergie de 20 à 100 keV, on peut convertir en lumière le rayonnement provenant de l'organe examiné au moyen d'un amplificateur d'images à rayons X du type classique. Le dispositif conçu à cet effet comprend les éléments suivants:

1. Un collimateur dont les caractéristiques sont déterminées par la résolution et la distance source-détecteur souhaitables;

2. Un amplificateur d'images à rayons X, électrostatique et focalisant, qui transforme les rayons X ou gamma collimatés en une image optique de forte luminosité;

3. Un ensemble de lentilles à grand angle d'ouverture, qui projette l'image dans l'appareil photographique ci-dessous;

4. Un appareil photographique «Polaroïd» chargé d'un film rapide (10 000 ASA) à fort contraste.

Les performances de ce dispositif en présence de photons de faible énergie sont supérieures à celles des scintigraphes classiques.

Les auteurs traitent de l'utilité de ce dispositif pour la visualisation des tumeurs du cerveau, des reins et de la thyroïde.

АВТОФЛУОРОГРАФИЯ С ПОМОЩЬЮ УСИЛИТЕЛЯ РЕНТГЕНОВСКОГО ИЗОБРАЖЕНИЯ. Визуальное наблюдение органов, содержащих радиоактивные изотопы, которые излучают рентгеновские кванты или гамма-кванты с энергиями в пределах от 20 до 100 кэв, достигается за счет превращения радиации органа в свечение с помощью усилителя рентгеновского изображения обычного типа. Сконструированный для этой цели аппарат состоит из следующих элементов:

1. Коллиматора, характеристики которого определяются разрешающей способностью и желаемым рабочим расстоянием.

2. Электростатического фокусирующего усилителя рентгеновского изображения, который превращает коллимированные рентгеновские кванты или гамма-кванты в оптическое изображение, имеющее большую яркость.

3. Объектива с большой диафрагмой, который проецирует изображение на камеру.

4. Камера "Полароид", заряженная высокочувствительной (10.000 ASA) пленкой с высокой контрастностью.

По качествам работы с фотонами малой энергии этот аппарат лучше, чем обычные сцинтискеннеры.

Обсуждается пригодность этого аппарата для визуального наблюдения опухолей мозга, почек и щитовидной железы.

AUTOFLUOROGRAFÍA CON UN AMPLIFICADOR DE IMAGEN DE RAYOS X. La visualización de órganos que contienen isótopos radiactivos emisores de fotones (rayos X o gamma) de energía comprendida entre 20 y 100 keV aproximadamente, puede lograrse convirtiendo en luz, mediante un amplificador de imagen de rayos X de tipo corriente, la radiación emitida por el órgano. El aparato construido con esta finalidad está constituído por los siguientes elementos:

1. Un colimador, cuyas características vienen determinadas por el poder de resolución y la distancia a que debe operar.
2. Un amplificador de imagen de rayos X de enfoque electrostático, que convierte los rayos X o gamma colimados en una imagen óptica muy brillante.
3. Un sistema de lentes de gran apertura que proyecta la imagen en la cámara mencionada a continuación.
4. Una cámara «Polaroid» cargada con película rápida (10 000 ASA) de gran contraste.

El rendimiento de este aparato para fotones de baja energía es superior al de los exploradores centelleográficos de tipo tradicional.

Los autores examinan su utilidad para visualizar tumores cerebrales, renales y tiroideos.

INTRODUCTION

The visualization by means of scintiscanning of organs or biological structures which concentrate compounds labelled with radioactive isotopes is now a well accepted clinical procedure. This procedure is carried out most commonly by means of a scintiscanner, which is basically a scintillation counter fitted with a collimating device, generally of the focussing type. The detector is attached to a mechanical device and scans the area under examination. The information carried by the gamma- or X-ray photons observed by the scintillation counter is converted into electrical signals which are in turn recorded in the form of a graphical pattern.

In the above apparatus, the collimator excludes most of the photons except those emitted from the volume of tissue "seen" by the detector. The photons originating outside this volume are wasted from the standpoint of the examination. It appears desirable to conceive a system which would overcome this limitation by "looking" continuously at the whole field of examination.

Several apparatuses have been designed which embody the above described advantage, that is they look continuously at the whole field of examination. Two of them [1, 2], designed by ANGER, and BENDER and BLAU are successfully used. Although these instruments differ somewhat in concept, they exhibit the common feature of using a crystal-photomuliplier tube combination for detecting ionizing radiations.

The purpose of this report is to describe a scintillation camera, the radiation detector component of which is an X-ray image amplifier.

The possibility of using an X-ray image amplifier for detecting and localizating the distribution of a radioactive element has been described by KELLERSHOHN and PELLERIN [3]. The authors attempted the visuali-

zation of a thyroid phantom containing radioactive iodine-131. The use of an X-ray image amplifier for detecting radiation emitted by radioactive iodine-125 was also suggested by MYERS and VANDERLEEDEN [4]. TER-POGOSSIAN et al. [5] described an apparatus embodying this principle for the visualization of the thyroid gland.

THE APPARATUS

The detailed description of an X-ray image amplifier is outside the scope of this discussion. In general terms, this apparatus converts into light the energy of X-rays impinging upon its sensitive surface; in turn, the light is used to accelerate electrons. These electrons are handled by a system of electron lenses and they form an optical image of the input screen of the apparatus. A typical light gain which can be thus obtained by the apparatus is approximately 6000. The input screen of a conventional image intensifier, designed for detecting X-rays used in diagnostic radiology, is thin and it absorbs efficiently only low-energy photons. It seems that the use of such an apparatus for detecting and localizing gamma- or X-ray emitting radioactive elements is most practical for isotopes emitting electromagnetic radiations with energies lower than approximately 150 keV. If higher energies are used the input screen of the image amplifier is so inefficient that the system seems to be undesirable for the projected purpose. It may appear that, in limiting the usefulness of the image amplifier for detecting electromagnetic radiations with energies lower than approximately 150 keV, its clinical applications may be seriously hindered simply because it restricts the number of radioactive isotopes with which it can be used. However, the situation is not as bad as it may appear. In the first place, low electromagnetic radiation is easy to collimate and particularly efficient collimators can be designed which considerably raise the figure of merit of the examination [6, 7]. Secondly, there are now numerous radioactive isotopes emitting electromagnetic radiations of low energy which, if necessary, can replace virtually all the other radioactive isotopes used routinely for scanning purposes. For example, both iodine-125 and technicium-99 m can be used for the visualization of the thyroid, mercury-197 is very suitable for the visualization of kidneys and of brain tumours, and xenon-133 is suitable for the visualization of the lungs. Technicium-99 m can also be used for liver scans. Each of these isotopes emits electromagnetic low-energy radiations; they are very practical for clinical purposes and generally they are superior to higher energy gamma-ray emitters.

The apparatus used in this study consists of four components, namely, (1) a collimator, (2) an X-ray image amplifier tube, (3) an optical lens system, and (4) a Polaroid camera.

(1) Several collimators were designed and used. These collimators can be divided into two categories: (a) High-resolution collimators designed for the visualization of the thyroid gland by means of iodine-125; these collimators are similar in resolution to the Picker X-ray Corporation Magnascanner collimator with 31 holes, and (b) collimators of low resolution designed for the visualization of brain tumours, kidneys and liver;

these collimators are similar in their resolving power to the 19-hole "Magnascanner" collimator.

The high-resolution collimator, which was found to be most suitable for the visualization of the thyroid, has a square field of 10×10 cm, holes approximately 1 mm in diam. and 5 mm high. The material used in the construction of the collimator is silver, approximately six-thousandths of an inch thick. Silver is selected because it exhibits a K-absorption discontinuity at an energy slightly higher than that of the electromagnetic radiation emitted by iodine-125 [8]. Silver is therefore a particularly suitable absorber for this radiation.

The lower resolution collimator covers a circular field 8 in in diam. The holes are 5 mm in diam., and the height of the collimator is 5 cm at its centre. The collimator is made of lead and one of its surfaces is concave to accomodate the convexity of the glass envelope of the image amplifier.

The image amplifier used in this study was manufactured by the Rauland Corporation in Chicago. It has a useful input diam. of 8 in, a measured gain of approximately 2400. The output screen is 1 in in diam. The tube is fitted with an ion pump, and it requires a power supply of approximately 30 000 V for operation.

The image appearing on the output screen of the image intensifier is transferred by means of a fast lens system with a numerical aperture slightly lower than 1.

The Polaroid camera is conventional in design. It was used in all of the reported studies with Polaroid 410 film with an ASA rating of 10 000.

The described detector is mounted on a stand for easy positioning.

RESULTS

The described system was used with different phantoms simulating various organs usually visualized by scintiscanning, viz. (1) A thyroid phantom with suitable defects (Picker X-ray Corporation) containing iodine-125. Suitable images were obtained in approximately 3 min when the phantom contained about 1 $\mu c/cm^3$ of iodine-125. (2) A phantom "head" containing a phantom "tumour" with mercury-197 was used to simulate brain-tumour localization. Suitable images were obtained within 15 min when the tumour contained approximately 2 $\mu c/cm^3$ of mercury-197. (3) Different containers were used to simulate lungs containing xenon-133, and (4) autoradiograms were also obtained of the kidneys of patients who received mercury-197 for brain scans.

All the results obtained indicate that suitable pictures could be obtained with times comparable or shorter than necessary with a scintiscanning system.

DISCUSSION

The question which must be answered is whether or not a system such as the one described above presents fundamental and practical advantages over a conventional scintiscanner. In order to compare the two systems

from the fundamental standpoint, it is necessary to compare their information gathering efficiencies. This study consists essentially in comparing the photon gathering efficiencies of the two systems. Let us assume that the comparison is carried out between a conventional scintiscanner (Picker "Magnascanner") fitted with a 19-hole collimator focused at a distance of 10 cm from the surface of the collimator, and "looking" at a circle 1 cm in diam., and an amplifier camera designed to achieve a similar resolution at a similar distance from the face of the collimator. Under such conditions the comparison of the photon-gathering efficiencies of the collimators indicate that the camera "sees" an area approximately 20 times greater than the area "seen" by the 19-hole focused scanning collimator. On the other hand, the efficiency of the large crystal used in the scintiscanner for detecting photons which strike it is greater than that of the thin fluorescent screen in the camera. These efficiencies vary depending upon the energy of the gamma radiation emitted by the isotope used. For the radiation emitted by mercury-197 the crystal is about three times more efficient than the camera screen. In such circumstances, taking into account both the relative efficiencies of the collimators used and the efficiencies with which the X- or γ-ray photons are detected by the two systems, it appears that the camera is approximately six to seven times more efficient than the scintiscanner.

From a practical standpoint, the autofluoroscope apparatus is simple in design with uncomplicated electronics and needs little maintenance. The most delicate part of the instrument is an X-ray image amplifier which is basically a rugged piece of equipment powered by a simple unregulated high-voltage power supply, which has been found to be trouble-free.

CONCLUSION

It appears that a scintillation camera constructed with an X-ray image intensifier offers several advantages over a conventional scintiscanner. From the information gathering standpoint, it is several times more efficient than a conventional scintiscanner. The autofluoroscope is also a simple, rugged and reliable instrument which does not embody any complicated electronics. But the autofluoroscope suffers from several disadvantages as compared to a scintiscanner. First, it does not contain any circuitry which allows either background erasing or enhancement of contrast, both of these operations being readily accomplished in a scintiscanner. This is a deficiency which is partially compensated by the high contrast obtained by using Polaroid-410 film. Also, the useful field of the autofluoroscope is restricted by the size of the image intensifier. It is difficult to build image intensifiers with fields greater than approximately 8 to 9 in in diam., whereas the scintiscanner can be made to scan any desired area. This, however, does not appear to be an appreciable drawback because, in most clinical applications, a circular field of 8 in in diam. is probably adequate.

The autofluoroscope which is described in the present report was not used for clinical purposes because we feel that this apparatus must be considerably improved before it can be applied practically. We are now in the

process of developing, in co-operation with The Rauland Corporation, an image amplifier specifically designed for use in a scintillation camera. This tube will embody an input screen thicker than normally used in X-ray amplifiers, which will result in greater photon stopping power. Furthermore, this tube will provide a very high light gain achieved by means of two-stage light amplification. It is hoped that with such a tube the X-ray amplifier scintillation camera will become a very useful tool for scintiscanning.

REFERENCES

[1] ANGER, H.O., Rev. scien. Instrum. 29 (1958) 27-33.
[2] BENDER, M.A. and BLAU, M., J. nucl. Med. 1 (1960) 105.
[3] KELLERSHOHN, C. and PELLERIN, P., C.R. Soc. Biol. CXLIX (1955) 533-536.
[4] MYERS, W.G. and VANDERLEEDEN, J.C., J. nucl. Med. 1 (1960) 149-164.
[5] TER-POGOSSIAN, M., KASTNER, J. and VEST, T.B., Radiology 81 No.6 (1963) 984-988.
[6] BECK, R.N., J. nucl. Med. 2 (1961) 314-324.
[7] STANG, Jr., L.G. and RICHARDS, P., Nucleonics 22 No.1 (1964) 46-49.
[8] FINE, S. and HENDEE, C.F., Nucleonics 13 (1955) 36-37.

DISCUSSION

A. LANSIART: You said that your silver collimator has holes 1 mm in diameter and 5 mm long and that it is made with foils one six-thousandth of an inch thick. Can you tell us how it is constructed?

M. TER-POGOSSIAN: The collimator is constructed by compressing silver foils one six-thousandth of an inch thick in concertina fashion; these are then assembled by welding so as to produce a square-holed grid.

A. LANSIART: How far from the collimator was the thyroid phantom?

M. TER-POGOSSIAN: Almost 2 cm.

A. LANSIART: It is generally very difficult to obtain pulses above background level with an X-ray source, a zinc-sulphide screen and a photomultiplier. The screen on the photocathode side of the X-ray image-amplifier tube seems less suitable than a NaI (Tl) or CsI (Tl) crystal for scintiscanning.

M. TER-POGOSSIAN: A NaI (Tl) or CsI (Tl) screen would probably be better. With a zinc-sulphide screen, however, we obtain very good images without any background.

M. BLAU: I cannot agree with Dr. Ter-Pogossian's statement that there are no disadvantages in using instruments which are capable of seeing only low-energy gamma-emitting isotopes. In the first place, the low-energy gamma-rays are strongly absorbed in the tissues and this makes scanning of large or deep organs difficult. Serious problems also arise with such isotopes because of radiation scattered in the tissues with little or no energy loss and producing smeared scan images. Moreover, the restriction to low-energy emitters leaves the chemist less scope in developing the most effective labelled compound for a given procedure. Some of the clinical procedures in current use could not be employed if we were restricted to low-energy isotopes.

W. NIKLAS: I should like to comment on the energy sensitivity of X-ray and gamma-ray image tubes developed by our research laboratories. The X-ray image tube used by Dr. Ter-Pogossian and Dr. Eichling was of the Rauland 6175-R-P type and had an input phosphor screen whose quantum absorption, effective energy conversion and resolution are optimized for approximately 120-kVp radiation, that is for normal X-ray fluorography. Tubes of this type have, however, been utilized very successfully in the 400-keV region for non-destructive testing in conjunction with isotope sources. Experiments have also indicated that they respond to energies somewhat in excess of 1 MeV.

Image tubes with a different pick-up pack with an internal lead converter are in use for the region between 1 MeV and 40 MeV, betatrons and linear accelerators being utilized as sources.

It is not difficult to increase the pick-up screen absorption so that optimization is achieved around 200 keV, and that is now being done. Furthermore, alkali halide pick-up screens are being developed; mosaic-type structures may also be considered for the pick-up pack.

Image tubes of essentially the same design as those used by Dr. Ter-Pogossian and Dr. Eichling are used in astronomy for electronography and permit exposure times of several hours without yielding density values above the chemical fogging level of typical electronographic emulsions such as Ilford G-5.

Thus, X-ray image tubes appear to have the proper energy response and the necessary low background to render them ideally suited for autofluorography at energy levels up to at least 200 keV.

M. TER-POGOSSIAN: In spite of the higher absorption of the lower-energy gamma rays in tissues, such low-energy emitters appear to be extremely useful, even in the visualization of deep-seated organs. A good example of this is the use of Hg^{197} (which is now in the process of replacing Hg^{203}) for localizing brain tumours.

H. WAGNER: I was very glad to learn that this instrument may be useful for radionuclides with energies up to 150 keV. I should also like to mention the possibility of interposing a thin sodium iodide crystal between the collimator and the photocathode of the image-intensification tube. Gamma rays that might otherwise pass through the photocathode might then produce photoelectric interactions in the crystal.

I should like to ask Dr. Blau if he could indicate the clinical studies which cannot be done with isotopes emitting radiation with energies of less than 200 keV.

M. BLAU: According to my experience, studies which cannot be performed with lower-energy isotopes include pancreas scanning, bone scanning and heart visualization.

M. TER-POGOSSIAN: I think that, at low energies, scatter may not appreciably affect the resolution of a scan.

W.G. MYERS: As a fellow chemist, I heartily agree with Dr. Blau that it is premature at this time to stress physical and technical problems relating to the detection of photons of various energies which might discourage and limit the chemist in his efforts to produce new labelled compounds. Professor George Hevesy, the discoverer of the isotopic method of analysis, emphasized in his Faraday Lecture in 1951 that isotopes are primarily new

forms of chemical reagents, and that gamma-emitting isotopes provide unique opportunities to perform biochemical and physiological analyses in vivo in patients.

I foresee that, in future, 511-keV annihilation radiation, especially that from the positrons of C^{11}, will play an important part in nuclear medicine.

I think that Dr. Ter-Pogossian's instrument may soon be developed in such a way that it will be particularly useful in the range of about 15 - 150 keV, where it will nicely overlap with Anger's scintillation camera which covers the range of about 125 - 750 keV. The Anger positron camera is, of course, especially attractive for all positron-emitting isotopes, e.g. C^{11}, N^{13}, O^{15}, F^{18}, Fe^{52}, Ga^{68}, As^{71}, etc.

I would like to ask Dr. Ter-Pogossian whether he feels that the instrument he is developing might become useful for gamma rays with energies as high as approximately 160 keV? Should this be possible, it might be especially useful to study the distribution of I^{123}, which has a half-life of 13.3 hours and emits 159-keV gamma rays and X-rays of about 28 keV. The radiation exposure would be trifling and pictures could be repeated frequently by comparison with I^{125} or I^{131}. A second picture could be made with a thin layer of suitable metal covering the collimator to absorb the X-rays but transmit almost all the gamma rays. The two pictures should indicate the depth at which I^{123} is localized because of the large differences in attenuation of the two radiations by the intervening tissues. The same method might be used with Xe^{131m} and Xe^{133} or other gamma-emitting isotopes of atomic number greater than approximately 35, the disintegration of which involves electron capture and/or internal conversion.

M. TER-POGOSSIAN: I am quite sure that our camera is still useful at about 160 keV, and that it might therefore be suitable for the visualization of I^{123}. In fact, it was your excellent study of the advantages offered by this isotope which to a large extent aroused our interest in developing a scintillation camera suitable for low-energy gamma emitters. Your idea of using both radiations of I^{123} separately is most interesting. I think that might be particularly useful in the relatively selective observation of tissue at different depths.

W. PAUL: Assuming that there are few energy limitations in future instruments of this type, would there be a further advantage in using a second image amplifier at the output of the first?

M. TER-POGOSSIAN: I am quite sure there would; we are now developing a two-stage, high-gain amplifier.

C. KELLERSHOHN: With regard to the comments made by Dr. Blau, I should like to point out that it is frequently stated in the literature that I^{125} is the best radionuclide for thyroid scanning. In the Biology Department of the French Atomic Energy Commission (Service Hospitalier Frédéric Joliot) we have considerable experience in using Hg^{197} and we have never found that kidney scans obtained with Hg^{197}-Neohydrin, or even with $Hg^{197}Cl_2$, were inferior in quality to those obtained with Hg^{203}-Neohydrin. I realize that it is difficult to avoid contamination of direct radiation by Compton scatter when low-energy emitters are used, and that in any case such isotopes cannot be used in certain circumstances because of the absorption of radiation by the tissues. Nevertheless, in the applications I have mentioned, the ad-

vantages of these two radionuclides far outweigh their disadvantages and make them particularly useful.

M. BLAU: I^{125} is no doubt adequate for an organ like the thyroid which is near the surface, and perhaps Hg^{197} is adequate for kidney scanning, although I suspect it would be difficult to see small tumours with the latter isotope. I cannot believe, however, that Hg^{197} yields the best results in brain tumour localization. In the paper he presented at this Symposium*, Dr. Glass told us that he can estimate the blood flow in the brain cortex with Xe^{133} because there is no response from the Xe^{133} in lower layers. Xe^{133} has the same gamma-ray energy as Hg^{197}. Surely Hg^{197} is unsuitable for finding deep brain tumours. It might be possible to localize large tumours with high uptake; a small deep tumour with low uptake could be diagnosed with Hg^{203} but not with Hg^{197}.

M. TER-POGOSSIAN: The neuro-surgeons in the Department of Isotopes at our Institute, after making about 300 conventional brain scans with Hg^{203}, decided to use Hg^{197} instead.

M. TUBIANA: Would it not be possible to eliminate at least some of the scattered photons by using a thin lead filter instead of a discriminator or electronic selector?

M. TER-POGOSSIAN: You are quite right. I think the method you suggest would be very useful.

C. HARRIS: If I am correct, there is no opportunity for pulse-height discrimination in your instrument. Its energy-response curve will thus be that of the screen, which will be similar to any other scintillator. We have all seen the folly of trying to scan without pulse-height discrimination. The literature is full of spectra showing "patient scatter" recorded over intensely active regions. What we do not find in the literature, however, are spectra from regions in the neighbourhood of active regions. Because of the effects of scatter in such regions, I think you will find the clinical scans disappointing.

M. TER-POGOSSIAN: I doubt whether the problem of scatter is very serious with low-energy radiation. We have found that it is not too troublesome with I^{125} in thyroid and brain phantoms. I agree, however, that this may become a problem with high-energy radiation and with large organs. The matter should be investigated further.

R. HERBERT: What fraction of incident energy at 70 keV is absorbed in the best screen?

M. TER-POGOSSIAN: For Hg^{197} radiation, with an energy of about 70 keV, it is approximately 20% in a conventional screen.

C.M.E. MATTHEWS: I think Hg^{197} is very different from I^{125} for scanning, since the photoelectric absorption coefficient in tissue increases rapidly between 70 and 30 keV. I do not think, therefore, that I^{125} would be suitable for scanning organs deeper than the thyroid. However, Hg^{197} has a high enough energy to be used for brain tumour localization; I have found that one can detect tumours in the centre of a phantom head with Bi^{206} X-rays which have an energy of 77 keV. This isotope would be difficult to use in

---

* GLASS, H.I., "A depth focusing collimator for the investigation of the brain cortex" (SM-51/27), these Proceedings I.

practice owing to the high background due to the body activity, but the experiments show that X-rays of this energy can be used.

M. TER-POGOSSIAN: I have seen some good kidney scans obtained with Tc^{99m}.

V

DISPLAY SYSTEMS

AN ANALYSIS OF QUANTITATIVE COLOUR DISPLAY FOR SCANNING

J.R. MALLARD, M.H. DUGGAN, M.J. MYERS and R.J. WILKS
DEPARTMENT OF MEDICAL PHYSICS,
HAMMERSMITH, LONDON, ENGLAND

Abstract — Résumé — Аннотация — Resumen

AN ANALYSIS OF QUANTITATIVE COLOUR DISPLAY FOR SCANNING. In colour scanning, first described by Mallard and Peachey in 1958, colour is used to present quantitative information in the display. Six colours are used for six equal divisions of count-rate across a ratemeter scale. In high count-rate scans (> 50 cps) the statistical spread of count-rate is small and the eye can see bands of colour on a scan and perceive boundaries between colours, these boundaries being isocount lines. In low count-rate scans (< 5 cps) the larger statistical spread results in overlap and marks appearing in the neighbouring colours. The relative proportion of marks in neighbouring colours can be calculated for a given count-rate and compares well with observation. Although isocount lines can no longer be perceived at these low count-rates, the colour changes between target and non-target areas lead to visual perception of differences in count-rate as low as one standard deviation; this is below that possible with monochrome printing without background suppression. A recent modification to improve the visual contrast still further has been to make the width of the mark, as well as the colour, change with count-rate. Several other methods of colour scanning have been developed by other workers.

Having established the lowest limit of count-rate difference which can be detected (approximately one standard deviation) it is possible to use a very simple phantom using disc tumours 1 cm thick, from which predictions can be made of the smallest size of any shape of tumour which can just be perceived at any concentration ratio and depth. Figures are given for the colour display used with a long-focusing 'depth-independent' collimator. It is predicted and shown that 2.5 cm cylinders at a depth of 12 cm can be perceived at 8 : 1 concentration ratio.

ÉTUDE CRITIQUE DE LA REPRÉSENTATION DES DIVERS NIVEAUX D'ACTIVITÉ PAR DES COULEURS DIFFÉRENTES AUX FINS DE SCINTIGRAPHIE. Décrite pour la première fois en 1958 par Mallard et Peachey, cette méthode de scintigraphie consiste à représenter divers niveaux d'activité par des couleurs différentes. Les auteurs utilisent six couleurs correspondant à six divisions égales de l'échelle d'un débitmètre. Pour les intensités élevées (> 50 cps), le scintigramme accuse une faible dispersion statistique des intensités; on peut distinguer à l'œil nu les bandes de couleur, dont les frontières constituent des lignes isodoses. Pour les faibles intensités (< 5 cps), la dispersion statistique est plus forte et il en résulte un chevauchement et des marques dans les couleurs avoisinantes. On peut calculer la proportion relative des marques dans les couleurs voisines pour une intensité donnée. Les résultats obtenus concordent bien avec les observations. Bien que l'on ne puisse plus, dans ce cas, distinguer de lignes isodoses, la différence de couleur entre la cible et le reste du champ exploré donne une représentation visuelle de différences d'intensité de l'ordre de un écart-type, seuil inférieur à celui de scintigrammes monochromes sans suppression du bruit de fond. On a pu récemment modifier le dispositif pour augmenter le contraste en faisant varier, non seulement la couleur, mais aussi la largeur des marques avec l'intensité. Il existe plusieurs autres méthodes de scintigraphie en couleur qui ont été élaborées par d'autres spécialistes.

Après avoir déterminé le seuil minimum de détection des variations d'intensité (un écart-type environ), on peut utiliser un fantôme très simple, formé de disques de 1 cm d'épaisseur stimulant des tumeurs, pour établir quelle dimension minimum doit avoir une tumeur de forme quelconque pour pouvoir être visualisée indépendamment du taux de concentration et de la profondeur. Le mémoire contient des données numériques pour la gamme de couleurs utilisée en conjonction avec un collimateur à grande distance focale et à profondeur de champs indifférente. Les auteurs démontrent qu'il est possible de détecter des cylindres de 2,5 à 12 cm de profondeur pour un taux de concentration de 8:1.

ПРОБЛЕМЫ ЦВЕТНОГО СКЕННИРОВАНИЯ. При цветном сканировании, впервые описанном в 1958 году Моллардом и Пичи, цвет используется для представления количествен-

ной информации в воспроизводящем устройстве. Для шести равных делений скорости счета на шкале измерителя берется шесть цветов. Для сценнограмм с большой скоростью счета (50 отсчетов/сек.) статистический разброс скорости счета невелик, и на сценнограмме можно увидеть цветные линии и проследить границы между цветами, представляющие собой изосчетные линии. Для сценнограмм с низкой скоростью счета (5 отсчетов/сек) больший статистический разброс выражается в перекрытии на границах соседних цветов. Можно подсчитать относительное количественное соотношение отметок в соседних цветах для данной скорости счета, и оно хорошо сравнивается с данными наблюдения. Хотя изосчетные линии нельзя наблюдать продолжительное время при низких скоростях счета, цветовые изменения между областью мишени и областью вне мишени приводят к визуальному восприятию такой низкой скорости счета, которая равна одному стандартному отклонению; это ниже, чем на монохромном отпечатке без подавления фона. Последнее усовершенствование для еще большего улучшения визуальной контрастности направлено на то, чтобы добиться изменения размера отметки, а также цвета вместе со скоростью счета. Были разработаны некоторые другие способы цветного сценнирования.

После установления наиболее низкого поддающегося обнаружению предела разности скорости счета (приблизительно одно стандартное отклонение) можно использовать очень простой фантом, представляющий опухолевый диск толщиной 1 см, с помощью которого можно определять очень мелкие опухоли любой формы при любом коэффициенте концентрации и глубине. Приведены рисунки, изображающие устройство для цветного воспроизведения с длиннофокусным "независимым от глубины" коллиматором. Предполагается и показывается возможность прослеживания цилиндров величиной 2,5 см до глубины 12 см при коэффициенте концентрации 8:1.

ANÁLISIS CUANTITATIVO DE LA ACTIVIDAD CORRESPONDIENTE A LOS DIFERENTES COLORES EN CENTELLEOGRAFÍA POLICROMA. La centelleografía policroma descrita por primera vez en 1948, consiste en representar diversos niveles de actividad por colores diferentes. Se emplean seis colores que corresponden a otras trantas divisiones iguales de la escala de recuento del integrador. En centelleogramas de elevado índice de recuento (> 50 cuentas/s) la dispersión estadística de este índice es pequeña y a simple vista se pueden ver bandas de color y percibir los límites entre las zonas coloreadas, que representan las líneas de isorrespuesta. En centelleogramas de bajo índice de recuento (< 5 cuentas/s) la dispersión estadística es mayor y da lugar a una superposición parcial de los trazos correspondientes a colores colindantes. La proporción relativa de trazos que aparecen en zonas de colores colindantes se puede calcular para cualquier índice de recuento y concuerda satisfactoriamente con los resultados experimentales. Aunque las líneas de isorrespuesta no son perceptibles cuando los índices de recuento son bajos, los cambios de color entre las zonas de interés y las otras permiten observar visualmente diferencias de índice de recuento de sólo una desviación standard, es decir, con un contraste mejor que el que se consigue por impresión monocroma sin supresión del fondo. Otra modificación introducida en fecha reciente para mejorar el contraste visual consiste en lograr que no sólo el color, sino también la anchura del trazo, varíe en función del índice de recuento. Existen algunos otros métodos de centelleografía policroma ideados por otros investigadores.

Una vez determinado el límite inferior de la diferencia entre índices de recuento que puede detectarse (una desviación standard, aproximadamente) es posible utilizar tumores simulados muy sencillos, en forma de discos de 1 cm de espesor, con ayuda de los cuales puede predecirse el tamaño menor de un tumor, sea cual fuere su forma, que puede percibirse a cualquier razón de concentración y profundidad. Se facilitan datos numéricos relativos a la representación policroma obtenida con ayuda de un colimador de enfoque largo, independiente de la profundidad. Se predice y demuestra que, para una razón de concentración 8 : 1, es posible percibir cilindros de 2,5 cm a una profundidad de 12 cm.

1. INTRODUCTION

The picture displayed as the end product of an isotope scan is required to show deviations from the normal pattern expected for that isotope in that particular part of the body. Ideally the abnormality should be described in terms of its position, shape and size, and the level of isotope concentration relative to the normal region; in many circumstances it is possible

to relate this information to pathological or histological findings. In the original hand-mapping technique the digital information of count-rate was available which enabled isocount contours to be drawn directly on the scan [1-3], and which helped to establish the presence of an abnormality and to define its extent.

Automatic scintiscanning machines began to come into general use in the early 1950s [4-6]. Although they were time-saving compared with the hand-mapping techniques and the type of shadow picture was undoubtedly very useful, all the available information was not displayed to the best advantage. A simple method was required which would display the numerical count-rate information in an immediately obvious manner.

At about this time other techniques of display were tried [4]. The printing of an even array of numbers to represent the count-rate, similar to that described by BEATTIE and BRADT [7], was considered here, but rejected in view of the lack of pictorial effect. It is interesting to note that very recently SIMPSON [8] has revised this idea with a special printing fount such that the numbers 1 to 9 are printed to give an area of ink proportional to the number itself; this helps to restore the visual effect and the numbers remain comparatively legible.

In 1958, a simple machine was described by MALLARD and PEACHEY [9] which was able to display some count-rate information without destroying the pictorial effect. The underlying principle was that the eye is easily capable of distinguishing between marks of different colour without doubt. The display consisted of an even array of marks, the colour of each mark being determined by the count-rate. A given colour represented a defined range of count-rates and it was possible to visualize a scan in terms of areas of colour, the boundary line between adjacent colours thus representing isocount lines of known count-rate. In early 1960 our present machine was described [10], a version of which is now commercially available. This combines both the familiar scintiscan principle with the colour system, in which the colours of the marks are changed as well as their spacing.

2. THE SCANNING MACHINE

Figure 1 is a block diagram of this machine. It differs from other scanners not only in the introduction of colour but also in that the couch-top is mechanized with variable speed drives to move the patient to and fro beneath the scintillation counter which is stationary. This has proved to be a particularly convenient and cheap way of obtaining the scanning raster because the couch and printer are completely independent of the counter system which can be changed at will with no limitations due to overloading of the scanning mechanisms.

The printer [10-12] is mounted at the end of the couch-top and moves to and fro with it over paper on the stationary table. The output from the counter is fed simultaneously to a scaler and a ratemeter; the scaler operates the tapping arm of the printer to give the scintiscan information, whilst the ratemeter output voltage triggers one of six transistor trigger units, which operates a solenoid system to move the appropriate colour band of a 6-coloured ribbon beneath the tapper. The ratemeter deflection thus se-

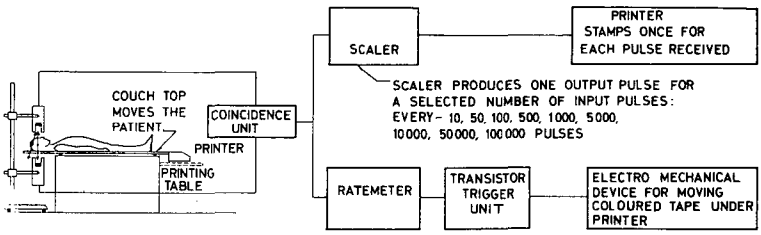

Fig. 1

Block diagram of colour scanning machine.
(The ratemeter range is adjusted to any value using a DC amplifier.)

lects the colour of mark to be printed at that moment. The colour scale is not limited to the ranges usually found on a ratemeter, for by means of a DC amplifier the ratemeter range can be adjusted so that the colour scale can be fitted to any scanning problem. Black-and-white carbon copies are produced simultaneously with the colour scan. The system has been in constant use for clinical and physical programmes for over five years and has proved to be a reliable and useful one.

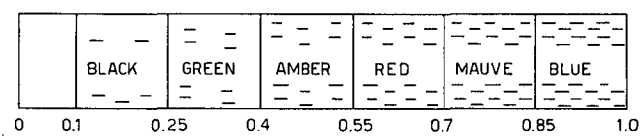

Fig. 2

The colour scale related to ratemeter range

The colour scale used is shown in Fig. 2. A linear colour scale has been adopted in which the six colours each cover a range of one and a half divisions of the ratemeter scale. It seems to us that the adjacent colours should have as much colour contrast as possible so that small changes in count-rate are rendered more obvious to the eye and so that the isocount boundaries between colours are readily visible. In our opinion this is to be preferred to a colour system which graduates the shades of colours with increasing count-rate; although the impression of 'hills and valleys' is enhanced, this effect really only applies to high count-rate scans and we feel that the extra contrast in low count-rate scans is of more value. The colour sequence used here is one for which a multi-colour tape is commercially available, and is not necessarily the very best from the point of view of contrast.

By adjusting the voltages at which the transistor trigger circuits operate it is possible to use non-linear scales for the colour changes, e.g. a logarithmic one or one based on standard deviations. However, a linear scale is thought to have more general application and gives a simpler immediate numerical interpretation. It is interesting to realize that some of the other displays are more limited in their response characteristics, e.g. photoscanners are limited to a logarithmic scale [13-14] and are prone to saturation effects [15].

3. THE ROLE OF COLOUR

Scintiscans may be divided into two arbitrary classes. Firstly, those in which the count-rate is fairly high, say 50 cps or more as one might obtain in liver or thyroid scanning, in which statistical deviations of count-rate become comparatively unimportant and the marks become comparatively close together. Secondly, those in which the count-rate is low, say 5 cps typical of brain-tumour or spleen scanning, where the marks are spaced out and the statistical fluctuations of count-rate are large and important.

In the high count-rate scans the role of colour is shown in Fig. 3. Figure 3 (a) shows a scan of radioactive colloidal gold which has been injected into a knee joint for treatment of persistent knee effusions [16]. The isocount lines stand out very clearly and more information is immediately available from the colour scan than from the black-and-white scan. Figure 3 (b) shows a liver scan using Au^{198} colloid. Two regions of reduced uptake, one very deep, are readily perceived on the colour scan. The outline and the deeper indentation are not nearly so clearly perceived on black and white and of course the colour gives the count-rate from point to point e.g. the main lobe is almost twice the count-rate of the indentation. Tumour was found in both indentations.

For the other group of low count-rate scans, brain-tumour scanning is typical. Figure 2 of a later paper [27] in this Symposium shows an obvious brain tumour which stands out very clearly on both AP and lateral views. Figure b of Ref. [27] shows the AP scan of another brain tumour which is very close to the limits of detection of the system. It can be visualized first by comparing the left with the right side, one side having more green marks than the other. The lateral scan of the same tumour [Figure b] [27] contains a region with more green marks than in the surrounding normal area and indeed more green marks than one normally expects in this region for scans of this count-rate range (see section 5 of Ref. [27]). The eye is able to detect quite small variations from the normal colour pattern whereas small variations from the corresponding normal black-and-white pattern are not easily perceived. Having located the region of deviation from the normal then the count-rate in this region can be determined, and its statistical significance examined. In this particular case, the count-rate was found to be five standard deviations (S.D.) greater than normal and a tumour, which was thought to be a glioblastoma, was found in the region indicated.

Thus, in the low count-rate scans, the role of colour is to make areas of slightly different count-rates more readily apparent, and to extend the limits of detection of abnormalities.

In the high count-rate scans colour is a means of printing on to one picture isocount lines and quantitative information which would have required additional experiments if photographic and television playback systems [14] were used. Colour also provides six built-in levels of background suppression which are immediately displayed and the scan need not be played back as with a magnetic-tape system [17]. As DI CHIRO has pointed out [18] background erase is not a desirable trend because accurate localization of a lesion requires presentation of the background structure of the scan related

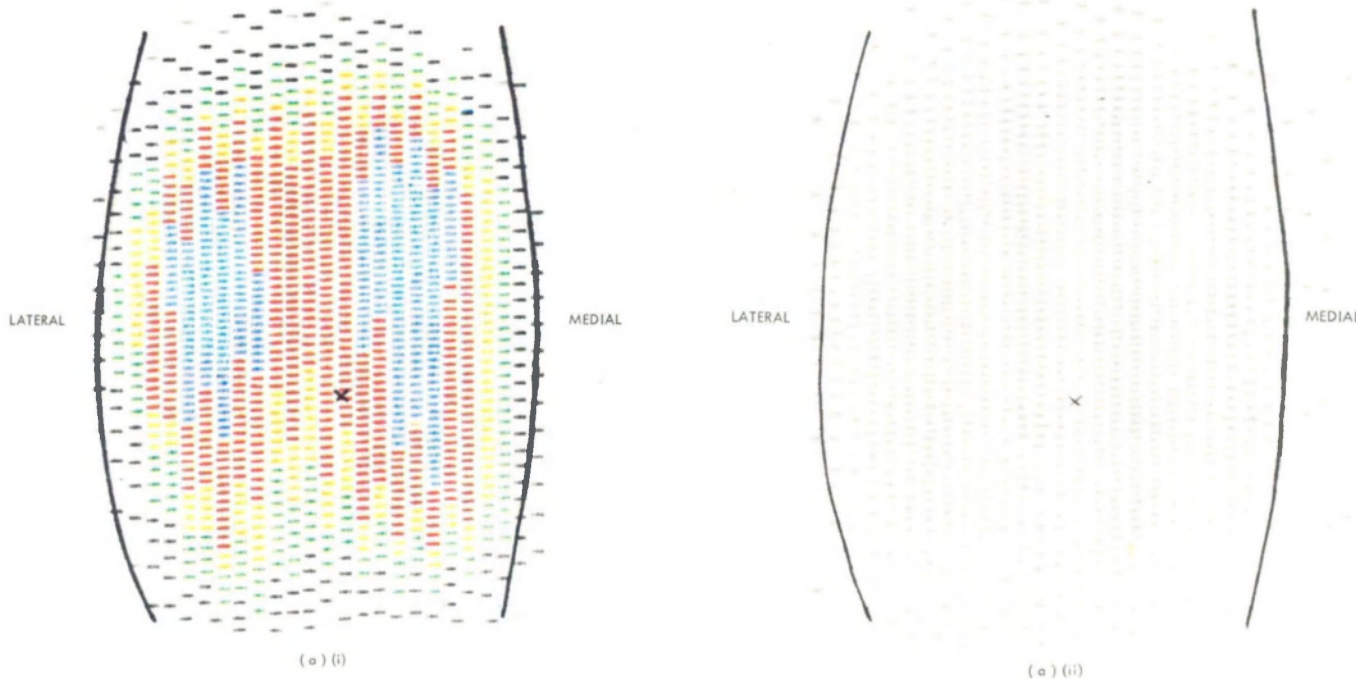

Fig. 3 (a)

Colour scan and black-and-white scan of Au^{198} colloid in knee joint to persistent effusion [16]

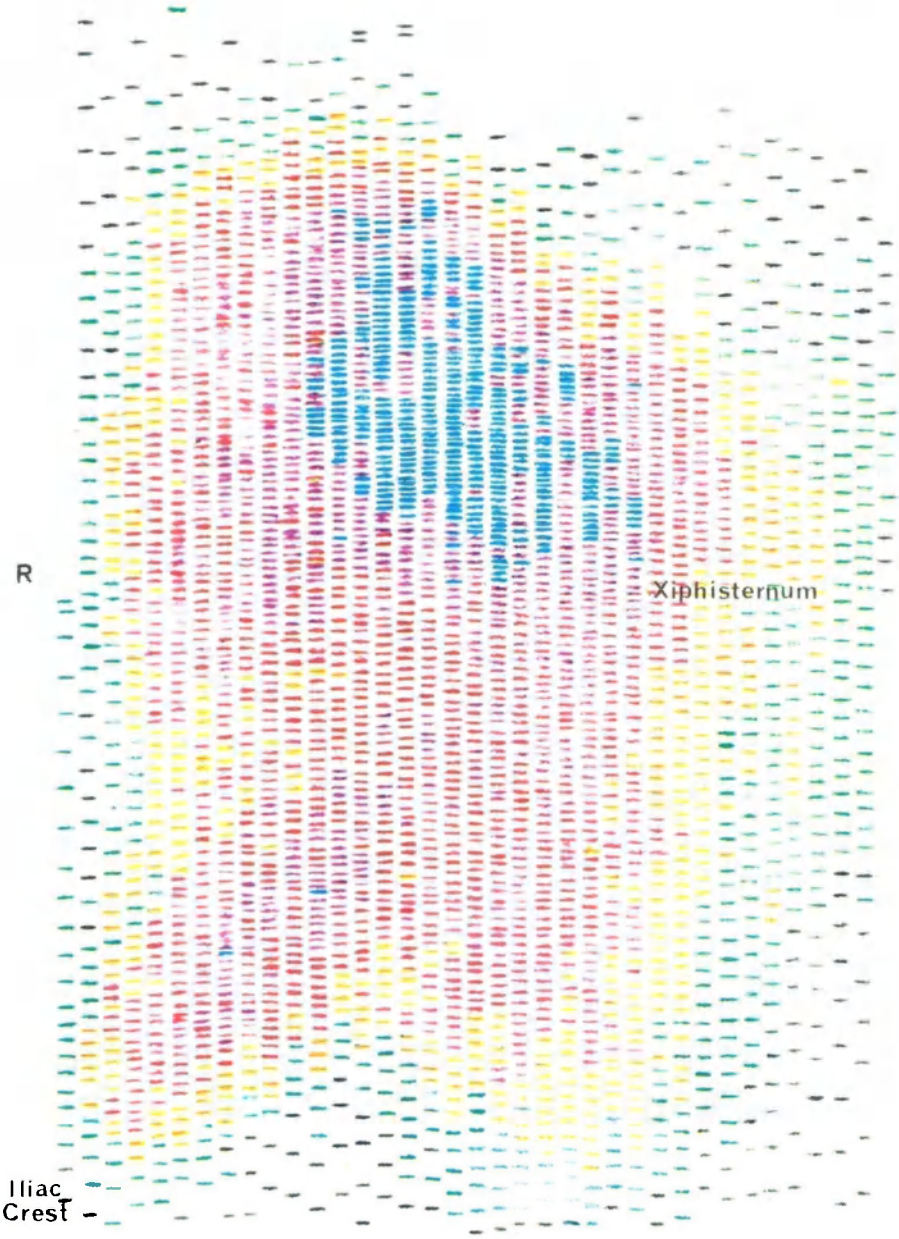

Fig. 3(b)

Colour scan of liver using Au^{198} colloid.
Two tumour masses can be seen as abnormal indentations in the red-yellow isocount line not seen so easily in the black-and-white scan (see page 430).

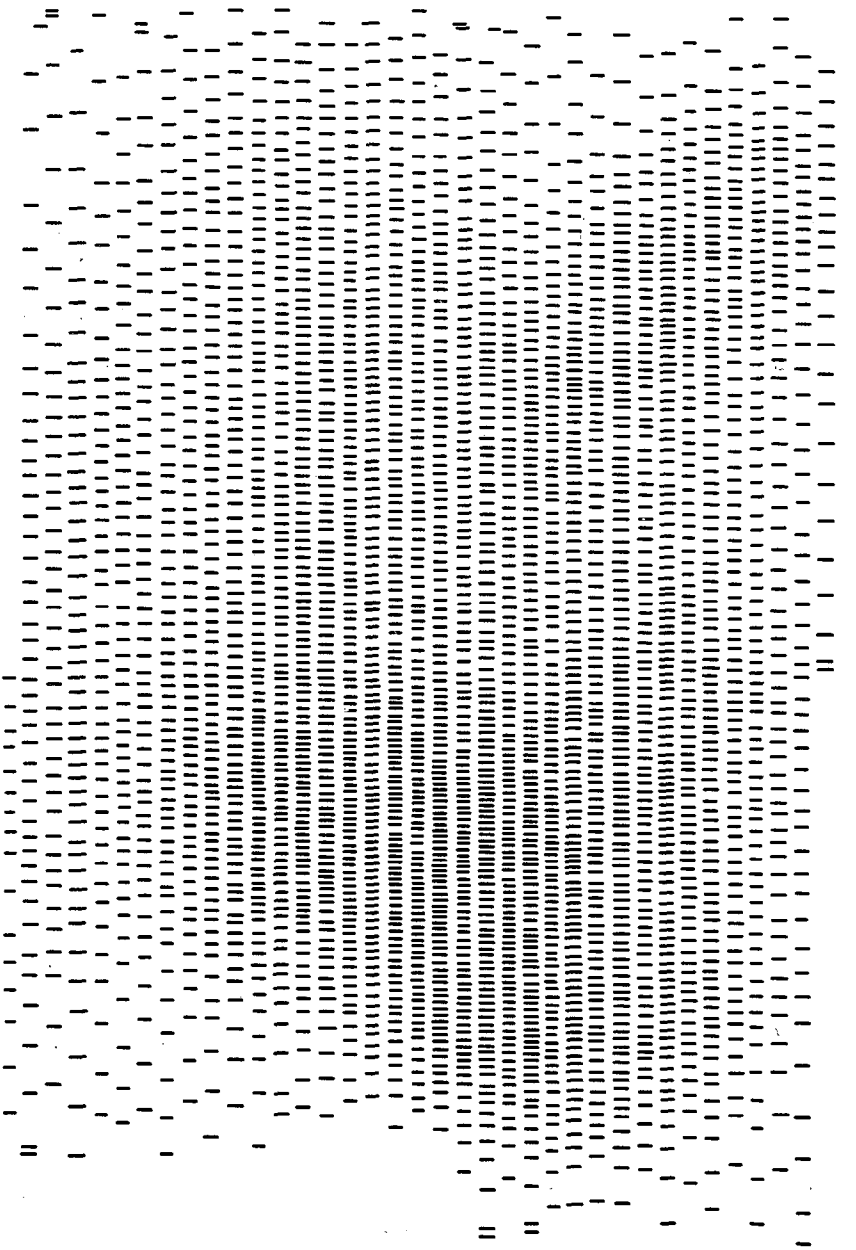

Fig. 3(b)

Black-and-white scan of liver using Au^{198} colloid.
Two tumour masses can be seen as abnormal indentations in the red-yellow isocount line (see page 429) not seen so easily in the black-and-white scan.

to the anatomy. With colour printing, all the available information is present on one scan and the colour helps to distinguish lesion from background.

4. THE EFFECT OF RATEMETER TIME CONSTANT

Figure 4 (a) shows the results of feeding into the ratemeter a sudden increment of count-rate from 200 cps to 1000 cps for 15 s, this period being equivalent to 5 cm of couch movement. The tapper was set to print at a constant rate throughout. The colours change through the complete range, from black up to blue, as the ratemeter deflection increases. As the time constant is increased the response of the ratemeter to the step function becomes slower and the bands of colour become correspondingly broader. The leading and the trailing edges of the square wave, when passed through the ratemeter become two curves, an exponential growth curve followed by an exponential decay curve. As one would expect the top colour blue, which appears at 85% of full-scale deflection, is reached at approximately two time constants after the beginning of the square wave.

At the longer time constants the colour pattern is displaced geometrically from the centre of the true peak. Since the couch of the scanning machine moves to and fro this gives rise to a 'stagger' effect whereby alternate lines of a scan are displayed in colour relative to one another. Figure 4 (b) illustrates this effect. The colour boundaries of adjacent lines do not coincide exactly whereas alternate lines, which are made with the printer moving in the same direction, do coincide. This 'stagger' tends to spoil the immediate impact of high count-rate colour scans by making colour boundaries less clear. The degree of stagger depends on the couch speed. The black-and-white scintiscan, controlled by a scaler with a low integrating time, does not exhibit this stagger effect.

The ratemeter time constant introduces a further error when a small area of increased count-rate is scanned. The ratemeter does not have time to reach the true peak count-rate over the 'hill' so that a quantitative estimation of concentration ratios may be incorrect.

There is a need for a colour control circuit which does not possess an appreciable time constant, but for practical purposes a time constant of 1 - 2 s does not introduce serious error.

5. THE EFFECTS OF COUNTING STATISTICS

5.1. High count-rate scans

In scanning, a consideration of counting statistics and its effect on the colour pattern is important [15, 17a]. In the high count-rate group of scans at 50 cps, for example, with a 2-s time constant (t) of the ratemeter, the standard deviation of the count-rate, $(\sqrt{n/2t})$, is approximately 3.6 cps. Since the ratemeter will be on the 0 - 100-cps range, a colour band extends over 15 cps, which is 4.2 standard deviations. As a result, at a given mean

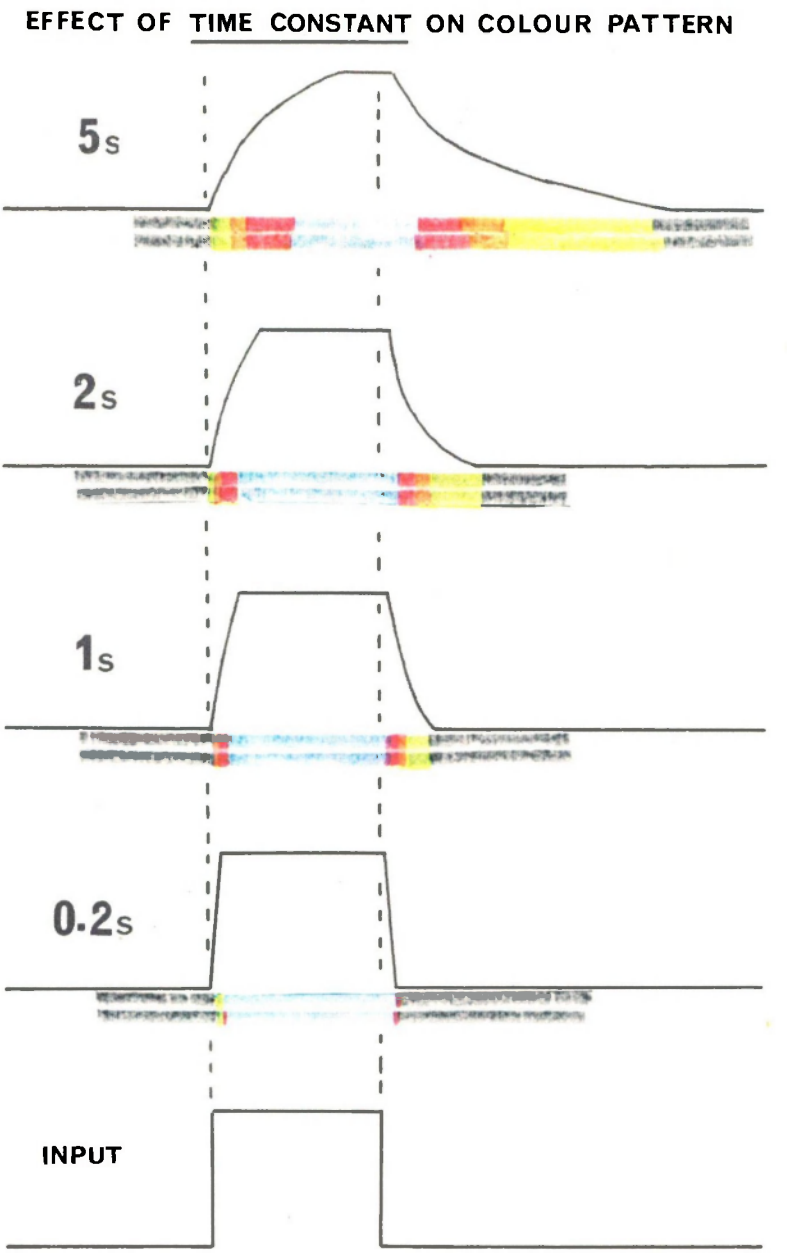

Fig. 4 (a)

The effect of ratemeter time constant.
The colour pattern follows the exponential growth and fall curves determined by the time constant.

Fig. 4 (b)

Stagger in alternate lines of colour scan.
The time-constant delay of the colour changes is the same
for alternate lines in which the scanning raster is in the same direction.

count-rate represented by a certain colour, there is a small chance that a mark may appear in the adjacent colour of higher or lower count-rate.

Each coloured mark made on a scan represents a measurement of count-rate. For any chosen mean value of count-rate it is possible to calculate the probability that a measurement of count-rate has a certain deviation from the mean using the statistical normal distribution for a large number of measurements. It is thus possible to determine the expected proportion of dots which will be recorded in the colour corresponding to the mean count-rate, and also in the adjacent colours.

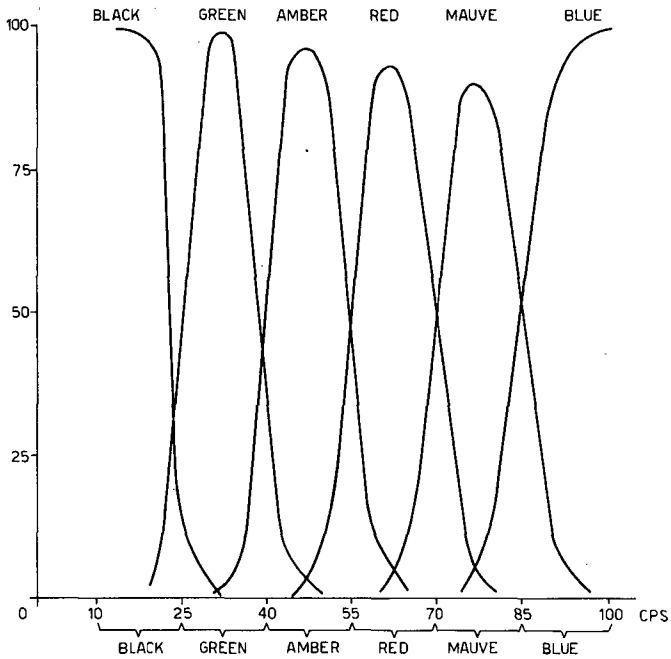

Fig. 5 (a)

The proportion of marks printed in the appropriate colour for high count-rates (0-100-cps ratemeter range, 2-s ratemeter time-constant).

Figure 5 (a) shows the results of such calculations for the 0 - 100-cps range of the ratemeter. At a count-rate of 62.5 cps, for example, in the middle of the red range, one should expect for a large number of dots, 92% red and only 4% amber (the lower colour) and 4% mauve (the higher colour). The colour discrimination between adjacent regions is almost, but not quite, complete, and the isocount boundaries are therefore quite clearly defined by the eye; for example, as the count-rate changes from 52 - 58 cps (a colour boundary at 55 cps), which is a count-rate difference of 1.2 standard deviations of difference ($\sqrt{(n_1+n_2)/2t}$), the pattern changes from 85% amber, 15% red to only 15% amber but 85% red, a change which is clearly visible to the eye. At the count-rate equal to the boundary itself, it will be half of each colour. As a result the colour pattern of the region of interest can instantly be related to the count-rate range and, in addition, if there is a region on a scan which has a different predominant colour from its surroundings, then it could represent a count-rate change of as little as one standard deviation even for small areas (cf. section 5.2).

At still higher count-rates above 100 cps, the ratemeter range being chosen accordingly, the curves of Fig. 5 (a) become more flat-topped with steeper sides so that the separation of colours is even more complete and still smaller fractional changes of count-rate can be perceived. At these very high count-rates the range of count-rate represented by one colour could be reduced so that more information is printed on the scan, either

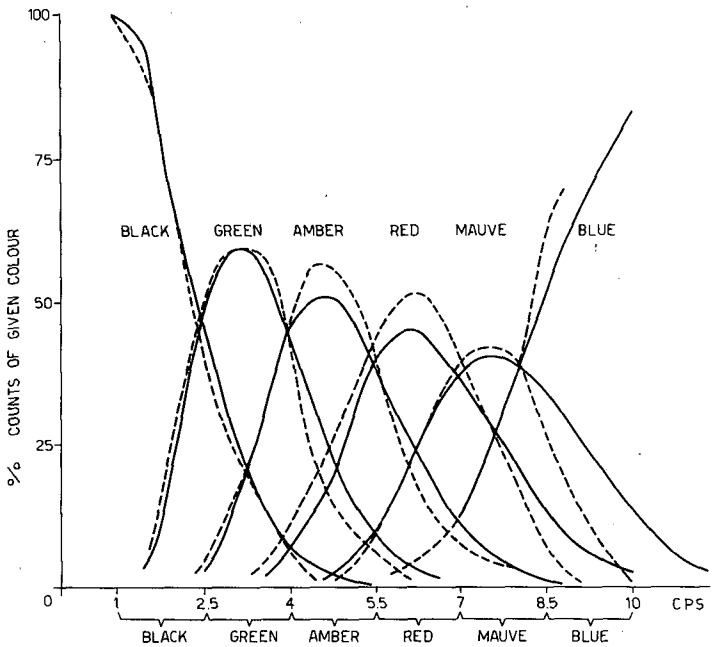

Fig. 5 (b)

The proportion of marks printed in the appropriate colour at low count-rates (0 - 10 cps ratemeter range, 2-s ratemeter time constant).

by introducing extra colours, or by taking only part of the ratemeter range for all six colours. For the count-rate range below 100 cps, however, the colour range is sufficiently narrow for any clinical purpose, and, if narrower, would not be so meaningful statistically.

5.2. Low count-rate scans

It is interesting to apply this analysis to the low count-rate scans where the statistical spread of count-rate is larger and where any increase in the amount of information printed is valuable. At 5 cps with a 2-s time constant, the standard deviation of the count-rate is approximately 1.1 cps. On the 0 - 10 cps range of the ratemeter a colour band is 1.5 cps and therefore represents a range of only 1.4 standard deviations (S.D.). There is thus a good chance of printing any one of several colours at any time and a particular mean count-rate will be represented, not by one colour, but by a distribution pattern of several colours.

The net result is seen in Fig. 6 which shows the colour and the black and white patterns obtained when the counter scans eight uniform distributions of radioactivity at various levels throughout this count-rate range. As the average count-rate is increased the average spacing between marks gets smaller and the predominant colour changes. It is much easier to per-

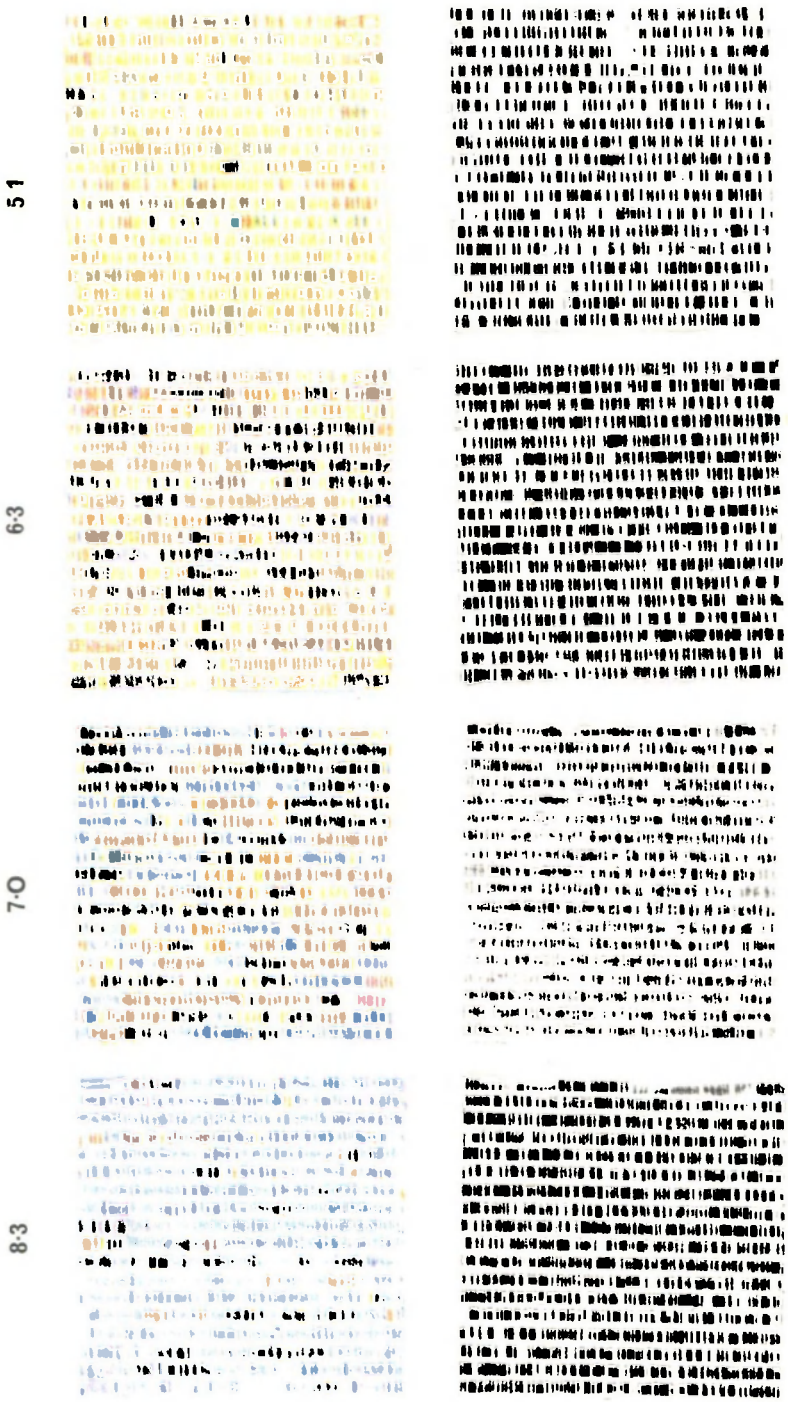
5·1
6·3
7·0
8·3

COMPARISON OF COLOUR AND BLACK AND WHITE PATTERNS FOR VARIOUS CONSTANT COUNTS/SEC.

Fig. 6

Colour and black-and-white patterns when viewing a series of uniform activities in the low count-rate range (0 - 10 cps)

ceive the changes of count-rate between adjacent scans through the colour sequence than through the black and white sequence and if one chooses two adjacent patterns which can definitely be seen to be different, e.g. 5.1 and 6.3 cps, then a count-rate change of 0.7 S.D. has been perceived. Also it is seen from Fig. 6 that, owing to statistical fluctuations, small areas on an individual scan will appear to represent a statistically significant change in count-rate, although they may not have any real significance. This fact must be borne in mind when considering scans at low levels, and also applies to black-and-white scans.

Figure 5 (b) shows the results of the calculations of the colour distribution for the 0 - 10-cps range of the ratemeter. The curves are much broader than those for the 0 - 100-cps range and overlap much more; they express the reduced colour separation which was seen in Fig. 6 which makes the drawing of isocount lines very difficult. At a count-rate of 6.25 cps for example, in the centre of the red range, 46% of the marks are the correct red, 24% are mauve (the higher colour), 24% are amber (the lower colour), and 6% are blue and 6% are green, the next but one colours higher and lower. If the count-rate changes down to 5.1 cps, 2% black appears, green increases from 6 to 15%, amber almost doubles from 24 to 45%, red decreases from 46 to 30% and mauve from 24 to 8%; this change of colour pattern has been shown in Fig. 6 to be a perceptible one. The observed distribution patterns of Fig. 5 (b) (dotted lines) are seen to agree closely with those calculated, the differences between them being due to small inaccuracies in the triggering voltage of the circuits which control the count-rate at which the colour is changed.

Figures 5 (b) and 6 show that in the low count-rate scans, although the colour is not nearly such a clear-cut indication of count-rate as at higher count-rates, the colour pattern still serves as a visible guide to count-rate and small changes of the order of 0.7 S.D. can be perceived between the patterns shown. The corresponding limit of visible perception for black-and-white scans is somewhat greater, (about two or three times), near the top of the scale, a value in good agreement with the statistical theory of contrast perception [26].

Now these changes, which may be thought to be very small, have only been perceived because, in the scans of Fig. 6, a considerable number of marks were viewed (approximately 900 in the middle of the range) over an area of $3\frac{1}{2}$ in square. The resulting standard deviation of these 900 determinations of the count-rate (standard deviation of the mean) is therefore small, so that the difference in count-rate between it and its neighbouring scan is statistically significant and is therefore perceived. We have, however, for convenience, expressed this count-rate difference as a multiple of a standard deviation calculated for only one ratemeter measurement of each of the two neighbouring count-rates, which is, of course, much larger.

As the area of scans which are compared is reduced, the number of marks in each becomes smaller, and the standard deviation of the mean becomes larger. As a result the difference in count-rate which is perceptible increases (inversely as the square root of the number of marks) as the area of scan decreases. It does not increase indefinitely, however,

as the area of the scans is reduced, as it does in black-and-white pictures because 'colour exclusion' comes into play. Two scans can be seen to be different if one contains many marks of a given colour but the other contains none at all. As a result, a count-rate change (see Fig. 5 (b)) from 3.25 to 1 cps (2.2 S.D.) or 3.25 to 7 cps (2.3 S.D.) is certainly perceived since there is a negligible probability of recording a green mark at less than 1 cps and at more than 7 cps.

The ultimate limit is reached when there are only very few marks printed. The graphs of Fig. 5 (b) now represent the probability of a certain colour being printed for a given count-rate. Consider two marks only, of different colour, one green and the other mauve. There is a much smaller probability that they could represent the same count-rate than there is that they could represent different count-rates because there is only a small region of overlap of the green and mauve curves. It is most probable that they represent a count-rate difference from the peak at 3.3 to the peak at 7.8 cps (2.7 S.D.). In these circumstances, monochrome printing would not be able to display a difference in count-rate. The colours chosen were two colours apart and it is apparent that for adjacent colours, due to greater overlap, one could not be very certain of the limit of perceptible count-rate difference without further analysis.

To sum up, with colour printing as used here, at low count-rates the perceptible difference in count-rate can be as low as about 1 S.D. or less for a large number of marks or for large areas of constant count-rate, rising to about 3 S.D. for very small numbers of marks. For small areas of scan with a moderate number of marks, the perceptible count-rate difference lies between these limits.

6. THE DETECTION OF 'TUMOURS' BY SCANNING

For scanning to be as useful as possible as a diagnostic procedure it is necessary to detect and display the smallest possible tumours for the tumour-to-background concentration ratio which is found for the tumour type and contrast material used.

Before one begins to scan a patient it would be very valuable to have a precise knowledge of the limits of tumour size which the scanning machine is able to detect in given circumstances. Indeed such information would also enable an intercomparison of scanning techniques to be made. The smallest tumour which is detectable will depend upon the following factors:

(i) The depth in a tissue equivalent phantom;
(ii) The concentration ratio of tumour to background radioactivity;
(iii) The γ-ray energy and width of spectrum utilized (positrons being a special case); and
(iv) Scanning machine characteristics, such as crystal size and collimation (which affect count-rate), couch speed, time constant and display features (e.g. print-out rate or background suppression features).

6.1. A phantom experiment using disc tumours

A simple phantom experiment has been devised which gives a considerable amount of information on the minimum tumour size detectable. It is applied here to one of the counters used in conjunction with the colour scanner display. The results presented are preliminary, and form part of an investigation of the parameters listed above.

The counter had a $3\frac{1}{2}$-in-diam., 3-in-thick NaI crystal fitted with a lead focusing collimator (19-hole) with a geometrical focus at a distance from the collimator of twice the collimator length; it is a 'long-focusing' one with point-source characteristics which show only a small depth dependence in a water phantom. It can loosely be described as a 'depth-independent' collimator; collimators of this type [19] are described in more detail in Ref. [27].

A phantom system was used which is a modification of a sectional one first described by MacINTYRE and CHRISTIE [20-21]. A 30 cm square tank, 12 cm thick, was used as a body phantom with hollow cylindrical discs as tumours of diameters 2, 3, 4 and 6 cm, each 1 cm thick. The discs were filled with a known activity concentration of I^{131} (A_{disc}) and the photopeak count-rate (gate-width 250 keV - 500 keV) was determined from them when placed at a series of depths in the tank filled with water (not I^{131}). Count-rates were determined for each depth over the middle of the discs (C_{MID}) and the results are shown in Fig. 7. (The count-rates were also determined over the edge of the discs (C_{EDG}) and are discussed later (section 6.3).) The count-rate ($C_{B.G.}$) was also determined over the centre of the tank filled with an activity concentration ($A_{B.G.}$) of I^{131} (without any discs at all).

Much information can be obtained from this one experiment with disc tumours in a water tank, together with the simple measurement of $C_{B.G.}$.

(i) The variation of count-rate over the middle of the discs can be shown as a function of disc diameter at a chosen depth in water phantom. Also, the dependence of this function on depth is presented. Since the discs are essentially two dimensional, such results should be capable of theoretical interpretation.

(ii) From the measurements of C_{MID} and $C_{B.G.}$ the functions given in (i) can be calculated for any concentration ratio of disc to body phantom. The fractional count-rate increment ($\Delta N/N$) over the centre of the phantom on introducing a disc tumour at a certain depth, Z, for a concentration ratio $A_{disc}/A_{B.G.}$ is therefore

$$\Delta N/N = \frac{C_{MID.Z}}{A_{disc}}\left(\frac{A_{disc}}{A_{B.G.}} - 1\right) / \frac{C_{B.G.}}{A_{B.G.}}$$

and can be calculated for the disc sizes and depths at which C_{MID} has been measured, for any concentration ratio.

It is worth noting here that a negative tumour or hole or void produces the same change in count-rate as a position one of twice the background activity

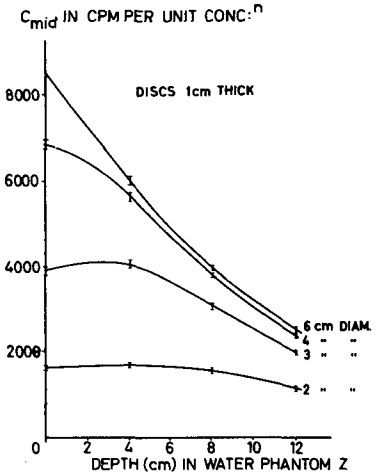

Fig. 7

Count-rates determined over the centre of various disc sizes of phantoms (1 cm thick) at a series of depths in a water tank, determined with a $3\frac{1}{2}\times3$-in NaI crystal and a 19-hole long-focusing 'depth-independent' collimator.

concentration but opposite in sign, as pointed out by BENDER [22] which we confirm experimentally.

(iii) From (ii) the variation of count-rate over the middle of the disc and also $\Delta N/N$ is obtained as a function of depth for each disc diameter at chosen concentration ratios. Such information, combined with knowledge of the count-rate changes which can be perceived by a given scanning display, enables predictions to be made of the minimum size of disc tumours which can be perceived for chosen concentration ratios and depths.

(iv) The same parameters as (iii) can be calculated for any chosen thicknesses of cylindrical tumour, e.g. the contribution from a cylinder 2 cm thick at a given depth of its top surface, is equal to the sum of the contribution from a 1-cm disc at that depth from Fig. 7 plus that of a 1-cm disc at a depth 1 cm lower, also from Fig. 7. In this way the graphs can be constructed to show fractional count-rate changes over cylinders which have the same thickness as their diameter, for example, the shape of which may be regarded as similar to clinical tumours. From these graphs, as above, the minimum size of cylinder which is perceivable can be predicted.

(v) By building up a chosen tumour shape from a number of discs of appropriate diameter, each 1 cm thick, the simple experiment (Fig.7) yields information on the perception of tumours of any shape or size, at any depth, and at any concentration ratio.

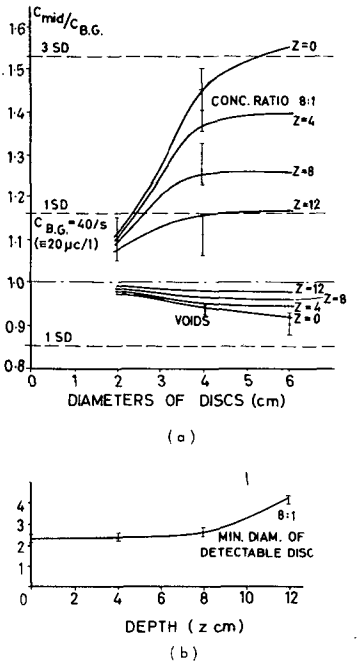

Fig. 8

Ratio of count-rate over the centre of various sizes of disc phantom (1 cm thick) to the count-rate over the tank background (without discs) for a concentration ratio of 8:1 at four depths in the tank.
($1+\Delta N/N$ calculated from Fig. 7)
Voids correspond to a concentration ratio of 2:1.
(b) shows the minimum size of disc detectable ($C_{B.G.} \approx 40$ cps) in the colour display where 1 S.D. of count-rate difference can be perceived

6.2. Comparison of derived limits of perception with scanning

Figures 8 and 9 show the results of applying the above calculations to the measurements shown in Fig. 7 for a concentration ratio 8:1; Fig. 8 applies to discs whilst Fig. 9 applies to cylinders of thickness equal to diameter. The background activity level has been chosen to be 20 μc/l, a level similar to that in liver scanning which, with the counter used here, gives a count-rate of 40 cps. The results are expressed as a ratio of the counts over the middle of the disc to the body phantom background count and are shown also for negative discs or voids. Also plotted on these graphs are the values obtained by direct experiment using disc tumours in the tank with 8:1 concentration ratio and using solid perspex discs as voids. The agreement between the values derived from the above calculations and these observed is good.

For the colour-scanning display it was shown in section 5 that one should be able to 'see' a count-rate change of one standard deviation. The line of 1 S.D. change in count-rate is marked in Figs. 8 and 9 and shows that the

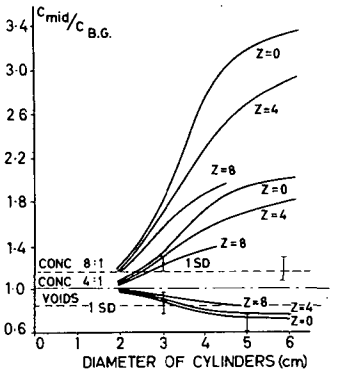

(a)

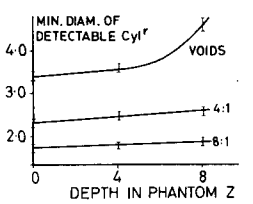

(b)

Fig. 9

Ratio of count-rate over the centre of various sizes of cylindrical tumour (thickness = diameter) to the count-rate over the tank background (without cylinders) for a concentration ratio of 8:1, 4:1 and 2:1 (voids). ($1+\Delta N/N$ calculated from Fig. 7.)
(b) shows the minimum size of cylindrical tumour detectable ($C_{B.G.} \approx 40$ cps) in the colour-scanning display where 1 S.D. of count-rate difference can be perceived

minimum detectable discs should be as shown in Fig. 8 (b). Close to the surface of the phantom one should see 2.3-cm-diam. discs at 8:1 concentration ratio and possibly no voids at all. The depth independent characteristics of the collimator come into play, and at 8-cm depth it is still possible to see discs of 2.5-cm-diam. but by 12-cm depth the minimum tumour detectable has risen to 3.5-cm-diam. It must be stressed here that other collimators with different resolution diameters and depth characteristics would show different performance figures.

Figure 10 shows scans carried out on a disc of 4 cm diam. at four different depths with a concentration ratio 8:1 and phantom level 20 μc/l. It is readily perceived on the surface and at depths 4 and 8 cm but is less easily distinguishable at 12 cm. This performance agrees very well with Fig. 8 (b) so that the detectable limit of 1 S.D. count-rate change is verified.

The black-and-white scintiscans of Fig. 10 do not show such low limits of perception, the limit being about 2.8 S.D. count-rate change. Thus with

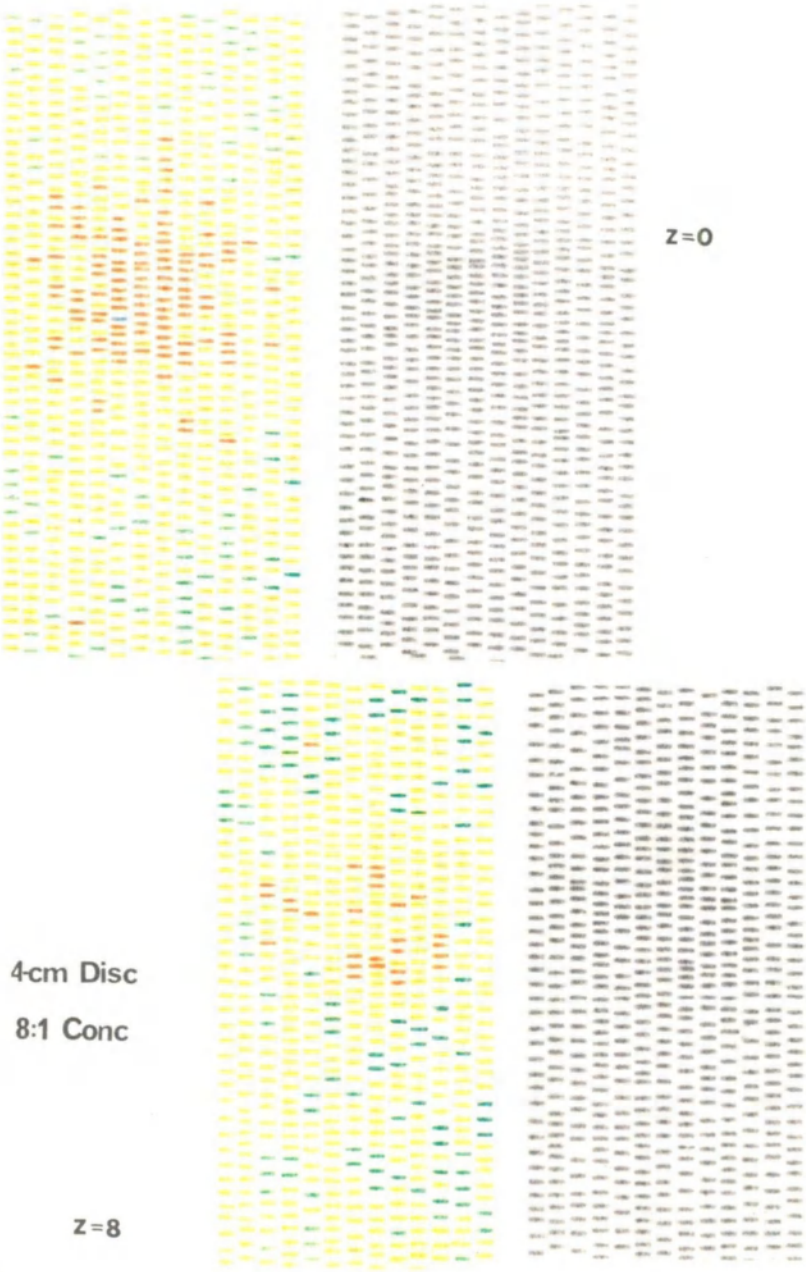

Fig. 10

Colour and black-and-white scans of a 4-cm disc (1 cm thick) with a concentration ratio 8:1 at four depths in a tank containing approximately 20 μc/l (background approximately 40 cps)

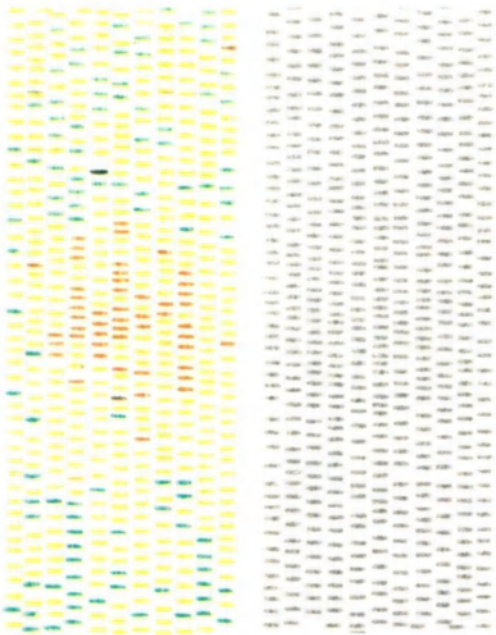

z=4

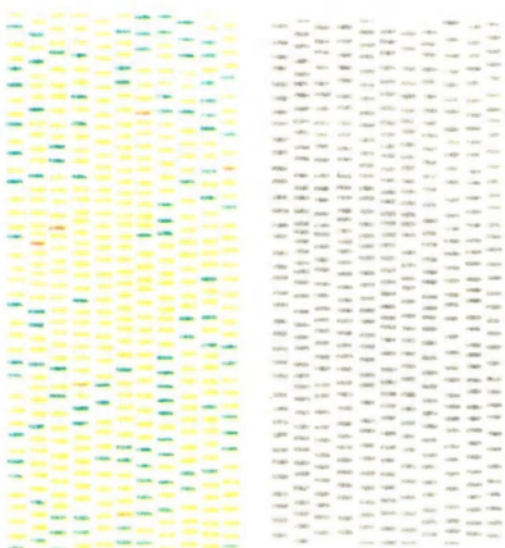

z=12

Fig. 10 (cont'd)

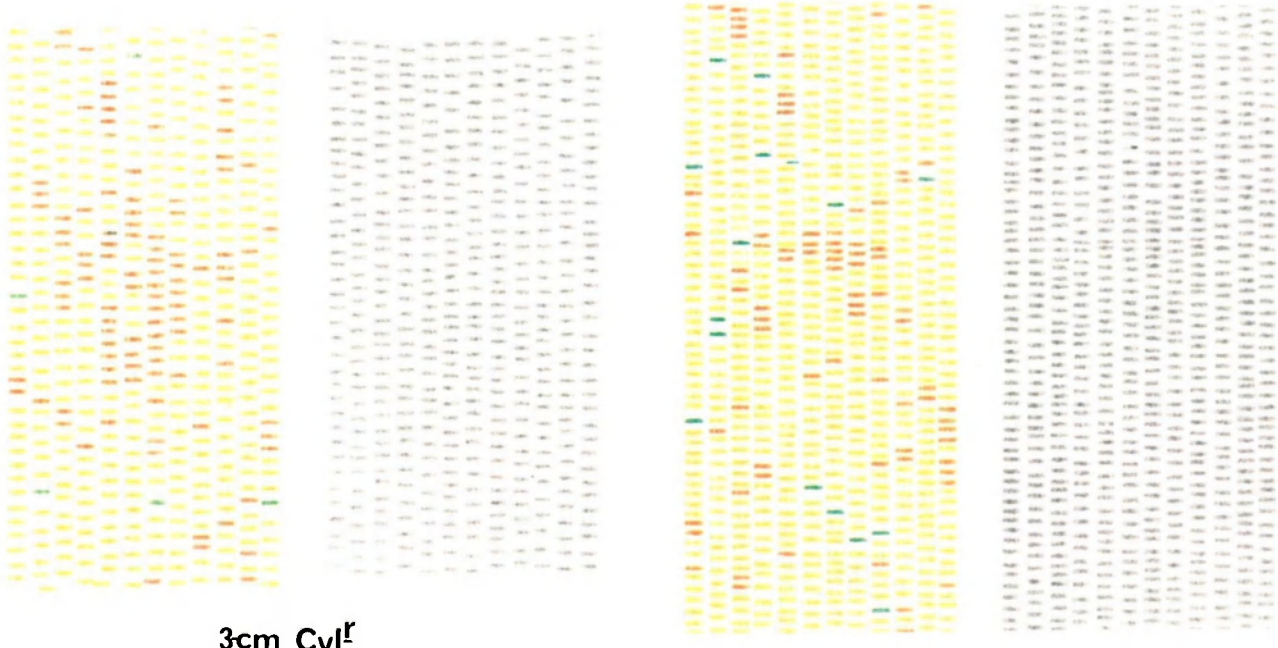

z-8 4:1 Conc.

Fig. 11

Colour and black-and-white scans of two cylinders (thickness = diameter) at 4:1 concentration. The 3-cm one is perceived but the 2-cm one is hardly perceived in colour (see Fig. 9). Neither of them are perceived in black and white.

the black-and-white display one can only perceive discs of about twice the diameter, or a given diameter at only about one third of the depth or at about twice the concentration.

Figure 9 (a) shows the curves derived from Fig. 7 for cylindrical tumours. Assuming again that 1 S.D. change of count-rate can be perceived then for positive cylinders at a concentration ratio 8:1 the minimum detectable size should be 1.9 cm at 8-cm depth and 1.8 cm at 4-cm depth. Figure 9 (b) shows the minimum perceptible sizes of cylinder for 8:1 concentration ratio and also at 8-cm depth for 4:1 concentration ratio. Figure 11 shows scans of 2-cm and 3-cm cylinders at 8-cm depth at 4:1 concentration ratio. The 3-cm one can definitely be seen but the 2-cm one is doubtful which is in good agreement with Fig. 9 (b). Again the depth-independent characteristics of the collimator are seen to be of value and the colour display reduces the limits by a useful factor e.g. from a 3-cm minimum perceptible diameter cylinder for black-and-white printing, to a 2-cm one in colour at concentration ratio 4:1 and depth 8 cm. Again, it must be stressed that these figures apply only to the long-focusing collimator and counter used here.

Finally in the low count-rate scans below 10 cps comparable to brain-tumour scanning with a body phantom background of 3 μc/l, it was shown in section 5 that for tumour detection over small areas of scan, 3 S.D. represent the limit of perceptible tumours. Figure 9 (a) shows that for this limit at 8-cm depth, a 3-cm-diam. cylinder should just be perceived at a concentration ratio 8:1, and at 4-cm depth a 2.8-cm-diam. cylinder can be perceived.

6.3. The size of tumours

The results of the measurements of C_{EDG}, the count-rate over the edge of the discs (see section 6.1) contain the information required to obtain the edge of tumours on the scan. We have not as yet been able to investigate this problem in detail but preliminary measurements [19] indicate that for cylindrical discs greater in diameter than the 50% resolution diameter of the collimator, the 'edge' can be taken as the isocount line half-way in count-rate between the peak count-rate and the body-background count-rate over the whole range of depth in phantom.

7. CONCLUSION

Colour display, which is a combined digital-analogue method [25] has been seen to be of value in both high and low count-rate scans; in both cases the statistical interpretation of colour patterns is possible. The quantitative information from region to region is immediately available in high count-rate scans and the colour contrast reduces the limit of tumour detection; although in low count-rate scans the quantitative information is not so

immediately obvious, the limits of tumour detection are still reduced. A simple phantom system has proved to be of great value in determining limits of tumour detection for a given collimator, counter and display system and may well have general value for intercomparison of scanning techniques.

The addition of colour printing to a scintiscan machine is not difficult and the cost is small. It can be argued that more sophisticated displays are more versatile but they are more costly. Now that two commercial versions of a colour scanner are available, this simple process will help the growth of a more quantitative and precise approach to clinical scanning.

ACKNOWLEDGEMENTS

We wish to thank the Medical Research Council who have granted equipment and financial support to J.R.M. and M.M. respectively. We are deeply indepted to the workshop and electronic staff for their skill in building the equipment and to the photographic and secretarial staff for their assistance.

REFERENCES

[1] ALLEN, H.C. and GOODWIN, W.E., Radiology 58 (1952) 68.
[2] MAYNEORD, W.V., Brit. J. radiol. Suppl. 2 (1950) 280.
[3] VEALL, N., Brit. J. Radiol. 21 (1950) 347.
[4] ALLEN, H.C. and RISSER, J.R., Nucleonics 13 (1955) 28.
[5] BROWNELL, G.L. and SWEET, W.H., Nucleonics 11 (1953) 40.
[6] CASSEN, B., CURTIS, L., READ, C. and LIBBY, R., Nucleonics 9 (1951) 46.
[7] BEATTIE, J.W. and BRADT, G., I.R.E. Transactions on Bio-Medical Electronics BME-8 (1961) 24.
[8] SIMPSON, D.C., (1963) Private Communication.
[9] MALLARD, J.R. and PEACHEY, C.J., Brit. J. Radiol. 32 (1959) 652.
[10] MALLARD, J.R. and PEACHEY, C.J., Proc. 3rd Int. Conf. Med. Elect. (1960) 511.
[11] MALLARD, J.R., FOWLER, J.F. and SUTTON, M., Brit. J. Radiol. 34 (1961) 562.
[12] MYERS, M.J., DUGGAN, M.H. and MALLARD, J.R., Proc. Rome Symp. on Scintigraphy (1963) In Press.
[13] ANGER, H.O., Amer. J. Roentgenol. 70 (1953) 605.
[14] BENDER, M.A. and BLAU, M., Medical Radioisotope Scanning, IAEA, Vienna (1959) 34.
[15] TUBIANA, M. and ALBEREDE, P., Ann. Radiol. 5 (1962) 173.
[16] ANSELL, B.M., CROOK, A., MALLARD, J.R. and BYWATERS, E.G.L., Ann. Rheumatic Diseases 21, 2 (1962) 218.
[17] BERNE, E. and JONSSON, U., Nucl. Med. 1 (1959) 80.
[17a] BASCHIERI, L. and D'APUZZO, B., Nucl. Med. 2 (1962) 290.
[18] DI CHIRO, G., Progress in Medical Radioisotope Scanning, Oak Ridge, USA (1962) 347.
[19] MYERS, M.J. and MALLARD, J.R., Int. J. appl. Rad. Isotopes (1964) In Press.
[20] CHRISTIE, J.H. and MACINTYRE, W.J., Progress in Medical Radioisotope Scanning, Oak Ridge, USA (1962) 405.
[21] MacINTYRE, W.J. and CHRISTIE, J.H., Proc. Amer. Ass. Phys. Med., Phys. Med. Biol. 9 (1964) 100.
[22] BENDER, M.A., Medical Radioisotope Scanning IAEA, Vienna (1959) 251.
[23] DEWEY, W.C., HEIDELBERG, J.G. and MOORE, E.B., J. nucl. Med. 3 (1962) 51.
[24] HERBERT, R., Brit. J. Radiol. 36 (1963) 770.

[25] HARRIS, C.C., BELL, P.R., FRANCIS, J.E., JORDAN, J.C. and SATTERFIELD, M.M., Progress in Medical Radioisotope Scanning, Oak Ridge, USA (1962) 66.
[26] ROSE, A., J. Optical Soc. Amer. (1948) 196.
[27] DUGGAN, M.H. Miss, et al., Scanning techniques for brain-tumour localization, these Proceedings.

A NEW METHOD FOR COLOUR SCANNING

H. KAKEHI, N. ARIMIZU AND G. UCHIYAMA
DEPARTMENT OF RADIOLOGY, CHIBA UNIVERSITY,
CHIBA, JAPAN

Abstract — Résumé — Аннотация — Resumen

A NEW METHOD FOR COLOUR SCANNING. In the original colour-scanning system reported by the authors, a ratemeter which had a seven-coloured fan-shaped filter on its pointer was inserted in a dark box between a 35-mm colour film and a lamp lit synchronously with the counting impulses. This system needed to be improved since a long scanning time was required to get a good colour scintigram, whilst the 35-mm colour film was too small for diagnostic purposes.

To improve these defects of the original method, a new colour-scanning method has been developed with the support of the Japanese Ministry of Education. This new method, referred to as the "fixed-time counter method", uses no ratemeter but an electronic gating circuit. Ten gates intercept the signals from the detector and at any one time only one of these is opened, depending on the number of counts recorded at a fixed time. Each gate actuates a chosen colour filter which filters the light from a xenon discharge tube. The filtered light is then used to form a photographic picture. Colour-printing papers are used instead of 35-mm colour films to get scintigrams of the natural size of organs and also to save the time needed for developing film.

Using this method, the one-way scanning that was adopted to get a good quality scan in original system type is no longer necessary, because the movement of the colour filter rapidly follows changes in the counting rate. Image distortion is thus avoided and scanning time is reduced.

Clinical results with the new system are presented.

UNE NOUVELLE MÉTHODE DE SCINTIGRAPHIE EN COULEURS. Dans le premier système de scintigraphie en couleurs mis au point par les auteurs, un débitmètre dont l'aiguille entraînait un filtre en éventail à sept couleurs était placé dans une chambre noire entre une pellicule en couleurs de 35 mm et une lampe qui s'allumait en synchronisation avec les impulsions du compteur. Ce système était loin d'être parfait: l'exploration devait durer assez longtemps si l'on voulait obtenir un bon scintigramme en couleurs; en outre, le format de 35 mm était trop réduit pour les besoins du diagnostic.

Pour remédier à ces inconvénients, les auteurs ont mis au point un nouveau procédé de scintigraphie en couleurs, leurs travaux recevant l'appui du Ministère de l'éducation. Dans le nouveau système, appelé «méthode du nombre de coups dans un temps donné», le débitmètre est remplacé par un circuit électronique à portes. Dix portes interceptent les signaux du détecteur, mais une seule peut s'ouvrir, selon le nombre de coups enregistrés dans un laps de temps donné. Chaque porte actionne un filtre d'une couleur déterminée, qui intercepte la lumière émise par un tube au xénon. La lumière ainsi colorée donne une image photographique. On utilise du papier sensible aux couleurs au lieu de la pellicule de 35 mm; cela permet d'obtenir un scintigramme grandeur nature et, en outre, de gagner le temps nécessaire au développement de la pellicule.

Avec le nouveau système, l'exploration en sens unique adoptée avec l'ancien système pour obtenir une image de bonne qualité n'est plus nécessaire, car le changement de filtre suit rapidement les fluctuations du comptage. On évite ainsi la distorsion de l'image et on diminue la durée de l'exploration.

Les auteurs présentent les résultats cliniques obtenus avec le nouveau système.

НОВЫЙ МЕТОД ЦВЕТНОГО СКЕННИРОВАНИЯ. В первоначальной системе для цветного скеннирования, о которой сообщали авторы, интенсиметр, имевший семицветный веерообразный фильтр, был установлен в темной коробке между 35-мм цветной пленкой и лампой, зажигающейся синхронно со счетными импульсами. Эта система требовала некоторого усовершенствования, так как для получения хорошей цветной сцинтиграммы требовалось длительное время скеннирования, и кроме того, 35-мм цветная пленка слишком мала для диагностических целей.

Для устранения этих недостатков первоначального метода при поддержке Министерства образования Японии был разработан новый метод цветного сканнирования—"метод счетчика *фиксированного времени*". Он основан на применении не интенсиметра, а электронной селекторной схемы. Десять селекторов прерывают сигналы от детектора, и в каждый данный момент открыт только один из них в зависимости от числа импульсов, зарегистрированных в фиксированное время. Каждый селектор возбуждает определенный цветной фильтр, который фильтрует свет от ксеноновой газоразрядной лампы. Прошедший через фильтр свет используется затем для получения фотографического изображения. Вместо 35-мм цветной пленки используется цветная фотобумага, что позволяет получать сцинтиграммы органов в натуральную величину и экономить время, необходимое для проявления пленки.

При этом методе уже не требуется одностороннее сканнирование, применявшееся для получения сканнограмм хорошего качества в первоначальной системе, так как движение цветного фильтра следует сразу же за изменениями скорости счета. Таким образом устраняется искажение изображения и сокращается время сканнирования.

Приводятся клинические результаты, полученные с помощью новой системы.

NUEVO MÉTODO DE CENTELLEOGRAFÍA POLICROMA. En el primer sistema de centelleografía policroma ideado por los autores, se insertó un integrador cuya aguja movía un filtro en abanico de siete colores, dentro de una cámara oscura, entre una película en colores de 35 mm y una lámpara que se encendía sincrónicamente con los impulsos. Este sistema distaba mucho de ser perfecto: para lograr un buen centelleograma policromo, la exploración debía durar mucho tiempo; además, el formato de 35 mm era demasiado reducido para las necesidades del diagnóstico.

A fin de subsanar estos inconvenientes, los autores han preparado un nuevo procedimiento de centelleografía policroma; sus trabajos han recibido el apoyo del Ministerio de Educación. En el nuevo sistema, denominado «método de recuento en un tiempo dado», no se utiliza un integrador sino un circuito electrónico de puertas. Las señales procedentes del detector son interceptadas por diez puertas, pero sólo puede abrirse una según el número de impulsos registrados en un tiempo dado. Cada puerta acciona un filtro de color determinado que filtra la luz emitida por un tubo de descarga de xenón. La luz filtrada da una imagen fotográfica. Se utiliza papel sensible a los colores, en lugar de la película de 35 mm; de esta manera se obtienen centelleogramas de tamaño natural y, además, se ahorra el tiempo necesario para revelar la película.

Con el nuevo sistema no se precisa la exploración unidireccional adoptada en el primero para obtener una imagen de buena calidad, ya que el cambio de filtro sigue rápidamente las variaciones del índice de recuento. De esa manera se evita la distorsión de la imagen y se reduce el tiempo de exploración.

Los autores presentan los resultados clínicos obtenidos con el nuevo sistema.

1. INTRODUCTION

Since 1961 the Radiological Department of Chiba University has been investigating a method of colour recording to improve visualization and contrast in radioisotope scanning.

In the former colour-recording system the ratemeter, which had a seven-coloured, fan-shaped filter on its pointer, was inserted between a 35-mm colour film and a xenon-discharge tube in the dark box of a conventional photoscanner. The ratemeter, together with the colour filter and light source, moved back and forth in the dark box, while the colour film was fixed at an appropriate, predetermined distance. The discharge of the xenon-discharge tube was triggered by the dotting impulse normally used to make a conventional black-and-white scintigram. Further details of the mechanical and electronic system were reported in 1962 to the Oak Ridge Symposium on Progress in Medical Radioisotope Scanning [1]. Using this system, tumours in the liver, brain or other organs could be detected more easily and distinctly than with the conventional black-and-white scanning [2-5].

2. DISADVANTAGES OF THE FORMER COLOUR-RECORDING SYSTEM

The former system, however, had several disadvantages.

(1) The delay of the ratemeter in recording changes in count rate necessitated one-way scanning to eliminate stagger effects in the recorded image. Even with one-way scanning there remained some distortion due to the time-lag of the ratemeter, especially in regions where the count rate was decreasing. Moreover, one-way scanning takes much time, during which the patient must remain motionless under the scanner.

(2) Since it takes a long time to have the 35-mm colour film developed (about one week), the colour-scintigram cannot be viewed immediately after scanning. Besides, the colour-scintigram is too small for clinical observation.

To obviate these disadvantages, it was suggested that the ratemeter should be eliminated and that colour-printing paper, which can be easily developed in the laboratory, might be used to obtain a full-size image of the colour recording [5].

3. THE PRINCIPLE OF THE NEW COLOUR-RECORDING METHOD

The new colour-recording method uses no ratemeter, but has a special counter including an electronic gating circuit (Fig. 1). Signals from the detector come to ten gates, only one of which can open at a time. This gate then causes a certain colour filter to move into position to filter the light that comes from the xenon-discharge tube. The choice of gate and colour filter depends on the count rate of the incoming signals and may be made by one of two methods, described as the 'fixed-time counter method' and 'fixed-count counter method' respectively. In the former, one of the ten gates controlling the filter is selected according to the number of counts recorded in a fixed time. In the latter, the gates are opened according to the time required for accumulation of a fixed number of counts.

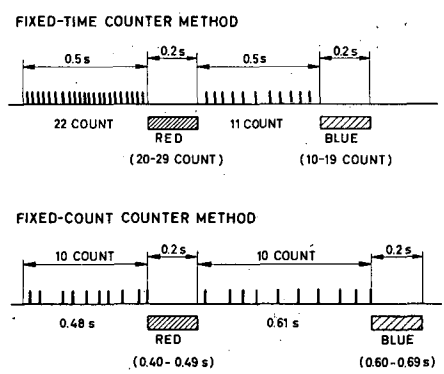

Fig. 1

Principles of choosing the colour filter by the fixed-time counter and the fixed-count counter

4. THE CONSTRUCTION OF THE APPARATUS AND ITS OPERATION

The construction of the apparatus is similar to the original system. However, neither ratemeter nor colour film are used, but instead a fixed-time counter, a fixed-count counter and colour-printing paper (Fig. 2). The apparatus is divided into two main parts:

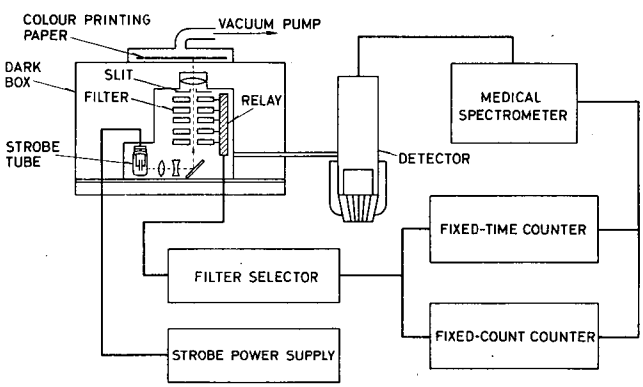

Fig. 2

Schematic diagram of the essential components of the new colour-recording system

(1) The dark box including a light source, its optical system and a group of electromagnetic relays (Fig. 3). The light source, the optical system and the relays are in one unit and move in the dark box synchronously with the detector of a conventional scinti-scanner.

A xenon-discharge tube or "strobo-tube" is used as light source. The light from this tube, which is triggered by the incoming signals, passes through one of the groups of ten gelatin colour filters which are connected mechanically with the relays. It then passes through the slit and lens and so reaches the colour-printing paper. Two kinds of slit, 1 mm × 4 mm or 0.5 mm × 3 mm are available according to the size of the scanning field.

The colour-printing paper has a specific spectral sensitivity and it was necessary to carry out preliminary experiments to show what kind of gelatin colour filters are suitable for obtaining the best colour arrangements. These experments were done at the Faculty of Photoengineering of the Department of Technology, Chiba University,

(2) The control circuit including the two kinds of counters, ignition power supply to the xenon-discharge tube and the high-voltage supply (Fig. 4).

The control panel provides three kinds of terminals: Ten of these correspond to the fixed-time counter, ten to the fixed-count counter, and ten to the colour filters. Each colour-filter terminal can be connected with any counter terminal. For example, in liver scanning using the fixed-time counter method, about 400 microcuries of Au^{198} are injected intravenously. Using a 2 in × 2 in crystal and honeycomb collimator with a focal distance of 10 cm, the maximum count rate comes to about 50 counts per second. Setting the fixed time to 0.5 s, a filter producing the colour of maximum intensity is connected to the 20-count terminal (which corresponds with 40

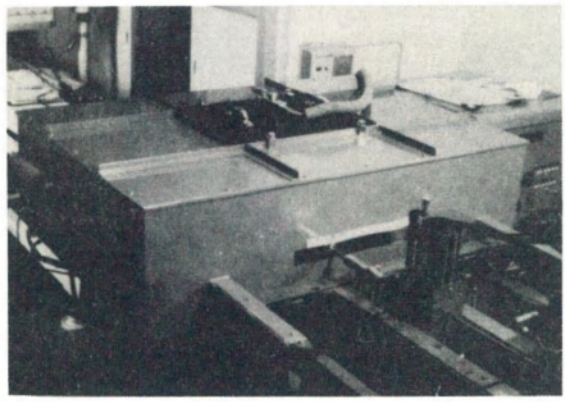

Fig. 3

Dark box and colour-paper holder
Light source with colour filters moving in the dark box back and forth
in synchronization with the detector.

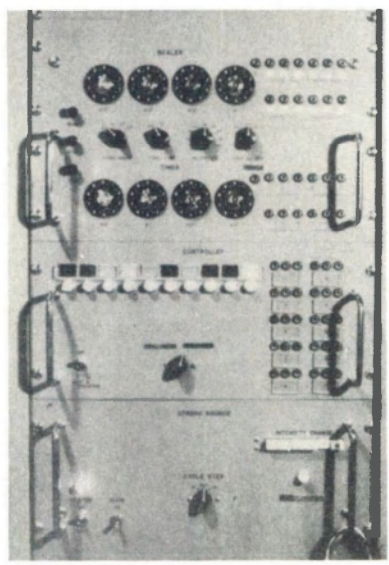

Fig. 4

Control panel
Fixed-time counter and fixed-count counter at the top,
colour filter terminals in the middle and ignition power supply at the bottom.

to 58 counts/s) and a filter producing the background colour is connected to the 1-count terminal. The background can be erased with a black filter. Intermediate filters are connected to intermediate fixed-time count terminals as required.

In the fixed-count counter method similar arrangements are made using the fixed-count time terminals.

5. RECORDING OF THE COLOUR SCINTIGRAM

The new colour-recording system has no time-lag in recording colour changes. Therefore, two-way scanning can be used without distortion. In other words, a high-fidelity colour scintigram can be obtained in half the time required by the original system.

Colour-printing paper is easily developed in the laboratory by a simplified method devised at the Faculty of Photoengineering of the Chiba University, and a scintigram can be obtained within 10 to 30 min after scanning.

It may be mentioned that the intervals between colour spots in the colour scintigram are variable in the fixed-count counter and constant in the fixed-time counter.

6. COLOUR SCINTIGRAMS OF LIVER AND THYROID PHANTOMS

A liver phantom, with a 1200-cm^3 capacity filled with I^{131} and containing seven defects corresponding to tumours 2 cm and 3 cm in diameter, was made for colour recording. This liver phantom was then buried in a rice body phantom. Figs.5 and 6 show scintigrams obtained with this phantom.

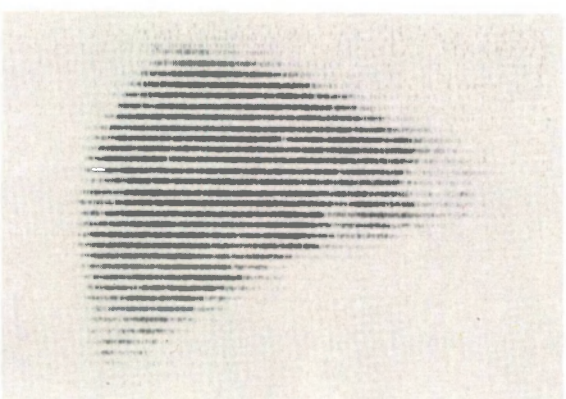

Fig. 5

Conventional scintigram of the liver phantom containing seven tumours

In the monochromatic scintigram, the respective tumour masses appear as lighter round areas against dark surroundings. In the colour scintigram they appear as areas whose colour represents a lower count rate, surrounded by regions whose colour represents a higher count rate. For example, a tumour in the upper part of right lobe is hardly visible in the monochromatic

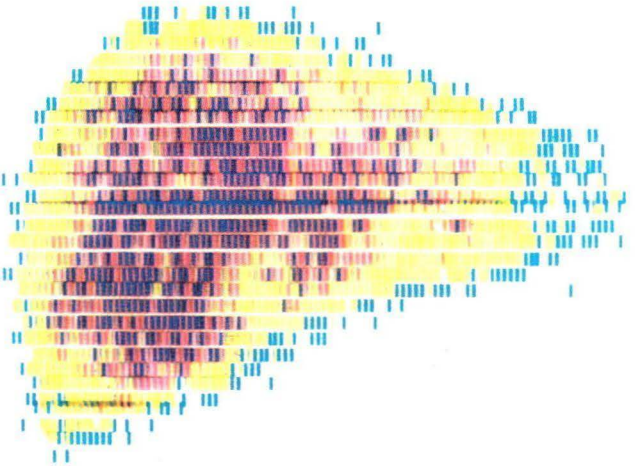

Fig. 6

Colour scintigram of the liver phantom
(Compare with Fig. 5)

scintigram, but in the colour scintigram it is clearly seen from the difference of colour. These scintigrams of the liver phantom were taken by the fixed-time counter method. It may be noted that the boundary lines between each colour are not distorted.

Figure 7 shows colour scintigrams of the thyroid phantom made in a similar way.

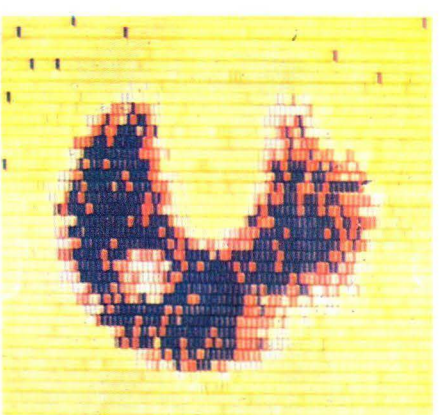

Fig. 7

Colour scintigram of thyroid phantom containing $\mu c\ I^{131}$

7. CLINICAL STUDIES

The colour scintigrams of all the cases below were made by the scanner with a 2-in crystal and 19-hole honeycomb collimator.

Fig. 8 shows a colour scintigram of normal liver; background is erased by the black filter;

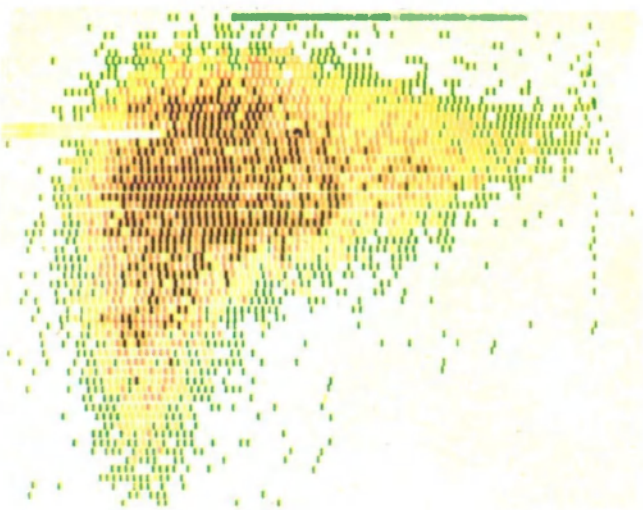

Fig. 8

Colour scintigram of normal liver

Fig. 9 shows a colour scintigram of thyroid; 50 μc I^{131} was administered and the uptake was 60% at 24 h;

Fig. 10 shows a colour scintigram of thyroid cancer;

Fig. 11 shows a colour scintigram of the pancreas with Se^{75}-selenomethionine; when scanning the pancreas contrast enhancement techniques must be used to delineate it clearly, because of the high background. The colour-recording technique is useful in such a case. Finally

Fig. 12 shows a colour scintigram of a normal kidney.

8. DISCUSSION

In our former colour-scanning system, a ratemeter was used for either dot- or colour-scans, whereas no ratemeter is used in our new system. Moreover, the result can be obtained immediately after scanning with the new system, since the colour-printing paper is developed in our own laboratory. The inclusion of two types of counters and ten colour filters permits various experimental arrangements with different advantages and disadvantages. The fixed-count counting method has the merit of rapidity in changing colours

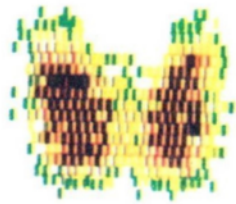

Fig. 9

Colour scintigram of thyroid: hyperthyroidism

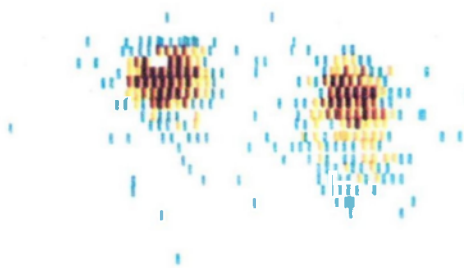

Fig. 10

Colour scintigram of thyroid: thyroid cancer
The lower part of the thyroid is affected.

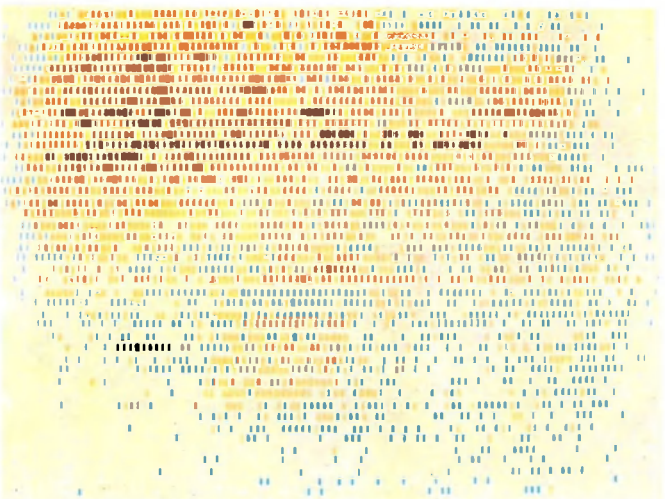

Fig. 11

Colour scintigram of pancreas made after administration of 400 μc Se^{75}-selenomethionine

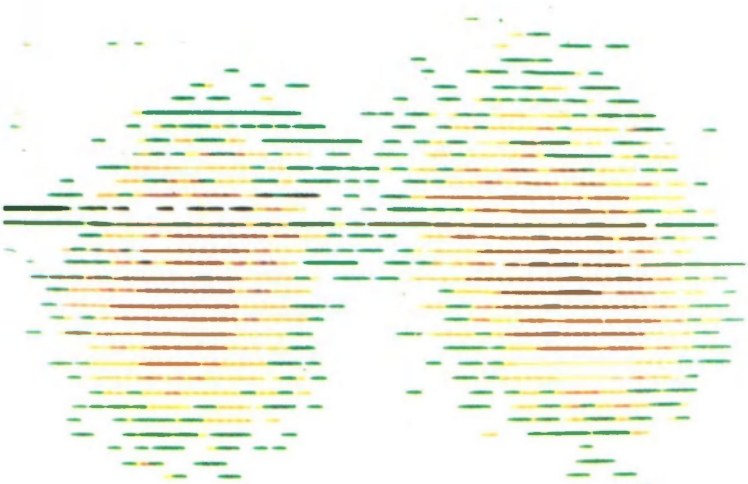

Fig. 12

Colour scintigram of a normal kidney
Slit size is reduced in length because of inadequate focussing distance.

and its density variation might be theoretically superior, but, in practice, the fixed-time counter method proves superior because the colour spots are more regularly spaced on the scintigram.

The isoresponse zones formed by spots of each colour can be more clearly recognized in the fixed-time counter method and the pattern is superior to that obtained by the fixed-count counter method because of the lack of interspaces between each colour spot.

The number of colour filters selected for a clinical application is determined by the doses of a radionuclide administered. When the activity in the organ to be examined is low, statistical fluctuations of counts are so much accentuated that the use of too many colours will distort the records. As a result, five or six kinds of colours will be sufficient. With high activities, a greater number of colours may be used.

The delay time in selecting the colour filter with the aid of electromagnetic relays in the present method is about 0.15 seconds. The shorter this delay, the better the scintigram. It is suggested that the delay may be shortened even further by using a system of several xenon-discharge tubes, each with a separate colour filter for a given count range.

The application of colour recording to rescanning method as a contrast enhancement technique is now being considered. A single colour rescanning might give the desired information and could avoid the repeated rescanning at various levels required in monochromatic rescanning.

The fixed-time counter has one strong advantage in that the count rate over a specified region is known accurately. Thus actual quantitative comparisons may be made between colour scintigrams or between parts of the same colour scintigram.

9. CONCLUSION

The original colour-scanning system has been improved by improving the quality and size of the picture and by shortening the time both for scanning and for developing the resulting scintigram.

ACKNOWLEDGEMENTS

The authors wish to thank Dr. C.C. Harris and Mrs. B. Anderson for their kind advice on translating into English.

REFERENCES

[1] KAKEHI, H., ARIMIZU, N. and UCHIYAMA, G., Scan recording in color, in Progress in Medical Radioisotope Scanning, (KNISELEY, R.M., ANDREWS, G.A. and HARRISON, C.C., Eds.) USAEC Rpt TID-7673 (1963) 111-31.

[2] KAKEHI, H., Acta radiol. Japonica 22 (1962) 415-47.

[3] UCHIYAMA, G., Acta radiol. Japonica 22 (1962) 929-32.

[4] UCHIYAMA, G., ARIMIZU, N. and KAKEHI, H., Proc. 1st Ann. Meeting Jap. Assoc. Nucl. Med., Jap. Radioisotope Assoc., Tokyo (1962) 18-19.
[5] KAKEHI, H., ARIMIZU, N. and UCHIYAMA, G., Genshiryoku Kogyo (Atomic Power Industry) 9 (1963) 26-31.

DISCUSSION

(On the two foregoing papers)

D. KUHL: Dr. Kakehi, what scan speed did you use for the colour scans of the liver?

H. KAKEHI: We used a commercially available machine for the colour scan; the scan speed was about 10 cm/min.

H. WAGNER: Both these papers make the point that colour scanning is superior to a dot system of data presentation, in which differences in counting rate are shown as differences in dot proximity. In view of the fact, however, that photo-recording has the advantage of permitting variation from white to black over the same region and is a system of proven superiority to dot-recording, would it not be more reasonable to compare colour-recording with photo-recording rather than with dot-recording.

J. MALLARD: I agree, but I think that colour-recording is still the best system since it provides quantitative information all over the picture. Even in regions where the photo-scan is completely white, as for example in the background region, it is possible to display information which is valuable in determining tumour-to-background ratio in identifying the margins of regions of high or low uptake, and so on.

E.E. POCHIN: I should like to take Dr. Wagner's point a little further. Why not compare this technique with more purely quantitative methods rather than with other semi-quantitative methods? What is the advantage of colour-recording compared with a numerical print-out? We may easily arrange a print-out device which moves with, or at half-scale to, the detector and which incorporates three discs with the digits 0 to 9 round their rims. While the detector remains stationary in each counting position, the discs rotate as counts, or groups of counts, occur and, at the end of 10 seconds the print-out stamps out through carbon paper the number of counts. The discs recycle to zero while the detector moves to the next counting position.

We normally count at 1-cm intervals in the belief that, if information is collected at intervals closer than the collimation justifies, the collimation is being studied rather than the patient.

J. MALLARD: I hope I have succeeded in showing that these colour patterns do make it possible to come very close indeed (within one standard deviation usually) to the correct counting rate in any particular region. The technique is possibly something more than semi-quantitative. Perhaps one could describe it as three-quarters or even seven-eighths quantitative.

L. Van STEKELENBURG: Dr. Mallard, is the colour ribbon moved continuously or stepwise in your system? If it is moved stepwise, then I suppose there must be delays in recording a change in counting rate apart from the delay of the ratemeter.

J. MALLARD: The colour ribbon is moved discontinuously and there is a delay, but in practice this is very small, particularly with commercial machines. Its only effect is to add very slightly to the stagger effect described for the ratemeter.

I. BASCHIERI: Your use of a linear scale for colour change seems to me to be open to criticism. Unless a logarithmic scale is used, is there not a danger of losing valuable information from those zones in the organ which, because of their thickness, have an activity lower than the maximum activity that can be detected?

J. MALLARD: In our opinion, the very best scale is one that is based on standard deviation, where a colour change is statistically significant at all points of the scale. As is shown in our paper, the linear scale is also capable of statistical interpretation in a way that is quite simple in practice and which, moreover, does not distort the visual effect. One cannot conveniently plot graphical contour maps on a non-linear scale because one needs a linear visual display in order to interpolate quickly.

R. KNISELEY: Do colour-blind persons have difficulty in reading these colour scans?

J. MALLARD: This is a snag, although many colour-blind people are able to distinguish differences between colours even if they do not actually see the same colours as ordinary individuals. An important requirement is that there should be sufficient contrast between adjacent colours. In any case, the interpretation of the colour scans is usually done by the scanning personnel and black-and-white copies duly marked with the abnormalities appearing on the colour scan are sent to the clinical department.

A. BAPTISTA: A colour system is, I think, useful in situations, such as occur in thyroid scanning, where there is a high target/non-target ratio. I should have thought, however, that a high-contrast system would be better where the differences in radioactivity to be detected are small, for instance, in liver scanning. I suppose that a combination of both methods is the answer.

CONTRAST ENHANCEMENT BY MULTICOLOUR PRINT-OUT OF THYROID, KIDNEY, LIVER AND BRAIN SCANS

G.J. HINE, D.H. PATTEN AND B.A. BURROWS
RADIOISOTOPE SERVICE, VETERANS ADMINISTRATION HOSPITAL
AND
BOSTON UNIVERSITY SCHOOL OF MEDICINE
BOSTON, MASS., UNITED STATES OF AMERICA

Abstract — Résumé — Аннотация — Resumen

CONTRAST ENHANCEMENT BY MULTICOLOUR PRINT-OUT OF THYROID, KIDNEY, LIVER AND BRAIN SCANS. Quantitative information can be obtained from a scan if the colour of the print-out changes with the count-rate. The printing pattern shows then the radioisotope distribution and the printing colour serves as a code for a digital evaluation of the scan. This can delineate areas with small differences in count-rate more clearly than other read-out methods.

A stylus hits one of several coloured typewriter ribbons mounted on a common carriage. Its movement is controlled by a count-rate meter with a time constant of 0.3 s. The first ribbon covering the lowest count-rate interval is uninked. This suppresses coloured prints at count-rates of less than 12.5% of the 100% maximum adjusted for each scan when eight coloured ribbons are used. However, all counts are preserved in black on carbon copies.

The clinical advantage of the colour scan is to recognize immediately differences in count-rate which outline areas of varying radioisotope concentration. The colour cut-off at low count-rates yields an improved visualization of areas such as brain lesions, which are difficult to localize due to high tissue background. The colour scan outlines the contours corresponding to the thickness of functioning liver tissue which are not easily seen otherwise. Compared with normal liver scans, areas of fibrosis and tumour infiltration are more readily recognized. The same is true for kidney scans where a change in colour may indicate ischemic, cystic or tumour areas. For thyroid scans, the colour print-out provides semi-quantitative comparison of radioiodine uptake in different areas.

ACCENTUATION DES CONTRASTES DANS LES SCINTIGRAMMES POLYCHROMES DU CERVEAU, DU FOIE, DU REIN ET DE LA THYROÏDE. Un scintigramme peut fournir des renseignements quantitatifs si la couleur de l'épreuve photographique varie suivant le taux de comptage. Le dessin de l'épreuve indique alors comment se répartit le radioisotope, et sa coloration est utilisée comme code pour l'évaluation numérique du scintigramme. Cette technique permet de déterminer, plus clairement que d'autres méthodes de lecture, le contour de zones où les différences de taux de comptage sont faibles.

Des rubans de machines à écrire de diverses couleurs sont montés sur un chariot unique; un stylet, dont le mouvement est commandé par un débitmètre, avec une constante de temps de 0,3 s, frappe l'un des rubans. Le premier ruban, qui correspond à la gamme des taux de comptage la plus basse, n'est pas encré; ainsi, il n'y a pas de marques colorées pour les taux de comptage inférieurs à 12,5% du maximum, qui est ajusté pour chaque scintigramme lorsque les huit rubans colorés sont utilisés en même temps. Toutefois, tous les coups sont enregistrés en noir sur des copies carbone.

Du point de vue clinique, le scintigramme polychrome a l'avantage de faire apparaître immédiatement les différences de taux de comptage qui délimitent des zones où la concentration du radioisotope n'est pas la même. La suppression de la couleur, pour les taux de comptage peu élevés, permet de mieux distinguer certaines zones difficiles à localiser par suite de l'intensité du bruit de fond dû aux tissus, par exemple les lésions cérébrales. Le scintigramme polychrome fait apparaître les contours correspondant à l'épaisseur du tissu hépatique qui participe aux fonctions du foie et qu'il est difficile de voir autrement. Il permet d'identifier plus aisément les zones de fibrose et d'infiltration néoplasique, en le comparant avec des scintigrammes de foies normaux. Il en est de même pour des scintigrammes de reins, où une modification de la couleur peut indiquer la présence de zones ischémiques, cystiques ou tumorales. Le scintigramme polychrome de la thyroïde

permet de procéder à des comparaisons semi-quantitatives de la fixation du radioiode entre les différentes zones.

КОНТРАСТНОЕ УСИЛЕНИЕ С ПОМОЩЬЮ МНОГОЦВЕТНОГО ОТПЕЧАТКА СКЕННОГРАММ ЩИТОВИДНОЙ ЖЕЛЕЗЫ, ПОЧЕК, ПЕЧЕНИ И ГОЛОВНОГО МОЗГА. С помощью сценнограммы можно получить количественную информацию, если цвет снимка изменяется вместе с интенсивностью счета. Образцы снимков показывают распределение радиоизотопов, а цветные отпечатки служат в качестве кода для цифровой оценки сценнограммы. Это дает возможность установить очертания участков с небольшими расхождениями в скорости счета гораздо лучше, чем при других методах снятия показаний.

Перо оставляет след на одной из нескольких цветных лент пишущей машинки, смонтированных на общей каретке. Его движения контролируются измерителями скорости счета с постоянной времени в 0,3 секунды. На первую ленту, соответствующую самой низкой скорости счета, чернила не наносятся. Это исключает цветной отпечаток при скорости счета меньшей 12,5% от максимума в 100% для каждой сценнограммы, соответствующего использованию 8 цветных лент. Однако, все вычисления сохраняются на копиях в черном цвете.

Клиническое преимущество цветной сценнограммы заключается в непосредственном определении различий в скорости счета, которые определяют районы различной концентрации радиоизотопов. Выпадение цвета при низкой скорости счета улучшает возможность наблюдения в таких районах, как участки пораженного головного мозга, которые трудно локализовать в результате высокого фона тканей. Цветная сценнограмма определяет контуры в соответствии с толщиной функционирующей ткани печени, которую иначе трудно увидеть. При сравнении нормальных сценнограмм печени участки фиброза опухолевой инфильтрации распознаются гораздо легче. Это справедливо и для сценнограмм почек, где изменения цвета могут указать на ишемические, кистозные или опухолевые участки. Что касается сценнограмм щитовидной железы, то цветные отпечатки дают возможность провести полуколичественное сравнение поглощения радиойода в различных участках.

AUMENTO DEL CONTRASTE EN LOS CENTELLEOGRAMAS POLICROMOS DE LA TIROIDES, EL RIÑÓN, EL HÍGADO Y EL CEREBRO. Un centelleograma puede proporcionar datos cuantitativos si el color de la impresión varía según el índice de recuento. La estructura de la impresión indica entonces la repartición de los radioisótopos; su color sirve de clave para la evaluación numérica del centelleograma. Esta técnica permite delimitar más claramente que otros métodos de lectura las zonas en que las diferencias del índice de recuento son muy reducidas.

En un mismo carro se montan cintas de máquina de escribir de diferentes colores; un punzón, cuyo movimiento está regido por un integrador, con una constante de tiempo de 0,3 s, golpea una de las cintas. La primera, que corresponde al intervalo más bajo del índice de recuento, no tiene tinta; así, no hay señales en color para los índices de recuento inferiores al 12,5 por ciento del valor máximo, que se ajusta para cada centelleograma cuando se utilizan las ocho cintas de color. Sin embargo, todos los impulsos quedan registrados en copias sacadas con papel carbón.

Desde el punto de vista clínico, el centelleograma policromo tiene la ventaja de que hace aparecer inmediatamente las variaciones del índice de recuento que delimitan zonas con concentraciones de radioisótopos distintas. La supresión del color para los índices de recuento poco elevados permite distinguir mejor ciertas zonas que son difíciles de visualizar a consecuencia de la intensidad de la actividad de fondo debida a los tejidos, por ejemplo, las correspondientes a lesiones cerebrales. Los centelleogramas policromos hacen aparecer los contornos correspondientes al espesor del tejido hepático que participa en las funciones del hígado y que difícilmente pueden observarse de otra manera. Permiten identificar mejor las zonas de fibrosis y de infiltración tumoral comparándolos con centelleogramas de tipo corriente. Lo mismo puede decirse de los centelleogramas del riñón en los que un cambio de color puede indicar la presencia de zonas isquémicas, císticas o tumorales. Los centelleogramas policromos de la tiroides permiten proceder a una comparación semicuantitativa de la concentración del yodo radiactivo en las diferentes zonas.

1. INTRODUCTION

The choice of a suitable display for scanning is as important as the development of an efficient γ-ray detector system. The same information

is contained by all recording systems, provided no data have been sacrificed by use of an erase method or by exposing photographic film to saturation density. For the interpretation of scans, however, different methods of data display show various virtues based on the information communicated by the scan. The eye does not judge spacing of dots as easily as relative blackness or variations in colour. The gray scale used for photoscanning can be evaluated only qualitatively.

The multicolour print-out system described here allows a semi-quantitative analysis of count-rate variations [1]. The results are immediately available in final form without further processing. The data display is full size, allowing easy judgement of anatomical abnormalities and comparisons with radiographic data. All these aspects are of importance for the operation of a scanner in clinical practice. More elaborate read-out systems may be useful for research applications.

2. PRINCIPLE OF COLOUR SCANNING

For colour printing eight parallel, coloured, typewriter ribbons are employed. The coloured ribbons are mounted on a carriage which moves them beneath the printing stylus (Fig. 1). The movement of the carriage is controlled by a count-rate meter with a time constant of 0.3 s. A single

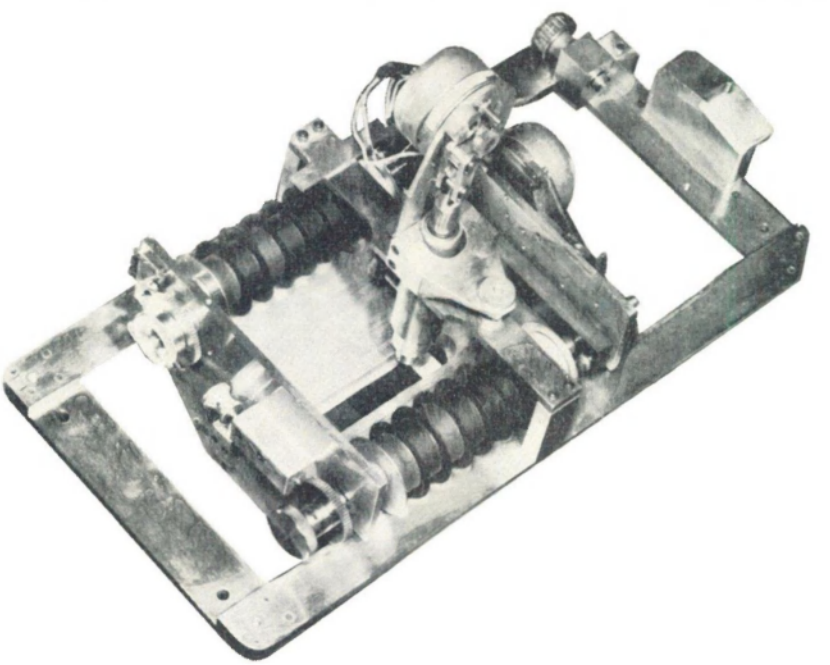

Fig. 1

Colour ribbon assembly.

Eight rolls of coloured typewriter ribbons are mounted on both sides of a carriage with a slit at the centre where the printing stylus hits the ribbons. The whole assembly follows the scanning motions.

5-cm wide ribbon containing eight colours has been developed for a commercial version of our colour read-out system*.

The area of greatest radioisotope concentration must be located to adjust the colour print-out. The output of the count-rate meter is varied so that a particular colour corresponds to that count rate. If the maximum count rate is low, ~1000 counts/min, as in most brain tumour scans, only the first few colours are employed. The large statistical variations would make any attempt at a more detailed count-rate analysis meaningless and would result in a confusing mixture of colours. At higher count rates, above 3000 counts/min, the statistical accuracy is sufficiently improved to warrant more gradations between background and maximum count rate. For thyroid, kidney and liver scanning, the area of maximum count rate is not difficult to locate before starting the scan, and full use of all eight colours can be made. However, dividing the count rate into more than eight intervals does not add more information.

The colours are arranged according to the rainbow spectrum with areas of high count rates printed red and those of low count rate printed purple. Actually, only seven colours are used, since the first ribbon, corresponding to the lowest count-rate interval, is colourless. This produces a low level count-rate cut-off on the colour print-out. However, in contrast to other systems employing a background cut-off, no information is lost, since all prints are shown on the carbon copies. A comparison of the colour print-out with the carbon copy is especially useful at low count rates with radioisotope concentrations close to tissue background (see Fig. 2).

The interpretation of the multicolour scans is not based on the colour distribution alone. The frequency of the prints varies with the count rate as in any symbol print-out. The colour serves as a code for a digital evaluation of the scan and also delineates areas of different count rates enhancing the contrast of count-rate variations.

3. CLINICAL RESULTS

Since March 1963 about 600 colour scans have been obtained with a scanner employing a scanning bed, a 4-in diam. sodium iodide crystal and several multi-hole collimators with a focal length of 3 in. For thyroid scans (130 patients) I^{131} is used as sodium iodide. Kidney (90 patients) and brain tumour scans (150 patients, one to three views each) are performed with Hg^{203}-chlormerodrin. For liver scans (70 patients) colloidal Au^{198} is used.

Thyroid scans are usually requested for patients who have nodules or when an abnormal distribution of radioiodine within one lobe or between the lobes is suspected. The colour print-out helps to accentuate any observed difference in function between the nodules and the rest of the gland or between different portions of the gland. Areas of relatively increased or decreased uptake are more easily seen and evaluated with a multicolour print than is possible with a black-and white scan. Another advantage is gained in the more accurate delineation of the actual size and shape of the gland by the removal of tissue background counts. The halo effect around the gland often seen on the carbon copy is absent on the colour scan.

* Picker Nuclear, White Plains, New York

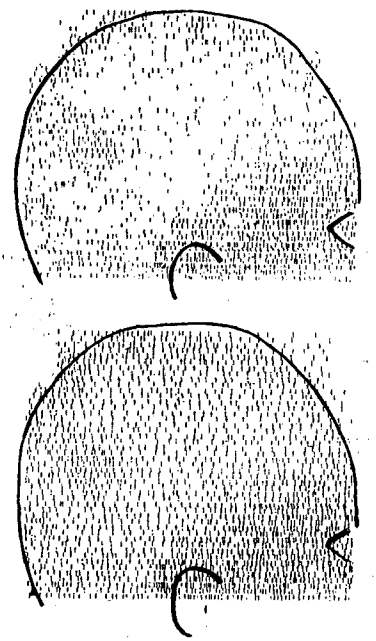

Fig. 2

Colour scan and carbon copy of a brain scan with 10 μc/kg of Hg^{203}-Neohydrin (scanning speed 25 cm/min, print factor of 8)
The presence of a lesion (metastasis from carcinoma of the lung) becomes apparent on the colour scan due to suppression of the low-level count rate. It would be difficult to detect it with certainty on the carbon copy due to large statistical variations.

Kidney scans become a more valuable clinical aid with the colour print-out. Slight variations in renal function can be noticed by comparing the predominant colours of each kidney. The information from the multicolour scan together with the results of the radio-Hippuran renal function test gives valuable aid in the diagnosis of renovascular disease. The elimination of the tissue background makes the kidney outline appear more distinct, revealing aberrations in contour. Localized areas of abnormal colour change could be related to old inflammatory disease, infarction, cyst or tumour. Such conditions sometimes cause only minor variations in count-rate which may be overlooked in a black-and-white read-out.

Liver scanning has been the subject of many recent publications. It has been pointed out that it is desirable to delineate areas of uniform count rates. In black and white this is only possible by displaying in parallel several scans employing different cut-off levels [2]. This requires an elaborate print-out system and the interpretation of the scans suffers from the need to compare many individual pictures instead of a single superimposition.

The contour effect, which is clearly visible only in a large organ such as the liver, is shown in Fig. 3. Normally the liver appears colour-contoured

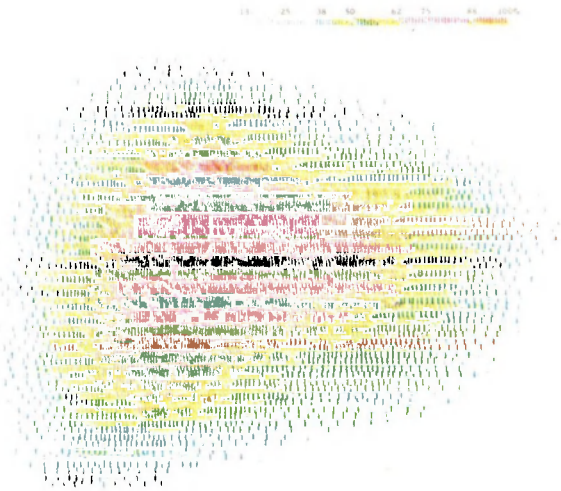

Fig. 3

Colour scan of a normal liver with 300 μc Au^{198}
(scanning speed 35 cm/min, print factor of 64)
The areas of uniform count rate are clearly separated by the various colours.

according to its thickness, but shows wide variation in actual shape. This normal contouring is lost or distorted in the abnormal scan. A mass may not change the general shape of the liver but will usually alter the colour distribution.

The limitations of 3-in focussing collimators have to be kept in mind when interpreting scans of either thick or deep-seated organs. The response to extended sources diminishes rapidly with increasing depth of the γ-ray emitting source. The count-rate along the central axis is shown in Fig. 4 for a 25-ml source in air and water. Though the data were obtained with I^{131}, the results with Au^{198} would be essentially identical. The focussing effect, which is well demonstrated with a point source in air, is completely lost with a volume source in water. Radiation emitted from the front of a thick source is detected with much greater efficiency than that emitted from within. Therefore, though colour changes of liver scans can be related to variations in thickness, the relationship is by no means a simple one. The use of 5-in focussing collimators would result in a significant improvement, since they show an increasing depth response up to 4 in (Fig. 4), which would allow a thick organ to be scanned with fairly uniform sensitivity.

Brain scans have improved in our hands considerably by using the multi-colour print-out. As mentioned above, the count rates are usually so low that a full colour display would only accentuate statistical variations. The low-level colour cut-off, however, provides improved visualization in areas where there is a low ratio of counts in the lesion to counts in the surrounding tissue. Sometimes an area on the black-and-white copy is equivocal but the colour scan brings out the presence of a lesion (Fig. 2). Some brain tumours

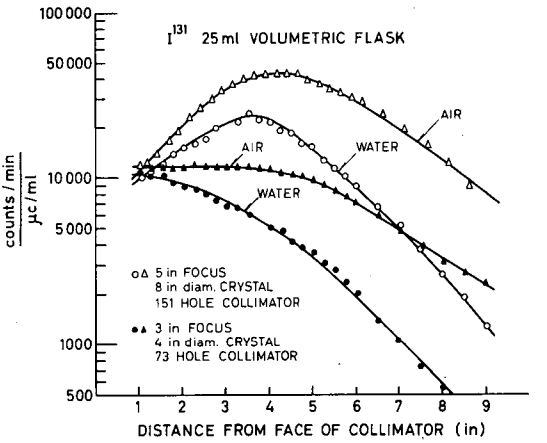

Fig. 4

Response of two focussing collimators to a 25-ml spherical source in air and water. As the source is positioned at increasing distances from the face of the collimator, the count rate decreases nearly exponentially for the source in water using a 3-in focal length. However, with a 5-in focus, the maximum sensitivity is reached at a depth of 4-in where it is twice that at the surface.

stand out sufficiently well so that subtler changes in count rate are not as important.

Besides the simplicity of producing the colour scan, it is important for clinical purposes that abnormalities in the scan can be easily recognized even by the inexperienced observer. This has stimulated the desire to extend scanning for routine diagnostic purposes.

REFERENCES

[1] HINE, G.J., Colour-coded digital print-out for radioisotope scanning, J.Nucl.Med. 4 (1963) 439.

[2] CHRISTIE, J.H., MacINTYRE, W.J., CRESPO, G.G. and KOCH-WESER, D., Radioisotope scanning in hepatic cirrhosis, Radiology 81 (1963) 455.

LE SCINTIGRAMME EN COULEURS DU FOIE

T. SPÂRCHEZ, B. GHEORGHESCU, A. STECLACI, E. MERCULIEV ET M. POPOVICI
CLINIQUE MÉDICALE, BUCAREST, ROUMANIE

Abstract — Résumé — Аннотация — Resumen

EXPERIENCE WITH A NEW COLOUR-SCINTILLOGRAPHIC METHOD FOR DIAGNOSING LIVER TUMOURS AND INFLAMMATORY LIVER DISORDERS. In order to obtain a better picture of the structural details of the diseased parenchyma of the liver, we have been using a device which has been adapted for use with the Scanner-Tracerlab and which produces liver scans made up of seven colours. The colours are chosen arbitrarily, each one corresponding to a given number of counts and representing zones of isoradioactivity, i.e. zones of liver tissue of relatively equivalent volume. The white in these colour scintigrams represents the radiation background and the black corresponds to the peak activity in the centre of the liver, where the parenchyma is thickest. The colours in between correspond to the different zones of isoradioactivity. This method has been used to examine 150 patients suffering from malignant (primary and secondary) and benign tumours, 80 patients suffering from chronic hepatitis and cirrhosis and 50 normal subjects. In most of the cases studied, intravenous injections of colloidal gold-198 (Amersham, UK) were used.

In numerous cases parallel studies were carried out with mechanical scans, black-and-white photoscintigrams and colour scintigrams. Diagnoses were checked by means of punctures, laparoscopy, laparophotography or cinematography, biopsic punctures, surgery and necropsy. Colour scintillography brings out more clearly the variations in the intensity of the radioactivity, i.e. the disorganization of the parenchyma of the liver or its substitution by tumoral processes.

EXPÉRIENCE D'UNE NOUVELLE MÉTHODE D'ENREGISTREMENT SCINTIGRAPHIQUE EN COULEURS, POUR LE DIAGNOSTIC DES TUMEURS HÉPATIQUES ET DES AFFECTIONS INFLAMMATOIRES DU FOIE. Pour obtenir des images qui reflètent mieux les détails de structure du parenchyme hépatique modifié par la maladie, les auteurs ont adapté au Scanner-Tracerlab un dispositif à l'aide duquel on obtient des cartes hépatiques en sept couleurs. Chaque couleur, choisie arbitrairement, correspond à un nombre d'impulsions et représente des zones d'isoradioactivité, c'est-à-dire de tissu hépatique de volume relativement égal. Dans le scintigramme en couleurs, le blanc représente la radioactivité de fond, tandis que le noir représente l'activité maximum, située au centre du foie où le parenchyme est plus épais. Les couleurs intermédiaires correspondent aux différentes zones d'isoradioactivité. Les auteurs ont étudié, à l'aide de cette méthode, 150 cas de tumeurs hépatiques malignes (primitives et secondaires) et de tumeurs bénignes, 80 cas d'hépatite chronique et de cirrhose et 50 cas normaux. Dans la majorité des cas, ils ont utilisé l'or-198 colloïdal (Amersham-Angleterre) injecté par voie intraveineuse.

Ils ont effectué parallèlement, dans un grand nombre de cas, des mécanogrammes, photoscintigrammes en blanc et noir et scintigrammes en couleurs. Le diagnostic a été vérifié par ponction, laparoscopie, laparophoto ou cinématographie, ponction biopsique, intervention chirurgicale ou nécropsie. La méthode scintigraphique en couleurs permet de mieux distinguer les variations d'intensité de la radioactivité, c'est-à-dire la désorganisation ou la substitution du parenchyme hépatique par processus tumoraux.

ОПЫТ ИСПОЛЬЗОВАНИЯ НОВОГО МЕТОДА ЦВЕТНОЙ СЦИНТИГРАФИИ ДЛЯ ДИАГНОСТИКИ ПЕЧЕНОЧНЫХ ОПУХОЛЕЙ И ВОСПАЛИТЕЛЬНЫХ ПРОЦЕССОВ ПЕЧЕНИ. Для получения изображений, лучше отражающих подробности структуры пораженной печеночной паренхимы, к лабораторному аппарату для сканнирования с самописцем было приспособлено особое устройство, позволяющее получать сканнограммы печени в семи цветах. Каждый произвольно выбранный цвет соответствует определенному числу импульсов и отграничивает зоны с одинаковой радиоактивностью, т.е. приблизительно равные по объему зоны печеночной ткани. На такой цветной сцинтиграмме белый цвет отражает фоновую радиоактивность, тогда как черный соответствует максимальной радиоактивности в центре печени, т.е. в месте наибольшей толщины паренхимы. Промежуточные цвета соответствуют различным зонам с одинаковой радиоактивностью.

С помощью этого метода изучено 150 случаев как злокачественных (первичных и вторичных), так и незлокачественных опухолей печени, 80 случаев хронического гепатита и цирроза и проведено 50 исследований печени у здоровых людей.

В большинстве случаев для внутривенных инъекций использовалось коллоидальное золото-198 (фирмы Амершем, Англия).

Во многих случаях одновременно были получены механограммы, черно-белые фотосцинтиграммы, а также цветные сцинтиграммы. Диагноз подтвердился с помощью пункции лапароскопии, фотографической и кинематографической съемок брюшной полости, пункций со взятием биопсии, хирургических операций или вскрытия.

Метод цветной сцинтиграфии дает возможность лучшего распознавания вариаций интенсивности радиоактивности, т.е. степени поражения или замещения печеночной паренхимы опухолевыми процессами.

ENSAYO DE UN NUEVO MÉTODO DE REGISTRO CENTELLEOGRÁFICO POLICROMO, PARA EL DIAGNÓSTICO DE TUMORES HEPÁTICOS Y DE INFLAMACIONES DEL HÍGADO. Para obtener imágenes que reflejasen mejor los detalles de la estructura del parénquima hepático modificado por la enfermedad, los autores adaptaron al aparato Scanner-Tracerlab un dispositivo gracias al cual se pueden obtener diagramas hepáticos en siete colores. Cada color, elegido arbitrariamente, corresponde a un número dado de impulsos y representa zonas de isorradiactividad, es decir, de tejido hepático de volumen relativamente igual. En el centelleograma policromo, el blanco representa la radiactividad de fondo, mientras que el negro representa la actividad máxima, situada en el centro del hígado, donde el parénquima es más espeso. Los colores intermedios corresponden a las diferentes zonas de isorradiactividad. Recurriendo a este método, los autores estudiaron 150 casos de tumores hepáticos malignos (primitivos y secundarios) y de tumores benignos, 80 casos de hepatitis crónica y de cirrosis, y 50 casos normales. En la mayoría de los casos utilizaron el oro-198 coloidal (Amersham -Reino Unido) inyectado por vía endovenosa.

En un gran número de casos, efectuaron paralelamente mecanogramas, fotocentelleogramas en blanco y negro y centelleogramas policromos. Verificaron el diagnóstico mediante punción, laparoscopia, laparofotografía o cinematografía, punción biópsica, intervención quirúrgica o necropsia. El método centelleográfico policromo permite distinguir mejor las variaciones de intensidad de la radiactividad, es decir, da una idea más cabal de la desorganización o sustitución del parénquima hepático provocadas por los procesos tumorales.

I. INTRODUCTION

Actuellement, le scintigramme est une méthode courante pour le diagnostic des maladies hépatiques. De nombreux auteurs [1, 2, 3, 4, 5, 6, 7, 8, 9, 10, 11] ont contribué à l'amélioration des enregistrements scanographiques et photoscintigraphiques. Chaque méthode est un progrès dans le domaine de la détection des lésions diffuses ou localisées du foie.

A notre connaissance, les premières communications concernant le scintigramme en couleurs, ont été faites par MALLARD [12, 14] et BASCHIERI [13]. Personnellement, nous avons tenté de réaliser une carte physique du foie dans laquelle les courbes de niveau isoradioactives sont représentées par des couleurs différentes [6]. Nos premiers résultats de scintigramme en couleurs ont été communiqués en 1963 [15].

II. MATÉRIEL ET MÉTHODE

Nous avons modifié l'appareil Scanner Tracerlab et le spectrophotomètre à mécanisme d'inscription sur papier en y ajoutant un dispositif pour l'obtention des images en couleurs. Nous avons présenté cette technique

au Congrès de Gastro-entérologie de Bruxelles en 1964. Cette technique nous permet d'éliminer le fond (en filtrant le signal spécifique de l'isotope utilisé), d'amplifier le signal et l'inscription des variations de la radioactivité à l'aide de l'instrument de mesure.

Nous avons injecté par voie intra-veineuse 4 μc de ^{198}Au/kg (Amersham, Angleterre) et nous avons effectué simultanément le scanogramme, le photoscintigramme en blanc-noir et le photoscintigramme en couleurs au cours des premières 24 h suivant l'injection.

Le scintigramme en couleur ainsi obtenu a un fond blanc et l'intensité maximum de radioactivité (noire) est située au centre du foie; les couleurs intermédiaires, jaune, bleu clair, bleu foncé, marron, rouge et rose, correspondent aux différents niveaux d'isoradioactivité, respectivement aux zones de tissu hépatique, d'épaisseur approximativement égale.

Cette méthode nous a permis d'examiner 333 patients dont 179 présentaient des affections inflammatoires diffuses, (115 hépatites chroniques, 64 cirrhoses) et 154 des tumeurs hépatiques, (118 tumeurs malignes dont 68 primitives, 50 secondaires et 36 bénignes dont 6 hémangiomes et 30 kystes hydatiques). Le diagnostic a été confirmé cliniquement par explorations fonctionnelles (électrophorèse, BSP, enzymes sériques), laparoscopie, biopsies hépatiques (tableau I).

III. RÉSULTATS

Sur le scintigramme en couleurs on distingue nettement le contour et les dimensions du foie normal, et sa surface composée de zones colorées différemment, concentriques, régulières (fig. 1).

A. Affections inflammatoires diffuses, hépatites chroniques (115 cas)

Le diagnostic a été confirmé chez 23 patients par laparoscopie, chez 41 patients par ponction biopsique, chez 5 par intervention, chez 3 patients par nécropsie. Ce groupe a donné 9,5% des scintigrammes faussement positifs indiquant des hépatites infirmés par l'évolution ultérieure, et biopsie hépatique.

Des scintigrammes (3,4%) sont faussement négatifs: ils présentent un aspect normal tandis que l'examen microscopique démontre la présence d'un processus inflammatoire. Il est probable que le pourcentage de résultats faussement positifs et faussement négatifs soit en réalité un peu plus élevé, car tous les cas étudiés n'ont pas été vérifiés à l'aide de méthodes strictement objectives. Pourtant, jusqu'à présent, l'évolution clinique confirme le diagnostic établi.

Le scintigramme a corrigé le diagnostic clinique faussement positif dans 6% des cas et faussement négatif dans 3,4% des cas.

Dans les hépatites chroniques, le scintigramme en couleur fait voir les dimensions normales ou plus grandes du foie. Le contour est généralement régulier. Dans les formes légères de la maladie, l'architecture normale du parenchyme - visible par la disposition concentrique relativement régulière des zones d'isoradioactivité - est conservée. Dans les formes plus sévères, on constate une extension des couleurs périphérique (bleu)

TABLEAU I

CONFIRMATION DES DIAGNOSTICS

	Diagnostic	Nombre de cas confirmés par laparoscopie	Nombre de cas confirmés par biopsie	Nombre de cas confirmés par intervention chirurgicale	Nombre de cas confirmés par nécropsie	Nombre de cas de diagnostics cliniques		Scintigrammes	
						a) faussement positifs	b) faussement négatifs	a) faussement positifs	b) faussement négatifs
I. Affections inflammatoires	Hépatite chronique 115	23	41	5	3	7	4	11	4
	Cirrhose 64	15	21	7	5	3	2	5	2
II. Tumeurs malignes	Malignes primitives 68	25	8	13	7	2	10	2	6
	Malignes secondaires 50	12	3	10	3	3	3	1	3
Tumeurs bénignes	Hémangiomes 6	6	-	5	-	-	1	-	2
	Kystes hydatiques 30	10	8*	29	1	1	10	-	2
Total	333	91	81	69	19	16	30	19	19
Pourcentage		27,3%	24,3%	20,7%	5,7%	4,8%	9,45%	5,7%	5,7%

* Biopsie hépatique intra-opératoire; hépatite d'association: 8 cas.

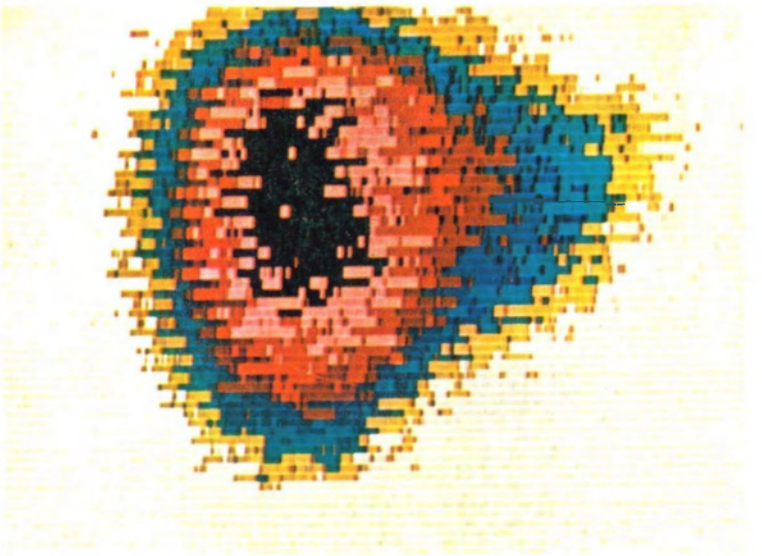

Figure 1

Scintigramme normal en couleurs:
succession concentrique régulière des couleurs.

correspondant à une réduction du tissu hépatique. Dans le centre on remarque la diminution accentuée des zones de radioactivité maximum (noir, rose), ce qui indique une absorption diffuse réduite du radioisotope par le parenchyme altéré par inflammation.

Les figures 2 et 3 montrent la gradation de ces modifications allant de l'aspect presque normal (fig. 2) jusqu'à l'aspect quelque peu désordonné (fig. 3), où le foie présente un contour irrégulier ainsi qu'une absorption médiocre d'isotope dans la partie centrale.

B. Cirrhoses hépatiques (64 cas)

Vingt et un cas sont confirmés par biopsie, 15 par laparoscopie, 7 par intervention chirurgicale et 5 par nécropsie. Dans ce groupe nous avons obtenu 5 scintigrammes faussement positifs et 2 faussement négatifs (tableau I).

L'aspect du scintigramme en couleur varie en fonction des modifications structurelles du parenchyme et de l'intensité des processus de régénération et de cicatrisation.

On remarque une interférence des zones d'isoradioactivité sur la surface du foie; généralement, les couleurs représentant un nombre réduit ou moyen d'impulsions s'étendant vers le centre, ne conservant plus leur emplacement normal et leur disposition concentrique. La portion centrale, normalement plus épaisse (noir) est plus réduite: seules les zones irrégulières de parenchyme à radioactivité élevée sont conservées. Les irrégularités de distribution de la radioactivité reflètent la désorganisation du parenchyme, déterminée par des processus de régénération (nodules) et de cicatrisation (fig. 4 et 5).

Figure 2

Extension des zones périphérique.
Diminution de l'absorption dans le centre (absence de noir).

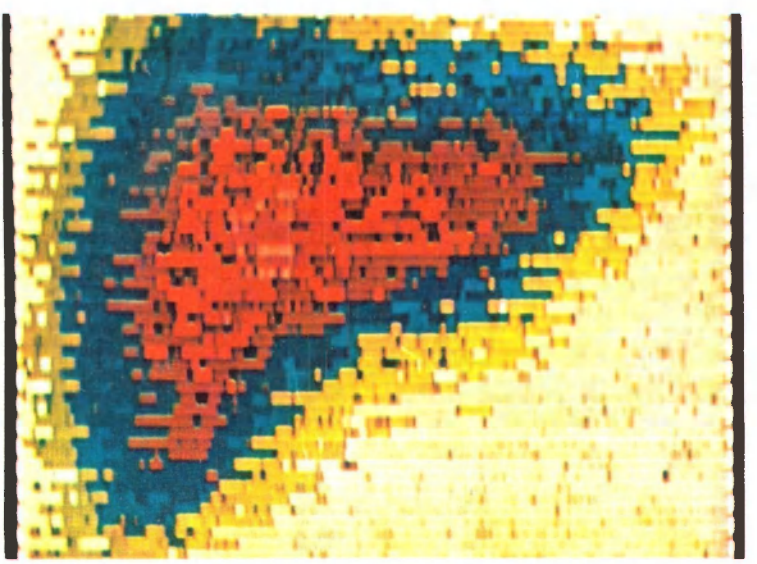

Figure 3

Aspect plus accentué;
les couleurs indiquant la radioactivité maximum normale (noir-rose) sont absentes,
étant substituées par la couleur marron.
Hépatite chronique sévère confirmée par biopsie et laparoscopie.

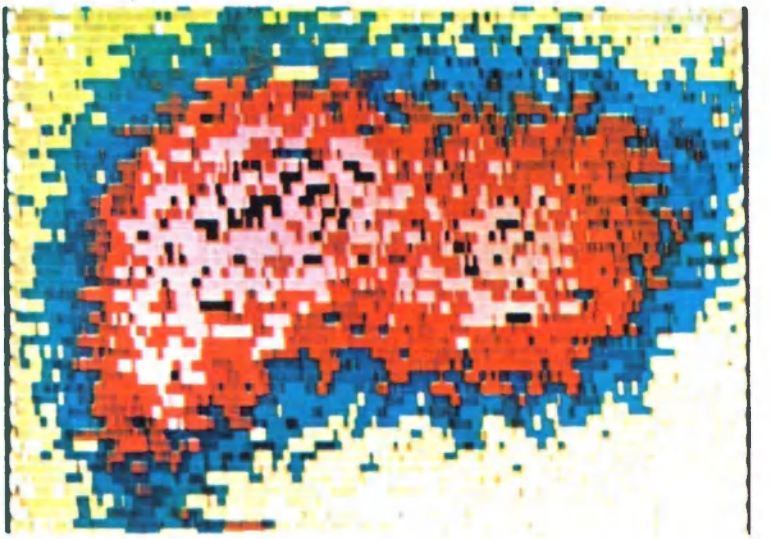

Figure 4

Foie aux marges irrégulières, zone périphérique (bleu clair) plus étendue.
L'interférence des zones colorées et de taches disséminées
irrégulièrement reflètent l'intensité variée de la radioactivité jusqu'aux bords.
Cirrhose confirmée par laparoscopie et biopsie.

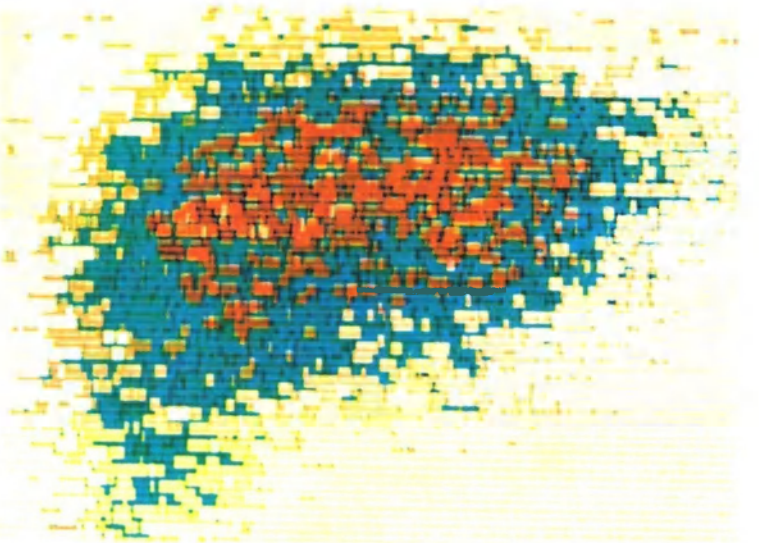

Figure 5

Foie réduit, contour irrégulier des zones complètement privées de radioactivité (blanc).
Aspect de mosaïque d'ensemble.
Le bleu clair (représentant des impulsions réduites) arrive jusqu'au centre;
le noir et le rose sont complètement absents.
Ce qui est frappant dans ce cas, c'est la désorganisation totale de l'architecture du foie.

Dans 50 cas, la fixation de l'or colloïdal sur la rate suggère une augmentation de circulation sanguine splénique ou d'hyperplasie réticulo-endothéliale [16].

C. Tumeurs hépatiques malignes primitives

Sur le scintigramme en couleurs les tumeurs apparaissent comme des lacunes irrégulières, où la radioactivité dans la zone marginale ou vers le centre du parenchyme est absente ou fort réduite.

La désorganisation architectonique du tissu hépatique autour de la tumeur se manifeste par l'interférence des couleurs, le déplacement des zones périphériques vers le centre et l'absence de zones à radioactivité élevée (fig. 6 et 7).

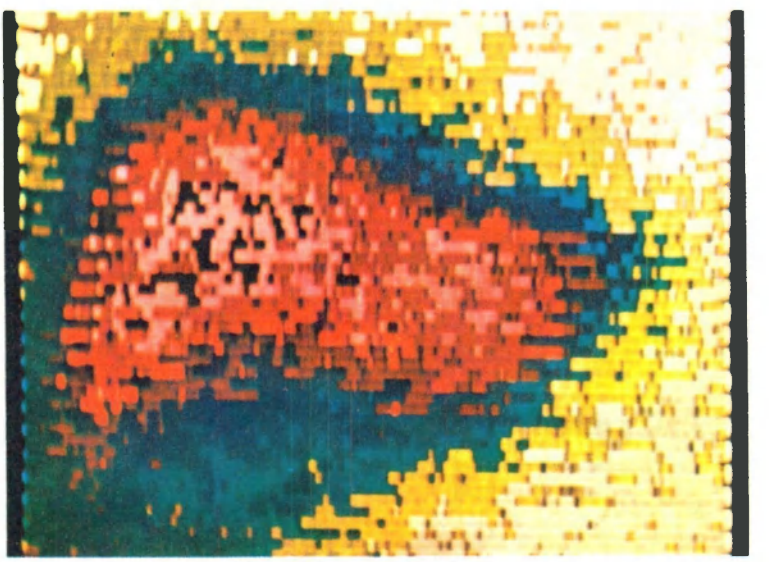

Figure 6

Sur la marge inférieure du foie se dessine un déplacement de zones périphériques vers le centre, sur une surface relativement étendue correspondant à la diminution du tissu fonctionnel. Le diagnostic de tumeur a été vérifié par laparoscopie et par examen anatomo-pathologique

Dans les cas de cancers métastatiques, le scintigramme montre, dans le foie, des lacunes irrégulières de dimensions variées correspondant aux nodules tumoraux froids. Les lacunes marginales sont complètement dépourvues de radioactivité tandis que celles du centre sont revêtues d'un parenchyme fonctionnel réduit, captant une petite quantité d'isotopes (couleurs périphériques), (fig. 8).

D. Tumeurs bénignes

Les hémangiomes donnent des images lacunaires. La nature bénigne de ces tumeurs a été établie seulement par laparoscopie et par intervention chirurgicale (fig. 9).

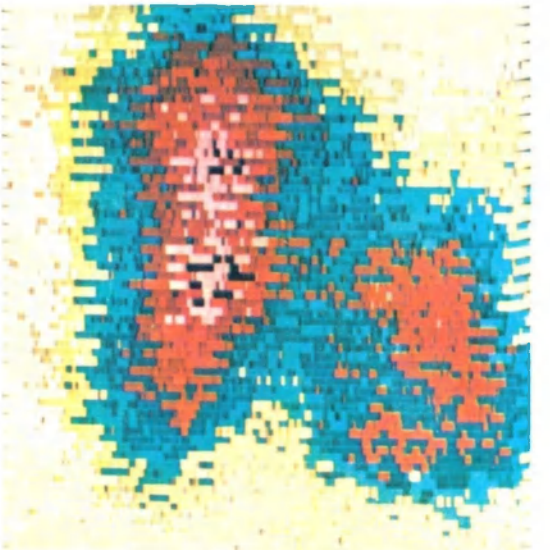

Figure 7

On observe le foie paraissant divisé en deux segments par des lacunes.
Au niveau de la tumeur, le parenchyme hépatique est fin,
l'épaisseur correspondant à l'épaisseur périphérique.

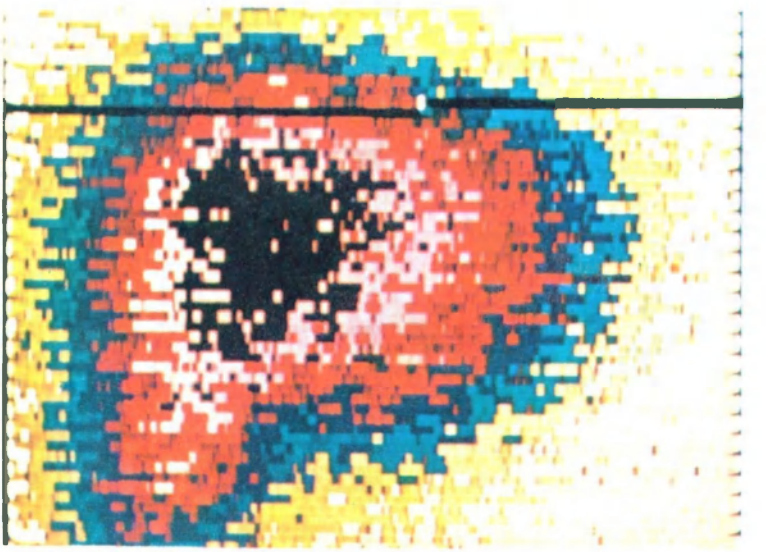

Figure 8

Sur la marge inférieure du foie on observe une petite lacune au contour irrégulier.
Diagnostic vérifié par laparoscopie puis par intervention chirurgicale:
néoplasme des voies biliaires avec métastases hépatiques.

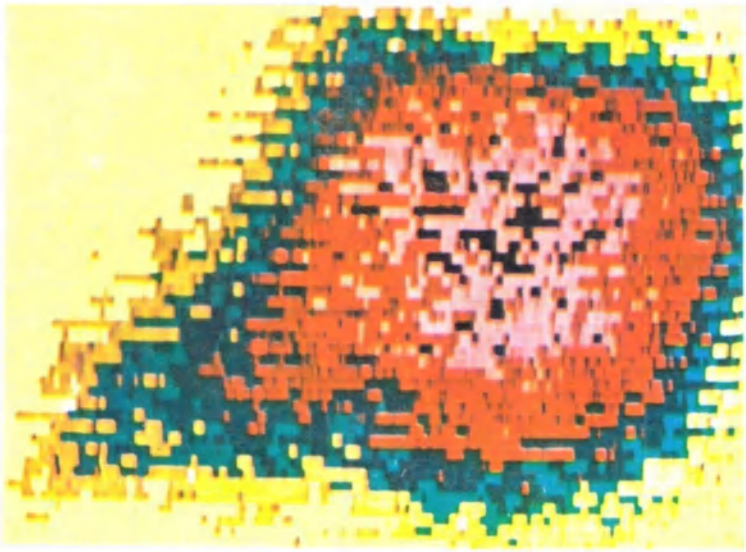

Figure 9

On observe une grande lacune dans la fixation de l'isotope sur la marge latérale droite du foie.
Dans le centre, la structure du parenchyme est désorganisée (noir réduit) avec aspect de cirrhose.
Diagnostic par laparoscopie: hémangiome du lobe droit.

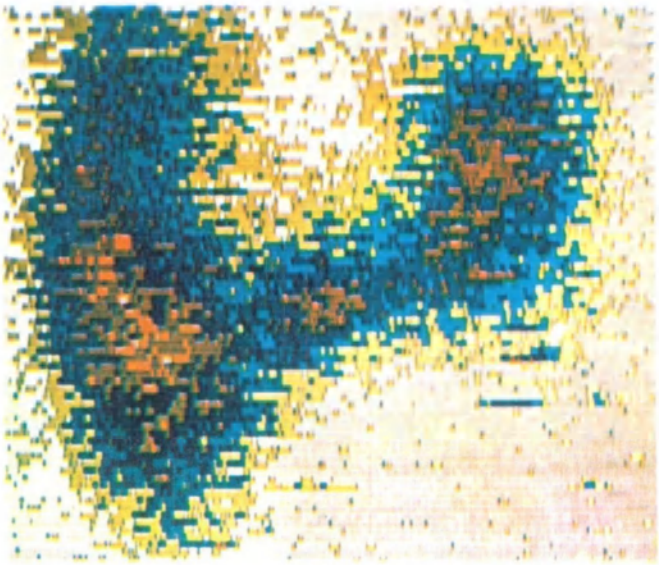

Figure 10

Kyste hydatique de grandes dimensions englobant la partie supérieure du foie.
La lacune, à marge régulière arrive à la partie inférieure du foie.
Le reste du parenchyme paraît désorganisé
vu les compressions et les altérations cirrhogènes provoquées par le kyste.
Le diagnostic a été vérifié par laparoscopie et intervention chirurgicale et par biopsie préopératoire.

E. Kystes hydatiques

L'image scintigraphique est caractérisée par la présence d'une lacune régulière (fig. 10).

IV. DISCUSSION

L'analyse des données montre que le scintigramme en couleurs est une méthode utile pour le diagnostic des maladies hépatiques. Notre expérience nous permet de constater l'efficacité de la méthode par le nombre de cas diagnostiqués correctement (89,6%). Les erreurs de diagnostic sont plus fréquentes dans les cas d'hépatites et de tumeurs de petites dimensions.

Le scintigramme n'est donc pas une méthode souveraine pour le diagnostic des maladies hépatiques vu qu'il existe des possibilités d'erreurs. Toutefois, la méthode donne un taux élevé de résultats corrects, les meilleurs étant obtenus les cas de kystes hydatiques. L'efficacité de la méthode augmente si les données cliniques biologiques et les données de laboratoire sont coordonnées.

La valeur du scintigramme est spécialement limitée dans les lésions tumorales au-dessous de 2 cm de diamètre et dans celles situées en profondeur du parenchyme.

Nous avons effectué parallèlement, dans tous les cas que nous avons étudiés, le scanogramme et le photoscintigramme en blanc-noir, les variantes donnant presque toutes généralement de bons résultats. Nous avons l'impression que le scintigramme en couleurs délimite mieux le contour des lésions et qu'il peut faire apparaître surtout les altérations discrètes de la structure du parenchyme qui se manifestent par l'interférence des couleurs.

L'altération de la séquence régulière et concentrique des zones d'isoradioactivité fait apparaître la diminution de l'absorption d'isotopes, soit par inflammation diffuse (hépatite), soit par un excès de tissur conjonctif (cirrhose), soit par la substitution partielle du parenchyme par un tissu tumoral bénin ou malin.

Comme toute méthode de diagnostic, le scintigramme en couleurs est de valeur limitée, mais les possibilités d'amélioration sont loin d'être épuisées.

V. CONCLUSIONS

Nous avons examiné 333 cas d'affections hépatiques inflammatoires et d'affections tumorales malignes et bénignes par scintigrammes en couleurs, parallèlement au scanogramme et au photoscintigramme en blanc et noir.

Nous avons obtenu des résultats corrects dans 89,6% des cas, faussement positifs dans 5,7% des cas et faussement négatifs dans 5,7% des cas.

Le photoscintigramme en couleurs dessine une carte physique du foie avec des «courbes de niveau» de 7 couleurs différentes, chaque couleur représentant une zone d'isoradioactivité équivalant à une zone de parenchyme d'épaisseur approximativement égale.

Dans les processus inflammatoires diffus et scléreux (hépatites chroniques, cirrhoses) l'image scintigraphique en couleurs fait apparaître une altération de la structure du parenchyme avec diminution de la quantité de tissu fonctionnel et désorganisation de l'architectonique normale.

Dans les tumeurs, on observe des images lacunaires reflétant la substitution partielle ou totale de la masse de tissu fonctionnel à ce niveau, par un nombre réduit d'impulsions radioactives se traduisant par des couleurs qui sont situées normalement à la périphérie de l'organe.

Dans les tumeurs malignes primitives ou secondaires les lacunes paraissent généralement irrégulières, tandis que dans les tumeurs bénignes elles sont nettement délimitées, le parenchyme restant étant relativement intègre.

RÉFÉRENCES

[1] KUHL, D. E., Rotational scanning of the liver, Radiol. 71 (1958) 875.

[2] BENDER, M. A. and BLAU, M., A versatile high contrast photoscanner for the localization of human tumors with radioisotopes, Int. J. Appl. Radioisotopes, 4 (1959) 154.

[3] McINTYRE, J. A., A method for the visualization of the configuration and structure of the liver, Amer. J. Roentgenol., 77 (1957) 455.

[4] BONTE, J. F., KROHMER, J. S., ELMENSDORF, E., PRESLEY, N. L. and ANDREWS, G. J., Scintillation scanning of the liver, Amer. J. Roentgenol., 88 (1962) 275.

[5] FAUVERT, R. et LOVERDO, A., Scintillographie hépatique par la technique de l'or colloïdal radioactif, Rev. intern. d'hépatol. 10 (1960) 1143.

[6] STECLACI, A., Le photoscintigramme en couleurs. Rev. méd. int. de photo, cinéma et télévision, 112 (1963) 43.

[7] CAROLI, J., Valeur diagnostique de la scintillographie hépatique, Arch. de mal. de l'app. dig. 51 (1962) 55.

[8] SCHUMACHER, W., Die Diagnostik von Leber- und Gallenwegerkrankungen einschliesslich der Tumoren mit Hilfe radioaktiv markierter Verbindungen, Dtsch. med. Wschr. 87 (1962) 347.

[9] SPÂRCHEZ, T., GHEORGHESCU, B., MERCULIEV, E., VASILESCU, V. V., KINSKY, S. et STECLACI, A., Le diagnostic des tumeurs hépatiques à l'aide des photoscintigrammes, Rev. intern. d'hépatol., 13 (1963) 67.

[10] NAGLER, W., BENDER, M. A. and BLAU, M., Radioisotope photoscanning of the liver, Gastroenterol. 44 (1963) 36.

[11] WAGNER, H. N., McATEE, J. and MOSLEY, J., Diagnosis of liver diseases by radioisotopes scanning, Arch. int. méd. 107 (1961) 324.

[12] MALLARD, J. R. and PEACHEY, C. J., A quantitative automatic body scanner for the localization of radioisotopes in vivo. Brit. Radiol. 32 (1959) 652.

[13] BASCHIERI, L. et D'APUZZO, B., Possibilités et limites de la scintigraphie. Nucl. Med. 2 (1962) 290.

[14] MALLARD, J. R., Registratione - Colori, Min. Nucl. 7 (1963) 161.

[15] SPÂRCHEZ, T., GHEORGHESCU, B., STECLACI, A. et MERCULIEV, E., Scintigrama hepatica in culori, Soc. de Gastroentérol. 17. V. 1963.

[16] BARBIERI, L. L., MANARESI, A., VANCINI, B. et PUDDU, P., Visualizzazione della milza nell' epato-scintigrama, Min. Nucl. 7 (1963) 149.

DISCUSSION

(On the two foregoing papers)

C. KELLERSHOHN: Dr. Hine, you showed a number of scintigrams of normal livers with colloidal Au^{198} but you said that it was not possible to

make scintigrams of normal kidneys with Hg^{203}-Neohydrin because the radiation dose would have been too high. Could you not have used Hg^{197}-Neohydrin? With this material the radiation dose for a kidney scintigram would be about ten times less than the dose delivered in a colloidal Au^{198} liver scintigram.

G. HINE: We have been using Hg^{203} mainly for convenience.

B. BODFORSS: Dr. Hine points out that it is difficult to obtain the correct settings in photoscanning. While this is true, I think that the difficulty can be overcome to a certain extent by using three layers of film instead of one. The first film then acts as a filter for the ones below, etc. Figure 1 shows density curves for the different layers as a function of lamp current

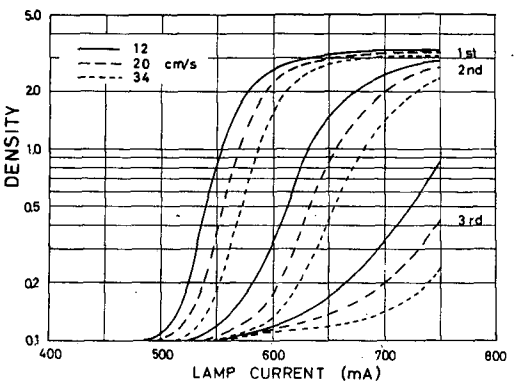

Fig. 1

Variation of density with lamp current for different layers of film and different scanning speeds

and the different scanning speeds. A brain scan obtained by this method is shown in Fig. 2.

We can obtain the same result by re-scanning with a closed-circuit television system, but the method described is cheap and offers a simple safety factor against over-exposure.

G. HINE: I think this method would give you good pictures but it does not offer much scope for quantitative interpretation. I do not believe there is any ideal read-out method. A combination of two relatively simple methods is probably the most practical proposition. The advantage of our mechanical colour print-out is that the results are immediately available as soon as the scan is ready. You can see what is going on while the process is in operation. In any photographic method - even with the paper-photographic method - there is always a delay.

E. LUBIN: In spite of this impressive presentation of colour scanning, I really fail to see that this technique is in any way better than conventional black-and-white scanning. The large lesions of the liver which were demonstrated could have been brought out just as well in black and white. As for the smaller lesions, one is faced with exactly the same sort of difficulties with both methods.

G. HINE: Obviously, colour scanning cannot eliminate the difficulties inherent in scanning, which are mostly connected with the detector. It mere-

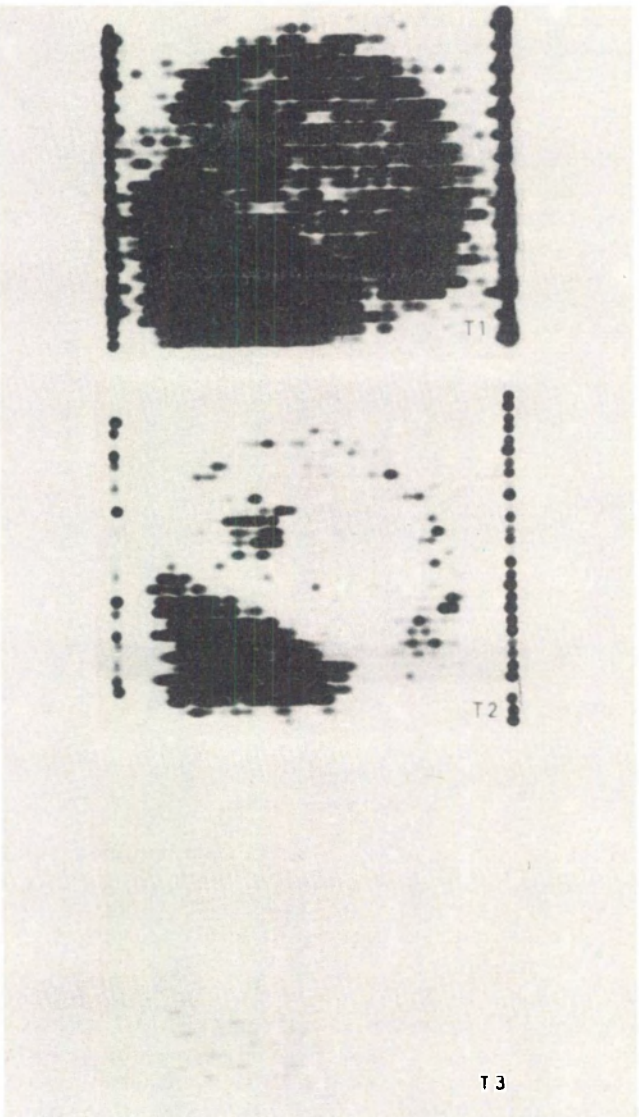

Fig. 2

Brain scans recorded on three superimposed layers of film

ly simplifies the interpretation. It does not provide any information that cannot be obtained by other methods. Experience does show, however, that physicians, and especially physicians relatively untrained in this field, find it easier to read colour scans than black-and-white scans or photoscans.

P. HARPER: Since the interpretation of colour scans involves subjective decisions, I wonder whether anyone has explored the possibilities of viewing such scans through colour filters.

G. HINE: Colour filters would certainly be useful. Colour-blind individuals, for example, could see which areas blacked out when a given filter was used and they could identify the colours by reading the names on the filter.

J. MALLARD: We have tried using colour filters to make the gamma-camera display quantitative. Using a storage tube, the display can be set at a selected contrast and photographed through a colour filter, set at another and re-photographed through another filter, and so on. Several colours then display the isocount lines of the camera display. The method is rather complicated.

M. TUBIANA: There has been a good deal of discussion so far on the need for improving the quantitative presentation of data. Colour scanning is certainly a step in this direction but it is still only a semi-quantitative method. The so-called profile method remains one of the simplest quantitative methods available. It is also one of the oldest. We have been using it since 1951 in conjunction with area-by-area counting [TUBIANA, M. and SUE, P., Presse méd. 59 (1951) 1027]; similar methods have been used by Pochin, by MacIntyre and by Doering [POCHIN, E.E., MYANT, N.B., HILTON, G., HONOUR, A.J. and CORBETT, B.D., Brit.Med.J.II (1952) 1115; MacINTYRE, W.J., GOMEZ-CRESPO, G. and CHRISTIE, J.H., J.nucl.Med.I (1960) 262; DOERING, P., Medical Radioisotope Scanning, IAEA, Vienna (1959) 158].

The method consists in moving a collimated probe over a radioactive area and recording the counting rate. This supplements the subjective scintigram with quantitative information. Figure 3 shows for instance the results of continuous registration of the counting rate by means of a counting ratemeter and a recorder.

This procedure reveals significant differences in counting rate that are difficult to distinguish on the scintigram.

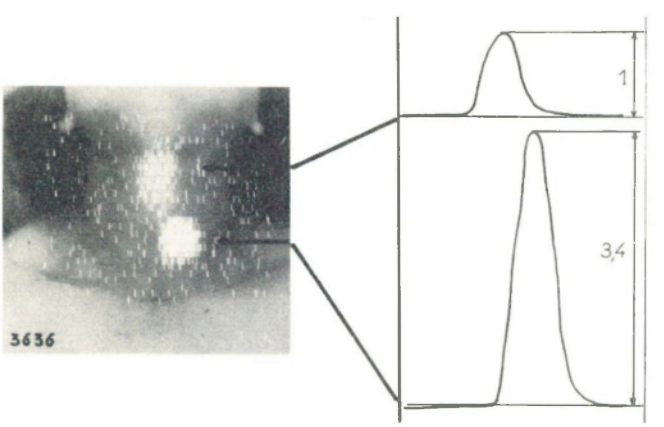

Fig. 3

Profile scans of thyroid gland with counting ratemeter and recorder
The heights of the different peaks in the profile scans give information about the activities of different regions.

The method does, however, have one drawback - it produces a distortion in the recorded counting rate and the shape of the observed profile curve due to the finite time constant of the counting ratemeter. In order to overcome this difficulty we have, together with P. Albarède and R. Di Paola, developed a modified system, in which a scintiscanner and a spectrometer are fitted with (a) a memory circuit connected by means of a stepping timer to a multichannel (64 channels) pulse-height analyser, used as a multiscaler, and (b) an XY graphic recorder.

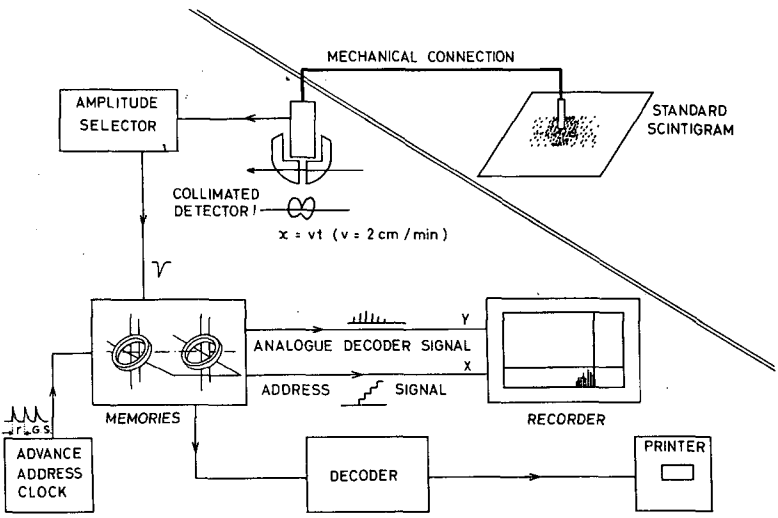

Fig. 4

Block diagram of apparatus

Figure 4 shows a block diagram of the circuit:

In practice, a conventional scintiscan is first performed. Then, without moving the patient, the areas under suspicion which require a more detailed study are marked. These selected levels are then scanned linearly at a much lower speed (2 cm/min). The number of counts accumulated by the detector in each successive period of 6 s is stored in one of the memory banks of the multichannel analyser. At the end of the pre-determined period, the accumulated counts are read out in digital binary form, passed to an analogue converter and recorded as a histogram on the XY recorder. The pen of the graphic recorder is then moved one space. Meanwhile, the next channel of the analyser is being used to accumulate counts.

The system is fully automatic and registers the profile scan as a histogram. Typical results are shown in Fig. 5, which shows measurements on a thyroid gland in which a cold nodule barely distinguishable on the scan is obvious on the profile scan.

The minimum in profile scan 1 may represent the interlobar space, and scans 2 and 3 clearly show central depressions from a hypofunctioning nodule.

This method has two advantages. Firstly, it exhibits the information quantitatively; and secondly, although it increases the examination time

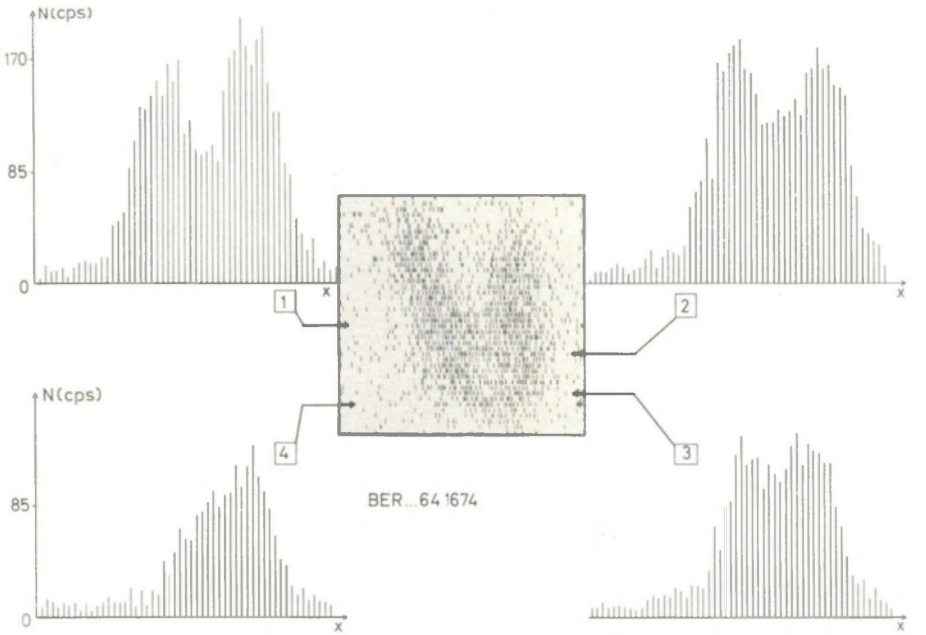

Fig. 5

Profile scans of thyroid gland with improved system

only slightly, it increases appreciably the amount of information recorded from any suspicious area, thus improving statistical accuracy.

G. HINE: I agree that there are other methods that can give more information. Unfortunately, however, these methods also increase the cost of the equipment, and it is important to keep costs down as much as possible in order to make the methods available to the greatest possible number of people.

P. CZERNIAK: Dr. Spârchez gave the results of more than 300 liver examinations carried out with the colour-scanning technique. False negative results were obtained for echinococcus cysts and for liver tumours in 7 - 9% of cases and for hepatitis in only 3% of cases. With normal scanning procedures the results are reversed, better results being obtained for the detection of hydatid liver cysts. The space-occupying lesions are mainly situated in the large right lobe of the liver and I wonder whether the reason for this discrepancy is not to be sought in the colour scan. Colour scanning is certainly extremely useful in areas where there are no great differences in relative activities. In the case of the right lobe, however, where the central activity is many times higher than in the border regions, it is possible that colour differentiation is inadequate to reveal the lesions.

T. SPÂRCHEZ: We think that 3% false negatives for chronic hepatitis is a reasonable result - our diagnoses have been checked by various exploratory techniques. In the case of liver tumours the figure of 7% is higher because of the fact that it is not easy to diagnose small tumours situated deep in the liver. Good results can be obtained by a combination of

black-and-white and colour techniques. With the latter method, however, the structural details of the functional parenchyma can be brought out more clearly. I do not think that the results can be improved by increasing the number of colours used for recording over the centre of the liver.

In general, of course, the diagnosis of small tumours remains a difficult problem in scanning.

ELECTRONIC MODIFICATION OF THE SCINTIGRAM AND ITS LIMITATIONS

B. CONRAD AND W. HORST
UNIVERSITY CLINIC FOR RADIOTHERAPY AND NUCLEAR MEDICINE
CANTONAL HOSPITAL, ZURICH, SWITZERLAND

Abstract — Résumé — Аннотация — Resumen

ELECTRONIC MODIFICATION OF THE SCINTIGRAM AND ITS LIMITATIONS. An investigation of the basic principles of contrast enhancement is presented. Certain fundamental laws should be observed in the design of transforming systems as well as in their application in order to visualize a maximum of information. These laws are developed using the following parameters and functions, which in general characterize all kinds of transforming systems:

(1) The elementary cell of primary information, defined by time intervals or pre-selected number of counts etc;

(2) The information-transforming function, according to which the elementary cell is represented in the scintigram (by the degree of blackening of a photo-dot, for example). Often this function is regarded as the final characteristic of the transforming system; this is true, however, only when statistical fluctuations are negligible.

The behaviour of a transforming system including statistical fluctuations is described by the following functions, which show the quality of a scintigram in quantitative terms.

(3) The picture-generating function, according to which the mean value of counting rate over an area is transformed into a mean blackening of the corresponding area in the scintigram. This function gives the contrast enhancement.

(4) The significance function, which describes the loss of information caused by the transformation. This function gives the degree of regularity of representation.

On the basis of the above definitions, the paper deals with the following problems: optimal "size" of the primary information cell, depending on the resolution of the detector; optimal shape of transforming function for various purposes; some electronic circuits for realization of such functions.

In particular, an apparatus is described in detail which gives an optimum of linear presentation using a suitable selected non-linear transforming function. Thus the range of net counting rate between background and maximal counting rate is projected to the full range of blackening in the scintigram in a manner that provides a minimum of falsification of data. Also other kinds of presentation can be selected, for example various quasi-logarithmic characteristics.

The problem of contrast enhancement in the case of extremely small differences, for example in brain-tumour scanning, is discussed in detail.

It should be noted that the principles described could be applied not only to scanners, but also to stationary detectors of every kind.

MODIFICATION ÉLECTRONIQUE DES SCINTIGRAMMES: LIMITATIONS. Les auteurs étudient les principes qui sont à la base de l'accentuation du contraste. Certaines lois fondamentales devraient être observées dans la réalisation et l'utilisation des systèmes de conversion, afin de permettre la visualisation d'un maximum d'informations. Pour déterminer ces lois, on a utilisé les paramètres et fonctions ci-après, qui caractérisent en règle générale tous les systèmes de conversion:

1. L'élément fondamental d'information primaire, qui est défini par les intervalles de temps, le nombre de coups déterminé à l'avance, etc.

2. La fonction de conversion de l'information, qui permet de représenter l'élément fondamental dans le scintigramme (par exemple, degré de noircissement d'un point photographique). Cette fonction est souvent considérée comme étant la caractéristique essentielle du système de conversion, mais cela n'est vrai que si les fluctuations statistiques sont négligeables.

Le comportement d'un système de conversion, y compris les fluctuations statistiques, est décrit par les fonctions suivantes, qui expriment quantitativement la qualité d'un scintigramme:

3. Fonction de production d'images, qui exprime la valeur moyenne du taux de comptage au-dessus d'une zone par un noircissement moyen de la zone correspondante du scintigramme; cette fonction assure l'accentuation du contraste.
4. Fonction d'évaluation, qui indique les pertes d'informations dues à la conversion. Elle montre le degré de régularité de la représentation.

En s'appuyant sur les définitions ci-dessus, les auteurs traitent des problèmes ci-après: «dimension» optimum de l'élément d'information primaire, en fonction du pouvoir de résolution du détecteur; forme optimum de la fonction de conversion suivant l'objet de l'examen scintigraphique; circuits électroniques permettant de réaliser ces fonctions.

En particulier, les auteurs décrivent en détail un appareil qui assure une présentation linéaire optimum grâce à une fonction de conversion non linéaire appropriée. Ainsi, la gamme des taux de comptage nets, allant du bruit de fond au taux de comptage maximum, se trouve représentée dans le scintigramme par toutes les nuances de noircissement, d'une manière qui réduit à un minimum l'altération des données. On peut aussi choisir d'autres genres de présentation, par exemple différentes caractéristiques quasi-logarithmiques.

Le problème de l'accentuation du contraste lorsque les nuances sont très faibles, par exemple dans l'exploration des tumeurs du cerveau, sera traité de manière détaillée.

Il est à noter que les principes exposés peuvent s'appliquer non seulement aux détecteurs mobiles utilisés en scintigraphie, mais aussi aux détecteurs stationnaires de tous genres.

ЭЛЕКТРОННОЕ УСОВЕРШЕНСТВОВАНИЕ СЦИНТИГРАММЫ И ЕГО ОГРАНИЧЕНИЯ. Представлено исследование основных принципов контрастного усиления. При разработке трансформирующих систем, а также при их применении необходимо соблюдать некоторые основные закономерности для того, чтобы получить максимум информации. Эти закономерности разработаны при использовании следующих параметров и функций, которые в целом характеризуют трансформирующие системы всех видов:

1. Элементарная ячейка первичной информации, определяемая интервалами времени или предварительно отобранным числом отсчетов, и т.д.
2. Функция преобразования информации, в соответствии с которой элементарная ячейка представляется на сцинтиграмме (например, степенью потемнения фотопятна). Часто эта функция рассматривается как окончательная характеристика трансформирующей системы; однако это справедливо только при незначительных статистических колебаниях.

Поведение трансформирующей системы, включая статистические колебания, описывается следующими функциями, которые показывают качество сцинтиграммы с количественной точки зрения.

3. Функция генерации снимка, в соответствии с которой средняя величина скорости счета в зоне трансформируется в среднее потемнение соответствующей зоны на сцинтиграмме. Эта функция дает контрастное усиление.
4. Функция достоверности, которая описывает потерю информации, причиненную трансформацией. Эта функция дает степень правильности воспроизведения изображения.

На основе вышеуказанных определений в докладе рассматриваются следующие проблемы: оптимальный "размер" ячейки первичной информации в зависимости от разрешающей способности детектора; оптимальная форма трансформирующей функции для различных целей; некоторые электронные контуры для реализации таких функций.

В частности будет подробно описан прибор, который дает оптимальное значение линейного представления при использовании соответствующим образом подобранной нелинейной трансформирующей функции. Таким образом, интервал чистой скорости счета в промежутке между фоновой и максимальной скоростью счета проецируется как потемнение в полном интервале на сцинтиграмме таким образом, что это обеспечивает минимальное искажение данных. Можно также отобрать другие виды представления, например различные квази-логарифмические характеристики.

Подробно обсуждается проблема контрастного усиления в случае чрезвычайно малых различий, например на скенноограмме мозговой опухоли.

Следует отметить, что вышеописанные принципы могут применяться не только к скеннерам, но и к стационарным детекторам любого вида.

MODIFICACIÓN ELECTRÓNICA DE LOS CENTELLEOGRAMAS; SUS LIMITACIONES. Los autores estudian los principios básicos del aumento del contraste. Al realizar y utilizar los sistemas de conversión deberían

observarse ciertas leyes fundamentales a fin de permitir la visualización del máximo de informaciones. Para determinar esas leyes se han utilizado los siguientes parámetros y funciones, que caracterizan, en general, todos los sistemas de conversión:

1. El elemento fundamental de información primaria, definido por los intervalos de tiempo, el número predeterminado de impulsos, etc.
2. La función de conversión de las informaciones, que permite representar el elemento fundamental en el centelleograma (el grado de ennegrecimiento de un punto luminoso, por ejemplo). A menudo esta función se considera como la característica esencial del sistema de conversión, pero esto sólo es cierto si las fluctuaciones estadísticas son despreciables.

El comportamiento de un sistema de conversión, incluidas las fluctuaciones estadísticas, es descrito por las funciones siguientes, que expresan cuantitativamente la calidad de un centelleograma:

3. Función de producción de imágenes: expresa el valor medio del índice de recuento correspondiente a una zona con un ennegrecimiento medio de la zona correspondiente del centelleograma. Esta función asegura el aumento del contraste.
4. Función significativa, que indica las pérdidas de información debidas a la conversión. Esta función muestra el grado de regularidad de la representación.

Basándose en dichas definiciones, los autores estudian los siguientes problemas:

«Dimensión» óptima del elemento de información primario en función del poder de resolución del detector. Forma óptima de la función de conversión según el objeto de la exploración centelleográfica. Circuitos electrónicos que permiten realizar dichas funciones.

En particular, los autores describen detalladamente un aparato que da una presentación lineal óptima gracias a una función de conversión no lineal apropiada. Así el intervalo de los índices netos de recuento comprendidos entre el fondo y el índice de recuento máximo se halla representado en el centelleograma por grados de ennegrecimiento de una manera que reduce al mínimo la alteración de los datos. Se pueden seleccionar otros tipos de presentación, por ejemplo, diferentes características cuasilogarítmicas.

Los autores estudian detenidamente el problema del aumento del contraste cuando las diferencias son extremadamente pequeñas, por ejemplo, en la exploración de tumores cerebrales.

Conviene advertir que los principios enunciados pueden aplicarse no sólo a los detectors móviles, sino también a los detectores fijos de cualquier tipo.

1. INTRODUCTION

A scintigram may be regarded as unmodified if every single pulse that is measured is visible on the scan; that means, the primary measurement of the spatial distribution of single pulses is given directly. With a scanner we have the single pulses distributed in lines and with a gamma camera we have the single pulses spread continuously over an area. Such a record must be transformed by eye to obtain the specific density of pulses within certain areas - up to very large areas, i.e. to determine the isoimpulse zones. The total transformation consists of the integration over very small areas at first with statistically very little information content, combining them step by step to give successively larger units, while at the same time taking into account the resolution of the detector, anatomical concepts and continuously estimating the statistical fluctuations. This very difficult task can be made easier by including a part of this total transformation in the scintigram itself. This, in fact, is what is normally done, if only by the use of a scale factor, in the case of the scanner, or by smearing together the single dots in the oscillogram of a gamma camera.

In this paper we will consider what are the optimal modifications for this purpose, i.e. which transformations will do a maximum of the preliminary work. In this respect the different types of final presentation (dots on paper, blackening on film, etc.) may be regarded as being less important,

as this is more a matter of personal taste. It is far more a question of deciding which electronic transformations will give the best presentation, in regard to contrast and minimal loss of information. In every transformation (except for a linear transformation without subtraction, i.e. without contrast enhancement) there is always a loss of information. This information may be lost in two ways: (1) a certain count-rate region is transformed with a diminished statistical significance; and (2) the spatial resolution of the transformed scintigram will not be as good as the primary resolution of the detector. First we shall consider the transformations with respect to this count-rate information loss and contrast enhancement.

2. COUNT-RATE INFORMATION LOSS AND CONTRAST ENHANCEMENT IN TRANSFORMING SYSTEMS

2.1. General criteria by which a transformation may be judged

The basis of every transformation (except the linear transformation without subtraction) is that there is a primary cell of information. We may consider the number of pulses N contained in an area of, say, 1 cm^2 as such an elementary cell. The resulting grid of numbers N_i is now transformed into a grid of "blackenings" B_i by means of an information-transforming function φ, so that every information cell is represented by a corresponding blackening. Figure 1 shows a step-function as an example of such an in-

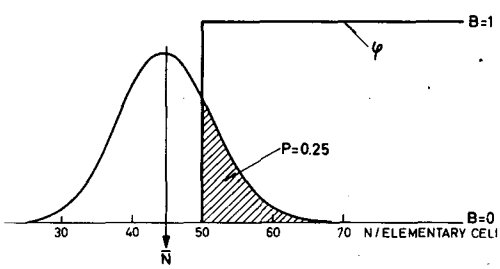

Fig. 1

Influence of statistics on an information-transforming system

$\bar{N}$ = true mean count rate per information cell
φ = information-transforming function
B = blackening of transformed elementary cell
P = 0.25 probability of giving a "black" area if $\bar{N} = 45$

formation-transforming function. Each information cell with $N \geq 50$ will give a completely black area ($B = 1$) and each cell with $N < 50$ will give a completely white area ($B = 0$).

A large area with constant count rate consists of many information cells with, for example, a true mean value of $\bar{N} = 45$, and will therefore because of the Poisson distribution be represented in the scan by a mixture of black and white dots with mean blackening $\bar{B} = 0.25$. The mean blackening, as a function of the different values of $\bar{N}$, is given in Fig. 2. For generality the

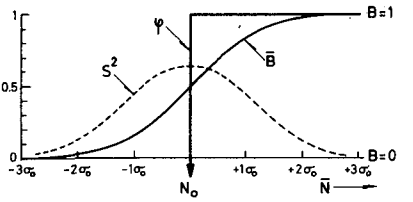

Fig. 2

Transformation by a step-function
$\bar{B}$ =mean blackening as function of mean count rate/ elementary cell
S^2=significance (information retained expressed as relative count rate)

scale of the abscissa is not given as a direct count rate but is expressed in σ units about a central value of N_0. This S-shaped curve gives the actual relationship between the count rate over an area and the corresponding mean blackening of the scintigram, as induced by the statistical fluctuations of the single elementary cells. Thus $\bar{B}$ represents the actual contrast. This function alone, however, is not a sufficient criterion of how well one can distinguish two different areas with mean count rates $\bar{N}_1$ and $\bar{N}_2$, because the corresponding blackenings $\bar{B}_1$ and $\bar{B}_2$ are only mean values. In addition one must consider the way in which the statistical fluctuations are transformed:

$$\bar{N}_1 \pm \sigma_1 \longrightarrow \bar{B}_1 \pm \sigma_{B_1}$$

$$\bar{N}_2 \pm \sigma_2 \longrightarrow \bar{B}_2 \pm \sigma_{B_2} .$$

It is doubtful whether a contrast enhancement in which the statistical variations - the fluctuations from elementary cell to elementary cell within each area - are more strongly contrasted than the mean blackenings of the areas is really of any help to the eye, because it is precisely the variations of blackening within surfaces which make the scintigram so difficult to read. It is for this very reason that a contrast enhancement is so much to be desired.

In fact, with the above step function, even if one counts the dots and computes the blackening from the scintigram, the statistical probability of distinguishing different areas in the scan is lowered. We can express this by a "significance function" as follows:

$$S = \frac{\overline{\Delta B}}{\sigma_B} \Big/ \frac{\overline{\Delta N}}{\sigma_N} < 1 .$$

This means that the original mean differences in count rate stand out from the statistical fluctuations more than the corresponding mean differences in blackening of the scintigram. By taking infinitely small differences we can obtain a general expression, so that the significance function can be written as:

$$S = \frac{\sigma_N}{\sigma_B} \frac{d\bar{B}}{d\bar{N}} .$$

For σ here, we can of course use the standard deviation of the single information cell. To picture this more clearly, one may say that the information in the scintigram is statistically more uncertain than the primary information and express this as if the scintigram were based on a count rate smaller than the primary one. The amount of information which comes through the transforming system is thus given as an equivalent count rate and is exactly equal to S^2. The loss of information is then the difference between unity and S^2.

The significance function S^2 for the step-function transformation is given in Fig. 2, together with $\overline{B}$ and φ. Only in this combined presentation do we have a complete description of the transforming system. For the sake of generality it is based on infinitely small differences. In the practical case of finite differences, the significance lies between the single significances for the corresponding count rates, i.e. in practice the maximum value $S^2 = 0.64$ is never reached. (The presentation in Fig. 2 is based on the normal distribution, so is strictly valid only for large count rates. However, large alternations occur only in the case of very small count rates per elementary cell, e.g. $N_0 < 5$.)

2.2. The maximal possible contrast

The step function considered above gives the maximal possible contrast within a certain count-rate region, but it should not be used, because it destroys so much information. It is much better if we take a transformation with a modified step, i.e. a linear increase in the blackening over a certain small region, for example $2\sigma_0$ (see Fig.3). This means that within the count-rate region $2\sigma_0$ the primary information cells are represented by different shades of grey, instead of only the sharp difference between black and white. The effective contrast $\overline{B}$ is scarcely any smaller than in the case of the "sharp" step, but now a small region of count rates is transformed with almost full information content, so that this transformation produces the maximal contrast really possible.

For practical purposes, however, one requires a plateau of significance, i.e. a somewhat larger region in which $S^2 \approx 1$. To meet this requirement, the information-transforming function should rise linearly over at least the range of $4\sigma_0$. In Fig. 4 $\overline{B}$ and S^2 are shown for the three transformations: for the "sharp step" transformation, the $2\sigma_0$-transformation and the $4\sigma_0$-transformation. The plateau of significance of the $4\sigma_0$-transformation can be regarded as being at least $2\sigma_0$ broad.

An an example of the use of this transformation in scanning, let us take a maximum count rate of 5400 pulses/min, with a background of 22%. The single information cell may correspond to a measuring time of one second. Then the count-rate region between 20 pulses and 90 pulses/cell is to be presented. This is optimally done by means of a series of five single presentations, each made with a 4σ-transformation, namely in the regions 20-30 pulses (25 ± 5), 30-42 (36 ± 6) ..... up to 72-90 (81 ± 9) pulses. The corresponding significance plateaus overlap considerably so that the single pictures are not isolated.

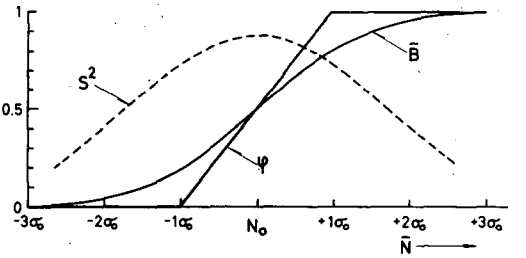

Fig. 3

Modified step transformation ($2\sigma_0$-transformation)

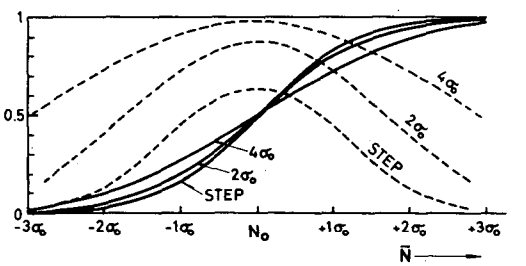

Fig. 4

Comparison of transformations
(Sharp step, $2\sigma_0$- and $4\sigma_0$-transformations)
—— $=\bar{B}$ ---- $=S^2$

The information-transforming function φ with a step, i.e. a sudden change between white and black, is used in colour scintigraphy, except that there the step is a change between two colours so that in one presentation there are a number of steps. The colour alone, as follows from the above discussions, makes only part of the full information visible and it is doubtful if the additional presentation of different dot densities can compensate for this information loss. The optimum would undoubtedly be to have a gradual transition in the colour of the single elementary cells, in the sense of the above 4σ-transformation; the necessary overlapping of the different colour-transformations would, however, lead to a multi-colouring of even the elementary cells. Accordingly it would perhaps be better to separate this into several colour-scans, in which the zones of colour transition are displaced in relation to each other. A large range of count rates (in σ-units) could then be presented in a smaller number of scans than is possible with merely black-and-white representations.

2.3. Elimination of background

The most widely used modification of the scintigram is that of background elimination. The simplest technical means of doing this is that of suppression. A more difficult, but better, form of transformation is the subtraction of background and the linear presentation of the net count rate [1, 2]; or, the net count rate may be presented in any desired non-linear

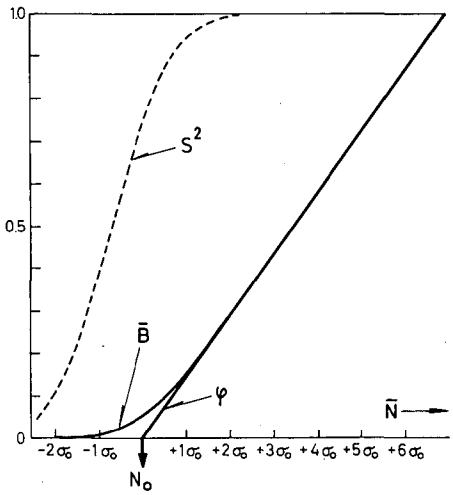

Fig. 5

Linear subtraction

form. The situation in regard to "linear subtraction" (subtraction and linear presentation) is shown in Fig. 5. The picture-generating function $\bar{B}$ only reaches the linear characteristic outside the region of statistical fluctuations of N_0 (i.e. the foot of φ); that means, that only there is the full contrast reached. Also full information is given there ($S^2 = 1$). If the full information is to be transformed, complete elimination of background is impossible; only a reduction in background can be made. But in general one might intend to eliminate the background almost completely; in which case the information-transforming function φ will be adjusted so that the background is somewhat below N_0. This is wrong from the standpoint of preserving information. It may be done only on aesthetic grounds, or perhaps because it is the only way in which the margins of large organs can be estimated. The information loss in this type of presentation cannot be avoided; it is possible, however, to improve the contrast somewhat. This can be done by a linear information-transforming function with additional suppression at the very beginning (see Fig. 6). A suppression of $1.5\,\sigma_0$ has proved to give optimal conditions.

As an example, we have in Fig. 7 a comparison of both types of subtraction for the following conditions: a 30% subtraction referred to a maximum count rate of 50 pulses/elementary cell (corresponding to a maximum count rate of 6000 counts/min and a measuring time of one second per elementary cell), whereby the background produces a residual blackening of 1% of the maximum blackening. With the additional suppression the blackening function $\bar{B}$ comes closer to the desired linear characteristic than without this device.

While the suppression of count rates up to $2\,\sigma_0$ may be considered to be a permissible "trick", a high step diminishes the information considerably. In Fig. 8, for example, the situation is given for a suppression of $5\,\sigma_0$. The high step destroys the information in its neighbourhood in the same way as did the "sharp step" (black-and-white transformation) above.

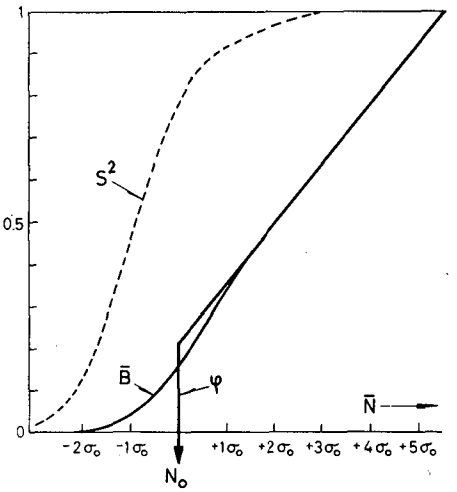

Fig.6

Linear subtraction with additional small suppression ($1.5\sigma_0$)

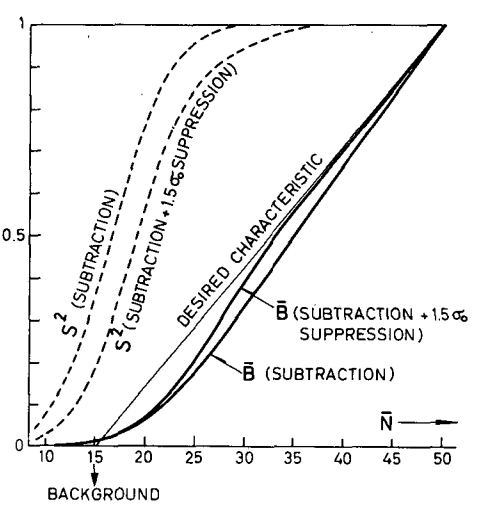

Fig.7

Comparison of linear subtraction with and without a $1.5\sigma_0$ suppression

For the sake of comparison these characteristics (for pure suppression) are given together in Fig. 9 with the characteristics of a linear subtraction without suppression for the previous example of a 30% background and a maximum count rate of 50 pulses.

Suppression is considerably poorer than linear subtraction in two respects. First, the significance S^2 is low, and, as the count rate rises, the rise of S^2 towards unity is much more delayed so that a very large count rate region is given in the scintigram with diminished information. Secondly,

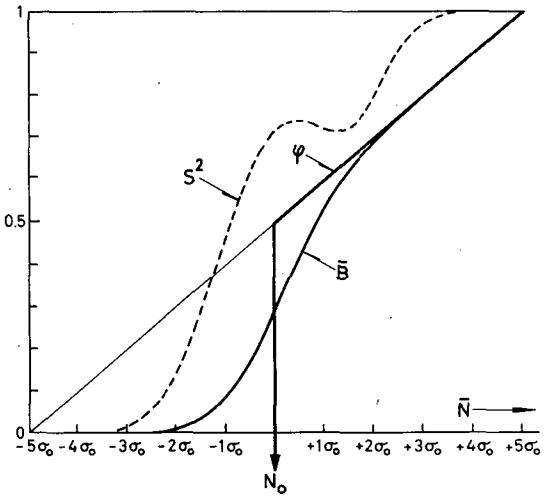

Fig. 8

High suppression ($5\sigma_0$)

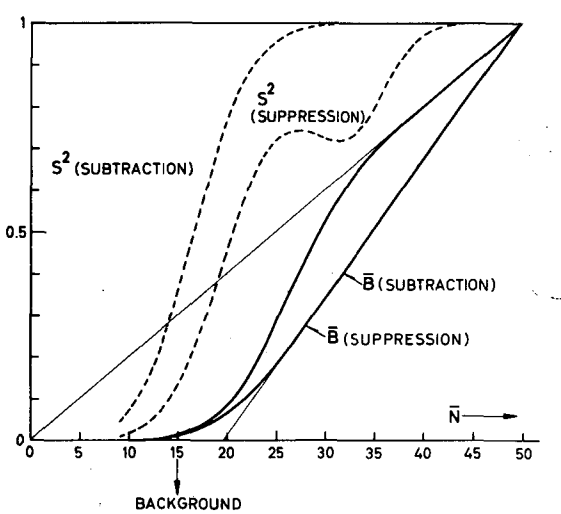

Fig. 9

Comparison of linear subtraction and suppression
(30% background elimination)

in the range of small count rates the contrast is very high, hence a large part of the total contrast range is wasted in this region of small significance. This means that in the margins of organs, one sees only fluctuations instead of information and in the inner part of the organ there is no contrast enhancement compared to the primary measurement. Without regard to the significance S^2, one might consider the blackening function $\bar{B}$ of the suppres-

sion as being at least well-suited for the mapping of the contours of organs, because of its quasi-logarithmic features. Such curved characteristics may in fact be used, but they should not be produced by the influence of the statistics; rather they should be pre-formed in the information-transforming function φ (i.e. φ should not start with a step but with a moderate increase as in the 4σ-transformation and a gradual flattening).

Of course, in the case where a small background, say 10%, is to be eliminated, there will not be very much difference between suppression and subtraction, but if, say, 50% is to be eliminated, the information lost by suppression is very much larger, Also if the counting statistics are very good, the region of lost information is not so large compared to the total range of net count rate, but the wastage of the contrast in the range of diminished significance always remains the same.

3. THE SIZE AND "SHAPE" OF THE ELEMENTARY CELL

Since the contrast and information loss of a transformation depend on the size of the statistical fluctuations and hence on the number of pulses N in the primary information cell, the single cells must be as statistically powerful as possible; therefore, they must be as large as the limits of resolution of the collimator will permit. In this the type of integration that leads to the information cell, one may say the shape of the information cell, is of interest. We limit ourselves here to the principles of integrating in the case of a continuously moving scanner, therefore we consider only the one-dimensional integration.

There are two different types of information cells, the constant-time information cell (e.g. the ratemeter) to which the characteristics considered above can be applied directly, and the variable-time information cell (e.g. the scaler). In our comparison of the two types we may consider that the constant-time cell is represented by a continuous blackening - the electronic realization of this will follow in the next section - whereas in the case of the scaler, the blackening is to be regarded as the time density (hence spatial density) of the output pulses.

3.1. The constant-time elementary cell

The most convenient manner of realizing this elementary cell is by the use of the ratemeter. The most normal method of mathematical analysis of statistical data is that of the sliding average; this, however, can also be realized electronically. There are two different types of "memory" at time t_0 for the pulses that have come in in the preceding time. The memory of the ratemeter is exponentially decreasing but of infinitely long extent, whereas the sliding average is a memory of constant weight over a limited time (see Fig.10). As is well known, the statistical fluctuations of a ratemeter with a time constant RC give rise to an equivalent measuring time of $t = 2RC$, so the sliding average over $t = 2RC$ builds up an elementary cell of equal statistical power. Variations in count rate are at first followed more quickly by the ratemeter than by the sliding average, but later there is a delay in actually reaching the new value. It is possible, however, to confine the

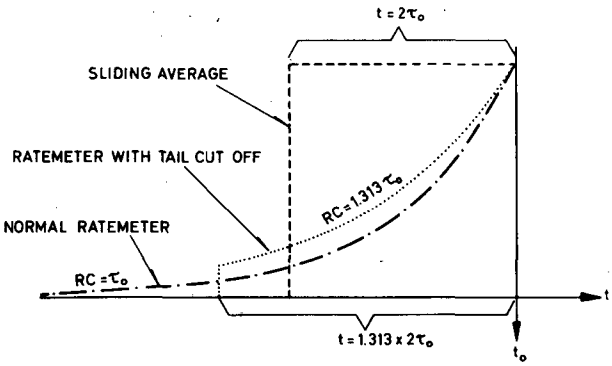

Fig. 10

Elementary cells of information with different types of "memory"

memory of the ratemeter to just the time 2RC; the time constant must then of course be somewhat greater to give an equivalent statistical power. From the statistical theory of the ratemeter [3, 4] can be derived:

$$RC_{\text{(Ratemeter with tail cut off)}} = 1.313\ RC_{\text{(Normal ratemeter)}}.$$

(The electronic realization of the sliding average and the cut-off tail ratemeter may be accomplished by the use of a number of condensers in cyclic operation, of which only one is loaded for a very short time according to the incoming pulse-rate N, while the voltages of the others are added to give the memory.)

The behaviour of these three types of elementary cells in the presentation of typical basic forms of scintigrams is seen in Figs. 11 to 13. These examples refer to a coarse-focus collimator which picks up 70% of the count rate within a diameter of 2 cm and a scan speed of 1 cm/s is assumed. The time constant of the ratemeter is RC = 2 s = 2 cm, so the sliding average is taken over 4 s = 4 cm. Figure 11 shows how the margins (ascending and descending) of a relatively large organ are presented in the scintigram. (Cylindrical model, radius of curvature 5.5 cm, I^{131} - photopeak only, no additional absorption by tissues.) There is a large displacement of up to 3 centimetres in the scan direction, so that in a normal to-and-fro scan there would be a hysteresis of up to 6 centimetres. By automatically displacing the writing point a distance of half the sliding average in the momentary direction of scanning, i.e. 2 cm, we obtain a relatively good fit between the scintigram and the primary measurement (see Fig. 12), except for the tail of the normal ratemeter, which may give additional hysteresis in the case of good statistics. The scanner should therefore have automatic compensation for hysteresis, or else it should be possible to scan in one direction only, with a very rapid retrace; otherwise, on aesthetic grounds, the information cell will be much too small. This means that there is better spatial resolution than is required, while count-rate contrast and information content are very poor. In Fig. 13 we have the presentation of a sphere of activity of 2 cm diameter under the same conditions, i.e. the "smear-out" of the smallest object which can be measured by the collimator in question.

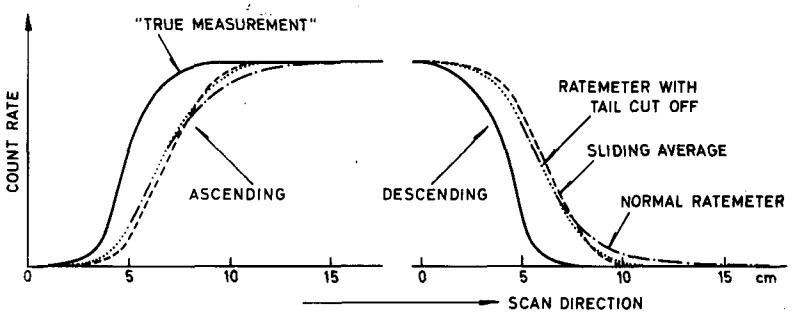

Fig. 11

Presentation of the margins of a large organ
(No hysteresis compensation)

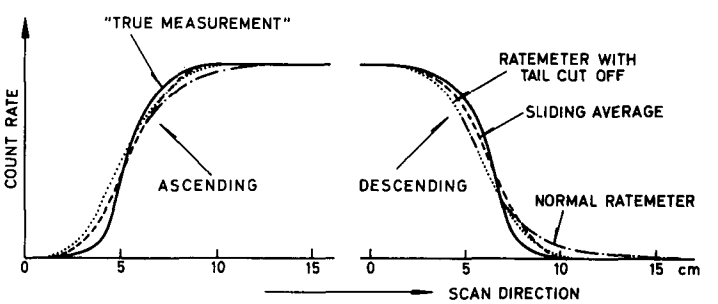

Fig. 12

As in Fig. 11, but with hysteresis compensation
(=half sliding average)

3.2. The variable-time information cell

A scaler can be used to make a subtraction transformation by feeding into it a constant pulse-rate (pulse generator) "backwards", while the incoming count rate, that is to be transformed, comes in "forwards" [5]. The statistical power of this information cell is governed by the scale factor, since its extension in time can be regarded as the distance between two output pulses. In comparison with the sliding average, this gives us a variable-time cell, for the sampling time is very short at high count rates and very long at low count rates, which means a small excess over background. In the scintigram, therefore, every count rate will give a different spatial "smear-out".

The calculation of the blackening functions $\overline{B}$ and the significances S^2 leads to characteristics which are very similar to those for linear subtraction in the case of a constant-time elementary cell if the scale factor is four or higher and no negative storage is assumed. A comparison can be made, therefore, in the following way:

For every sliding average with a measuring-time of 2τ, and for every count rate N_0/s that is to be subtracted, there exists a certain scale factor

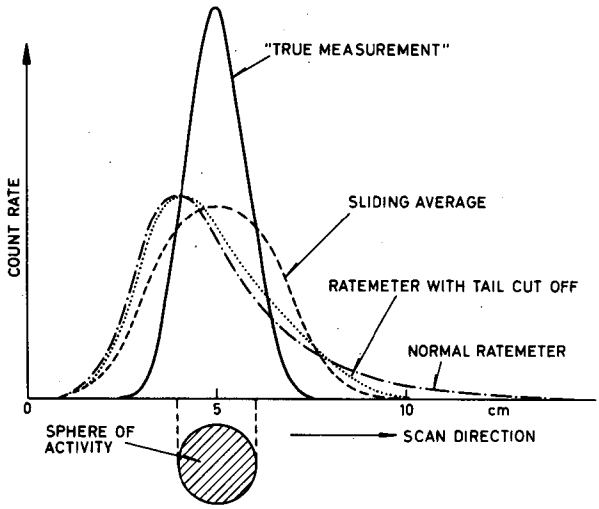

Fig. 13

As in Fig. 12, but for a small object
(With hysteresis compensation)

such that the blackenings $\overline{B}$ and significances S^2 in both systems are almost equal. With this scale factor the following result is obtained: An excess over background N_0, which is just sufficient to be presented with full contrast and full significance, gives rise to output pulses in the scaler with a mean time-distance of exactly 2τ. Thus, just at this count rate, the spatial smear-out of the scaler is the same as may be produced by the sliding average (Fig. 13). The scaler may have a slight advantage in that high count rates are given with less spatial "smear-out"; on the other hand, the ratemeter may have a slight advantage in that in regions of low count rates the lower significance and lower contrast are not accompanied by a large "smear-out" as well.

The scaler can also be used to make a suppression transformation [6]. This is done by suppressing all pulses which are separated from the previous pulse by more than a pre-determined time t. This situation is then very similar to the case of suppression for a constant-time elementary cell (Figs. 8 and 9).

4. ELECTRONIC REALIZATION OF TRANSFORMATION

The main conclusions of the foregoing sections about the realization of scintigram modifications are:

(1) Statistical fluctuations make a scintigram difficult to read. A transformation should therefore contrast the various mean greying of surfaces as sharply as possible, without contrasting the statistical fluctuations within these surfaces even more strongly (information loss).

(2) Any transformation is able to do this only to a limited extent; moreover this becomes worse as its spatial resolution is improved. The primary

information cell must therefore be carefully adapted to the limits of resolution (collimator), i.e. it must be as large as possible.

(3) The information-transforming function, given by the mechanism of the transforming system, can be freely chosen only within certain limits. Count-rate suppression, in many cases, destroys a large part of the information content; a linear subtraction is considerably better. In any case, one should be able to see clearly the type of transformation that has been made, and its quality should not be dependent on such parameters as the absolute maximum count rate, percentage of background to be eliminated, etc. The adjustments of such an apparatus should be clearly reproducible.

As an example, a system for direct registration (dash-scintigram) may be given. The block diagram (Fig. 14) shows the transforming elements of such a system.

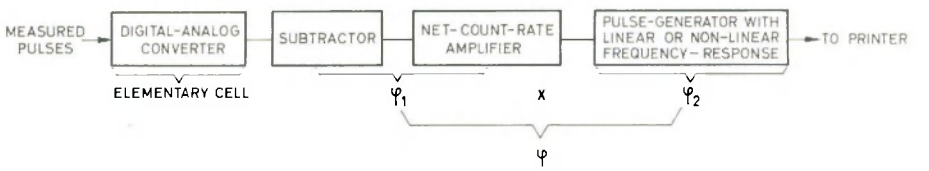

Fig. 14

Block diagram of a transforming system
(Direct registration)

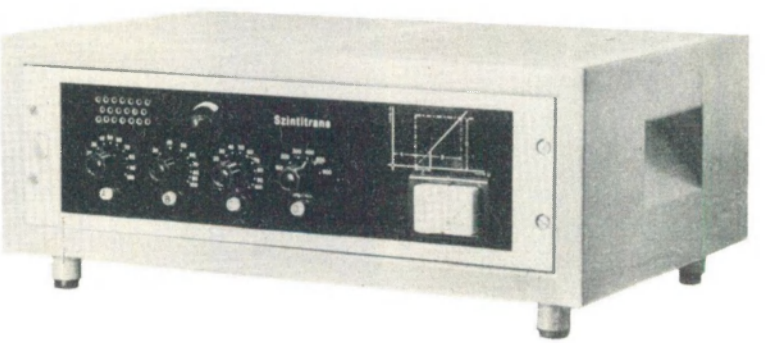

Fig. 15

A transistorized apparatus for making a Linear Subtraction Transformation

A transistorized apparatus for making a linear subtraction according to this system is seen in Fig. 15. It is used in the following way:

The maximum count rate and the background to be adjusted are read from the ratemeter. Then there is a linear frequency-dependence of the output pulses in the range of the net count rate (without regard to statistics). The maximum count rate is always set to the same frequency (same density of dots). This frequency is chosen according to the scan speed to be precisely that at which the dots can be counted out directly, up to the maximum count rate (quantitative evaluation). According to the statistical fluc-

tuations, an additional suppression is used - the range of the suppression is read on a dial calibrated directly in percentage of net count rate. Thus one can check that this "trick" is used only with great care.

ACKNOWLEDGEMENTS

In conclusion we wish to acknowledge the assistance of Miss J. Hayward and Dr. W. Müller-Duysing in extended discussions on this theme, Miss S. Hinrichs for numerical calculations and Mr. H.D. Vogt for developing a transistorized version of our transformation system.

REFERENCES

[1] HORST, W., HEYMANN, H.-J. and TEPE, H.-J., Strahlentherapie 106 (1958) 191-201.
[2] HORST, W., THIEMANN, H.-J. and TRALAU, G., Fortschr. Röntgenstr. 93 (1960) 343-9.
[3] SCHIFF, L.I. and EVANS, R.D., Rev. Sci. Instr. 7 (1936) 456.
[4] KIP, A.F. et al., Rev. Sci. Instr. 17 (1946) 323, 515.
[5] JORDAN, K. and WINKLER, C., Sonderband z. Strahlentherapie 53 (1963) 67-78.
[6] PRÄG, R., Strahlentherapie 119 (1962) 569-83.

DISCUSSION

C. HARRIS: The profiles shown in our paper* were made with a sliding-average count rate device that was very similar to yours. I am making this point not in order to advertise our own work but so that anyone interested can refer to an actual profile obtained by this method.

B. CONRAD: Thank you. Of course the problem is to decide what type of integration one should use. The normal ratemeter is certainly not ideal. As can be seen in Fig. 13 in our paper, one obtains a better spatial resolution for the detection of a small "tumour" with the ratemeter with tail cut-off than with the sliding-average device. It is difficult to say what method of weighting is best as a general rule.

C. HARRIS: How do you obtain the time constant with tail cut-off?

B. CONRAD: This can be done by using a number of condensers. At the moment we are building a device designed on the following lines:

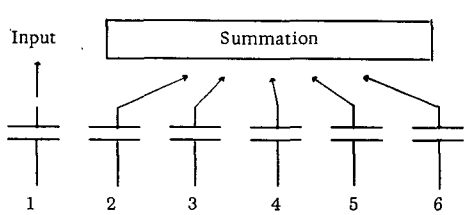

* HARRIS, C.C. et al., "The design and performance of a large high resolution focusing collimator" (SM-51/59), these Proceedings I.

Each condenser in turn is charged for a short time Δt, the charge collected depending on the incoming pulses within Δt. While condenser 1 is being charged, condensers 2-6 are connected to a memory circuit which measures their total charge. They are thus equivalent to the large tank condenser of a ratemeter. An exponential discharge of the memory is achieved by giving each condenser a discharge resister, as it is important not to mix the charges of the different condensers. After Δt, condenser 6 is disconnected from the summation circuit, discharged and connected to the input, while condenser 1 is connected to the summation circuit, and so on. The cyclical switching can be done by means of a step-by-step mechanical switch, though it may be better to use electronic switching.

TECHNIQUES WHICH AID IN QUANTITATIVE INTERPRETATION OF SCAN DATA

D. B. CHARLESTON, R. N. BECK, P. EIDELBERG AND M. W. SCHUH
ARGONNE CANCER RESEARCH HOSPITAL*,
CHICAGO, ILL., UNITED STATES OF AMERICA

Abstract — Résumé — Аннотация — Resumen

TECHNIQUES WHICH AID IN QUANTITATIVE INTERPRETATION OF SCAN DATA. This paper discusses a range of techniques which assist in evaluating and interpreting scanning read-out display. This range extends from simple internal calibration for photographic read-out to fairly elaborate auxiliary equipment for presentation of accumulated digital scan information to a computer programme.

The direct and remarkably useful method of using a random pulse generator to produce a calibrated step-wedge of spots, which are projected on to a film by the same projection light source as is used during the scan, allows the viewer to compare exposure densities of regions of interest on the scan to similar regions on the wedge which are calibrated directly in count-rate units.

Auxiliary equipment, such as a multichannel analyser used in the multiscaling mode, permits the accumulation of digital information for a "total count per scan line" display for each index step.

Small animal scans have been made which accumulate and display "counts per scan line" for each index step. This produces an accurate quantitative measure of the distribution of activity over the animal and a profile display of activity similar to the slit scan display of a linear scanning system.

The same multiscaling technique is carried further by accumulating digital information for a "count per unit area" display. A profile curve is obtained for each scan line of each index step. From this it is possible to visualize or construct an area profile of count-rate.

Scan displays with or without contrast enhancement and with or without "time lag" from integrating circuitry and scans with various spot sizes and shapes have been produced under identical statistical conditions by means of multiple read-outs while scanning a phantom with a single-detector system. Direct comparison of displays combined with the "count per unit area" mapping technique aid in the interpretation of scan results.

Precise position information must be included with the data record. Computations of percentage difference of activity in regions of interest on opposite sides of the head are made from data accumulated by multiscaling in the Argonne Cancer Research Hospital's brain-scanning system.

MÉTHODES FACILITANT L'INTERPRÉTATION QUANTITATIVE DES SCINTIGRAMMES. Les auteurs du mémoire examinent une série de méthodes qui facilitent l'évaluation et l'interprétation des scintigrammes. Ces méthodes vont du simple étalonnage intérieur en vue d'une représentation photographique à l'utilisation d'un matériel auxiliaire assez complexe permettant d'introduire les données du scintigramme sous forme numérique dans le programme d'un ordinateur.

Une méthode directe et très efficace consiste à réaliser, au moyen d'un générateur d'impulsion, une échelle de densités étalonnée qui est projetée sur un film au moyen de la même source lumineuse employée pour l'établissement du scintigramme; cette méthode permet à l'observateur de comparer les densités d'exposition des régions intéressantes sur le scintigramme à celles de l'échelle de référence, qui est étalonnée directement en unités de taux de comptage.

A l'aide d'un matériel auxiliaire, tel qu'un sélecteur à canaux multiples fonctionnant en multi-échelle, on parvient à accumuler des données sous forme numérique en vue d'une représentation de «tous les coups par ligne de balayage» pour chaque degré de densité de l'échelle.

On a établi des scintigrammes de petits animaux qui accumulent et reproduisent les «coups par ligne de balayage» pour chaque degré de densité de l'échelle. On obtient ainsi une mesure quantitative précise de la répartition de l'activité dans l'ensemble du corps de l'animal ainsi qu'une représentation en profil de cette activité, semblable à celle que donne un scintigramme linéaire établi au moyen d'un collimateur à fentes.

* Operated by the University of Chicago for the United States Atomic Energy Commission

La même méthode fondée sur l'emploi d'une multi-échelle peut être étendue de manière à accumuler les données numériques en vue d'une représentation des «coups par unité de surface». On obtient une courbe en profil pour chaque ligne de balayage correspondant à un degré de densité de l'échelle. Ces courbes permettent la visualisation du taux de comptage pour la région considérée ou l'établissement d'une carte en profil.

Des scintigrammes avec ou sans accentuation du contraste et avec ou sans «retard» dû au circuit d'intégration, et des scintigrammes à traces de dimensions et de formes différentes ont été obtenus dans les conditions statistiques identiques, au moyen de relevés multiples, lors de l'exploration d'un fantôme à l'aide d'un système à un seul détecteur. La comparaison directe de scintigrammes, associée à la représentation cartographique des coups par unité de surface, facilite l'interprétation des résultats.

Les positions exactes des appareils doivent être indiquées dans les enregistrements. La différence relative (exprimée en pourcentage) de l'activité qu'accusent les régions à examiner sur les faces opposées de la tête est calculée à partir des données accumulées grâce à la multi-échelle dont est muni le dispositif de scintigraphie du cerveau du Cancer Research Hospital d'Argonne.

МЕТОДЫ,ОБЛЕГЧАЮЩИЕ КОЛИЧЕСТВЕННУЮ ИНТЕРПРЕТАЦИЮ ДАННЫХ СКЕННИРОВАНИЯ. В настоящем докладе обсуждается ряд методов, облегчающих оценку и интерпретацию данных сканирования. Этот ряд простирается от простой внутренней калибровки для расшифровки фотопленок до довольно сложного вспомогательного оборудования для представления накопленных цифровых данных сканирования в виде, пригодном для составления программ для электронных пересчетных устройств.

Непосредственный и чрезвычайно полезный метод использования генератора беспорядочных импульсов служит для нанесения калиброванных уступчато-клинообразных отметок, которые проектируются на пленку тем же самым источником света, который используется во время сканирования; это дает возможность просмотровой головке сравнивать плотность облучения изучаемых зон сканирования с аналогичными зонами на клинообразных отметках, которые калиброваны непосредственно в единицах скорости счета.

Вспомогательное оборудование, как например многоканальный анализатор, используемых при способе множественных счетов, позволяет накоплять цифровую информацию для получения "общего числа счетов на строчку сканирования" для каждого шага показателя.

Было проведено сканирование мелких животных, которое позволяет накоплять данные и давать "число счетов на строчку сканирования" для каждого шага показателя. Это дает точное количественное измерение распределения активности в теле животного, а также изображает профиль активности, аналогичный тому, который получается при щелевом линейном сканировании.

Тот же самый метод множественных счетов применяется и далее путем накопления численной информации для получения "числа счетов на единицу площади". Для каждой строчки сканирования каждого шага показателя получается отдельная кривая профиля. Это дает возможность определять скорость счета или строить соответствующий профиль для каждой площади.

Показания сканирования с усилением контраста или без него, а также с "отставанием" или без него в интегрирующем контуре диаграммы сканирования с различными размерами и формами пятен были получены в идентичных статистических условиях при помощи многократного сканирования фантома одним детектором. Непосредственное сравнение этих показаний совместно с методом составления графиков "числа счетов на единицу площади" облегчает толкование результатов сканирования.

Зарегистрированные данные должны включать информацию о точном положении детектора.

На основании данных, накопленных в Аргонской больнице по изучению рака прибором для сканирования мозга, были подсчитаны процентные расхождения радиоактивности в изучаемых противоположных частях головы.

TÉCNICAS QUE FACILITAN LA INTERPRETACIÓN CUANTITATIVA DE LOS DATOS CENTELLEOGRÁFICOS. La memoria trata de diversas técnicas que facilitan la evaluación e interpretación de los datos centelleográficos. La más sencilla es la simple calibración interna de representaciones fotográficas; en las más complicadas se emplea un equipo auxiliar bastante complejo para alimentar una calculadora electrónica con los datos numéricos acumulados durante la exploración.

Un método directo y sumamente útil consiste en emplear un generador de impulsos aleatorios para producir una cuña escalonada y calibrada de puntos que se proyecta sobre una película por medio de la misma

fuente luminosa empleada durante la exploración. Ese método permite comparar las densidades de exposición en las regiones de interés del centelleograma con regiones similares de la cuña, directamente calibradas en unidades de índice de recuento.

El equipo auxiliar, entre el que figura un analizador multicanal empleado en forma de multiescalímetro, permite acumular la información numérica para obtener para cada escalón del índice una presentación según el «recuento total por línea de exploración».

Por este procedimiento se han explorado animales pequeños y se ha obtenido una medición cuantitativa exacta de la distribución de la actividad en todo el animal y un perfil de actividad similar al que se obtiene al emplear un sistema de exploración lineal mediante rendija.

Esa técnica multiescalimétrica se completa acumulando información numérica para presentarla en forma de «cuentas por unidad de superficie». Se obtiene un perfil para cada línea de exploración correspondiente a cada escalón del índice y el conjunto de estos perfiles permite construir el diagrama tridimensional del índice de recuento en aquella área. Los autores han explorado un simulador con un detector único. Empleando lecturas múltiples han obtenido en idénticas condiciones estadísticas representaciones centelleográficas con o sin acentuación del contraste y con o sin retardo en el circuito integrador, y centelleogramas de puntos de diversas formas y tamaños. La comparación directa de las representaciones combinada con el trazado de un gráfico de «cuentas por unidad de superficie» ayuda a interpretar los resultados de la exploración.

Al registro de los datos deben añadirse informaciones exactas sobre la posición. El sistema de exploración del cerebro del Argonne Cancer Research Hospital permite calcular las diferencias percentuales de actividad en las regiones de interés situadas en lados opuestos de la cabeza, a partir de los datos reunidos por multiescalimetría.

INTRODUCTION

As scanning systems have become more sophisticated and we become more critical of artifacts, there has been a trend towards the increased use of auxiliary equipment and techniques which aid in the interpretation of scan data.

Conventional scanning systems must be designed to avoid irregularities in mechanical function. Scanning speed and index step widths must be precise and consistent to avoid the introduction of modulation by speed variation and irregularities in line width structure. Studies of human perception indicate that contours which are discontinuous [1] or imbedded in a system of parallel lines [2, 3] tend to be concealed. In a fairly uniform scan picture (Fig. 1) small gaps in mechanical operation can be most disturbing. For example, the line seen in the middle of the scan appears to be an omitted scan pass in our 0.0625-in (0.158-cm) index step pattern. Actually it is a mechanical error which presents a gap of 0.008 in (0.02 cm) between the two halves of the scan. It is most obvious to the eye and upsets the viewers' interpretation of the scan film. An overlap of the same magnitude is equally disturbing. Even with the elimination of machine-made irregularities, statistical deviations alone present the observer with enough confusion to warrant the use of aids for the interpretation of scan pictures. Some of the aids presented in this paper have been incorporated into the Argonne Cancer Research Hospital's brain scanning system, which has four scintillation detector channels (two on each side of the head) that operate simultaneously.

The Argonne Cancer Research Hospital's brain scanning system produces two films simultaneously, each representing activity distributions for opposite sides of the head. The opposing pairs of detectors have direct mechanical linkage with the projector pairs which produce the Gaussian spots

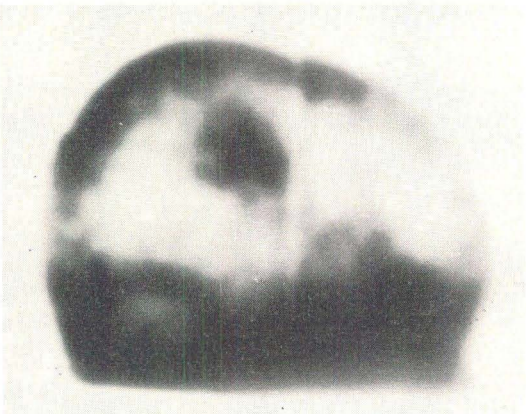

Fig. 1

Reproduction of a scan read-out film which demonstrates how obvious a small (0.008 in) gap can be in an otherwise uniform and smooth display

on separate films. It is possible to compare relative count levels on opposite sides of the head by film examination. An off-centreline "hot spot" or tumour will show a greater intensity on the film corresponding to the side nearest the tumour. A mid-line tumour will show equally well on both sides.

With relatively low-energy isotopes, tumours on one side of the head are most likely to be seen by the detector on that side only; the opposing detector can sense very little because of attenuation through the greater path length in the head. It has been shown [4] that the optimum energy for scanning a standard 16-cm head is approximately 100 keV, if scatter effects are neglected.

With use of higher energy gammas the off-centre tumour may be seen by both detectors, and it becomes increasingly important to determine which side receives the greater number of counts so that tumour depth may be estimated.

The tumour position might be determined accurately by making both anterior-posterior and lateral scans of the head. In some cases, however, the tumour may be evident in one view and hidden by normally active regions in line with the tumour in the other. In such cases additional data that aid in estimating the position of the tumour are most welcome.

The technique used to aid interpretation of scan data may be divided into two categories, digital (or numeric) and analogue.

DIGITAL OR NUMERIC TECHNIQUES

These techniques make use of the numbers of counts detected in small regions of the total area scanned.

When fast sweep speeds are employed, ratemeters and integrators are too slow to follow abrupt changes in count rate without spatial displacement or "scalloping", and fast digital recording is therefore preferable to ana-

logue read-out. A multichannel analyser system was used as a digital data logging and read-out device for feasibility studies. The digital recorder (in this case a multichannel analyser) with a direct linear read-out display is convenient for these measurements.

A multichannel analyser used in the multi-scaling mode can be a useful aid for scan data interpretation. The technique is simple. Each single channel of a multichannel analyser can be used to act as a separate scaler or count register for any predetermined interval of time, at the end of which the analyser can be switched to the next higher channel or "scaler". The unit therefore can substitute for a number of scalers or counters.

For use in scanning systems the multi-scalers can be employed to accumulate the total count for each scan sweep in a separate channel (every index step advances the multi-scaler to the next higher channel). This accumulated count-per-scan-line will hereafter be referred to as "count-per-index" to differentiate it from another method which uses the multi-scaler to accumulate counts within fixed increments of the distance along the sweep line. This approach will be referred to as the "count-per-increment" method.

The digital count-per-index data display is comparable to a linear scanner display obtained with a slit collimator, ratemeter and an analogue read-out. Both systems present a profile display along the axis of the region scanned.

The Argonne Cancer Research Hospital's small animal scanner system [5] uses the count-per-index technique to plot a profile of the distributed activity (Fig. 2). The linear display feature of the multichannel analyser is a direct quantitative aid to eye interpretation of the mouse scan photo read-out.

The scan in Fig. 2 was produced by indexing horizontally with 1/24 in steps, and vertically with the scanning sweep motion. It is obvious that a profile display produced with the mouse rotated 90° would be less helpful for interpretation of the scan picture. A combination of the two views might be of help, but a repeat scan would be necessary.

From the data accumulated in this way it is possible to determine quantitatively the total amount of activity in the animal (a sum of all counts accumulated, divided by the scan time over the animal), and the percentage of total activity in any region of the scan.

Scanning of large organs presents a much more complex problem to this method of quantitative interpretation of data. For large, usually rectangular scans of liver, pancreas, lungs, kidneys, thyroids or brain, the count-per-index system will accumulate information about activity within the entire rectangular scan region in such a way that it is impossible to separate regions of interest from regions of non-interest that are in the same line as the scan sweep.

A more useful technique for large area scans can be achieved by producing a profile display for each scan sweep.

Studies have been made using the Argonne Cancer Research Hospital's brain scanning system with multichannel analyser in the multi-scaling mode, where each channel corresponds to the count accumulation in 1/4 in (0.635 cm) increments along each scan sweep.

A simple phantom study was undertaken to establish the feasibility of the count-per-increment method, using as phantom a 6-in diam. (15.24 cm)

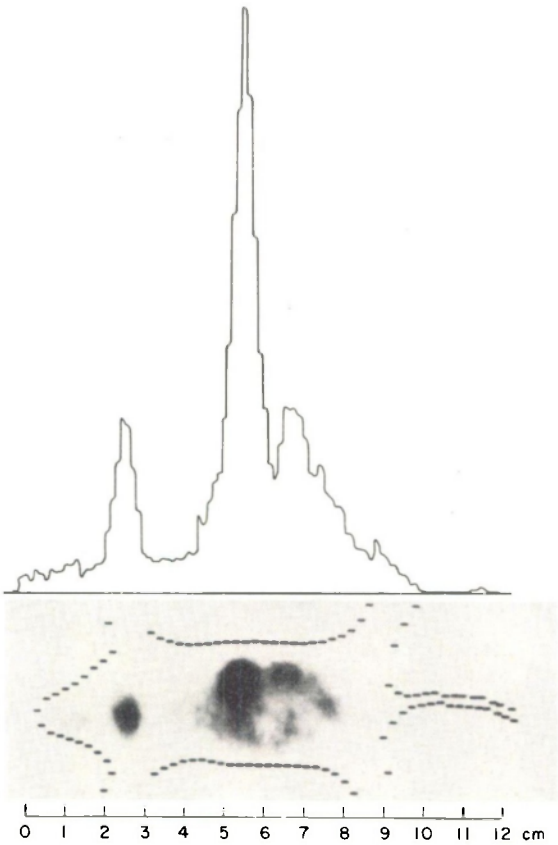

Fig. 2

Above

A profile graph of the activity distribution recorded on a multichannel analyser

Below

A scan picture presentation of the distribution of Tc^{99m} in a mouse four hours after injection. Note the absence of gross line and spot structure.

plastic container filled with a mercury solution containing 0.2 μc per cm^3 of Hg^{203}.

Three "tumours" were positioned off centre line in the container (Fig. 3). These tumours were made up as 1 in, 3/4 in and 1/2 in diam. spheres, each filled with Hg^{203} in a concentration 7 times that of the surrounding liquid to simulate a 7 to 1 uptake ratio.

Scans were made with 1/16 (0.158 cm) index steps, each scan sweep being broken up into 1/4 in sections which were recorded sequentially in separate channels of a multichannel analyser.

Each scan sweep profile accumulation was stored on magnetic tape, and adjacent profiles were summed in blocks of 4 to construct a matrix layout of 1/4 × 1/4-in squares over the scanned area (Fig. 4). The read-out film was analysed by direct comparison with a number overlay on the film.

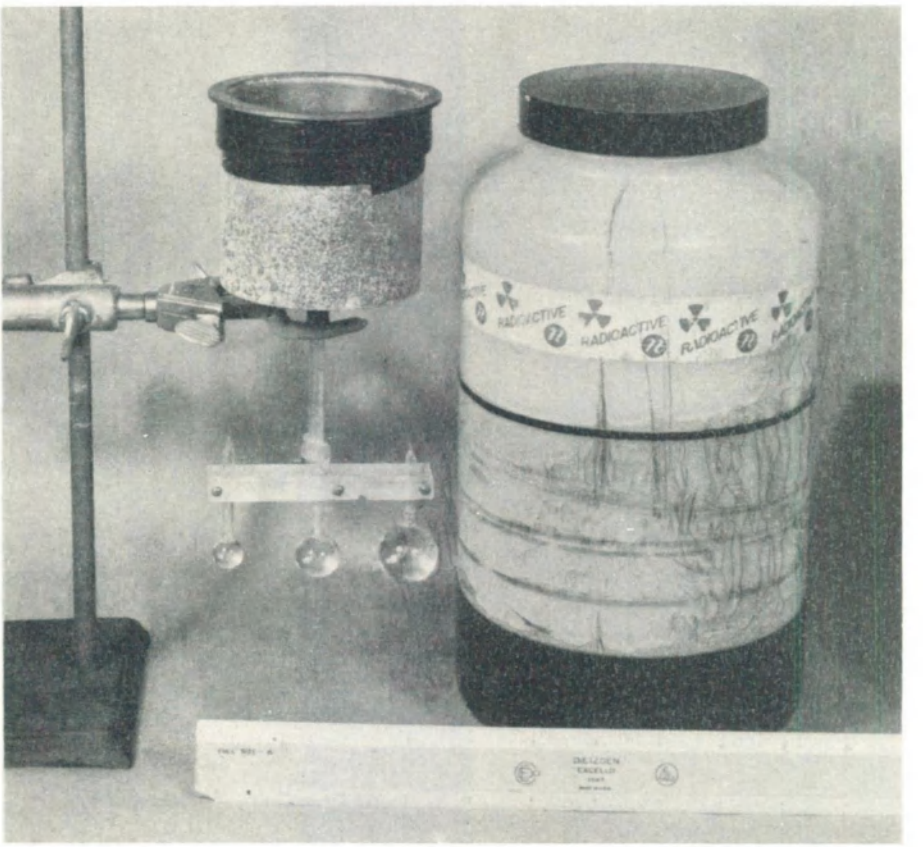

Fig. 3

Photograph of the "head" phantom used to produce test films and data for both digital and analogue data processing. The sealed glass vials represent the "tumours" which may be positioned anywhere within the container.

By photographing the count-per-increment digital read-out in a slightly displaced sequence, an apparent three-dimensional display is produced (Fig. 5) which can be compared directly with the read-out photograph. Position information must be retained to interpret this count rate profile.

The curve A in Fig. 5 is equivalent to the count-per-index accumulation display and represents the sum of all the curves on the left side of the picture. Curves B and C indicate positively that there is increased activity in two of the tumours. Display D is made by scanning off the tumour region and it outlines the container activity alone. The series of curves gives a better insight into the count distribution over an area of interest.

A model (Fig. 6) was constructed using the digital information obtained from the phantom studies previously described. The numbers displayed in the matrix of Fig. 4 were used to determine the scale length of the 1/4-in-diam. rods. To make a model for each scan would be unreasonable, but

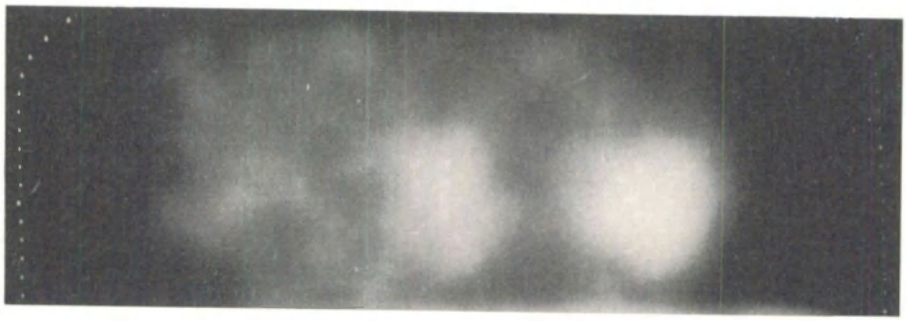

	1	2	3	4	5	6	7	8	9	10	11	12	13	14	15	16	17	18	19	20	21	22	23	24
1	49	72	111	124	130	140	144	147	147	150	152	158	147	150	139	147	150	155	144	140	120	100	72	40
2	46	66	125	126	132	145	137	150	140	156	159	175	139	154	140	151	149	149	130	158	121	108	80	35
3	45	83	102	116	127	125	134	172	143	170	144	166	171	153	162	163	180	183	164	167	124	113	73	33
4	47	75	110	129	120	140	157	147	156	163	167	193	167	170	129	164	195	214	204	152	134	108	76	41
5	51	79	116	130	147	154	162	165	143	197	174	197	194	159	169	171	219	208	242	190	144	99	91	31
6	52	89	111	133	133	158	130	156	145	170	167	162	145	152	169	157	178	207	190	168	128	115	79	41
7	56	89	92	124	132	155	138	167	159	146	173	166	160	167	135	159	152	165	146	145	145	100	86	49
8	46	80	109	121	135	141	143	145	157	135	147	153	152	154	163	115	159	159	154	124	110	98	68	24

Fig. 4

A photocopy of a film read-out made from a phantom scan is shown over a matrix display of the actual counts accumulated per unit area during the scan

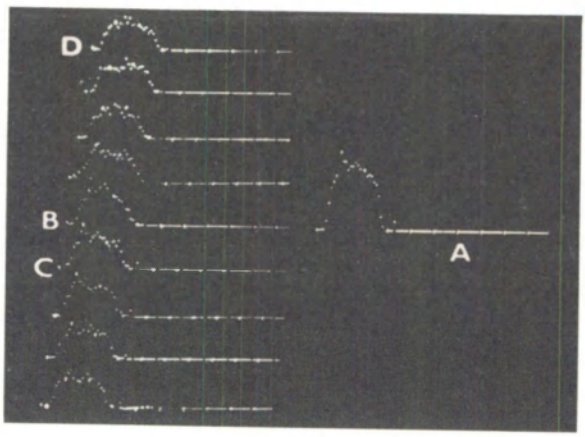

Fig. 5

Reproduction of a polaroid photograph of displaced scan sweep count-rate profiles. Nine "slices" are displayed on the left, and the sum of these profiles is shown at the right.

the example does demonstrate the difficulty inherent in the detection of small tumours in a large volume of surrounding activity with any degree of statistical validity.

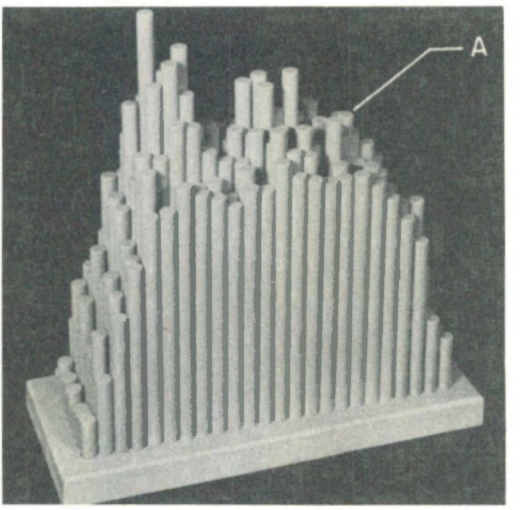

Fig. 6

Photograph of a model constructed using the data accumulated from a brain phantom scan. The rod lengths were scaled to represent the numbers stored in the matrix of Fig. 4.

It can be seen from the model that the 1/2-in "tumour" (A in Fig. 6) would not have been verified from the scan photograph. There is a faint indication on the film, but statistically this would not justify a positive decision. The same scan made with contrast enhancement can produce a darker spot in this region, but is likely to produce a "false positive" spot in some other region due to statistical fluctuations.

Data accumulated and stored by the multi-scaling method can be presented by tape to a digital computer programmed to produce a series of matrices with numbers printed in each area cell similar to the small section shown in Fig. 4 from which our model was constructed. A series of cell areas with varying sizes can be printed out by the computer, summing groups of smaller cells to make a coarse cell matrix. A two-dimensional matrix display of this type is difficult to interpret by itself, but is useful as an overlay on a film read-out for direct comparison.

A 7094 computer was programmed to perform a variety of statistical measurements on such matrices of numbers, with the idea of comparing each cell with its neighbours (or groups of neighbours) to determine whether or not the measurements were significantly different. It might be expected that any tumour that was detectable by visual inspection could be found with at least equal reliability by a computer programmed to determine the statistical significance of the data. Although several (admittedly simple) programmes were tried, they tended to reveal more problems than they solved. The statistical analysis may be formulated as follows. If N_0 and N_t are the numbers of counts in adjacent cells, the question is whether or not these counts come from the same "population" or the same true mean count-rate. Such counts are Poisson distributed and therefore have standard deviations of $\sqrt{N_0}$ and $\sqrt{N_t}$ respectively. The difference, $(N_0 - N_t)$, has a standard deviation of $\sqrt{N_0 + N_t}$. To test the statistical significance of the difference we

form the "null hypothesis" that the observed counts do in fact represent the same count-rate. This hypothesis is rejected whenever the observed difference exceeds a certain "critical level" corresponding to a certain number of standard deviations. The standardized variable, Z, is defined by $Z = (N_0 - N_t)/(N_0 + N_t)^{\frac{1}{2}}$. Thus, when Z exceeds the critical level, Z_c, the hypothesis is rejected. Even when the hypothesis is true, there is a certain probability of observing a difference that exceeds the critical level, and this probability depends on where Z_c is set. For $Z_c = 1$, the probability of deciding incorrectly that the count-rates are different is about 32%; for $Z_c = 2$, this probability drops to about 5%. By making Z_c large, this kind of error ("false positive" or error of the 1st kind; also called α error) can be made arbitrarily small, resulting in an increased probability of deciding that there is no difference when one actually exists (this amounts to not finding tumours which exist, and is sometimes called an error of the 2nd kind or a β error). One solution is to set the critical level, Z_c, midway between zero and the observed standard variable, i.e. $Z_c = Z/2$. This indicates the value that might be given Z_c to establish a test that would take into account both types of error.

Stored data from the matrix and film strip shown in Fig. 4 demonstrate the digital computer techniques used in the search for a method to aid in the evaluation of scan data.

In this simple example the smallest unit area "cell" was the 1/4-in square. The counts-per-unit cell varied from about 40 to 240 counts, with an average of approximately 120 counts. A tumour will present itself as a sum of counts over an area which is proportional to the cross-sectional area of the tumour. To determine the presence of a tumour from the stored data, the number Z_c as defined previously was calculated for any two given areas. The problem of defining the area which is to be compared to the unknown tumour area was approached in three different ways.

The computer was programmed to determine the Z_c between a unit cell area with each of its neighbour cells, with the average for any three neighbour cells, and with the average for the sum of its eight neighbour cells.

These three methods offered little in the way of a definite demonstration of tumour size or location when referred to the model of Fig. 6. Other computer programmes have been written to compare the unit cell with groups of adjoining cells. This study is still under way and the results will be presented in a subsequent paper. It could be argued that the cell and area sizes selected for comparison were too small, but it would be almost impossible to define these areas without some pre-knowledge of the suspect region.

A fourth method, which used the information derived from the film readout, was employed. The indicated tumour areas were compared with areas round the tumour that were equivalent in terms of their geometric form as well as size. These calculations were considered meaningful, and confirmed the opinion that a small tumour could not be verified with any degree of confidence.

A digital computer can be programmed to produce contour displays from stored scan data. Contour studies have been made of frequency distributions obtained from multi-parameter analysers for fission fragment experiments [6]. The basic studies differ, but the data display and reduction techniques are directly applicable to scanning data reduction.

Contour plots can be generated by computer from the digital numbers obtained per unit area from a scan matrix but these plots are sensitive to the pre-selected contour intervals. Peaks can be falsely indicated or omitted by selection of improper intervals. If many intervals are taken the observer is faced with a massive quantity of information, a wide range of contours, and great numbers of false peaks. It is more difficult to evaluate a series of contour plots produced by a computer than it is to analyse a film read-out display directly by eye.

Although much has been done to improve digital computer analysis and read-out presentation of virtual three-dimensional information, especially in the field of nuclear physics utilizing multi-parameter analysers, the programmes are highly sophisticated, the auxiliary equipment is expensive, and the machine time is considerable.

ANALOGUE TECHNIQUES AS AIDS FOR INTERPRETATION OF SCANNING DATA

Film can be used as both a read-out display and a storage medium for further data reduction. It is possible to operate on the information content of the film to obtain considerable aid to quantitative interpretation.

The logarithmic response of film permits it to accept several decades of exposure between the lower fog level and the upper saturation region. If each detected event produces a spot density just above the fog level of the film, it is possible to display one or one thousand spots in one place without reaching the saturation level. This rate exceeds the highest expected display rate in any one spot because the scanner is always moving.

Counts are stored on film as they are detected without the "cell size" position ambiguity inherent in direct digital data logging for computer use.

Provided no data manipulation such as enhancement control, background erase, integrating circuitry time-lag, or mechanical modulation, enter into producing the film read-out, it is possible to store and retrieve nearly all information from the film and to perform the data manipulation with simple inexpensive auxiliary equipment. Contrast enhancement and background erase manipulations can be performed on the film read-out after the scan is completed by the closed-circuit television enhancement technique introduced by M.A. BENDER in 1959 [7], or by direct photocopy of the original with different contrast film and/or varying exposures (Fig.7). The closed-circuit television method has advantages in that it is simple to operate and the original film can be examined visually for direct comparison with the television picture.

The Argonne Cancer Research Hospital's brain scanner has an internal calibration system which produces a graduated step-wedge display of random pulses. This unit has been a valuable aid to quantitative analysis of scan film displays (Figs.8 and 9).

The basic components of the step-wedge calibrator are: a line source of β activity (thallium-204), a low (0.76 MeV) energy β with a fairly long half-life (3.6 yr), a stepped window-like shield (C) and a simple Geiger counter detector system with a shield (E). The line source is sealed in a thin polyethylene tube which is inserted (B) into a shield consisting of an

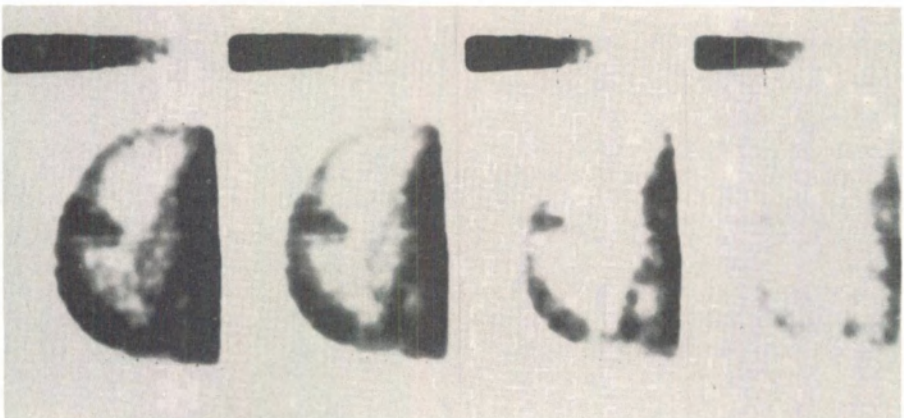

Fig. 7

A series of photocopies which were made by varying the exposure time for printing. The same effect can be obtained by use of closed-circuit television enhancement.

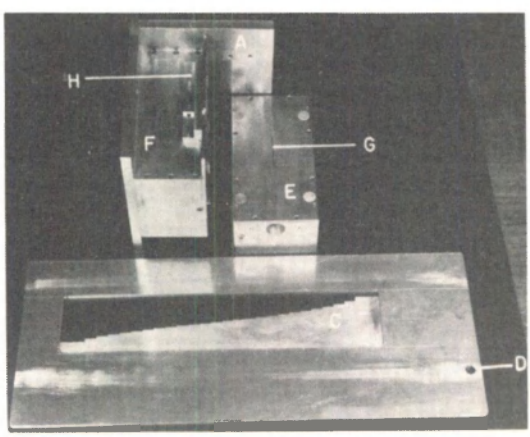

Fig. 8

Photograph of component parts of the step-wedge calibration device which is permanently mounted to the brain scanner.

aluminium inner liner (to eliminate Bremsstrahlung radiation) and a lead outer shield (F). The source is held vertically in the same plane as the Geiger tube centre wire. Both the Geiger tube and the line source have slit collimation (G) to ensure good resolution of the step-wedge. The source collimation slit is made adjustable (H) to correct for the beta source half-life.

The step-wedge (C) is made of an aluminium-lead-aluminium laminate to prevent Bremsstrahlung radiation effects. The step-wedge window is designed to generate 20% changes in count-rate per step for 26 steps over

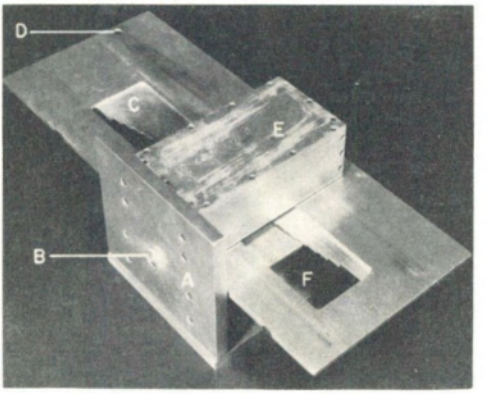

Fig. 9

Assembled step-wedge random pulse calibrator.

the count-rate range of 100 to 9500 counts/min as the window is drawn between the source and detector. The detector and source shields are held in a frame (A) and mounted to a stationary part of the machine, and the step-wedge window is fastened at (D) to the moving scan mechanism so that it may be drawn back and forth between the source and detector. As the unit scans, a graduated line of exposure densities is projected on a section of the film by the same projector light system used for producing the actual scan picture. The width of this calibrated exposure wedge can be adjusted by changing the number of index steps used.

A device of this type, constructed for use with the Argonne Cancer Research Hospital's brain scanning system, has been a valuable aid for film interpretation. Similar units will be incorporated into our other scanning systems.

Although the unaided eye can compare any region of a scan picture's exposure density to an equivalent exposure density on the calibration wedge, it is even more helpful if viewed by means of the closed-circuit television technique. As the contrast and intensity controls are varied, regions of interest can be enhanced or erased, and equivalent regions on the calibration wedge will be enhanced or erased to the same degree. One can quickly evaluate the density of the darkest spot on the scan picture by erasing all but that region and comparing it directly against the remaining edge of the exposure wedge (Fig. 7). Exposure densities of 20% differences can be distinguished.

A densitometer or flying-spot-scanner can be used to plot film density contour lines (count rate contours) to aid the visual interpretation of films. Provided the film exposure densities are continuous, useful flying-spot plots of contour lines can be made without gross line or spot structure. Small index steps, fast scanning, and projection of relatively large Gaussian spots on film, are combined to produce smooth film displays from the Argonne Cancer Research Hospital's brain scanner.

A comparison of contour plots made from films that contained identical statistical data but used different spot sizes is shown in Fig. 10. The larger 1/2-in Gaussian spots produce a smoother picture and smoother contour

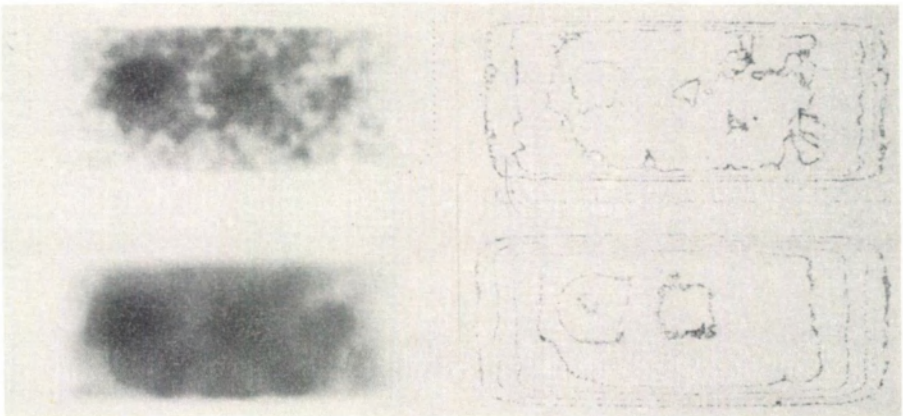

Fig. 10

Photographs of isodensity contour plots made from the films on the left. The spot sizes used were 1/4-in Gaussian for the upper pictures and 1/2-in Gaussian for the lower pictures.

lines. One-quarter-inch Gaussian spots produced the more ragged, less informative, contour plot.

A typical brain scan isodensity plot is shown in Fig. 11. The upper picture was produced by normalizing the upper level of the isodensity plotter to the most dense region on the film and then plotting the 90%, 80%, 60%, 40%, 20% and 10% contour lines. The lower picture shows only the 90%, 80%, 50% and 20% lines. The full range of isodensity lines at 10% intervals can be plotted simultaneously or singly at any density level selected. These lines can be compared with the calibration step-wedge by mapping each contour level separately and noting the corresponding line or the wedge. A flying-spot-scanner system would be faster and more versatile. A dual-beam system is at present being devised which will combine the features of the closed-circuit television read-out and the isodensity plotter and will be used to compare count-rate information contained in the two films (left and right sides of the head) produced simultaneously by the brain scanner. A simple analogue system will be arranged to compute and read out the percent differences in count-rate between identical regions on the two films.

CONCLUSIONS

While the digital techniques offer accurate, undistorted (except for finite cell size) recording of the scan data, the computer techniques for manipulating the data are quite complex. The analogue techniques are less accurate, in the sense that the numerical data is lost, but appear at present to offer a wider range of simple convenient manipulative procedures.

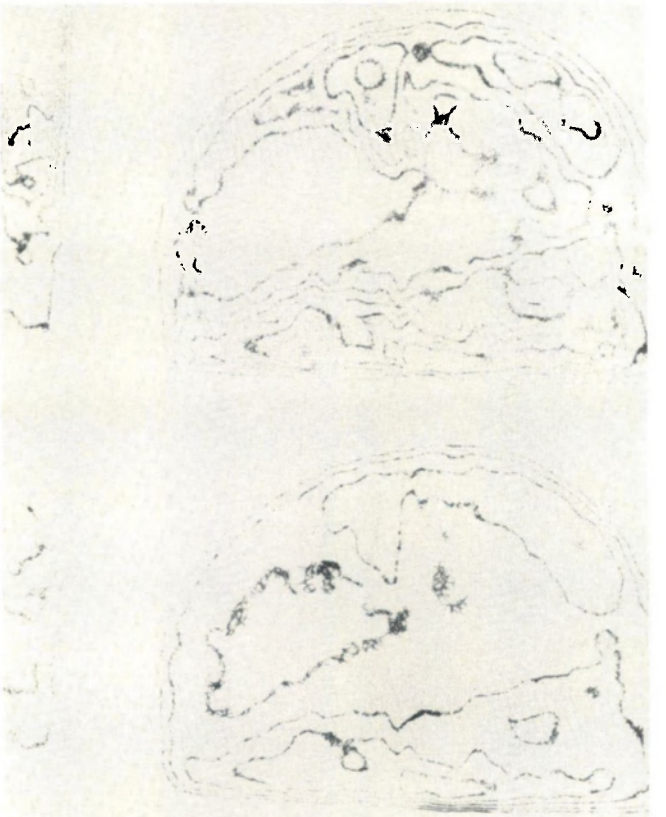

Fig. 11

Above
Photograph of a brain scan contour plot showing six contour intervals.

Below
The same scan showing only four contour intervals.
In both cases the top line of the step-wedge on the left indicates the level of the most dense spot on the film.

ACKNOWLEDGEMENTS

The authors wish to thank Dr. L.O. Jacobson and Dr. Paul V. Harper for their continued interest and active support of these studies.

REFERENCES

[1] TITCHNER, E.B., A Textbook of Psychology, Macmillan Co., New York (1911) 327.
[2] OSGOOD, C.E., Method and Theory in Experimental Psychology, Oxford University Press, New York (1953) 230.

[3] WOODWORTH, R.S. and SCHLOSBERG, H., Experimental Psychology, Henry Holt, New York (1956) 415.
[4] HARPER, P.V., BECK, R.N., CHARLESTON, D. and LATHROP, K.A., Nucleonics 22 (1964) 50-4.
[5] BECK, R.N. and CHARLESTON, D., Intern. J. appl. Radiat. Isotopes 15 (1964) 101.
[6] Proceedings, Conference on the Utilization of Multiparameter Analyzers in Nuclear Physics, November 1962, Columbia University, New York. Office of Technical Services, Department of Commerce, Washington, D.C. CU(PNPL)-227, NYO-10595.
[7] BENDER, M.A. and BLAU, M., in Medical Radioisotope Scanning, IAEA, Vienna (1959) 31.

DISCUSSION

R. HERBERT: I was interested in your use of a random stepwedge for the calibration of photoscans. We use a regular pulse train produced by a signal generator and we vary the frequency. Do you think that random pulses are preferable to regular pulses and, if so, do you think they could be conveniently produced by an electronic noise generator?

R. BECK: I believe there are advantages in using a random wedge. The first calibrator we built produced regular pulses but we had a certain amount of difficulty in associating the regular density patterns with the regions on the scan that were produced by the same, though random, count rate. As for the noise generator, I do not know of any simple way of accurately controlling the frequency of such a device in the manner that would be required. I suppose this is mainly a practical problem of coupling the generator to the scanner.

R. HINDEL: I have a question in connection with the bell-shaped density function of the photo-dots. Did you correlate this with the design of the collimator or was it just part of the attempt to obtain a smooth photoscan?

R. BECK: The original idea was to record a spot which would duplicate the point-source response pattern at the focal distance. In our brain-scanning system we have not quite done this. Our collimators have a $\frac{3}{4}$-in-diam. field of view at the focal distance and we record $\frac{1}{2}$-in-diam. bell-shaped spots. This is large enough to produce a smooth photoscan with almost no line structure or spot structure. We think that the smooth photoscan is preferable to one containing either line or spot structures, especially if contour-plotting or contrast-enhancement techniques are used.

M. TUBIANA: We also make use of a system in which the profiles are recorded at each sweep of the detector. We obtain so many curves, however, that we find it difficult to analyse them. I suppose the only solution is to use a computer, as you do.

R. BECK: I agree that the quantity of data presents a real problem. A computer certainly helps but there is always the problem of deciding what sort of analysis should be carried out. Contour plots can be made fairly simply from numerical profile data but no more simply than from a photorecording.

M. TUBIANA: The information obtained with this technique is presented quantitatively but there is no increase in the actual number of items of information. Usually, however, scintigrams contain zones of minor interest side by side with suspicious zones. The latter may cover only a small surface area but it is often necessary to accumulate a considerable amount of information from them for the clinical interpretation. In such cases, do

you not think it would be better to make a fairly rapid scintigram and then follow up with a detailed study of the critical regions? It seems to me that this would yield the maximum amount of clinically useful information in the time available.

R. BECK: We have not attempted such a division of the scanning time, but it might in certain situations be valuable. With Tc^{99m} the total scanning time for simultaneous lateral brain scans is only about 15 minutes, so that there is no reason to divide it.

VI

DISPLAY SYSTEMS
(cont.)

ANALYSIS OF SCAN RECORDS WITH A RECORDING DENSITOMETER*- THE "RE-SCANNER"

C. C. HARRIS, P. R. BELL, M. M. SATTERFIELD, D. A. ROSS
AND J. C. JORDAN
OAK RIDGE NATIONAL LABORATORY, TENN.
UNITED STATES OF AMERICA

Abstract — Résumé — Аннотация — Resumen

ANALYSIS OF SCAN RECORDS WITH A RECORDING DENSITOMETER – THE "RE-SCANNER". The impact of improvements in scanning equipment has not been fully felt at the clinical level, largely because of deficiencies in scan recording. In an attempt to improve visualization and contrast in scan records, various instrumental methods of analysis have been devised.

We have devised a simple and comparatively inexpensive recording densitometer for "re-scanning" scan records. A light-sensor scans the record just as a scanner scans a patient. The output of the device is a pulse rate proportional to the opacity (or transmission) of the record, and may be used to make a new, or "re-scan", record. The area of the record over which information is integrated is set by sensor aperture. The wide range of output pulse-rates (zero to 15 000 parts/s) causes large and adjustable contrast amplification. A threshold control provides any "cut-off level" of choice. Operation is rapid, and a record can be re-scanned in a small fraction of the time required to obtain the original record.

Studies on clinical scans of almost every organ or area of interest show that the re-scanner reveals information not at first evident in original scan records. It has been particularly useful in determining the statistical significance of small variations in counting rate in a scan record.

In scan records of large dynamic range where no single cut-off level satisfactorily shows all regions of interest, re-scans at several cut-off levels were once necessary. A two-region sensor, that views a region of the record around the field of view of the main sensor, has been used in an attempt to overcome this difficulty. At least three modes of operation are possible with the two-region sensor: (1) "normal" operation; (2) ignoring general record density and responding only to small variations, thus setting its own cut-off level; and (3) reporting only abrupt changes in record density. Other modes seem to be possible.

This relatively simple and inexpensive device is proving to be of valuable assistance in the interpretation of scan records.

ANALYSE DE SCINTIGRAMMES A L'AIDE D'UN DENSITOMÈTRE ENREGISTREUR. Les perfectionnements des appareils de scintigraphie n'ont pas eu d'effet comparable sur le plan clinique, surtout en raison des imperfections des enregistrements scintigraphiques. En vue d'améliorer la visualisation et le contraste des scintigrammes, on a mis au point divers appareils d'analyse.

Les auteurs ont conçu un densitomètre enregistreur, assez simple et relativement peu coûteux, qui permet de «scintigraphier» les scintigrammes. Une cellule photoélectrique explore le scintigramme, tout comme un détecteur à scintillation explore le patient. Les impulsions à la sortie de l'appareil sont proportionnelles à la densité du scintigramme et elles peuvent être utilisées pour établir un nouvel enregistrement. La surface du scintigramme pour laquelle on intègre les informations est déterminée par l'ouverture de la cellule. La gamme étendue des impulsions à la sortie (de zéro à 15 000 impulsions/s) permet d'amplifier fortement et à volonté le contraste. Un dispositif spécial permet de choisir à l'avance un «seuil de coupure». L'opération est rapide, si bien qu'un scintigramme peut être exploré en une fraction du temps qui avait été nécessaire pour l'établir.

L'étude de scintigrammes cliniques de presque tous les organes ou régions intéressants a permis de constater que le densitomètre enregistreur révèle des informations qui n'apparaissaient pas clairement sur le scintigramme. Cet appareil a été particulièrement utile pour déterminer la signification statistique de légères variations du taux de comptage dans un scintigramme.

* Research sponsored by the United States Atomic Energy Commission under contract with the Union Carbide Corporation.

Pour les scintigrammes représentant de fortes variations de la radioactivité, où un seul seuil de coupure du densitomètre ne donne pas une image satisfaisante de toutes les zónes intéressantes, il fallait autrefois faire plusieurs explorations avec différents seuils de coupure. Pour surmonter cette difficulté, on a eu recours à une cellule à deux plages qui explore le scintigramme autour du champ de vision de la cellule principale. On peut l'utiliser d'au moins trois manières: a) normalement; b) sans tenir compte de la densité générale du scintigramme, pour n'accuser que de faibles variations de la densité (en fixant alors son propre seuil de coupure); c) pour n'enregistrer que de brusques variations de la densité du scintigramme. Il semble que d'autres modes d'utilisation soient également possibles.

Cet appareil, relativement simple et peu coûteux, se révèle extrêmement utile pour l'interprétation des scintigrammes.

АНАЛИЗ СКЕНОГРАММ С ПОМОЩЬЮ РЕГИСТРИРУЮЩЕГО ДЕНСИТОМЕТРА–"РЕСКЕННЕР". Влияние усовершенствований в скеннирующем оборудовании не чувствовалось полностью на клиническом уровне в значительной мере ввиду недостатков регистрации скеннограмм. Для улучшения изображения и контрастности при скенниоровании были разработаны различные инструментальные методы анализа.

Авторы создали простой и сравнительно недорогостоящий регистрирующий денситометр для "повторного скеннирования" скеннограмм. Легкий чувствительный элемент скеннирует диаграмму точно также, как скеннер пациента. Мощность устройства является равной коэффициенту импульса, пропорциональному непрозрачности (или передаче) изображения и может использоваться для того, чтобы сделать новое или "рескеннированное" изображение. Площадь диаграммы, с которой обобщается информация, устанавливается отверстием, снабженным чувствительным элементом. Широкий диапазон коэффициентов мощности импульсов (от 0 до 15 000 импульсов в секунду) вызывает значительное и регулироемое увеличение контрастности. Пороговый контроль дает любой "сокращенный уровень" выбора. Работа проводится быстро, и диаграмма может быть рескеннирована в течение небольшого промежутка времени, необходимого для получения первоначального изображения.

Исследования в области клинического скеннирования почти любого органа или района, представляющего интерес, показывают, что реразвертыватель дает информацию, не видимую сначала на диаграммах при первоначальном скеннировании. Это было особенно полезным при определении статистического значения небольших изменений в коэффициенте счета при скеннирующем изображении.

При диаграммах, полученных методом скеннирования, большого динамического диапазона, гле никакой отдельный сокращенный уровень удовлетворительно не показывает все районы, представляющие интерес, вновь были необходимы реразвертыватели на некоторых сокращенных уровнях. В попытке преодолеть эту трудность использовался двухдиапазонный чувствительный элемент, который охватывает район регистрации вокруг области наблюдения главного чувствительного элемента. По крайней мере, возможны три вида эксплуатации прибора с двухдиапазонным чувствительным элементом: 1) "нормальная" эксплуатация; 2) игнорирование общей плотности изображения и реакция только на небольшие изменения, устанавливая таким образом свой собственный сокращенный уровень; 3) сообщение только о внезапных изменениях в плотности регистрации. По-видимому, возможны также другие виды.

Это сравнительно простой и недорогостоящий прибор обеспечивает оказание ценной помощи в интерпретации диаграмм, произведенных методом скеннирования.

ANÁLISIS DE CENTELLEOGRAMAS CON UN NUEVO DENSITÓMETRO REGISTRADOR. El perfeccionamiento de los aparatos de centelleografía no ha repercutido como debiera en los estudios clínicos debido, en gran parte, a las deficiencias de los centelleogramas. Para mejorar la visualización y acentuar el contraste se han estudiado diversos métodos instrumentales de análisis.

Los autores han ideado un densitómetro registrador sencillo y poco costoso para «reexplorar» centelleogramas. Un elemento fotosensible analiza el centelleograma de la misma manera que el detector explora al paciente. Ese elemento responde con impulsos de frecuencia proporcional a la opacidad (o capacidad de transmisión) del registro y puede utilizarse para hacer otro nuevo (registro de «reexploración»). El área del registro respecto a la cual se integra la información, se determina fijando la apertura del elemento fotosensible. El amplio margen de la frecuencia de los impulsos de salida (entre 0 y 15 000 impulsos/s) da lugar a un gran aumento del contraste, que es posible graduar. Un regulador de umbral permite preseleccionar

cualquier « nivel de corte ». La operación es rápida y es posible reexplorar un registro en una pequeña fracción del tiempo que se necesitó para obtenerlo.

El estudio de centelleogramas clínicos de casi todos los órganos o zonas de interés muestra que la reexploración proporciona datos que no eran evidentes en los centelleogramas originales. Ese método resulta especialmente útil para determinar la significación estadística de pequeñas variaciones del índice de recuento en un centelleograma.

Con los centelleogramas de intervalo dinámico muy amplio, en los que un solo nivel de corte no revela todas las regiones de interés, era preciso anteriormente trabajar a diversos niveles. Para allanar esta dificultad, los autores han tratado de emplear un elemento fotosensible bizonal que analiza una región del centelleograma situada alrededor del campo de visión del elemento principal. Este dispositivo se puede emplear, por lo menos, de tres maneras diferentes: a) de manera «normal»; b) prescindiendo de la densidad general del registro y respondiendo solamente a pequeñas variaciones, fijando así su propio nivel de corte; c) indicando solamente cambios bruscos de densidad. También parecen posibles otros procedimientos de empleo.

Ese dispositivo relativamente sencillo y poco costoso es sumamente útil para la interpretación de centelleogramas.

The clinical usetulness of the "scan record" - a plane projection of a map of the radioactivity in a patient, roughly comparable to an X-ray picture - has brough the relatively new (13 years old) procedure of scanning into widespread use. Detectors, electronic systems, and recording methods have all been immensely improved since the early machines were built, and today more problems occur in the interpretation of a scan record than in its production. What a doctor sees in a scan is in a large measure dependent on whether the technician guessed correctly in setting up the scanner, and it is unreasonable to expect a technician always to do an optimum job, working - as he usually must - on a one-shot basis. This puts a premium on a policy under which a technician's assignment is to get all possible information safely stored in the original scan. This would not always make the most readable record, so the clinician could be provided with a secondary device that uses the information in the primary scan record to produce an interpretable record without destroying the original. If the first attempt at the secondary record turns out unhappily, another try could be made quickly, without involving the patient in another hour or so of lying motionless under a scanner.

Several ideas of this sort have been advanced [1, 2]; our "re-scanner" merely represents one possible approach that has the virtue of using rather simple and inexpensive equipment. The only complicated equipment needed is a scanner itself. A fast, light scanner mechanism is desirable but its only advantage is that of speed.

The system diagram of the re-scanner is shown in Fig. 1. A light sensor is used to scan a scan record just as a gamma-ray detector is used to scan a patient. The area that this sensor sees, and hence over which it integrates information, is controlled by selection of one of several defining apertures. The output of the sensor and its associated amplifier is a voltage that is proportional to the blackness (or, at your choice, whiteness) of the primary scan. This voltage then modulates the frequency of an oscillator comparable to "howlers" used for listening to the radioactivity of a patient [3]. The oscillator's output-pulses are delivered into the regular recording channels of the scanner used to move the sensor.

The threshold control is used to make the oscillator disregard all shades of blackness below a chosen level, and thus provides "background erase"

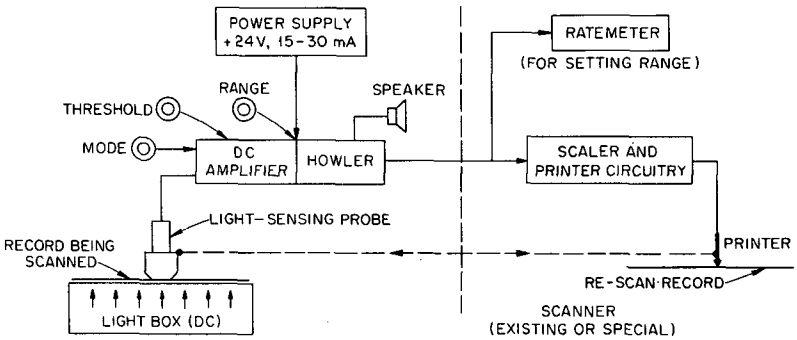

Fig. 1

A block diagram of the complete re-scanner system
The scanner used may be a standard machine, or one with specially fast sweep speeds.

of any degree desired, down to zero. A range control chooses the frequency corresponding to maximum blackness, available range being zero to about 15 000 Hz. Audible signals are provided for setting the threshold and a ratemeter can be used in setting range.

The basic device has been reported [4] and was shown to provide great contrast enhancement and a widely variable "background erase". The purpose of this presentation is to show further examples of the practical usefulness of the re-scanner, and to show some results obtained by the use of an additional sensor that sees an area surrounding the original, single sensor.

The light sensor assembly currently used is sketched in Fig. 2. When the outer sensor is disconnected, the operation is the same as the original device; we call this the "simple" sensor. When the outer sensor is added, the assembly becomes a "compound" sensor. The sensor elements are 1 cm by 1 cm silicon photosensitive diodes. The amplifier input has a high impedance, hence the diodes operate as photovoltaic devices.

Since the revelation of the basic device is relatively recent, we review some of the results obtained with the original, simple sensor. Figure 3A is a reproduction of a negative paper print of a pulse-type photorecording from an antero-posterior brain scan. The primary scan was done with a 3-in gold-tungsten collimator 48 h after injection of I^{131}-human serum albumin. Figure 3B is from a re-scan of the primary record, recorded by the same photo-recorder. The threshold was set for only a slight amount of "background erase". In the primary record a rather obvious lesion is demonstrated; this was shown at autopsy, two months later, to be metastatic carcinoma. Although photorecorder light intensity and scaling factor were not optimum for the re-scan, the contrast-enhancing capacity of the instrument is apparent.

Another use of the original re-scanner is shown in Figs. 4 and 5. Figure 4 is a reproduction of a positive paper print of a Rose Bengal liver scan (I^{131}), recorded by a multi-stylus mechanical tapper [5]. Figure 5 shows a sequence of re-scans, printed with a conventional, but fast, mechanical

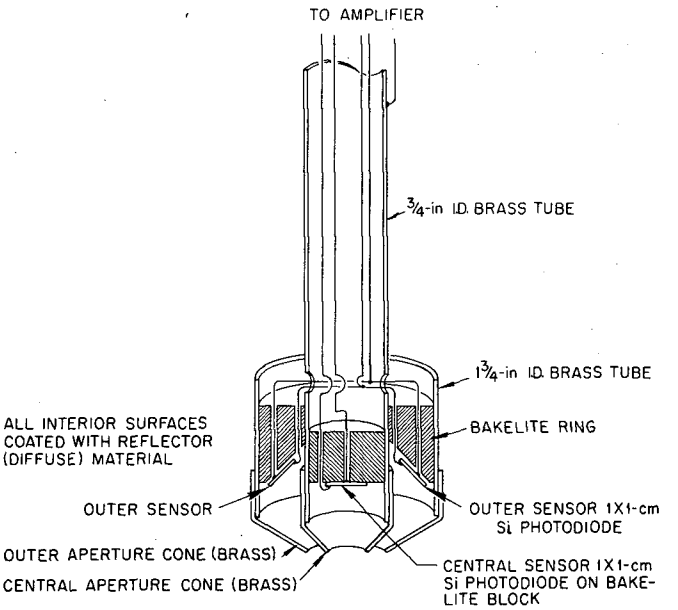

Fig. 2

Section drawing of the current compound sensor
The outer sensor consists of two or more silicon photodiodes connected in parallel.

tapper. The threshold was set higher for each succeeding re-scan. Note the emergence of new information at each cut-off level.

Another useful property of the original device with the simple sensor has been its ability to "rejuvenate" a photorecording in which density or contrast is so weak that interpretation is difficult. Such a scan record seems to result all too often from a failing light source, improper recorder settings, or from weak developer solution. Figure 6 shows on the left a photorecording of a right lateral brain scan done 24 h after administration of I^{131}-human serum albumin. There is a large shadow in the posterior fossa, due to the post-surgical regrowth of a cerebellar astrocytoma. The original recording was, however, so faint that boundaries of the shadow were hard to see. A simple-sensor re-scan (Fig. 6, right), done with a $\frac{1}{4}$-in aperture and a low threshold, successfully rejuvenated the scan and permitted much easier interpretation.

The re-scanner has been specially useful in clarifying, with the help of iodinated albumin, the pattern of the normal structures within the human head. Use of the re-scanner on a set of these normal records has brought out the appearance of the vascular system described by DI CHIRO [6]. In the original scans, it takes all the skill of an experienced neurosurgeon to find evidence of these vascular groups. Re-scan records show them clearly, provided sufficient information is present in the primary records, and in addition, demonstrate some sinuses not visible at all in the primary record - except in retrospect after seeing the re-scan.

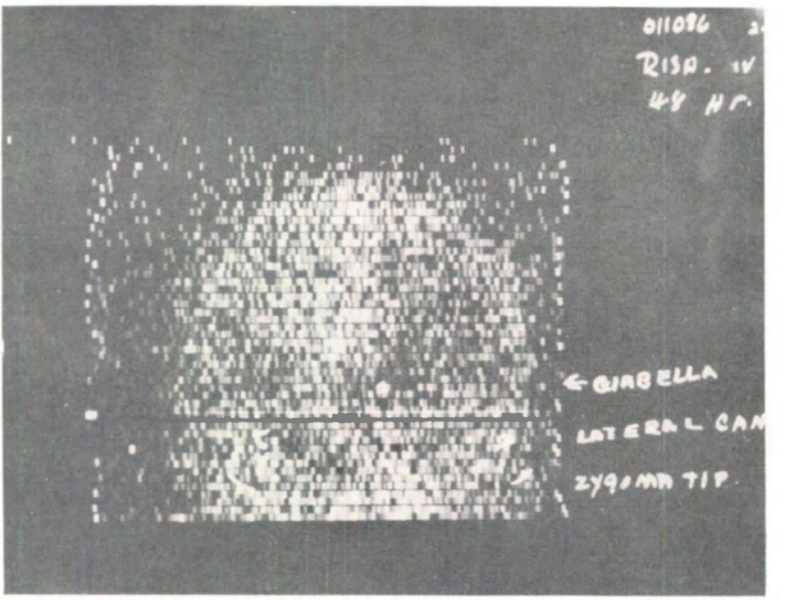

Fig. 3A

Antero-posterior brain scan record, negative print of a pulse-type photorecording
Tumour (metastatic carcinoma) is above and to the viewer's left (patient's right) of glabella.
Other areas of activity are considered normal with I^{131}-human serum albumin as the tracer material.

Fig. 3B

Re-scan of Fig. 3A, pulse-type photorecording
Re-scanning aperture 3/16 in, speed 24 in per min.
Light intensity and scaling factor were not optimum, but the contrast enhancement is evident.

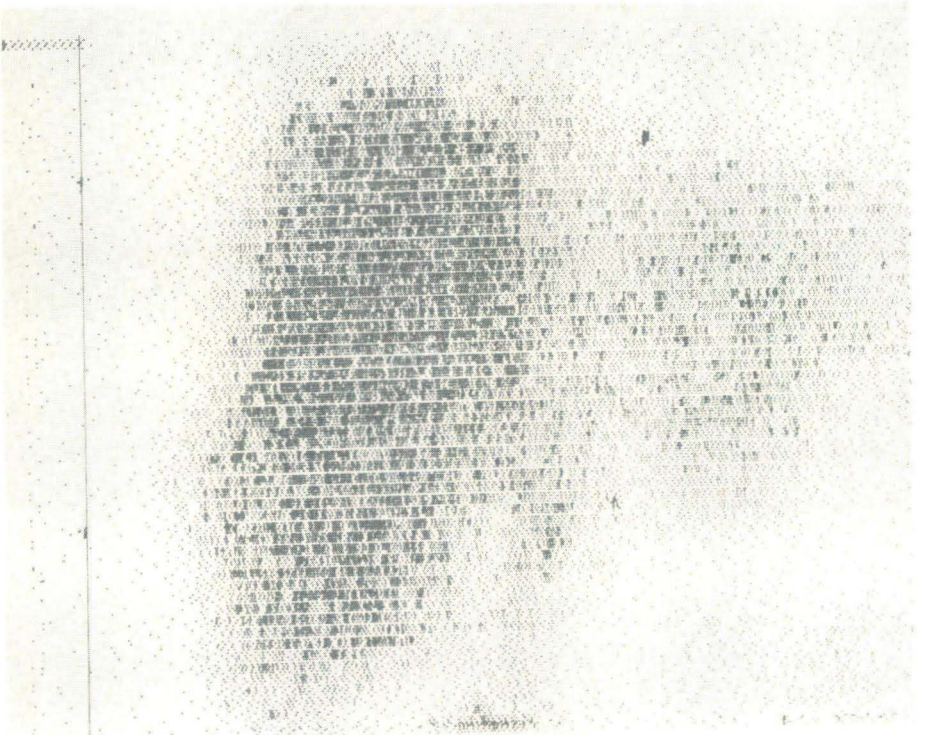

Fig. 4

Primary scan of liver, 30-60 min after Rose Bengal I^{131};
recording on white paper by "multidotter"
(Reprinted from Progress in Medical Radioisotope Scanning, USAEC TID 7673).

In these studies, and in the re-scanning of liver scans, the large dynamic density range of the primary records may make it impossible to see, with a single threshold setting, all the targets of interest. The compound sensor was designed to deal with this problem, by using, in effect, the information reaching the outer sensor to adjust the threshold for the inner one. Under this mode of operation the re-scan registers the degree of contrast between the small area viewed by the inner sensor, and the average density of a surrounding belt viewed by the outer one, whatever this density may be. Thus the outer sensor tends automatically to set the threshold for the inner sensor.

The first operation tried was with the output of the outer sensor opposing that of the central sensor; we called this "inhibit" operation. A control, labelled "Mode" in Fig. 1, was added to vary the relative contributions of the two sensors. At one end of the range of this control the outer sensor is suppressed, and "normal" re-scanner operation results. At the other end, the inhibiting effect of the outer element is maximum. For most primary scan records, the best operation occurs about midscale on the mode control.

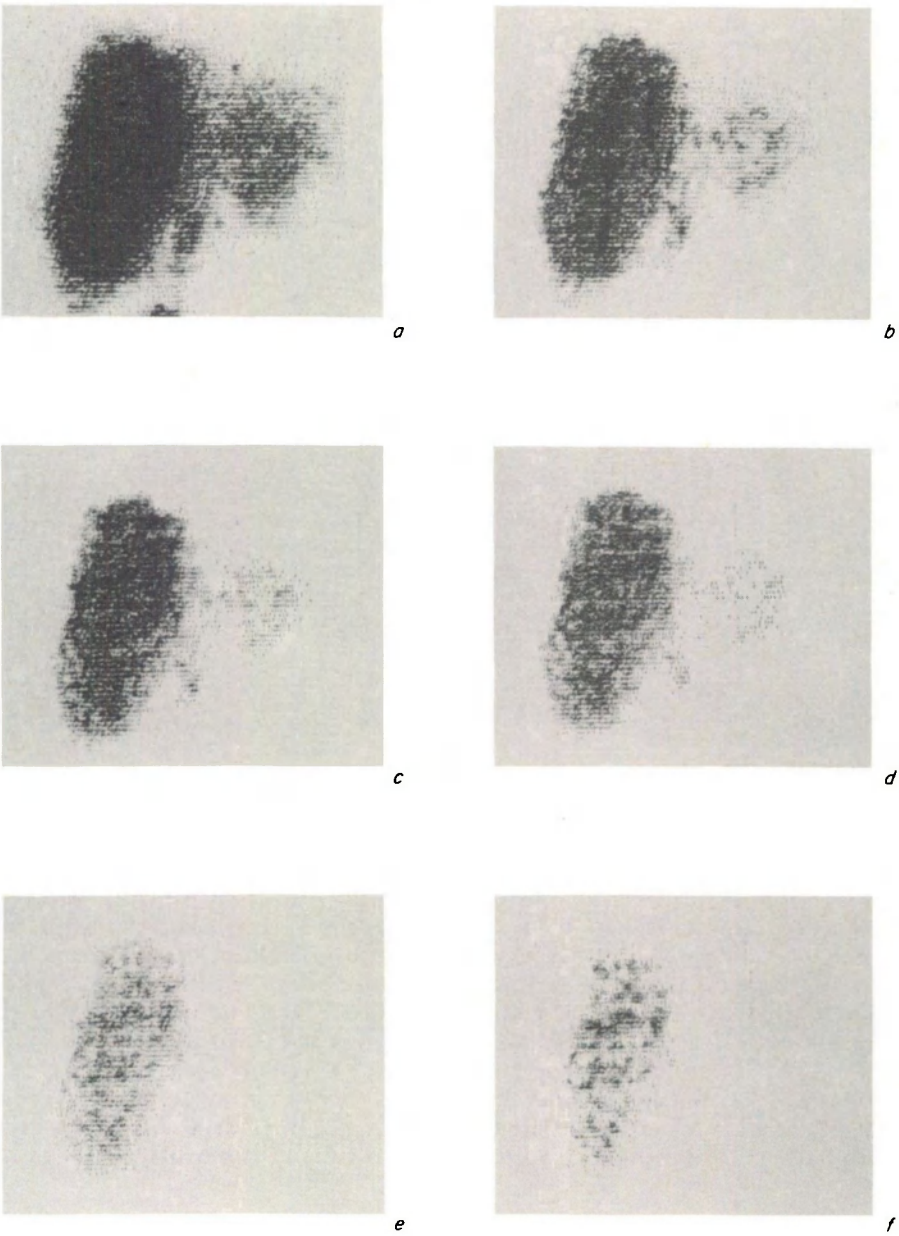

Fig. 5

Re-scans of Fig. 4, with threshold progressively rising, (a) through (f)
Sensor aperture 3/16 in; single-line printer.
(Reprinted from Progress in Medical Radioisotope Scanning, USAEC TID 7673).

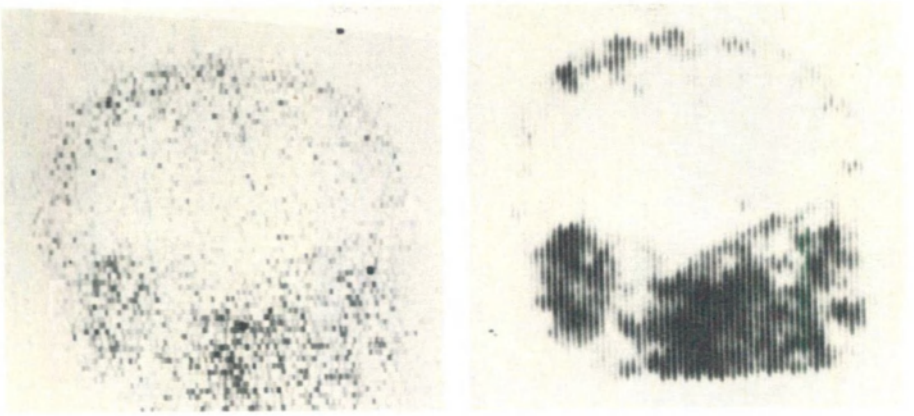

Fig. 6

A one-sensor re-scan of a right lateral brain scan
In the primary scan (left) the activity in the subtentorial region is poorly outlined;
in the re-scan (right) the tumour (a recurring cerebellar astrocytoma) is clearly visible.

An example of the useful effect of the compound sensor is shown in Fig. 7. The primary scan record is shown at the lower left; it is an AP brain scan after administration of I^{131} albumin. The patient had no evidence of intracranial disease. The simple-sensor re-scan is shown at the upper right; the aperture was 3/8 in. Note that radioactivity in the middle cerebral vessels (Sylvian fissure) merges almost completely into the dark shadow of the facial activity. This is in spite of a moderately high threshold. The re-scan obtained with the compound sensor is shown at the upper left. The central aperture was the same as before, and the outer sensor was looking at a 1/8-in ring around the inner sensor's viewing area. For this comparison, the appearance of the areas at the top of the cranium was made to be similar to that in the simple-sensor re-scan. Note the emergence of detail in the facial activity. This mode of operation also offers the privilege of running liver re-scans with a single threshold setting.

If an area of density is large enough to cover the field of the outer sensor, the resultant strong, "inhibit" signal may prevent adequate recording in a compound re-scan - or may permit recording only around the edges of the dark area, where the change is sudden. This effect may prove to be useful for the demonstration of a void swamped in a sea of surrounding activity; the compound re-scan will show a "rim" around the void.

Another interesting use of the outer sensor was obtained when its polarity was reversed, so that instead of opposing the central sensor, the output voltage of the outer sensor added to that of the inner element. We call this the "enhancing mode". It is almost like using a large aperture with a single sensor, except that the contribution from the outer sensor is kept small. Thus, a contribution from the outer sensor is required for the rescanner to acknowledge a given blackness seen by the central sensor. This mode has been useful in bringing out areas of low-level and diffuse activity in the primary scan record, without the smearing that a single, larger sen-

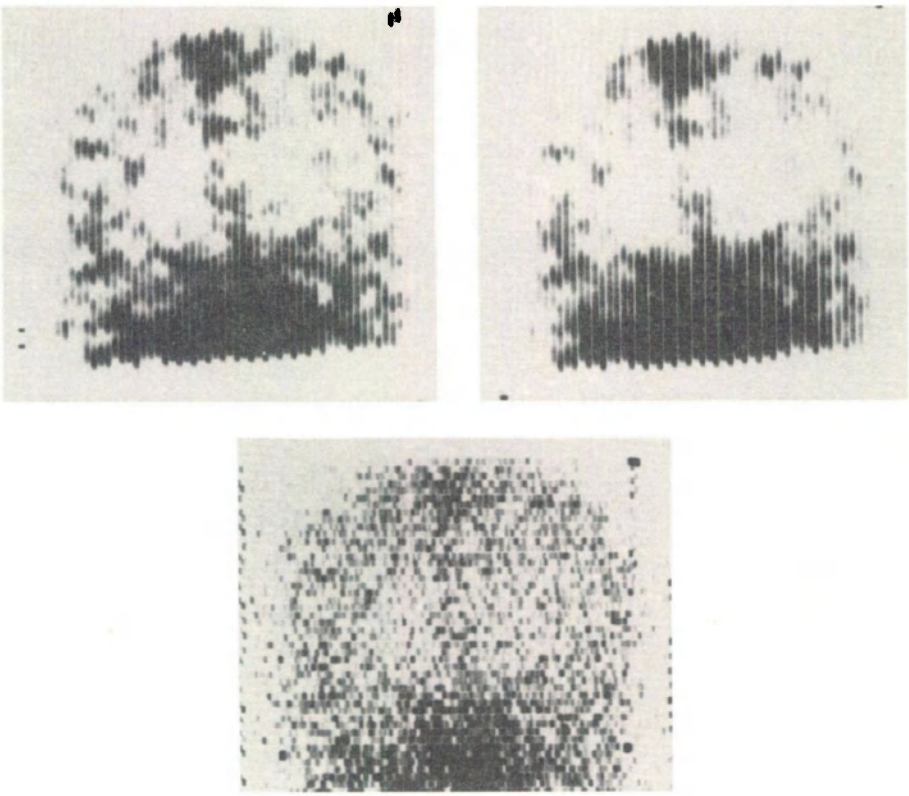

Fig. 7

Illustrating the action of the re-scanner in the "inhibiting" mode
The original scan (lower left) is an antero-posterior view of the head;
note the dark area, without apparent structure, in the facial region.
In the simple re-scan (upper right) the shadow is hardly more informative;
in the "inhibit" re-scan (upper left) the vasculature at eye level begins to come out.

Upper left. A compound (two-sensor) re-scan, outer sensor inhibiting
inner sensor, 3/8-in aperture
outer sensor, 5/8-in outer diameter
Upper right. A simple (one-sensor) re-scan, 3/8-in aperture
Lower left. The original scan record
Patient W. A., antero-posterior view
$RI^{131}HSA$ IV
Patient believed normal

sor would cause. In addition, the "enhanced" re-scanner does not go wild upon viewing a single very black mark such as an anatomical landmark on a single scan line.

Figure 8 shows an example of the use of the enhancing mode. The original record was made 22 h after the injection of iodinated albumin into a patient showing evidence of a parasagittal lesion in the left parietal area. This primary scan, a left lateral, is shown at lower left in Fig. 8, and it was not

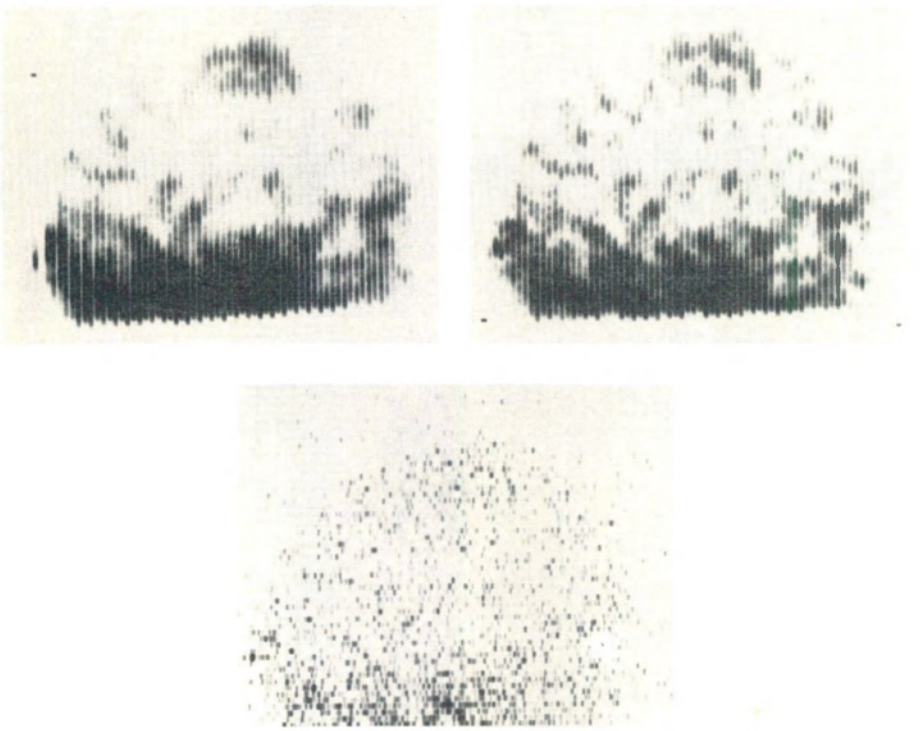

Fig. 8

Illustrating the action of the re-scanner in the "enhancing" mode
The original scan (lower left) is a left lateral view of the head;
the parasagittal, left parietal tumour is difficult or impossible to see.
It is brought out to some extent without enhancement (upper right),
but much better with (upper left) enhancement.

Upper left. A compound (two-sensor) re-scan, outer sensor enhancing
inner sensor, 3/8-in aperture
outer sensor, 5/8-in outer diameter
Upper right. A simple (one-sensor) re-scan, 3/8-in aperture
Lower left. The original scan record
Patient D. P., left lateral view
Scan 22 hours after 600 μc RI^{131}HSA IV

at all remarkable. Simple-sensor re-scans (upper right), though more suggestive of abnormal activity in the parasagittal region, were not wholly convincing either. But when an "enhancing" compound re-scan was done (upper left) the result left no doubt that there was left parietal trouble. Meanwhile the patient, in a distant city, underwent a "subtotal resection of an infiltrating astrocytoma, left parietal parasagittal".

Certain conclusions, rather obvious in retrospect, have been formed as a result of use of the re-scanner.

(1). The higher the quality and information content of the primary scan

record, the more the re-scanner will bring out. But it cannot create quality where none existed.

(2). Ordinarily we find very little in a re-scan record that could not be seen by reviewing the primary record and examining it carefully. The re-scanner has been helpful in showing where to look on the primary record. Re-scans should always be interpreted by comparing them closely with the primary records. Lately, however, use of the compound sensor has brought out information nearly invisible in the primary record.

(3) Because it is really a densitometer that integrates over a chosen area, the re-scanner can quantitatively perform a function done only with difficulty by the human eye. This is its basic function. Since it is an electronic device, modifications of its operation can be made rather easily.

APPENDIX

CIRCUIT OPERATION

The re-scanner's schematic circuit is shown in Fig. 9. It consists basically of the sensors, a DC amplifier, and an oscillator. For "inhibiting" operation of the compound sensor, the outer sensor diodes are connected as shown; for "enhancing" operation their connections are reversed. The DC amplifier consists of the two

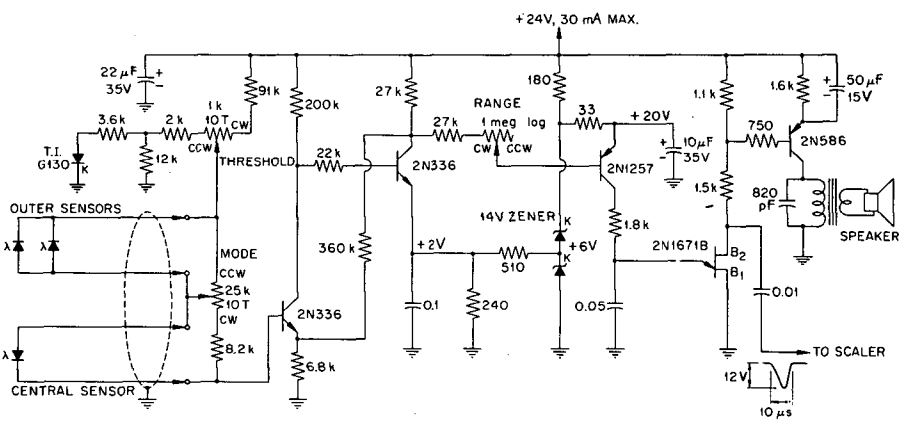

Fig. 9

Schematic diagram of re-scanner for compound sensor

2N336 transistors and associated components; almost any reasonably high-beta silicon transistors are satisfactory. Voltage signals at the base of the first 2N336 are amplified and appear at the collector of the second 2N336; 22-V swing at this collector represents full output. The unijunction device 2N1671B is the oscillator. The 2N1257 acts as a rheostat to control the charging current to the capacitor connected to the emitter of the 2N1671B, and thus acts as a control on the oscillator frequency. Collector current flow in the 2N1257 is changed by conversion of the voltage swing at the collector of the second 2N336 into base current into the 2N1257.

The threshold control operates by determining how much the voltage output of the sensors must be changed to affect the collector current in the first 2N336. The mode control determines the relative voltage contri-

butions from the inner and outer sensors. The range control simply sets a limit on the base current of the 2N1257 for a given voltage change at the collector of the second 2N336.

For a more detailed circuit description, the reader is referred to reference [4] in which the original circuit is discussed.

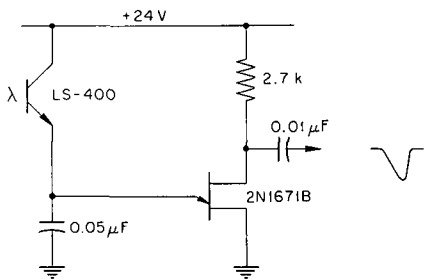

Fig. 10

Experimental circuit for a new, simple sensor, which shows promise
Threshold and range controls have yet to be added.

A greatly simplified circuit with which we are currently experimenting is shown in Fig. 10. The Texas Instruments LS-400 sensor is a silicon phototransistor. Its high output (a collector current change of 7 μA per foot-candle at 600 foot candles) eliminates the need for a voltage amplifier. This sensor is equipped with a lens, and must be used with directed light. Because of its small size, it is especially suited for re-scanning copy negatives of scan records. This device has not yet been "tamed", but shows considerable promise.

ACKNOWLEDGEMENTS

The authors gratefully acknowledge the tireless efforts of Ann Miller, Oak Ridge National Laboratory, in preparing this material for publication. We thank Brena Stevens and Ray Cockreham for their expert help in reproducing copies for use at the Symposium. The work of W. C. Colwell, W. N. Tillery and their groups in preparing the illustrations is also gratefully acknowledged.

REFERENCES

[1] BENDER, M. A. and BLAU, M., Medical Radioisotope Scanning, IAEA, Vienna (1959) 83-6.

[2] DEWEY, W. C., HEIDELBERG, J. G. and MOORE, E. B., J. nucl. Med. 3 (1962) 51-62.

[3] HARRIS, C. C., BIGELOW, R. R., FRANCIS, J. E., Jr., KELLEY, G. G. and BELL, P. R., Nucleonics 14 11 (1956) 102-8.

[4] HARRIS, C. C., BELL, P. R., FRANCIS, J. E., Jr., JORDAN, J. C. and SATTERFIELD, M. M., Progress in Medical Radioisotope Scanning, USAEC TID 7673 (1963) 81-97.

[5] HARRIS, C. C., BELL, P. R., FRANCIS, J. E., Jr., JORDAN, J. C. and SATTERFIELD, M. M., Progress in Medical Radioisotope Scanning, USAEC TID 7673 (1963) 77-81.

[6] DI CHIRO, G., Progress in Medical Radioisotope Scanning, USAEC TID 7673 (1963) 347-70.

DISCUSSION

A. DESGREZ: From what information density per unit surface can contrast amplifiers of this type distinguish defects which correspond to anatomical facts from those due to amplification of statistical fluctuations? Are these devices a practical proposition if one uses types of detectors in current use or does one have to use very high-efficiency collimators? I should be interested to hear a figure if one can be given because, for some time, we have been using a magnetic recording device employing variable contrast read-out together with a scanner with a good commercial collimator. So far we have been unable to show up defects that could not be seen in the original picture.

C. HARRIS: Unfortunately, I cannot give you a precise figure. Regarding your second question, I feel that, in general, one must use some judgement in interpreting records of this type. For example, one cannot attach significance to a defect which is smaller than the resolution of the collimator.

H.A.B. SIMONS: Subjective factors may play a part in the recognition of areas of different information density. I should like to know, therefore, whether you have tried to record scintigrams using marks of different form, e.g. open circles, triangles or filled circles.

C. HARRIS: No. There were, I fear, quite a lot of things that could not be done, since the work was carried out in our spare time. I am very grateful for your suggestion.

L. DONATO: The papers and discussions on display systems which we have been hearing stress the need for quantitative scans and the importance of having some sort of contrast enhancement device of the photo-scanning type. I agree with Dr. Pochin's remarks during the discussion on the papers by Dr. Mallard and Dr. Kakehi et al.* concerning the importance of quantitative data and I think one should adopt this approach consistently. Colours may be pretty, but it must be remembered that, for a long time past, the most generally accepted method of quantitating something has been by using numbers.

Digital ratemeters seem to me the natural and ideal instruments to do this job properly and at low cost. We have had one for over a year, and they are now commercially available from several firms. Using them, it is possible to obtain numerical maps at very low cost. It may be thought that numerical maps do not give such an immediate idea of the activity distribution as one gets with conventional display systems. But it is easy to obtain a conventional display from, or even simultaneously with, a numerical map. We do this at present using a principle very similar to that used in reproducing black and white pictures in newspapers. The marks are equally spaced and their size varies with the counting rate. One may choose any scale, contrast or background suppression level, and make any number of scans one wishes. In this way it is easy to obtain a range of blackening from minimum to maximum, even for very small changes in counting rate, without the need for complex or costly instrumentation.

---

* MALLARD, J.R., "An analysis of quantitative colour display for scanning" (SM-51/25) and KAKEHI, H., ARIMIZU, N. and UCHIYAMA, G., "A new method for colour scanning" (SM-51/7), these Proceedings I.

I. BASCHIERI: I am quite sure that magnetic recording is the most appropriate method to use in scinti-scanning. All the pulses can then be stored and used later to make scintigrams with different cut-off levels and to calculate the statistical significance of their frequency variations. We have, however, tried to develop a simple method which would increase contrast in scinti-scanning, since the use of more complicated methods takes more time and, when a good deal of routine work has to be done, there is too little time to re-examine the data, especially from the statistical point of view. This is all the more true in that - at least in Italy - there are not enough technicians able to do this work.

The advantages of the technique described are that it significantly enhances the contrast, does not necessitate the use of very expensive equipment and leaves scope for further development.

D. FOLLETT: Dr. Harris' system of re-scanning with a compound detector would seem to be almost tantamount to cross-correlation between the central and surrounding light detectors. Were the outputs from the detectors actually combined to give cross-correlation?

C. HARRIS: The system does not involve a real cross-correlation. The outputs of the sensors are merely added or subtracted, whereas they would have to be multiplied in a real cross-correlation, and that would be very difficult. It might be possible to solve the problem in a comparatively simple manner by using Hall-effect amplifiers.

E. von SABSAY: How long does it take to re-scan the picture? I should like to know, in particular, whether your method offers any advantage compared with replaying from magnetic tape, which can be done about ten times faster then the original scan.

C. HARRIS: The speed is limited, for all practical purposes, only by the method of moving the sensor in relation to the film. In our re-scans, there were some zig-zag lines due to the time constant of the detector which comprises voltage source with large capacitance feeding a high impedance. This can be eliminated by using the sensor as a current source feeding a low impedance. The only advantage of the re-scanner over tape, or any other system, is its simplicity and the fact that it makes a full-size re-scan recording. We have also used magnetic tape to record and later reproduce scans. One reason why we have not used tape recording to a greater extent is that our laboratory is situated in an unfavourable magnetic environment. Stray fields from controlled fusion experiments have caused deterioration of some tapes.

PERSPECTIVES D'EMPLOI D'UN NOUVEAU SYSTÈME D'ENREGISTREMENT A CONTRASTE ACCENTUÉ

I. BASCHIERI ET A. SCOGNAMIGLIO
INSTITUT DE PATHOLOGIE SPÉCIALE,
UNIVERSITÉ DE ROME, ITALIE

Abstract — Résumé — Аннотация — Resumen

PROSPECTS FOR THE USE OF A NEW SYSTEM OF INTENSIFIED CONTRAST RECORDING. The normal recording systems used to give a scintigraphic image are not capable of yielding sufficient contrast for the identification of two radioactive zones when the difference in concentration of the radioisotope is less than 20%. The authors examine the technical procedures adopted by different writers in order to get more exact information from scintigraphic examinations. They then discuss the advantages and disadvantages of each of these procedures.

A new technical solution of the problem is then proposed. It consists in varying the width and height of each mark in relation to the time between two successive marks, not to the average pulse frequency.

The recording element is controlled electronically: the circuit presented examines precisely the time interval between one pulse and the preceding one and produces a pulsating voltage which varies with the separation of the pulses. This pulsating voltage selectively controls the recorder: in this way variation of the recorded mark is obtained. The new system makes it possible to obtain adequate contrast between radioactive zones with a difference of activity of about 10%. Finally, the first experimental results are given.

PERSPECTIVES DE L'EMPLOI D'UN NOUVEAU SYSTÈME D'ENREGISTREMENT A CONTRASTE ACCENTUÉ. Les systèmes normaux d'enregistrement employés afin d'obtenir l'image scintigraphique ne sont pas capables de fournir un contraste suffisant pour l'identification de deux zones radioactives lorsque la différence de concentration en radioélément est inférieure à 20%. Les auteurs examinent les solutions techniques adoptées par les différents auteurs dans le but d'obtenir des informations plus précises des examens scintigraphiques. Ils considèrent ensuite les avantages et les inconvénients de chacune d'elles.

Une nouvelle solution technique du problème est proposée. Elle consiste dans la variation de la largeur et de la hauteur de chaque marque en rapport, non pas avec la fréquence moyenne des impulsions, mais avec le temps intercurrent entre deux marques successives.

L'élément enregistreur est commandé par voie électronique: le circuit présenté examine justement l'intervalle de temps entre une impulsion et la précédente, et produit une tension impulsive variable avec la distance des impulsions. Cette tension impulsive commande en manière sélective l'enregistreur: on obtient ainsi une variation de la marque enregistrée. Le nouveau système permet d'obtenir un contraste suffisant entre les zones radioactives dont la différence d'activité est de l'ordre de 10%. Pour terminer, les premiers résultats expérimentaux sont présentés.

ПЕРСПЕКТИВЫ ИСПОЛЬЗОВАНИЯ НОВОЙ СИСТЕМЫ РЕГИСТРАЦИИ С БОЛЬШИМ КОНТРАСТОМ. Нормальные системы регистрации, используемые для получения сцинтиграфического изображения, не способны обеспечить контрастность, достаточную для идентификации двух радиоактивных зон тогда, когда разница в концентрации радиоэлементов ниже 20%. Авторы изучают технические решения, к которым пришли другие авторы, в целях получения более точной информации о сцинтиграфических исследованиях. Затем они рассматривают положительные и отрицательные стороны каждого из этих решений.

Далее предлагается новое техническое решение проблемы. Оно заключается в изменении ширины и высоты каждой отметки в зависимости не от средней частоты импульсов, а от промежуточного времени между двумя последовательными метками.

Регистрирующий элемент получает команды от электронных приборов: представленная схема дает возможность изучать интервал времени между двумя последовательными импульсами, а также в основе импульсное напряжение, изменяемое в зависимости от расстояния

импульсов. Это импульсное напряжение дает селективно команду регистратору: таким путем получают изменение регистрирующей отметки. Новая система позволяет получать достаточную контрастность между двумя радиоактивными зонами, разница в активности которых составляет, примерно, 10%. В заключение приводятся первые экспериментальные результаты.

PERSPECTIVAS DE UN NUEVO SISTEMA DE REGISTRO CON CONTRASTE ACENTUADO. Los sistemas corrientes de registro empleados para obtener una imagen centelleográfica no dan el contraste suficiente para identificar dos zonas radiactivas cuando la diferencia entre las concentraciones radioisotópicas es inferior al 20%. Los autores examinan las soluciones técnicas adoptadas para obtener una información más precisa mediante el examen centelleográfico y exponen las ventajas y los inconvenientes de cada una de ellas.

Seguidamente proponen una nueva solución que consiste en variar la anchura y la altura de cada marca en relación, no con la frecuencia media de los impulsos, sino con el tiempo que transcurre entre los impulsos correspondientes a dos marcas sucesivas.

El elemento registrador se rige electrónicamente: el circuito presentado examina precisamente el intervalo entre un impulso y el precedente y origina una tensión impulsiva que varía con la distancia entre los impulsos. Esta tensión gobierna selectivamente el registrador, y así se obtiene una variación de la marca. El sistema descrito permite obtener un contraste suficiente entre zonas radiactivas con una diferencia de actividad del orden del 10%. En la memoria se presentan los primeros resultados experimentales del nuevo sistema.

Les systèmes d'enregistrement scintigraphique habituellement utilisés fournissent des images dans lesquelles il n'est pas possible de repérer des variations modérées de la fréquence des hachures [1, 2].

Plusieurs auteurs ont envisagé la possibilité d'améliorer l'enregistrement afin d'obtenir un contraste plus accentué entre deux zones dont la différence d'activité est relativement faible, et nombreuses sont actuellement les solutions techniques proposées à cet égard [3, 4, 5, 6, 7, 8, 9, 10, 11, 12].

Elles présentent toutefois certains défauts, dont nous avons déjà fait mention dans une note précédente [13].

En résumant, on peut dire que:

1. Les systèmes utilisant des circuits de «cut-off» nécessitent l'exécution de plusieurs enregistrements simultanés ou non, ou bien ils exigent l'élaboration ultérieure des données obtenues directement sur le malade.

2. L'adoption de variation de couleur des hachures suppose la parfaite connaissance du code des couleurs sans quoi l'interprétation de l'image scintigraphique est impossible, et d'autre part il est assez difficile de disposer d'une gamme étendue de couleurs qui aient, entre elles, un contraste suffisant.

3. Les deux solutions mentionnées ci-dessus ont été le plus souvent réalisées en utilisant des intégrateurs d'impulsions; on introduit alors une constante de temps qui, quoique modeste, produit une image en «damier».

4. La suppression des impulsions au dessous d'une fréquence prédéterminée, ou la variation de la couleur ont été en général réalisées par division en parties égales d'une échelle centésimale. Ceci ne semble pas correct pour diverses raisons: d'abord il n'est pas toujours aisé d'établir avec une approximation satisfaisante le niveau d'activité «maxima» auquel on est supposé appliquer la valeur 100. En deuxième lieu, les organes explorés n'ont pas toujours la même épaisseur sur toute leur étendue et l'activité détectée sera donc variable: or pour repérer sur le scintigramme une lésion au niveau de la portion de l'organe qui, en raison de son épaisseur

réduite, a, déjà dans des conditions normales, une activité de 50%, il sera nécessaire qu'elle produise une perte de comptage double en pourcentage par rapport à celle nécessaire à l'identification d'une lésion au niveau de la zone dont l'activité est «maxima».

A la suite de ces considérations nous avons pensé à réaliser un nouveau système d'enregistrement qui permette de repérer, sur un même scintigramme, une gamme assez étendue de niveaux d'activité et ceci sans recourir ni à la variation de couleur des hachures, ni à l'emploi d'un intégrateur d'impulsions.

Le nouvel enregistreur a été conçu en se basant sur la remarque déjà faite par un de nous selon laquelle en registrant des impulsions statistiques, l'œil n'est pas capable de déceler une variation de la fréquence des hachures si celle-ci est inférieure à 20% [1] en raison du fait que le contraste entre les zones est insuffisant.

Cependant si l'on fait varier convenablement les dimensions des hachures par rapport au temps entre deux impulsions successives, on pourrait obtenir un contraste suffisant même lorsque la réduction de la fréquence des impulsions est inférieure à la limite mentionnée ci-dessus.

Pour la réalisation de notre projet nous avons utilisé comme enregistreur une machine à écrire électrique (OLIVETTI 84) modifiée dans notre laboratoire (fig. 1): le déplacement du chariot se fait en sens inverse et à la même vitesse que celui de la sonde a scintillation au moyen d'une paire de moteurs répétiteurs électriques synchrones.

Sur douze des barres du clavier, les caractères normaux ont été remplacés par des «I» convenablement modifiés de façon que chaque caractère imprimé ait une surface inférieure de 20% à celle du précédent. Les douze touches respectives sont actionnées par des électroaimants.

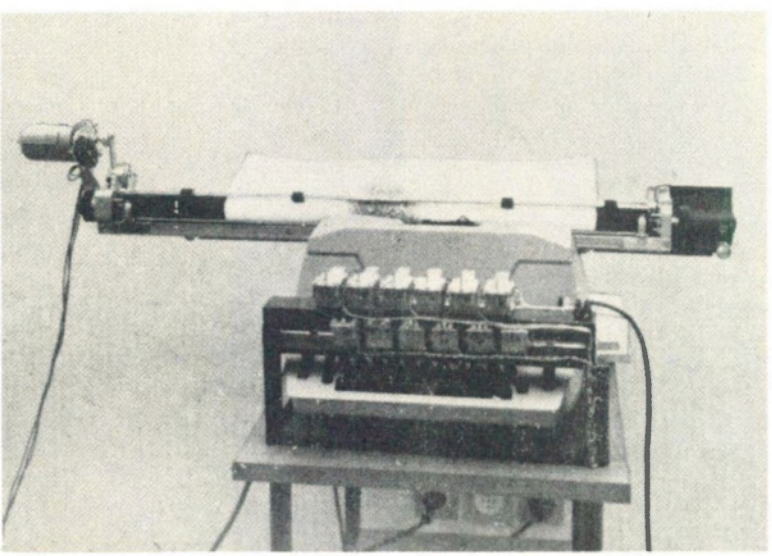

Figure 1

Groupe mécanique d'enregistrement.

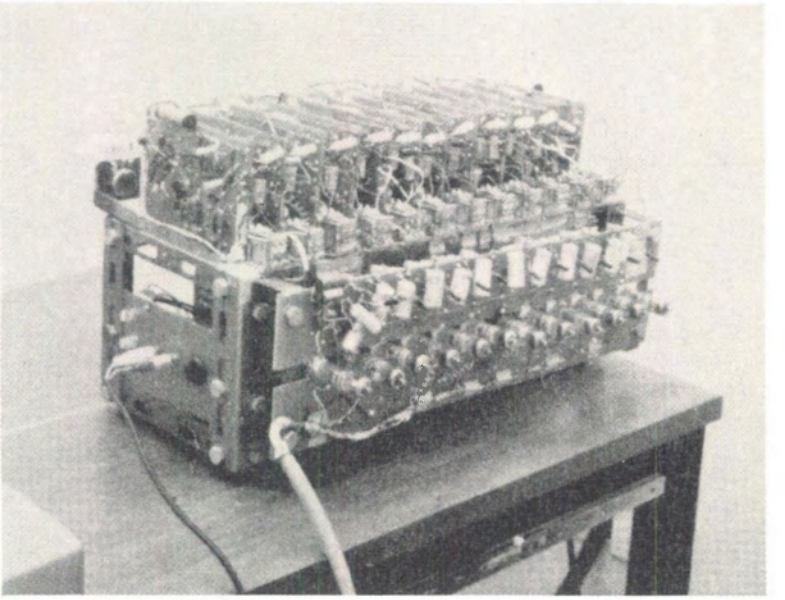

Figure 2

Groupe électronique à 12 canaux pour la discrimination des impulsions d'après leur fréquence instantanée.

La sélection de la touche est opérée par un discriminateur électronique multicanal (fig. 2) qui sélectionne les impulsions d'après l'intervalle de temps s'écoulant entre deux impulsions successives (fig. 3).

Le discriminateur est constitué par l'assemblage de circuits logiques qui trient les impulsions dans douze canaux d'utilisation correspondants aux douze caractères de la machine à écrire.

Chaque canal permet seulement le passage des impulsions qui sont séparées de la précédente par un temps compris entre les limites de temps propres au canal même. Chaque canal commence où se termine le précédent.

La première impulsion de la série provoque, moyennant la formation d'une onde rectangulaire d'une durée de 370 ms*, l'ouverture du premier canal: la deuxième impulsion permettra la frappe du premier caractère à condition qu'elle atteigne le canal dans sa période d'ouverture.

Lorsque ceci se produit, on a, en même temps que l'impression du caractère, la fermeture prématurée du canal et sa réouverture immédiate afin de permettre la discrimination de l'impulsion suivante.

Si, par contre, la deuxième impulsion arrive après un temps plus long que le temps d'ouverture du premier canal, la fermeture de celui-ci produit dans le deuxième circuit une onde rectangulaire d'une durée de 41 ms qui

* On a choisi comme limite de temps du premier canal 370 ms pour les raisons suivantes: la largeur du premier caractère étant d'environ 1 mm et la vitesse de déplacement du détecteur habituellement employée par nous étant de 3, 5 mm/s, il suffit d'imprimer trois caractères par seconde (= 3 Hz) pour obtenir un noircissement complet. Puisque le changement des caractères se produit pour une variation de fréquence de 10%, le premier canal devra avoir une largeur maxima égale au temps entre deux impulsions de fréquence 2, 7 Hz, ce qui correspond à 370 ms.

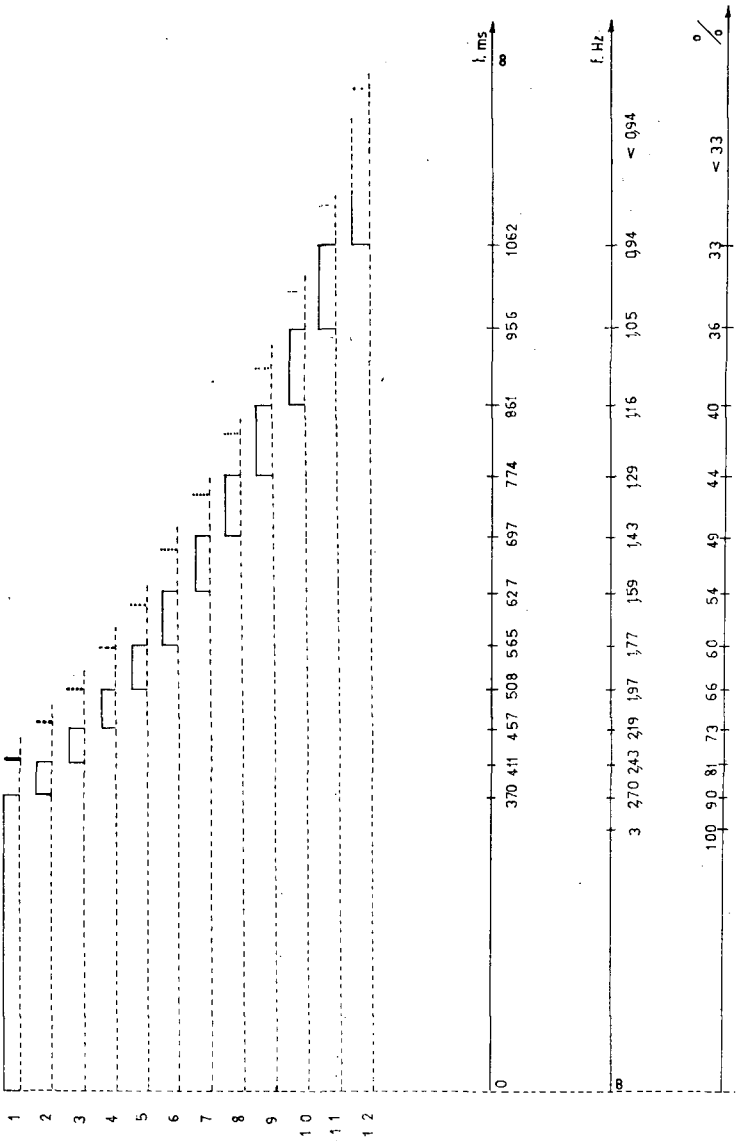

Figure 3

Schéma de principe du discriminateur temporel des impulsions (à côté de chaque canal figure de caractère d'impression respectif).

permet pour conséquence l'ouverture, pendant un temps équivalent, du deuxième canal. Si l'impulsion arrive pendant ce temps la deuxième touche sera actionnée, et il se produira la fermeture prématurée du second canal et la réouverture du premier; dans le cas contraire la fermeture du canal au bout du temps normal, produit l'ouverture du troisième et ainsi de suite jusqu'au douzième canal. Celui-ci restera ouvert pendant un temps infini * ou plus exactement jusqu'à l'arrivée d'une impulsion: la douzième touche sera alors actionnée et en même temps se produira la fermeture du canal correspondant et la réouverture du premier.

Les caractères changent selon une échelle des temps à décroissance constante (fig. 4): ceci devrait permettre d'apprécier des variations d'activité de 10% soit qu'on ait commis une erreur en excès dans la détermination de l'activité «maxima», soit que l'altération qui produit la variation de comp-

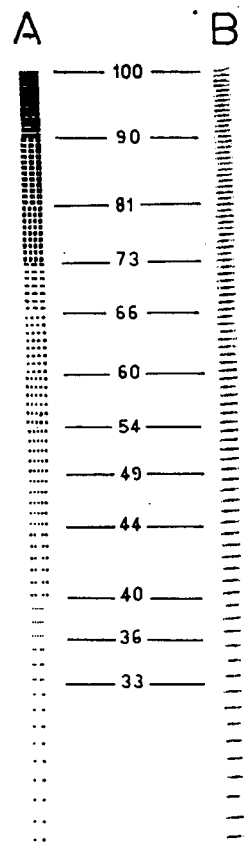

Figure 4

Enregistrements des impulsions régulières engendrées par un oscillateur à fréquence variable effectués avec la nouvelle méthode (A) et avec le système classique (B).
(Les enregistrements scintigraphiques (A) et (B) ont été effectués simultanément.)

* De même que les autres canaux, le douzième peut rester ouvert pendant un temps prédéterminé. Dans ce cas, l'on pourra obtenir la suppression du bruit de fond.

tage se trouve dans une portion de l'organe où, en raison de l'épaisseur, l'activité est dans les conditions physiologiques, inférieure à l'activité «maxima».

L'on pourrait nous objecter que le temps entre deux impulsions peut varier statistiquement de plus de 10%; en effet c'est seulement lorsqu'on emploie un facteur de démultiplication supérieur à 100 que la déviation standard est inférieure à cette limite.

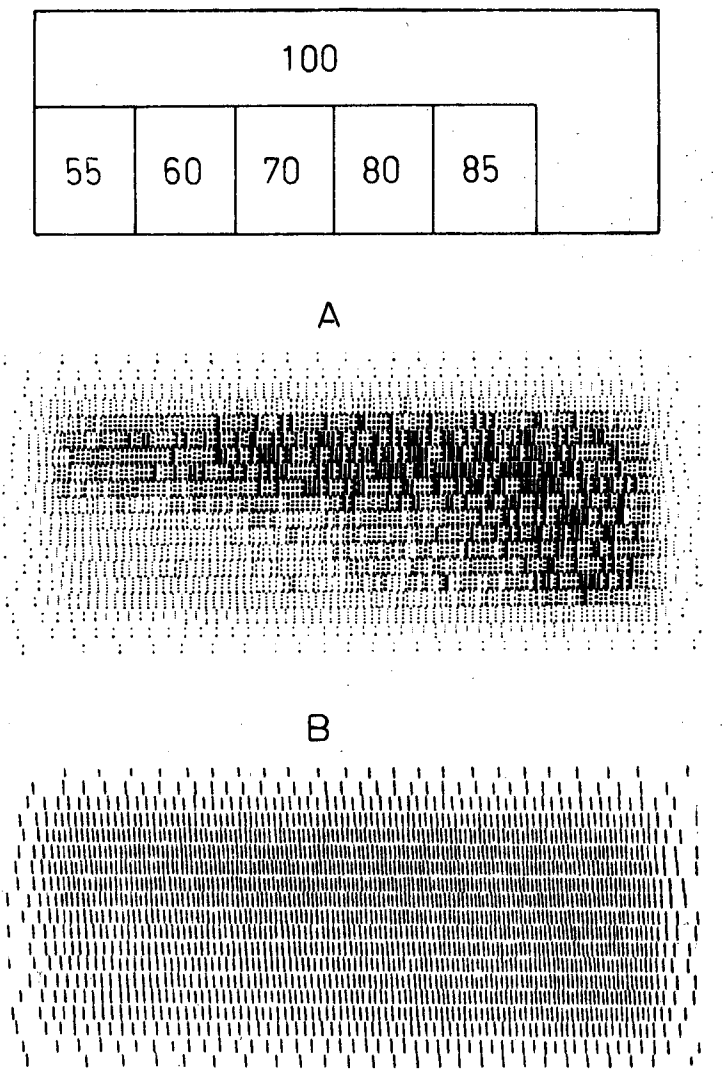

Figure 5

Scintigrammes effectués sur fantôme:
(A) enregistrement à contraste accentué,
(B) enregistrement selon la technique classique.
Les variations d'activité entre les différentes zones sont bien plus marquées sur (A).

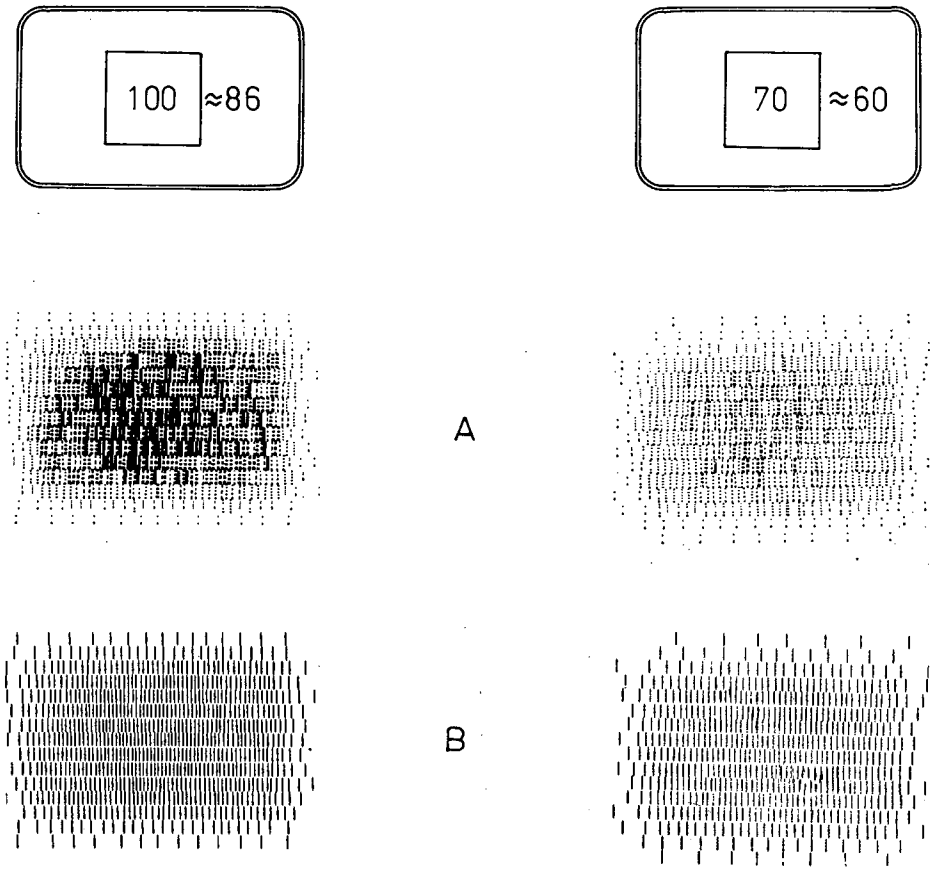

Figure 6

Scintigrammes effectués sur fantômes: la partie externe est moins active (-14%) que la partie centrale, l'activité étant dans un cas (schéma de gauche) égale à 100, dans l'autre 70. La zone centrale plus active est plus facilement reconnaissable sur les scintigrammes effectués avec la nouvelle méthode (A).

On doit cependant remarquer que l'identification d'une zone plus ou moins active ne se base pas sur la présence d'une hachure de type différent mais sur le contraste produit par l'ensemble de toutes les hachures enregistrées sur une zone de l'organe, laquelle n'aura pas, forcément, une étendue inférieure à quelques centimètres carrés.

Il va de soi, par ailleurs, que le contraste sera d'autant meilleur et plus significatif que le facteur de démultiplication sera plus élevé.

Les premières recherches expérimentales sur fantômes montrent que la méthode que nous avons mise au point, fournit une augmentation significative du contraste de l'image scintigraphique et permet, en conséquence, un repérage plus aisé des zones qui ont une activité inférieure ou supérieure de 10% par rapport aux zones environnantes (fig. 5 et 6).

Ces données expérimentales sont confirmées par les examens cliniques (fig. 7, 8, 9, 10, 11a et 11b).

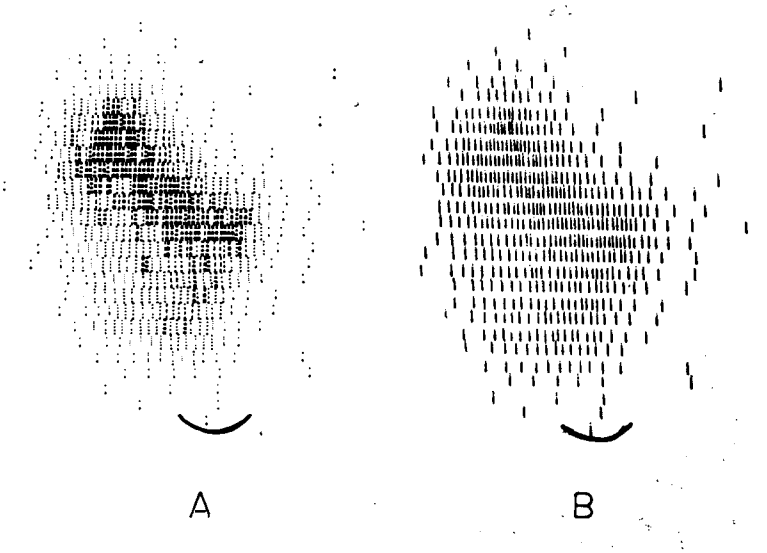

Figure 7

Scintigrammes thyroïdiens (adénome hyperfonctionnant avec dégénération kystique): l'enregistrement à contraste accentué (A) permet une différenciation plus nette des variations d'activité.

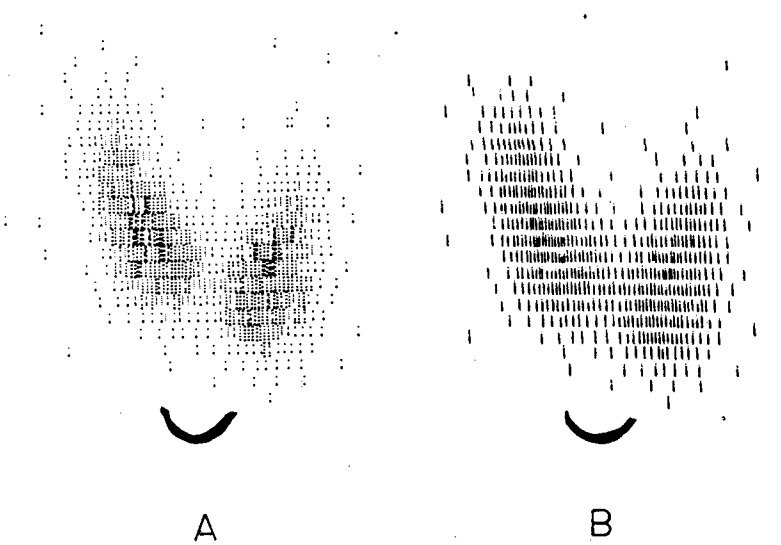

Figure 8

Scintigrammes thyroïdiens (sujet normal): l'enregistrement à contraste accentué (A) permet de reconnaître dans chaque lobe l'existence de 3 niveaux d'activité à mettre en rapport avec la variation d'épaisseur du tissu thyroïdien. (Etant donné que la dose de ^{131}I administrée était modeste, l'enregistrement a été effectué à la vitesse de 1, 75 mm/s et l'activité «maxima» n'a jamais atteint la valeur 100).

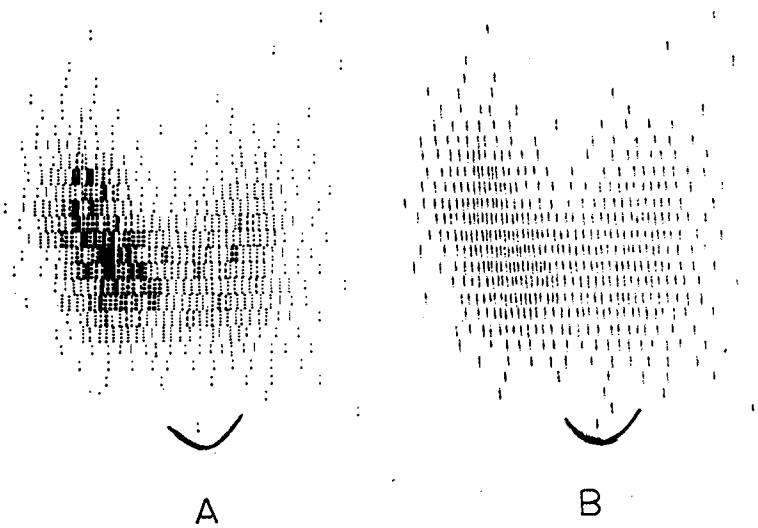

Figure 9

Scintigrammes thyroïdiens (sujet avec hyperplasie modeste du lobe droit): sur l'enregistrement (A) la différence entre les activités des deux lobes est plus nette.

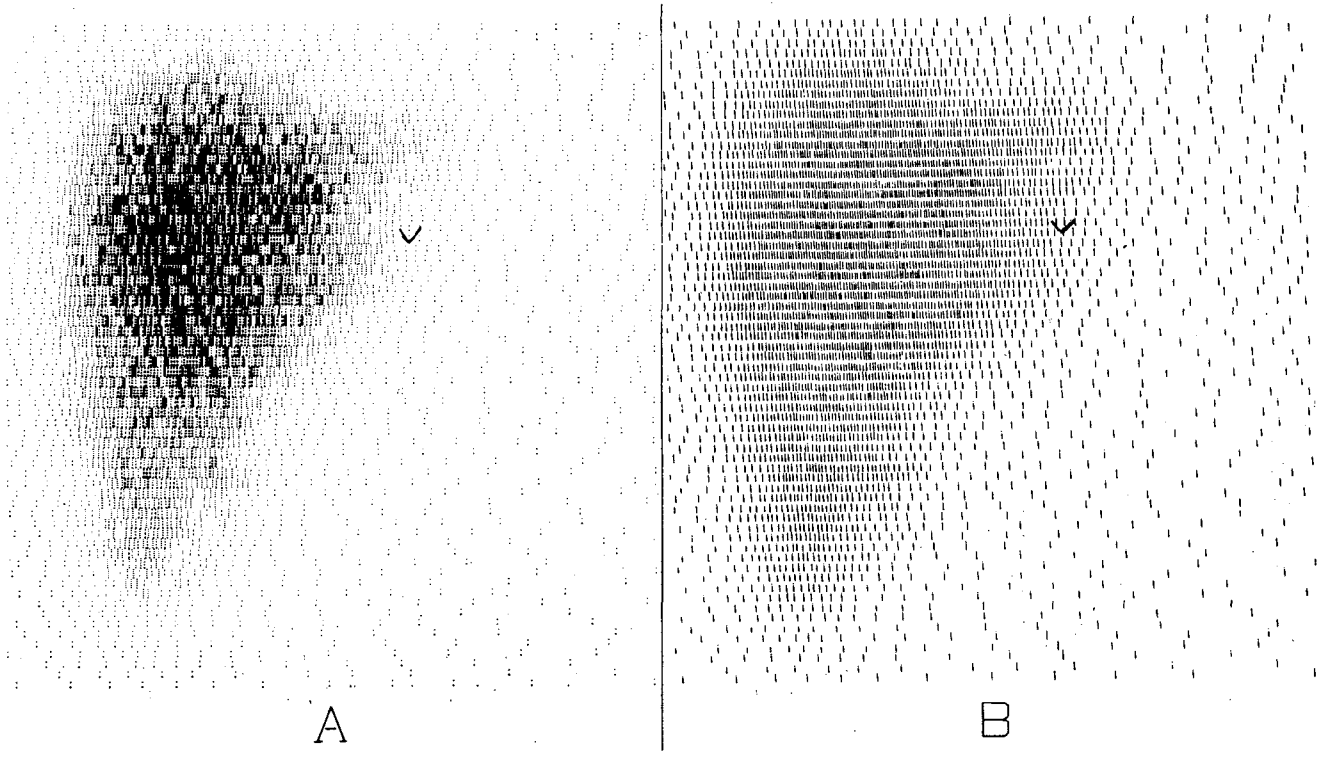

Figure 10

Hépatoscintigrammes avec ^{198}Au colloïdal (hépatomégalie modeste):
sur l'enregistrement (A) il est plus aisé reconnaitre les différents niveaux d'activité.

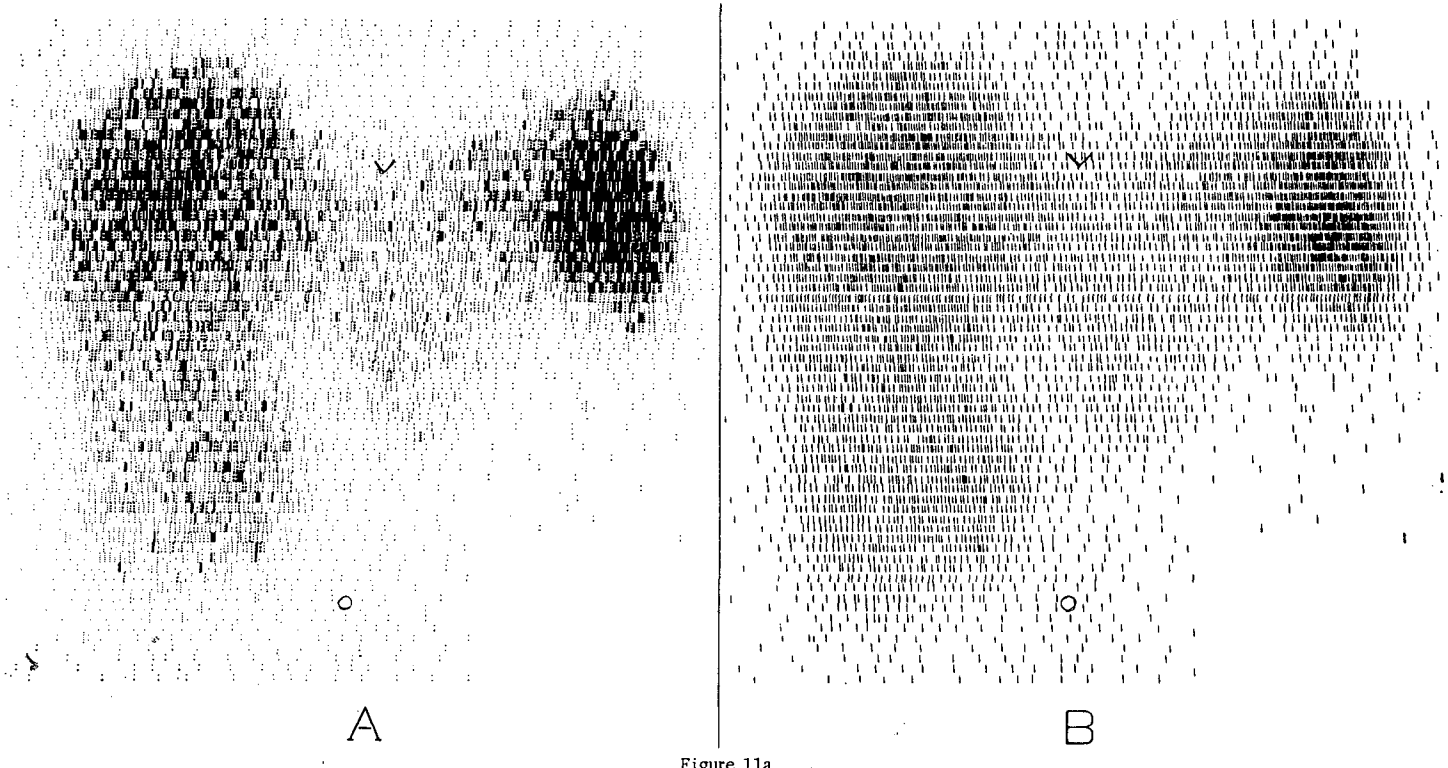

Figure 11a

Hépatoscintigrammes avec ^{198}Au colloïdal (cirrhose hypertrophique (?)):
les variations d'activité sont plus marquées sur le scintigramme effectué avec la nouvelle méthode (A);
sur cet enregistrement on peut de même reconnaître que la zone active dans la partie médiane de
l'hypocondre gauche appartient à la rate. Ceci est confirmé par l'enregistrement postérieur simultané
(fig. 11b).

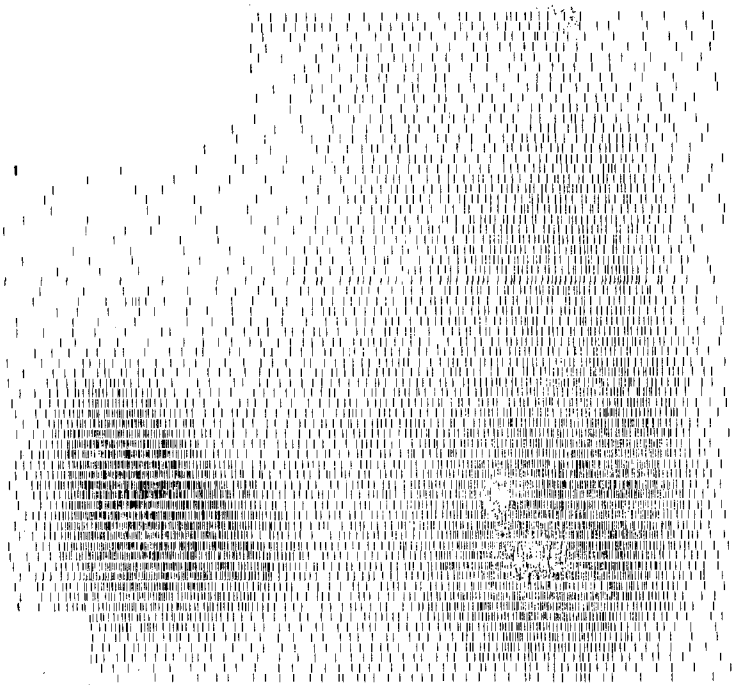

Figure 11b

Confirmation par enregistrement postérieur simultané.

Il nous semble donc pouvoir conclure que la méthode d'enregistrement réalisée présente quelques avantages par rapport à celles employées jusqu'à maintenant, et nous pensons pouvoir lui apporter des améliorations ultérieures en modifiant le code des caractères initialement employé.

RÉFÉRENCES

[1] BASCHIERI, I. et D'APUZZO, B., Nucl.- Med., 2 (1962) 290.

[2] TUBIANA, M. et ALBARÈDE, P., Ann. Radiol. 5 (1962) 173.

[3] FRIEDELL, H.L., Mac INTYRE, W.J. and REJALI, A.M., Amer. J. Roentgenol., 77 (1957) 455.

[4] DOERING, P., Medical Radioisotope scanning, AIEA, Vienne (1959) 114.

[5] MARZANO, E., Nunt. Radiol. 4 (1961) 296.

[6] BERNE, E. and JONSSON, U., Nucl.-Med. 1 (1959) 80.

[7] BENDER, M.A. and BLAU, M., Int. J. appl. Rad., 4 (1959) 154.

[8] MALLARD, J.R. and PEACHEY, C.J., Brit. J. Radiol. 32 (1959) 652.

[9] MALLARD, J.R. and PEACHEY, C.J., Proc. Third Int. Conf. Medical Electronics III London (1960) 511.

[10] KAKEHI, H., ARIMIZU, N., UCHIYAMA, G., GENTA, H. et KUBO, S., Simposio su «Le applicazioni della scintigrafia nella ricerca clinica». Roma (1963) sous presse.

[11] HINE, G.J., J. nucl. Med., 4 (1963) 439.

[12] HAWLICZEK, F. and ZITA, G., Nucl.-Med. 3 (1963) 312.

[13] BASCHIERI, I., Simposio su «Le applicazioni della scintigrafia nella ricerca clinica». Roma (1963) sous presse.

SYMPOSIUM ON MEDICAL RADIOISOTOPE SCANNING

HELD IN ATHENS, 20-24 APRIL 1964

CHAIRMEN OF SESSIONS

Session 1	B. MALAMOS	Dept. of Clinical Therapeutics, University of Athens
Session 2	L. G. LARSSON	World Health Organization, Geneva
Session 3	W. J. MacINTYRE	Highland View Hospital, Cleveland, Ohio
Session 4	E. E. POCHIN	World Health Organization, Geneva and International Commission on Radiological Protection
Session 5	G. BROWNELL	Physics Research Laboratory, Massachusetts General Hospital, Boston
Session 6	G. PANTAZIS	University of Athens
Session 7	T. SPÂRCHEZ	Faculté de Médecine, Bucarest
Session 8	L. DONATO	Centro di Medicina Nucleare, University of Pisa
Session 9	K. SCHEER	Universitäts-Strahlenklinik, Heidelberg
Session 10	M. TUBIANA	Institut Gustave Roussy, Villejuif (Seine)

SECRETARIAT OF THE SYMPOSIUM

Scientific Secretaries:	H. BELCHER	Division of Isotopes, IAEA
	G. GÓMEZ-CRESPO	Division of Isotopes, IAEA
Editor:	A. M. HAMENDE	Division of Scientific and Technical Information, IAEA
Records Officer:	N. W. A. JONES	Division of Languages, IAEA
Administrative Secretary:	H. H. STORHAUG	Division of Scientific and Technical Information, IAEA

IAEA SALES AGENTS

Orders for Agency publications can be placed with your bookseller or any of our sales agents listed below:

AUSTRALIA
Hunter Publications,
23 McKillop Street
Melbourne, C.1

AUSTRIA
Georg Fromme & Co.
Spengergasse 39
Vienna V

BELGIUM
Office international de librairie
30, avenue Marnix
Brussels 5

BRAZIL
Livraria Kosmos Editora
Rua do Rosario, 135-137
Rio de Janeiro

Agencia Expoente Oscar M. Silva
Rua Xavier de Toledo, 140-1° Andar
(Caixa Postal No. 5.614)
São Paulo

BYELORUSSIAN SOVIET SOCIALIST REPUBLIC
See under USSR

CANADA
The Queen's Printer
Ottawa, Ontario

CHINA (Taiwan)
Books and Scientific Supplies Service, Ltd.,
P.O. Box 83
Taipei

DENMARK
Ejnar Munksgaard Ltd.
6 Nörregade
Copenhagen K

FINLAND
Akateeminen Kirjakauppa
Keskuskatu 2
Helsinki

FRANCE
Office international de
documentation et librairie
48, rue Gay-Lussac
Paris 5e

GERMANY, Federal Republic of
R. Oldenbourg
Rosenheimer Strasse 145
Munich 8

ISRAEL
Heiliger and Co.
3 Nathan Strauss Street
Jerusalem

ITALY
Agenzia Editoriale Internazionale
Organizzazioni Universali (A.E.I.O.U.)
Via Meravigli 16
Milan

JAPAN
Maruzen Company Ltd.
6, Tori Nichome
Nihonbashi
(P.O. Box 605)
Tokyo Central

MEXICO
Libraría Internacional
Av. Sonora 206
Mexico 11, D.F.

NETHERLANDS
N.V. Martinus Nijhoff
Lange Voorhout 9
The Hague

NEW ZEALAND
Whitcombe & Tombs, Ltd.
G.P.O. Box 1894
Wellington, C.1

NORWAY
Johan Grundt Tanum
Karl Johans gate 43
Oslo

PAKISTAN
Karachi Education Society
Haroon Chambers
South Napier Road
(P.O. Box No. 4866)
Karachi, 2

POLAND
Ośrodek Rozpowszechniana
Wydawnictw Naukowych
Polska Akademia Nauk
Pałac Kultury i Nauki
Warsaw

SOUTH AFRICA
Van Schaik's Bookstore (Pty) Ltd.
Libri Building
Church Street
(P.O. Box 724)
Pretoria

SPAIN
Librería Bosch
Ronda de la Universidad 11
Barcelona

SWEDEN
C.E. Fritzes Kungl. Hovbokhandel
Fredsgatan 2
Stockholm 16

SWITZERLAND
Librairie Payot
40, rue du Marché
Geneva

TURKEY
Librairie Hachette
469, Istiklâl Caddesi
Beyoğlu, Istanbul

UKRAINIAN SOVIET SOCIALIST REPUBLIC
See under USSR

UNION OF SOVIET SOCIALIST REPUBLICS
Mezhdunarodnaya Kniga
Smolenskaya-Sennaya 32-34
Moscow G-200

UNITED KINGDOM OF GREAT BRITAIN AND NORTHERN IRELAND
Her Majesty's Stationery Office
P.O. Box 569
London, S.E.1

UNITED STATES OF AMERICA
National Agency for
International Publications, Inc.
317 East 34th Street
New York, N.Y. 10016

VENEZUELA
Sr. Braulio Gabriel Chacares
Gobernador a Candilito 37
Santa Rosalía
(Apartado Postal 8092)
Caracas D.F.

YUGOSLAVIA
Jugoslovenska Knjiga
Terazije 27
Belgrade

IAEA publications can also be purchased retail at the United Nations Bookshop at United Nations Headquarters, New York, at the news-stand at the Agency's Headquarters, Vienna, and at most conferences, symposia and seminars organized by the Agency.

In order to facilitate the distribution of its publications, the Agency is prepared to accept payment in UNESCO coupons or in local currencies.

Orders and inquiries from countries where sales agents have not yet been appointed may be sent to:

Publications Sales Unit, International Atomic Energy Agency,
Kärntner Ring 11, Vienna I, Austria

INTERNATIONAL
ATOMIC ENERGY AGENCY
VIENNA, 1964

PRICE: USA and Canada: US $11.50
Austria and elsewhere: S 241,50
(£3.9.0; F.Fr. 46,-; DM 40,25)